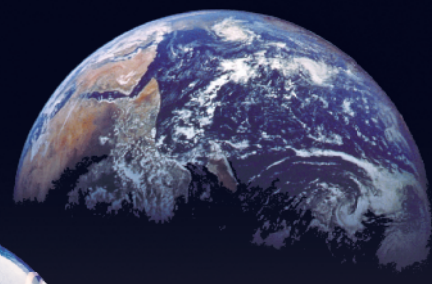Majid Amidpour ·
Mohammad Ebadollahi ·
Farkhondeh Jabari ·
Mohammad-Reza Kolahi ·
Hadi Ghaebi   *Editors*

Synergy Development in Renewables Assisted Multi-carrier Systems

Springer

Green Energy and Technology

Climate change, environmental impact and the limited natural resources urge scientific research and novel technical solutions. The monograph series Green Energy and Technology serves as a publishing platform for scientific and technological approaches to "green"—i.e. environmentally friendly and sustainable—technologies. While a focus lies on energy and power supply, it also covers "green" solutions in industrial engineering and engineering design. Green Energy and Technology addresses researchers, advanced students, technical consultants as well as decision makers in industries and politics. Hence, the level of presentation spans from instructional to highly technical.

Indexed in Scopus.

Indexed in Ei Compendex.

More information about this series at https://link.springer.com/bookseries/8059

Majid Amidpour · Mohammad Ebadollahi ·
Farkhondeh Jabari · Mohammad-Reza Kolahi ·
Hadi Ghaebi
Editors

Synergy Development in Renewables Assisted Multi-carrier Systems

Editors
Majid Amidpour
Faculty of Mechanical Engineering
K. N. Toosi University of Technology
Tehran, Iran

Farkhondeh Jabari
Department of Power System Operation
and Planning
Niroo Research Institute
Tehran, Iran

Hadi Ghaebi
Faculty of Engineering
University of Mohaghegh Ardabili
Ardabil, Iran

Mohammad Ebadollahi
Faculty of Mechanical Engineering
K. N. Toosi University of Technology
Tehran, Iran

Mohammad-Reza Kolahi
Energy and Environmental Research Center
Niroo Research Institute
Tehran, Iran

In memory of maestro Mohammad-Reza Shajarian...

Preface

Due to the environmental pollution caused by fossil fuels and the non-permanent nature of these resources, the move toward the use of renewable energy has accelerated. Renewable energy systems are stable, do not pollute the environment, and lead to sustainable development in the countries. In recent years, many attempts have been made to improve the energy systems' performance by using multi-generation units and analyzing them from energy, exergy, economics, and the environment. This book's primary goal is the effort to introduce new methods for assessing and upgrading the synergy. Therefore, the book explores sustainable practices such as water-energy-food nexus in poly-generation units and novel desalination systems.

One of the significant issues in these energy systems is the storage methods; for instance, carbon capture to reduce environmental pollution and the hydrogen store for the utilization of supplementary fuel. In this regard, the elimination of carbon dioxide, the application of clean fuels such as renewable energy, and the special considerations in energy storage with the approach of improving the welfare of society are the other purposes of this book. Also, robust optimization, uncertainty and risk-aware probabilistic analysis, energy management, and power supply of sensitive places such as oil rig platforms by renewables are considered other aims of the book. Meanwhile, the uncertainty of these units has led to main concerns regarding the reliability and flexibility of the smart grids. Therefore, uncertainty analysis is performed to help store energy, especially in variable loads such as solar and wind energies.

This book is written with comprehensive and simultaneous approaches to all these concepts. While complementing previous books in this field, it adds several new methods and procedures. The authors propose a book as an appropriate reference for energy system specialists, academic researchers, and developers from energy sectors and environmental organizations.

This book retains its comprehensiveness and integrity, despite its extensive content. The book targets an interdisciplinary field, which is dedicated to energy systems and seeks to address the lack of fully inclusive references in this field. It presents exciting topics from introductory to advanced chapters and meets the needs of many enthusiasts in this field. Because the subject area of this book is broad, the authors focused on balancing each chapter's theoretical and practical aspects.

Finally, the authors hope that the book will be helpful to undergraduate and graduate students, researchers, and engineers, who are trying to solve and learn deep concepts in the field of energy engineering in renewable assisted multi-carrier systems.

Tehran, Iran   Majid Amidpour
Tehran, Iran   Mohammad Ebadollahi
Tehran, Iran   Farkhondeh Jabari
Tehran, Iran   Mohammad-Reza Kolahi
Ardabil, Iran   Hadi Ghaebi

Contents

Part I
Efficiency Improvement from Energy, Exergy, Economic, and Environmental Viewpoints, and Water, Energy, and Food Nexus

Chapter 1
Exergoeconomic Analysis of Energy Conversion Systems: From Fundamentals to Applications

Muhammad Ahmad Jamil, Haseeb Yaqoob, Talha S. Goraya, Muhammad Wakil Shahzad, and Syed M. Zubair

Abstract Exergoeconomic analysis, a simultaneous investigation of exergetic and monetary performance has attained significant attention to analyze and improve the performance of energy conversion systems. This combined analysis allows an individual audit of all the components in the system. The research is particularly useful for multi-component systems to get a better understanding of how effectively each component consumes energy and economic capital. This chapter aims to present a comprehensive theoretical framework for exergoeconomic study of thermal systems. For this purpose, the framework is initially developed for standalone heat exchangers and then extended to commercial-scale thermal desalination systems consisting of preheaters, pumps, evaporators, and compressors, etc. The exergetic and economic values of each stream in the system were evaluated using the developed framework. The sensitivity and parametric analysis of different thermodynamic and economic parameters on the system performance was conducted to study the performance variations. The presented model can be generalized for performance analysis of other systems.

M. A. Jamil (✉) · M. W. Shahzad
Mechanical and Construction Engineering Department, Northumbria University, Newcastle Upon Tyne N1 8ST, UK
e-mail: muhammad2.ahmad@northumbria.ac.uk

M. W. Shahzad
e-mail: muhammad.w.shahzad@northumbria.ac.uk

H. Yaqoob · T. S. Goraya
Department of Mechanical Engineering, Khwaja Fareed University of Engineering and Information Technology, Rahim Yar Khan 64200, Pakistan
e-mail: haseeb.yaqoob@kfueit.edu.pk

S. M. Zubair
Department of Mechanical Engineering, King Fahd University of Petroleum & Minerals, KFUPM Box # 1474, Dhahran 31261, Saudi Arabia
e-mail: smzubair@kfupm.edu.sa

Nomenclature

Variables

A	Area, m^2
C	Cost, \$/s
h	Enthalpy, kJ/kg
$\dot{m}$	Mass flow rate, kg/s
P	Pressure, *kpa*
$\dot{Q}$	Heat transfer rate, kW
s	Entropy, kJ/kg K
T	Temperature, ° C
$\dot{W}$	Work, kW
x	Specific exergy, kJ/kg
X	Exergy, kW

Greek Letters

Λ	Operational availability
β	Chevron angle °
ε	Effectiveness
Δ	Change in quantity
η	Efficiency, %

Subscripts/Superscripts

cap	Capital
ch	Chemical
comp	Compressor
D	Distillate
ele	Electricity
ene	Energy
eq	Equivalent
G	Generator
i	Inlet
misc	Miscellaneous
o	Outlet
ren	Renewable

the   Thermal
y   Amortization period
0   Dead state

Abbreviations

AD   Adsorption
CF   Conversion factor
CRF   Capital recovery factor
FF   Forward feed
GA   Genetic algorithm
HX   Heat exchanger
MED   Multi-effect desalination
MVC   Mechanical vapor compression
PCF   Parallel cross feed
PF   Parallel feed
PHX   Plate heat exchanger
PR   Performance ratio
RO   Reverse osmosis
STHX   Shell and tube heat exchanger
UPR   Universal performance ratio

1.1 Introduction

The economic efficiency of energy conversion systems is particularly focused on the last few decades because of soaring power requirements, optimal design constraints, environmental concerns, and high investments [1, 2]. Some of the major areas in this regard include power plants, air conditioning units, water desalination systems, and energy recovery heat exchangers [3–5]. This is because these areas have a direct impact on the human life cycle. For instance, power plants fulfill the energy demands [6], the air conditioning systems maintain the comfortable working and living environment [7], desalination systems supply drinking water [8], and the energy recovery sections enhance the performance efficiency of these systems through waste heat recovery [9]. Therefore, significant research is conducted in all these sectors to enhance their performance efficiencies from energy, economic and environmental standpoints. For instance, in the power plant sector, new power cycles [10], and the cooling industry sustainable technologies with low energy consumption and minimal environmental impacts [11] are being developed.

   Likewise, various developments in energy recovery heat exchangers and thermal desalination systems (which are the focus of this study) have been made [12, 13]. In

this regard, the commonly used heat exchangers for liquid phase energy recovery are shell-and-tube heat exchangers (STHX) and plate heat exchangers (PHX) [14, 15]. For STHX, the major interest has been the performance improvement through variation in design parameters including the number and orientation of baffles, and diameter, length, layout, and the number of tubes [16, 17]. Besides, the economic optimization of these HXs has also been conducted using different numerical techniques [18, 19]. For instance, Iyer et al. [20] achieved up to 52% cost reduction of STHX using Adaptive range and Genetic Algorithm (GA). Mirzaei et al. [21] used Constructal Theory and GA which reduced the investment cost by 32%. Tharakeshwar et al. [22] reported a 14% reduction using GA and Bat Algorithm. Segundo et al. [23], achieved a 54% reduction using the Differential Evolution algorithm. Rao and Siraj [24] attained a 33% decrement in the total cost using Elitist-Jaya Algorithm. Dhavle et al. [25], reported 52%, Hajabdollahi et al. [26] 35% and Mohanty [27] 29% using Cohort Intelligence Algorithm, sensitivity based GA and Firefly Algorithm, respectively.

While for plate heat exchangers the research focus has been on the plate features including length, width, protrusion/chevron angle (β), and enlargement factor [28, 29]. Nilpueng et al. [30] investigated the influence of surface roughness, chevron angle, and Reynolds number. They found that the heat transfer coefficient and pressure drop of 30° angle plates were 2.5 and 1.8 times greater than those of 60° angle plates, respectively. The 30° angle plates with the highest surface roughness and lowest Reynolds number had the best overall results. Turk et al. [31] used artificial neural networks to investigate the effect of mixed angle plates and found that they had no substantial effect on thermal performance. Similarly, Kumar et al. [32] reported that an increasing the chevron angle from (30°/30°) to (60°/30°) and then to (60°/60°) increased ΔP by 22.05% and 37.9%, respectively.

For desalination systems, the focus has been on energy and cost optimization particularly for thermal systems which are suitable for harsh feeds [33, 34]. The common systems in this regard include multi-effect desalination [35], multi-stage flash, mechanical/thermal vapor compression [36], electrodialysis [37], and other hybrid systems like MED hybrid with AD [38, 39]. Though, significant research has been conducted to improve the performance of desalination systems the equivalent energy consumption of conventional systems hover around 3.7–8 kWh/m^3 for RO, 14.45–21.35 kWh/m^3 for MED, and 19.58–27.25 kWh/m^3 for MSF [40, 41]. These energy consumptions are significantly higher (~5–30 times) than the minimum separation work (0.72 kWh/m^3 at 35 g/kg and 25 °C) [42]. Therefore, some novel systems like domestic scale units [43], hybrid systems [44], greener desalination technologies [45], integrated cooling and water production systems [46], and cogeneration plants [47] are also investigated.

It is important to mention that almost all the developments presented above either involve design modifications or the integration of new components. For the case of standalone components, the design modifications require a robust computational facility for the execution of a complex optimization algorithm. While for the multicomponent system, this approach is not viable because of being computationally expensive due to the combinatory effect of parameters. Moreover, most multicomponent systems are analyzed treating the whole system as a single unit. The total

expenditures, i.e., purchasing, chemical, labor, recurring, operation, and maintenance costs spent at system boundaries, are divided by the product (electricity, freshwater, cooling capacity, etc.) to calculate the unit product cost. Therefore, the approach provides a quick initial estimation of the product cost, however, it is difficult to locate the most sensitive parameters/components for performance improvement.

In this regard, the exergoeocnomic analysis method presented in this study has a significant potential for a detailed design and analysis of standalone as well as multi-component systems [48]. The method works by taking thermodynamics as well as economic parameters into account and investigating their individual as well as a combined effect on the system performance. Each component is analyzed individually to evaluate how efficiently the input thermodynamic (energy, exergy, etc.), as well as economic resources, are utilized on local as well as overall performance scale. Moreover, the approach also offers flexibility for design improvement and fault diagnosis. The current study presents a systematic procedure for exergoeocnomic analysis of thermal systems with applications. Two energy recovery heat exchangers and three industrial-scale mechanical vapor compression-based desalination systems are presented as an example. Based on the discussions made in the study, the method can also be extended to analyze other systems involving energy conversion mechanisms.

The remaining chapter is organized as follows, in Sect. 1.2, the exergoeconomic mathematical framework is formulated with examples of key components (pump, compressor, evaporator, etc.). Section 1.3 covers illustrative examples for an application of exergoeocnomic analysis on standalone (heat exchangers) and multicomponent systems (desalination systems). The conclusion is presented in Sect. 1.4.

1.2 Problem Formulation

A comprehensive framework for exergoeconomic analysis of energy conversion systems is formulated in this study. The analysis is employed as a combined application of thermodynamic and economic analyses. The analysis proceeds by calculating the exergetic and monetary values of all the fluid streams in the systems as they pass through each component. The exergy value is calculated based on temperature, pressure, and chemical potential. While the monetary value is calculated based on the capital and operational expenses of each component individually. The product is characterized by the main function of the parts, such as high-pressure water for a pump, compressed vapor for a compressor, and evaporated vapors for evaporators. In the first step, the significance of selecting appropriate input energy calculation metrics (i.e., exergy) is presented by reviewing different available models. Then a systematic procedure for developing cost balance equations for different key components is established. Finally, the illustrative examples of heat exchangers as a standalone system and thermal desalination systems as a multi-component system analysis are presented.

1.2.1 On Energy Metrics

The input energy metric is very important in desalination system calculations because of being a decisive parameter for selection among different systems. The accurate calculation of energy consumption requires an equal emphasis on its quantitative, qualitative, and source characteristics. This is because the same quantity (W) of different energy grades like thermal, mechanical, or electrical, etc. correspond to different metrics and costs. Both factors must be considered for a fair comparison of unit energy usage of multiple desalination systems working with different energy forms. Therefore, to handle the potential discrepancies in performance metrics due to variations in input energy calculations, the following notable efforts have been made.

The exergy-based calculation model [49, 50] asserts that all the calculations in the thermal systems should be based on the exergy of streams (which represents the maximum theoretical work) rather than energy. Where the stream exergy was defined based on a uform dead state as given below [51].

$$X(kW) = \dot{m}\,x = \dot{m}\left[\{(h - h_0) - T_0(s - s_0)\} + x_{ch}\right] \tag{1.1}$$

where h and S denote the stream enthalpy and entropy while, h_0, S_0 represents the dead state enthalpy and entropy (T_0, P_0) and x_{ch} denotes the chemical exergy.

An equivalent electricity consumption model was proposed to cumulate secondary energy inputs (electricity) with the primary energy inputs (steam) using electrical energy units [52]. It refers to the amount of electrical work that might have been produced if the desalination system had been supplied with steam. This electrical work is estimated by expanding an equivalent amount of steam in a theoretical steam turbine as given below [52].

$$\dot{W}(kW) = \dot{m}\,\eta_G(h_i - h_o) \tag{1.2}$$

where η_G is the generator efficiency (taken 95%), steam outlet temperature 35 °C, and the turbine efficiency as 85% [52]. The equivalent electricity consumption is calculated as.

$$E_{eq}(kWh/m^3) = \frac{\dot{W}}{3.6\,\dot{m}_D} \tag{1.3}$$

A universal performance ratio model was proposed to assess the desalination system performance on a common platform using primary energy [53]. The model is important for a cogeneration system that observes inappropriate distribution among energy given for electricity and desalination. Unlike the conventional performance ratio (PR) formula (based on derived energy), in the proposed UPR the derived energies are corrected with conversion factors (CF) as given below [54].

$$UPR = \frac{evaporative\ energy}{primary\ energy\ input}$$

$$= \frac{h_{fg}}{3.6\{CF_1\left(\frac{kWh}{m^3}\right)_{ele} + CF_2\left(\frac{kWh}{m^3}\right)_{the} + CF_3\left(\frac{kWh}{m^3}\right)_{ren}\}} \tag{1.4}$$

According to the above discussion, exergy is the true indicator of plant input energy in the plant. Therefore, the calculation model presented below is based on the exergetic cost of fluids streams.

1.2.2 Components of Exergoeconomic Analysis

The economic analysis involves the calculation of capital cost, input energy cost, operation and maintenance cost, and other applicable miscellaneous costs heads as product post-treatment, storage, distribution cost, etc. Among these different components, the capital cost represents the purchasing cost obtained from the market or calculated using well-established correlations [55]. It depends upon component capacity, material, efficiency, and local market situation. While the energy cost depends upon input energy type, consumption, and unit cost. Similarly, the maintenance cost depends upon the shutdown time and parts replacement. Therefore, the total cost rate equation is given as:

$$C_{total}(\$/s) = C_{cap} + C_{ene} + C_{O\&M} + C_{ch} + C_{misc} \tag{1.5}$$

It is important to mention that all the costing terms in the above equation should correspond to same units i.e., *($/s)*. For this purpose, the capital cost ($) is multiplied with the capital recovery factor (CRF) using interest rate, and amortization period given as below [56].

$$CRF = \frac{i \times (1+i)^y}{(1+i)^y - 1} \tag{1.6}$$

$$C_{cap} = \frac{\overline{C}_{cap} \times CRF}{365 \times 24 \times 3600 \times \Lambda} \tag{1.7}$$

Similarly, the energy cost is obtained in $/s by multiplying the energy consumption (kW) with the unit energy cost ($/kJ). Likewise, the other costs i.e., labor, chemical, maintenance, etc. are also converted into *$/s* using appropriate unit rates and consumption rates.

In conventional economic analysis, the total cost calculated using Eq. 1.5 is finally divided by the output which is different for different systems e.g., for power plants it is electricity, for refrigeration systems it is cooling capacity, for heat exchangers, it is energy recovered, and for desalination systems, it is desalinated water.

While, in the exert economic analysis, each component is investigated individually using a cost balance equation consisting of its local inputs, outputs, and fixed cost rate as given below [57].

$$C_{outputs}(\$/s) = \Sigma \, C_{inputs} + C_{cap} \tag{1.8}$$

It's worth mentioning that the output cost of the equipment with a single output stream (such as compressors, pumps, and blowers) is measured as shown above. Meanwhile, additional supplementary calculations are needed to solve the cost balance equation for components with several outlet streams (e.g., evaporators, heat exchangers, etc.). For a system with "J" outlet streams, a "J-1" number of supplementary equations based on the equality of the average cost of inlet and outlet streams are needed to solve the system as given below [58].

$$\frac{C_{inlet}}{X_{inlet}} = \frac{C_{outlet}}{X_{outlet}} \tag{1.9}$$

The sample cost equations for the common system component are given in Table 1.1.

1.3 Illustrative Examples and Discussions
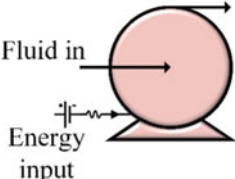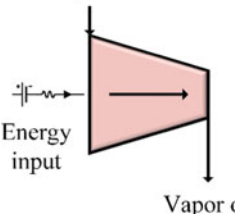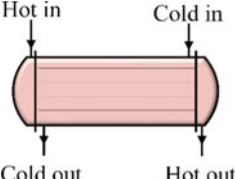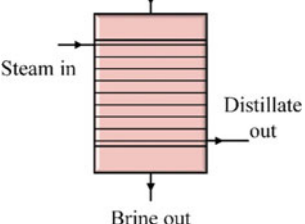
The exergoeconomic analysis investigates every system component (either standalone or multi-component) as a complete system with its local inputs, outputs, and capital cost. For instance, in the case of pumps, the local output is pressurized water while the local inputs are water stream and electricity. Similarly, for heat exchangers, the local inputs are cold-and-hot fluid inlet streams, while the outputs are cold-and-hot fluid outlet streams. However, the single major output of HXs is decided to depend upon their main function i.e., whether it is used as a cooler (e.g., lubricating oil coolers in power generation), or as a heater (e.g., feed heater/preheater in the desalination systems). Similarly, for multicomponent systems, besides defining local inputs and outputs, and overall production of the system is optimized. For instance, in the case of a power plant, the electricity production cost is the global output, while for a desalination system, it is the freshwater production cost. The below section presents the effect of major input parameters on the output stream cost for standalone as well as multi-component systems.

1.3.1 Standalone Component (Heat Exchanger Analysis)

For standalone system example, two different heat exchangers i.e., a shell and tube heat exchanger (STHX) and a plate heat exchanger (PHX) are considered. These heat
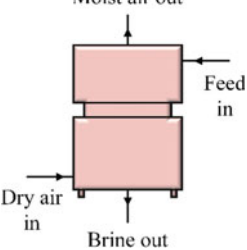
Table 1.1 The cost balance equations for some common thermal system components [59, 60]

Sr	Component & cost function	Cost balance equation
1	**Pump**: $\overline{C}_{cap} = f(\dot{m}, \dot{W}, \eta, P)$ 	$C_{fluid,\,out} = C_{fluid,\,in} + C_{ele}\,\dot{W}_{Pump} + C_{cap,\,pump}$
2	**Compressor**: $\overline{C}_{cap} = f(\dot{m}, \dot{W}, \eta, P)$ 	$C_{vapor,\,out} = C_{vapor,\,in} + C_{ele}\,\dot{W}_{comp} + C_{cap,\,comp}$
3	**Heat exchanger**: $\overline{C}_{cap} = f(\dot{m}, \dot{Q}, \varepsilon, A, \Delta P, \Delta T)$ 	$C_{cold,\,out} =$ $C_{cold,\,in} + C_{hot,\,in} - C_{hot,\,out} + C_{cap,\,HX}$ $\frac{C_{hot,\,in}}{X_{hot,\,in}} - \frac{C_{hot,\,out}}{X_{hot,\,out}} = 0$ or $C_{hot,\,out} =$ $C_{cold,\,in} + C_{hot,\,in} - C_{cold,\,out} + C_{cap,\,HX}$ $\frac{C_{cold,\,in}}{X_{cold,\,in}} - \frac{C_{cold,\,out}}{X_{cold,\,out}} = 0$
4	**Evaporator**: $\overline{C}_{cap} = f(\dot{m}, \dot{Q}, \varepsilon, A, \Delta P, \Delta T)$ 	$C_{Vapor,\,out} = C_{Feed,\,in} + C_{Steam,\,in} - C_{Brine,\,out}$ $- C_{Distillate,\,out} + C_{cap,\,Evap}$ $\frac{C_{Steam,\,in}}{X_{Steam,\,in}} - \frac{C_{Distillate,\,out}}{X_{Distillate,\,out}} = 0$ & $\frac{C_{Feed,\,in}}{X_{Feed,\,in}} - \frac{C_{Brine,\,out}}{X_{Brine,\,out}} = 0$

Table 1.1 (continued)

Sr	Component & cost function	Cost balance equation
5	**Humidifier**: $\overline{C}_{cap} = f(\dot{m}, \varepsilon, \Delta T, A)$ Moist air out Feed in Dry air in Brine out	$C_{moist\,air,\,out} = C_{dry\,air,\,in} + C_{Feed,\,in}$ $- C_{Brine,\,out} + C_{cap,\,Hum}$ $C_{Feed,\,in} = C_{Brine,\,out}$

A = area (m^2), $\dot{m}$ = mass flow rate (kg/s), $\dot{Q}$ = heat capacity (kW), ε = effectiveness (%), ΔP = pressure differential (kPa), ΔT = temperature differential (°C).

exchangers work as energy recovery heat exchangers with the purpose to preheat the intake water by recuperating the waste heat. The STHX is analyzed with three different methods including Kern, Bell-Delaware, and Wills-Johnston methods as presented in a recent study by Jamil et al. [61]. The operating parameters used in the analysis are presented in Table 1.2. In the first step, the cost flow diagram exhibiting the stream cost at the inlet and outlet of the pumps and HX is presented in Fig. 1.1. It is important to note that, the intake cost, in this case, is negligible (taken as 0$) because the normal lake water without any pretreatment is pumped to the heat exchanger. However, it varies in the case of chemicals/chemically treated water. After that, the effect of cold-water flow rate on the stream outlet cost is studied with three methods. The analysis showed that (refer to Fig. 1.2) an increase in the cold (shell-side) flow rate increased the cold product/stream outlet ($C_{cold,\,out}$) cost. As the mass flow rate of the cold fluid is increased from 15 to 45 kg/s, the commodity cost

Table 1.2 Heat exchangers operating parameters [61, 62]

Parameter	Value	
	STHX [61]	PHX [62]
Mass flow rate (hot/cold), kg/s	28/69	13/13
Hot fluid temperature (inlet/outlet), °C	95/40	63/23
Cold fluid temperature (inlet/outlet), °C	25/40	21/57
Heat transfer area, m^2	279	245
Overall heat transfer coefficients, kW/m^{2}K	0.84	4.9
Pumping power, kW	1.73	1.56

$C_{hot, in} = 0.11$ \$/h

$C_{cold, in} = 0.11$ \$/h

$C_{cap, STHX} = 106$ k\$

$C_{cap, Pump} = 1.1$ k\$

$C_{hot.out} = 0.0027$ \$/h $C_{cold.out} = 2.62$ \$/h

$C_{hot, in} = 0$ \$/h $C_{cold, in} = 0$ \$/h
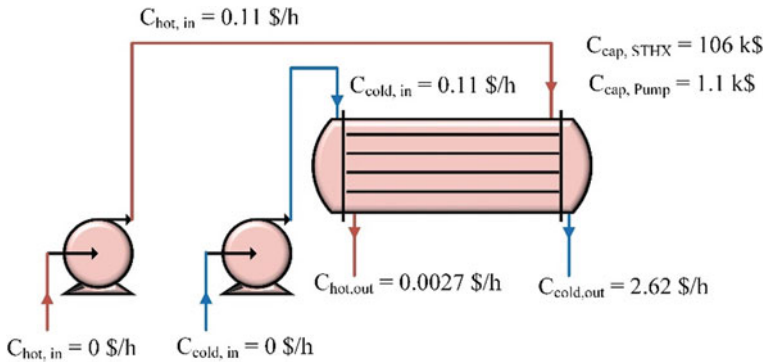
Fig. 1.1 Cost flow diagram for STHX

$m_t = 68.9 \ kg/s, \ i = 10\%, C_{ele} = 0.09(\$/kWh), \ \Lambda = 7000(h/y),$
$C_{h,i} = C_{c,i} = 0 \ (\$/h)$
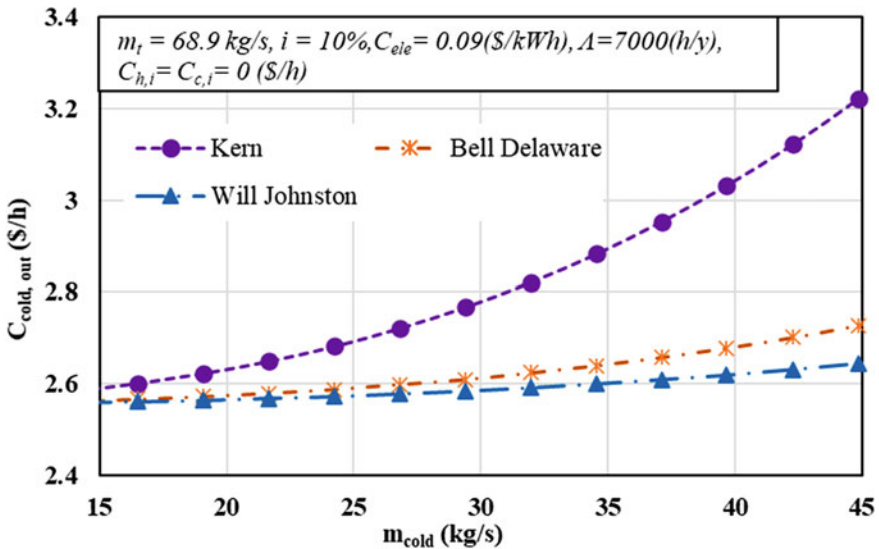
Fig. 1.2 Variation in cold fluid outlet cost versus cold fluid flow rate for STHX

for the Bell-Delaware and Wills-Johnston methods increased by 6–8 percent, and the Kern method increased by about 20%. This increase in stream cost is because of an increase in the pressure drop which increased the pumping power and energy cost. Moreover, the remarkable difference in the calculations made using the Kern method gives very high-pressure drop values particularly at high flow rates because of a less accurate and very simple formulation. As a result, the other two approaches can be used to reduce resources and economic investments with a realistic design.

Similarly, Fig. 1.3, shows the cost flow diagram for PHX used as a preheater for the desalination system. The intake cost is taken as 4.6\$/h as the chemically treated seawater is fed to pumps and heat exchangers to mitigate fouling issues. Then the

$C_{hot, in} = 4.7$ $/h $C_{hot,out} = 0.52$ $/h

$C_{cold, in} = 4.7$ $/h

$C_{cold,out} = 12$ $/h

$C_{cap, PHX} = 161$ k$

$C_{cap, Pump} = 1.2$ k$

$C_{hot, in} = 4.6$ $/h $C_{cold, in} = 4.6$ $/h
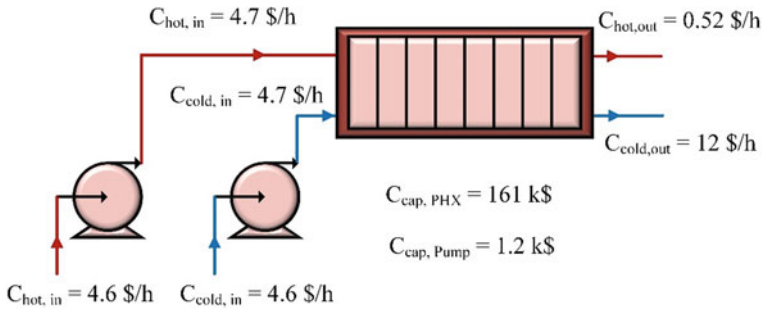
Fig. 1.3 Cost flow diagram for PHX

variation in the product cost for a PHX with different chevron angles at varying flow rates is studied. The input data for the analysis is given in Table 1.2 and the design procedure used is presented in detail in a recent study by Jamil et al. [62]. The analysis showed that (refer to Fig. 1.4) product/cold stream outlet cost $C_{cold,\ out}$ increased by 2–6% with increasing flow rate from 2–20 kg/s because of the increasing pressure drop that increased the pumping power. Similarly, for chevron angles, the $C_{cold,\ out}$, followed the following order $\beta = 30° > 45° > 50° > 60°$.

$m_h = 13$ kg/s, $i = 10\%$, $C_{ele} = 0.09$ $/kWh, $\Lambda = 7000$ h/y, $C_{c,i} = C_{h,i} = 4.9$ $/h

$C_{cold,\ out}$ ($/h)

- $\beta = 30°$ $\beta = 45°$
- $\beta = 50°$ $\beta = 60°$

m_{cold} (kg/s)
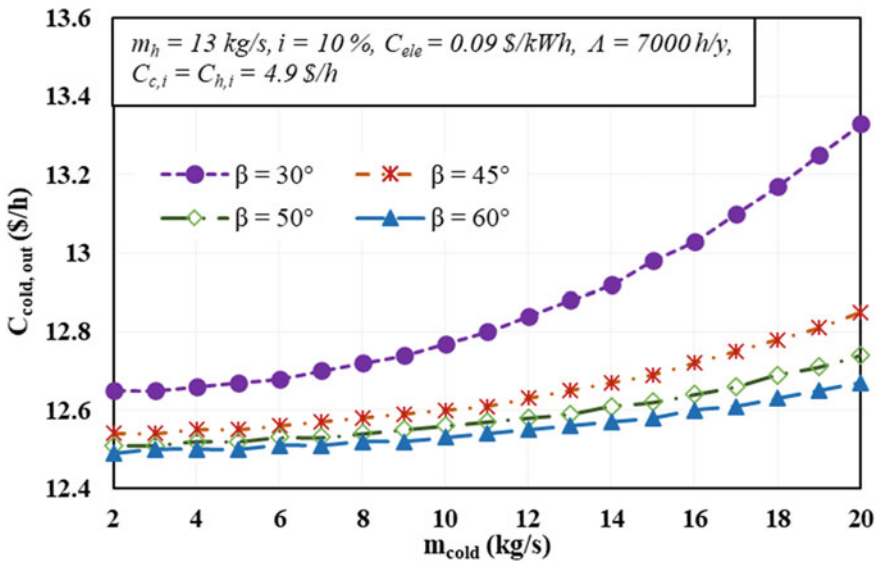
Fig. 1.4 Variation in cold fluid outlet cost versus cold fluid flow rate for PHX

1.3.2 Multi-Component System (Desalination System Analysis)

A mechanical vapor compression desalination device with a water output capacity of 35 kg/s is provided as an example of a multi-component system. Forward feed (FF), parallel feed (PF), and parallel crossfeed (PCF) are the three common feed flow configurations used by the system. The design specifications and operating conditions used in the analysis are adopted from a detailed study by Jamil and Zubair [63]. In the first step, the cost flow diagram representing the stream cost for all three feed configurations is developed and presented in Fig. 1.5. After that, a detailed parametric analysis is conducted for all three systems. As an example, the impact of compressor efficiency on the cost of freshwater output is discussed. The effect of compressor efficiency η_{comp} is more dominant at a lower number of evaporators (refer to Fig. 1.6) than at a higher number. As a result, rising η_{comp} substantially reduced the product cost C_P. As there are more evaporators, though, the capital cost governs the running cost, and the cost of producing water becomes less sensitive to compressor performance. For example, in the FF case, C_P decreased by 20% for a 2-effect system with η_{comp} ranging from 55 to 85%. While the 5-effect system showed only a 17% decrease for the same variation in η_{comp}. Similar behavior is observed for other flow arrangements with slightly different magnitudes (Figs. 1.7 and 1.8).
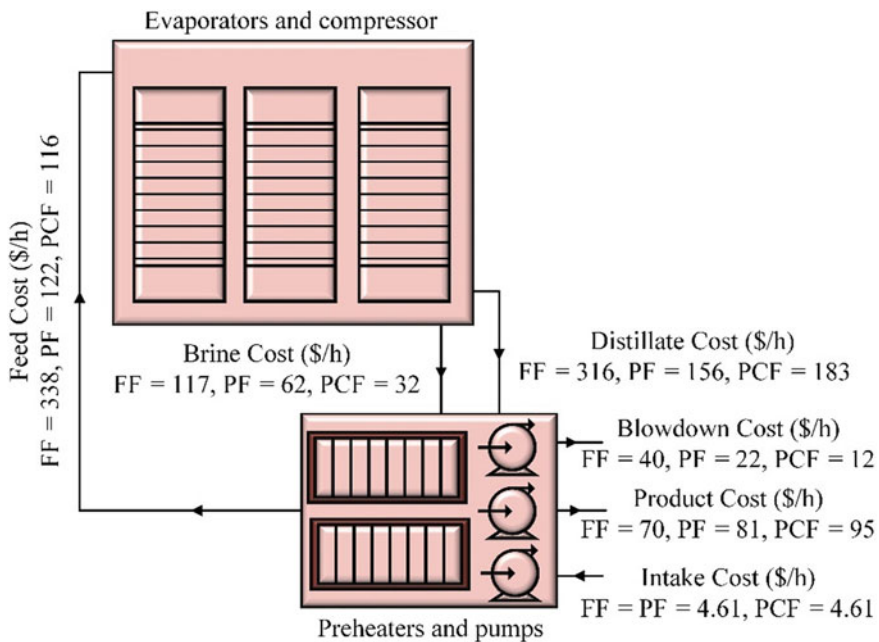
Fig. 1.5 Cost flow diagram for multi-effect MVC system under forward (FF), parallel (PF), and parallel crossfeed (PCF) arrangement
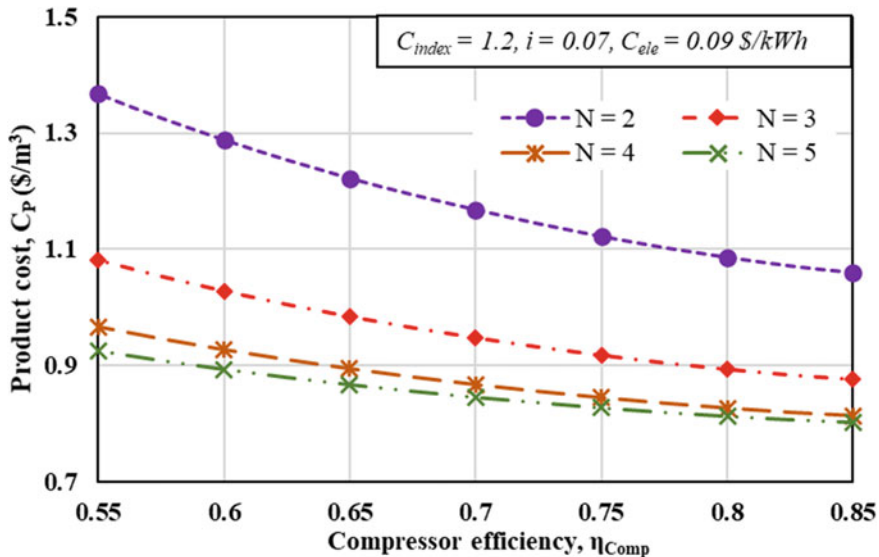
Fig. 1.6 Variation in cold fluid outlet cost versus cold fluid flow rate for PHX
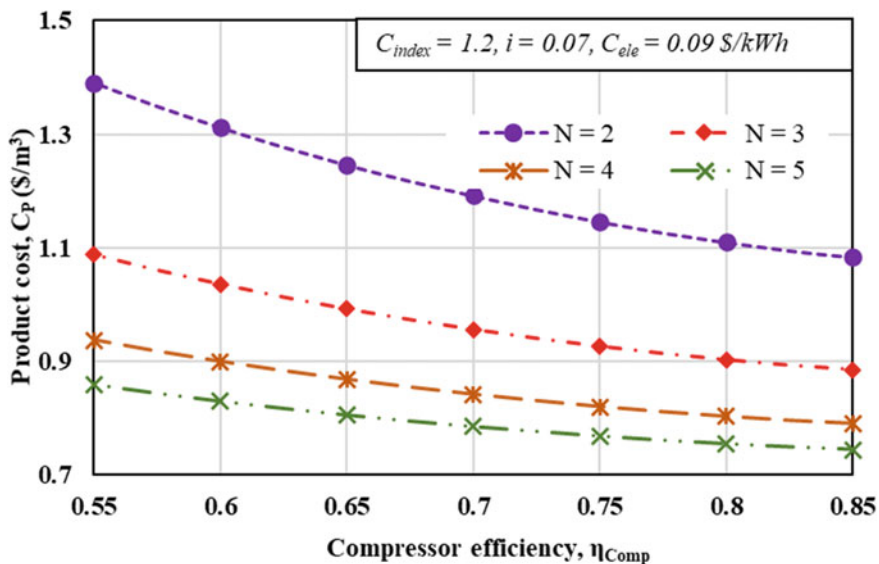
Fig. 1.7 Variation in cold fluid outlet cost versus cold fluid flow rate for PHX
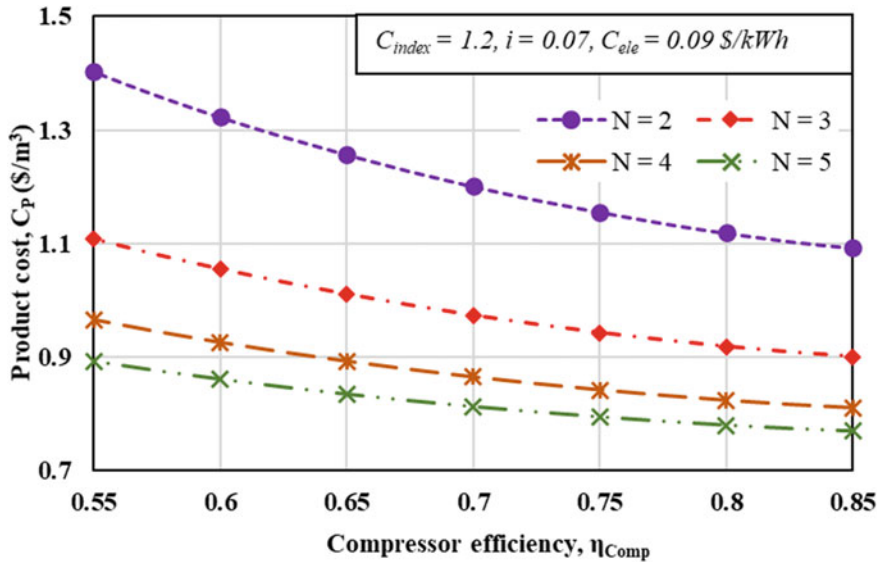
Fig. 1.8 Variation in cold fluid outlet cost versus cold fluid flow rate for PHX

1.4 Conclusion

The chapter presents a comprehensive theoretical framework for exergoeocnomic analysis of standalone and multi-component systems. The presented model is equally important for investigation, malfunction detection, and simultaneous thermodynamic and economic performance optimization of energy conversion systems. Two distinct energy recovery exchangers i.e., shell-and-tube heat exchanger and plate heat exchanger are solved using the proposed method as an example of standalone system analysis. Similarly, a multi-effect mechanical vapor compression desalination system operating under three different feed flow arrangements is analyzed as a multi-component system example. In the first step, cost flow diagrams depicting stream cost ($/h) are developed for all these systems. These diagrams indicate the contribution of each component in the system (from both capital and operational cost perspectives) in achieving the final product cost. After that, a parametric analysis using output stream cost against different input parameters is conducted.

In the case of heat exchangers (both STHX and PHX), the study revealed that increasing the flow rate raised the production cost due to higher pressure drop, which increased pumping power and energy usage. Meanwhile, it is also important to note that higher flow rate results in a higher heat transfer coefficient, however, a higher flow rate is not recommended above a certain range because of an exponential rise in pressure drop and operational cost. In the case of STHX, for example, increasing the shell side flow rate from 15 to 45 kg/s raised the cold stream outlet cost by 6 to

8%. Likewise, for PHX, the increase in stream outlet cost was observed 2–6% for different chevron angles when the flow rate increased from 2–20 kg/s.

In the case of a desalination system, the effect of compressor efficiency on the water production cost is studied. For instance, for the forward feed case, the product cost sowed a 20% decrease for a 2-effect system, when compressor efficiency varied from 55–85%. While the 5-effect system, showed only a 17% decrease for the same variation in the compressor efficiency. Therefore, it is observed that that at a lower number of evaporators, the effect of compressor efficiency η_{comp} is dominant than that at the higher number because of the major contribution of operating cost.

Overall, it is concluded that in conventional thermodynamic analysis the economic part is missing while in economic analysis the effect of monetary parameters is studied only. Although the presented framework allowed for simultaneous investigation of the impact of thermodynamic parameters on the economic performance of thermal systems.

References

1. N. Chitgar, M. A. Emadi, A. Chitsaz, M. A. Rosen, Investigation of a novel multigeneration system driven by a SOFC for electricity and fresh water production. Energy Convers. Manag. 196 (June), 296–310 (2019). https://doi.org/10.1016/j.enconman.2019.06.006.
2. T. Gholizadeh, M. Vajdi, H. Rostamzadeh, Exergoeconomic optimization of a new trigeneration system driven by biogas for power, cooling, and freshwater production. Energy Convers. Manag. **205** (August 2019), 112417 (2020)
3. M. A. Jamil, B. B. Xu, L. Dala, M. Sultan, L. Jie, M. W. Shahzad, Experimental and normalized sensitivity based numerical analyses of a novel humidifier-assisted highly efficient indirect evaporative cooler. Int. Commun. Heat Mass Transf. **125**, 105327 (2021). https://doi.org/10.1016/j.icheatmasstransfer.2021.105327.
4. M.A. Jamil, Z.U. Din, T.S. Goraya, H. Yaqoob, S.M. Zubair, Thermal-hydraulic characteristics of gasketed plate heat exchangers as a preheater for thermal desalination systems. Energy Convers. Manag. **205** (October 2019), 112425 (2020). https://doi.org/10.1016/j.enconman.2019.112425.
5. M.J. Rahimi, B. Ghorbani, M. Amidpour, M.H. Hamedi, Configuration optimization of a multigeneration plant based on biomass gasification. Energy **227**, 120457 (2021). https://doi.org/10.1016/j.energy.2021.120457
6. H. Wei, X. Huang, L. Chen, L. Yang, X. Du, Performance prediction and cost-effectiveness analysis of a novel natural draft hybrid cooling system for power plants. Appl. Energy **2020**(262), 114555 (2019). https://doi.org/10.1016/j.apenergy.2020.114555 (December)
7. M. W. Shahzad, M. Burhan, D. Ybyraiymkul, S. J. Oh, K. Choon, An improved indirect evaporative cooler experimental investigation. Appl. Energy **256** (September), 113934 (2019)
8. H. Rostamzadeh, A.S. Namin, H. Ghaebi, M. Amidpour, Performance assessment and optimization of a humidification dehumidification (HDH) system driven by absorption-compression heat pump cycle. Desalination **447**(June), 84–101 (2018)
9. S. DeAntonellis, L. Cignatta, C. Facchini, P. Liberati, Effect of heat exchanger plates geometry on performance of an indirect evaporative cooling system. Appl. Therm. Eng. **173** (July 2019), 115200 (2020). https://doi.org/10.1016/j.applthermaleng.2020.115200
10. B. Ghorbani, M. Amidpour, Energy, exergy, and sensitivity analyses of a new integrated system for generation of liquid methanol, liquefied natural gas, and crude helium using organic rankine cycle, and solar collectors. J. Therm. Anal. Calorim. (2021). https://doi.org/10.1007/s10973-021-10659-9

11. M.W. Shahzad, J. Lin, B.B. Xu, L. Dala, Q. Chen, M. Burhan, M. Sultan, W. Worek, K.C. Ng, A spatiotemporal indirect evaporative cooler enabled by transiently interceding water mist. Energy **217**, 119352 (2020). https://doi.org/10.1016/j.energy.2020.119352

12. V.C. Onishi, M.H. Khoshgoftar, R. Salcedo-díaz, A. Caballero, Thermo-economic and environmental optimization of a solar-driven zero-liquid discharge system for shale gas wastewater desalination rub ´. Desalination **511**(April), 115098 (2021). https://doi.org/10.1016/j.desal.2021.115098

13. S.E. Shakib, M. Amidpour, M. Boghrati, M.M. Ghafurian, A. Esmaieli, New approaches to low production cost and low emissions through hybrid MED-TVC+RO desalination system coupled to a gas turbine cycle. J. Clean. Prod. **295**, 126402 (2021). https://doi.org/10.1016/j.jclepro.2021.126402

14. Z. Zhang, D. Ma, X. Fang, X. Gao, Experimental and numerical heat transfer in a helically baffled heat exchanger combined with one three-dimensional finned tube. Chem. Eng. Process. Process Intensif. **47**(9–10), 1738–1743 (2008)

15. R.V. Rao, V. Patel, Multi-objective optimization of heat exchangers using a modified teaching-learning-based optimization algorithm. Appl. Math. Model. **37**(3), 1147–1162 (2013). https://doi.org/10.1016/j.apm.2012.03.043

16. B.A. Abdelkader, S.M. Zubair, The effect of a number of baffles on the performance of shell-and-tube heat exchangers. Heat Transf. Eng. **40**(1–2), 39–52 (2019). https://doi.org/10.1080/01457632.2017.1404806

17. B.A. Abdelkader, M.A. Jamil, S.M. Zubair, Thermal-hydraulic characteristics of helical baffle shell-and-tube heat exchangers. Heat Transf. Eng. (2019). https://doi.org/10.1080/01457632.2019.1611135

18. E. Kayabasi, H. Kurt, Simulation of heat exchangers and heat exchanger networks with an economic aspect. Eng. Sci. Technol. an Int. J. **21**(1), 70–76 (2018). https://doi.org/10.1016/j.jestch.2018.02.006

19. U. Roy, M. Majumder, Economic optimization and energy analysis in shell and tube heat exchanger by meta-heuristic approach. Vacuum **2019**(166), 413–418 (2018). https://doi.org/10.1016/j.vacuum.2018.12.052 (December)

20. V.H. Iyer, S. Mahesh, R. Malpani, M. Sapre, A.J. Kulkarni, Adaptive range genetic algorithm: a hybrid optimization approach and its application in the design and economic optimization of shell-and-tube heat exchanger. Eng. Appl. Artif. Intell. **2019**(85), 444–461 (2018). https://doi.org/10.1016/j.engappai.2019.07.001 (September)

21. M. Mirzaei, H. Hajabdollahi, H. Fadakar, Multi-objective optimization of shell-and-tube heat exchanger by constructal theory. Appl. Therm. Eng. **125**, 9–19 (2017). https://doi.org/10.1016/j.applthermaleng.2017.06.137

22. T.K. Tharakeshwar, K.N. Seetharamu, B. Durga Prasad, Multi-objective optimization using bat algorithm for shell and tube heat exchangers. Appl. Therm. Eng. **110**, 1029–1038 (2017). https://doi.org/10.1016/j.applthermaleng.2016.09.031

23. E.H. de Vasconcelos Segundo, A.L. Amoroso, V.C. Mariani, L. dos S. Coelho, Economic optimization design for shell-and-tube heat exchangers by a Tsallis differential evolution. Appl. Therm. Eng. **111**, 143–151 (2017). https://doi.org/10.1016/j.applthermaleng.2016.09.032

24. R.V. Rao, A. Saroj, Constrained economic optimization of shell-and-tube heat exchangers using elitist-jaya algorithm. Energy **128**, 785–800 (2017). https://doi.org/10.1016/j.energy.2017.04.059

25. S.V. Dhavle, A.J. Kulkarni, A. Shastri, I.R. Kale, Design and economic optimization of shell-and-tube heat exchanger using cohort intelligence algorithm. Neural Comput. Appl. **30**(1), 111–125 (2018). https://doi.org/10.1007/s00521-016-2683-z

26. H. Hajabdollahi, M. Naderi, S. Adimi, A comparative study on the shell and tube and gasket-plate heat exchangers: the economic viewpoint. Appl. Therm. Eng. **92**, 271–282 (2016). https://doi.org/10.1016/j.applthermaleng.2015.08.110

27. D.K. Mohanty, Application of firefly algorithm for design optimization of a shell and tube heat exchanger from economic point of view. Int. J. Therm. Sci. **102**, 228–238 (2016). https://doi.org/10.1016/j.ijthermalsci.2015.12.002

28. C. Gulenoglu, F. Akturk, S. Aradag, N.S. Uzol, S. Kakac, Experimental comparison of performances of three different plates for gasketed plate heat exchangers. Int. J. Therm. Sci. **75**, 249–256 (2014). https://doi.org/10.1016/j.ijthermalsci.2013.06.012

29. K. Sarraf, S. Launay, L. Tadrist, Complex 3D-flow analysis and corrugation angle effect in plate heat exchangers. Int. J. Therm. Sci. **94**, 126–138 (2015). https://doi.org/10.1016/j.ijthermalsci.2015.03.002

30. K. Nilpueng, T. Keawkamrop, H.S. Ahn, S. Wongwises, Effect of chevron angle and surface roughness on thermal performance of single-phase water flow inside a plate heat exchanger. Int. Commun. Heat Mass Transf. **91**, 201–209 (2018). https://doi.org/10.1016/j.icheatmasstransfer.2017.12.009

31. C. Turk, S. Aradag, S. Kakac, Experimental analysis of a mixed-plate gasketed plate heat exchanger and artificial neural net estimations of the performance as an alternative to classical correlations. Int. J. Therm. Sci. **109**, 263–269 (2016). https://doi.org/10.1016/j.ijthermalsci.2016.06.016

32. B. Kumar, A. Soni, S.N. Singh, Effect of geometrical parameters on the performance of chevron type plate heat exchanger. Exp. Therm. Fluid Sci. **91**, 126–133 (2018). https://doi.org/10.1016/j.expthermflusci.2017.09.023

33. M.W. Shahzad, M. Burhan, D. Ybyraiymkul, K.C. Ng, Desalination processes ' efficiency and future roadmap. Entropy **21**(1), 84 (2019). https://doi.org/10.3390/e21010084

34. M.W. Shahzad, M. Burhan, L. Ang, K. Choon Ng, Energy-water-environment nexus underpinning future desalination sustainability. Desalination **413**, 52–64 (2017). https://doi.org/10.1016/j.desal.2017.03.009

35. A. Abid, M. A. Jamil, N. us Sabah, M. U. Farooq, H. Yaqoob, L.A. Khan, M.W. Shahzad, Exergoeconomic optimization of a forward feed multi-effect desalination system with and without energy recovery. Desalination, **499** (July 2020), 114808 (2020). https://doi.org/10.1016/j.desal.2020.114808

36. M.A. Jamil, S.M. Zubair, On thermoeconomic analysis of a single-effect mechanical vapor compression desalination system. Desalination **420**(July), 292–307 (2017)

37. S. Al-Amshawee, M.Y.B.M. Yunus, A.A.M. Azoddein, D.G. Hassell, I.H. Dakhil, H.A. Hasan, Electrodialysis desalination for water and wastewater: a review. Chem. Eng. J. **380** (March 2019) (2020). https://doi.org/10.1016/j.cej.2019.122231

38. K.C. Ng, K. Thu, S. J. Oh, L. Ang, M.W. Shahzad, A.B. Ismail, Recent developments in thermally-driven seawater desalination: energy efficiency improvement by hybridization of the MED and AD cycles. Desalination **356**, 255–270 (2015). https://doi.org/10.1016/j.desal.2014.10.025

39. K.C. Ng, M.W. Shahzad, Sustainable desalination using ocean thermocline energy. Renew. Sustain. Energy Rev. **2018**(82), 240–246 (August 2017)

40. A. Al-Karaghouli, L.L. Kazmerski, Energy Consumption and water production cost of conventional and renewable-energy-powered desalination processes. Renew. Sustain. Energy Rev. **24**, 343–356 (2013). https://doi.org/10.1016/j.rser.2012.12.064

41. M.W. Shahzad, M. Burhan, D. Ybyraiymkul, K.C. Ng, Desalination processes' efficiency and future roadmap. Entropy **21**(1), 84 (2019)

42. J.H. Lienhard, K.H. Mistry, M.H. Sharqawy, G.P. Thiel, Thermodynamics, exergy, and energy efficiency in desalination systems (2017). https://doi.org/10.1016/B978-0-12-809791-5.00004-3

43. M.A. Jamil, H. Yaqoob, M.U. Farooq, Y.H. Teoh, B. Bin Xu, K. Mahkamov, M. Sultan, K.C. Ng, M.W. Shahzad, Experimental investigations of a solar water treatment system for remote desert areas of Pakistan. Water, **13** (8), 1070 (2021). https://doi.org/10.3390/w13081070

44. H.S. Son, M.W. Shahzad, N. Ghaffour, K.C. Ng, Pilot studies on synergetic impacts of energy utilization in hybrid desalination system: multi-effect distillation and adsorption cycle (MED-AD). Desalination **2020**(477), 114266 (October 2019). https://doi.org/10.1016/j.desal.2019.114266

45. R. Alrowais, C. Qian, M. Burhan, D. Ybyraiymkul, M. Wakil, K. Choon, A greener seawater desalination method by direct-contact spray evaporation and condensation (DCSEC): experiments. Appl. Therm. Eng. **179**(June), 115629 (2020). https://doi.org/10.1016/j.applthermaleng.2020.115629

46. Q. Chen, M. Burhan, M. Wakil, D. Ybyraiymkul, Simultaneous production of cooling and freshwater by an integrated indirect evaporative cooling and humidification-dehumidification desalination cycle. Energy Convers. Manag. **221**(May), 113169 (2020). https://doi.org/10.1016/j.enconman.2020.113169

47. M.H. Khoshgoftar Manesh, S. Kabiri, M. Yazdi, F. Petrakopoulou, Thermodynamic evaluation of a combined-cycle power plant with MSF and MED desalination. J. Water Reuse Desalin. 1–12 (2020). https://doi.org/10.2166/wrd.2020.025

48. S. Keshavarzian, M.V. Rocco, F. Gardumi, E. Colombo, Practical approaches for applying thermoeconomic analysis to energy conversion systems: benchmarking and comparative application. Energy Convers. Manag. **150**(August), 532–544 (2017)

49. M.A. Darwish, F.A. Yousef, N.M. Al-Najam, Energy consumption and costs with a multi-stage flashing (MSF) desalting system. Desalination **109**, 285–302 (1997)

50. H. Esen, M. Inalli, M. Esen, K. Pihtili, Energy and exergy analysis of a ground-coupled heat pump system with two horizontal ground heat exchangers. Build. Environ. **42**(10), 3606–3615 (2007)

51. G. Tsatsaronis, Definitions and nomenclature in exergy analysis and exergoeconomics. Energy **32**(4), 249–253 (2007)

52. G.P. Narayan, R.K. Mcgovern, S.M. Zubair, V.J.H., Lienhard, High-temperature-steam-driven, varied-pressure, humidification-dehumidification system coupled with reverse osmosis for energy-efficient seawater desalination. Energy **37** (1), 482–493 (2012)

53. M. W. Shahzad, M. Burhan, K.C. Ng, A Standard primary energy approach for comparing desalination processes. npj Clean Water 2 (1), 1–7 (2019)

54. M.W. Shahzad, M. Burhan, H. Soo Son, S. Jin Oh, K. Choon Ng, Desalination processes evaluation at common platform: a universal performance ratio (UPR) method. Appl. Therm. Eng. **134** (October 2017), 62–67 (2018)

55. L. Galanti, A.F. Massardo, Micro gas turbine thermodynamic and economic analysis up to 500 KWe size. Appl. Energy **88**(12), 4795–4802 (2011)

56. M.A. Jamil, S.M. Zubair, Design and analysis of a forward feed multi-effect mechanical vapor compression desalination system : an exergo-economic approach. Energy **140**, 1107–1120 (2017). https://doi.org/10.1016/j.energy.2017.08.053

57. M.A. Jamil, S. M. Elmutasim, S.M. Zubair, Exergo-economic analysis of a hybrid humidification dehumidification reverse osmosis (HDH-RO) system operating under different retrofits. Energy Convers. Manag. 158 (September 2017), 286–297 (2018). https://doi.org/10.1016/j.enconman.2017.11.025

58. A. Lazzaretto, G. Tsatsaronis, SPECO: a systematic and general methodology for calculating efficiencies and costs in thermal systems. Energy **31**(8–9), 1257–1289 (2006)

59. M.A. Jamil, B.A. Qureshi, S.M. Zubair, Exergo-economic analysis of a seawater reverse osmosis desalination plant with various retrofit options. Desalination **401**, 88–98 (2016)

60. M.A. Jamil, M.W. Shahzad, S.M. Zubair, A comprehensive framework for thermoeconomic analysis of desalination systems. Energy Convers. Manag. **222** (June), 113188 (2020). https://doi.org/10.1016/j.enconman.2020.113188

61. M.A. Jamil, T.S. Goraya, M.W. Shahzad, S.M. Zubair, Exergoeconomic optimization of a shell-and-tube heat exchanger. Energy Convers. Manag. **226** (September), 113462 (2020). https://doi.org/10.1016/j.enconman.2020.113462

62. M.A. Jamil, T.S. Goraya, K.C. Ng, S.M. Zubair, B. Bin, M.W. Shahzad, Optimizing the energy recovery section in thermal desalination systems for improved thermodynamic, economic, and environmental performance. Int. Commun. Heat Mass Transf. **124**, 105244 (2021). https://doi.org/10.1016/j.icheatmasstransfer.2021.105244

63. M.A. Jamil, S.M. Zubair, Effect of feed flow arrangement and number of evaporators on the performance of multi-effect mechanical vapor compression desalination systems. Desalination **429** (September 2017), 76–87 (**2018**). https://doi.org/10.1016/j.desal.2017.12.007

Chapter 2
Efficiency Improvement and Cost Analysis of a New Combined Absorption Cooling and Power System

Farzin Javanfam, Hamed Ghiasirad, and Rahim Khoshbakhti Saray

Abstract Serious concerns like population growth, environmental pollution due to excessive waste disposal, fossil fuels consumption in order to provide high energy demands, global warming, ozone depletion, and acid rainfalls have led energy policy-makers to recommend solutions to resolve these challenges. In this regard, the cogeneration of electricity and cooling is a technology to solve the mentioned formidable obstacles. The present study introduces a practical but straightforward simultaneous power and cooling plant executed by a natural gas-fired open Brayton cycle. The bottoming process utilizes an ammonia-water mixture. To be more specific, the thermodynamic and thermoeconomic model of the process was assessed in the engineering equation solver (EES). The effect of the significant variables of the proposed cycle is also studied based on the overall system performance criteria. As a result, the highest exergy destruction is for the Brayton cycle, 44.89% of the total irreversibility, followed by the boiler and mixer in the absorption cycle, and the smallest amount of irreversibility belongs to the evaporator, with 0.14%. The parametric study results demonstrate that minimizing the air temperature entering the combustor will improve the studied system. To deduce, the cogeneration unit is optimized based on the second law efficiency as an objective function. In turn, the optimization results illustrate an enhancement in exergy efficiency and unit cost of products by 21.73% and 4.13%.

Keywords Gas turbine · Goswami cycle · Combined cooling and power (CCP) · Exergoeconomic analysis · Efficiency enhancement

F. Javanfam · H. Ghiasirad · R. Khoshbakhti Saray (✉)
Faculty of Mechanical Engineering, Sahand University of Technology, Sahand New Town, Tabriz, Iran
e-mail: khoshbakhti@sut.ac.ir

H. Ghiasirad
e-mail: h_ghiasirad@sut.ac.ir

23

Nomenclature

Symbols

$\dot{E}$	Exergy rate (kW)
$\dot{m}$	Mass flow rate (kg/s)
P	Pressure (bar)
LHV	Lower heating value (kJ/kg)
P	Density (kg/m^3)
y	Exergy destruction ratio
$\dot{Q}$	Heat transfer rate (kW)
h	Specific enthalpy (kJ/kg)
s	Specific entropy (kJ/kgK)
T	Temperature (K)
$\dot{W}$	Power (kW)
PEC	Purchased Equipment Cost ($)
$\dot{C}$	Cost rate ($/h)
c	The unit cost of exergy ($/GJ)
$\dot{Z}$	Purchased Equipment Cost rate ($/h)
$CCHP$	Combined cooling, heating, and power
SG	Steam generator
AC	Air compressor
$cond$	Condenser
Eva	Evaporator
EV	Expansion valve

Greek Letters

Δ	Difference
η	Thermal efficiency (%)
η_{II}	Exergy efficiency (%)

Superscripts

CH	Chemical
PH	Physical
th	Thermal
0	Dead state

Subscripts

F	Fuel (exergy)
P	Product (exergy)
D	Destruction
L	Loss
is	Isentropic
CV	Control Volume
v	Vapor
l	Liquid
sys	System
0	Dead state
s	Isentropic
in	Inlet
LMTD	The logarithmic mean temperature difference
Mix	Mixer
PP	Pinch point
s	Constant entropy

2.1   Introduction

The rapid growth in the consumption of various fossil fuels, namely oil, coal, and natural gas, has caused climate change. Therefore, these non-renewable resources are the primary factor in greenhouse effects caused by carbon dioxide emissions. Among various sectors involved in fossil fuel consumption, power plants are responsible for a significant percentage of the consumption of these fuels and the emission of greenhouse gases. Thus, it is essential to eliminate their obnoxious effects [1].

It is an essential task for scientists and engineers to tackle this situation and provide optimal systems to augment power plants' performance and diminish greenhouse gas emissions. In line with this goal, proposing optimal energy systems and presentation of 3E data as well as results in safety and reliability of different components of cycles to the designers can be a promising solution to renovate old industries. This encourages researchers to come up with new ideas to address the problems related to energy shortages. Therefore, different sources of renewable energy are used to redirect hybrid energy systems. Also, the capacity of renewable energy technologies increases in various ways due to population growth [2].

Optimization of a CHP system, including a gas turbine, was investigated by Nami et al. [3]. The high-temperature combustion gases leave the gas turbine to undergo the supercritical cycle of carbon dioxide and then generate heat in the steam generator. Also, for cooling the carbon dioxide entering the main compressor, its energy is transferred to an organic Rankine cycle. The results revealed that the cost of final products falls by 2.8% compared to the base condition. The outputs of the gas

turbine cycle and the integrated solid oxide fuel cell were tested by Gholamian and Zare [4]. Then they considered the organic Rankine cycle and the Kalina cycle to the system as two alternatives for bottoming cycles. They also compared the systems regarding thermodynamics and environmental principles. Their study includes three systems: SOFC-GT, SOFC-GT with organic Rankine Cycle, and SOFC-GT with Kalina cycle. The results showed that the total output power and energy/exergy efficiency of the gas turbine system and fuel cell system increase by a combination of organic Rankine and Kaline cycles. Also, the exergy efficiency of the whole unit with organic Rankine and Kalina systems was 62.35% and 59.53%, respectively. Alklaibi et al. [5] conducted the thermodynamic study of the gas turbine cycle with three new cycles and compared the energetic and exergetic results of the cycles in their investigation. According to their design, the base cycle consists of two compressors, two turbines, a combustion chamber, a central cooler, a heat exchanger, and a preheater. The air is compressed by compressors and is mixed with the fuel in the combustion chamber. Then, the combustion gases go to the turbine and expand to generate power. In the second cycle, the two base cycles are connected by a heat exchanger. This part performs as a combustion chamber in the second cycle supplied by the exhaust gases from the turbine in the first cycle. In the third cycle, the three base cycles are combined. The combustion chamber only exists in the first cycle, and the next two cycles are fed by the exhaust gases from the turbine of the upstream cycle. In their results, the combined cycle of gas turbine and downstream air showed 4.78% higher energy efficiency than the cycle with a simple gas turbine; meanwhile, the exergy destruction in the cycle is reduced by 6%. Besides, the exergy loss in combustion products decreased by 16% in the combined cycle. A combination of solar and SOFC-GT systems and an ammonia fuel cell was designed by Siddiqui and Dincer [6] to supply the necessary power for a multigeneration system. The energy and exergy efficiencies are 39.1% and 38.7%, implying a 19.3% and 17.8% increase in energy and exergy efficiencies of the multigeneration system compared to the single-generation one. Exergy-economic analysis of a CCHP system with a wastewater treatment plant was studied by Mirmasoumi et al. [7]. They evaluated thermophilic digestion and thermal pretreatment of sewage sludge. Then, the wastewater is converted to biogas and goes to the combustion chamber of the gas turbine cycle after the anaerobic digestion process. The turbine generates power, and then high-temperature waste gases are taken to provide the heat for digestion, hot water, and cooling process in the absorption refrigeration cycle. They concluded that the combustion chamber, the third heat exchanger, and the digester undergo the most exergy destruction in winter. Also, the combustion chamber, the first evaporator, and the digester had the most exergy destruction in summer. On the other hand, digestion, combustion chamber, and economizer in winter, and digestion, combustion chamber, and absorber accounted for the highest total costs. Thermo-economic optimization of a system for cogeneration of power, cooling, and freshwater was investigated by Behzadi et al. [8]. In this system, carbon dioxide is absorbed and used as an oxidizer for municipal solid waste. The synthetic gas with air then enters the solid oxide fuel cells, afterburner, and gas turbine, and combustion gases transfer thermal energy to a double-effect LiBr-Water absorption refrigeration system for ambient

cooling production. The extra power of this system is also transferred to the reverse osmosis desalination plant to provide the required freshwater. The results indicated that the gas generator was the most destructive part in terms of exergy, and the exergy-economic factor of the refrigeration system components was less than 20%. Sensitivity analysis of various parameters also necessitated minimizing the fuel cell temperature difference, compressor pressure ratio, and carbon dioxide feed ratio. Chen et al. [9] investigated the economic optimization of a two-objective energy system comprising a supercritical carbon dioxide power cycle, a gas turbine, and a solid oxide fuel cell. After optimization, they observed that the optimum condition of the Pareto frontiers had a second law efficiency of 68% and electricity cost of $ 0.075 per kilowatt-hour. The multi-objective optimization of a cogeneration system was analyzed by Habibollahzadeh et al. [10]. The system was driven by municipal solid waste. Air, enriched air, oxygen, and carbon dioxide as oxidizers enter the gas generator. Then, the generated synthesis gas was led to a solid oxide fuel cell, after-burner, and gas turbine to convey the excess generated power and produce hydrogen from the incoming air. The study's main goals were to investigate the second law of thermodynamics, total product cost, emission of greenhouse gases, and the rate of hydrogen production. They concluded that a pure oxygen oxidizer is the best option for the product cost and exergy efficiency. Darabadi et al. [11] carried out a two-objective exergo-economic optimization by considering a genetic algorithm for a CHP system. Natural gas and municipal solid waste were used as fuels in this system. The biomass is converted to biogas after the anaerobic digestion process and mixed with natural gas. The combustion gases of the gas turbine split and supply the heat required by both digester and steam generator. In their study, two methods were used for optimization in the system. The ratio of natural gas and biogas mixing was one of the decision variables in the first method. In the second method, this parameter was considered constant and equal to 50%. The combustion chamber and digestion had the highest irreversibility in their results. Also, the combustion chamber and steam generator had the highest total investment costs and exergy destruction costs. Optimization by the first method caused a 6.66% improvement in exergy efficiency, and the costs decreased by 1450 $/h. Moreover, the second optimization method indi-cated a 2.15% rise in exergy efficiency and a 363 $ per hour reduction in costs. A novel design for cogeneration of power and cooling was proposed by Barkhordarian et al. [12]. They studied the cycle from energy and exergy viewpoints. Their recommended cycle includes a Goswami cycle, an ejector refrigeration system, ammonia-water as a working fluid, and two evaporators with different temperature ranges and cooling loads. The cycle had 19% thermal efficiency and 38.97% exergy efficiency. Ghaebi et al. [13] coupled the Kalina cycles and ejector to provide the ejector's initial flow after proceeding with two preheating processes using the flow rate extracted from the turbine. On the other hand, the secondary flow was a solution extracted from the turbine after only one preheating process. Optimal first and second law efficien-cies were 15% and 47.8%. Hosseinpour et al. [14] investigated a combined power and refrigeration unit using wood gasification. After the gasification of wood, the mixture of produced gases and air enters the solid oxide fuel cell. Then, it goes to the afterburner. Combustion gases then transfer thermal energy to the Goswami

power cycle and refrigeration. In the proposed system, the gas generator and boiler were the most destructive exergy, and the absorber and recovered heat exchanger have the least irreversibility. In 2018, Rostamzadeh et al. [15] carried out an analytical study on a cogeneration system and looked over the influence of an ejector in low-temperature thermal source systems such as Kalina. The reported energy and exergy efficiencies were 33.65% and 10.78%, while the total product cost was $ 256.1 /GJ. Behnam et al. [16] developed a hybrid cycle encompassing EKalina and ejector refrigeration cycles with ammonia-water working fluid. They employed two-phase ejectors to improve power generation and cooling. The condenser and steam generator accounted for the highest exergy destruction, with 47.66% and 31.94%, respectively. Besides, the second ejector with 3.94%, had the lowest irreversibility. They found out that the influence of turbine inlet pressure on energy efficiency was not sensible, but increasing the inlet pressure from 20 to 30 bars reduced the efficiency of the second law from 12 to 8%. Also, they obtained 10.23% and 9.55% energy and exergy efficiencies in their result.

In recent years, the growth in the economic and thermodynamic assessment of combined and modern energy systems has been hastened. In addition, scientists have exploited the absorption system to meet the cooling needs of these energy systems. Therefore, a hybrid power and refrigeration system based on a gas turbine cycle and a hybrid electricity and refrigeration cycle with ammonia-water working fluid is presented, driven by methane gas entering the combustion chamber. In this system, the gas turbine output, which includes high-temperature combustion gases, enters the boiler and rectifier of the absorption system. Other innovations of the present cogeneration system are discussed in the system description section.

2.2   System Description

The flowchart of the studied power generation and refrigeration cycle is shown in Fig. 2.1.

As observed in the scheme of the combined cycles, the gas turbine cycle is the upper cycle, and the bottoming process is the ammonia water cogeneration of power and cooling.

At the first stage, the air enters the compressor and is compressed, and then it is heated in the preheater and mixed with the input fuel (methane gas) of the combustion chamber, and combustion takes place. The hot gases enter the gas turbine after leaving the combustion chamber to expand and produce power. Afterward, the combustion gases are transferred to the boiler in the bottoming cycle for cooling and power generation. The bottoming process comprises ammonia-water working fluid, which is intended to generate power and cooling by the waste heat of the gas turbine cycle. In this cycle, the working fluid (ammonia-water) entering the boiler (state 11) and gaining the heat from the topping cycle splits into two flows. The flow with higher density (state 12) enters the rectifier, and the flow with lower density (state 18) goes to the solution heat exchanger (SHE). The ammonia-water entering the rectifier
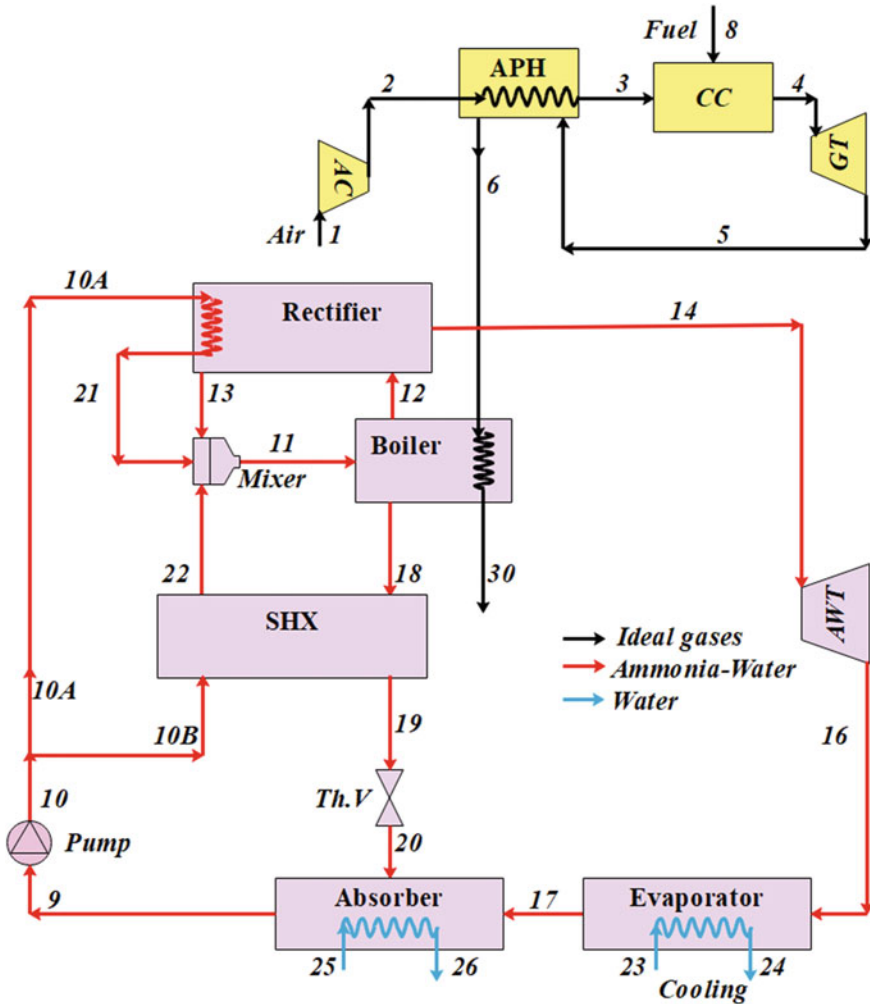
Fig. 2.1 Flowchart of the considered cogeneration power and refrigeration system

transfers the heat to the flow 10A to increase the density of the output stream (state 14). High-quality ammonia enters the turbine and generates power. After leaving the turbine (state 16), it goes to the evaporator for cooling production. Then, it enters the absorber and is blended with the ammonia-water from the expansion valve (state 20) and gives its heat to the ambient resulting in a reduction of its density. It should be noted that the output stream enters the SHE from state 18, gives its heat to the opposite stream (state 19), and its pressure drops by the expansion valve (state 20).

The output stream from the pump is divided into two parts: 10A and 10B. Stream 10A goes to the rectifier and gains heat from the rectifier (state 21). On the other hand, stream 10B goes to the SHE and heats up (state 22). Finally, the two streams

are mixed with the output stream from the rectifier (state 13). The output of these three streams enters the boiler after mixing in the mixer.

2.3 System Modeling and Simulation

2.3.1 Assumptions and Input Data

Several hypotheses for a comprehensive evaluation of the studied cogeneration cycle are sorted as follows:

1. A steady-state analysis is considered in the system evaluation [1].
2. The processes in pumps, turbines, and compressors are isentropic [1].
3. The physical and chemical exergies of components are assumed in the evaluation of the second law, and the potential and kinetic exergies are ignored [2].
4. The composition of air is assumed at 77.48% of N_2, 20.59% of O_2, 0.03% of CO_2, and 1.9% of H_2O [17].
5. The inlet pressure and temperature of the compressor are at reference conditions, and chemical exergy is zero at its entrance [17].
6. The air preheater is assumed to have a 5% pressure drop [18].
7. Methane fuel enters the combustion chamber at ambient temperature and 12 bar [18].
8. The temperature in state 12 and state 18 is assumed to be equal [19].
9. The temperature in state 13 and state 14 is assumed to be equal [19].

In addition, some of the input data required to design the system are shown in Table 2.1.

2.3.2 Energy Analysis

To analysis the cycle, components are assumed under the steady-state, and the mass, energy, and exergy balances are executed [1]:

$$\sum \dot{m}_{in} - \sum \dot{m}_{out} = 0 \tag{2.1}$$

$$\sum (\dot{m}h)_{in} - \sum (\dot{m}h)_{out} + \sum \dot{Q}_{in} - \sum \dot{Q}_{out} + \dot{W} = 0 \tag{2.2}$$

In the above equations, $\dot{m}$ and h represent the specific mass flow rate and enthalpy. Also, $\dot{W}$ and $\dot{Q}$ represent the power and heat transfer rate in the control volume.

Using the assumptions and explanations of the following sections and applying the above equations to components, the simplified and final forms of relations for energy analysis are presented.

Table 2.1 Input data required for system design

Parameters	Symbol	Value	Ref.
Reference temperature	$T_0(K)$	298.15	[20]
Reference pressure	$P_0(bar)$	1.013	[20]
Compressor pressure ratio	$R_{Copmressor}$	10	[20]
Inlet air temperature to the combustion chamber	$T_3(K)$	850	[20]
Exhaust gas temperature from the combustion chamber	$T_4(K)$	1520	[20]
Inlet fuel pressure to the combustion chamber	$P_8(bar)$	12	[20]
Isentropic efficiency of gas turbine	$\eta_{is,Gas\ Turbine}(\%)$	86	[20]
Isentropic efficiency of the compressor	$\eta_{is,Comp}(\%)$	86	[20]
the net power output of the gas turbine cycle	$\dot{W}_{net,GasTur}(MW)$	30	[20]
Pump inlet temperature	$T9$	303.15	[19]
Pump pressure ratio	R_{Pump}	6	[19]
Isentropic efficiency of the turbine	$\eta_{is,AWM\ Turbine}$	85	[19]
Isentropic efficiency of the pump	$\eta_{is,Pump}$	85	[19]
Pinch point temperature difference	$\Delta T_{Pinch\ Point}$	5	[19]
Pump inlet concentration	x_9	0.524	[19]
Rectifier temperature	T_{14}	353.15	[19]
Boiler temperature	T_{12}	383.15	[19]
Quality of saturated liquid in states 9, 13 and 18	$Q_9 \& Q_{13} \& Q_{18}$	0	[19]
Quality of saturated steam in states 12 and 14	$Q_{12} \& Q_{14}$	1	[19]

To calculate the molar mass of the ideal gas mixtures, the following equation is used [1]:

$$MW_{mix} = \sum x_i MW_i \tag{2.3}$$

The enthalpy of the mixture is also calculated from the following equation [17]:

$$\overline{h}_{mix} = \sum x_i (\overline{h}_{f,i}^0 + \Delta \overline{h}_i) \tag{2.4}$$

In the above equations, $\Delta \overline{h}_i$ is the sensible enthalpy difference of species and $\overline{h}_{f,i}^0$ is the species enthalpy of formation.

Also, the entropy of the gas mixtures is obtained from the following equation [17]:

$$\overline{s}_{mix} = \sum x_i \left[\overline{s}_{T,P_0,i} - \overline{s}_{T_0,P_0,i} - \overline{R}Ln(x_i \frac{P}{P_0}) \right] \tag{2.5}$$

The chemical reaction in the combustion chamber is considered as follows [20]:

$$\lambda CH_4 + 0.7748N_2 + 0.2059O_2 + 0.0003CO_2$$
$$+0.019H_2O \rightarrow (1+\lambda)(x_{N_2}N_2 + x_{O_2}O_2 + x_{CO_2}CO_2 + x_{H_2O}H_2O) \qquad (2.6)$$
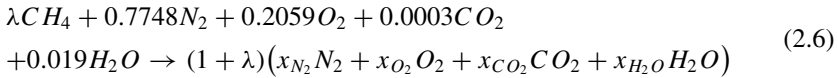
In the above equation, the following relations are taken to calculate the unknown mole fractions of the combustion products [20]:

$$x_{CO_2} = (0.0003 + \lambda)/(1+\lambda) \qquad (2.7)$$

$$x_{O_2} = (0.2059 - 2\lambda)/(1+\lambda) \qquad (2.8)$$

$$x_{H_2O} = (0.019 + 2\lambda)/(1+\lambda) \qquad (2.9)$$

$$x_{N_2} = 0.7748/(1+\lambda) \qquad (2.10)$$

2.3.3 Exergy Analysis

Exergy is the most considerable amount of theoretical and beneficial work achievable when the systems affect the equilibrium, including heat transfer with the environment. [18]. Depending on the system's stability with the ambient, the system can have chemical, physical, potential, and kinetic exergies.

The exergy equation for components is written as follows [2].

$$\dot{E}_{F,k} = \dot{E}_{P,k} + \dot{E}_{D,k} \qquad (2.11)$$

where, $\dot{E}_{F,k}$ and $\dot{E}_{P,k}$ are the fuel exergy of a component and its produced exergy, respectively. Besides, $\dot{E}_{D,k}$ is the exergy destruction of the considered components. The system's boundaries used in the exergy balance are presumed to be at the reference temperature (T0). Hence the exergy balance in the whole system is as follows [2].

$$\dot{E}_F = \dot{E}_P + \sum \dot{E}_D + \dot{E}_L \qquad (2.12)$$

Also, it is worth mentioning that just the boiler and combustion chamber include exergy losses in this study, which is due to waste heat of combustion chamber and exhaust gases at state 30 [2].

The ratio of product exergy to the fuel exergy identifies the exergy efficiency of each component of the system [2]:

$$\varepsilon_k = \frac{\dot{E}_{P,k}}{\dot{E}_{F,k}} = 1 - \frac{\dot{E}_{D,k}}{\dot{E}_{F,k}} \tag{2.13}$$

For the kth stream, the total exergy is [2]:

$$\dot{E}_k = \dot{E}_{ph,k} + \dot{E}_{ch,k} \tag{2.14}$$

$$\dot{E}_{ph,k} = \dot{m}((h - h_0) - T_0(s - s_0))_k \tag{2.15}$$

$$\dot{E}_{ch,k} = \dot{n}_i \left(\sum_i y_i \overline{e}_i^{CH,0} + \overline{R}T_0 \sum_i y_i ln y_i \right) \tag{2.16}$$

where the standard chemical exergy values ($\overline{e}_i^{CH,0}$) for the various components of a mixture can be found in Ref. [21].

Table 2.2 indicates the energy and exergy equations of the equipment employed in the studied cycle.

2.3.4 Exergoeconomic Evaluation

The most common method for assessment of the cost of each stream to calculate the exergy unit cost of products in the literature is the specific exergy cost method developed by Tsatsaronis et al. [18]. To calculate an economic assessment using the specific exergy costing, cost balance and auxiliary equations are presented for the components [18]. The specific exergy cost method consists of the following three steps that should be applied to each element in a cycle:

1. Recognizing the exergy streams.
2. Recognizing the exergy of fuel and product.
3. Writing cost balance and auxiliary equations.

The first and second steps were described in the previous sections. In this section, the third step is applied to each component, and the results find the unit cost of products.

The cost rate of inlet and outlet streams with the maintenance, operation ($\dot{Z}^{OM}$), and capital investment ($\dot{Z}^{CI}$) are determined by the following cost balance equations [21]:

$$\dot{C}_{Q,k} + \sum \dot{C}_{in,k} + \dot{Z}_{total}^{CI} + \dot{Z}_{total}^{OM} = \dot{C}_{W,k} + \sum \dot{C}_{out,k} \tag{2.17}$$

$$\dot{C}_k = c_k \dot{E}_k \tag{2.18}$$

Table 2.2 Equations related to different equipment in the cycle

Equipment	Mass continuity and energy balance equations	Exergy balance equations
Pump	$\dot{W}_{Pum1} = \dot{m}_9(h_{10} - h_9)$ $\eta_{is,Pump1} = (h_{10s} - h_9)/(h_{10} - h_9)$ $\dot{m}_9 = \dot{m}_{10},\ \dot{m}_{10} = \dot{m}_{10A} + \dot{m}_{10B}$	$\dot{E}_F = \dot{W}_{Pump}$ $\dot{E}_P = (\dot{E}_{10} - \dot{E}_9)$
Gas turbine	$\dot{W}_{Tur1} = \dot{m}_4(h_4 - h_5)$ $\eta_{is,Tur1} = (h_4 - h_5)/(h_4 - h_{5s})$ $\dot{m}_4 = \dot{m}_{air} + \dot{m}_{fuel}$	$\dot{E}_F = (\dot{E}_4 - \dot{E}_5)$ $\dot{E}_P = \dot{W}_{GasTurbine}$
Compressor	$\dot{W}_{AC} = \dot{m}_1(h_2 - h_1)$ $\eta_{is,AC} = (h_{2s} - h_1)/(h_2 - h_1)$ $\dot{m}_1 = \dot{m}_2 = \dot{m}_3 = \dot{m}_{air}$	$\dot{E}_F = \dot{W}_{Air\ Compressor}$ $\dot{E}_P = (\dot{E}_2 - \dot{E}_1)$
Heat exchanger	$\dot{Q}_{SHX} = \dot{m}_{18}(h_{18} - h_{19}) = \dot{m}_{22}(h_{22} - h_{10B})$ $\dot{m}_{18} = \dot{m}_{19},\ \dot{m}_{10B} = \dot{m}_{22}$	$\dot{E}_F = (\dot{E}_{18} - \dot{E}_{19})$ $\dot{E}_P = (\dot{E}_{22} - \dot{E}_{10B})$
Combustion chamber	$\dot{m}_8 h_8 + \dot{m}_3 h_3 = \dot{m}_4 h_4 + \dot{Q}_{L,CC}$ $\dot{Q}_{L,CC} = -0.02 \times \dot{m}_{fuel} \times LHV_{fuel}$ $\dot{m}_8 = \dot{m}_{fuel}$	$\dot{E}_F = \dot{E}_3 + \dot{E}_8$ $\dot{E}_P = \dot{E}_4$ $\dot{E}_{L,CC} = \dot{Q}_{L,CC}(1 - \frac{T_0}{T_4})$
Preheater	$\dot{Q}_{APH} = \dot{m}_2(h_2 - h_3) = \dot{m}_5(h_5 - h_6)$ $\dot{m}_6 = \dot{m}_5 = \dot{m}_4$	$\dot{E}_F = (\dot{E}_5 - \dot{E}_6)$ $\dot{E}_P = (\dot{E}_3 - \dot{E}_2)$
Boiler	$\dot{m}_6 h_6 + \dot{m}_{11} h_{11} = \dot{m}_{30} h_{30} + \dot{m}_{12} h_{12} + \dot{m}_{18} h_{18}$ $\dot{m}_{11} x_{11} = \dot{m}_{12} x_{12} + \dot{m}_{18} x_{18}$ $\dot{m}_{11} = \dot{m}_{12} + \dot{m}_{18}$ $\dot{m}_6 = \dot{m}_{30}$	$\dot{E}_F = \dot{E}_6$ $\dot{E}_P = \dot{E}_{12} + \dot{E}_{18} - \dot{E}_{11}$ $\dot{E}_L = \dot{E}_{30}$
Rectifier	$\dot{m}_{10A} h_{10A} + \dot{m}_{12} h_{12} = \dot{m}_{13} h_{13} + \dot{m}_{14} h_{14} + \dot{m}_{21} h_{21}$ $\dot{m}_{12} x_{12} = \dot{m}_{13} x_{13} + \dot{m}_{14} x_{14}$ $\dot{m}_{12} = \dot{m}_{13} + \dot{m}_{14}$ $\dot{m}_{10A} = \dot{m}_{21}$	$\dot{E}_F = \dot{E}_{12} - \dot{E}_{13} - \dot{E}_{14}$ $\dot{E}_P = \dot{E}_{21} - \dot{E}_{10A}$
Absorber	$\dot{m}_{17} h_{17} + \dot{m}_{20} h_{20} + \dot{m}_{25} h_{25} = \dot{m}_9 h_9 + \dot{m}_{26} h_{26}$ $\dot{m}_{17} x_{17} + \dot{m}_{20} x_{20} = \dot{m}_9 x_9$ $\dot{m}_{17} + \dot{m}_{20} = \dot{m}_9$ $\dot{m}_{25} = \dot{m}_{26}$	$\dot{E}_F = \dot{E}_{17} + \dot{E}_{20} - \dot{E}_9$ $\dot{E}_F = \dot{E}_{26} - \dot{E}_{25}$
Evaporator	$\dot{m}_{16} h_{16} + \dot{m}_{23} h_{23} = \dot{m}_{17} h_{17} + \dot{m}_{24} h_{24}$ $\dot{m}_{16} = \dot{m}_{17},\ \dot{m}_{24} = \dot{m}_{25}$	$\dot{E}_F = \dot{E}_{16} - \dot{E}_{17}$ $\dot{E}_P = \dot{E}_{24} - \dot{E}_{23}$
Ammonia-water turbine	$\dot{W}_{AWT} = \dot{m}_{14}(h_{14} - h_{16})$ $\eta_{is,AWT} = (h_{14} - h_{16})/(h_{14} - h_{16s})$ $\dot{m}_{16} = \dot{m}_{14}$	$\dot{E}_F = (\dot{E}_{14} - \dot{E}_{16})$ $\dot{E}_P = \dot{W}_{AW\ Turbine}$
Expansion valve	$\dot{m}_{19}(h_{19} - h_{20}) = 0$ $\dot{m}_{19} = \dot{m}_{20}$	$\dot{E}_F = \dot{E}_{19}$ $\dot{E}_P = \dot{E}_{20}$

Table 2.2 (continued)

Equipment	Mass continuity and energy balance equations	Exergy balance equations
Mixer	$\dot{m}_{13}h_{13} + \dot{m}_{21}h_{21} + \dot{m}_{22}h_{22} = \dot{m}_{11}h_{11}$ $\dot{m}_{13}x_{13} + \dot{m}_{21}x_{21} + \dot{m}_{22}x_{22} = \dot{m}_{11}x_{11}$ $\dot{m}_{13} + \dot{m}_{21} + \dot{m}_{22} = \dot{m}_{11}$	$\dot{E}_F = \dot{E}_{13} + \dot{E}_{21} + \dot{E}_{22}$ $\dot{E}_P = \dot{E}_{11}$

Here, c_k is the cost per unit of energy (\$/GJ).

According to Eq. (2.17), the total costs of the output exergy stream from a component (right hand of the equation) is the total costs of the inlet exergy stream of the component and the cost of operation, including the cost of investment and maintenance. For the kth component, the cost rate of exergy destruction is assessed by the following equation [21]:

$$\dot{C}_{D,k} = c_{P,k}\dot{E}_{D,k} \ (If \ \dot{E}_{F,k} = Constant) \tag{2.19}$$

For the kth component, the total cost rate is calculated by summation of the significant investment ($\dot{Z}^{CI}$) and maintenance and operations ($\dot{Z}^{OM}$) [21]:

$$\dot{Z}_k = \dot{Z}_k^{CI} + \dot{Z}_k^{OM} \tag{2.20}$$

Using capital recovery factor (CRF), the total cost rate can be calculated as follows [22]:

$$\dot{Z}_k = Z_k \times CRF \times \frac{\phi_r}{\tau} \tag{2.21}$$

$$CRF = \frac{i_r(1 + i_r)^N}{(1 + i_r)^N - 1} \tag{2.22}$$

where, Z_k is the purchased equipment cost, and N refers to life duration (N = 20). Also, ϕ_r, i_r, τ are the maintenance factor ($\phi_r = 1.06 \ 1$), the interest rate ($i_r = 0.12$), and the annual system's operating hours ($\tau = 8000$) [22].

For the kth component, the exergoeconomic factor (f_k) and the relative cost difference (r_k) are determined as follows, respectively [23]:

$$r_k = (c_{P,k} - c_{F,k})/c_{F,k} \tag{2.23}$$

$$f_k = \dot{Z}_k/(\dot{Z}_k + \dot{C}_{D,\ k}) \tag{2.24}$$

Table 2.3 The overall heat transfer coefficient of heat exchangers in the proposed cycle

Equipment	$U(kW/(m^2 \cdot K))$	Ref.
Evaporator	1.1	[22]
Solution heat exchanger	0.7	[19]
Preheater	0.018	[18]
Boiler	0.5	[19]
Absorber	0.8	[19]
Rectifier	0.9	[19]

The total heat exchanger area can be calculated by the following equation [23] using the total heat transfer coefficient and LMTD (average logarithmic temperature difference).

$$A_k = \frac{\dot{Q}_k}{U_k \Delta T_{LMTD}} \qquad (2.25)$$

For heat exchangers, the overall heat transfer coefficient is shown in Table 2.3.

The equations related to purchasing cost for the components can be found in Tables 2.4 and 2.5.

Table 2.6 reveals the cost balance and auxiliary equations for the involved components independently, while the investment and maintenance costs have already been assessed. Accordingly, the exergy cost rate ($\dot{C}$) and exergy unit cost (c) can be calculated for all streams. It should be noted that some auxiliary equations are stated based on the equality of unit cost in hot streams. It implies that the input and output streams of the energy transfer in heat exchangers have the exact unit cost. Also, air and water entering the system have a unit cost of zero. Turbine inputs and outputs have the same unit cost. Since the production capacity of turbines supplies the power consumption of pumps and compressors, the unit cost of their power consumption is also equal. [18].

2.3.5 Evaluation Parameters of the Cogeneration System

In the present cycle, $\dot{W}_{net}$ as the net power is calculated as follows:

$$\dot{W}_{net,total} = \dot{W}_{AWMTurbine} + \dot{W}_{GASturbine} - \dot{W}_{Pump} - \dot{W}_{Compressor} \qquad (2.26)$$

The energy efficiency of the cogeneration cycle of power and cooling can be written as follows:

$$\eta_{en} = \frac{\dot{W}_{net,total} + \dot{Q}_{cooling}}{(\dot{m} * LHV)_{fuel}} \qquad (2.27)$$

Table 2.4 Purchasing cost, cost balance, and auxiliary equations for each component

Equipment	Purchasing cost	Ref.
Heat exchanger	$Z_{AHP} = \left(\frac{CEPCI_{2018}}{CEPCI_{1995}}\right) * 4122 * (A_{APH})^{0.6}$	[18]
Combustion chamber	$Z_{CC} = \left(\frac{CEPCI_{2018}}{CEPCI_{2009}}\right) * (\frac{\dot{m}_{air}+\dot{m}_{fuel}}{628.5})^{(0.67)*21.9*1000000}$	[24]
Gas turbine	$Z_{GT} =$ $\left(\frac{CEPCI_{2018}}{CEPCI_{2011}}\right) * 1318.5 * (\dot{w}_T - 98.328) * \dot{w}_T * Ln(\dot{w}_T)$	[25]
Boiler	$Z_{Boiler} = \left(\frac{CEPCI_{2018}}{CEPCI_{2000}}\right) * 17500 * (A_{Boiler}/100)^{0.6}$	[23]
Rectifier	$Z_{Rec} = \left(\frac{CEPCI_{2018}}{CEPCI_{2000}}\right) * 1700 * (A_{REC}/100)^{0.6}$	[23]
Ammonia water turbine	$Z_{AWM} = \left(\frac{CEPCI_{2018}}{CEPCI_{1996}}\right) * C_{0AWMturbine} * fm_t$ $log(C_{0AWT}) =$ $k_{1,T} + k_{2,T} * Log(\dot{W}_{AWT}) + k_{3,T} * (Log(\dot{W}_{AWT}))^2$	[21]
Evaporator	$Z_{Eva} = \left(\frac{CEPCI_{2018}}{CEPCI_{2000}}\right) * 16000 * (A_{Eva}/100)^{0.6}$	[23]
absorber	$Z_{ABS} = \left(\frac{CEPCI_{2018}}{CEPCI_{2000}}\right) * 16500 * (A_{ABS}/100)^{0.6}$	[23]
mixer	$\dot{Z}_{Mixer} = 0$	[23]
Pump	$Z_p = \left(\frac{CEPCI_{2018}}{CEPCI_{1996}}\right) * C_{0_p} * (b_{1,P} + b_{2,P} * fm_P * fp_P)$ $log(C_{0p}) = k_{1,P} + k_{2,P} * Log(\dot{W}_p) + k_{3,P} * (Log(\dot{W}_p))^2$ $log(fp_P) = c_{1,P} + c_{2,P} * Log(p_P) + c_{3,P} * (Log(p_p))^2$	[21]
Solution heat exchanger	$Z_{SHE} = \left(\frac{CEPCI_{2018}}{CEPCI_{2000}}\right) * 12000 * (A_{SHE}/100)^{0.6}$	[23]
compressor	$Z_{Comp} = \left(\frac{CEPCI_{2018}}{CEPCI_{2003}}\right) * 91562 * (\dot{w}_{Comp}/445)^{0.67}$	[22]
Expansion valve	$Z_{TV} = \left(\frac{CEPCI_{2018}}{CEPCI_{2018}}\right) * 114.5 * \dot{m}_{20}$	[21]

Table 2.5 Coefficients for the calculation of purchased equipment costs of turbine and pump [21]

Component	Turbine	Pump
k_1	2.2476	3.3892
k_2	1.4965	0.0536
k_3	−0.1618	0.1538
c_1	–	0.3935-
c_2	–	0.3957
c_3	–	−0.0023
b_1	–	1.89
b_2	–	1.35
f_m	3.5	1.6

Table 2.6 Cost balance and auxiliary equations of different equipment

Equipment	Cost balance equations	Auxiliary equations
Compressor	$\dot{C}_1 + \dot{Z}_{comp} + \dot{C}_{w,comp} = \dot{C}_2$ $\dot{C}_{w,comp} = c_{w,comp} * \dot{w}_{comp}$	$c_1 = 0$ $c_{w,comp} = c_{w,tur}$
Preheater	$\dot{C}_2 + \dot{C}_5 + \dot{Z}_{APH} = \dot{C}_3 + \dot{C}_6$	$c_5 = c_6$
Combustion chamber	$\dot{C}_8 + \dot{C}_3 + \dot{Z}_{CC} = \dot{C}_4$	$c_8 = 3.365$[1]
Gas turbine	$\dot{C}_4 + \dot{Z}_{GT} = \dot{C}_5 + \dot{C}_{w,tur}$ $\dot{C}_{w,tur} = c_{w,tur} * \dot{w}_{Gastur}$	$c_4 = c_5$
Boiler	$\dot{C}_{11} + \dot{C}_6 + \dot{Z}_{Boiler} =$ $\dot{C}_{12} + \dot{C}_{18} + \dot{C}_{30}$	$c_6 = c_{30}$ $\dfrac{\dot{C}_{12} - \frac{\dot{m}_{12}}{\dot{m}_{11}}\dot{C}_{11}}{\dot{E}x_{12} - \frac{\dot{m}_{12}}{\dot{m}_{11}}\dot{E}x_{11}} = \dfrac{\dot{C}_{18} - \frac{\dot{m}_{18}}{\dot{m}_{11}}\dot{C}_{11}}{\dot{E}x_{18} - \frac{\dot{m}_{18}}{\dot{m}_{11}}\dot{E}x_{11}}$
Rectifier	$\dot{C}_{12} + \dot{C}_{A10} + \dot{Z}_{Rec} =$ $\dot{C}_{13} + \dot{C}_{14} + \dot{C}_{21}$	$c_{21} = c_{10,A}$ $\dfrac{\dot{C}_{13} - \frac{\dot{m}_{13}}{\dot{m}_{12}}\dot{C}_{12}}{\dot{E}x_{13} - \frac{\dot{m}_{13}}{\dot{m}_{12}}\dot{E}x_{12}} = \dfrac{\dot{C}_{14} - \frac{\dot{m}_{14}}{\dot{m}_{12}}\dot{C}_{12}}{\dot{E}x_{14} - \frac{\dot{m}_{14}}{\dot{m}_{12}}\dot{E}x_{12}}$
Ammonia-water turbine	$\dot{C}_{14} + \dot{Z}_{AWM} =$ $\dot{C}_{16} + \dot{C}_{w,AWMturbine}$ $\dot{C}_{w,AWMturbine} =$ $c_{w,AWMturbine} * \dot{w}_{AWMtur}$	$c_{14} = c_{16}$
Evaporator	$\dot{C}_{16} + \dot{C}_{23} + \dot{Z}_{Eva} = \dot{C}_{17} + \dot{C}_{24}$	$c_{16} = c_{17}$ $c_{23} = 0$
Absorber	$\dot{C}_{17} + \dot{C}_{20} + \dot{C}_{25} + \dot{Z}_{ABS} =$ $\dot{C}_9 + \dot{C}_{26}$	$c_{25} = 0$ $\dfrac{\dot{C}_{17} + \dot{C}_{20}}{\dot{E}x_{17} + \dot{E}x_{20}} = \dfrac{\dot{C}_9}{\dot{E}x_9}$
Pump	$\dot{C}_9 + \dot{C}_{w,pump} + \dot{Z}_{pump} = \dot{C}_{10}$ $\dot{C}_{w,pump} = c_{w,pump} * \dot{w}_{pump}$	$c_{w,pump} = c_{w,AWMturbine}$
Mixer	$\dot{C}_{13} + \dot{C}_{21} + \dot{C}_{22} + \dot{Z}_{Mixer} =$ $\dot{C}_{11}$	$\dot{Z}_{Mixer} = 0$
Solution heat exchanger	$\dot{C}_{18} + \dot{C}_{10B} + \dot{Z}_{SHE} =$ $\dot{C}_{19} + \dot{C}_{22}$	$c_{18} = c_{19}$
Expansion valve	$\dot{C}_{19} + \dot{Z}_{TV} = \dot{C}_{20}$	$c_{19} = c_{20}$

Besides, the exergy efficiency of the cogeneration cycle of power and cooling is determined as follows:

$$\eta_{ex} = \frac{\dot{W}_{net,Total} + \dot{E}x_{Cooling}}{\dot{E}x_{fuel}} \tag{2.28}$$

$$\dot{E}_{cooling} = \dot{E}_{24} - \dot{E}_{23} \tag{2.29}$$

The overall product cost for the power and cooling cogeneration cycle is written as follows:

Table 2.7 Model validation of gas turbine cycle between this study and Bejan et al. [18]

State	Working fluid	T (k)		P (bar)		h (kJ/kg)	
		[18]	This work	[18]	This work	[18]	This Work
1	Ideal gas	298.2	298.2	1.013	1.013	−164.6	−164.6
2	Ideal gas	603.7	603.7	10.13	10.13	160.5	160.5
3	Ideal gas	850	850	9.624	9.624	437.2	437.2
4	Ideal gas	1520	1520	9.142	9.142	329.3	329.3
5	Ideal gas	1016	1016	1.157	1.157	−300.9	−300.9
6	Ideal gas	789.8	789.8	1.122	1.122	−527.7	−527.7
7	Ideal gas	377.8	377.8	1.122	1.122	−995.4	−1044
8	Fuel	298.2	298.2	12	12	−4667	−4667

$$c_{pr,total}\left(\frac{\$}{GJ}\right) = \left(\frac{\dot{Z}_{Total} + \dot{C}_{fuel}}{\dot{W}_{net,Total} + \dot{E}_{Cooling}}\right) \tag{2.30}$$

2.4 Results and Discussion

2.4.1 Validation

This study contains two primary cycles, namely gas turbine and Goswami cycles, so they should be appropriately modeled. In this regard, these cycles are separately modeled in engineering equation solver (EES) to evaluate their validity according to similar studies. Therefore, their results are compared with Ref. [18] and [19] in Tables 2.7 and 2.8, respectively. As can be seen, an exceptionally well compatibility exists between the literature results and those of the present work.

2.4.2 Numerical Results

The thermodynamic characteristics of the operating states in the combined cycles are shown in Table 2.9.

As shown in this table, the thermodynamic characteristics of all states are obtained after exergy analysis.

Also, the net and cooling powers and exergy efficiency of the cycle are given in Table 2.10.

Table 2.11 shows the exergoeconomic assessment in different components. Accordingly, the highest exergy destruction and cost of exergy destruction rates occurred in the combustion chamber and boiler, where there is a large amount of fuel

Table 2.8 Model validation of Goswami cycle between this study and Zare et al. [19]

State	Working fluid	T (k)		P (bar)		x		h (kJ/kg)	
		[19]	This work	[19]	This work	[19]	This work	[19]	This work
9	AWM	303.2	303.2	4.1	4.1	0.524	0.524	−104.5	−104.5
10	AWM	303.4	303.4	24.6	24.6	0.524	0.524	−101.5	−101.5
11	AWM	372.8	372.8	24.6	24.6	0.5252	0.5252	230.2	230.2
12	AWM	383.2	383.2	24.6	24.6	0.9682	0.9682	1496	1496
13	AWM	353.1	353.2	24.6	24.6	0.6541	0.6541	163.7	162.7
14	AWM	353.2	353.2	24.6	24.6	0.9949	0.9949	1376	1376
16	AWM	273.8	273.8	4.1	4.1	0.9949	0.9949	1183	1183
17	AWM	293.2	293.2	4.1	4.1	0.9949	0.9949	1305	1305
18	AWM	383.2	383.2	24.6	24.6	0.4658	0.4658	265.3	265.3
19	AWM	308.4	308.4	24.6	24.6	0.4658	0.4658	−79.27	−79.27
20	AWM	308.8	308.8	4.1	4.1	0.4658	0.4658	−79.27	−79.27
21	AWM	322.6	322	24.6	24.6	0.524	0.524	−15.18	−17.94
22	AWM	378.6	379.1	24.6	24.6	0.524	0.524	334.7	340.9
23	Water	298.2	298.2	1	1.013	–	–	104.8	104.8
24	Water	288.2	288.2	1	1.013	–	–	63.01	63.01
25	Water	303.2	278.2	1	1.013	–	–	21.12	21.12

exergy in fuel and compressed air streams, which have high-temperature differences with outlet combustion gases. Additionally, combustion chamber and boiler equipment lose a large amount of exergetic cost because of their waste heat or exhaust gases, which can be minimized using optimization methods. It is noteworthy to mention that the gas turbine and combustion chamber have enormous investment costs, so they should be appropriately designed for the manufacturers to spend the lowest amount of money.

2.4.3   Sensitivity Analysis

This section discusses the influence of various thermodynamic parameters on the second law efficiency and total cost rate. Other parameters are ignored due to their slight impact on the proposed cycle performance.

Table 2.9 Thermodynamic and thermo-economic results for each stream of the proposed cycle

State	Working fluid	T (K)	P (bar)	x	Qu	$\dot{m}$ ($\frac{kg}{s}$)	h ($\frac{kJ}{kg}$)	S ($\frac{kJ}{kg.K}$)	$\dot{E}$ (kW)	c ($/GJ)
1	Ideal gas	298.2	1.013	–		94.79	−164.6	6.958	0	0
2	Ideal gas	603.7	10.13	–		94.79	160.5	7.036	28,602	10.45
3	Ideal gas	850	9.624	–		94.79	437.2	7.435	43,556	9.877
4	Ideal gas	1520	9.142	–		96.49	329.3	8.345	106,139	7.116
5	Ideal gas	1016	1.157	–		96.49	−300.9	8.451	42,299	7.116
6	Ideal gas	789.8	1.122	–		96.49	−572.7	8.451	24,515	7.116
7	Ideal gas	377.8	1.122	–		96.49	−1044	7.319	3190	7.116
8	fuel	298.2	12	–		1.705	−4667	–	88,454	3.365
9	AWM	303.2	4.1	0.524	0	249.4	−104.5	0.2908	2,596,000	5.503
10	AWM	303.4	24.6	0.524	−0.001	249.4	−101.5	0.2923	2,597,000	5.505
11	AWM	372.8	24.6	0.5252	0.008359	251.7	230.2	1.272	2,638,000	5.492
12	AWM	383.2	24.6	0.9682	1	29.75	1496	4.559	583,666	8.097
13	AWM	352.2	24.6	0.6541	0	2.329	162.7	1.034	30,415	6.53
14	AWM	353.2	24.6	0.9949	1	27.42	1376	4.233	552,088	8.117
16	AWM	273.8	4.1	0.9949	1	27.42	1183	4.356	545,948	8.117
17	AWM	293.2	4.1	0.9949	0.9333	27.42	1305	4.79	545,811	8.117
18	AWM	283.2	24.6	0.4658	0.9893	222	265.3	1.371	2,068,000	4.794
19	AWM	308.4	24.6	0.4658	0	222	−79.27	0.3719	2,058,000	4.794
20	AWM	308.4	4.1	0.4658	−0.001	222	−79.27	0.3798	2,058,000	4.794
21	AWM	322	24.6	0.524	−0.001	76.48	−17.94	0.5597	798,875	5.505
22	AWM	379.1	24.6	0.524	−0.001	172.9	340.9	1.565	1,817,000	5.484
23	Water	298.2	1.013	–	0.07643	79.77	104.8	0.3669	199.3	0
24	Water	288.2	1.013	–		79.77	63.01	0.2242	256.5	5.521
25	Water	278.2	1.013	–		2111	21.12	0.04625	11,482	0
26	Water	283.2	1.013	–		2111	42.09	0.151	8721	5.273

Table 2.10 Power, cooling, and efficiencies of the first and second laws

$\dot{W}_{net\ total}$ (kW)	$\dot{Q}_{eva}$ (kW)	η_{Energy} (%)	η_{Exergy} (%)
34,533	3337	44.41	39.11

Table 2.11 Exergoeconomic results for each component of the designed CCP unit

Components	$\dot{E}_D$(kW)	$\dot{E}_L$(kW)	ϵ(%)	$\dot{C}_D$($/h)	$\dot{C}_L$($/h)	$\dot{Z}$($/h)
AC	2206	0	92.84	73.17	0	44.09
APH	2830	0	84.09	72.48	0	27.47
CC	25,870	414.4	80.4	495.2	2256	135.3
Gas turbine	3033	0	95.25	77.7	0	381.1
Rectifier	866.2	0	25.46	34.98	0	0.5677
Boiler	7585	3190	56.05	194.3	22,698	1.995
Mixer	7986	0	99.7	158.2	0	0
SHE	476.8	0	95.61	7.791	0	9.271
Pump	109.7	0	85.15	4.616	0	9.368
AWM turbine	936.5	0	84.92	27.56	0	39.11
Evaporator	80.17	0	41.66	2.36	0	0.9605
Absorber & Th.V	5417	0	33.76	107.4	0	3.465

2.4.3.1   Effect of Isentropic Efficiency of Gas Turbine

Figure 2.2 indicates the effect of the isentropic efficiency of the gas turbine on the total cost rate and exergy efficiency. When the isentropic efficiency of the gas turbine increases, it causes a rise in the exergy efficiency. Because the enthalpy and mass flow
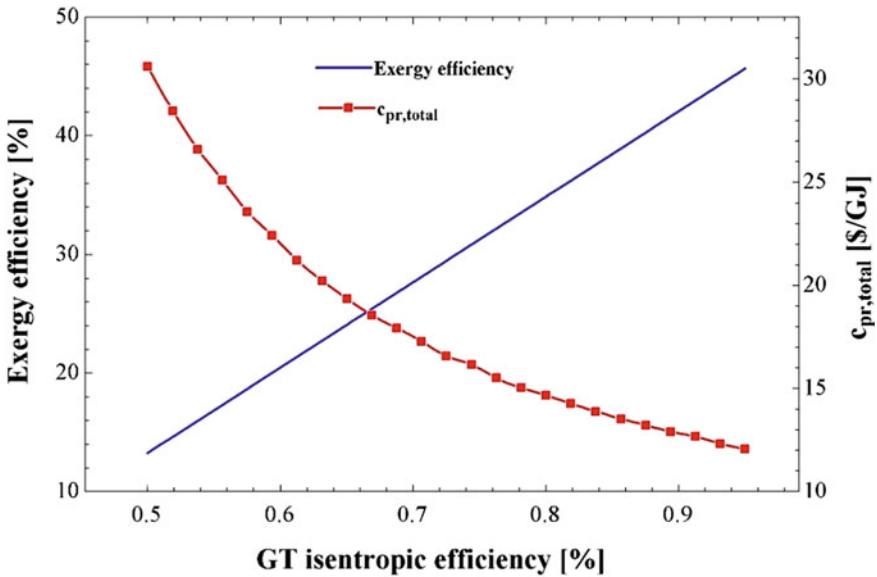
Fig. 2.2 The effect of turbine isentropic efficiency on exergy efficiency and total cost rate of the system

rate of the output stream from the turbine (stream 5) decreases, leading to a decrease in $\dot{W}_{nettotal}$. On the other hand, fuel exergy and $\dot{Ex}_{Cooling}$ are reduced (while the enthalpy of stream 4 remains constant). Since the reduction in fuel exergy is higher than $\dot{Ex}_{Cooling}$ and $\dot{W}_{net\,total}$, this raises the exergy efficiency of the cycle. Also, a decrease in $\dot{c}_8$ due to reducing the rate of inlet fuel and air as well as decreasing $\dot{Z}_{total}$ results in a decrement of $c_{pr,total}$.

2.4.3.2 Effect of Isentropic Efficiency of the Compressor

The influence of the isentropic efficiency of the compressor on the exergy efficiency and the total cost rate is demonstrated in Fig. 2.3. Accordingly, rising the isentropic efficiency of the compressor improves the exergy efficiency of the cycle. As the isentropic efficiency of the compressor increases, the enthalpy of the output stream from the compressor (stream 2) decreases, leading to the decrement of the compressor's power consumption. Since the net output power of the open Brayton cycle is constant, lowered power consumption in the compressor contributes to reducing fuel consumption. Consequently, the amount of $\dot{W}_{nettotal}$, $\dot{Ex}_{Cooling}$, and $\dot{Ex}_{fuel}$ decreases. Also, since the ratio of fuel exergy reduction to $\dot{Ex}_{Cooling}$ and $\dot{W}_{nettotal}$ is high, it increases the total exergy efficiency. By enhancement of compressor's isentropic efficiency, the rate of inlet fuel and air decreases. It causes a reduction in $\dot{C}_{fuel}$ and decreasing $\dot{Z}_{total}$, in turn, results in a decrement of $c_{pr,total}$.
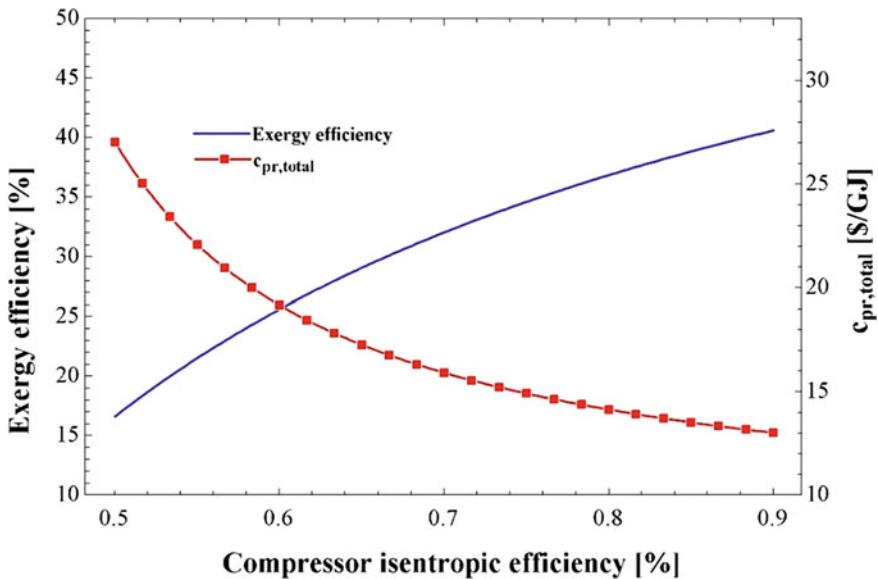
Fig. 2.3 The effect of compressor isentropic efficiency on exergy efficiency and total cost rate of the system
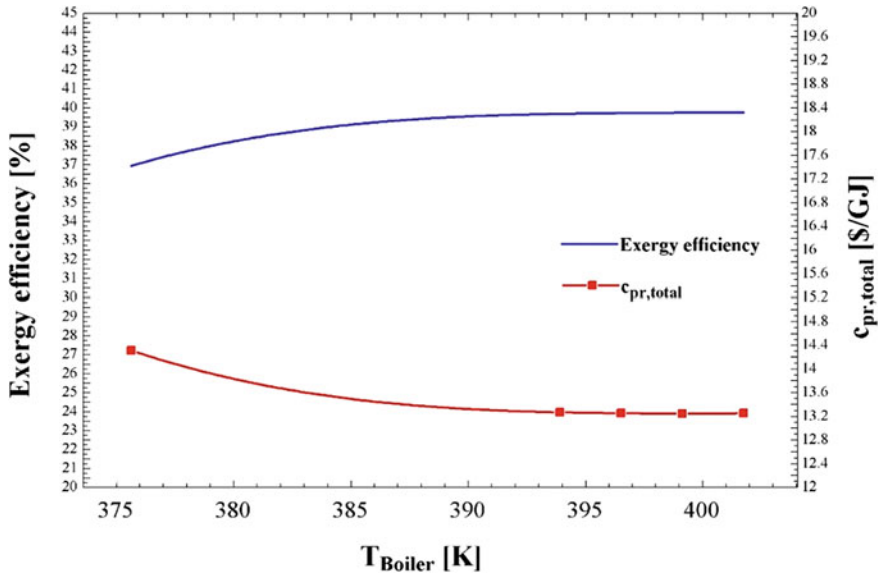
Fig. 2.4 The effect of boiler temperature on exergy efficiency and total cost rate of the system

2.4.3.3 Effect of Boiler Temperature

Regarding Fig. 2.4, by an increase in the gas turbine's inlet temperature, the cycle's exergy efficiency improves. According to the minimum and maximum temperature studied for the inlet temperature of the gas turbine (375.6 K and 410 K), the exergy efficiency of the cycle changes from 37.76% to 39.77%. As the boiler temperature rises, the mass flow rate and enthalpy of stream 12 increase, and the mass flow rate of stream 18 decreases. This increases the power production of the AWM turbine and reduces the power consumption in the pump. As a result, $\dot{W}_{nettotal}$ increases in the cycle. Moreover, with an increasing flow rate of state 16, $\dot{Ex}_{Cooling}$ increases leading to an improvement in exergy efficiency. Since $\dot{c}_8$ is constant and $\dot{Z}_{total}$ decreases while $\dot{Ex}_{Cooling}$ and $\dot{W}_{nettotal}$ increase, and consequently, it leads to a decrement of $c_{pr,total}$.

2.4.3.4 Effect of Air Temperature Entering the Combustion Chamber

One of the effective parameters studied in sensitivity analysis is the air temperature entering the combustion chamber. It has a remarkable influence on the exergy efficiency and the total cost rate of the system, as seen in Fig. 2.5. According to this figure, an augmentation in the air temperature at the inlet of the combustion chamber causes an improvement of exergy efficiency and reduction of the total cost rate. Variation of the temperature from 700 to 900 K improves the exergy efficiency from 34.38%
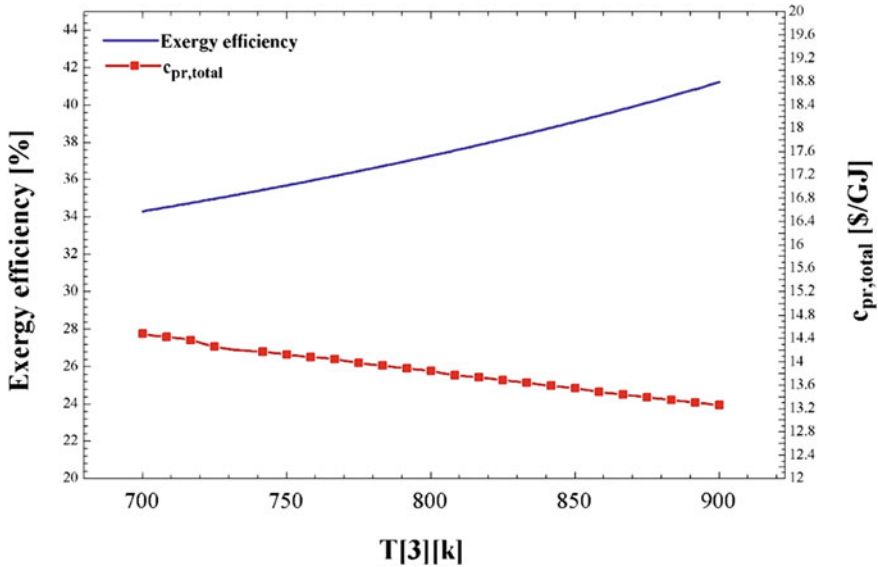
Fig. 2.5 The effect of air temperature entering the combustion chamber on exergy efficiency and the total cost rate of the system

to 41.32%. This achievement is due to the output power of the turbine, which occurs as a result of increased flow and enthalpy of inlet air. Also, a dramatic reduction in fuel exergy enhances the rate of improvement in exergy efficiency. Moreover, the variation mentioned above in the inlet air temperature of the combustor leads to a fall in the total cost rate from $ 14.39 GJ to $ 13.14 GJ. Overall, as the airflow rate rises, the fuel rate decreases significantly, which causes $c_{pr,total}$ to decrease as well. On the other hand, decreasing $\dot{W}_{nettotal}$ in high-level results in a decrement of $c_{pr,total}$.

2.4.3.5   Effect of Gas Turbine Inlet Temperature

Another effective parameter studied in sensitivity analysis is the flame temperature. The influence of flame temperature is shown in Fig. 2.6. A rise in flame temperature causes a decrement in exergy efficiency and reduces the total cost rate. Variation of the flame temperature from 1300 to 1700 K reduces the exergy efficiency from 39.95% to 38.68%. It is due to the exergy loss by combustion at higher temperatures in the combustion chamber of the gas turbine cycle.

On the other hand, this variation in the exhaust gases temperature leads to a fall in the total cost rate of the process from $39.95GJ to $38.68 GJ. As the temperature of the exhaust gases rises, the amount of consumed fuel diminishes, which must run the gas turbine cycle and provide 30 MW net output power. So, there will be a lower amount of energy to produce power and cooling in the Goswami cycle. Therefore,
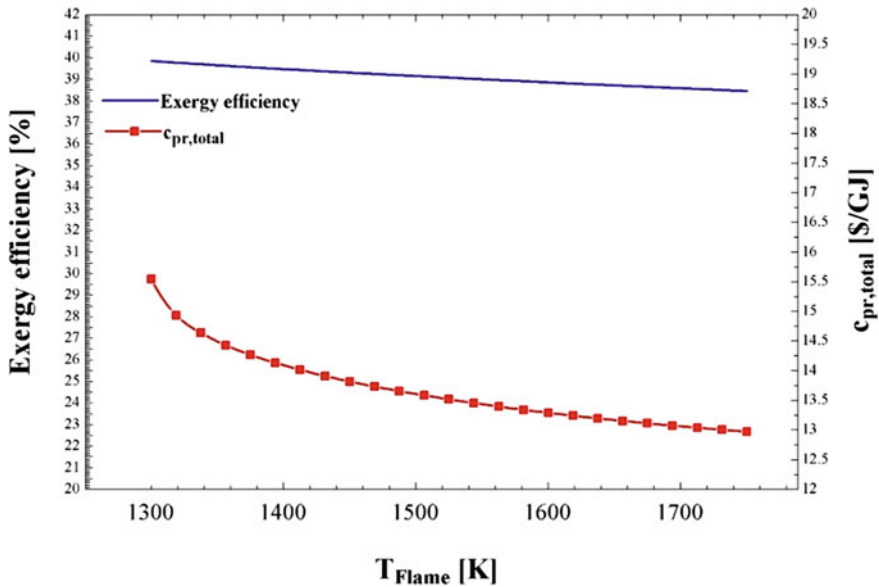
Fig. 2.6 The effect of flame temperature on exergy efficiency and the total cost rate of the system

the lowered capacity of cooling and total net output power causes a fall in exergy efficiency. Also, a lower amount of fuel consumption leads to reducing the unit cost of products.

2.4.4 Cycle Optimization

Optimization refers to a strategic search for identifying a system's maximum or minimum value utilizing available tools or methods. Depending on needs, it can be single-objective or multi-objective. Optimization includes the objective functions, the decision variables, and mainly the conditional functions. In an optimization process, the aim is to determine the optimal values for variables. There are different methods for optimizing a problem, and the one-objective optimization method with EES software is employed to fulfill this aim in the present study.

2.4.4.1 Single-Objective Optimization

The exergy efficiency is taken into consideration for single-objective optimization of the studied cycle. By assuming a constant value for economic factors, the objective function is the proportion of efficacy improvement of the system by increasing

the exergy efficiency and minimizing the cost or preventing its rise simultaneously. Regarding this, the objective function is written as follows:

$$\eta_{ex} = \frac{\dot{W}_{net,Total} + \dot{Ex}_{Cooling}}{\dot{Ex}_{fuel}} \tag{2.31}$$

2.4.4.2 Decision Variables

Sensitivity analysis is considered for each parameter for selecting the decision variables. The variable with a significant effect on the objective function is regarded as a decision variable. In this study, six decision variables are identified to optimize the system, as below.

1. Isentropic efficiency of the gas turbine ($\eta_{Gas\,turbine}$)
2. Isotropic efficiency of the ammonia-water turbine ($\eta_{AWM\,turbine}$)
3. Isentropic efficiency of the compressor ($\eta_{compressor}$)
4. The inlet temperature of the AWM turbine (T_{boiler})
5. The inlet temperature of the gas turbine(T_4)
6. The inlet air temperature to the combustion chamber (T_3)

The decision variables constraints are based on a parametric study and are considered in accordance with the operating conditions of the proposed cycle as follows:

$$0.6 < \eta_{Gas\,turbine} < 0.85$$

$$0.7 < \eta_{AWM\,Turbine} < 0.95$$

$$0.7 < \eta_{comp} < 0.95$$

$$380 < T_{boiler} < 410$$

$$1300 < T_4 < 1700$$

$$700 < T_3 < 900$$

Table 2.12 Comparison of the objective functions in optimal and primary conditions

Optimized condition	Basic condition	Objective function
η_{ex}	39.11%	47.61%
C_{pr}	13.55 $/GJ	14.11 $/GJ

Table 2.13 Decision variables in the primary and optimized modes

Optimized condition	Basic condition	Objective function
$\eta_{Gas\,turbine}(\%)$	86	85
$\eta_{AWM\,turbine}(\%)$	85	95
$\eta_{compressor}(\%)$	86	95
$T_{boiler}(K)$	353	402
$T_4(K)$	1520	1435
$T_3(K)$	850	900

2.4.4.3 Results of the Optimized Cycle

After the optimization, the achieved values for the considered objective function are shown and compared with the results obtained before the optimization in Table 2.12. It shows that optimization results in an 8.5% increase in exergy efficiency, which is significant, while the total cost rate rises by about $ 0.56 / GJ.

The comparison between the values of the decision variables in the primary and optimal conditions is shown in Table 2.13.

As can be inferred, the values of the isentropic efficiency of the compressor, the compressor pressure ratio, the inlet air temperature to the combustion chamber, and the boiler temperature increase after optimization compared to the primary mode. Besides, the value of variables such as isotropic efficiency of the turbine, pinch point temperature difference in the heat exchanger, inlet flow temperature to the gas turbine, rectifier temperature, flame temperature, and pump pressure ratio decreases relative to the primary mode.

2.5 Conclusion

1. Increasing the inlet air temperature of the combustion chamber, the isentropic efficiency of the gas turbine and compressor, and the compressor pressure ratio improved the thermodynamic performance of the system and reduced the final cost rate of the system.
2. Increasing the flame temperature reduced the exergy efficiency of the system. In contrast, the isentropic efficiency of the turbine and the inlet exhaust gas temperature to the gas turbine could increase or decrease the total cost rate of the system.

3. The most destructive unit is the gas turbine cycle, which equals 44.89% of the total exergy destruction. Following that, the boiler and mixer (in the bottoming process) are the most irreversible ones. Also, the lowest amount of exergy destruction is 0.401% for the evaporator.
4. The exergy efficiency of the system rises from 39.11% to 47.61% by optimizing the system, while the total cost rate increases only by $ 0.56 / GJ.

References

1. M.-R. Kolahi, A. Nemati, M. Yari, Performance optimization and improvement of a flash-binary geothermal power plant using zeotropic mixtures with PSO algorithm. Geothermics **74**, 45–56 (2018)
2. H. Nasrollahi, F. Ahmadi, M. Ebadollahi, S. Najafi Nobar, M. Amidpour, The greenhouse technology in different climate conditions: a comprehensive energy-saving analysis. Sustain. Energy Technol. Assessments **47**, 101455 (2021)
3. H. Nami, S.M.S. Mahmoudi, A. Nemati, Exergy, economic and environmental impact assessment and optimization of a novel cogeneration system including a gas turbine, a supercritical CO2 and an organic Rankine cycle (GT-HRSG/SCO2). Appl. Therm. Eng. **110**, 1315–1330 (2017)
4. E. Gholamian, V. Zare, A comparative thermodynamic investigation with environmental analysis of SOFC waste heat to power conversion employing Kalina and Organic Rankine Cycles. Energy Convers. Manag. **117**, 150–161 (2016)
5. A.M. Alklaibi, M.N. Khan, W.A. Khan, Thermodynamic analysis of gas turbine with air bottoming cycle. Energy **107**, 603–611 (2016)
6. O. Siddiqui, I. Dincer, Analysis and performance assessment of a new solar-based multigeneration system integrated with ammonia fuel cell and solid oxide fuel cell-gas turbine combined cycle. J. Power Sources **370**, 138–154 (2017)
7. S. Mirmasoumi, R.K. Saray, S. Ebrahimi, Evaluation of thermal pretreatment and digestion temperature rise in a biogas fueled combined cooling, heat, and power system using exergo-economic analysis. Energy Convers. Manag. **163**, 219–238 (2018)
8. A. Behzadi, A. Habibollahzade, V. Zare, M. Ashjaee, Multi-objective optimization of a hybrid biomass-based SOFC/GT/double effect absorption chiller/RO desalination system with CO2 recycle. Energy Convers. Manag. **181**, 302–318 (2019)
9. Y. Chen et al., Parametric analysis and optimization for exergoeconomic performance of a combined system based on solid oxide fuel cell-gas turbine and supercritical carbon dioxide Brayton cycle. Energy Convers. Manag. **186**, 66–81 (2019)
10. A. Habibollahzade, E. Gholamian, A. Behzadi, Multi-objective optimization and comparative performance analysis of hybrid biomass-based solid oxide fuel cell/solid oxide electrolyzer cell/gas turbine using different gasification agents. Appl. Energy **233–234**, 985–1002 (2019)
11. A.D. Zare, R.K. Saray, S. Mirmasoumi, K. Bahlouli, Optimization strategies for mixing ratio of biogas and natural gas co-firing in a cogeneration of heat and power cycle. Energy **181**, 635–644 (2019)
12. O. Barkhordarian, A. Behbahaninia, R. Bahrampoury, A novel ammonia-water combined power and refrigeration cycle with two different cooling temperature levels. Energy **120**, 816–826 (2017)
13. H. Ghaebi, T. Parikhani, H. Rostamzadeh, B. Farhang, Proposal and assessment of a novel geothermal combined cooling and power cycle based on Kalina and ejector refrigeration cycles. Appl. Therm. Eng. **130**, 767–781 (2018)

14. J. Hosseinpour, A. Chitsaz, B. Eisavi, M. Yari, Investigation on performance of an integrated SOFC-Goswami system using wood gasification. Energy **148**, 614–628 (2018)
15. H. Rostamzadeh, H. Ghaebi, T. Parikhani, Thermodynamic and thermoeconomic analysis of a novel combined cooling and power (CCP) cycle. Appl. Therm. Eng. **139**, 474–487 (2018)
16. P. Behnam, M. Faegh, M.B. Shafii, Thermodynamic analysis of a novel combined power and refrigeration cycle comprising of EKalina and ejector refrigeration cycles. Int. J. Refrig. **104**, 291–301 (2019)
17. H. Ghiasirad, R. Khoshbakhti Saray, B. Abdi, K. Bahlouli, Energy, exergy, and exergo-economic analyses of Urmia sugar factory: a case study of Iran, in The 11th International Chemical Engineering Congress & Exhibition (IChEC) 6 (IChEC, 2020)
18. A. Bejan, G. Tsatsaronis, M. Maran, *Thermal Design and Optimization* (Wiley, John, 1996)
19. V. Zare, S.M.S. Mahmoudi, M. Yari, An exergoeconomic investigation of waste heat recovery from the Gas Turbine-Modular Helium Reactor (GT-MHR) employing an ammonia–water power/cooling cycle. Energy **61**, 397–409 (2013)
20. N. Asgari, R. Khoshbakhti Saray, S. Mirmasoumi, Energy and exergy analyses of a novel seasonal CCHP system driven by a gas turbine integrated with a biomass gasification unit and a LiBr-water absorption chiller. Energy Convers. Manag. **220**, 113096 (2020)
21. H. Ghiasirad, H. Rostamzadeh, S. Nasri, Design and evaluation of a new solar tower-based multi-generation system: Part II, Exergy and exergoeconomic modeling, in Integration of Clean and Sustainable Energy Resources and Storage in Multi-Generation Systems 103–120 (Springer International Publishing, 2020). https://doi.org/10.1007/978-3-030-42420-6_6
22. H. Rostamzadeh, H. Ghiasirad, M. Amidpour, Y. Amidpour, Performance enhancement of a conventional multi-effect desalination (MED) system by heat pump cycles. Desalination **477**, 114261 (2020)
23. H. Ghiasirad, N. Asgari, R. Khoshbakhti Saray, S. Mirmasoumi, Thermoeconomic assessment of a geothermal based combined cooling, heating, and power system, integrated with a humidification-dehumidification desalination unit and an absorption heat transformer. Energy Convers. Manag. **235**, 113969 (2021)
24. F. Petrakopoulou, Comparative Evaluation of Power Plants with CO2 Capture: Thermodynamic, Economic and Environmental Performance. (TU-Berlin, 2010)
25. Y.C. Ledón, P. González, S. Concha, C.A. Zaror, L.E. Arteaga-Pérez, Exergoeconomic valuation of a waste-based integrated combined cycle (WICC) for heat and power production. Energy **114**, 239–252 (2016)

Chapter 3
Reliability and Availability Consideration in Design of an Ammonia-Water CHP System for a Low-Temperature Geothermal Source

Hadi Rostamzadeh, Afshin Yaghoubi, Saeed Ghavami Gargari, Majid Amidpour, and Weifeng He

Abstract Reliability consideration in design process of CHP (combined heat and power) systems can be an encouraging approach to a complete analysis of power plants working with renewable sources such as geothermal since the estimated cost of products can be more viable and reliable. With regard to this point, an ammonia-water CHP system applicable for the Sabalan geothermal well is considered in this chapter. The devised system consists of a Kalina cycle (KC) and an absorption-compression heat pump cycle (ACHPC). First, the devised CHP unit is evaluated from thermodynamics and thermoeconomics perspectives. Next, the state-space continuous Markov method is used to compute various considered sub-system's repair and failure rates, and the results are integrated with the results of thermoeconomic analysis. The devised CHP unit generated net electricity and heating load of 3,235 kW and 70,328 kW, respectively, while achieving energy efficiency of 61.01% and exergy efficiency of 22.21% under this circumstance. The condenser/desorber was introduced as source of irreversibility between all elements. Taking reliability of different elements of the proposed CHP unit into account, it is found that the unit cost of electricity, unit cost of heating, and OPCS (overall product cost of the system) are increased by 5.75%, 6.41%, and 6.5%, respectively.

H. Rostamzadeh
Department of Aerospace Engineering, Sharif University of Technology, Azadi Ave, Tehran, Iran

A. Yaghoubi
Department of Industrisal Engineering, Sharif University of Technology, Azadi Ave, Tehran, Iran

S. G. Gargari
Department of Mechanical Engineering, University of Mohaghegh Ardabili, Ardabil, Iran

M. Amidpour (✉)
Department of Mechanical Engineering, K.N. Toosi University of Technology, Tehran, Iran
e-mail: amidpour@kntu.ac.ir

W. He
Energy Conservation Research Group (ECRG), College of Energy and Power Engineering, Nanjing University of Aeronautics and Astronautics, Nanjing 210016, Jiangsu, China
e-mail: wfhe@nuaa.edu.cn

Nomenclature

Symbols

A	Area (m^2)
Av	Availability
B	Basic solution
c	Cost per exergy unit ($.kWh^{-1})
$\dot{C}$	Cost rate ($.h^{-1})
CHP	Combined heating and power
CR	Compressor ratio
CRF	Capital recovery factor
ex	Exergy per unit mass (kW.kg^{-1})
$\dot{Ex}$	Exergy rate (kW)
GF	Geofluid
h	Specific enthalpy (kJ.kg^{-1})
k	Interest rate
KC	Kalina cycle
$\dot{m}$	Mass flow rate (kg.s^{-1})
N	Stochastic transitional probability matrix
N	Annual number of hours (h)
n$_r$	Components expected life
OPCS	Overall product cost of the system ($/GJ)
P	Pressure (bar)
P$_{ij(t)}$	Probability of transition from state i to state j
PR	Pump ratio
s	Specific entropy (kJ.kg^{-1}.K^{-1})
T	Temperature (°C)
TTD	Terminal temperature difference
U	Overall heat transfer coefficient (kW.m^{-2}K^{-1})
ACHPC	Absorption-compression heat pump cycle
$\dot{W}$	Power (kW)
w	Weight function
X	Ammonia concentration
Z	Investment cost of components ($)
$\dot{Z}$	Investment cost rate of components ($.h^{-1})

Greek Symbols

η	Efficiency (%)
φ	Maintenance factor
ε	Effectiveness
λ	Failure rate (per year)
μ	Repair rate (per year

Subscripts and Supercripts

Abs	Absorber
CD	Condenser/Desorber
ch	Chemical
CI	Capital investment
Com	Compressor
c.v.	Control volume
D	Destruction
Des	Desorber
elec	electricity
en	Energy
ex	Exergy
exi	Exit
F	Fuel
h	Heating
Geo	Geothermal
HS	Heat source
in	Inlet
is	Isentropic
i	ith component
L	Loss
Mix	Mixer
Net	net value
OM	operating & maintenance
out	Outlet
P	Product
ph	Physical
PP	Pinch point
Pu	Pump
q	Heat transfer
R	Reliability
Rg	Regenerator
s	Constant entropy

Sep	Separator
SHE	Solution heat exchanger
Sup	Superheater
sys	System
tot	Total
Tur	Turbine
Th.V	Throttling valve
VG	Vapor generator
w	Work
1, 2, …	States
0	Dead state

3.1   Introduction

As a core concept in design of CHP (combined heat and power) systems, their constituents should be more reliable and available through the entire time of operation and so does the whole system. Any dearth of attention to reliability of CHP systems may culminate in irreparable damages to the society due to shortfall in power/heating storage. Any enhancement in reliability of energy systems will offer some surplus expenditure for provision of installation of new devices or maintenance of the previous installed ones. Increasingly productive efforts have been dedicated to model reliability and availability of cogeneration systems along with economic aspect of the systems in order to reveal how reliability deliberation for an entire plant could influence products cost. Broadly speaking, only after estimating cost of a reliable power plant could one make a deduction about cost-effectiveness of the recommended amendments by weighing the expended cost and the aggregated product cost before and after the reliability consideration. Carazas et al. [1] evaluated reliability and availability of two HRSGs (heat recovery steam generator) in a 500 MW combined power plants. They showed that the availability is highly influenced by feed-water pump failure. They also proposed some enhancement procedure for monitoring of the operated device. Sabouhi et al. [2] assessed and quantified the repair and maintenance effects in terms of reliability and availability indices for three different power plants, namely CHP systems, gas turbine (GT) systems, and steam turbine (ST) systems. They derived a new mathematical relation for availability, repair rate, and failure rate at steady state. They found that the ST systems are highly reliable than the GT and CHP systems. They also deduced that the MTTF (system mean time to failure) and MTTF1 (system mean time to first failure) of all three examined set-ups are equal. Hosseini et al. [3] pondered the impact of reliability on economic aspect of a combined power and distilled water system using a GT system and a MSD (multi-stage desalination) unit. Using the continuous Markov approach incorporated with thermoeconomic assessment, they demonstrated that the distilled

water and extracted electricity costs could increase up to 6.4% and 4.1%, respectively, as reliability analysis is deliberated in calculations. Dev et al. [4, 5] computed reliability indices of combined power plants based on the graph theory and matrix method. They developed a function for reliability that led to a better reliability as the numerical values are substituted in the relation. Wang et al. [6] analyzed performance and cost of a building CHP (BCHP) system with considering reliability and availability of the system, using a GT as the topping cycle. They discovered that the reliability and availability of the non-redundant BCHP unit for heating and cooling is lower than the single generation scenario. In another study, Wang et al. [7] considered reliability in cost analysis of a trigeneration system fueled by biomass. The authors understood that the unit cost associated with electricity/cooling is mainly influenced by the repair and failure rates of the gasification unit. Also, the OPCS (overall product cost of the system) is augmented 16% as reliability is taken into cost evaluation. Zare [8] performed exergoeconomic evaluation of a GT-MHR (modular helium reactor) system and a combined GT-MHR/ORC system under reliability consideration. The scholar also optimized performance of both systems and found that the availability of the GT-MHR unit is relatively significant than that of the combined set-up due to its less complexity. Pouyan-Rad et al. [9, 10] devised a new hybrid approach in reliability-cost deliberation in the utility systems based on the continuous Markov approach and thermoeconomic assessment. They argued that their proposed approach is more apt for thermoeconomic optimization. They also notified that the OPCS is decreased as the system availability increases. Nearly all substantiated the idea of repairing and adjusting of these systems than renewing the constituents.

In addition to reliability implementation in cogeneration systems, several ventilation systems (heating or air-conditioning) are designed with reliability accounting in the analysis [11]. Wang et al. [12] employed reliability and availability concepts to estimate risk and rigorous solutions for a hybrid cooling system and concluded that the hybrid cooling system has a better reliability than the conventional cooling system.

3.2 Description of Layout

The layout of the introduced ammonia-water CHP unit fueled by the Sabalan geothermal well is displayed in Fig. 3.1. The NH_3-H_2O solution is fed into a separator, in which the rich solution in ammonia is directed to a turbine for power generation, while the lean solution is directed to the regenerator to heat the sub-cooled flow entering the vapor generator and expanded to the condenser pressure thereafter. These two streams (states 6 and 8) merge with each other and the outcome is liquefied through a condenser. The liquid is then pressurized back to the regenerator to be heated up prior to completing the cycle.

In the ACHPC, the KS's waste energy is used for the desorber to generate heating load. While exiting as a mixture (point 13), it is segregated into the vapor mode (point 14) and liquid mode (point 16). While, the vapor part is compressing to the
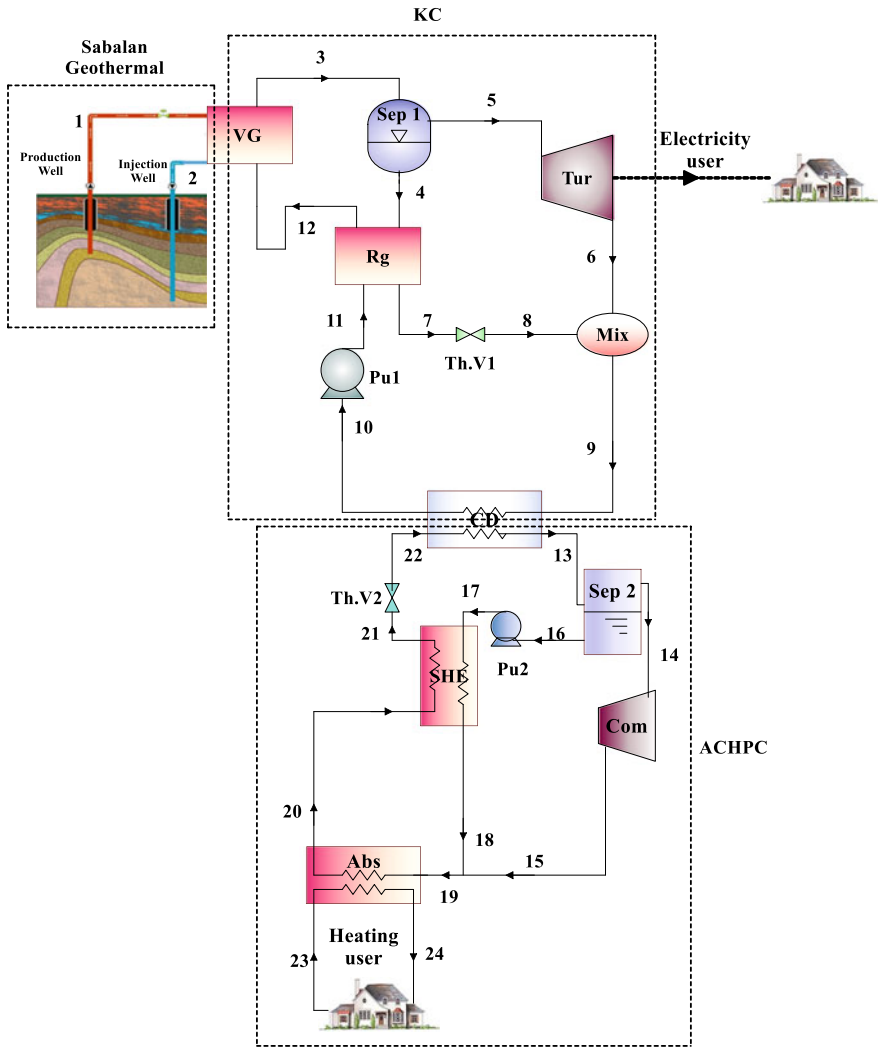
Fig. 3.1 Layout of the devised CHP system applicable for the Sabalan geothermal well with low-temperature well

absorber pressure by a compressor (point 15), the saturated liquid lean in ammonia is pressurized to the absorber pressure via pump 2 (point 17) and is heated up by a solution heat exchanger (SHE) thereafter (point 18). This flow is merged with the stream outflowing from the compressor and then the merged flow enters the absorber (point 19), leading to the heat release (point 24). Next, the liquid mixture (point 20) exiting from the absorber is chilled (point 21) and is throttled to a two-phase flow thereafter (state 22), completing the ACHPC operation.

3.3 Materials and Methods

3.3.1 Thermodynamic Analysis

Under steady state assumption, the chief governing equations needed for thermodynamic analysis of a unit can be expressed as [13]:

Mass balance:

$$\sum \dot{m}_{in} = \sum \dot{m}_{out} \tag{3.1}$$

Energy balance:

$$\sum \dot{Q}_{in} - \sum \dot{Q}_{out} = \sum (\dot{m}h)_{in} - \sum (\dot{m}h)_{out} + \dot{W} \tag{3.2}$$

By assuming that a proportion of the input exergy rate is lost or destroyed through operation of a system, the exergy balance relation can be stated as [13]:

$$\dot{Ex}_{D,i} = \sum_{i=1}^{n} \dot{Ex}_{in,i} - \sum_{i=1}^{n} \dot{Ex}_{out,i} \tag{3.3}$$

or, expressing Eq. (3.3) in other forms, we have:

$$\dot{Ex}_{D,i} = \dot{Ex}_{Fu,i} - \dot{Ex}_{Pr,i} - \dot{Ex}_{L,i} \tag{3.4}$$

where, $\dot{Ex}_{Fu,i}$, $\dot{Ex}_{Pr,i}$, $\dot{Ex}_{D,i}$, and $\dot{Ex}_{L,i}$ are called the exergy rate of fuel, product, destruction, and loss, respectively.

For insignificant amount of potential and kinetic exergy rate, the exergy rate for the ith flow can be calculated by summing the chemical and physical exergy rates altogether as [14]:

$$\dot{Ex}_i = \dot{Ex}_{ph,i} + \dot{Ex}_{ch,i} \tag{3.5}$$

where,

$$\dot{Ex}_{ph,i} = \dot{m}((h - h_0) - T_0(s - s_0))_i) \tag{3.6}$$

$$\dot{Ex}_{ch,i} = \dot{m}\left(\left[\frac{ex^0_{ch,a}}{M_a}\right]X_a + \left[\frac{ex^0_{ch,b}}{M_b}\right](1 - X_a)\right)_k \tag{3.7}$$

At the end, the exergy efficiency can be iterated as:

$$\eta_{ex,i} = \frac{\dot{Ex}_{Pr,i}}{\dot{Ex}_{Fu,i}} \tag{3.8}$$

The detailed thermodynamic equations applied to the devised CHP unit based on the state points available in Fig. 3.1 are listed in Table 3.1.

Table 3.1 Energetic and exergetic relations for different elements of the CHP unit

Component	Energy balance equation	Exergy balance equation
Vapor generator	$\dot{Q}_{VG}=\dot{m}_1(h_1-h_2)$, $\dot{Q}_{VG}=\dot{m}_3(h_3-h_{12})$	$\dot{Ex}_{D,VG} =$ $(\dot{Ex}_1-\dot{Ex}_2)-(\dot{Ex}_3-\dot{Ex}_{12})$
Separator 1	$\dot{m}_3 h_3 = \dot{m}_5 h_5 + \dot{m}_4 h_4$, $\dot{m}_3 = \dot{m}_4 + \dot{m}_5$, $\dot{m}_3 X_3 = \dot{m}_5 X_5 + \dot{m}_4 X_4$,	$\dot{Ex}_{D,Sep1}=\dot{Ex}_3 - (\dot{Ex}_4 + \dot{Ex}_5)$
Regenerator	$\dot{m}_4(h_4-h_7) = \dot{m}_{11}(h_{12}-h_{11})$, $\varepsilon_{Rg1} = \frac{T_4-T_7}{T_4-T_{11}}$	$\dot{Ex}_{D,Rg} =$ $(\dot{Ex}_4-\dot{Ex}_7)-(\dot{Ex}_{12}-\dot{Ex}_{11})$
Turbine	$\dot{W}_{Tur} = \dot{m}_5(h_5-h_6)$, $\eta_{is,Tur} = (h_5-h_6)/(h_5-h_{6s})$	$\dot{Ex}_{D,Tur} = (\dot{Ex}_5-\dot{Ex}_6)-\dot{W}_{Tur}$
Pump 1	$\dot{W}_{Pu1} = \dot{m}_{10}(h_{11}-h_{10})$, $\eta_{is,Pu1} = (h_{11s}-h_{10})/(h_{11}-h_{10})$	$\dot{Ex}_{D,Pu1} =$ $\dot{W}_{Pu1} - (\dot{Ex}_{11}-\dot{Ex}_{10})$
Mixer	$\dot{m}_6 h_6 + \dot{m}_8 h_8 = \dot{m}_9 h_9$, $\dot{m}_6 + \dot{m}_8 = \dot{m}_9$	$\dot{Ex}_{D,Mix} = (\dot{Ex}_6 + \dot{Ex}_8)-\dot{Ex}_9$
Throttling valve 1	$h_7 = h_8$	$\dot{Ex}_{D,TV1} = \dot{Ex}_7 - \dot{Ex}_8$
Desorber	$\dot{Q}_{Des}=\dot{m}_9(h_9-h_{10})$, $\dot{Q}_{Des}=\dot{m}_{22}(h_{13}-h_{22})$ $\Delta T_{PP,Des} = T_9 - T_{13}$	$\dot{Ex}_{D,Des} =$ $(\dot{Ex}_9-\dot{Ex}_{10})-(\dot{Ex}_{13}-\dot{Ex}_{22})$
Separator 2	$\dot{m}_{13} h_{13} = \dot{m}_{14} h_{14} + \dot{m}_{16} h_{16}$, $\dot{m}_{13} = \dot{m}_{14} + \dot{m}_{16}$ $\dot{m}_{13} X_{13} = \dot{m}_{14} X_{14} + \dot{m}_{16} X_{16}$	$\dot{Ex}_{D,Sep2}=\dot{Ex}_{13} - (\dot{Ex}_{14} + \dot{Ex}_{16})$
Pump 2	$\dot{W}_{Pu2} = \dot{m}_{16}(h_{17}-h_{16})$, $\eta_{is,Pu2} = (h_{17s}-h_{16})/(h_{17}-h_{16})$	$\dot{Ex}_{D,Pu2} =$ $\dot{W}_{Pu2} - (\dot{Ex}_{17}-\dot{Ex}_{16})$
Solution heat exchanger	$\dot{m}_{20}(h_{20}-h_{21}) =$ $\dot{m}_{17}(h_{18}-h_{17})$, $\varepsilon_{SHE} = \frac{T_{20}-T_{21}}{T_{20}-T_{17}}$	$\dot{Ex}_{D,SHE} =$ $(\dot{Ex}_{20}-\dot{Ex}_{21})-(\dot{Ex}_{18}-\dot{Ex}_{17})$
Compressor	$\dot{W}_{Com} = \dot{m}_{14}(h_{15}-h_{14})$, $\eta_{is,Com} = (h_{15s}-h_{14})/(h_{15}-h_{14})$	$\dot{Ex}_{D,Com} =$ $\dot{W}_{Com} - (\dot{Ex}_{15}-\dot{Ex}_{14})$
Absorber	$\dot{Q}_{Abs}=\dot{m}_{29}(h_{29}-h_{30})$, $\dot{Q}_{Abs}=\dot{m}_{23}(h_{24}-h_{23})$ $\Delta T_{PP,Abs} = T_{19} - T_{24}$	$\dot{Ex}_{D,Abs} =$ $(\dot{Ex}_{19}-\dot{Ex}_{20})-(\dot{Ex}_{24}-\dot{Ex}_{23})$
Throttling valve 2	$h_{21} = h_{22}$	$\dot{Ex}_{D,TV2} = \dot{Ex}_{21} - \dot{Ex}_{22}$

3.3.2 Thermoeconomic Analysis

The cost balance equation for a unit can be expressed as [13]:

$$\sum \dot{C}_{w,i} + \dot{C}_{out,i} = \sum \dot{C}_{q,i} + \dot{C}_{in,i} + \dot{Z}_{tot}^{OM} + \dot{Z}_{tot}^{CC} \tag{3.9}$$

$$\dot{Z}_i = \dot{Z}_i^{OM} + \dot{Z}_i^{CC} = CRF \times \frac{\phi_r}{N} \times Z_i \tag{3.10}$$

$$CRF = \frac{i_r(1+i_r)^{n_r}}{(1+i_r)^{n_r} - 1} \tag{3.11}$$

where, $\dot{C}_{out,i}$, $\dot{C}_{w,i}$, $\dot{C}_{in,i}$, $\dot{C}_{q,i}$, and $\dot{Z}_i$ are the cost rate associated with the outlet flow, power, inlet flow, heat, and total investment cost, respectively. Hence, we have:

$$\dot{C}_{w,i} = c_{w,i}\dot{E}x_{W,i}, \dot{C}_{out,i} = c_{out,i}\dot{E}x_{out,i}, \dot{C}_{q,i} = c_{q,i}\dot{E}x_{q,i}, \dot{C}_{in,i} = c_{in,i}\dot{E}x_{in,i} \tag{3.12}$$

Equation (3.9) can also be re-expressed as [13]:

$$\dot{C}_{Pr,tot} = \dot{C}_{Fu,tot} + \dot{Z}_{tot}^{CI} + \dot{Z}_{tot}^{OM} \tag{3.13}$$

The cost rate as cost penalty associated with exergy destruction can be calculated for each element as [13]:

$$\dot{C}_{D,i} = c_{Fu,i}\dot{E}x_{D,i}(If : \dot{E}x_{Pr,i} = Constant) \tag{3.14}$$

The main exergoeconomic relations for each component are listed in Table 3.2. Also, the overall heat transfer coefficients for different heat exchangers are listed in Table 3.3.

3.3.3 Reliability Modeling

In literature, reliability is defined as the probability of equipment carrying out its duty aptly for a specific course of time under the encountered working conditions [16]. It is imperative to note that the validity of the performed reliability analysis for a set-up is straightforwardly related to the validity of the model used through the evaluation. Regarding this point, it has already been proved that the state-space Markov method can lead to results with maximum reliability for energy systems [7, 8, 12]. Before proceeding further, it is imperious to quantify failure and repair of the different constituents of a system. Failure rate (λ) and repair rate (μ) can respectively be defined as [16]:

Table 3.2 Exergoeconomic relations for different elements of the proposed CHP unit

Components	Cost balance equations	Auxiliary relations	Investment cost functions
Vapor generator	$\dot{C}_1 + \dot{C}_{12} + \dot{Z}_{VG} = \dot{C}_3 + \dot{C}_2$	$c_1 = c_2$	$\dot{Z}_{VG} = 1397 \times (A_{VG})^{0.89}$
Separator 1	$\dot{C}_3 + \dot{Z}_{Sep1} = \dot{C}_4 + \dot{C}_5$	$c_4 = c_5$	$\dot{Z}_{Sep1} = 280.3 \times (\dot{m}_3)^{0.67}$
Regenerator	$\dot{C}_4 + \dot{C}_{11} + \dot{Z}_{Rg} = \dot{C}_7 + \dot{C}_{12}$	$c_4 = c_7$	$\dot{Z}_{Rg} = 2143 \times (A_{Rg})^{0.514}$
Turbine	$\dot{C}_5 + \dot{Z}_{Tur} = \dot{C}_6 + \dot{C}_{W,Tur}$	$c_{15} = c_{16}$	$\dot{Z}_{Tur} = 4405 \times (\dot{W}_{Tur})^{0.89}$
Pump 1	$\dot{C}_{10} + \dot{C}_{W,Pu1} + \dot{Z}_{Pu1} = \dot{C}_{11}$	$c_{W,Pu1} = c_{W,Tur}$	$\dot{Z}_{Pu1} = 1120 \times (\dot{W}_{Pum1})^{0.8}$
Mixer	$\dot{C}_{16} + \dot{C}_{18} + \dot{Z}_{Mix} = \dot{C}_{19}$	–	$\dot{Z}_{Mix} = 0$
Throttle valve 1	$\dot{C}_7 + \dot{Z}_{TV1} = \dot{C}_8$	–	$\dot{Z}_{TV1} = 114.5 \times \dot{m}_{17}$
Desorber	$\dot{C}_9 + \dot{C}_{22} + \dot{Z}_{Des} = \dot{C}_{13} + \dot{C}_{10}$	$c_9 = c_{10}$	$\dot{Z}_{Des} = 2143 \times (A_{Des})^{0.514}$
Separator 2	$\dot{C}_{13} + \dot{Z}_{Sep2} = \dot{C}_{14} + \dot{C}_{16}$	$c_{14} = c_{16}$	$\dot{Z}_{Sep2} = 280.3 \times (\dot{m}_{23})^{0.67}$
Pump 2	$\dot{C}_{16} + \dot{C}_{W,Pu2} + \dot{Z}_{Pu2} = \dot{C}_{17}$	$c_{W,Pu2} = c_{W,Tur}$	$\dot{Z}_{Pu2} = 1120 \times (\dot{W}_{Pu2})^{0.8}$
Solution heat exchanger	$\dot{C}_{17} + \dot{C}_{20} + \dot{Z}_{SHE} = \dot{C}_{18} + \dot{C}_{21}$	$c_{20} = c_{21}$	$\dot{Z}_{SHE} = 2143 \times (A_{SHE})^{0.514}$
Compressor	$\dot{C}_{14} + \dot{C}_{W,Com} + \dot{Z}_{Com} = \dot{C}_{15}$	$c_{W,Com} = c_{W,Tur1}$	$\dot{Z}_{Com} = 10167.5 \times (\dot{W}_{Com})^{0.46}$
Absorber	$\dot{C}_{19} + \dot{C}_{23} + \dot{Z}_{Abs} = \dot{C}_{24} + \dot{C}_{20}$	$c_{19} = c_{20}$	$\dot{Z}_{Abs} = 2143 \times (A_{Abs})^{0.514}$
Throttling valve 2	$\dot{C}_{21} + \dot{Z}_{TV2} = \dot{C}_{22}$	–	$\dot{Z}_{TV2} = 114.5 \times \dot{m}_{21}$

Table 3.3 The overall heat transfer coefficient for heat exchangers [15]

Component	$U\,(kW/m^2 K)$
Vapor generator	1.6
Desorber/Absorbers	0.85
Solution heat exchanger	1.1
Regenerator	1.1

$$\lambda = \frac{\text{number of failures of a constituent in the given period of time}}{\text{total period of time the constituent was operating}} \qquad (3.15)$$

$$\mu = \frac{\text{number of repairs of a constituent in the given period of time}}{\text{total period of time the constituent was being repaired}} \qquad (3.16)$$

Consider a system that consists of n independent binary states. In this case, the state space for this system can be defined as $S = \{s_1, s_2, \ldots, s_{2^n}\}$. If the probability of transition from state i to state j of a system is designated by P_{ij} (which is occurred with the rate of λ_{ij}), then Kolmogorov differential equations can be used to express the probability of state i at any time t as [17]:

$$\frac{dP_i(t)}{dt} = \sum_{j=1}^{n} \lambda_{ji} P_j(t) - P_i(t) \sum_{j=1}^{n} \lambda_{ij}; \, i = 1, 2, \ldots, n \qquad (3.17)$$

where,

$$\sum_{i=1}^{n} P_i(t) = 1 \qquad (3.18)$$

Characterizing the failure and repair rates of the ith constituent of a system by λ_i and μ_i, respectively; then the failure (λ_{sys}) and repair rates (μ_{sys}) of the system can be respectively defined as [17, 18]:

$$\lambda_{sys}(\lambda_1, \ldots, \lambda_n) = \sum_{i=1}^{n} \lambda_i \qquad (3.19)$$

$$\mu_{sys}(\mu_1, \ldots, \mu_n) = \frac{\sum_{i=1}^{n} \lambda_i}{\sum_{i=1}^{n} \left(\frac{\lambda_i}{\mu_i}\right)} \qquad (3.20)$$

For reliability analysis of the proposed CHP system, three sub-systems of geothermal fluid (GF), KC and ACHPC are connected in series. Operation and failure mechanisms of the proposed system are as follows. When three sub-systems operate, the proposed CHP system can produce heating and electricity, simultaneously. When one of the GF or KC fails, the entire system breaks down, whilst any failure in the ACHPC culminates in only electricity generation. Assuming two conditions of operating (O) and failed (F) for each sub-system, eight ($2^3 = 8$) possible states for the proposed CHP system can be defined. Figures 3.2 and 3.3 depict the block diagram and state space diagram of the proposed geothermal-based CHP system, respectively.

The steady state probabilities can be found as follows:

$$\dot{P}(t) = NP(t) \qquad (3.21)$$
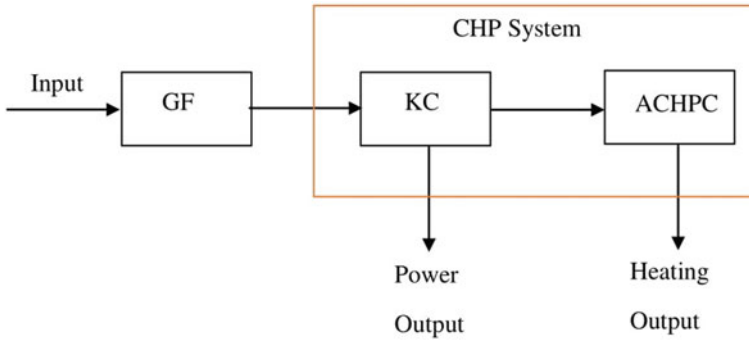
Fig. 3.2 Reliability block diagram for the proposed geothermal-based CHP system

where, $P(t)$ is the steady state probability vector and N is the stochastic transitional probability matrix. For the proposed CHP system, the transitional probability matrix can be articulated as:

$$
N =
\begin{bmatrix}
-(\lambda_{GF}+\lambda_{KC}+\lambda_{ACHPC}) & \mu_{GF} & \mu_{KC} & \mu_{ACHPC} & 0 & 0 & 0 & 0 \\
\lambda_{GF} & -(\mu_{GF}+\lambda_{KC}+\lambda_{ACHPC}) & 0 & 0 & \mu_{KC} & \mu_{ACHPC} & 0 & 0 \\
\lambda_{KC} & 0 & -(\mu_{KC}+\lambda_{GF}+\lambda_{ACHPC}) & 0 & \mu_{GF} & 0 & \mu_{ACHPC} & 0 \\
\lambda_{ACHPC} & 0 & 0 & -(\mu_{ACHPC}+\lambda_{KC}+\lambda_{GF}) & 0 & \mu_{KC} & \mu_{GF} & 0 \\
0 & \lambda_{KC} & \lambda_{GF} & 0 & -(\mu_{KC}+\mu_{GF}+\lambda_{ACHPC}) & 0 & 0 & \mu_{ACHPC} \\
0 & \lambda_{ACHPC} & 0 & \lambda_{KC} & 0 & -(\mu_{ACHPC}+\mu_{KC}+\lambda_{GF}) & 0 & \mu_{GF} \\
0 & 0 & \lambda_{ACHPC} & \lambda_{GF} & 0 & 0 & -(\mu_{ACHPC}+\mu_{GF}+\lambda_{KC}) & \mu_{KC} \\
0 & 0 & 0 & 0 & \lambda_{ACHPC} & \lambda_{GF} & \lambda_{KC} & -(\mu_{ACHPC}+\mu_{GF}+\mu_{KC})
\end{bmatrix}
$$
$$(3.22)$$

where,

$$
P(t) =
\begin{bmatrix}
P_1(t) \\
P_2(t) \\
P_3(t) \\
P_4(t) \\
P_5(t) \\
P_6(t) \\
P_7(t) \\
P_8(t)
\end{bmatrix}
\tag{3.23}
$$

Based on the above calculations, the steady state probability vectors are calculated and are listed in Table 3.4. According to Table 3.4 and Fig. 3.3, the availability of electricity, heating, and cogeneration of heating/electricity can be obtained respectively as follows:

$$
Av_{elec} = P_1 + P_4 = 0.9455 \tag{3.24}
$$

$$
Av_{CHP} = Av_h = P_1 = 0.9385 \tag{3.25}
$$
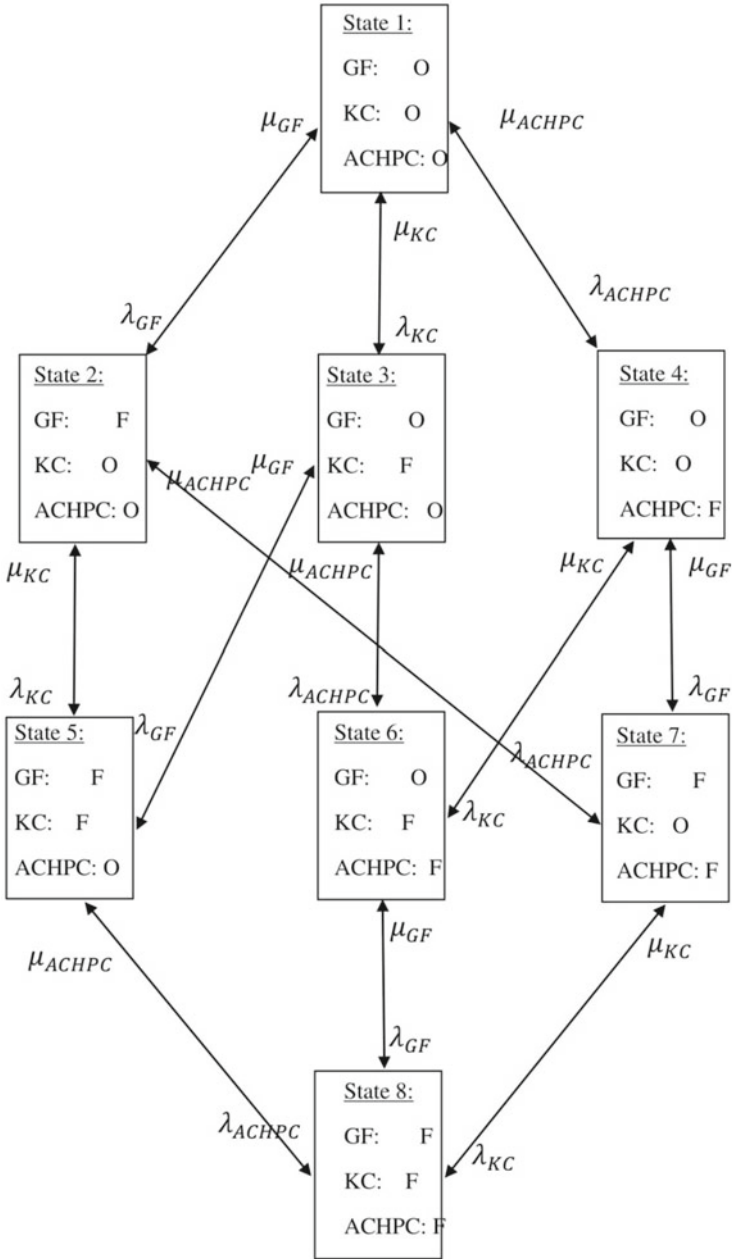
Fig. 3.3 State transition diagram of the proposed geothermal-based CHP system

Table 3.4 The calculated steady state probability vectors

State	Probability (%)
1	0.9385
2	0.0464
3	0.007
4	0.007
5	0.00034
6	0.00044
7	0.00032
8	0.00000

3.3.4 Main Performance Metrics

The energetic efficiency of the power cycle (i.e., KC) and proposed CHP system may be stated respectively as follows [19]:

$$\eta_{en,KC} = \frac{\dot{W}_{Tur} - \dot{W}_{Pu1}}{\dot{Q}_{VG}} \tag{3.26}$$

$$\eta_{en,CHP} = \frac{\dot{W}_{Net} + \dot{Q}_{Abs}}{\dot{Q}_{VG}} \tag{3.27}$$

where, $\dot{Q}_{Abs}$ is the obtained heating load and $\dot{W}_{Net}$ is the net electricity defined as:

$$\dot{W}_{Net} = \dot{W}_{Tur} - \dot{W}_{Com} - \dot{W}_{Pu1} - \dot{W}_{Pu2} \tag{3.28}$$

The exergetic efficiency of the KC and proposed CHP system are respectively iterated as below:

$$\eta_{ex,KC} = \frac{\dot{W}_{Tur} - \dot{W}_{Pu1}}{\dot{Ex}_1 - \dot{Ex}_2} \tag{3.29}$$

$$\eta_{ex,CHP} = \frac{\dot{W}_{Net} + \left(\dot{Ex}_{24} - \dot{Ex}_{23}\right)}{\dot{Ex}_1 - \dot{Ex}_2} \tag{3.30}$$

The unit cost of electricity and heating without reliability consideration may be stated respectively as follows:

$$c_{elec} = \frac{\dot{C}_{elec,Net}}{\dot{W}_{Net}} \tag{3.31}$$

$$c_h = \frac{\dot{C}_{24}}{\dot{Ex}_{24}} \tag{3.32}$$

Accounting reliability for electricity and heating, the unit cost of electricity and heating with reliability consideration are iterated respectively as below:

$$c_{elec-R} = \frac{c_{elec}}{Av_{elec}}$$ (3.33)

$$c_{h-R} = \frac{c_h}{Av_h}$$ (3.34)

The overall product cost of the system (OPCS) for the proposed CHP system without reliability consideration may be stated as follows:

$$OPCS_{CHP} = \frac{\dot{C}_{elec,Net} + \dot{C}_{24}}{\dot{W}_{Net} + \dot{Ex}_{24}}$$ (3.35)

where, $\dot{C}_{elec,Net}$ is the cost rate associated with the net power of the introduced CHP system and is defined as $\dot{C}_{elec,Net} = \dot{C}_{elec,Tur} - \dot{C}_{elec,Com} - \dot{C}_{elec,Pu1} - \dot{C}_{elec,Pu2}$. Also, $\dot{C}_{24}$ is the cost rate of heating. The OPCS with reliability consideration may be stated as follows:

$$OPCS_{CHP-R} = \frac{OPCS_{CHP}}{Av_{CHP}}$$ (3.36)

3.4 Results and Discussion

3.4.1 Main Results

The main input data for thermodynamic, thermoeconomic, and reliability analysis of the described ammonia-water CHP unit are listed in Table 3.5.

Table 3.6 discloses calculated results for the introduced CHP system with and without reliability deliberation. From the 1st law of thermodynamics vantage point, proposing a CHP system with the prior discussed features could substantially enhance energy efficiency by as high as four times. In fact, the energy efficiency of power generation system is surged from 12.03% to 61.01%. However, the exergy efficiency is lessened from 38.1% to 22.21% as the proposed cogeneration system has being installed. Through this integration, the extracted electricity and heating load are attained 3,235 kW and 70,328 kW, respectively. These outputs generation costs approximately 675.3 $/GJ for the overall system (without reliability deliberation), which is increased to 719.6 $/GJ as reliability is taken into account of the designer (augmented nearly 6.5%). The impact of a reliable design on separate production of heating and power is also presented in Table 3.6. Based on the computed results, the heating unit cost without reliability contemplation is attained 1,091 $/GJ which is

Table 3.5 Complete list of input data

Parameter	Value	Reference
Reference pressure, $P_0 (bar)$	1.013	[20]
Reference temperature, $T_0(K)$	298.15	[20]
Geothermal water mass flow rate, $\dot{m}_{Geo}$ (kg/s)	53	[21]
Geothermal inlet temperature, $T_{in,Geo}$ (K)	438	[21]
Vapor generator pinch point temperature difference, $\Delta T_{PP,VG}$ (K)	10	[20]
Pump1 inlet temperature, $T_{in,Pu1}$ (K)	313.15	[22]
Geothermal inlet pressure, $P_{in,Geo}$ (bar)	7	[23]
Turbine inlet pressure, $P_{in,Tur}$ (bar)	25	[24]
Compressor inlet pressure, $P_{in,Com}$ (bar)	4.957	[25]
Regenerators effectiveness, $\varepsilon_{Rg}(\%)$	95	[26]
Solution heat exchanger effectiveness, $\varepsilon_{SHE}(\%)$	80	[27]
Terminal temperature difference of Vapor generator, $TTD_{VG}(K)$	5	[20]
Absorber pinch point temperature difference, $\Delta T_{PP,Abs}$ (K)	10	[25]
Desorber pinch point temperature difference, $\Delta T_{PP,Des}$ (K)	15	[25]
Basic ammonia concentration of KC, $X_{B,KC}$	50	[28]
Basic ammonia concentration of ACHPC, $X_{B,ACHPC}$	50	–
Kalina pump isentropic efficiency, $\eta_{is,Pu1}(\%)$	75	[20]
ACHPC pump isentropic efficiency, $\eta_{is,Pu2}(\%)$	85	[27]
Turbine isentropic efficiency, $\eta_{is,Tur}$ (%)	85	[20]
Compressor polytropic efficiency, $\eta_{P,Com}(\%)$	0.9051–0.0422(CR_{Com})	[27]
Compressor compression ratio, CR_{Com}	3	[27]
Pump 2 ratio, PR_{Pu2}	3	–
Total operating hours, N (h)	7000	[20]
Components lifetime, n_r (years)	20	[20]
Maintenance factor, $\varnothing_r$	1.06	[20]
Annual interest rate, k_i	0.15	[20]
Geothermal unit cost, $c_{Geo}(\$/GJ)$	1.3	[29]
GF failure rate, λ_{GF}(per day)	0.00236	[18]
GF repair rate, μ_{GF}(per day)	0.04752	[18]
KC failure rate, λ_{KC}(per day)	0.00274	[8]
KC repair rate, μ_{KC}(per day)	0.14	[8]
ACHPC failure rate, λ_{ACHPC}(per day)	0.00082	[30]
ACHPC repair rate, μ_{ACHPC}(per day)	0.10958	[30]

Table 3.6 Results of energy, exergy, economic analysis with and without reliability considerations

Performance parameters	Amount
Turbine output power, $\dot{W}_{Tur}(kW)$	14,745
Pump 1 consumption power, $\dot{W}_{Pum1}(kW)$	2,374
Pump 2 consumption power, $\dot{W}_{Pum2}(kW)$	3,585
Compressor consumption power, $\dot{W}_{Com}(kW)$	10,914
Heating capacity, $\dot{Q}_{Abs}(KW)$	70,328
Net output power, $\dot{W}_{Net}(KW)$	3,235
Energy efficiency of KC, $\eta_{en,KC}(\%)$	12.03
Exergy efficiency of KC, $\eta_{ex,KC}(\%)$	38.1
Energy efficiency of CHP system, $\eta_{en,CHP}(\%)$	61.01
Exergy efficiency of CHP system, $\eta_{ex,CHP}(\%)$	22.21
Heating unit cost without reliability, c_h (\$/GJ)	1091
Heating unit cost with reliability, c_{h-R} (\$/GJ)	1161
Net electricity unit cost without reliability, c_{elec} (\$/GJ)	6.452
Net electricity unit cost with reliability, c_{elec-R} (\$/GJ)	6.823
Overall production cost of the system without reliability, OPCS$_{CHP}$ (\$/GJ)	675.3
Overall production cost of the system with reliability, OPCS$_{CHP-R}$ (\$/GJ)	719.6

increased up to 1,161 \$/GJ with reliability consideration (increased nearly 6.41%). In the same order, the electricity cost without reliability contemplation is attained 6.452 GJ which is increased up to 6.823 \$/GJ with reliability consideration (increased nearly 5.75%).

Table 3.7 has outlined the chief exergy and exergoeconomic outputs for the devised CHP unit. On the basis of the obtained results, condenser/desorber distinctively contributes to the largest exergy destruction rate by 7,992 kW. The overall CHP system accounted for 27,156.89 kW exergy destructed through its operation. The highest investment cost rate is attributed to separators since they have large volumetric flow rate. The total investment cost of the devised CHP unit is calculated 20,787.61 \$/h.

3.4.2   Parametric Study

3.4.2.1   Impact of the Geothermal Inlet Temperature on the System

The impact of geothermal inlet temperature on the heating load, energy efficiency, net electricity, exergy efficiency, and OPCS with and without reliability considerations is outlined in Fig. 3.4. Accordingly, with the rise of the geothermal inlet temperature the net electricity is raised up since the power generated by turbine increases, while the consumption electricity by pumps and compressor decreases. By contrast, the

Table 3.7 Major exergy and exergoeconomic outcomes for different elements

Component	$\dot{Ex}_P^i$ (kW)	$\dot{Ex}_F^i$ (kW)	$\dot{Ex}_D^i$ (kW)	η_{ex}^i (%)	$\dot{C}_{D,k}$ ($/h)	$\dot{Z}_k$ ($/h)
Vapor generator	32,244	38,074	5830	84.69	75.78	240.9
Seperator 1	1,387,636.9	1,388,029.8	392.9	99.97	4.77	7513
Regenerator	7204	7590	386.6	94.91	5.067	2.238
Turbine	14,745	16,818	2072	87.68	48.13	546.7
Pump 1	180.9	237.4	56.46	76.22	2.393	2.154
Mixer	1,362,601	1,363,077	476	99.96	5.785	0
Throttling valve 1	365,639	365,790	151	99.96	1.834	0.2016
Desorber	4,723	12,715	7992	0.3714	5742.16	5.094
Separator 2	2,873,550.7	2,873,551.4	0.7	99.99	0.953	12,446
Pump 2	293.4	358.5	65.12	81.83	2.513	2.995
Solution heat exchanger	3,314	3,493	178.5	94.89	310.5	6.982
Compressor	9,396	10,914	1,518	86.09	43.82	17.72
Absorber	5220	12,423	7203	42.02	28,263	2.826
Throttling valve 2	2,868,828.82	2,869,662.51	833.7	99.97	1,375	0.7967
Total system	8,935,576.72	8,962,733.61	27,156.89	22.21	35,881.71	20,787.61

heating capacity decreases as the geothermal inlet temperature increases since the flow rate of the external stream is decreased. In KC, rising up the geothermal inlet temperature augments input heat received by vapor generator which is significantly meaningful than the net electricity increment, and hence the energy and exergy efficiencies of KC is declined slightly. Since heating load has a dominant influence on the energy efficiency of the CHP system, it can be stated that an increase in the geothermal inlet temperature also reduces energy efficiency of the suggested CHP system. However, from second-law standpoint, the exergy efficiency of CHP system is augmented as the geothermal inlet temperature augments since the net electricity augmentation has a dominant effect. Additionally, both energy and exergy efficiencies of the recommended CHP system surpasses over those of the KC in the examined range (as it was expected), nevertheless its impact at high geothermal temperatures is reduced.

The results of exergoeconomic evaluation underline the fact that the cost associated with the net electricity increases with the rise of the geothermal inlet temperature, whilst the heating cost is declined during this alteration. The decrement of heating cost rate has more appreciable impact on the OPCS (for both with and without reliability) due to its huge decrement value. Hence, the OPCS of the CHP unit will be decreased with the rise of the geothermal inlet temperature. Additionally, it can be
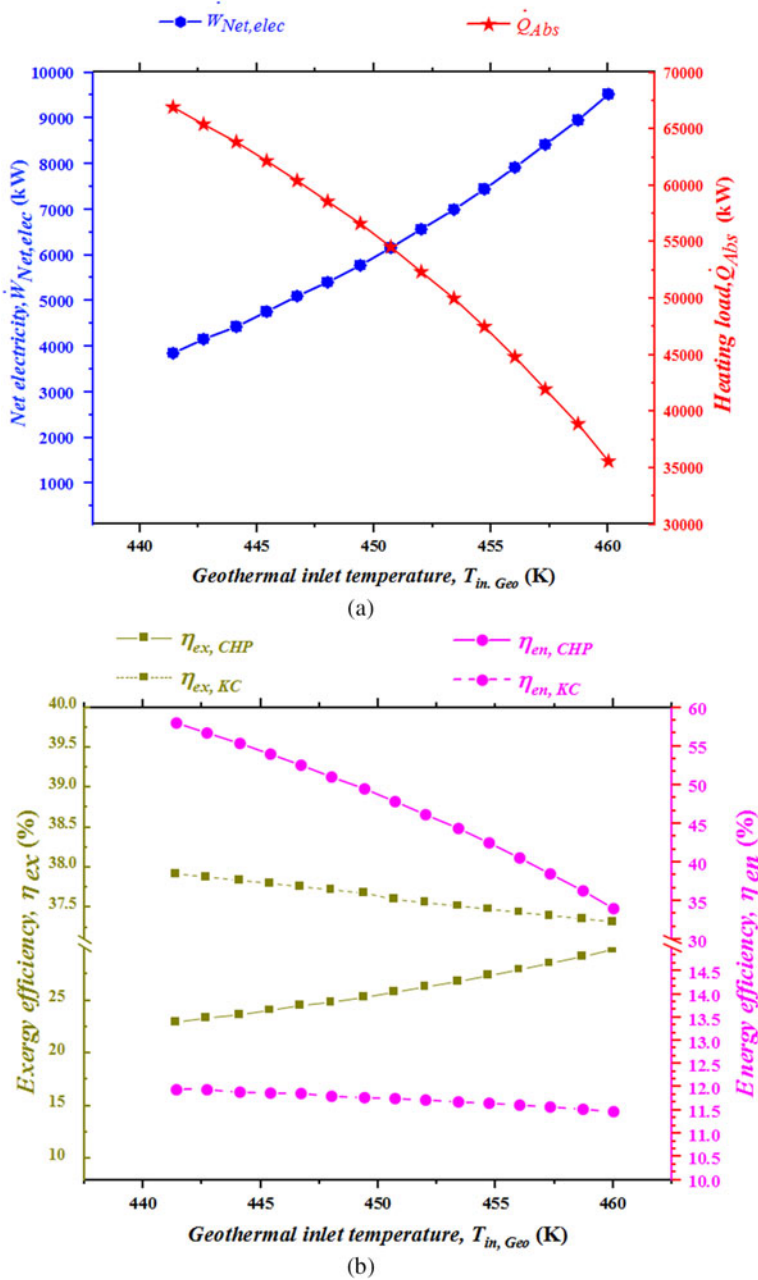
Fig. 3.4 Impact of geothermal inlet temperature on the: **a** net electricity and heating load, **b** energy and exergy efficiencies, and **c** OPCS with and without reliability considerations

Fig. 3.4 (continued)

deduced according to this figure that considering reliability in cost of the recommended CHP system will lead to the increase of cost which is more observable at low geothermal temperatures.

3.4.2.2 Impact of the Pump 1 Inlet Temperature on the System

The effect of pump 1 inlet temperature on the heating load, energy efficiency, net electricity, exergy efficiency, and OPCS with and without reliability consideration is displayed in Fig. 3.5. On the basis of the results portrayed in Fig. 3.5 it can be iterated that the net power is dropped with the rise of the pump 1 inlet temperature since the power generated by turbine is decreased substantially. Similarly, the heating load is declined as the pump 1 inlet temperature augments since the mass flow rate of the heated water is reduced. As a result of these trends, the energy and exergy efficiencies of both KC and CHP system are decreased with an increase in the pump 1 inlet temperature. Additionally, both energy and exergy efficiencies of the recommended CHP system surpasses over those of the KC in all ranges. The results of exergoeconomic evaluation underline the fact that the cost rate associated with the net power and heating is declined as pump 1 inlet temperature increases. However, since decrement rate of electricity and heating cost rates is lower than the decrement rate of electricity and exergy of heating, thus the OPCS of the CHP system will surged upward as pump 1 inlet temperature augments. Additionally, it

Fig. 3.5 Impact of pump1 inlet temperature on the: **a** net electricity and heating load, **b** energy and exergy efficiencies, and **c** OPCS with and without reliability considerations
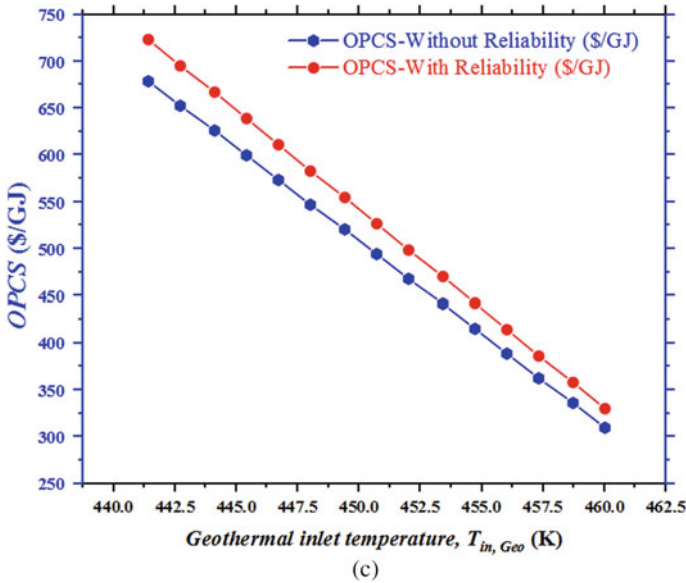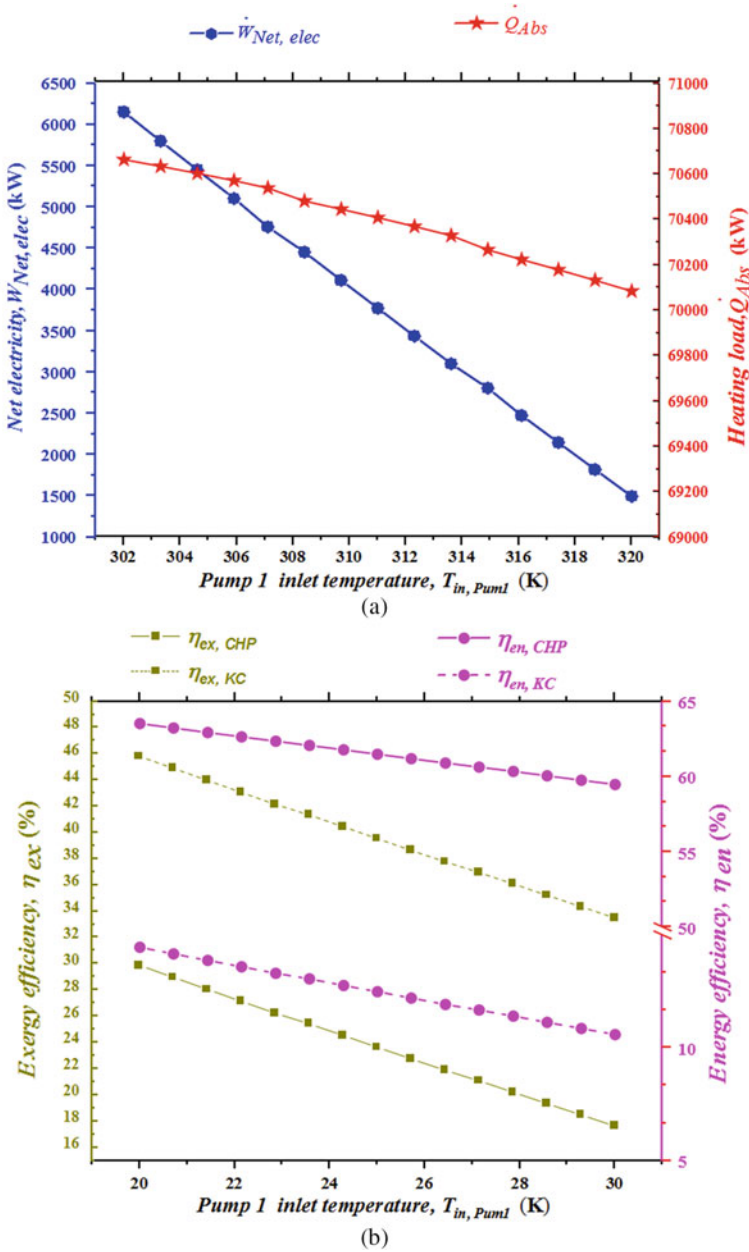
Fig. 3.5 (continued)

can be deduced according to this figure that considering reliability in cost of the recommended CHP system will lead to the increase of cost.

3.4.2.3 Impact of the Vapor Generator Pressure on the System

The impact of vapor generator pressure on the heating load, net electricity, energy efficiency, exergy efficiency, and OPCS with and without reliability considerations is sketched in Fig. 3.6. According to this sketch, increasing the vapor generator pressure decreases the net electricity up to vapor generator pressure of 22.17 bar and increases it thereafter. The heating load is aggrandized as the vapor generator pressure augments since the mass flow rate of the heated water is increased. Due to the supreme impact of the heating load trend, the energy and exergy efficiencies of both KC and CHP system are increased with an increase in the vapor generator pressure. Additionally, both energy and exergy efficiencies of the recommended CHP system surpasses over those of the KC in all ranges. In terms of economics, the OPCS has a peak value with respect to the vapor generator pressure variation. Additionally, it can be deduced that considering reliability in cost of the recommended CHP system will lead to a substantial increase of cost.

Fig. 3.6 Impact of vapor generator pressure on the: **a** net electricity and heating load, **b** energy and exergy efficiencies, and **c** OPCS with and without reliability considerations at various NH$_3$ concentration
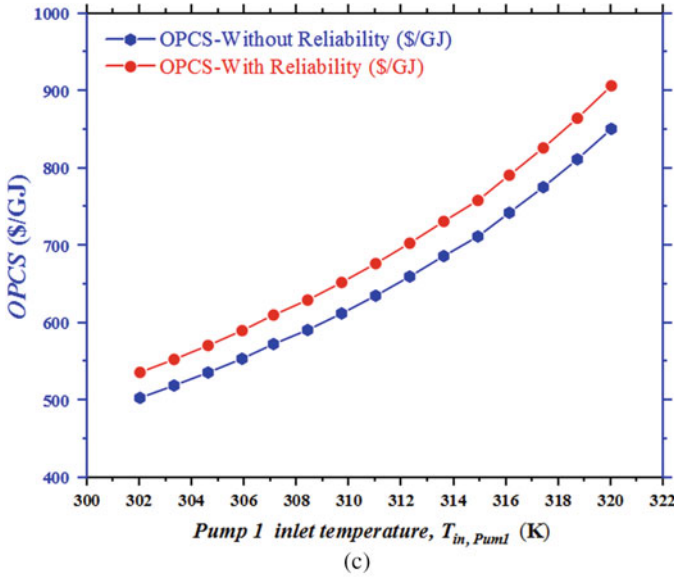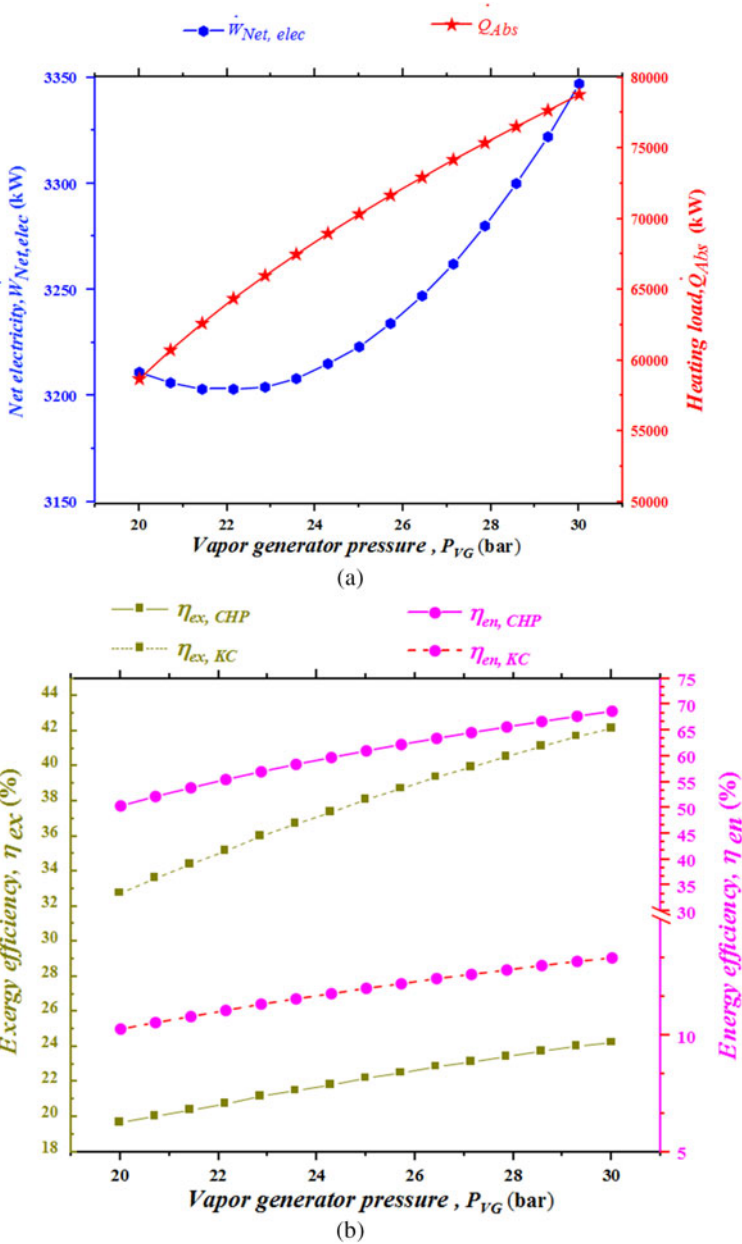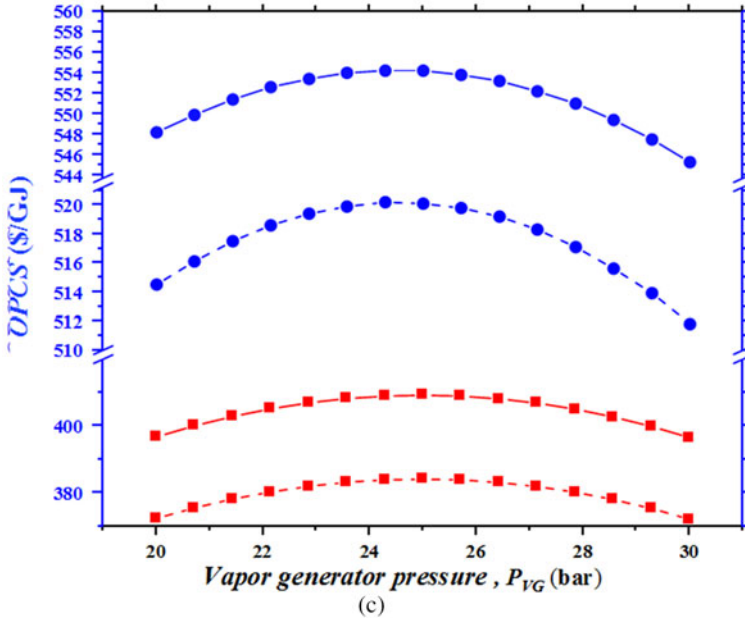
Fig. 3.6 (continued)

3.4.2.4 Impact of the Compressor Ratio on the System

The influence of the compressor ratio on the net electricity, heat capacity, energy efficiency, exergy efficiency, and OPCS with and without reliability considerations is outlined in Fig. 3.7. Accordingly, any increase in the compressor ratio decreases the net electricity since the power consumed by compressor is increased substantially. Whereas, the heating load is augmented as the compressor ratio augments since the mass flow rate and temperature of the heated water are increased. The energy and exergy efficiencies of KC and energy efficiency of CHP system is remained unvaried with any changes in the compressor ratio, while the exergy efficiency of the CHP system is decreased as the compressor ratio increases due to the decrement of net electricity. Also, the OPCS of the CHP system will be surged upward as compressor ratio augments. It is noteworthy to say that considering reliability in cost of the recommended CHP system will lead to the increase of cost in all compressor ratios.

3.4.2.5 Impact of the Ammonia Concentration on the System

Figure 3.8 shows altering trend of the pre-discussed main performance criteria and cost of the system with and without considering reliability analysis with varying the NH_3 concentration. The net electricity of the CHP unit increases with the rise of the

Fig. 3.7 Impact of compressor ratio on the: **a** net electricity and heating load, **b** energy and exergy efficiencies, and **c** OPCS with and without reliability considerations at various ammonia concentration
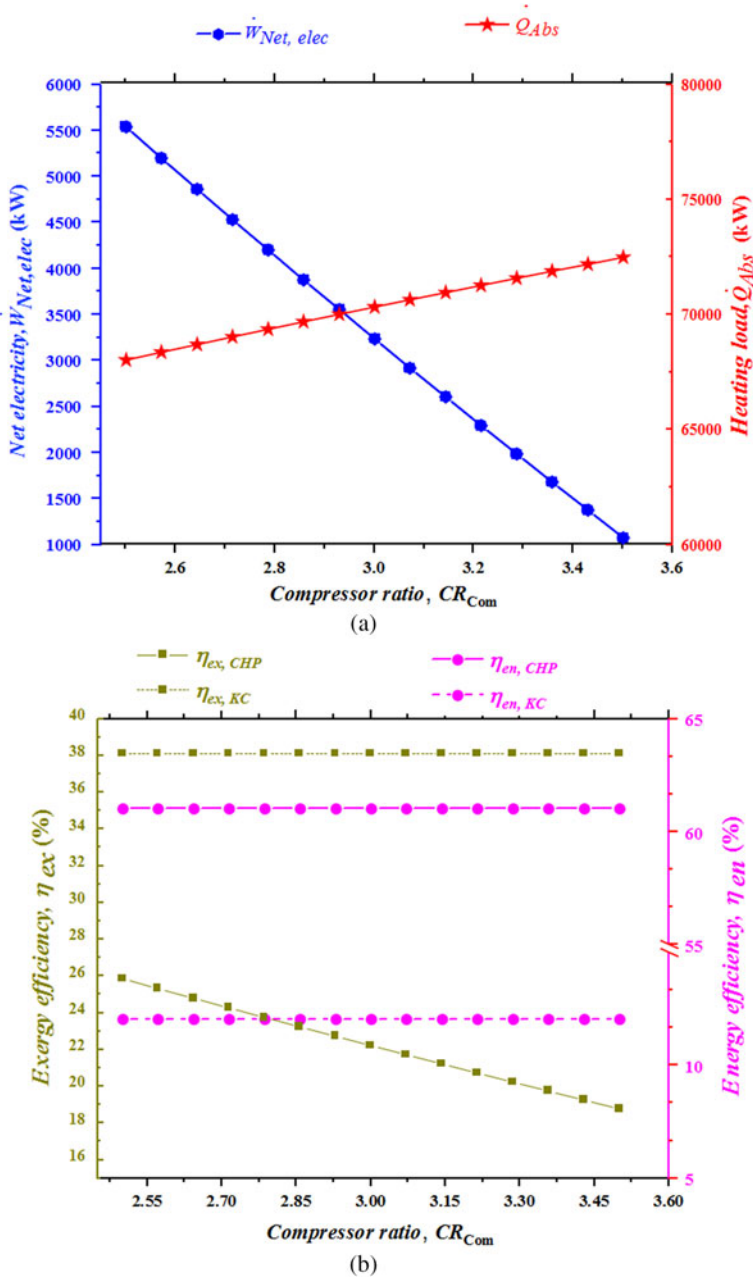
Fig. 3.7 (continued)

NH$_3$ concentration since the compressor consumption electricity is declined which is more appreciable than decrement of turbine electricity. Meantime, the heating capacity decreases immensely with the rise the ammonia concentration, whereas the influence of this parameter on the energy efficiency is more meaningful than that of power, thereby decreasing the energy efficiency with the rise of the NH$_3$ concentration. Needless to say, the energy of KC is also reduced with the rise of the NH$_3$ concentration since the electricity produced by the turbine is dipping. Another reason for these trends is increment rate of vapor generator capacity with the rise of the NH$_3$ concentration due to the pinch and energy balance relations. While the exergy efficiency of KC is declined with an increase in the NH$_3$ concentration, the exergy efficiency of the suggested CHP is maximized with respect to NH$_3$ concentration. From thermoeconomic standpoint, the OPCS with and without reliability considerations is exponentially declined as NH$_3$ concentration augments.

3.4.2.6 Impact of the Failure and Repair Rates of the System on the Availability and OPCS

The impact of system failure rate on the OPCS and availability of CHP system is portrayed in Fig. 3.9. According to this figure, as system failure rate increases, the OPCS is increased since the system's downtime associated with repair action augments. In addition, availability of the system is declined as the system failure rate

Fig. 3.8 Impact of NH$_3$ concentration on the: **a** net electricity and heating load, **b** energy and exergy efficiencies, and **c** OPCS with and without reliability considerations
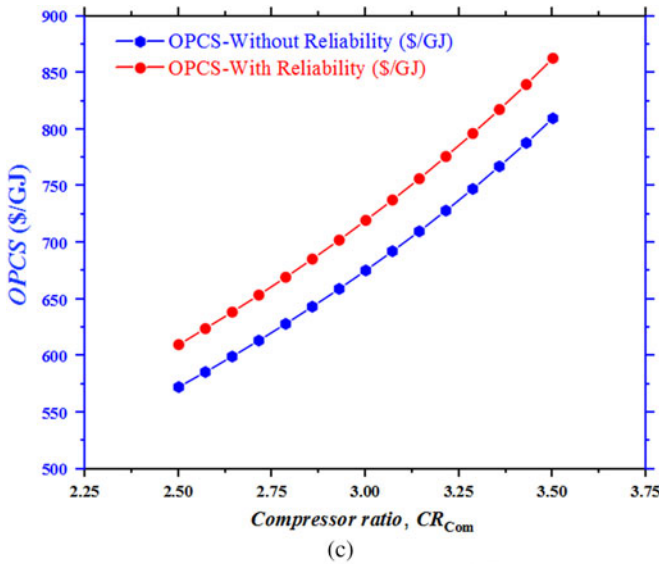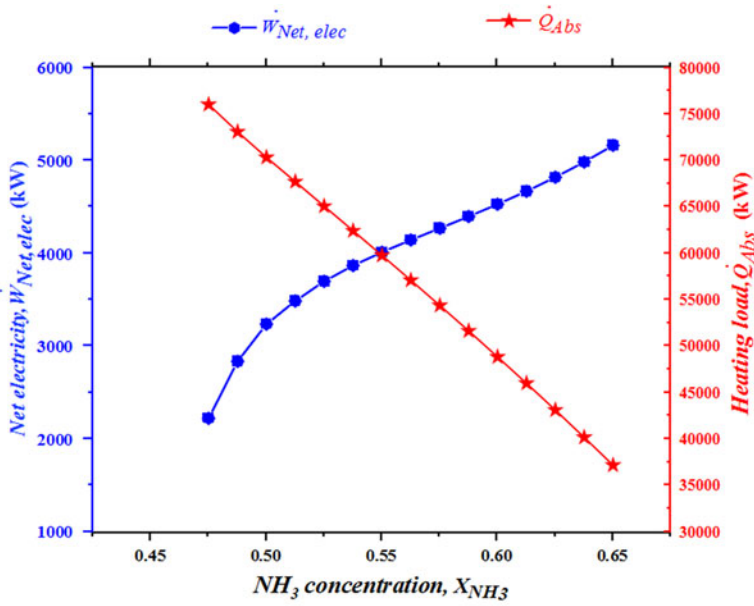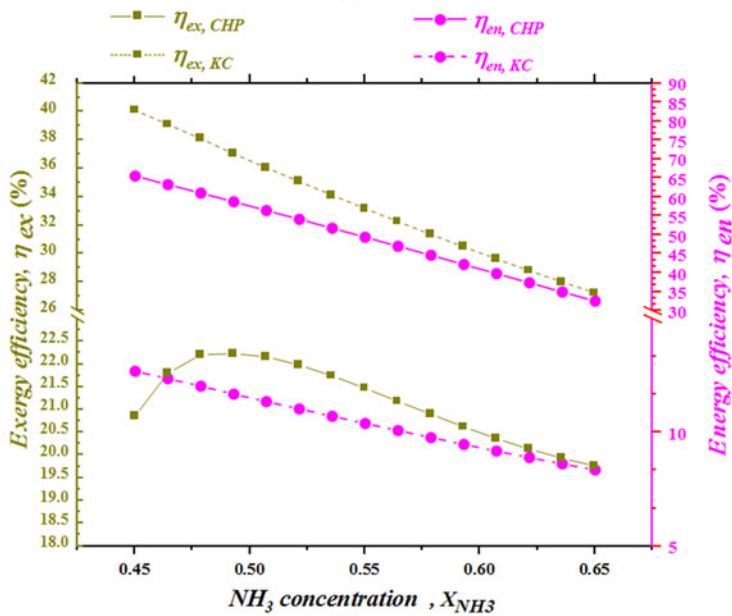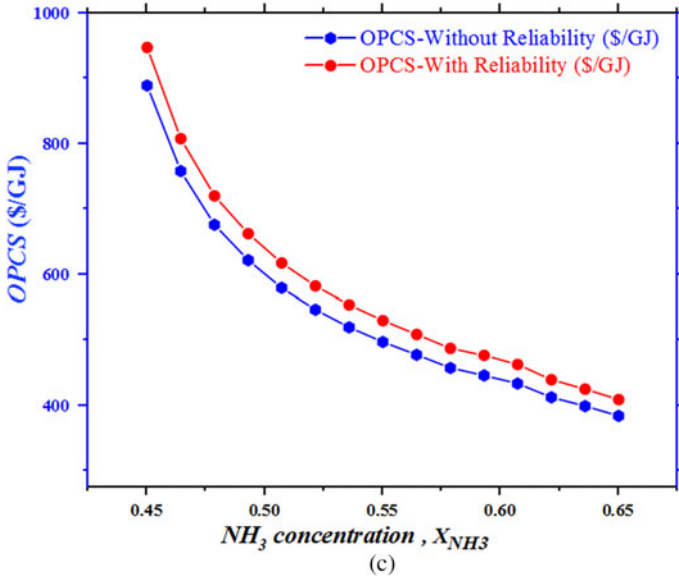
Fig. 3.8 (continued)
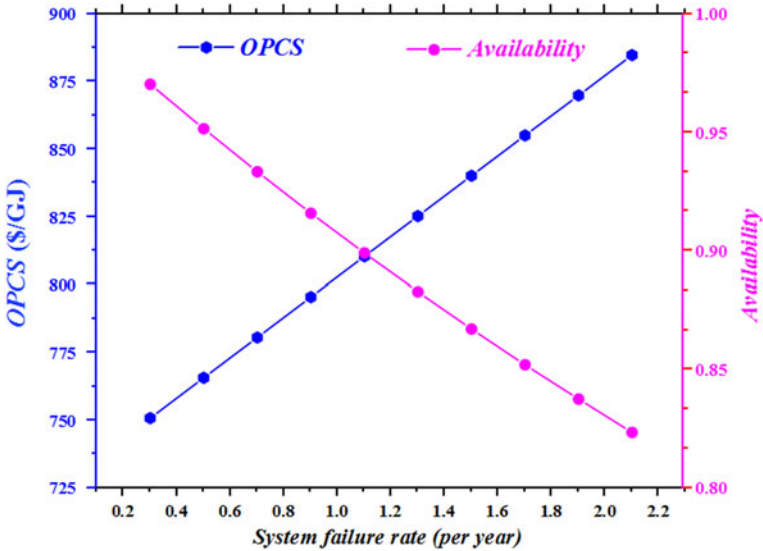
Fig. 3.9 Impact of system failure rate on the availability and OPCS with reliability consideration
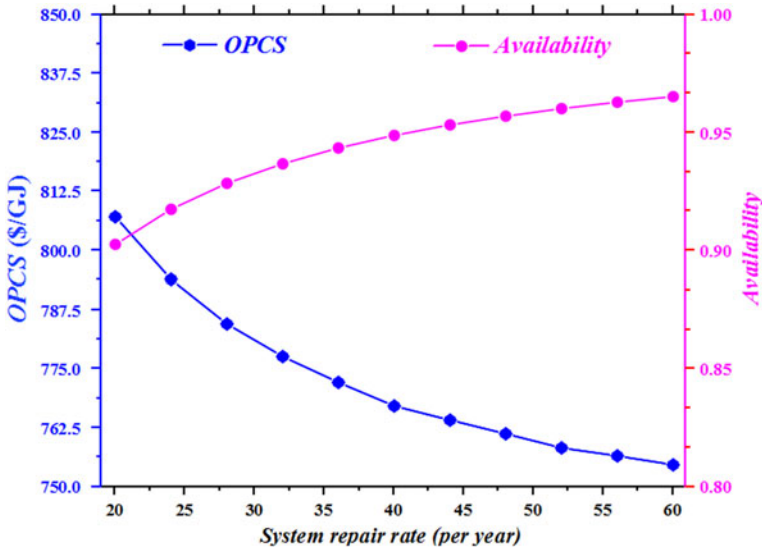
Fig. 3.10 Impact of system repair rate on the availability and OPCS with reliability consideration

augments which is also can be corroborated with findings of Zare [8]. The opposite trend is seen with respect to the system repair rate and the results are depicted in Fig. 3.10.

3.4.2.7   Impact of the Geofluid Unit Cost on the System

In order to further investigate impact of the pondered unit cost for Sabalan geothermal, Fig. 3.11 is presented. Based on this figure, the heating unit cost (with and without reliability) is increased as the geofluid cost augments, while the electricity unit cost is declined through this variation. Meantime, the OPCS goes up as the geothermal fluid cost augments which demonstrates the fact that OPCS mainly influenced by heating unit cost.

3.5   Conclusion

Feasibility study of a new ammonia-water CHP system applicable for the Sabalan geothermal well is carried out in this chapter by employing thermodynamics and thermoeconomics tools. In order to include availability of the components in the cost analysis, the reliability analysis of the system is performed as well. At the end, a complete parametric analysis is performed to investigate the varying trend of the main energetic, exergetic, cost, and reliability metrics versus key independent input
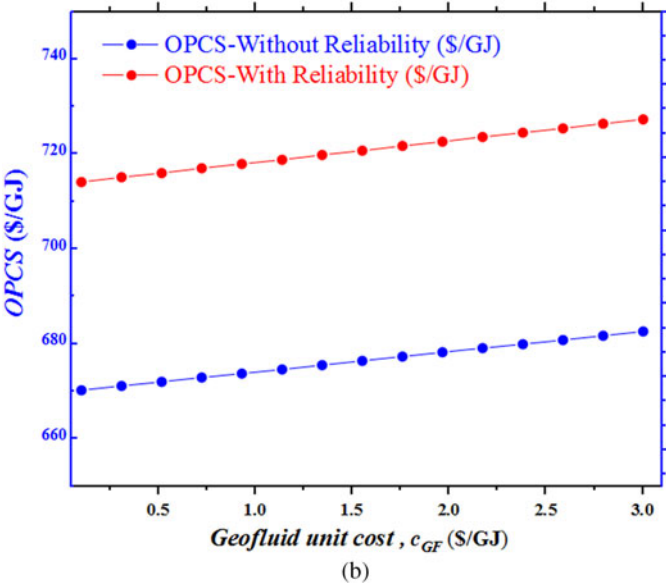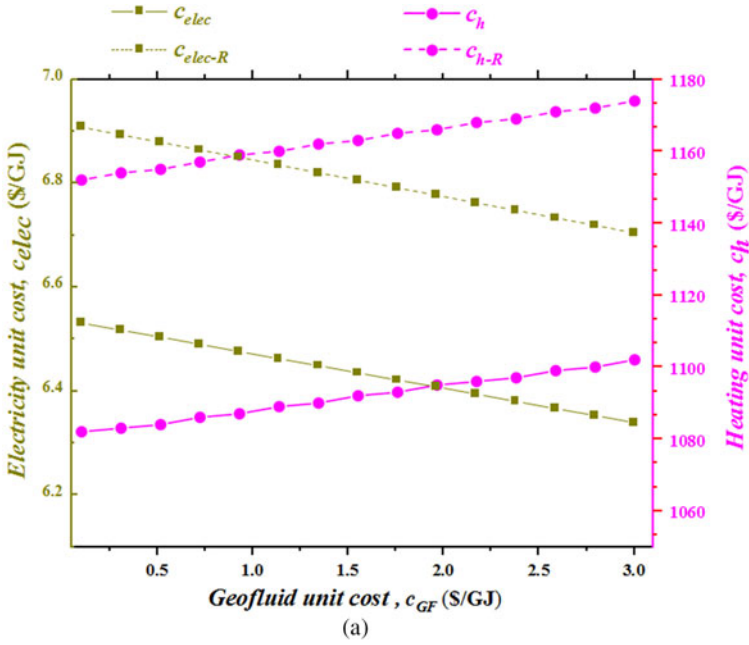
Fig. 3.11 Impact of geofluid unit cost on the: **a** electricity and heating unit costs and **b** OPCS

parameters. In the introduced CHP systems, the condenser/desorber attributed to the highest portion of exergy destruction. Also, the overall CHP system accounted for 632,266 kW exergy destructed through its operation. Also, the introduced cogeneration system generated net electricity of 3,235 kW and heating load of 70,328 kW. At this state, the overall energy and exergy efficiencies of CHP system were computed 61.01% and 22.21%, correspondingly. Higher energy efficiency may be attained with decreasing the geothermal inlet temperature, pump 1 inlet temperature, and NH3 concentration or with increasing the vapor generator pressure. Furthermore, higher exergy efficiency may be attained with decreasing the compressor ratio and pump 1 inlet temperature or with increasing the vapour generator pressure and geothermal inlet temperature. Lower OPCS may be attained with decreasing the compressor ratio, pump 1 inlet temperature, system failure rate, and geofluid unit cost or with increasing the geothermal inlet temperature, ammonia concentration, and system repair rate.

References

1. F. Carazas, C. Salazar, G.F.M.d. Souza, Availability analysis of heat recovery steam generators used in thermal power plants. Energy **36**(6), 3855–3870 (2011)
2. H. Sabouhi et al., Reliability modeling and availability analysis of combined cycle power plants. Int. J. Electr. Power Energy Syst. **79**, 108–119 (2016)
3. S.R. Hosseini, M. Amidpour, A. Behbahaninia, Thermoeconomic analysis with reliability consideration of a combined power and multi stage flash desalination plant. Desalination **278**(1–3), 424–433 (2011)
4. N. Dev, S. Kachhwaha, R. Attri, Development of reliability index for combined cycle power plant using graph theoretic approach. Ain Shams Eng. J. **5**(1), 193–203 (2014)
5. N. Dev, S. Kachhwaha, R. Attri, Development of reliability index for cogeneration cycle power plant using graph theoretic approach. Int. J. Syst. Assurance Eng. Manag. **5**(4), 700–710 (2014)
6. J. Wang et al., Multi-criteria performance analysis of BCHP system taking reliability and availability into consideration. Energy Procedia **61**, 2580–2583 (2014)
7. J. Wang et al., Modified exergoeconomic analysis method based on energy level with reliability consideration: cost allocations in a biomass trigeneration system. Renew. Energy **123**, 104–116 (2018)
8. V. Zare, Exergoeconomic analysis with reliability and availability considerations of a nuclear energy-based combined cycle power plant. Energy **96**, 187–196 (2016)
9. M.P. Rad et al., New procedure for design and exergoeconomic optimization of site utility system considering reliability. Appl. Therm. Eng. **94**, 478–490 (2016)
10. M.K. Manesh, M.P. Rad, M. Rosen, New procedure for determination of availability and reliability of complex cogeneration systems by improving the approximated Markov method. Appl. Therm. Eng. **138**, 62–71 (2018)
11. S. Myrefelt, The reliability and availability of heating, ventilation and air conditioning systems. Energy and buildings **36**(10), 1035–1048 (2004)
12. J. Wang et al., Reliability and availability analysis of a hybrid cooling system with water-side economizer in data center. Build. Environ. **148**, 405–416 (2019)
13. A. Bejan, G. Tsatsaronis, M.J. Moran, Thermal Design and Optimization (John Wiley & Sons, 1995)
14. A. Bejan, G. Tsatsaronis, Thermal Design and Optimization (John Wiley & Sons, 1996)
15. H. Rostamzadeh et al., A novel multigeneration system driven by a hybrid biogas-geothermal heat source, Part II: Multi-criteria optimization. Energy Convers. Manage. **180**, 859–888 (2018)

16. R. Billinton, R. N. Allan, Reliability Evaluation of Engineering Systems (Springer, 1992)
17. A.M. El-Nashar, Optimal design of a cogeneration plant for power and desalination taking equipment reliability into consideration. Desalination **229**(1–3), 21–32 (2008)
18. I. Felea, C. Panea, G. Bendea, Stochastic evaluation of the reliability of the geothermal energy exploitation systems. Revue roumaine des sciences techniques, Série Électrotechnique et Énergétique, 2014, pp. 141–151
19. M. Ebadollahi, et al., Proposal and multi-criteria optimization of two new combined heating and power systems for the Sabalan geothermal source. J. Cleaner Prod. (2019)
20. H. Ghaebi, A.S. Namin, H. Rostamzadeh, Performance assessment and optimization of a novel multi-generation system from thermodynamic and thermoeconomic viewpoints. Energy Convers. Manage. **165**, 419–439 (2018)
21. C. Yilmaz, Thermodynamic and economic investigation of geothermal powered absorption cooling system for buildings. Geothermics **70**, 239–248 (2017)
22. H. Ghaebi, T. Parikhani, H. Rostamzadeh, A novel trigeneration system using geothermal heat source and liquefied natural gas cold energy recovery: Energy, exergy and exergoeconomic analysis. Renew. Energy **119**, 513–527 (2018)
23. R. Wegeng, R. Diver, P. Humble, Second law analysis of a solar methane reforming system. Energy Procedia **49**, 1248–1258 (2014)
24. H. Rostamzadeh et al., Energy and exergy analysis of novel combined cooling and power (CCP) cycles. Appl. Therm. Eng. **124**, 152–169 (2017)
25. J.K. Jensen et al., Technical and economic working domains of industrial heat pumps: Part 2– Ammonia-water hybrid absorption-compression heat pumps. Int. J. Refrig **55**, 183–200 (2015)
26. H. Ghaebi, A.S. Namin, H. Rostamzadeh, Exergoeconomic optimization of a novel cascade Kalina/Kalina cycle using geothermal heat source and LNG cold energy recovery. J. Clean. Prod. **189**, 279–296 (2018)
27. S. R. Nordtvedt, Experimental and theoretical study of a compression/absorption heat pump with ammonia/water as working fluid (2005)
28. H. Ghaebi, T. Parikhani, H. Rostamzadeh, Energy, exergy and thermoeconomic analysis of a novel combined cooling and power system using low-temperature heat source and LNG cold energy recovery. Energy Convers. Manage. **150**, 678–692 (2017)
29. S.M. Bina, S. Jalilinasrabady, H. Fujii, Exergoeconomic analysis and optimization of single and double flash cycles for Sabalan geothermal power plant. Geothermics **72**, 74–82 (2018)
30. M.R. Haghifam, M. Manbachi, Reliability and availability modelling of combined heat and power (CHP) systems. Int. J. Electr. Power Energy Syst. **33**(3), 385–393 (2011)

Chapter 4
Thermodynamic, Economic and Environmental Study of a Combined Power Generation Cycle Using Biogas Fuel as a Primary Heat Source

Mohammad Ebadollahi, Omid Pourali, Hadi Ghaebi, and Majid Amidpour

Abstract Biogas is a promising renewable-based energy resource for several energy systems such as combined power plants. This chapter investigates the proposal of a high-efficient combined power generation set-up fueled by biogas integrating the Brayton cycle and Rankine cycle. Thermodynamic, exergoeconomic, and exergoenvironmental assessment of the proposed system can be revealed as the main aims of the research. The analysis outcomes showed that the combustion chamber has the maximum exergy destruction rate, cost destruction rate and environmental impact of destruction among all constituents. The recommended set-up could generate a net output power of 1372 kW, resulting in the energy efficiency, exergy efficiency, unit cost of product, and impact environmental of product of 37.57%, 21.27%, 21.46 $/GJ, and 6432 mPts/GJ, respectively. Furthermore, it is found that by increasing the condenser pressure, the energy efficiency, exergy efficiency, unit cost of product, and impact of the environmental product were reduced.

Keywords Biogas · Gas turbine cycle · Rankine cycle · Exergoeconomic assessment · Exergoenvironmental analysis

Nomenclature

Symbols

A   area (m^2)
$\dot{B}$ Environmental impact rate ($mPts.h^{-1}$)

M. Ebadollahi · O. Pourali · M. Amidpour (✉)
Faculty of Mechanical Engineering, Department of Energy System Engineering, K.N. Toosi University of Technology, Pardis Ave, Tehran, Iran
e-mail: amidpour@kntu.ac.ir

H. Ghaebi
Department of Mechanical Engineering, Faculty of Engineering, University of Mohaghegh Ardabili, P.O. Box 179, Ardabil, Iran

$\dot{C}$	cost rate ($.h^{-1})
CRF	capital recovery factor
EIP	Environmental impact of product (mPts.GJ^{-1})
$\dot{E}$	exergy rate (kW)
i	interest rate
LCA	life cycle assessment
N	annual number of hours (h)
n_r	componets expected life
TTD	terminal temperature difference
UCP	unit cost of product ($.GJ^{-1})
$\dot{Y}$	environmenatl impact of the constituent (mPts.h^{-1})
$\dot{Z}$	investment cost rate of components ($.h^{-1})

Subscripts and Superscripts

ch	chemical
cond	condenser
CI	capital investment
D	destruction
Di	disposal
ex	exergy
F	fuel
fg	flue gas
is	isentropic
i	ith component
OM	operating & maintenance
P	product
p	pump
ph	physical
tot	total
w	water

Greek Letters

η	efficiency (%)
ρ	density (kg $\cdot$ m^{-3})
σ	rupturing stress (MPa)
ϕ_r	maintenance factor

4.1 Introduction

Extravagant energy consumption is one of the most crucial international challenges. Besides that, finding novel approaches to reducing energy consumption using renewable energies, cogeneration systems, and simultaneous attention to the concept of energy, exergy, economic, and environment can be recommended as vital procedures [1–4]. Waste heat reduction from industrial zones is recognized as the usual procedure for decreasing greenhouse gases emissions as well as increasing performance of the base set-up for electricity augmentation. In this case, the waste heat from industrial processes (mostly heat) is utilized to generate more power or several high-add extra byproducts such as districted heat water, cooling, and pure water [5–8]. Waste heat is calculated as the heat of a carrier once it is cooled from its initial temperature. Normally, the released source of waste heat is cooling up to the ambient temperature unless there are some technical limitations such as the flue gases from diesel boilers which are not cooled below 120 °C for avoiding condensation of water vapor and the production of sulfuric acid [9].

One of the essential procedures to increase the efficiency of electricity generation plants is to use these set-ups in simultaneous power generation systems such as combined cycle power plants [10]. Numerous studies have been conducted on the combination of the natural gas-based power plants with the steam power plant on a large scale or with the organic Rankine cycle (RC) in the small scale power generation set-ups. Due to the high temperature of the output flue gas via the recovery heat exchanger (RHE), the combined system not only plays a significant role in generating more power but also has enough potential to utilize the removal energy in multi-generation systems.

Using waste heat of the topping cycle of a power plant via the concept of the integrated energy systems has been boosted in recent years due to the restriction policy on fossil fuel used across the globe. For example, Ebadollahi et al. [11] utilized waste heat of biogas combustion to generate more power via a combination of Brayton cycle (BC) and close Brayton Cycle (CBC) as well as inverse Brayton cycle (IBC) for power supplying of small companies and decentralized complexes. According to the results, the BC/CBS structure has a better performance with 45.16% of energy efficiency, 25.58% of exergy efficiency. Also, the unit cost and environmental product rates are reported 19.49 $/GJ and 6139 mPts/GJ, respectively. Ghaebi et al. [12] used removal energy of the biogas steam reforming unit for power production utilizing the organic Rankine cycle (ORC). Thermodynamic and optimization results showed that the critical parameters such as carbon dioxide/methane and steam/carbon ratios should set at 0.502 and 2.99, correspondingly. Jabari et al. [13] suggested a cogeneration set-up for cooling and power system utilizing a biogas-driven gas turbine (GT) for a hotel in Ahwaz city in Iran. By decreeing power utilization of the system and using the mixed-integer nonlinear program, the primary amount of the calculated whole product cost can be reduced. Zareh et al. [14] performed a novel heat/power set-up and presented its thermodynamic and thermoeconomic equations when the mixture of biogas and natural gas was used as a heat source. The authors showed that

the anaerobic digester and combustion chamber has a significant role in the system's total irreversibility. Also, they calculated that the total energy efficiency is raised from 46.94% to 50.64%, and unit cost product rate is reduced from 98.71 \$/MWh to 66.7 \$/MWh while NG is used instead of biogas.

In Sweden, Amiri et al. [15] developed a reliable optimization model for a biogas-driven combined heat and power (CHP) system. They discovered that CO_2 emission decreased by 21,000 ton/yr when the proposed model was used instead of the conventional coal-fired power system. Similarly, Zeng et al. [15] employed a porous media burner in the combustor of a CHP system with non-catalytic fuel to warrant a high-temperature and stable reformed syngas for a biogas-fueled solid oxide fuel cell (SOFC) to increase the starting time of the unit. The experimental results indicated that a reforming efficiency of 42.3% could be attained. Leonzio [17] designed a novel biogas-driven set-up for simultaneous cooling, heating, and electricity production for trigeneration applications. The recommended set-up generated 925 kW power, 2523 kW heating and 473 kW cooling. According to the results, the suggested set-up increased electricity by 28% and decreased CO_2 emission by 40%, respectively.

Regarding the application of biogas in hybrid CCHP systems, Su et al. [16] transformed biogas to the syngas via reforming reaction and then assisted solar energy to operate a new CCHP system. They outlined a higher operating performance of 5.41% for the hybrid solar-biogas CCHP system than the reference system. In another similar examination by these scholars [17], they upgraded the caloric value of biogas prior to combustion by proposing a thermochemical conversion process operated by solar thermal energy. Their procedure led to a substantial improvement in energetic and exergetic efficiencies of 46.8% and 26.49%, respectively, and reduction of 18.27% in CO2 emission compared with the reference system.

Over the last years, authors have conducted several cohesive studies in biogas-driven integrated energy systems to cover the existing scientific gap. According to the high potential of the biogas process for multi-generation purposes, its range of applications can be modified to have more yields. Some of these aims are achieved through previous research, although many investigations are still required to carry out. For example, Gholizadeh et al. [18] increased the performance of the biogas-fueled GT system by adding a modified ORC. After set-up optimization, it is calculated that the energy and exergy efficiencies, output electricity, and unit cost product rate are raised from 39.99% to 41.83%, 37.2% to 38.91%, 1308 kW to 1368 kW, and 17.45 \$/GJ to 17.2 \$/GJ, respectively. Liang et al. [19] performed a optimization procedure for a new solar-driven supercritical Brayton Cycle in terms of thermodynamic. In another investigation, Yang et al. [20] performed the economic factor in a multi-objective procedure for a CCHP set-up based on the supercritical Brayton Cycle. In other researches, the removal energy of the BC is utilized via an ORC-based power and cooling cogeneration set-up [21, 22] or used by a trigeneration of electricity, cooling, and freshwater system [23].

Based on the above extensively explained points and necessities associated with the proposal of advanced and high-efficient combined power set-ups fueled by biogas energy, the practicability of integrating the BC and the RC is investigated. The main targets of the current research can be declared as below:

- To use biogas instead of natural gas in the combustion chamber of a Brayton cycle.
- To utilize exhaust gas of Brayton cycle for more electricity generation, using a Rankine cycle.
- To investigate the performance of the recommended set-up from the energy and exergy standpoints.
- To assess the feasibility of the recommended set-up in terms of exergoeconomic and exergoenvironmental evaluation.
- To perform an extensive parametric study of the recommended set-up.

4.2 System Description

The figure of the proposed combined power systems is depicted in Fig. 4.1. The whole system includes two major sub-systems. The top system is a gas turbine cycle (GT) fueled by biomass as an energy source, and the bottoming system is the Rankine cycle (RC).

In the top system, called GT, air with ambient pressure and temperature enters the compressor (AC). As the air passes through the compressor, its pressure and temperature are increased and directed to the combustion chamber (CC). Also, biogas fuel injects into the CC for performing combustion. By combustion between fuel and air inside CC, flue gas with high temperature and pressure leaves CC and enters turbine 1 to generate power by lowering the pressure inside it.

Also, the Rankine cycle is considered for the bottoming system. By heat recovering inside the RHE, steam as working fluid enters turbine 2, which is named the steam turbine. Then, power is produced by expansion in turbine 2. The lean steam leaves turbine 2 to the condenser and loses heat to the surrounding. Afterwards, the stream
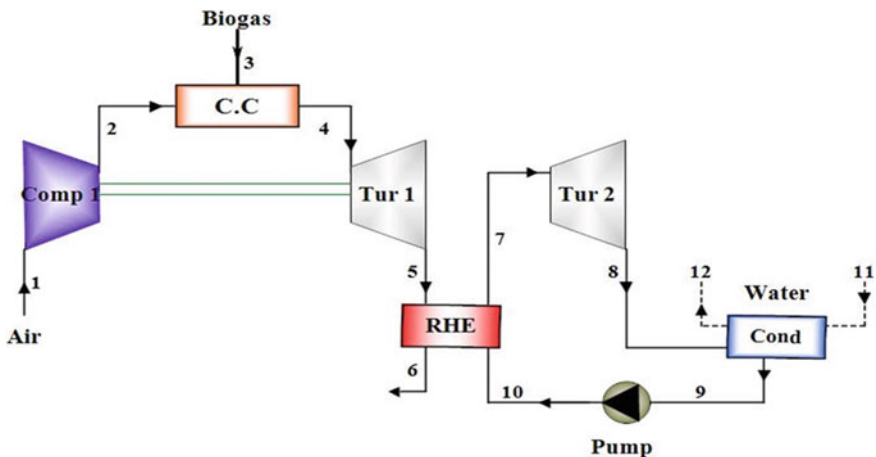
Fig. 4.1 Sketch of the introduced power system

is pumped in the form of a sub-cooled liquid and finally returns to the RHE with the recovered pressure to complete the cycle.

4.3 Methodology

4.3.1 Thermodynamic Presumptions

The assumptions used in this study are as follows: [18, 24–26]

- The set-up operates theoretically under steady-state condition.
- Gas mixtures are analyzed with ideal gas regulations for both air and flue gas.
- 2% of LHV_{biogas} is assumed as energy loss of the combustion chamber.
- Pressure drop in CC and heat exchangers are presumed 5% and 4%, correspondingly.
- The biogas content consists of 40% carbon dioxide and 60% methane.
- 77.48% of N_2, 20.59% of O_2, 0.03% of CO_2, and 1.9% of H_2O contain a mixture of inlet air to the compressor.

However, some main assumptions, a prerequisite for modelling the proposed power systems, are presented in Table 4.1.

Table 4.1 The main assumption for modelling the proposed power systems

Parameter	Value	Refs.
Reference temperature, T_0 (K)	293.15	[18]
Reference pressure, P_0 (kPa)	101.3	[18]
GT subsytem		
Isentropic efficiency of turbine 1,η_{t1} (%)	86	[18]
Isentropic efficiency of compressor 1,η_{comp1} (%)	86	[18]
Compressor 1 pressure ratio,r_{comp1}	10	[18]
inlet temperature of turbine 1, T_4 (K)	1250	[18]
Inlet pressure of biogas, P_3 (kPa)	1200	[18]
Inlet temperature of biogas, T_3 (K)	293.15	[18]
RC sub-system		
Isentropic efficiency of turbine 2, η_{t2} (%)	90	[27]
Inlet pressure of turbine 2, $P_{in,t2}$ (kPa)	9623	[27]
Pressure pf condenser, P_{cond} (kPa)	9.12	[27]
Isentropic efficiency of pump, η_{pu} (%)	95	[27]
Temperature of inlet water to condenser, $T_{w,cond}$ (K)	293.15	[27]
Temperature of inlet water to condenser, $P_{w,cond}$ (K)	101.3	[27]
TTD of condensr, TTD_{cond} (K)	15	[27]

4.3.2 Mathematical Simulation of GT Sub-System

In this subsection, the mathematical formulas for the GT simulation are given. The GT is explained in detail in the previous studies, and now the main relations are written in Table 4.2 [20, 23].

4.3.3 Energy and Exergy Assessment

At steady-state circumstance, the whole relations for evaluation of a thermodynamic set-up may be written as [28, 29]:

$$\sum \dot{m}_{in} - \sum \dot{m}_{out} = 0 \tag{4.1}$$

$$\sum \dot{Q}_{in} - \sum \dot{Q}_{out} + \dot{W} + \sum (\dot{m}h)_{in} - \sum (\dot{m}h)_{out} = 0 \tag{4.2}$$

Based on the 2nd law of thermodynamics, the exergy balance of a set-up is displayed as [28, 29]:

$$\dot{E}_{D,i} = \sum_{i=1}^{n} \dot{E}_{in,i} - \sum_{i=1}^{n} \dot{E}_{out,i} \tag{4.3}$$

By disregarding the impact of potential and kinetic exergies, the total exergy efficiency is written as below:

$$\dot{E}_k = \dot{E}_{ph,i} + \dot{E}_{ch,i} \tag{4.4}$$

The physical and chemical exergies are displayed as:

$$\dot{E}_{ph,i} = \dot{m}((h - h_0) - T_0(s - s_0))_i \tag{4.5}$$

$$\dot{E}_{ch,i} = \dot{n}_i (\sum_i y_i \overline{ex}_i^{ch,0} + \overline{R}T_0 \sum_i y_i ln y_i) \tag{4.6}$$

In the above relation, $\overline{ex}_i^{ch,0}$ shows the standard chemical exergy and y_i Indicates the ith component concentration [30].

The exergy efficiency of each constituent can be articulated as:

$$\eta_{ex,i} = \frac{\dot{E}_{out}}{\dot{E}_{in}} = \frac{\dot{E}_{P,i}}{\dot{E}_{F,i}} \tag{4.7}$$

Table 4.2 A summary of used mathematical formulas for simulation of GT sub-system [18]

Component	Parameters	Thermodynamic formulas
Compressor 1	Isentropic efficiency of compressor 1	$\eta_{comp1} = \frac{\overline{h}_{2s} - \overline{h}_1}{\overline{h}_2 - \overline{h}_1}$
	The output power of compressor 1	$\dot{W}_{comp1} = \dot{m}_1 \frac{(\overline{h}_2 - \overline{h}_1)}{M_1}$
Combustion chamber	The ratio of molar fuel to molar air	$\overline{\lambda} = \frac{\dot{n}_3}{\dot{n}_2} \, or \, \frac{\dot{n}_4}{\dot{n}_2} = 1 + \overline{\lambda}$
	Chemical relations regarding ratio of fuel to air	$\overline{\lambda}[0.4CO_2 + 0.6CH_4] + [0.7748N_2 + 0.2059O_2 + 0.0003CO_2 + 0.019H_2O] \rightarrow$ $[1 + \overline{\lambda}]\left[Y_{H_2O}H_2O + Y_{CO_2}CO_2 + Y_{O_2}O_2 + Y_{N_2}N_2\right],$ $Y_{H_2O} = \frac{0.019 + 1.2\overline{\lambda}}{1 + \overline{\lambda}},$ $Y_{CO_2} = \frac{0.0003 + \overline{\lambda}}{1 + \overline{\lambda}},$ $Y_{O_2} = \frac{0.2059 - 1.2\overline{\lambda}}{1 + \overline{\lambda}},$ $Y_{N_2} = \frac{0.7748}{1 + \overline{\lambda}}$
	Energy balance relation	$\dot{Q}_{CV} + \dot{n}_3\overline{h}_3 + \dot{n}_2\overline{h}_2 - \dot{n}_4\overline{h}_4 = 0$ $\dot{Q}_{CV} = -0.02\dot{n}_3\overline{LHV}$ OR $\overline{\lambda}\overline{h}_3 + \overline{h}_2 - (1 + \overline{\lambda})\overline{h}_4 = 0.02\lambda\overline{LHV}$
	Air enthalpy	$\overline{h}_2 = \left[0.7748\overline{h}_{N_2} + 0.2059\overline{h}_{O_2} + 0.0003\overline{h}_{CO_2} + 0.019\overline{h}_{H_2O}\right]_{T=T_2}$

Table 4.2 (continued)

Component	Parameters	Thermodynamic formulas
	Flue gas enthalpy	$\overline{h}_4 = \dfrac{[0.7748\overline{h}_{N_2} + (0.2059-1.2\lambda)\overline{h}_{O_2} + (0.0003+\lambda)\overline{h}_{CO_2} + (0.019+1.2\lambda)\overline{h}_{H_2O}]_{T=T_{Pr}}}{1+\overline{\lambda}}$ $\overline{\lambda} = \dfrac{0.7748\Delta\overline{h}_{N_2} + 0.2059\Delta\overline{h}_{O_2} + 0.0003\Delta\overline{h}_{CO_2} + 0.019\Delta\overline{h}_{H_2O}}{\overline{h}_3 - 0.02\lambda LHV - [1.2\lambda\overline{h}_{H_2O} - 1.2\lambda\overline{h}_{O_2} + \overline{h}_{CO_2}]_{T=T_4}}$
	Biogas enthalpy	$\overline{h}_3 = 0.6\overline{h}_{CH_4} + 0.4\overline{h}_{CO_2}$
	Biogas LHV	$LHV_{biogas} = H_{Pr} - H_{react} = \sum N_{Pr}\overline{h}_{f,Pr}^{\circ} - \sum N_{react}\overline{h}_{f,react}^{\circ} =$ $\left(N_{Pr}\overline{h}_f^{\circ}\right)_{CO_2} + \left(N_{Pr}\overline{h}_f^{\circ}\right)_{H_2O} - \left(N\overline{h}_f^{\circ}\right)_{CH_4} + \left(N_{react}\overline{h}_f^{\circ}\right)_{CO_2}$
	Combustion chamber pressure loss	$\dfrac{P_4}{P_2} = 1 - \Delta P_{CC}$
Turbine 1	Isentropic efficiency of turbine 1	$\eta_{t1} = \dfrac{\overline{h}_4 - \overline{h}_5}{\overline{h}_4 - \overline{h}_{5s}}$
	The power output of turbine 1	$\dot{W}_{t1} = \dot{m}_4 \dfrac{(\overline{h}_4 - \overline{h}_5)}{M_4}$

The destruction proportion is the ratio of constituent's destruction exergy to the total unit destruction, which may be noted as below:

$$y_{D,i} = \frac{\dot{E}_{D,i}}{\dot{E}_{D,tot}} \tag{4.8}$$

The major mass, energy, and exergy balance relations of the constituents are tabulated in Table 4.3.

Table 4.3 The main balance equations for separate constituents of each power generation system

Constituent	Energy balance	Exergy balance
GT sub-system		
Compressor 1	$\dot{W}_{comp1} = \dot{m}_1(h_2 - h_1),$ $\eta_{comp1} = \frac{h_{2s} - h_1}{h_2 - h_1}$	$\dot{E}_{D,comp1} = \dot{W}_{comp1} - (\dot{E}_2 - \dot{E}_1)$
Combustion chamber	$\overline{\lambda}\overline{h}_3 + \overline{h}_2 - (1 + \overline{\lambda})\overline{h}_4 = 0.02\overline{\lambda}\overline{LHV},$ $\dot{Q}_{cc} = \overline{LHV} * \dot{m}_3/M_3$	$\dot{E}_{D,CC} = (\dot{E}_2 + \dot{E}_3) - \dot{E}x_4$
Turbine 1	$\dot{W}_{t1} = \dot{m}_4(h_4 - h_5),$ $\eta_{t1} = \frac{h_4 - h_5}{h_4 - h_{5S}}$	$\dot{E}_{D,t1} = (\dot{E}_4 - \dot{E}_5) - \dot{W}_{t1}$
Recovery heat exchanger	$\dot{Q}_{RHE} = \dot{m}_5(h_5 - h_6),$ $\dot{Q}_{RHE} = \dot{m}_7(h_{14} - h_7)$	$\dot{E}_{D,RHE} = (\dot{E}_5 - \dot{E}_6) - (\dot{E}_7 - \dot{E}_{14})$
RC sub-system		
Turbine 2	$\dot{W}_{t2} = \dot{m}_7(h_7 - h_8),$ $\eta_{t2} = \frac{h_7 - h_8}{h_7 - h_{8S}}$	$\dot{E}_{D,t2} = (\dot{E}_7 - \dot{E}_8) - \dot{W}_{t2}$
Condenser	$\dot{Q}_{cond} = \dot{m}_8(h_8 - h_9),$ $\dot{Q}_{cond} = \dot{m}_{11}(h_{12} - h_{11})$	$\dot{E}_{D,cond} = (\dot{E}_8 - \dot{E}_9) - (\dot{E}_{12} - \dot{E}_{11})$
Pump	$\dot{W}_{pu} = \dot{m}_9(h_{10} - h_9),$ $\eta_{pu} = \frac{h_{10s} - h_9}{h_{10} - h_9}$	$\dot{E}_{D,pu} = \dot{W}_{pu} - (\dot{E}_{10} - \dot{E}_9)$

4.3.4 Exergoeconomic Evaluation

Exergoeconomic evaluation is one of the thermodynamics tools that combine the exergy and economic principles across the constituents of the system. Exergoeconomic analysis assists the designers in device profitable systems that is not obtainable by the usual economic assessment [28].

From the cost balance relation dedicated that, the sum of cost rates of inlet stream ($\sum \dot{C}_{in,i}$), heat transfer ($\dot{C}_{Q,i}$), operating and maintenance ($\dot{Z}^{OM}$), and capital investment ($\dot{Z}^{CI}$) is equal to the sum of cost rates of outlet stream ($\sum \dot{C}_{out,i}$), heat transfer ($\dot{C}_{Q,i}$) [28, 31]:

$$\sum \dot{C}_{in,i} + \dot{C}_{Q,i} + \dot{Z}_{tot}^{OM} + \dot{Z}_{tot}^{CI} = \sum \dot{C}_{out,i} + \dot{C}_{W,i} \tag{4.9}$$

here,

$$\dot{C}_{in,i} = c_{in,i} \dot{E}_{in,i} \dot{C}_{Q,i} = c_{Q,i} \dot{E}_{Q,i} \dot{C}_{out,i} = c_{out,i} \dot{E}_{out,i} \dot{C}_{W,i} = c_{W,i} \dot{E}_{W,i} \tag{4.10}$$

where, $c_{in,k}, c_{Q,k}, c_{out,k}$, and $c_{W,k}$ demonstrates the cost per exergy unit in $\$/kWh$ adapted to inlet stream, heat transfer, outlet stream, power of the ith constituent of each thermodynamic system, respectively.

As mentioned previously, the part of the exergy is destructed in the system, and the system must spend for this exergy destruction. The cost destruction rate of each constituent is denoted as [28]:

$$C_{D,i} = c_{F,i} \dot{E}_{D,i} \left(If : \dot{E}_{P,i} = Constant \right) \tag{4.11}$$

For calculating the total cost rate of the ith constituent, the amounts of investment cost must be added to operating and maintenance cost as below:

$$\dot{Z}_i = \dot{Z}_i^{CI} + \dot{Z}_i^{OM} \tag{4.12}$$

Regarding product and fuel cost rates concept, Eq. 4.9 may be articulated as [28]:

$$\dot{C}_{P,tot} = \dot{C}_{F,tot} + \dot{Z}_{tot}^{CI} + \dot{Z}_{tot}^{OM} \tag{4.13}$$

Capital investment must be turned into the cost rate, which purchased equipment cost is defined as:

$$\dot{Z}_i = CRF \times \frac{\phi_r \times 365 \times 24}{N} \times Z_i (4.14) \tag{4.14}$$

where the capital recovery factor is articulated as:

Table 4.4 The main input economics parameter of the systems [32]

Parameter	Value
Annual operating time, N (hr)	7000
Maintenance factor, ϕ_r	1.06
Interest rate, i_r (%)	15
Estimated lifetime, n_r	20

$$CRF = \frac{i_r(1+i_r)^{n_r}}{(1+i_r)^{n_r}-1}(4.15) \tag{4.15}$$

The parameters of the above equation are digested in Table 4.4.

The relative cost difference ($r_{c,i}$) and exergoeconomic factor ($f_{c,i}$) are articulated as two dominant dimensionless relationships that are defined for the cost comparison of the constituents.

$$r_{c,i} = (c_{P,i} - c_{F,i})/c_{F,i} \tag{4.16}$$

$$f_{c,i} = \dot{Z}_i/(\dot{Z}_i + \dot{C}_{D,i}) \tag{4.17}$$

The dominant exergoeconomic balance and auxiliary equations of each component of the power generation systems are portrayed in Table 4.5.

4.3.5 Exergoenvironmental Evaluation

Exergoenvironmental evaluation is a procedure to link the concepts of thermodynamics and the environment. The designer must consider the environmental impacts of the components and try to decrease these effects as possible. Three stages must be taken to account to assess the system from an exergoenvironmental vantage point. First, the exergy analysis must be completed; second, by utilizing life cycle assessment (LCA), the environmental impacts must be reckoned; finally, the exergy of flows and environmental impacts must be linked [34, 35].

Regarding concepts of fuel and product for each constituent, the main exergoenvironmental balance relation is noted as below [36]:

$$\dot{B}_{P,i} = \dot{B}_{F,i} + \dot{Y}_i \tag{4.18}$$

The summation of the fuel environmental impact rate ($\dot{B}_{F,i}$) and environmental impact of the constituent ($\dot{Y}_i$) is equal to the product environmental impact rate ($\dot{B}_{P,i}$) while the $\dot{B}_{F,i}$, $\dot{B}_{P,i}$ must be gotten by multiplying the total product/fuel exergy rate and specific environmental impact as below [36]:

Table 4.5 The main exergoeconomic equation of each constituent [18, 32, 33]

Constituents	Economic balance equations	Auxiliary equations	Cost function
GT sub-system			
Compressor 1	$\dot{C}_1 + \dot{Z}_{comp1} + \dot{C}_{W,comp1} = \dot{C}_2$	$c_{W,comp1} = c_{W,t1}$ $c_1 = 0$	$Z_{comp1} = (71.1\dot{m}_1(0.9 - \eta_{comp1}))(P_2/P_1)\ln(P_2/P_1)$
Combustion chamber	$\dot{C}_2 + \dot{C}_3 + \dot{Z}_{CC} + C_4$	$c_1 = 6.847$ [18]	$Z_{CC} = (46.08\dot{m}_2/(0.955 - P_4/P_2))[1 - \exp(0.018T_4 - 26.4)]$
Combustion chamber	$\dot{C}_2 + \dot{C}_3 + \dot{Z}_{CC} = \dot{C}_4$	$c_1 = 6.847$[18]	$Z_{CC} = (46.08\dot{m}_2(0.995 - P_4/P_2))[1 + exp(0.018T_4 - 26.4)]$
Turbine 1	$\dot{C}_4 + \dot{Z}_{t1} = \dot{C}_5 + \dot{C}_{W,t1}$	$c_4 = c_5$	$Z_{t1} = (479.34\dot{m}_4(0.92 - \eta_{t1}))\ln(P_5/P_4)[1 + exp(0.036T_4 - 54.4)]$
Recovery heat exchanger	$\dot{C}_5 + \dot{C}_{14} + \dot{Z}_{RHE} = \dot{C}_6 + \dot{C}_7$	$c_5 = c_6$	$Z_{RHE} = 130\times(A_{RHE}/0.093)^{0.78}$
RC sub-system			
Turbine 2	$\dot{C}_7 + \dot{Z}_{t2} = \dot{C}_8 + \dot{C}_{W,t2}$	$c_7 = c_8$	$Z_{t2} = 3880 \times \dot{W}_{t2}^{0.7}\left(1 + \left(\frac{0.05}{1-\eta_{t2}}\right)^3\right)(1 + 5 \times e^{(T_7-866)/10.42})$
Condenser	$\dot{C}_8 + \dot{C}_{11} + \dot{Z}_{cond} = \dot{C}_9 + \dot{C}_{12}$	$c_8 = c_9;$ $c_{11} = 0$	$Z_{cond} = 130\times(A_{cond}/0.093)^{0.78}$
Pump	$\dot{C}_9 + \dot{Z}_{pu} + \dot{C}_{W,pu} = \dot{C}_{10}$	$c_{W,pu2} = c_{W,t2}$	$Z_{pu} = 2100 \times \left(\frac{\dot{W}_{pu}}{10}\right)^{0.26}\left(\frac{1-\eta_{pu}}{\eta_{pu}}\right)^{0.5}$

$$\dot{B}_{P,i} = b_{P,i}\dot{E}_{P,i} \tag{4.19}$$

$$\dot{B}_{F,i} = b_{F,i}\dot{E}_{F,i} \tag{4.20}$$

The environmental impact of the constituents ($\dot{Y}_i$) is obtained by applying LCA method while this parameter is calculated through the summation of the environmental impact of the operation and maintenance ($\dot{Y}_i^{OM}$), construction ($\dot{Y}_i^{Co}$), and disposal ($\dot{Y}_i^{Di}$) as follows [36]:

$$\dot{Y}_i = \dot{Y}_i^{Co} + \dot{Y}_i^{OM} + \dot{Y}_I^{Di} \tag{4.21}$$

Since a part of the exergy is destructed in the process, the environmental impact of destruction may be reported as below.

$$\dot{B}_{D,i} = b_{F,i}\dot{E}_{D,i}(If : \dot{E}_{P,i} = Constant) \tag{4.22}$$

The exergoenvironmental factor ($f_{b,i}$) and relative difference ($r_{b,i}$) of the constituents are presented to evaluate the constituents' environmental impacts [36].

$$r_{b,i} = (b_{P,i} - b_{F,i})/b_{F,i} \tag{4.23}$$

$$f_{b,i} = \dot{Y}_i/(\dot{Y}_i + \dot{B}_{D,i}) \tag{4.24}$$

The parameter of $r_{b,i}$ demonstrates the decreasing potential environmental impact. Mainly, the environmental impact of constituents with a high relative difference index can be decreased. The ratio of constituent-related environmental impact to the total environmental impact of a constituent is defined as $f_{b,i}$ index. Whilst $f_{b,i}$ is more than 0.7, the constituent-related environmental impact has a prominent role compared to exergy destruction, and exergy destruction plays a key role when the factor is less than 0.3 [36].

The component weight function and Eco-indicator for materials of each constituent must be existed to calculate the environmental impacts. The Eco-indicator for constituents is tabulated in Table 4.6, and their weight function is explained as follows:

The weight of all gas turbines and compressors are extracted from SIEMENS catalogues [37, 38].

The combustion chamber weight is calculated by the rupturing pressure inside the cylindrical shell and mass flow rate of working fluid from the relations as below [39]:

Table 4.6 Eco-indicator for materials of the system components [34, 39]

Constituent	Material	Percent of material (%)	Material (mPts/kg)	Process (mPts/kg)	Disposal (mPts/kg)	Total (mPts/kg)
Compressor	Steel low alloy Steel Cast iron	45 33 22	131	11.7	−70	72.7
Turbine	Steel high alloy steel	75 25	202	11.7	−70	143.7
Combustion chamber	Steel high alloy Steel	77 23	729	20	−70	679
Recovery heat exchanger	Steel Copper	67 33	519	12.1	−70	461.1
Condenser	Steel	100	86	12.1	−70	28.1
Pump	Cast iron Steel	65 35	186	16.9	−70	132.9

$$\dot{m}_{in,cc} = \rho_{in,f}.vel_{cc}.A_{cc} \tag{4.25}$$

$$t_{cc} = \frac{p_{cc}.D_{cc}.FS_{cc}}{2\sigma} \tag{4.26}$$

$$V_{cc} = A_{cc}.L_{cc}, \, w_{cc} = \rho_{alloy}.V_{cc} \tag{4.27}$$

The amounts of flue gas velocity (vel), rupturing stress (σ), and safety factor (FS$_{CC}$) of the combustion chamber are estimated 6.2 m/s, 21 MPa and 2.0, respectively [39]. After calculating the combustion chamber area and thickness from Eqs. 4.25 and 4.26, constituent weight is obtained by determining the alloy density of the combustion chamber and its volume through the density relationship.

The weight function for the recovery heat exchanger is specified as [34].

$$w_{HE} = 2.14.\dot{Q}^{0.7} \tag{4.28}$$

The weight function for the condenser is depicted as [34]:

$$w_{cond} = 0.073.\dot{Q}^{0.99} \tag{4.29}$$

The weight function relation for steam turbine (GT sub-system turbine) and pump are stated as [34]:

$$w_{st} = 4.9.\dot{W}^{0.73} \tag{4.30}$$

$$w_{pu} = 0.175.ln(\dot{W}) - 1.06 \tag{4.31}$$

The exergoenvironmental balance and auxiliary equations of the components are reported in Table 4.7. The Eco-indicator of the carbon dioxide and methane are presumed 5.454 and 114.622 mPts, respectively [36]. Finally, the fuel Eco-indicator in mPts per gigajoule is calculated as below:

$$b_{biogas} = \frac{\dot{m}_{biogas}\left[(b_{CH4}Y_{CH4}) + (b_{CO_2}Y_{CO_2})\right] \times 1000000}{\dot{E}_{biogas}} \tag{4.32}$$

4.3.6 Performance Evaluation

The main target of the devised systems is power production, so the energy efficiency of each system is written as:

Table 4.7 The main exergoenvironmental relation of the components [36, 40]

Constituents	Economic balance equations	Auxiliary equations
GT subsystem (Fig. 4.1a)		
Compressor 1	$\dot{B}_1 + \dot{Y}_{comp1} + \dot{B}_{W,comp1} = \dot{B}_2$	$b_{W,comp1} = b_{W,t1}$ $b_1 = 0$
Combustion chamber	$\dot{B}_2 + \dot{B}_3 + \dot{Y}_{CC} = \dot{B}_4$	Equation (4.30)
Turbine 1	$\dot{B}_4 + \dot{Y}_{t1} = \dot{B}_5 + \dot{B}_{W,t1}$	$b_4 = b_5$
Recovery heat exchanger	$\dot{B}_5 + \dot{B}_{14} + \dot{Y}_{RHE} = \dot{B}_6 + \dot{B}_7$	$b_5 = b_6$
RC sub-system (Fig. 4.1b)		
Turbine 2	$\dot{B}_7 + \dot{Y}_{t2} = \dot{B}_8 + \dot{B}_{W,t2}$	$b_7 = b_8$
Condenser	$\dot{B}_8 + \dot{B}_{11} + \dot{Y}_{cond} = \dot{B}_9 + \dot{B}_{12}$	$b_8 = b_9;$ $b_{11} = 0$
Pump	$\dot{B}_9 + \dot{Y}_{pu} + \dot{B}_{W,pu} = \dot{B}_{10}$	$b_{W,pu2} = b_{W,t2}$

$$\eta_{en,sys} = \frac{\dot{W}_{net}}{\dot{n}_{biogas}.\overline{LHV}_{biogas}} \tag{4.33}$$

The net output power of the system is presented as below:

$$\dot{W}_{net} = \dot{W}_{t1} + \dot{W}_{t2} - \dot{W}_{comp} - \dot{W}_{pu} \tag{4.34}$$

The exergy efficiency of the recommended biogas power generation system can be articulated as:

$$\eta_{ex,sys} = \frac{\dot{W}_{net}}{\dot{n}_{biogas}.\overline{ex}^0_{ch,biogas}} \tag{4.35}$$

The unit cost of product (UCP) for the suggested set-up may be noted as:

$$UCP_{sys} = \frac{\dot{C}_{w,net}}{\dot{W}_{net}} \tag{4.36}$$

Finally, the impact of environmental product (IEP) rate for the power generation system are demonstrated as:

$$IEP_{sys} = \frac{\dot{B}_{w,net}}{\dot{W}_{net}} \tag{4.37}$$

where, $\dot{C}_{w,net}$, $\dot{B}_{w,net}$ are the cost rate and environmental impact rate of the net electricity.

4.4 Results and Arguments

4.4.1 Energy and Exergy Outcomes

Tables 4.8 and 4.9 show the energy, exergy, exergoeconomic, and exergoenvironmental assessment outcomes for the recommended system. According to the results of Table 4.9, the combustion chamber has the maximum value of exergy destruction of 3835 kW between all components, including more than 89% of the system exergy destruction. The whole exergy destruction of the set-up has been calculated 4276 kW. The pimp with 0.002% of the exergy destruction ratio has the minimum value of the component's exergy destruction. Based on an economic standpoint, the lowest and highest value of investment cost belongs to the pump and turbine 2 with 0.016 $/h and 5.829 $/h, respectively; the whole investment cost is reported 12.82 $/hr. However, due to the high exergy destruction rate, the cost and environmental destruction rates of the combustion chamber have the highest amounts. Also, turbine 2, with 63.76%, has the maximum exergoeconomic factor because of related considerable investment cost. Based on the exergoenvironmental point of view, compressor with 0.39% and condenser with 0.0008% have the outmost and lowest value of exergoenvironmental factor, respectively. Finally, the environmental impact of the whole set-up is reported

Table 4.8 The main outputs of the total system

Parameter	Value
Input energy of combustion chamber, $\dot{Q}_{CC}(kW)$	3652
Capacity of condenser, $\dot{Q}_{cond}(kW)$	523.9
Capacity of recovery heat exchanger, $\dot{Q}_{RHE}(kW)$	2523
Consumed work of compressor, $\dot{W}_{comp}(kW)$	1453
Generated work of turbine 1, $\dot{W}_{t1}(kW)$	2523
Generated work of turbine 2, $\dot{W}_{t2}(kW)$	304.7
Consumed work of pump, $\dot{W}_{p1}(kW)$	2.593
Net generated power, $\dot{W}_{net}(kW)$	1372
Toal energy efficiency, $\eta_{en,tot}(\%)$	37.57
Toal exergy efficiency, $\eta_{ex,tot}(\%)$	21.27
Toal unit cost of product, $UCP(\$/GJ)$	21.46
Toal environmental impact of product, $EIP(mPts/GJ)$	6432

Table 4.9 The detail results of exergy, exergoeconomic and exergoenvironmental assessment

Constituents	$\dot{E}_{D,i}$ (kW)	$\eta_{ex,i}$ (%)	$y_{D,i}$ (%)	$\dot{C}_{D,i}$ ($/h)	$\dot{Z}_i$ ($/h)	$r_{c,i}$	$f_{c,i}$ (%)	$\dot{B}_{D,i}$ (mPts/h)	$\dot{Y}_i$ (mPts/h)	$r_{b,i}$	$f_{b,i}$ (%)
Compressor	105.4	92.75	2.466	7.091	4.438	0.127	38.49	2245	8.948	0.078	0.39
Combustion chamber	3835	52.02	89.69	125.3	0.145	0.923	0.11	40,136	21.31	0.923	0.053
Turbine 1	146.4	94.52	3.424	9.203	1.921	0.07	17.27	2946	17.11	0.058	0.57
Recovery heat exchnager	125.9	74.77	2.945	7.915	0.206	0.346	2.54	2534	2.145	0.337	0.0084
Turbine 2	31.29	90.69	0.731	2.656	5.829	0.328	68.7	843.2	7.463	0.103	0.87
Condenser	31.78	19.91	0.743	2.697	0.264	4.418	8.94	856.3	0.007	4.023	0.0008
Pump	0.119	95.38	0.002	0.013	0.016	0.108	55.21	3.56	0.0008	0.048	0.0023
Total	4276	21.27	–	105.4	12.82	2.003	10.85	34,925	56.98	1.834	0.162

56.96 mPts/h, which is mostly concerned by the combustion chamber because of its high environmental impact of 21.31 mPts/h.

4.4.2 Parametric Study

4.4.2.1 The Impact of the Compressor Pressure Ratio on the System Performance

Figure 4.2. shows the impact of the compressor pressure ratio on the system performance. Rising the compressor pressure ratio leads to an increasing trend in the energy and exergy efficiencies because of increasing the consuming power of the compressor and subsequently decreasing the whole net power. Also, the environmental and power cost rates decline, and trades-off between these factors and net power lead to an increasing trend in the unit cost of product along with descending and then ascending trend in the impact of the environmental product (Eqs. 4.36, 4.37).
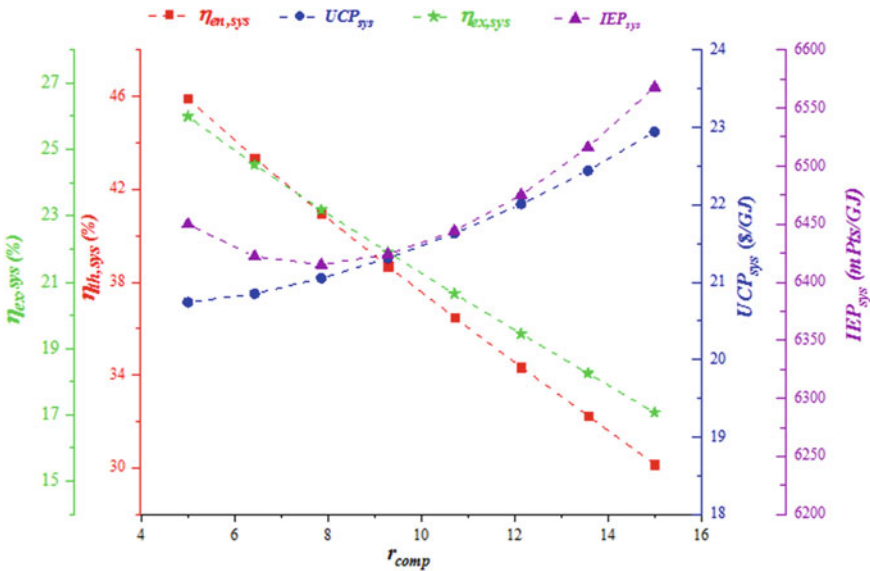

Fig. 4.2 The impact of the compressor pressure ratio on the system performance
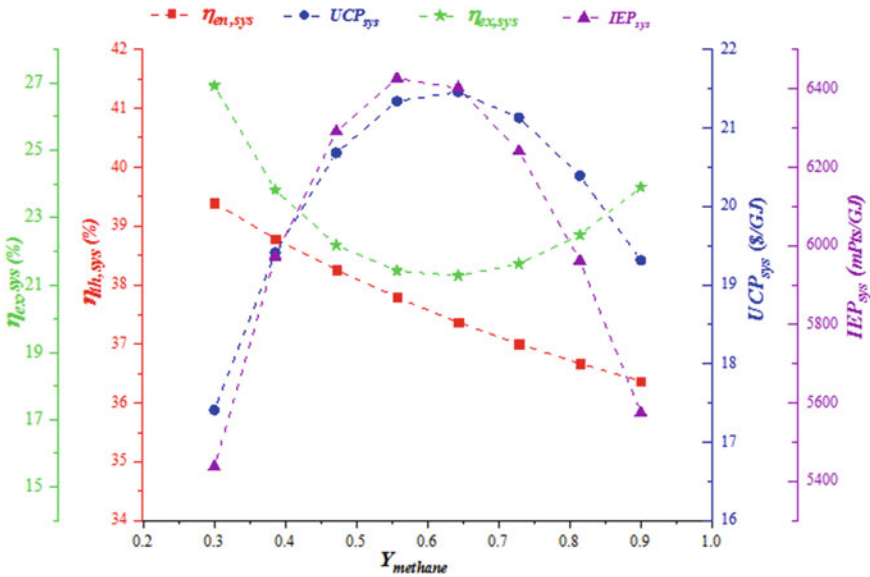
Fig. 4.3 The impact of the methane mole fraction on the system performance

4.4.2.2 The Impact of the Methane Mole Fraction on the System Performance

The effect of the methane mole fraction on the system performance is presented in Fig. 4.3. The energy efficiency is reduced by raising the methane molar mass. This trend can be expressed because the produced power declining as the fraction increases. Also, exergy efficiency shows a fluctuating trend. Since the cost of the net generated electricity has a rising trend with increasing methane mole fraction up to the range of 0.6 and then has a declining tendency. Moreover, regarding the declining direction of the net produced power, the unit cost of product and the impact of the environmental product first raised and then reduced.

4.4.2.3 The Impact of Combustion Chamber Outlet Temperature on the System Performance

Based on Fig. 4.4, by increasing the combustion chamber outlet temperature, the net generated power is increased owing to the augmented enthalpy difference between the inlet and outlet of turbine 1, in which the influence of this increase is more than the raised rate of the combustion chamber energy. The exergy efficiency has an ascending trend due to the fundamental impact of the net generated power rising than the fuel exergy. Because the cost and environmental impact of the net power rises with increasing the combustion chamber outlet temperature and the ascending trend
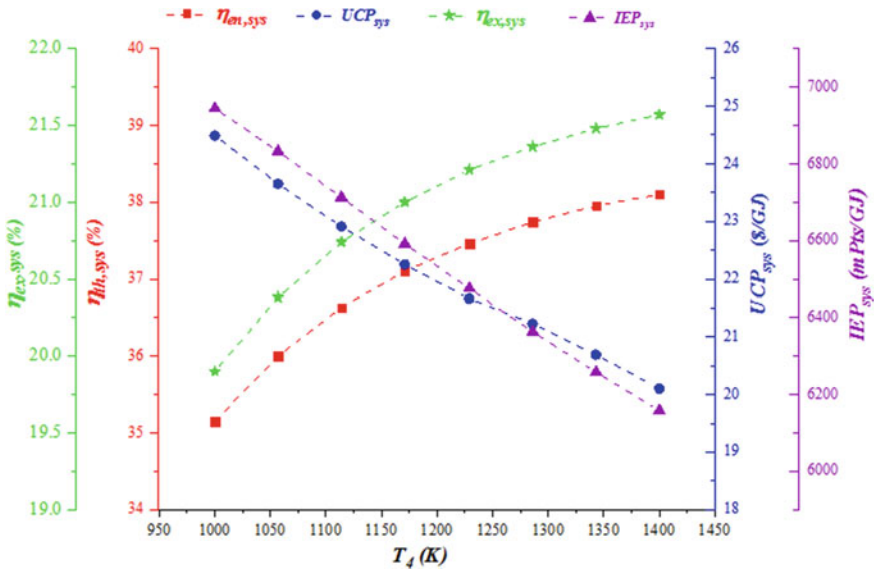
Fig. 4.4 The impact of combustion chamber temperature on the system performance

of the net generated electricity to calculate the unit cost of product and impact of the environment product, a trade-off is done between these parameters. Regarding the significant effect of the net generated electricity, the unit cost of product and impact of the environmental product is decreased.

4.4.2.4 The Impact of the Condenser Pressure on the System Performance

Figure 4.5 the impact of the compressor pressure ratio on the system performance. Rising the condenser pressure increases the enthalpy of the steam turbine output. This augmentation in enthalpy reduces the generated power of the steam turbine, and consequently, the net produced power of the system decreases. This reduction effect causes a decreasing trend in energy, exergy, cost, and environmental indicators.

4.5 Conclusions

Increasing power generation by using integrated energy systems is one of the promising technologies. This chapter studied the 4E analysis of the integrated power generation set-up by combining the Brayton and Rankine cycles as sub-systems. Also, the biogas is injected into the combustion chamber as a heat source instead of natural gas.
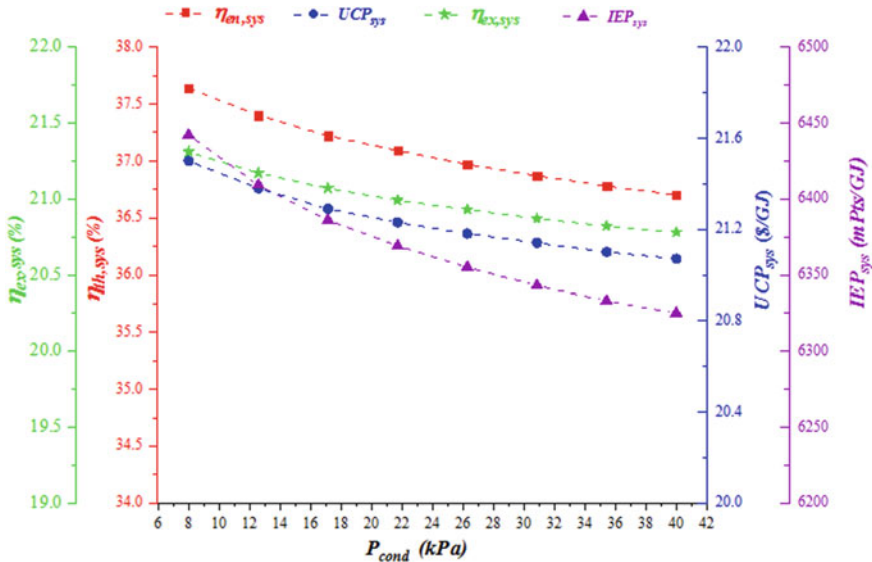
Fig. 4.5 The impact of the condenser pressure on the system performance

The prominent conclusions can be presented as below:

- The energy and exergy efficiencies of the system are reported 37.57% and 21.27%.
- The unit cost of product and impact environmental of product is are calculated 21.46 $/GJ, and 6432 mPts/GJ, respectively.
- The combustion chamber has the maximum value of exergy destruction of 3835 kW between all components.
- The cost and environmental destruction rates of the combustion chamber have the highest amounts
- By increasing the condenser pressure, the energy efficiency, exergy efficiency, unit cost of product, and impact of the environmental product are reduced.

References

1. M. Tajik Mansouri, M. Amidpour, J.M. Ponce-Ortega, Optimization of the integrated power and desalination plant with algal cultivation system compromising the energy-water-environment nexus. Sustain. Energy Technol. Assess. **42**, 100879 (2020). 2020/12/01
2. M.-R. Kolahi, M. Amidpour, M. Yari, Multi-objective metaheuristic optimization of combined flash-binary geothermal and humidification dehumidification desalination systems. Desalination **490**, 114456 (2020) 2020/09/15/
3. H. Nasrollahi, F. Ahmadi, M. Ebadollahi, S. Najafi Nobar, M. Amidpour, The greenhouse technology in different climate conditions: A comprehensive energy-saving analysis. Sustain. Energy Technol. Assess. **47**, 101455 (2020). 2021/10/01/

4. H. Rostamzadeh, H. Ghiasirad, M. Amidpour, Y. Amidpour, Performance enhancement of a conventional multi-effect desalination (MED) system by heat pump cycles. Desalination **477**, 114261 (2020). 2020/03/01/

5. H. Zhang et al., A review of waste heat recovery technologies towards molten slag in steel industry. Appl. Energy **112**, 956–966 (2013)

6. M. Tajik Mansouri, M. Amidpour, J.M. Ponce-Ortega, Optimal integration of organic Rankine cycle and desalination systems with industrial processes: Energy-water-environment nexus. Appl. Thermal Eng. **158**, 113740 (2020). 2019/07/25/

7. M.-R. Kolahi, A. Nemati, M. Yari, Performance optimization and improvement of a flash-binary geothermal power plant using zeotropic mixtures with PSO algorithm. Geothermics **74**, 45–56 (2018). 2018/07/01/

8. www.satba.gov.ir.

9. A. Bahadori, Estimation of combustion flue gas acid dew point during heat recovery and efficiency gain. Appl. Therm. Eng. **31**(8–9), 1457–1462 (2011)

10. A.H. Mosaffa, Z. Ghaffarpour, L. Garousi Farshi, Thermoeconomic assessment of a novel integrated CHP system incorporating solar energy based biogas-steam reformer with methanol and hydrogen production. Solar Energy **178**, 1–16 (2020). 2019/01/15/

11. M. Ebadollahi, H. Rostamzadeh, O. Pourali, H. Ghaebi, M.J.J.O.E.R.T. Amidpour, Close supercritical versus inverse Brayton cycles for power supply, using waste of a biogas-driven open Brayton cycle **143**(9), 092102 (2021)

12. H. Ghaebi, M. Yari, S.G. Gargari, H. Rostamzadeh, Thermodynamic modeling and optimization of a combined biogas steam reforming system and organic Rankine cycle for coproduction of power and hydrogen. Renew. Energy (2018)

13. F. Jabari, B. Mohammadi-ivatloo, M.-B. Bannae-Sharifian, H. Ghaebi, Design and performance investigation of a biogas fueled combined cooling and power generation system. Energy Convers. Manag. **169**, 371–382 (2018). 2018/08/01/

14. A.D. Zareh, R.K. Saray, S. Mirmasoumi, K. Bahlouli, Extensive thermodynamic and economic analysis of the cogeneration of heat and power system fueled by the blend of natural gas and biogas. Energy Convers. Manage. **164**, 329–343 (2018)

15. H. Zeng, Y. Wang, Y. Shi, N. Cai, Biogas-fueled flame fuel cell for micro-combined heat and power system. Energy Convers. Manage. **148**, 701–707 (2017)

16. B. Su, W. Han, Y. Chen, Z. Wang, W. Qu, H. Jin, Performance optimization of a solar assisted CCHP based on biogas reforming. Energy Convers. Manage. **171**, 604–617 (2018)

17. B. Su, W. Han, H. Jin, Proposal and assessment of a novel integrated CCHP system with biogas steam reforming using solar energy. Appl. Energy **206**, 1–11 (2017)

18. T. Gholizadeh, M. Vajdi, F. Mohammadkhani, Thermodynamic and thermoeconomic analysis of basic and modified power generation systems fueled by biogas. Energy Convers. Manag. **181**, 463–475 (2019). 2019/02/01/

19. Y. Liang, J. Chen, X. Luo, J. Chen, Z. Yang, Y. Chen, Simultaneous optimization of combined supercritical CO2 Brayton cycle and organic Rankine cycle integrated with concentrated solar power system. J. Clean. Prod. 121927 (2020)

20. Y. Yang, Y. Huang, P. Jiang, Y. Zhu, Multi-objective optimization of combined cooling, heating, and power systems with supercritical CO2 recompression Brayton cycle. Appl. Energy **271**, 115189 (2020)

21. T. Gholizadeh, M. Vajdi, H. Rostamzadeh, Energy and exergy evaluation of a new bi-evaporator electricity/cooling cogeneration system fueled by biogas. J. Clean. Prod. **233**, 1494–1509 (2019). 2019/10/01/

22. T. Gholizadeh, M. Vajdi, H. Rostamzadeh, A new biogas-fueled bi-evaporator electricity/cooling cogeneration system: Exergoeconomic optimization. Energy Convers. Manag. **196**, 1193–1207 (2019). 2019/09/15/

23. T. Gholizadeh, M. Vajdi, H. Rostamzadeh, Exergoeconomic optimization of a new trigeneration system driven by biogas for power, cooling, and freshwater production. Energy Convers. Manag. **205**, 112417 (2020)

24. M. Ebadollahi, H. Rostamzadeh, M.Z. Pedram, H. Ghaebi, M. Amidpour, Proposal and multi-criteria optimization of two new combined heating and power systems for the Sabalan geothermal source. J. Clean. Prod. **229**, 1065–1081 (2019). 2019/08/20/

25. M. Ebadollahi, H. Rostamzadeh, P. Seyedmatin, H. Ghaebi, M. Amidpour, Thermal and exergetic performance enhancement of basic dual-loop combined cooling and power cycle driven by solar energy. Thermal Sci. Eng. Progress 100556 (2020). 2020/04/27/

26. M. Kolahi, M. Yari, S.M.S. Mahmoudi, F. Mohammadkhani, Thermodynamic and economic performance improvement of ORCs through using zeotropic mixtures: Case of waste heat recovery in an offshore platform. Case Stud. Thermal Eng. **8**, 51–70 (2016). 2016/09/01/

27. A. Ganjehkaviri, M.N. Mohd Jaafar, P. Ahmadi, H. Barzegaravval, Modelling and optimization of combined cycle power plant based on exergoeconomic and environmental analyses. Appl. Thermal Eng. **67**(1), 566–578 (2014). 2014/06/01/

28. A. Bejan, G. Tsatsaronis, M.J. Moran, Thermal Design and Optimization (Wiley, New York, 1995)

29. H. Ghiasirad, N. Asgari, R. Khoshbakhti Saray, S. Mirmasoumi, Thermoeconomic assessment of a geothermal based combined cooling, heating, and power system, integrated with a humidification-dehumidification desalination unit and an absorption heat transformer. Energy Convers. Manag. **235**, 113969 (2021). 2021/05/01/

30. H. Rostamzadeh, K. Mostoufi, M. Ebadollahi, H. Ghaebi, M.J.I.J.O.E. Amidpour, Exergoeconomic optimisation of basic and regenerative triple-evaporator combined power and refrigeration cycles **26**(1–2), 186–225 (2018)

31. N. Hashemian, A. Noorpoor, Assessment and multi-criteria optimization of a solar and biomass-based multi-generation system: Thermodynamic, exergoeconomic and exergoenvironmental aspects. Energy Convers. Manag. **195**, 788–797 (2019). 2019/09/01/

32. M. Ebadollahi, H. Rostamzadeh, M.Z. Pedram, H. Ghaebi, M. Amidpour, Proposal and assessment of a new geothermal-based multigeneration system for cooling, heating, power, and hydrogen production, using LNG cold energy recovery. Renew. Energy **135**, 66–87 (2019). 2019/05/01/

33. C. Mata-Torres, A. Zurita, J.M. Cardemil, R.A. Escobar, Exergy cost and thermoeconomic analysis of a Rankine Cycle + Multi-Effect Distillation plant considering time-varying conditions. Energy Convers. Manag. **192**, 114–132 (2019). 2019/07/15/

34. W. Wang, J. Wang, Z. Lu, S. Wang, Exergoeconomic and exergoenvironmental analysis of a combined heating and power system driven by geothermal source. Energy Convers. Manag. **211**, 12765 (2020). 2020/05/01/

35. M.D. Madvar, F. Ahmadi, R. Shirmohammadi, A. Aslani, Forecasting of wind energy technology domains based on the technology life cycle approach. Energy Rep. **5**, 1236–1248 (2019). 2019/11/01/

36. L. Meyer, G. Tsatsaronis, J. Buchgeister, L. Schebek, Exergoenvironmental analysis for evaluation of the environmental impact of energy conversion systems. Energy **34**(1), 75–89 (2009). 2009/01/01/

37. Siemens, Siemens gas turbine portfolio, ed (2019)

38. A. Copco, General Catalog for Compressed Air, Gas and Vacuum Solutions (2010)

39. E.J.C. Cavalcanti, Exergoeconomic and exergoenvironmental analyses of an integrated solar combined cycle system, Renew. Sustain. Energy Rev. **67**, 507–519 (2017). 2017/01/01/

40. A. Boyano, A.M. Blanco-Marigorta, T. Morosuk, G. Tsatsaronis, Exergoenvironmental analysis of a steam methane reforming process for hydrogen production. Energy **36**(4), 2202–2214 (2011). 2011/04/01/

Chapter 5
A Biomass Assisted Solar-Based Multi-generation Plant with Hydrogen and Freshwater Production: Sustainability, Advanced Exergy and Advanced Exergo-Economic Assessments

Nasim Hashemian, Alireza Noorpoor, and Majid Amidpour

Abstract In this chapter, the sustainability, advanced exergy, and exergo-economic aspects of the biomass-assisted solar-based multi-generation plant for producing power load, heating load, cooling load, hydrogen, and freshwater are considered and investigated. To have more extensive knowledge of the recommended multi-generation plant operation, the examinations are undertaken to expand and to envision the simulations in Engineering Equation Solver software. The sustainability index of the plant has been estimated at 1.042. The advanced analyses of the multi-generation plant are examined under unavoidable, and ideal conditions. The advanced inquiries outcomes signify that in most elements, the destructed exergy has endogenous characters, and the parabolic trough solar collector, double-effect absorption chiller, and biomass combustor are holding the most potential to diminish destructed exergy. Additionally, advanced exergetic study shows that by changing the configuration variables of biomass combustor and turbine, 6240 and 4398 KW of these elements' destructed exergy can be avoided, sequentially. Trusted by the advanced exergo-economic investigation outcomes, the PEM electrolyzer holds the highest avoidable and endogenous cost rates and it is probable to avoid destruction near 33$/h internally. In conclusion, some recommendations for augmenting the performance of this multi-generation plant are made.

N. Hashemian · A. Noorpoor (✉)
School of Environment, College of Engineering, University of Tehran, Tehran, Iran
e-mail: noorpoor@ut.ac.ir

N. Hashemian
e-mail: nsm.hashemian@ut.ac.ir

M. Amidpour
Department of Energy System Engineering, Faculty of Mechanical Engineering, K. N. Toosi University of Technology, Tehran, Iran
e-mail: amidpour@kntu.ac.ir

Nomenclature

Abbreviations

ABS	Absorber
BC	Biomass Combustor
BPE	Boiling Point Elevation
c	Exergy cost per unit, $/J
$\dot{C}$	Rate of cost, $/s
Cond	Condenser
DEAC	Double Effect Absorption Chiller
Eco	Economizer
Eva	Evaporator
$\dot{E}$	Exergy rate, kW
HX	Heat exchanger
multi	Multi-generation
P	Pressure, kPa
PEM	Proton Exchange Membrane
TIP	Turbine Inlet Pressure
PTC	Parabolic Trough Collector
SRC	Steam Rankine Cycle
T	Temperature, K
Turb	Turbine
X	Steam quality

Greek Letters

η	Efficiency
Δ	Difference

Superscript

AV	Avoidable
EN	Endogenous

| EX | Exogenous |
| UN | Unavoidable |

Subscripts

0	Ambient condition
D	Destruction
f	Fuel
L	Loss
p	Product
tot	Total

5.1   Introduction

Now an exergy study stands as a very powerful way for deciding the energy carriers' quality, and the intelligent management of energy conversion. This aforementioned investigation may be involved in every energy-conversion operation. Exergy theory can be applied to improve operations that use energy reserves efficiently [1, 2]. The exergo-economic study implies an exergy-based approach that recognizes the position, quantity, objects, and expenses of thermodynamic inabilities into an energy-conversion operation. The exergo-economic study is carried out at the element of an energy-transformation plant and exposes the inclusive cost-efficacy [3]. The intensities and conditions of the conventional exergy and exergo-economic analyses have previously been considered in other studies [4–9]. As can be understood in the earlier researches, alone conventional exergy/exergo-economic approach has been implemented to increase energy conversion in multi-generation plants [10, 11]. Nevertheless, conventional exergy/exero-economic examinations cannot expose inefficiencies of the plant elements and extra developments. The advanced exergy-based study, submitted by Tsatsaronis et al. [12–14], enables the communications between elements and the ability to repair them. By the advanced exergy-based study, the conventional destructed exergy is divided toward endogenous/exogenous and unavoidable/avoidable pieces. Throughout this kind of study, the exactness of the general exergy-based investigation can be updated and expedite the advancement of any energy-conversion plants. Besides, advanced exergetic study has been implemented strongly in multiple multi-generation plants. Tan et al. [15] had investigated advanced exergetic aspects of the renewable-based system for producing district heating load. They probed a neighborhood heating plant by adopting an advanced exergetic approach toward recognizing the ability to repair and the ability for managing energy. Dai et al. [16] studied a complete assessment of advanced exergy and economic of a system for power generation. The outcomes revealed

that the exergetic efficiency was increased by nearly 20% by the advanced exergy investigation. The cost of endogenous avoidable was comparatively receptive to the temperature of the heat reservoir. Ebrahimi et al. [17] carried advanced exergetic examination of a grid-connected system with compressed air energy storage. The advanced exergetic examination sequences showed that 76.4% of the destructed exergy was avoidable. In another inquiry [18] a unit of separation of the air by a carbon dioxide power system was reviewed by advanced exergo-economic investigation. The report pointed that the destroyed exergy and cost rates of investment held endogenous characters, and the arrangement of the system had an important influence on costs. Kabiri et al. [19] introduced a system based on solar energy to repower steam power plants and conducted the advanced exerg and advanced exergo-economic inquiries to discover the augmentation in cycle operation throughout the repowering. A hydrogen liquefaction process was analyzed by employing advanced exergetic and exergo-economic investigations by Ansarinasab et al. [20]. Considering avoidable endogenous destroyed exergy cost rates, heat exchangers must be controlled via alterations. In another research [21], for examining the organic Rankine cycle-based combined plant, diagnosing the specific communications between elements of the plant, and developing the validity of exergy and exergo-economic investigations, the advanced exergy method was practiced. Based on the model developed by Li et al. [22], advanced exergy inquiry was carried on the hydrogen and power generation plant. Dividing the destructed exergy into avoidable and unavoidable sections in the mentioned work, showed that the betterment in the auxiliary elements would be an adequate way for the plant operation enhancement. To assess the operation of a cogeneration plant integrated with a desalination unit, advanced exergy, and exergo-economic investigations were conducted by You et al. [23]. The advanced study outcomes revealed that the significant share of plant destructed exergy had internal characters. In another work, advanced exergy and advanced exergo-economic inquiries respecting unavoidable and avoidable destructed exergy and rates of cost were carried in the research designated by Moharamian et al. [24]. According to revealed outcomes of advanced exergetic inquiry conducted by Caglayan et al. [25], chemical reactions happening in the combustion chamber make an increment in endogenous destructed exergy rate. Moreover, the unavoidable destructed exergy rates of the combustion chamber were more than its avoidable destructed exergy rates. Colorado [26] conducted an advanced exergetic study on a single-stage absorption unit, working with a solution of lithium bromide/water. The total avoidable portion of the destructed exergy was calculated at 14.78%. Mohammadi et al. [27] estimated the possibility of improving a system operation by determining the advanced exergo-economic study. They showed that the results concerned by the conventional exergetic study were varied from those obtained by the advanced exergetic study. Galindo et al. [28] made advanced exergetic investigation on a bottoming organic Rankine cycle system. Based on the obtained results from the advanced study, 36.5% of destructed exergy could be reduced by improvement in expander and pump.

According to the above-elaborated publications, some other researchers employed advanced exergetic-based investigation and described the importance of this approach for various energy conversion plants. Nevertheless, facing the best of the authors'

information, none of those previous publications concerned results for advanced exergy and advanced exergo-economic aspects for a biomass-assisted solar-based multi-generation plant with power, heating, cooling, hydrogen, and freshwater production purposes. This is the first time that advanced analyses of such a recommended multi-generation plant are conducted and in the following chapter, the divided destructed exergy plus the destructed exergy cost toward avoidable and unavoidable, endogenous and exogenous were evaluated as well as the multi-generation plant sustainability, which can satisfy the research gap in the aforementioned area. The next parts of this chapter are classified as follows: The description of the recommended multi-generation plant is addressed in Sect. 5.2. A conceptual description of the three different approaches for advanced studies, the supervising equations, and the hypothesis to develop the model are addressed in Sect. 5.3. By accurate plant simulation, the sustainability, advanced thermodynamic, and advanced thermo-economic aspects could be assessed, therefore, Sect. 5.4 gives numerical outcomes and associated discussions. The concluding points of this chapter are arranged in Sect. 5.5.

5.2 Description of the System

The arrangement of the recommended multi-generation plant has depicted in the following figure that is conceived up of parabolic trough solar collectors (PTC), biomass combustor (BC), steam Rankine cycle (SRC), double-effect absorption chiller (DEAC), proton exchange membrane (PEM) electrolyzer and multi-effect desalination (MED) unit. The main energy reservoir of this plant is solar power that is collected via PTC (state 1) and carries the heat of working fluid to the steam inside a single SRC. Under the BC unit, bagasse roles fuel-assisted, furthermore surplus air penetrated inside the bagasse combustor and fired. This process provides energy as an assisted fuel to fix the variation of periodic solar light. Under the SRC unit, the heat delivered by the BC unit provides superheated vapor (state 4) and generating electric power by the turbine (state 25). To accommodate the heating power of the plant, lost energy exodus from the turbine is utilized by HX1. Into the DEAC unit, via the heat of the exited steam from HX1, the refrigerant (water) is desorbed from the absorbent (lithium bromide). The water vapor catches in the low-temperature generator (LTG) and dense into the condenser to arrive at the cooling temperature. Consequently, the cooled water produces the cooling power inside evaporator2. The light water/lithium bromide solution moves in the high-temperature heat exchanger (HHX), low-temperature generator (LTG), and low-temperature heat exchanger (LHX), and the vapor originating from evaporator 2 is absorbed by the absorber. Heated exodus gasses of biomass burner insert HX2 (state10) to fulfill the demanded energy for the MED unit. Seawater penetrates the first effect of desalination (state12) and the preheater provides the distillation temperature of the feed water (state 23). Lastly, a share of produced power load by the plant and heated water (state 6) is used by the PEM electrolyzer to decay the water toward hydrogen (state
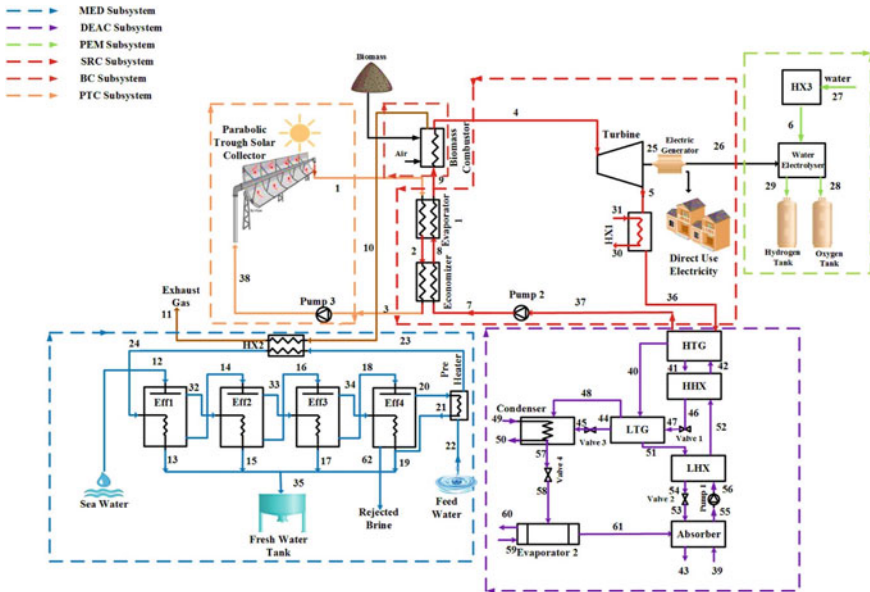
Fig. 5.1 Layout of the recommended multi-generation plant

29) and oxygen (state 28) during an electrolysis reaction. Figure 5.1 is displayed the multi-generation plant layout.

5.3 Process Assessment and Performance of Criteria

In this section, the description of sustainability, advanced exergy, and exergy-economic concepts as a stalwart means to the extra evaluation of the plant and their related equations will be described. To explain the developed model and make sustainability, advanced thermodynamic, and thermo-economic examination available, some right hypotheses are presented [29]:

- The temperature and pressure of ambient are $T_0 = 25$ °C, $P_0 = 100$ kPa.
- The inlet pressure of the turbine (TIP) is assumed to be 6000 kPa.
- The salinity of seawater is 40 g/kg.
- The plant works in a steady-state condition.
- This plant owns insignificant variations of kinetic, and potential energy, and exergy.
- All pumps and the turbine have isentropic efficiencies.
- Heat and pressure losses of piping and other auxiliary elements are insignificant.

Engineering Equation Solver (EES) software [30] as an applicable software is decided to make the developed modeling of the multi-generation plant. It should be

noted that founded upon the first and second laws of thermodynamics, an in-depth conventional energy, exergy, exergo-economic, and exergo-environmental investigations and parametric study of the recommended multi-generation plant were presented in the previous work [29] and all obtained results from conventional analyses and input data are employed in the present work for the sustainability/advanced examinations of the plant.

5.3.1 Sustainability Index Analysis

Before handling the sustainability report, it could be important to know that sustainable development has been described in many styles, however, the common and generally applied description quotes to "a development that satisfies the requirements of the now without hazarding the capacity of coming generations to satisfy their own demands" [31]. Actuality, sustainability evaluation holds an indication of sustainable development [32] that highlights the effective application of energy origins with the minimum energy loss. On the other hand, sustainability, and exergetic study are deeply associated with each other that aid to determine the sustainability criterion as below [33, 34]:

$$SI_{plant} = \frac{1}{D_{plant}} \qquad (5.1)$$

Here D_{plant} is a number of depletion, which is described as:

$$D_{plant} = \frac{E_{D,tot}}{E_{in,tot}} \qquad (5.2)$$

$E_{D,tot}$ is the plant's total destructed exergy and $E_{in,tot}$ is the total input exergy of the whole multi-generation plant.

5.3.2 Advanced Exergy Method

An advanced exergetic approach signifies an inherent method for extra appraising energy-conversion process and operation such as studying the rate of the destructed exergy below deeper circumstances wherever the general exergy study requires. Toward an advanced exergetic study, the rate of the destructed exergy of all elements has been classified into two subdivisions: The prime piece evaluates the irreversibility of the element itself so-called endogenous rate of destructed exergy ($\dot{E}_{D,k}^{EN}$). The second is the exogenous rate of destructed exergy ($\dot{E}_{D,k}^{EX}$) that exposes the irreversibilities that stay in the care of other elements. Unavoidable rate of destructed exergy ($\dot{E}_{D,k}^{UN}$) involves mechanical, technical, and financial boundaries of each plant and the
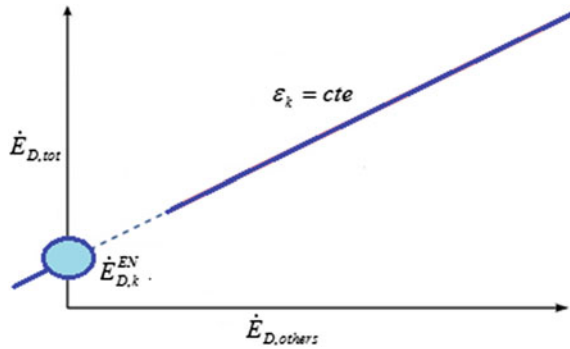
avoidable piece of the destructed exergy rate ($\dot{E}_{D,k}^{AV}$) could be described as the growth possibility or deficiency of each element. There are several different approaches for advanced studies like the thermodynamic cycle approach, the equivalent element approach, and the engineering approach [35]. The thermodynamic cycle approach remains relying on dividing the destructed exergy toward endogenous and exogenous sections considering the complete analysis of a thermodynamic cycle. In the equivalent element approach, the elements are drawn equivalent to each other, i.e., an ideal combustor is similar to a beau-ideal heat exchanger and amounts of the pressure and temperature in each state have been kept and the applied operating fluid through the system is alike. Applying different working fluids during inquiring about the real and the ideal operations is the chief problem of this approach. The engineering approach (also known as a graphical method) is applied to estimate endogenous exergy destruction by drawing a graph. For this purpose, Fig. 5.2 is illustrated based on the next equations:

$$\dot{E}_{F,tot} = \dot{E}_{P,tot} + \dot{E}_{D,tot} + \dot{E}_{L,tot} \tag{5.3}$$

$$\dot{E}_{D,tot} = \dot{E}_{D,k} + \dot{E}_{D,others} \tag{5.4}$$

Here $\dot{E}_{F,tot}$, $\dot{E}_{P,tot}$, and $\dot{E}_{L,tot}$ are the total fuel exergy, product exergy, and exergy loss of the plant, individually. Considering the endogenous destructed exergy holds the element exergy efficiency function (ε_k), the exergy efficiency of each element is required to be retained consistently while $\dot{E}_{D,others}$ is changing. While other elements of the system are close to the ideal performance, $\dot{E}_{D,others}$ leads to 0, and their corresponding exergy yields progress to 100%. Direct lines happen since $\dot{E}_{D,others}$ is diverse, as displayed in Fig. 5.2. This figure depicts the plant's total destructed exergy versus other elements' destructed exergy.

To study in this chapter, the thermodynamic cycle approach as the most common approach with believable accuracy has been adopted. A fundamental pattern for advanced study in this work is illuminated in Fig. 5.3.
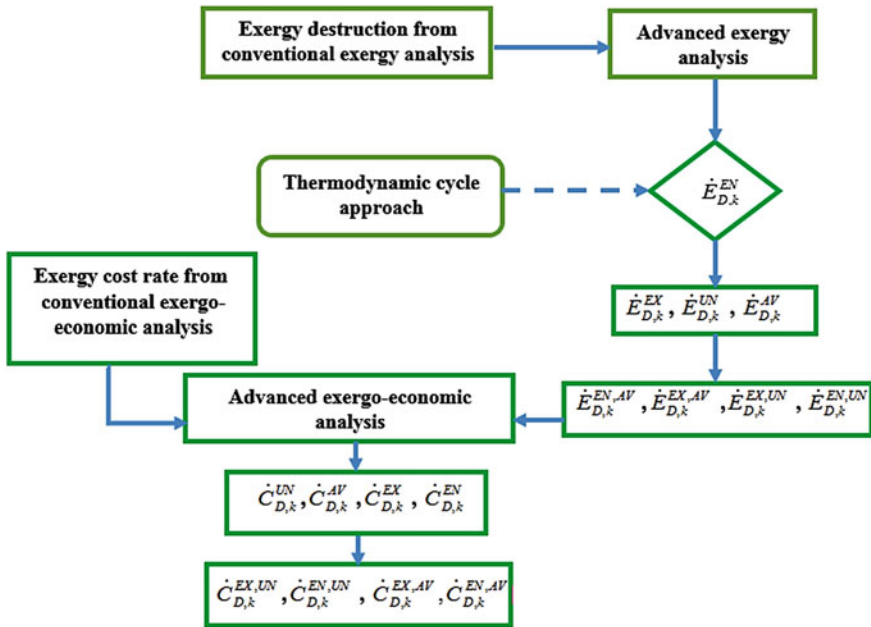
Fig. 5.3 Fundamental pattern for advanced study

Complete governing equations linked to advanced exergetic study are arranged in Table 5.1.

5.3.3 Advanced Exergo-Economic Method

The central opinion in the advanced exergo-economic study is to ascertain and link the parameters obtained from advanced exergy inquiry to economics. This method helps to make decisions on picking the most suitable procedure for decreasing total cost. In this study, cost rates linked to destructed exergy and the real possibility to economically enhance the operation are revealed within four divisions including their roots and capacity to evade: avoidable endogenous, avoidable exogenous, unavoidable endogenous, and unavoidable exogenous. Mentioned parameters aimed to understand the multi-generation plant behavior deeply. An unavoidable division of cost rates could not be evaded owing to technical and economical restrictions. The avoidable division of cost rates gives the ability to an element and whole multi-generation plant to increase efficiency. Avoidable endogenous division of element cost rates could be diminished by growing the thermodynamic efficiency of the element itself. Avoidable exogenous division of the element cost rates could be defeated by improving the efficiency of the other elements. The associated equations correspond to advanced exergo-economic study are given in Table 5.2.

Table 5.1 Governing equations linked to advanced exergetic study [36]

Idiom	Description	Number of equation
Exogenous destructed exergy rate of the kth element	$\dot{E}_{D,k}^{EX} = \dot{E}_{D,k} - \dot{E}_{D,k}^{EN}$	(5.5)
Unavoidable destructed exergy rate of the kth element	$\dot{E}_{D,k}^{UN} = \dot{E}_{P,k}^{\text{Real}} \left(\dfrac{\dot{E}_{D,k}}{\dot{E}_{P,k}} \right)^{UN}$	(5.6)
Avoidable destructed exergy rate of the kth element	$\dot{E}_{D,k}^{UN} = \dot{E}_{D,k} - \dot{E}_{D,k}^{AV}$	(5.7)
Unavoidable endogenous destructed exergy rate of the kth element	$\dot{E}_{D,k}^{UN,EN} = \dot{E}_{D,k}^{EN} \left(\dfrac{\dot{E}_{D,k}}{\dot{E}_{P,k}} \right)^{UN} = \dot{E}_{D,k}^{UN} \left(\dfrac{\dot{E}_{D,k}}{\dot{E}_{P,k}} \right)^{EN}$	(5.8)
Unavoidable exogenous destructed exergy rate of the kth element	$\dot{E}_{D,k}^{EX,UN} = \dot{E}_{D,k}^{UN} - \dot{E}_{D,k}^{EN,UN}$	(5.9)
Avoidable endogenous destructed exergy rate of the kth element	$\dot{E}_{D,k}^{EN,AV} = \dot{E}_{D,k}^{EN} - \dot{E}_{D,k}^{EN,UN}$	(5.10)
Avoidable exogenous destructed exergy rate of the kth element	$\dot{E}_{D,k}^{EX,AV} = \dot{E}_{D,k}^{EX} - \dot{E}_{D,k}^{EX,UN}$	(5.11)
Total destructed exergy rate of the kth element	$\dot{E}_{D,k}^{UN} + \dot{E}_{D,k}^{EN} + \dot{E}_{D,k}^{AV} + \dot{E}_{D,k}^{EX} = \dot{E}_{D,k}$	(5.12)

Presumptions for ideal, and unavoidable conditions for the multi-generation plant elements are tabulated in Table 5.3.

5.3.4 Verification of the Developed Model

Facing the best of the authors' information, the recommended configuration of the biomass-assisted solar-driven multi-generation plant providing electricity, heating power, cooling power, hydrogen, plus freshwater is firstly investigated in the advanced study area, due to the loss of data recorded for the same whole plant, and considering that the results of the advanced exergetic-based study for each element are carried out according to its unavoidable conditions and the ideal conditions of other elements of the plant, therefore, it is not a scientific decision to validate advanced studies results for subsystems individually except in the same plant cases. Unlike the advanced studies, the results of conventional analyses are suitable to validate individually and had been verified in the previous work [29].

Table 5.2 Associated equations correspond to advanced exergo-economic study [37]

Idiom	Description	Equation	Number of equation
Endogenous destructed exergy Cost rate	Considering the performance of all elements without the kth element, which works by its efficiency, following the ideal conditions leads to estimating the kth element cost as if named the cost of internal	$\dot{C}_{D,k}^{EN} = c_{f,k} \dot{E}_{D,k}^{EN}$	(5.13)
Exogenous destructed exergy cost rate	Via decreasing the kth element internal cost of the kth element total cost, the exogenous cost within the kth element is calculated	$\dot{C}_{D,k}^{EX} = \dot{C}_{D,k} - \dot{C}_{D,k}^{EN}$	(5.14)
Unavoidable destructed exergy cost rate	Owing to technological restriction, the unavoidable destructed exergy cost can be deducted	$\dot{C}_{D,k}^{UN} = c_{f,k} \dot{E}_{D,k}^{UN}$	(5.15)
Avoidable destructed exergy cost rate	Cost rate that stands shunned	$\dot{C}_{D,k}^{AV} = c_{f,k} \dot{E}_{D,k}^{AV}$	(5.16)
Unavoidable endogenous destructed exergy cost rate	Unavoidable cost rate in element kth linked with itself element performance	$\dot{C}_{D,k}^{EN,UN} = c_{f,k} \dot{E}_{D,k}^{En,UN}$	(5.17)
Unavoidable exogenous destructed exergy cost rate	Unavoidable cost rate in element kth induced by the other elements	$\dot{C}_{D,k}^{EX,UN} = \dot{C}_{D,k}^{UN} - \dot{C}_{D,k}^{EN,UN}$	(5.18)
Avoidable endogenous cost rate of destructed exergy	Avoidable cost rate of element kth correlated with itself element performance	$\dot{C}_{D,k}^{EN,AV} = \dot{C}_{D,k}^{EN} - \dot{C}_{D,k}^{EN,UN}$	(5.19)
Avoidable exogenous destructed exergy cost rate	Avoidable cost rate of element kth made by the other elements	$\dot{C}_{D,k}^{EX,AV} = \dot{C}_{D,k}^{EX} - \dot{C}_{D,k}^{EX,UN}$	(5.20)

5.4 Results and Discussion

Antecedent to the advanced analyses, the sustainability index for the biomass-assisted solar-based multi-generation plant has been calculated at 1.042. Figure 5.4 accompanies the trend of sustainability index of the multi-generation plant by accretion of evaporator1 temperature difference, TIP, and the HTG quality. From Fig. 5.4a, it can be understood that by increasing the evaporator1 temperature difference, obeyed

Table 5.3 Presumptions for ideal, and unavoidable conditions for the multi-generation plant subsystems [23, 38, 39]

| Elements	Ideal condition	Unavoidable destructed exergy condition
DEAC	$\Delta T_{\min(HXs,LTG,HTG,ABS,Eva2)} = 0\,°C$	$\Delta T_{\min(HXs,LTG,HTG,ABS,Eva2)} = 3\,°C$
	$\Delta T_{\min(cond)} = 0\,°C$	$\Delta T_{\min(cond)} = 5\,°C$
SRC	$\Delta T_{\min(Eva1,eco,HX1)} = 0\,°C$	$\Delta T_{\min(Eva1,eco,HX1)} = 3\,°C$
	$\eta_{is(turb,pump)} = 100\%$	$\eta_{is(turb,pump)} = 98\%$
MED	$BPE_{Seawater} = 0\,°C$	$BPE_{Seawater} = 0.4\,°C$
PTC	$\eta = 100\%$	$\eta = 75\%$
PEM	$T_{PEM} = 300\,°C$	$T_{PEM} = 350\,°C$
BC	$Q_L = 0\%$	$Q_L = 1\%$

by the biomass combustor input temperature, SRC running by more working fluid and producing more valuable products. Therefore, the sustainability of the plant increases following the total destructed exergy of the plant diminished. As implies in Fig. 5.4b, by enhancing the TIP, the sustainability of the plant increases. More TIP needs a more mass flow rate of the operating fluid and consequences to an increment in the amounts of valuable outputs of the plant and points to a decrement in the total quantity of destructed exergy of the plant. Relating to Fig. 5.4c, by the change of HTG inlet quality from 0.2 to 0.9, the quantity of cooling power production diminished. Owing to this decrement, the amount of the total destructed exergy generated by the plant improved, and the sustainability index of the plant drops about 15%.

The consequences of the divisions of destructed exergy of the multi-generation plant elements by advanced exergy are tabulated in Table 5.4. It can be detected that the rate of the internal destructed exergy stands more powerful than the rate of the exogenous destructed exergy for all the plant elements. In other words, the largest destructed exergy has belonged to the internal inefficiencies of the plant element itself. The endogenous destructed exergy holds the prevailing place for all the plant elements and indicates weak interactive interdependencies between plant elements. The rate of the exogenous destructed exergy of parabolic trough solar collector is considerably higher than other elements in the plant. Hence, a change in the other element efficiencies can point to a decrease in the rate of the destructed exergy of this element and enhance the plant efficiency. To assess the real potential of advancement for each plant element, the destructed exergy is divided into avoidable and unavoidable pieces, as noted in the fourth and fifth columns in Table 5.4. The outcomes reveal the heat exchanger 1, proton exchange membrane electrolyzer, turbine, and pump have larger avoidable destructed exergy than the unavoidable. The unavoidable part of the destructed exergy of the biomass combustor is higher than the avoidable part, due to the irreversibility of the combustion process. Also, the greatest share of the internal rate of destructed exergy amount is related to the parabolic trough solar collector, and this is owing to the large temperature difference among the receivers and the operating fluid. The negative value for parabolic trough solar collector avoidable destructed exergy means that its unavoidable destructed exergy is greater than the real value.
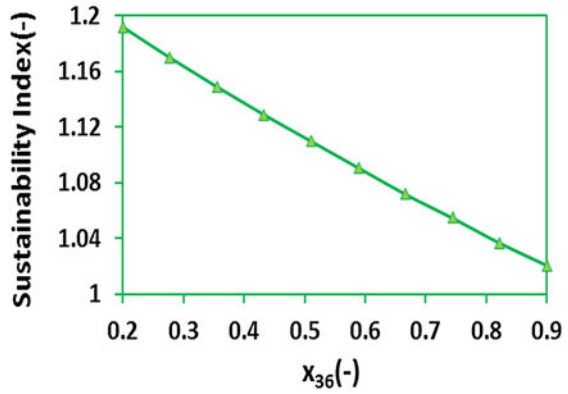
Fig. 5.4 Impression of the temperature difference of the evaporator 1 (**a**), TIP (**b**), and the HTG inlet quality (**c**) variations on the sustainability index of the plant
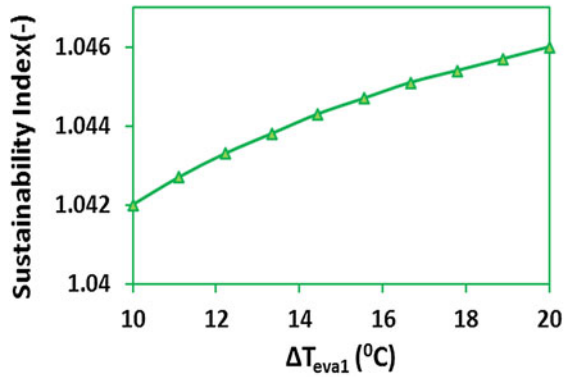
(a)
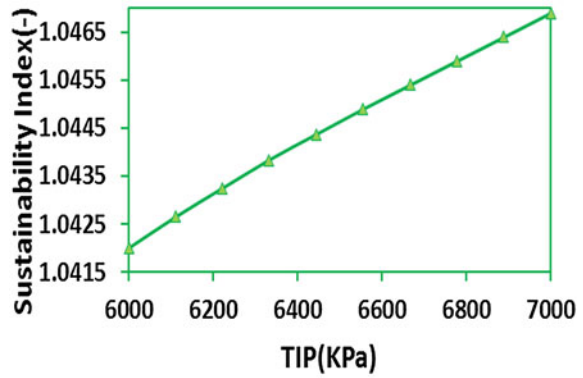
(b)

(c)

Table 5.4 Consequences of the divisions of destructed exergy of the multi-generation plant elements

Compnent	$\dot{E}_{D,k}^{EX}$ (kW)	$\dot{E}_{D,k}^{EN}$ (kW)	$\dot{E}_{D,k}^{AV}$ (kW)	$\dot{E}_{D,k}^{UN}$ (kW)	$\dot{E}_{D,k}^{EX,UN}$ (kW)	$\dot{E}_{D,k}^{EN,UN}$ (kW)	$\dot{E}_{D,k}^{EX,AV}$ (kW)	$\dot{E}_{D,k}^{EN,AV}$ (kW)
PTC	61,500	80,973	−4,641	217,114	299,817	−2,703	144,203	−18,844
BC	−9653	26,512	6240	10,619	6370	4249.9	−6,023	22,263
Eva1	144	4542	174.9	4511	4483	28.54	−4339	4513
Eco	457.1	2501	0.5568	2957	2373	584.5	−1916	1916
Turb	977	3996	4398	575.2	511.4	63.78	465.6	3932
Pump	92.26	154.9	235.4	11.77	8.607	3.162	83.65	151.8
HX1	567.4	582.6	738.9	411.1	343	68.09	224.3	514.5
MED	−3.429	111.5	34.48	73.62	−578	78.2	1.149	33.33
DE-AC	−3,683	65,328	20,588	21,057	−68,421	389,478	344,738	−24,150
PEM	476	1649	1482	643	−35.6	1579	1412	70.43

During applying the unavoidable conditions in the plant, following the increment in mass flow rate entering the parabolic trough solar collector, the difference among fuel and product exergies increases, and raises the destructed exergy. Negative values of exogenous, unavoidable exogenous, and avoidable exogenous destructed exergies for some elements mean that for the decrement in these element exergy destructions, it is necessary to increase the exergy efficiency of other components. According to Table 5.4, it can be stated that the double effect absorption chiller, biomass combustor, turbine, proton exchange membrane electrolyzer, and heat exchanger1 with the most avoidable destructed exergy values, respectively, have the powerful possibility for the plant thermodynamic operation improvement.

Figure 5.5a, b, c, d, e, f manifests the percentages of the endogenous/exogenous and avoidable/unavoidable destructed exergy for each subsystem of the plant.

According to the results achieved from advanced exergo-economic study and conforming to Table 5.5, all of the costs of destructed exergy in the elements comprise endogenously; Therefore, the destructed exergy cost cannot be affected by the element's interplays remarkably. The trends of the cost rates of destructed exergy for the SRC, PEM, and DEAC subsystem are alike to the trend of the rates of destructed exergy and remain avoidable. The outcomes show that the PEM electrolyzer has higher endogenous rates of destructed exergy than the other components. It is clear that the destructed exergy cost rates for PTC, BC, and MED subsystems are zero, owing to the zero exergy costs per unit for plant fuels.

The internal/exogenous and avoidable/unavoidable share of the cost rate of destructed exergy for the subsystems of the multi-generation plant is designated in Fig. 5.6. Acknowledging that the advanced exergo-economic study is a great means to recognize the possibility of cost decrement owing to inefficiencies inside the multi-generation plant, it can be understood, the subsystem that offers a vaster chance to a decrease of costs of the destructed exergy is the PEM electrolyzer followed by
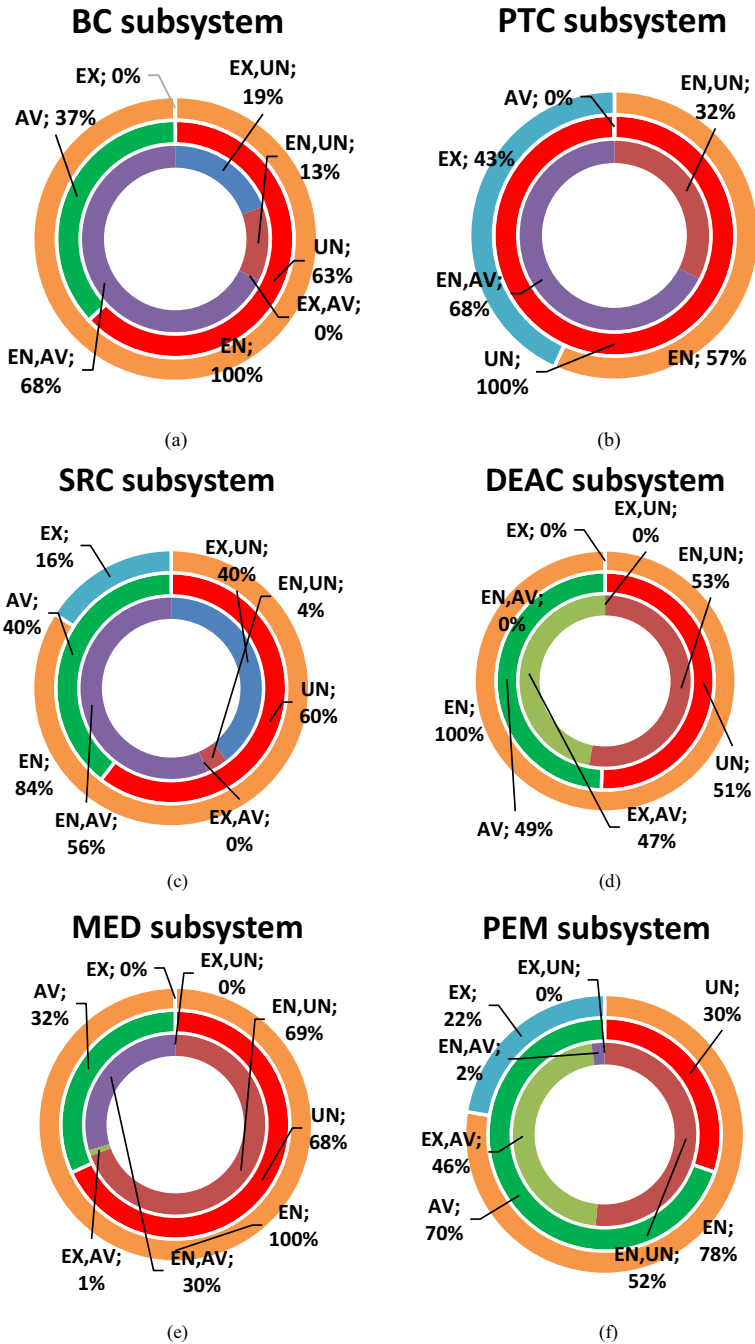
Fig. 5.5 Share of destructed exergy division for each subsystem (**a**, **b**, **c**, **d**, **e**, **f**)

Table 5.5 Consequences of the advanced exergo-economic study of the multi-generation plant elements

Component	$\dot{C}_{D,k}^{EX}$ ($/s)	$\dot{C}_{D,k}^{EN}$ ($/s)	$\dot{C}_{D,k}^{AV}$ ($/s)	$\dot{C}_{D,k}^{UN}$ ($/s)	$\dot{C}_{D,k}^{EX,UN}$ ($/s)	$\dot{C}_{D,k}^{EN,UN}$ ($/s)	$\dot{C}_{D,k}^{EX,AV}$ ($/s)	$\dot{C}_{D,k}^{EN,AV}$ ($/s)
Eva1	0.0003	0.0009	0.0000	0.0012	0.0012	0.0000	−0.0008	0.0009
Eco	0.0002	0.0005	0.0000	0.0007	0.0006	0.0001	−0.0003	0.0003
Turb	0.0067	0.0079	0.0087	0.0059	0.0057	0.0001	0.0009	0.0078
Pump	0.0031	0.0015	0.0023	0.0023	0.0023	0.0000	0.0008	0.0015
HX1	0.0016	0.0017	0.0022	0.0011	0.0009	0.0002	0.0006	0.0015
DEAC	−0.0701	0.1934	0.0609	0.0623	−1.091	1.1530	1.0210	−0.9598
PEM	0.0636	0.2201	0.1978	0.0859	−0.1248	0.2107	0.1884	0.0094
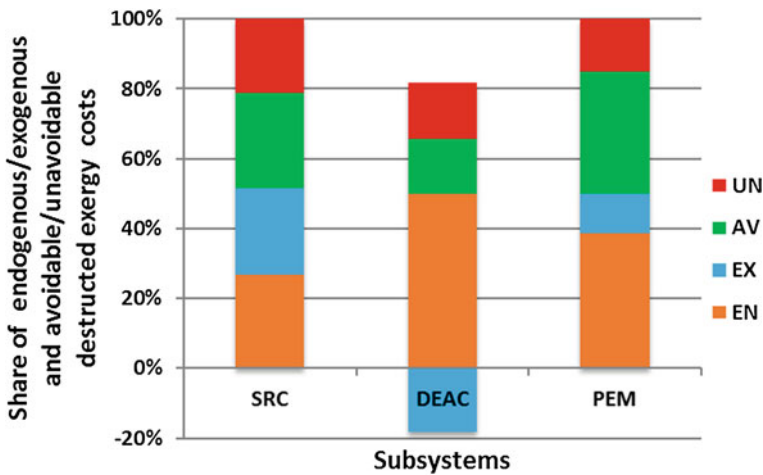
Fig. 5.6 Share of advanced destructed exergo-economic analysis for subsystems

the DEAC and the SRC. In the case of the PEM electrolyzer, it is probable to avoid destruction near 33 $/h internally by cooperating with the other multi-generation plant elements. In the case of non-cooperating by other elements, the destructed exergy cost of 720 $/h can continue avoided and the cost of 324 $/h cannot be avoided.

Figure 5.7 displays the whole plant exergy division cost rates to endogenous, exogenous, avoidable, and unavoidable. As can be detected in this figure, the significantly destructed exergy cost rates of the plant have endogenous and avoidable character.
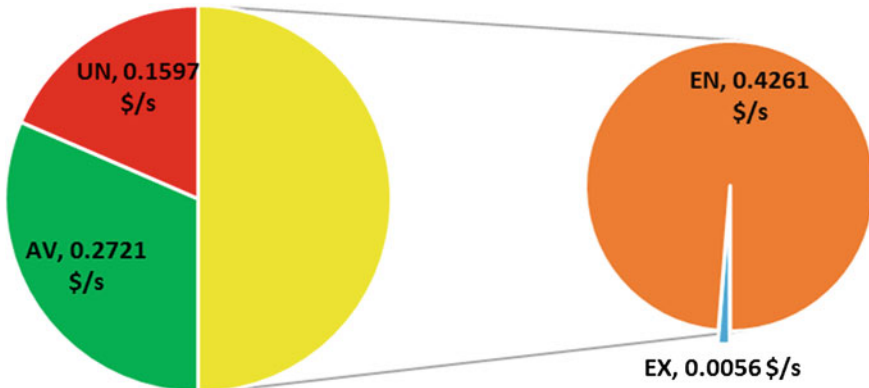
Fig. 5.7 The whole plant exergy division cost rates

5.5   Conclusions

In this chapter, the biomass-assisted solar-based multi-generation plant considering power, heating, cooling, hydrogen, and freshwater production was modeled in the EES software environment to accomplish sustainability, advanced exergetic, and advanced exergo-economic analyses. According to the obtained results, the concluding points are as follows:

1. The sustainability index of the plant has been estimated at 1.042. Matching to the outcomes acquired of the sensitivity assessment, the trends of sustainability index of the multi-generation plant by accretion of evaporator1 temperature difference, and TIP are ascending, and by the increment of HTG quality is descending.

2. Based on the advanced exergetic study the destructed exergy of most elements has endogenous characters and the PTC, DEAC, and BC are holding the most potentials to diminish destructed exergy. Additionally, advanced exergetic study shows that 6240 kW of destructed exergy inside the BC and 4298 kW of destructed exergy inside the turbine can continue avoided by changing the configuration variables of these elements.

3. Trusting on the advanced exergo-economic investigation, amongst whole elements, the PEM electrolyzer holds the highest avoidable and internal rates of cost and it is probable to avoid destruction near 33$/h internally with cooperating with the other multi-generation plant elements. By non-cooperating with other elements, 34% of the cost of destructed exergy can continue avoided and 16% of the cost cannot be avoided.

To diagnose the individual cooperation between elements, to develop the exactness of the conventional exergetic investigations, and to better understand the thermodynamic irreversibility of the overall plant, the advanced study was employed. In this regard, The PTC has notable amounts of exogenous destructed exergy rates.

Therefore, improvement in the other elements' efficiencies points to a decrease in the destructed exergy rate of PTC and makes an increase in the plant efficiency. DEAC has the most avoidable destructed exergy, therefore, has high potential and a significant role to improve the efficiency of the plant by increasing its performance. Also, it is important to mention that even technical improvement cannot prevent endogenous exergy destruction, completely.

References

1. J. Szargut, D.R. Morris, F.R. Steward, Exergy Analysis of Thermal, Chemical, and Metallurgical Processes (1987)
2. M.J. Moran et al., Principles of Engineering Thermodynamics. Wiley Global Education (2015)
3. A. Lazzaretto, G. Tsatsaronis, SPECO: a systematic and general methodology for calculating efficiencies and costs in thermal systems. Energy **31**(8–9), 1257–1289 (2006)
4. A. Noorpoor, D. Hamedi, N. Hashemian, Optimization of parabolic trough solar collectors integrated with two stage rankine cycle. J. Solar Energy Res. **2**(2), 61–66 (2017)
5. S.M. Parsa et al., Energy-matrices, exergy, economic, environmental, exergoeconomic, enviroeconomic, and heat transfer (6E/HT) analysis of two passive/active solar still water desalination nearly 4000m: Altitude concept. J. Clean. Prod. **261**, 121243 (2020)
6. A. Pirmohamadi et al., Exergoeconomic analysis of a novel hybrid system by integrating the kalina and heat pump cycles with a nitrogen closed brayton system. Energy Rep. **7**, 546–564 (2021)
7. B. Ghorbani, M. Amidpour, Energy, exergy, and sensitivity analyses of a new integrated system for generation of liquid methanol, liquefied natural gas, and crude helium using organic Rankine cycle, and solar collectors. J. Thermal Anal. Calorimetry 1–24 (2021)
8. P. Heidarnejad, Exergy based optimization of a biomass and solar fuelled CCHP hybrid seawater desalination plant. J. Thermal Eng. **3**(1), 1034–1043 (2017)
9. Y. Cao et al., A novel multi-objective spiral optimization algorithm for an innovative solar/biomass-based multi-generation energy system: 3E analyses, and optimization algorithms comparison. Energy Convers. Manag. **219**, 112961 (2020)
10. N. Hashemian, A. Noorpoor, P. Heidarnejad, Thermodynamic diagnosis of a novel solar-biomass based multi-generation system including potable water and hydrogen production. Energy Equip. Syst. **7**(1), 81–98 (2019)
11. A. Noorpoor et al., A thermodynamic model for exergetic performance and optimization of a solar and biomass-fuelled multigeneration system. Energy Equip. Syst. **4**(2), 281–289 (2016)
12. T. Morosuk, G. Tsatsaronis, Advanced exergy analysis for chemically reacting systems–application to a simple open gas-turbine system. Int. J. Thermodyn. **12**(3), 105–111 (2009)
13. T. Morosuk, G. Tsatsaronis, Advanced exergy-based methods used to understand and improve energy-conversion systems. Energy **169**, 238–246 (2019)
14. F. Petrakopoulou et al., Advanced exergoeconomic analysis applied to a complex energy conversion system. J. Eng. Gas Turbines Power **134**(3) (2012)
15. M. Tan, A. Keçebaş, Thermodynamic and economic evaluations of a geothermal district heating system using advanced exergy-based methods. Energy Convers. Manage. **77**, 504–513 (2014)
16. B. Dai et al., Evaluation of organic Rankine cycle by using hydrocarbons as working fluids: Advanced exergy and advanced exergoeconomic analyses. Energy Convers. Manag. **197**, 111876 (2019)
17. M. Ebrahimi et al., Conventional and advanced exergy analysis of a grid connected underwater compressed air energy storage facility. Appl. Energy **242**, 1198–1208 (2019)
18. M. Mehrpooya et al., Conventional and advanced exergoeconomic assessments of a new air separation unit integrated with a carbon dioxide electrical power cycle and a liquefied natural gas regasification unit. Energy Convers. Manage. **163**, 151–168 (2018)

19. S. Kabiri et al., New procedure for optimal solar repowering of thermal power plants and integration with MSF desalination based on environmental friendliness and economic benefit. Energy Convers. Manag. **240**, 114247 (2021)
20. H. Ansarinasab, M. Mehrpooya, A. Mohammadi, Advanced exergy and exergoeconomic analyses of a hydrogen liquefaction plant equipped with mixed refrigerant system. J. Clean. Prod. **144**, 248–259 (2017)
21. G. Liao et al., Advanced exergy analysis for organic rankine cycle-based layout to recover waste heat of flue gas. Appl. Energy **266**, 114891 (2020)
22. L. Li, et al., Conventional and advanced exergy analyses of a vehicular proton exchange membrane fuel cell power system. Energy **222**, 119939 (2021)
23. H. You, J. Han, Y. Liu, Conventional and advanced exergoeconomic assessments of a CCHP and MED system based on solid oxide fuel cell and micro gas turbine. Int. J. Hydrogen Energy **45**(21), 12143–12160 (2020)
24. A. Moharamian et al., A comparative thermoeconomic evaluation of three biomass and biomass-natural gas fired combined cycles using organic Rankine cycles. J. Clean. Prod. **161**, 524–544 (2017)
25. H. Caglayan, H. Caliskan, Advanced exergy analyses and optimization of a cogeneration system for ceramic industry by considering endogenous, exogenous, avoidable and unavoidable exergies under different environmental conditions. Renew. Sustain. Energy Rev. **140**, 110730 (2021)
26. D. Colorado, Advanced exergy analysis applied to a single-stage heat transformer. Appl. Therm. Eng. **116**, 584–596 (2017)
27. Z. Mohammadi, M. Fallah, S.S. Mahmoudi, Advanced exergy analysis of recompression supercritical CO2 cycle. Energy **178**, 631–643 (2019)
28. J. Galindo et al., Advanced exergy analysis for a bottoming organic rankine cycle coupled to an internal combustion engine. Energy Convers. Manage. **126**, 217–227 (2016)
29. N. Hashemian, A. Noorpoor, Assessment and multi-criteria optimization of a solar and biomass-based multi-generation system: Thermodynamic, exergoeconomic and exergoenvironmental aspects. Energy Convers. Manage. **195**, 788–797 (2019)
30. S. Klein, *Engineering Equation Solver (EES) V9, F-Chart Software*. Madison, *USA* (2015)
31. H. Nami, A. Anvari-Moghaddam, Geothermal driven micro-CCHP for domestic application–Exergy, economic and sustainability analysis. Energy **207**, 118195 (2020)
32. P. Ahmadi, I. Dincer, M.A. Rosen, Development and assessment of an integrated biomass-based multi-generation energy system. Energy **56**, 155–166 (2013)
33. P. Ahmadi, I. Dincer, M.A. Rosen, Energy and exergy analyses of hydrogen production via solar-boosted ocean thermal energy conversion and PEM electrolysis. Int. J. Hydrogen Energy **38**(4), 1795–1805 (2013)
34. P. Ahmadi, I. Dincer, M.A. Rosen, Exergo-environmental analysis of an integrated organic Rankine cycle for trigeneration. Energy Convers. Manage. **64**, 447–453 (2012)
35. S. Kelly, G. Tsatsaronis, T. Morosuk, Advanced exergetic analysis: Approaches for splitting the exergy destruction into endogenous and exogenous parts. Energy **34**(3), 384–391 (2009)
36. H. Nami, A. Nemati, F.J. Fard, Conventional and advanced exergy analyses of a geothermal driven dual fluid organic Rankine cycle (ORC). Appl. Therm. Eng. **122**, 59–70 (2017)
37. F. Petrakopoulou, G. Tsatsaronis, T. Morosuk, Evaluation of a power plant with chemical looping combustion using an advanced exergoeconomic analysis. Sustain. Energy Technol. Assess. **3**, 9–16 (2013)
38. A. Moharamian et al., Advanced exergy and advanced exergoeconomic analyses of biomass and natural gas fired combined cycles with hydrogen production. Appl. Therm. Eng. **134**, 1–11 (2018)
39. H.V. Modabber, M.H.K. Manesh, Optimal exergetic, exergoeconomic and exergoenvironmental design of polygeneration system based on gas Turbine-Absorption Chiller-Solar parabolic trough collector units integrated with multi-effect desalination-thermal vapor compressor-reverse osmosis desalination systems. Renew. Energy **165**, 533–552 (2021)

Chapter 6
Principle of Life Cycle Assessment and Cumulative Exergy Demand for Biodiesel Production: Farm-To-Combustion Approach

Ashkan Nabavi-Pelesaraei, Shahin Rafiee, Naghmeh Mohammadkashi, Kwok-wing Chau, and Fatemeh Mostashari-Rad

Abstract Decreasing petroleum sources and growing requests for emission attributes of fossil fuel combustion and energy lead to researches on clean, accessible, and inexpensive energy resources. On the other hand, environmental burden that is imposed on nature through biodiesel production and its combustion has also been considered in recent years. Previous studies also focused on the production process and sometimes the exhaust emissions. However, in order to adopt the right policies, a comprehensive analysis requires a review of the entire process from farm-to-combustion. Besides, environmental studies without considering the energy consumption cannot indicate the efficiency of the produced biodiesel. Therefore, the cumulative exergy demand (CExD) method, as a new approach in determining the amount of useful energy consumed in systems, has been used for several years and the lack of this approach can be seen in the study of biofuel production. Accordingly, in

A. Nabavi-Pelesaraei (✉)
Department of Mechanical Engineering of Biosystems, Faculty of Agriculture, Razi University, Kermanshah, Iran
e-mail: a.nabavi@razi.ac.ir

S. Rafiee
Department of Agricultural Machinery Engineering, Faculty of Agricultural Engineering and Technology, University of Tehran, Karaj, Iran
e-mail: shainrafiee@ut.ac.ir

N. Mohammadkashi
Department of Horticultural Science, Faculty of Agricultural Science & Engineering, University of Tehran, Karaj, Iran
e-mail: n.mohammadkashi@ut.ac.ir

K. Chau
Department of Civil and Environmental Engineering, Hong Kong Polytechnic University, Hung Hom, Kowloon, Hong Kong
e-mail: cekwchau@polyu.edu.hk

F. Mostashari-Rad
Department of Agricultural Biotechnology, Faculty of Agricultural Sciences, University of Guilan, Rasht, Iran
e-mail: mostashari@msc.guilan.ac.ir

this chapter, all stages of biodiesel production from cradle-to-grave including agricultural phase, oil extraction, biodiesel production, combustion and finally power generation are studied from life cycle assessment (LCA) and CExD point of view. Moreover, all these steps along with how to interpret the results are explained with examples.

Keywords Bioenergy · Biofuel · Environmental impact · Exergy · Oilseed

Nomenclature

$°C$	Celsius degree
ASTM	American society for testing and materials
B20	80% w/w diesel + 20% w/w biodiesel
B20A3	80% w/w diesel + 20% w/w biodiesel (97% biodiesel and 3% of glycerol additive)
B5	95% w/w diesel + 5% w/w biodiesel
B5A3	95% w/w diesel + 5% w/w biodiesel (97% biodiesel and 3% of glycerol additive)
bTDC	Before top dead center
BTE	Brake thermal efficiency
C_6H_6	Benzene
Cd	Cadmium
CH_4	Methane
CI	Compression ignition
CO	Carbon monoxide
CO_2	Carbon dioxide
Cr	Chromium
cSt	Centistokes
Cu	Copper
CV	Calorific value
DALY	Disability adjusted life years
DC	Direct current
EMA	Engine Manufacturers' Association
FAO	Food and Agriculture Organization
FU	Functional unit
GHG	Greenhouse gas
GHz	Gigahertz
GJ	Gigajoule
gr	Gram
h	Hour
H_2	Hydrogen
HC	Hydrocarbons
HCl	Hydrochloric acid

|	
Hg	Mercury
IC	Internal combustion
K$_2$O	Potassium
kg	Kilogram
kW	Kilowatt
L	Liter
LCA	Life cycle assessment
LCI	Life cycle inventory
LCIA	Life cycle impact assessment
m^3	Cubic meter
mg	Milligram
MHz	Megahertz
MJ	Mega joule
mm	Millimeter
N.m	Newton meter
N$_2$O	Dinitrogen monoxide
NaOH	Sodium hydroxide
NG	Natural gas
NH$_3$	Ammonia
Ni	Nickel
NMVOC	Non-methane volatile organic compound
NO$_3^-$	Nitrate
NOx	Nitrogen oxides
O$_2$	Oxygen
P$_2$O$_5$	Phosphate
Pa	Pascal
PAH	Polycyclic aromatic hydrocarbon
Pb	Lead
PO$_4^{3-}$	Phosphate
ppm	Parts per million
rpm	Revolutions per minute
s	Second
Se	Selenium
SI	Spark-ignition
SO$_2$	Sulfur dioxide
t.km	Ton in kilometer
USA	United States of America
USD2013	United States dollars for 2013
V	Volt
yr	Year
Zn	Zink
μm	Micrometer

6.1 Introduction

During the recent decade, many concerns have been raised around issues associated with the depletion of fossil fuels and the impacts of global warming, which have in turn strongly encouraged researching biofuel production. The production of vegetable-oil biofuels and biofuels extracted from bioethanol benefit largely from the current delivery systems and technology. In addition, CO_2 emissions associated with the combustion of biofuels are generally less than that of fossil fuels. In contrast, biofuel production technology has negative impact on the environment due to the increasing use of pesticides and fertilizers. Furthermore, such technologies can enhance competition for the land that are normally used for the production of food crops. Hence, using biofuels as an alternative to fossil fuels has been considered disputable and found to be controversial [1].

The increasing cost of petroleum in the global bazaar, along with reducing sources of non-renewable fossil fuels, have increased worries and triggered for renewable energy sources as the replacement for fossil fuels. Moreover, as previously recognized, the use of fossil fuels generate a huge amount of GHG emissions that eventually contaminate the environment [2].

The utilization of biodiesel as a substitute fuel can draw global attention from fossil fuels to biofuels. Biodiesel has caught the notice of researchers due to its great potential as part of a renewable energy mix and as a stable energy supply in the time to come. Biodiesel has a more beneficial combustion emission profile, in comparison with fossil fuels diesel, like having less emissions of CO, SO_2 and unburned HC. Biodiesel is obtained from renewable fatty substances like vegetable oils (virgin or used) or animal fats (tallow), mainly by utilizing transesterification procedure with an alcohol which has certain gases like methanol as well as ethanol plus consuming alkali catalyst or an acid. Fatty acid methyl and ethyl esters known as biodiesel are the outcomes as well as glycerol, which is considered as a byproduct [3]. FAO [4] reported that a universal biodiesel production will arrive at 39.3 billion L by 2027, equivalent to a 9% raise from the 2017 level. Figure 6.1 shows the physical amount of biodiesel production in the world.

Biodiesel is made from various types of oilseed crops as well as fats of some animals. Vegetable oil is gained from oilseed and also considered as a sort of renewable source, so it can be produced easily. In addition, its properties have similarities to diesel fuel [5]. The benefits of employing vegetable oils for diesel fuel are based on factors such as their abilities to be immediate available, inexhaustible and less sulfur in addition to fragrance and decomposability [6]. The utilization of vegetable oils as a useful source became possible for scientists when they recognized diesel engines [7, 8]. Diesel engines are important origin of potency for conveyances. In comparison with gasoline engines, diesel engines allocate the majority of universe sources which are effective in terms of energy. Most fuels are used by off road and on road conveyances, generators, nautical transporting, husbandry, industrial departments, etc. Because of the following reasons, diesel engines are more desirable than gasoline engines: economical fuel usage, great power transfer, inflexible structure
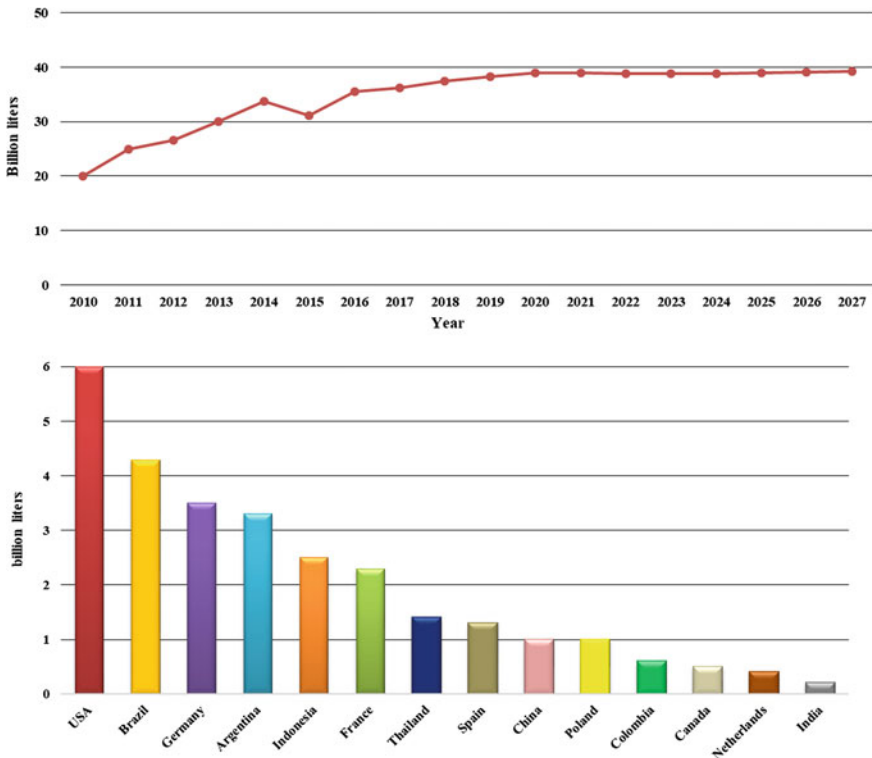
Fig. 6.1 Statistics of physical amount of biodiesel production in the world and the leading production countries

and superior BTE [9]. One of the remarkable parameters in diesel engines is the emission of pollutants like CO, HC, NOx, and smoke. Nowadays, scientists are trying to discover sources so that the structure of the engine does not change but the amount of emissions decreases. Persistent disposal of emission leads to suffocation, which affects lungs negatively and stings eyes [10].

Despite beneficial properties of biodiesel, there is still slight amount of pollutions, which is produced during the combustion process [11, 12]. For example, one of the main deficiency of biodiesel fuel is the excess NO_x emission via the use of biodiesel *versus* diesel [13, 14]. Accordingly, different methods have been used to lessen exhaust emissions of biodiesel including betterment of engines, improving the efficiency of fuel and characterization of emission through adding fuel supplement along with technologies related to exhaust gas purification [15]. Amongst all mentioned solutions, making a few corrections in fuel attributes in order to improve the combustion procedure is probably the best possible remedy because there is no need for engine correction and additional equipment. In this way, a variety of additives, which were based on metal, oxygenated supplements, enhancers of cold flow, antioxidants, etc., were used for biodiesel as well as combinations of biodiesel [15].

Actually, choosing suitable additives is important because they have fundamental effect in reducing costs and possible functional difficulties. It also decreases probable fuel special needs, otherwise that might cause difficulties or not possible in the absence of their application [15].

Selecting appropriate additives for use in biodiesel depends upon many factors including characteristics of fuel combination, economic feasibility, toxicity, water separation of the additive, fuel blend's viscosity, solvability of additive, flashing point for the mixture of fuel and water solvability for the mentioned mixture [16].

LCA facilitates all aspects of environmental assessment of a product to be undertaken from when the product is raw and/or at its extraction stage to when the final product is made and can continue until the product reaches its final disposal stage. As a result, LCA contains all different parts of a life cycle for an output [17]. LCA supports informed decision-making process by quantifying and assessing all relevant environmental inputs and outputs during a production containing the entire life cycle; and hence allows a complete comparative evaluation of existing and proposed technical solutions [18]. The framework for the LCA approach has been internationally adopted and is supported by several well-known practices and environmental standards such as ISO 14040 and ISO 14044, which are known for the assessment of requirements and the impacts of products, technologies and various processes [19]. LCA is generally utilized for evaluating environmental impacts within a system, activities or goods during the entire life cycle [20]. Certain main targets for undertaking LCA are known as providing comprehensive evaluation and comparing the environmental and social impacts of a product or a service to enable feasible comparisons for scoping and selection of the best alternative options [21]. LCA scope can differ with regards to accepted approaches. A cradle-to-grave approach is known as a comprehensive LCA, which begins at the resource extraction stage (cradle) and finishes at disposal stage (grave). However, cradle-to-gate is referred to partial life cycle for an outcome between the resource extractions (cradle) as well as the time it reaches the product factory gate and excludes the emissions that are associated with usage and disposal of the product [22]. From fuel (energy) production point of view, the above-mentioned terms can be modified to well-to-wheels and well-to-pump LCA. Well-to-wheel includes all emissions that are made and all energy that is required for the fuel production (well-to-pump) as well as emissions and operational energy related to vehicle technologies taking into account emissions associated with engine efficiency [17].

LCA can help to recognize chances to better environmental aspects of products from a different point of view in their life cycle; making decision in different places such as industrial, official or private establishments (e.g. targeted outlining, precedence ordering, design of goods, activities or reforming); choosing indexes related to environmental efficiency, containing techniques of measurement; and marketing (e.g. environmental assertion, eco-labelling design or environmental product annunciation) [23].

CExD is considered as a practical tool in this research. It clearly demonstrates the use of energy simulation for a particular process of the production line. It relates the system characteristics and the associated emissions because it is completely reliant

on the system condition as well as the environment [24]. As a matter of fact, CExD is well-known as one of the highly valuable methods for the reduction of exergy. The destruction of a cycle's exergy is shown by adding exergy destruction values within all processes comprising the cycle [25]. To verify the exergy destruction of a cycle, a unique exergy destruction formula is proposed considering that the complete cycle is a single process [26].

Table 6.1 summarizes various LCA studies that are performed on the production of biodiesel from agricultural raw materials and provides information on environmental impacts for the combustion of this type of biofuel.

The production of biodiesel from crops is the first generation of biofuels. However, it should be noted that biodiesel is 100% natural and is still one of the main clean alternatives to fossil fuels in the world. Moreover, most of biodiesel production is based on plant products. Many studies have been done on pollution emissions in this area. However, as shown in Table 6.1, each considered only part of the biodiesel production process and did not include all stages from field production to combustion. In addition, CExD as an indicator of the useful energy consumption has not yet been considered in the stages of fuel production as well as power generation. To this end, the present chapter intends to consider CExD of all the steps of this process, in addition to providing a complete and comprehensive instruction in relation to LCA and the actual study of cradle to grave in the production of biodiesel from farm production to power generation. In fact, the content of this chapter can be used as a set of principles for a comprehensive study of exergoenvironmental aspects in biodiesel production in any part of the world.

6.2 Farm-To-Combustion

6.2.1 Case Study, Data Collection and Oilseeds Production

The first stage of biodiesel production includes field production of oilseeds. Examining this step should fully follow the principles outlined below:

- Determining the physical amount of oilseed yield in the region
- Determining the amount of biodiesel production in the region from cultivated oilseeds
- Determining the geographical location of the studied area
- Checking the total number of farmers in the studied area to determine the sample size
- Determining necessary agricultural operations to produce oilseeds
- Compiling a standard questionnaire to obtain information related to each agricultural operation
- Gathering information, categorize and sort them.

Table 6.1 A summary of the studies carried out on different oil seed crop, biodiesel production and engine combustion

Surveyed study	Geographical scale	System boundary			Engine combustion	Exhaust emissions	LCA method	Reported results content
		Agricultural phase	Biodiesel production					
			Without additive	With additive				
Kim and Dale [27]	USA	☑	☑	✗	✗	✗	TRACI	Partially reviewed
Peiro et al. [28]	Spain	✗	☑	✗	☑	✗	CML	Full reviewed
Collet et al. [29]	France	☑	☑	✗	☑	✗	CML	Full reviewed
Oprescu et al. [30]	Romania	✗	✗	Glycerol derivatives	☑	☑	✗	Partially reviewed
Tarabet et al. [31]	Algeria	✗	☑	✗	☑	☑	✗	Partially reviewed
Lounici et al. [32]	Algeria	✗	☑	✗	✗	☑	✗	Partially reviewed
Lapuerta et al. [33]	Spain	✗	✗	✗	☑	☑	✗	Partially reviewed
Imtenan et al. [34]	Malaysia	✗	✗	n-butanol and diethyl ether	☑	☑	✗	Partially reviewed
Moecke et al. [35]	Brazil	✗	☑	✗	☑	✗	IPA	Partially reviewed
Zare et al. [36]	Australia	✗	✗	Triacetin	☑	☑	✗	Partially reviewed
Srinivasa Rao and Anand [37]	India	✗	☑	AlO (OH) nanoparticles	☑	☑	✗	Partially reviewed

(continued)

Table 6.1 (continued)

Surveyed study	Geographical scale	System boundary				Exhaust emissions	LCA method	Reported results content
		Agricultural phase	Biodiesel production		Engine combustion			
			Without additive	With additive				
Hosseini et al. [38]	Iran	☒	☒	alumina	☑	☑	☒	Partially reviewed
Sharma et al. [39]	India	☒	☒	Tyre pyrolysis oil	☑	☑	☒	Partially reviewed
Zareh et al. [40]	Iran	☒	☑	☒	☑	☑	☒	Partially reviewed
Paul et al. [41]	India	☒	☑	☒	☑	☑	☒	Partially reviewed
Forleo et al. [42]	Italy	☑	☑	☒	☒	☒	CML–IA	Full reviewed
Nabi et al. [43]	Australia	☒	☑	☒	☑	☑	☒	Partially reviewed
Sidhu et al. [44]	Canada	☒	☒	Glycerin	☑	☑	☒	Partially reviewed
Yıldızhan et al. [45]	Turkey	☒	☒	H_2	☑	☑	☒	Partially reviewed
Abed et al. [46]	Egypt	☒	☒	☑	☑	☑	☒	Partially reviewed

(continued)

Table 6.1 (continued)

Surveyed study	Geographical scale	System boundary					LCA method	Reported results content
		Agricultural phase	Biodiesel production		Engine combustion	Exhaust emissions		
			Without additive	With additive				
Thangaraj et al. [47]	India	☒	☒	☑	☑	☑	☒	Partially reviewed
Alloune et al. [48]	Algeria	☒	☒	☑	☑	☑	☒	Partially reviewed
Dinesha et al. [49]	India	☒	Diethyl ether	☑	☑	☑	☒	Partially reviewed
Asokan et al. [50]	India	☒	☒	☑	☑	☑	☒	Partially reviewed
Krishna et al. [51]	Thailand	☒	Ethanol	☑	☑	☑	☒	Partially reviewed
Raman et al. [52]	India	☒	☒	☑	☑	☑	☒	Partially reviewed
Devarajan et al. [53]	India	☒	Di-methyl-carbonate	☑	☑	☑	☒	Partially reviewed
Akbarian and Najafi [54]	Iran	☒	Glycerol triacetate	☑	☑	☑	☒	Partially reviewed
Cavalcanti et al. [55]	Brazil	☒	☒	☑	☑	☑	Eco-indicator 99	Partially reviewed

(continued)

Table 6.1 (continued)

Surveyed study	Geographical scale	System boundary				Exhaust emissions	LCA method	Reported results content
		Agricultural phase	Biodiesel production		Engine combustion			
			Without additive	With additive				
Ghasemi-Mobtaker et al. [56]	Iran	☑	☒	☒	☒	☒	ReCiPe2016	Full reviewed
Saranya and Ramachandra [17]	India	☒	☒	☒	☒	☒	Life cycle energy	Partially reviewed
Khanali et al. [57]	Iran	☑	☒	☒	☒	☒	IMPACT 2002 +	Full reviewed
Nabavi-Pelesaraei et al. [58]	Iran	☑	☒	☒	☒	☒	IMPACT 2002 +	Full reviewed

The amount of oilseeds production, their share in biodiesel production and the total amount of biodiesel production can be extracted and cited from the official statistics of national organizations such as the annual statistics of the Ministries of Agriculture, Industry and Commerce or can be obtained from international organizations such as FAO.

In explaining the geographical characteristics, the location of the study area, including the country and province, should be mentioned.

Adequate explanations in this section, in addition to creating a good knowledge of the studied area for readers, can show the importance of the case study in terms of oilseed production. It can provide the possibility of comparing different agricultural systems in other places for researchers and, in case of geographical similarities, they can generalize the results to their regions. It should be noted that this introduction will definitely be more effective if it is accompanied by schematic diagram.

An example of a description of a study area in Brazil is as follows:

This study is accomplished in Santa Catarina state, which is the major center of oilseeds and biodiesel production in Brazil. The state of Santa Catarina is specifically situated in the south district of Brazil, within 48° 19′ and 53° 50′ east longitude and 25° 57′ and 29° 24′ north latitude [59]. Furthermore, Santa Catarina is known as the ninth state, including 295 different city halls. Santa Catarina state consists 3.4% of the population in Brazil as well as managing 3.8% of the whole country's gross domestic product [60]. The location of this state in Brazil is shown in Fig. 6.2.

In most cases, the large number of farmers makes counting them and collecting operational information very time consuming and costly [61]. For this reason, in most agricultural studies, random sampling method is used for data collection but the important point in using this method is that the correct number of samples must be

Fig. 6.2 Location of Santa Catarina state in the south of Brazil as an example for case study

examined. Actually, choosing the right sample size is very important in the accuracy of results. One of the most reliable methods in determining the sample size is the Cochran method [62], which is described as follows:

$$n = \frac{\frac{z^2 pq}{d^2}}{1 + \frac{1}{N}(\frac{z^2 pq}{d^2} - 1)} \tag{6.1}$$

where:

d   is the allowable error ratio derived from the mean population (= 0.05),
p   is the measured proportion of an attribute within the population (= 0.5), q is 1-p (= 0.5).
n   is the entailed sample size.
z   is the reliability coefficient (= 1.96 at 95% confidence level), and.
N   is the whole population of farmers.

After that, the types of agricultural operations and their order should be examined. Different studies showed that the order of agricultural operations in oilseeds production usually included land preparation, including primary and secondary tillage, planting seeds, operations including fertilizing, spraying, irrigation, and finally harvesting of oilseeds yields [58, 63–68].

After having determined agricultural operations, a comprehensive questionnaire should be designed to collect information so that it contains all data related to all the above-mentioned operations and at the same time is concise and useful. An example of a common questionnaire in oilseed production is shown in Fig. 6.3.

6.2.2 Oil Extraction Process

Generally, oil extraction methods are divided into two categories, namely conventional and innovative techniques.

6.2.2.1 Conventional Methods of Oil Extraction

Solvent extraction as well as mechanical expression are two popular and widely practiced methods for oil extraction [69]. The solvent extraction approach is known as a typical extraction method frequently used for oilseeds with little oil, i.e., less than 20 percent of oil, such as soya bean. The mentioned method is known as one of the most effective approaches for extraction of vegetable oil, resulting in less residual oil remained in a muffin [70]. The selection of the solvent is mostly based on the maximum leaching limits of the appropriate solute substrate [71]. Common solvents that are normally used are hexane, petroleum ether, diethyl ether, and ethanol.

Fig. 6.3 An example for designed questionnaire for data collection

❖ Questionnaire No: …
❖ Date: 2021/…/…
❖ The total are under cultivation: …
❖ Duration of the production: …
❖ Total weight of seed use: …
❖ Yield per functional unit (ha): …
❖ Number of fixed labors: …
❖ Number of daily labors: ….
❖ Daily working hours: ….
❖ Machinery operation used: …
❖ Types of machinery used: …
❖ Total weight of machinery per year: …
❖ Types of fuel used: …
❖ Total fuel consumption: …
❖ Types of chemical fertilizers: …
❖ Total weight of chemical fertilizers from each type: ….
❖ Types of chemical biocides: ….
❖ Total weight of biocides from each type: …
❖ Total weight of FYM use: …
❖ Rate of electricity consumption for each implement: …
❖ Total electricity consumption: …

Mechanical expression includes the utilization of force via hydraulic or screw presses, which forces oil out of an oil-bearing material [69]. By employing the mentioned method, oil yield is improved by rising mechanical force on the oil-bearing material. Methods involving mechanical press are normally utilized for the extraction of vegetable oil from oilseeds that contain more than 20% oil content [72]. Usually, having low performance cost and making top quality and light-colored oil with minimum free fatty acid concentration are its advantages, but this method has approximately less performance in comparison with solvent extraction. Therefore, it is comparatively inefficient and often maintains a large portion of oil left in the meal or cake after extraction. In addition, this method is found to be time wasting and laboring [73]. For example, for castor oil extraction, mechanical pressing removes only around 45% of oil, and the remaining oil in the meal can only be extracted using the solvent extraction method [74]. Two types of mechanical press methods, named cold-press and hot-press methods, are available. Cold-press or scarification method is conducted at low temperature (less than 500 °C) and force whilst hot-press method can be undertaken at higher temperature and force. Cold-pressed seed oils are often found to be more secure than hot-pressed seed oils. This is due to the fact that adverse

effects may be caused by high temperatures in hot-pressed methods, which can be avoided in cold-pressed approaches. The reduction of oxidative solidity, decreasing oil storing condition as well as deterioration of worthy oil contents are some of the probable negative consequences. The purity and natural properties of seed oils can be maintained in cold-pressed oils [75].

6.2.2.2 Innovative Techniques of Oil Extraction

Several methods are known as innovative techniques for oil extraction. Among all methods, microwave-assisted extraction and ultrasonic-assisted extraction are main methods that are described as follows.

Microwave-assisted extraction is one of innovative methods to isolate vegetable oils from oilseeds. This has also been applied in the extraction of important oils [76]. This method is not complicated; however it is crucial for many other thermal methods that are utilized for extracting top quality vegetable oils. Pre-treatment of oilseed is performed in a microwave oven. This method uses telectromagnetic radiation for transporting well as turning energy to hotness at frequencies around 300 megahertz to 300 gigahertz [69]. Microwave radiation is used for processing oilseeds, which causes split of cytomembrane, making it feasible to achieve more extraction yield with a growth in mass transfer coefficients [75].

The advantages of this method are as follows [69]:

- Enhancing oil extraction quality as well as yield
- Reduction in the use of energy
- Straight extraction capacity
- Higher developing time
- Reduction in the use of solvent.

Ultrasonic-assisted extraction is considered to be a new innovative technique, which benefits from ultrasonic sound waves to rise hotness as well as vibrancy, and results in wall destruction of the rigid plant cells, hence enhancing the contact between solvent and the plant material [77]. Therefore, when joined with solvent extraction, the ultrasonic-assisted extraction method proves to be an innovative way for increasing extracted oil yield by making plant cell walls thinner, and then improving the interaction with the solvent.

The following are the benefits of the Ultrasonic-assisted extraction method [78]:

- Decrease in extraction time
- Being ecofriendly with minimal use of energy
- Higher processing and rise in extraction yield.

6.2.3 Biodiesel Production and Glycerol Additive

Histories of biodiesel and diesel engine are approximately the same. Rodulf Diesel presented the first diesel engine with the goal of operating on vegetable oil. He patented his engine in 1892. In 1900, Rodulf Diesel successfully applied the engine on peanut oil for some hours. He foretold in 1912 that vegetable oil would be a fuel similar to diesel oil in future [79].

Several methods have been so far established and are currently made available for production of biodiesel fuels. It was found sensible to modify the properties of crude oils by reducing their viscosity so that they become appropriate for combustion in engines. Many methods have been made accessible for this alteration of oils to produce a better quality of biodiesels. There are four main methods/procedures to achieve this modification: mixture of crude oils, pyrolysis, microemulsions and transesterification [80].

6.2.3.1 Blending of Crude Oils or Dilution

In order to enhance the viscosity of crude vegetable oils and remove issues related to high viscosities of pure vegetable oils in compression ignition engines, vegetable oils can be directly mixed or diluted with diesel fuel. In 1980, a 10% mixture of vegetable oil is used by Caterpillar Brazil in order to keep the total power of the engines without performing any modifications or adjustments to engines. For this, a mixture of 80% diesel fuel and 20% vegetable oil was used and reported to be successful [81]. Besides, a blend of 25% sunflower oil with 75% diesel fuel with a viscosity of 4.88 cDt at 40 °C was used and studied by Koh et al. [82]. In addition, the viscosity of a blend of 25 parts of high oleic sunflower oil and 75 parts of diesel fuel was described as 4.92 cSt at 40 °C, which successfully passed the 200 h EMA test.

6.2.3.2 Micro-Emulsification

Microemulsion is considered as another method for decreasing vegetable oil viscosity. Microemulsions have stability and they are clear isotropic fluids comprising three phases, namely an aqueous phase, an oil phase, and a surfactant. The aqueous phase might have salts or other constitution. The oil phase however may include a sophisticated mixture of various olefins as well as hydrocarbons. Explosive vaporisation of the little boiling which are in the micelles can be used at this ternary phase to enhance the spray characteristics. All micro-emulsions including hexanol, butanol and octanol are able to meet the maximum viscosity limits defined for diesel engines [82]. A 200 h EMA examination was conducted on a microemulsion by a mixture of methanol, soya bean oil, 2-octanol and cetane improver in the ratio of 52.7:13.3:33.3:1.0, and satisfactory results were obtained [83].

6.2.3.3 Pyrolysis

Pyrolysis is defined as the process of changing one element into another using heat or by means of a catalyst without air or oxygen. Pyrolysis can happen for various materials including vegetable oils, organic fatty acids, animal fat and methyl ester of fatty acids [82]. Using standard ASTM approach described for distilling, Soya bean oil can be thermally degraded in air. Pyrolysed soya bean oil, which has distilled, has a viscosity of 10.2 cSt at 37.8 °C. This is more than the range stated by ASTM for No.2 diesel fuel. However, this viscosity value is satisfactory since it is still well below soya bean oil viscosity [82].

6.2.3.4 Transesterification

Transesterification or alcoholysis is a process wherein an alcohol derived from an ester is replaced by another alcohol in a process similar to hydrolysis, except that in this process alcohol is consumed rather than water [84]. This process is utilized to decrease triglyceride's viscosity. Transesterification reaction is demonstrated via the following equations:

$$
\underset{\text{Ester}}{RCOOR^1} + \underset{\text{Alcohol}}{R^2OH} \underset{}{\overset{\text{Catalyst}}{\longleftrightarrow}} \underset{\text{Ester}}{RCOOR^2} + \underset{\text{Alcohol}}{R^1OH}
\tag{6.2}
$$

When methanol is utilized in this process, it is termed methanolysis. Triglyceride methanolysis is demonstrated in (6.3):

$$
\begin{array}{c}
CH_2 - OCOR^1 \\
| \\
CH - OCOR^2 \\
| \\
CH_2 - OCOR^3 \\
\text{Triglyceride}
\end{array}
+ \underset{\text{Methanol}}{3CH_3OH} \overset{\text{Catalyst}}{\longleftrightarrow}
\begin{array}{c}
CH_2OH \\
| \\
CHOH \\
| \\
CH_2OH \\
\text{Glycerol}
\end{array}
+
\begin{array}{c}
R^1COOCH_3 \\
R^2COOCH_3 \\
R^3COOCH_3 \\
\text{Methyl ester}
\end{array}
\tag{6.3}
$$
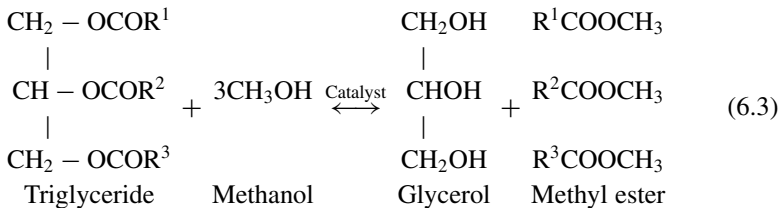
Transesterification is a reversible reaction and goes on necessarily via blending the reactants, although the addition of a catalyst (a strong base or acid) speeds up the conversion.

Glycerol and fatty acid alkyl esters are products of transesterification of triglycerides. A layer of glycerol would settle down at the bottom of the reaction container. The intermediate products in this process are diglycerides and mono-glycerides. The mechanism of transesterification is demonstrated in (6.4) [85]:

$$
\begin{array}{l}
\text{Triglyceride} + R^1OH \leftrightarrow \text{Diglyceride} + RCOOR^1 \\
\text{Diglyceride} + R^1OH \leftrightarrow \text{Monoglyceride} + RCOOR^1 \\
\text{Monoglyceride} + R^1OH \leftrightarrow \text{Glycerol} + RCOOR^1
\end{array}
\tag{6.4}
$$
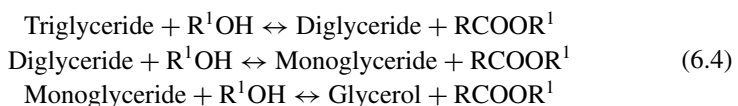
6.2.3.5 Additives

In order to minimize exhaust emissions associated with the combustion of biodiesels, different methods have been proposed so far. These methods include engine improvement, enhancement of emission characteristics using fuel additives, improvement of fuel performance as well as introduction of novel technologies to treat exhaust gases [15]. Amongst all methods, altering fuel characteristics to improve the combustion process is likely to be the most feasible option due to the fact that for this method no engine modification and/or extra equipment is required. Besides, many fuel additives including antioxidants, cold flow enhancers, oxygenated and metal-based additives have already been used and tested for various biodiesels and blends [86]. As a matter of fact, using additives is proven to be cost-effective. In addition, additives have been shown to be effective in reducing potential operational issues and complying with fuel specification requirements, which can be challenging to be met without the use of additives [15]. The selection of additives for biodiesels is dependent on a number of parameters including economic feasibility, solubility of additives, blending properties of fuels, toxicity and viscosity of fuel blend, water solubility in the fuel blend, and the additive water partitioning factor [16]. In general, using additives can resolve some major technical issues related to use of biodiesels [87].

6.2.4 Combustion Sector

Engines are the last stage of the life cycle of any fuel. Engine combustion is a series of sequence chemical reactions occurring between fuel molecules (reductant) and oxidant molecules such as oxygen. Combustion produces heat and mixture of gaseous emissions as its products. It should be noted that carbon and hydrogen are the main fuel elements that contribute to the combustion process regardless of what type of fuel being combusted. Hence, under a complete combustion condition (i.e. ideal condition), water and carbon dioxide are the only expected combustion products [88]. Nevertheless, under practical conditions, a complete combustion is unlikely to achieve and most likely a series of other gases and emissions such as CO, HC, NOx and PM, etc. will be generated [89]. Therefore, generally, emissions from combustion products generate both grave environmental effects such as climate change, global warming and greenhouse effects as well as grave impacts on human health [90].

The first stage of combustion evaluation is preparing fuel blends. Two types of B5 and B20 fuels are commonly used for engine test. After that, additives will be added. Pure combustion of diesel fuel is also determined as control treatment in different researches. It is important to note that whole blends are usually examined with 5 rates of engine load, namely, 0, 25, 50, 75 and 100% of full load. A single cylinder, 4-stroke, conventional diesel engine accompanied with DC generator is utilized to analyze the efficiency and emissions of various strategies on diesel/biodiesel blends. Furnishing characteristics of the engine is essential for better understanding of the test situation. In Table 6.2, the characteristics of a sample engine are presented.

Table 6.2 Specifications of a sample diesel engine test with the single cylinder and four-stroke

Engine parameter	Specification
Model	DEUTZ F1L511
Cylinder number	1
Engine type	4 cycle, Direct injection, naturally aspirated
Cooling method	Air-cool
Bore*stork (mm*mm)	100*105
Compaction ratio	17:1
Displacement (L)	0.824
Maximum torque (N.m)	44 N.m @ 900 rpm
Maximum power (kW)	5.7 kW@ 1500 rpm
Injection nozzle	4-Hole nozzle
Fuel delivery advance (° bTDC)	24
Fuel delivery pressure (MPa)	17.5
Net weight (kg)	110

Table 6.3 The accuracy of sample experimental equipment with the rate of parameters uncertainties that used in engine test

Item	Measuring instrument	Accuracy
DC generator	MEZ-BURNO	1 V
Fuel flow meter	Portable fuel consumption gauges FC-102–2	1 A/s
Air flow meter	Extech Division AN100	1 m^3/s
CO	AVL DiSmoke 4000 gas analyzer	0.01%
CO_2	AVL DiSmoke 4000 gas analyzer	0.01%
HC	AVL DiSmoke 4000 gas analyzer	1 ppm
NOx	AVL DiSmoke 4000 gas analyzer	1 ppm
O_2	AVL DiSmoke 4000 gas analyzer	0.01%

Exhaust emissions analysis is the last step of engine test for biodiesel. In this step, emissions to air related to combustion of produced blends such as NOx, CO, CO_2, HC, etc. should be measured by accurate emission analyzer. Characteristics of AVL DiSmoke 4000 emission analyzer are tabulated in Table 6.3 as an example.

6.3 LCA Method

LCA is found to be one of most powerful tools to evaluate environmental impacts of a product (for instance a biodiesel) during its process lifetime, from agricultural products and oil extraction to combustion and power generation [91]. Adequate and
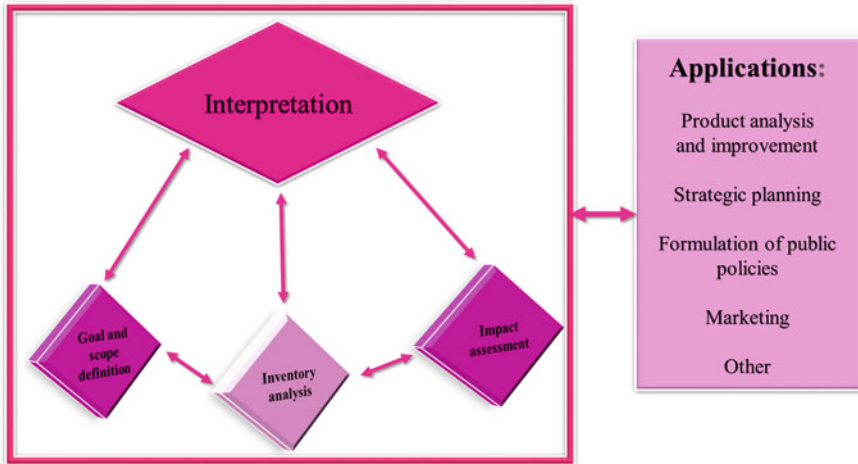
Fig. 6.4 Relation between four steps of LCA

useful information related to environmental impacts for the product chain can be obtained using this effective and organized method [92]. This information can then be used to form a decision-making tool to produce the best process design that can minimize environmental footprints [93]. Assessing input and output data of the net material and energy, an LCA provides the best estimates of environmental impacts associated with the process over its life cycle [94]. LCA includes four main stages and their relationship is shown in Fig. 6.4.

6.3.1   Goal and Scope Determination

One of the first steps to perform LCA is to define the scope and goal. For goal and scope definition, FU determination and system boundary definition are considered to be the main steps [56]. Target of studies related to biodiesel production is different depending on system boundary. In a comprehensive investigation, system boundary starts by agricultural production of oilseeds in farms and continues with biodiesel production and finally, its combustion in IC engine. An example of system boundary for a comprehensive study is shown in Fig. 6.5.

FU is defined as a measure to determine the system function from inputs and outputs provided within an LCA [95]. Therefore, the selection of FU significantly impacts the results of LCA [91]. In comprehensive studies, the physical amount of power generation by IC engine such as 1 kWh has been usually selected as FU. It should be noted that in different stages, depending on the nature of the issue, FU may be defined by different units. For example, for agricultural production of oilseeds, 1 t
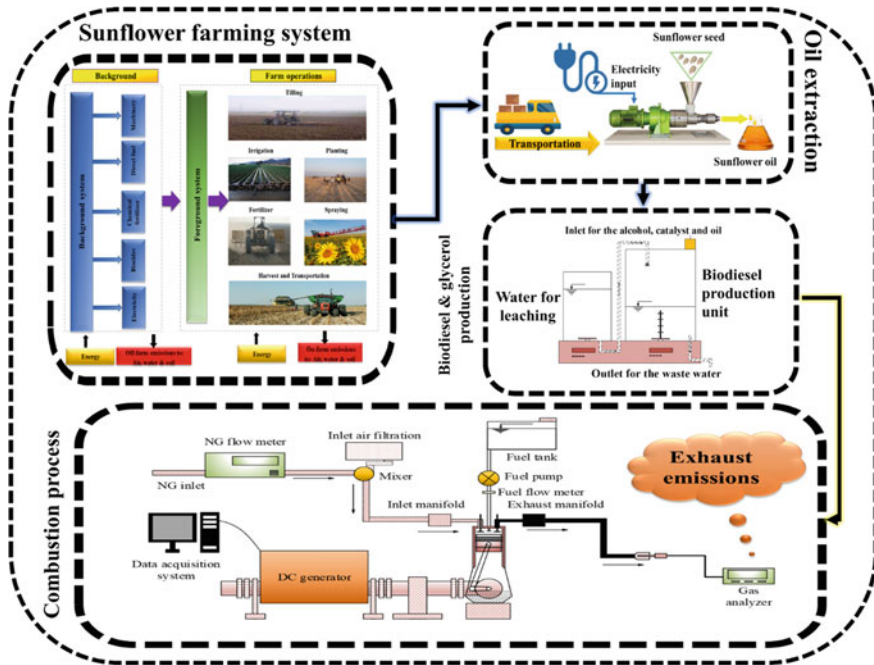
Fig. 6.5 System boundary including farm to combustion process of production and consumption of fuel samples

of harvested crop is usually defined as Fu but in the end, all of them must be based on the same engine production capacity in the system.

6.3.2 LCI

In LCI, the study is on all inputs and outputs of the environment comrades to a service or product, like using crude matter and energy, the emission of contaminant, and the flow dissipation [96]. Amid these steps, the LCI analysis produces a life-cycle model that involves all inputs with outputs of the FU process as well as collecting all relevant interventions, i.e., the release of environmental loads and resource consumption [97].

In a comprehensive study, to complete LCI, all inputs, energy and materials should be inserted from the first stage including the agricultural production of oilseeds (from the farm gate to harvest step), then the information about the oil extraction, data of the biodiesel production process with/without additives and finally fuel ignition into the CI engine and power generation based on the FU. During each of the mentioned stages, there are two categories of indirect and direct emissions. Indirect emissions are related to the production of any input outside the system and direct emissions are related to the consumption of some inputs in the system, which must be extracted

by various sources such as different databases. All direct emissions that should be considered during the farm-to-combustion process are explained in the following.

Two main steps that need computatin of indirect emissions are farm production of oilseeds and combustion of produced biodiesel in IC engine. In agricultural phase, first direct emissions are related to diesel fuel combustion in agricultural machinery so that extracted standard coefficients of EcoInvent®3.6 database [98] can be used for computing emissions to air and soil.

Second direct emissions are related to fertilizer consumption to air, and water [99] and emissions derived from heavy metals content to soil [100]. The mentioned standard coefficients are shown in Fig. 6.6.

Final direct emissions are related to biocides to soil, water, and air. Coefficients introduced by Margni et al. [101] can be used for biocide direct emissions to soil whilst biocide direct emissions to air and water can be attained by PestLCI 2.0 model. In fact, two different levels of emission distributions are used by PestLCI 2.0 model. Early processes, which occurred minutes after the biocide application, are covered by primary (or initial) mass distributions. However, secondary emission distributions can also cover impacts of additional degradation and transport processes, which may occur after the biocide application during a certain period of time (e.g. one day) [102]. Figure 6.7 displays the PestLCI 2.0 model concept.

The next step of direct emissions is associated with the combustion stage, which is called exhaust emission. In previous studies, NOx, HC, CO_2 and CO were presented as major contaminant factors that created spark ignition engine exhaust [103–105]. Thus, NOx, HC, CO_2 and CO or more emissions can be selected to analyze direct emissions for the combustion of various blends and their rates are computed by emission measure as mentioned above.

The last direct emission that is mutual between all stages is CO_2 emissions derived from human activity to air. For computation of this emission, standard coefficient of 0.7 kg CO_2 eq. per h of human labor working was applied in many researches [57, 106, 107]. Table 6.4 shows an example of a comprehensive LCI from farm-to-combustion.

6.3.3   LCIA

As a crucial step, environmental interventions shall be converted into environmental impacts, which is defined by classification of interventions into impacts in LCA [108]. In order to study the impacts, available data from the relevant databases, research publications together with data obtained from simulation research procedures are used by relevant software packages to investigate the impacts [109]. SimaPro is found to be one of the best software packages that are used for LCA due to its outstanding advantages. These include sensible decision-making capability, performing detailed and accurate computations, avoiding concealed assumptions, providing 100% transparency, having user-friendly features and utilizing complete control of LCA trainings.
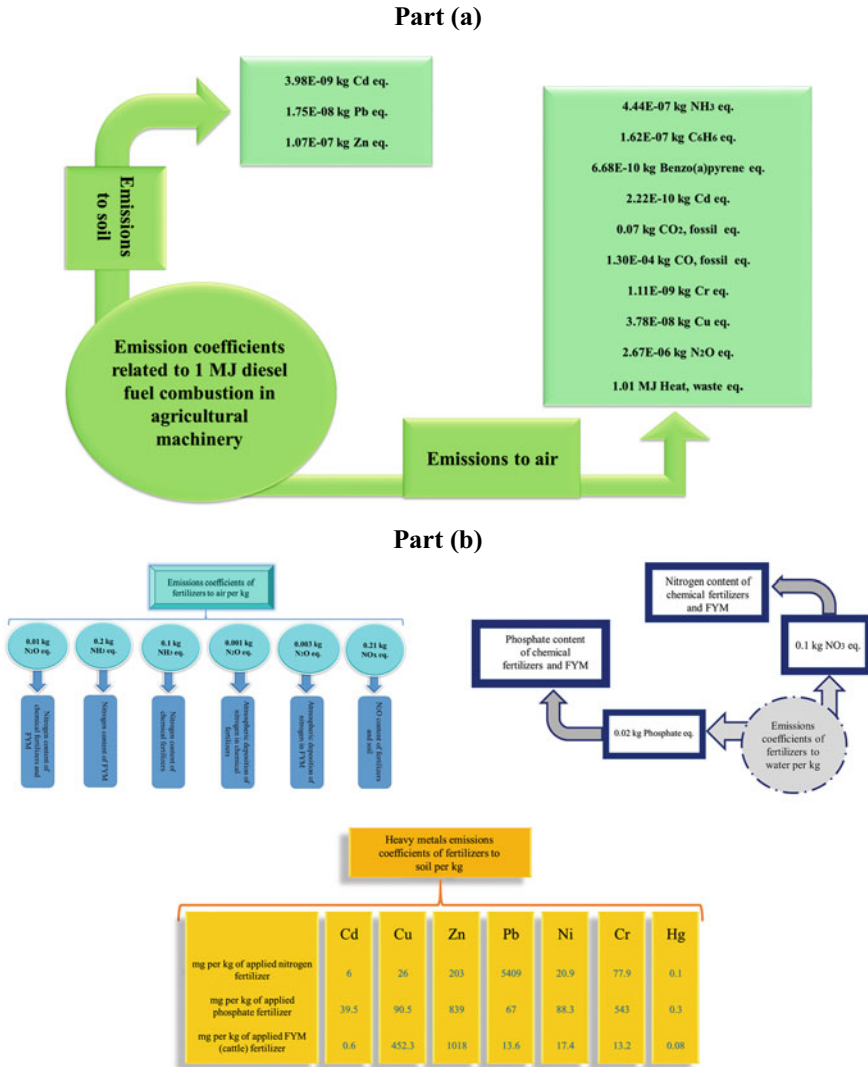
Fig. 6.6 Direct emissions coefficient related to diesel fuel combustion in agricultural machinery (**a**) and fertilizers consumption in the farms (**b**)

Various parameters and methods have been used in the literature to measure environmental impacts for a process. Some of these parameters can be considered equivalent to others [110]. For instance, the equivalent CO_2 emissions (g CO_2) can be measured from the energy input (MJ). Each method however estimates the impacts using different mixture of emitted gasses. For example, EU renewable energy method involves mainly three greenhouse gasses (GHGs) including CO_2, CH_4 and N_2O whereas ReCiPe covers up to 93 gases. Further, more gases are covered by both
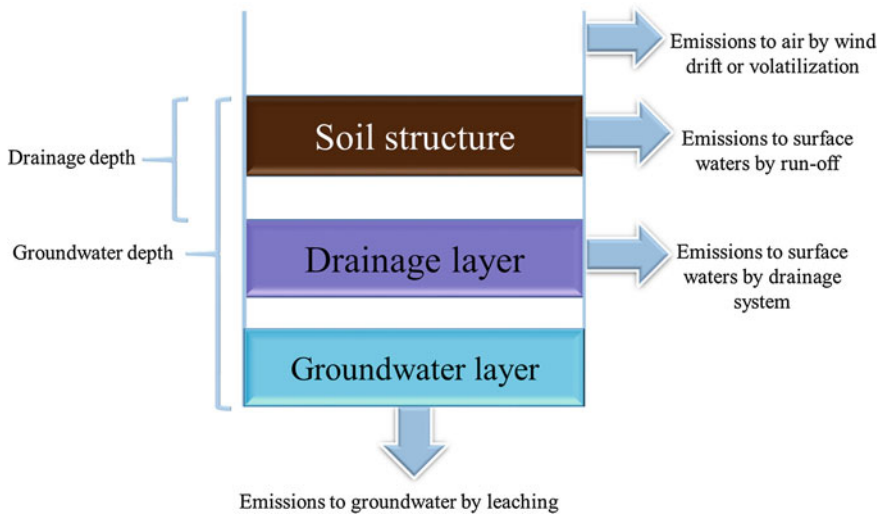
Fig. 6.7 Concept schematic of PestLCI 2.0 model

TRACI 2.1 and RECiPe-2013 than by CML-2013 [111]. Different models have different characteristics, which influences the results of LCA. Consequently, as an example, a weak result may falsely show that a process is not at its optimum status with regards to environmental impacts [112]. The following are some of the common methods that are generally used to evaluate environmental impacts [110]:

ReCiPe midpoint.
EDIP (2003).
IPCC guidelines.
CML method.
Eco-Indicator 2002 +
TRACI.
CA LCFS.

ReCiPe2016 has been found to be one of the most updated and complete methods for the evaluation of environmental impacts in recent years. Thus, ReCiPe2016 was the focus of many researchers around the world [56, 100, 113, 114]. This method is in fact the altered version of ReCiPe2008 introduced by Goedkoop et al. [115]. The latter method included 17 midpoints and finally summarized them in 3 midpoints for which the relationship was illustrated in Fig. 6.8.

Table 6.4 An example of LCI of farm to combustion of fuel blends samples

Item	Unit	Value
A. Sunflower production (FU = 1 t of sunflower yield)		
I. Indirect emissions		
1. Biocides	kg	2.31
2. Chemical fertilizers		
(a) Nitrogen	kg	72.75
(b) K_2O	kg	7.94
(c) P_2O_5	kg	14.55
3. Agricultural machinery	kg	18.83
4. Sunflower seed	kg	8.93
5. Electricity	kWh	367.14
6. Diesel fuel	kg	62.74
II. Direct emissions		
1. Emissions by diesel combustion in agricultural machinery to air		
(a) NH_3	kg	1.83E-03
(b) C_6H_6	kg	6.66E-04
(c) Benzo (a) pyrene	kg	2.74E-06
(d) Cd	kg	9.13E-07
(e) CO_2, fossil	kg	284.76
(f) CO, fossil	kg	0.54
(g) Cr	kg	4.56E-06
(h) Cu	kg	1.55E-04
(i) N_2O	kg	0.01
(j) Heat, waste	MJ	4145.70
(k) CH_4, fossil	kg	0.01
(l) Ni	kg	6.39E-06
(m) NOx	kg	3.56
(n) NMVOC	kg	0.20
(o) PAH	kg	2.99E-04
(p) Particulates, < 2.5 um	kg	0.45
(q) Se	kg	9.13E-07
(r) SO_2	kg	0.09
(s) Zn	kg	9.13E-05
2. Emissions by diesel combustion in agricultural machinery to soil		
(a) Cd	kg	1.63E-05
(b) Pb	kg	7.18E-05
(c) Zn	kg	0.04

Table 6.4 (continued)

Item	Unit	Value
3. Emissions by fertilizers to air		
(a) N_2O	kg	1.14
(b) NH_3	kg	8.80
4. Emission by atmospheric deposition of fertilizers to air		
(a) N_2O	kg	0.11
5. Emissions by fertilizers to water		
(a) NO_3^-	kg	1.05
(b) PO_4^{3-}	kg	0.17
6. Emission by N_2O of fertilizers and soil to air		
(a) NOx	kg	0.26
7. Emission by heavy metals of fertilizers to soil		
(a) Cd	mg	751.59
(b) Cu	mg	2679.91
(c) Zn	mg	21,520.12
(d) Pb	mg	394,048.37
(e) Ni	mg	2257.95
(f) Cr	mg	10,063.04
(g) Hg	mg	9.66
8. Emission by human labor to air		
(a) CO_2	kg	142.93
9. Emissions by biocides to air		
(a) Diazinon	kg	0.05
(b) Phosalone	kg	0.04
(c) Trichlorophenol	kg	0.04
(d) Trifluralin	kg	0.05
(e) Ethalfluralin	kg	0.04
10. Emissions by biocides to water		
(a) Diazinon	kg	0.02
(b) Phosalone	kg	0.02
(c) Trichlorophenol	kg	0.03
(d) Trifluralin	kg	0.03
(e) Ethalfluralin	kg	0.02
11. Emissions by biocides to soil		
(a) Diazinon	kg	0.43
(b) Phosalone	kg	0.36
(c) Trichlorophenol	kg	0.4
(d) Trifluralin	kg	0.45

(continued)

Table 6.4 (continued)

Item	Unit	Value
(e) Ethalfluralin	kg	0.33
B. Oil extraction process (FU = 1 t of sunflower oil)		
1. Transportation	t.km	900
2. Steel	kg	10
3. Electricity	kWh	1500
C. Biodiesel production (FU = 1 t of biodiesel)		
1. Steel	kg	0.91
2. Water	kg	946.24
3. HCl	kg	8.70
4. Methanol	kg	193.98
5. NaOH	kg	9.46
6. Wastewater	kg	28.39
7. Electricity	kWh	72.86
D. Glycerol production (FU = 1 t of Glycerol)		
1. Steel	kg	0.45
2. Water	kg	468.75
3. HCl	kg	4.31
4. Methanol	kg	96.09
5. NaOH	kg	4.69
6. Wastewater	kg	14.06
7. Electricity	kWh	36.09
E. Combustion of fuel samples (FU = 1 kWh power produced)		
I. Indirect emissions		
1. Sunflower	kg	Based on sunflower oil required
2. Sunflower oil	kg	Based on biodiesel and glycerol required
3. Biodiesel	kg	Based on type of fuel sample
4. Glycerol	kg	Based on type of fuel sample
6. Diesel	kg	Based on type of fuel sample
7. Engine body		
(a) Cast iron	kg	3.30E-05
(b) Aluminum	kg	2.00E-05
II. Exhaust emissions to air		
1. NOx	kg	Calculated by combustion of each blend

(continued)

Table 6.4 (continued)

Item	Unit	Value
2. HC	kg	Calculated by combustion of each blend
3. CO_2	kg	Calculated by combustion of each blend
4. CO	kg	Calculated by combustion of each blend
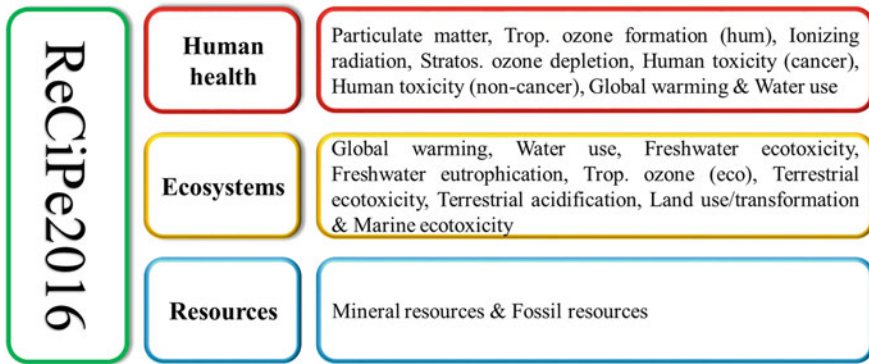
Fig. 6.8 Relationship between midpoints and endpoints in ReCiPe2016 LCIA

6.3.4 Life Cycle Interpretation

Life cycle interpretation is the final stage of LCA for which the results obtained from other stages are assessed considering overall data uncertainties and assumptions made during the course of the study [116].

6.4 CExD

CExD is considered as an indicator for the quantification of a specific product exergy demand during its life cycle and is defined as the exergy summation of all resources needed to provide a service, make a product or create a process [117]. CExD is identical to the definition of a parameter defined by Szargut [118] termed as cumulative exergy consumption. Both parameters measure the full exergy usage of a product. The cumulative exergy consumption was measured by Szargut et al. [119] by adding up the total requirement levels of a process over a certain period of time (for instance over one year). Exergy usage of the process output unit was then computed by
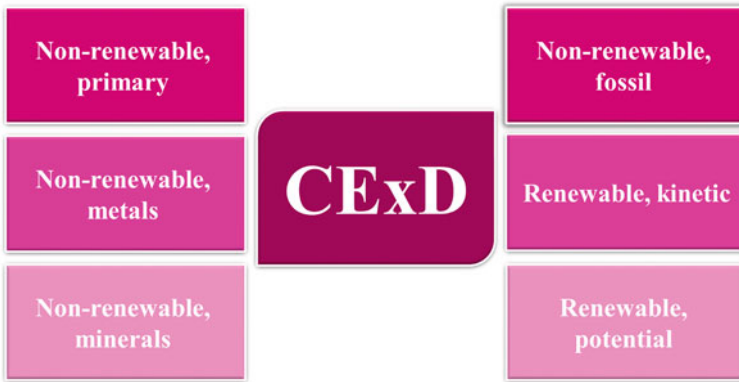
Fig. 6.9 List of energy forms of CExD

dividing amount of the total exergy usage by unit output numbers over this period. The development of large databases containing product/process life cycle data such as EcoInvent can facilitate life cycle assessment using a product-specific method. This is due to the fact that such databases provide the required information on resource demand for each process unit. Access to these databases can therefore improve the methods for computing CExD sources, which in turn results in direct measurement of the exergy demand of a single product. Being referenced in MJ equivalents, it is highlighted that CExD is not an inventory elementary flow but rather is an indicator for the impact assessment [117]. Several categories are included in CExD. Yet, only six energy methods are adequate for the evaluation of CExD for the production of biodiesel, which are shown in Fig. 6.9.

6.5 Interpretation of Results

6.5.1 Exhaust Emissions Analysis

The first part of presenting the results is usually for exhaust emissions of combustion process, because as mentioned in the LCI section, these emissions are used as direct emission to compute environmental damages of power generation. The results are usually presented in the form of bar charts and the amount of emission is reported for each load. For example, in Fig. 6.10, NOx emission throughout combustion of B5 with different rates of glycerol additive and NG are illustrated. It can be seen that, with adding 5% biodiesel to fuel, NOx emission increases. It is due to the increasing O_2 content of fuel, which improves the reaction conditions for producing more NOx. Furthermore, in this case, increasing temperature and pressure in-cylinder due to increasing engine load has a direct relationship with NOx emission. Increasing NG
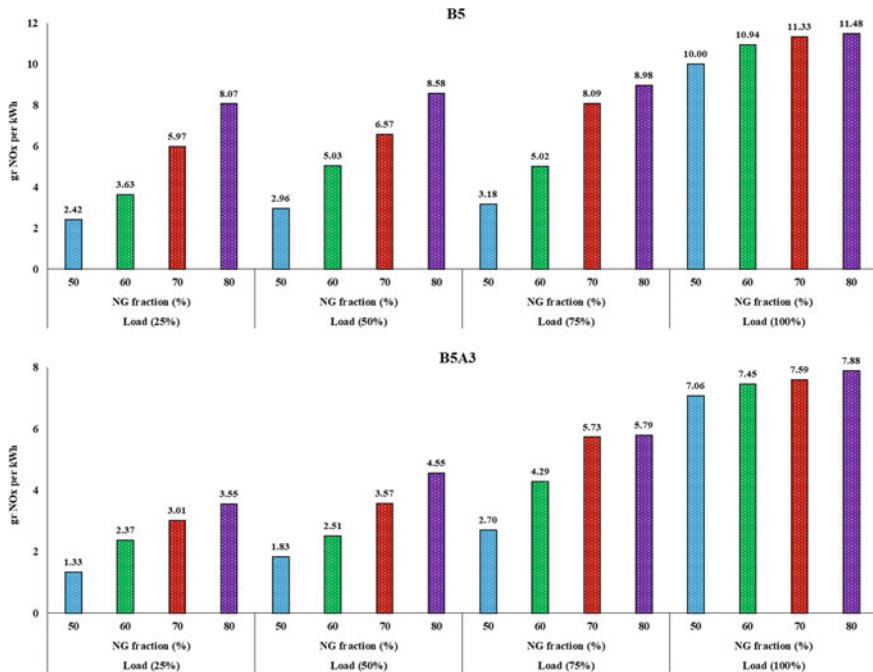
Fig. 6.10 An example of NOx emissions analysis during the combustion of B5 and B5A3 with different rate of NG

fraction has a direct relationship with NOx emission because, in higher NG fraction, pressure and temperature of combustion chamber increase and additional combustion of NG takes more time than diesel to produce NOx.

As can be seen, adding 3% of glycerol as additive in B5A3 has significant positive effects on NOx emission (mitigating NOx emission).

On the one hand, an advantage of an additive on combustion process is rendering combustion more uniformly and thus producing less NOx. On the other hand, glycerol, by absorbing temperature in combustion chamber, has a cooling effect in the power generation stage and results in mitigating NOx emission. However decreasing fuel CV and increasing fuel viscosity reduce fuel efficiency, and thus diminish additives advantages compared with B5A3.

6.5.2 Exergoenvironmental Damages Assessment for Farm to Biodiesel Production

Presenting and interpreting LCA-CExD results is in the order of the above-mentioned steps. Accordingly, the results of the exergoenvironmental assessment of oilseeds

production in agricultural phase, oil extraction process and biodiesel production should be presented.

Generally, the presentation of LCA results for each stage consists of four main parts:

1. Explaining the physical value of each environmental damage
2. Describing the share of each input in emission of each environmental damage.
3. Determining physical amounts of energy forms based on CExD method
4. Contribution of each input to each CExD category.

Of course, observing the following points is also necessary in providing the best analysis:

- Providing these 4 steps is essential for each system step.
- The interpretation of results of tables of physical values is the same for all stages and is accompanied only by mentioning the value of each damage.
- The interpretation of share charts include explanation of most effective inputs in all damages and study of each damage separately.

Table 6.5 shows an example for presenting physical amounts of environmental damages. Based on the sample results, human health is computed as 0.0026, 0.0011, and 0.0003 DALY, ecosystems is computed as about 4742, 228, and 28 species.yr and resources category is computed as about 20,457, 25,471, 7883 USD2013 for agricultural phase of oilseeds production, oil extraction and biodiesel production, respectively.

Figure 6.11 displays an example showing each input share to environmental damages. This figure includes three parts, namely Part (a), Part (b), and Part (c) for farm production, oil extraction and biodiesel production, respectively. Based on Part (a) of Fig. 6.11, direct emission is the most effective factor for human health and ecosystems damages; while in resources category, this item is related to electricity. The following suggestions can be offered for improving environmental-friendly status of sunflower production:

- Applying reduced tillage and No tillage systems for reducing diesel fuel.
- Performing timely maintenance of agricultural equipment for reducing diesel fuel consumption.
- Using bio fertilizers instead of chemical fertilizers especially nitrogen.

Table 6.5 An example of the damages results for different steps of biodiesel production based on ReCiPe2016

Damage category	Unit	Amount		
		Agricultural phase	Oil extraction	Biodiesel production
Human health	DALY	0.0026	0.0011	0.0003
Ecosystems	species.yr	4741.97	227.63	27.97
Resources	USD2013	56.72	31.27	1.27

Part (a)

Part (b)

Part (c)
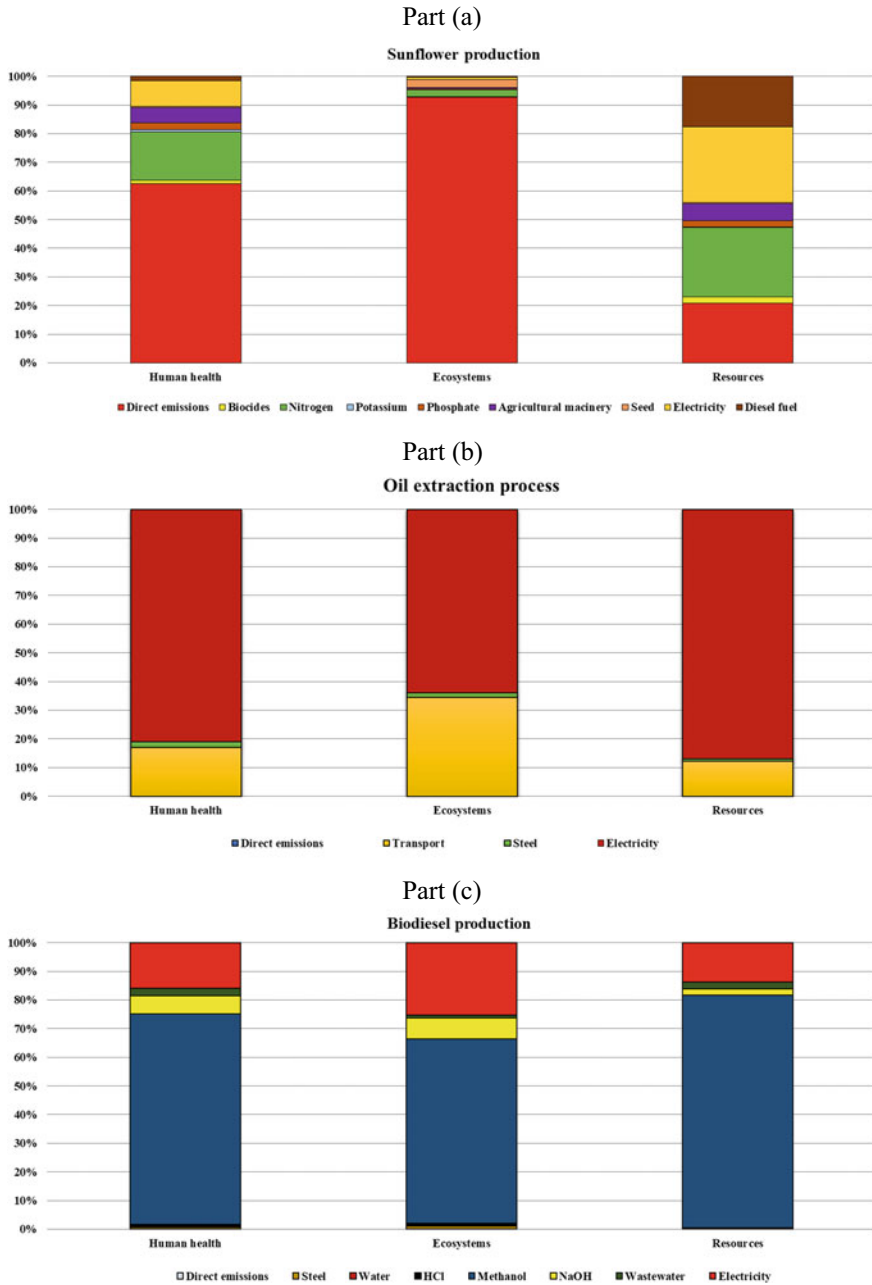
Fig. 6.11 The share of each inputs to form environmental damages of farming system, oil extraction and biodiesel production

Part (b) of Fig. 6.11 reveals that electricity and transport are the main hotspots for oil extraction process. The followings are the main reasons causing environmental consequences of sunflower oil extraction:

- Environmental consequences due to electricity generation (given that in Iran about 1% of electricity is produced from renewable sources [120]).
- Lack of timely maintenance
- Lack of optimized pattern for transportation.

As can be seen Part (c) of Fig. 6.11, methanol consumption is the dominant factor for environmental impacts of its production. In human health damage categories, it is because of CO, CO_2 and PM emissions at distillation and reforming steps in the conventional method of producing methanol and increased damage in midpoint damages on carcinogenic, respiratory and ozone layer depletion. In ecosystems damage category, methanol consumption has major impacts due to increased aquatic ecotoxicity, aquatic acidification and aquatic eutrophication at water-cooling in methanol production process. In resource damage category, the fundamental role of methanol consumption is due to the use of non-renewable resources (fossil fuels) as raw material for methanol production.

Table 6.6 shows an example for energy form amounts in farming system of oilseeds, oil extraction, and biodiesel production. It is obvious that non-renewable, fossil has the maximum amounts in comparison with other energy forms in all steps. Moreover, total CExD is computed as about 13,456, 9565, and 7455 MJ for agricultural phase, oil extracting process and biodiesel production, respectively.

In the next step to present CExD results, showing input share in each energy form is essential for all studied steps. Figure 6.12 shows an example for the investigation of farming system (Part (a)), oil extraction (Part (b)), and biodiesel production (Part (c)) from CExD point of view. Farming system reveals that electricity, diesel fuel and nitrogen are the most exergy consumer among all inputs. In oil extraction process, electricity with significant difference has the most share in CExD categories. As can be seen in Part (c) of Fig. 6.12, methanol and electricity have the first and second rank in all energy forms for biodiesel production, respectively.

Table 6.6 An example of the energy forms of CExD for different steps of biodiesel production

Damage category	Unit	Amount		
		Agricultural phase	Oil extraction	Biodiesel production
Non-renewable, fossil	MJ	11,942.41	8509.20	6733.60
Renewable, kinetic	MJ	44.54	34.27	25.13
Renewable, potential	MJ	280.94	191.47	122.73
Non-renewable, primary	MJ	324.04	207.02	163.51
Non-renewable, metals	MJ	404.04	269.02	180.51
Non-renewable, minerals	MJ	459.87	353.94	229.97
Total CExD	MJ	13,455.83	9564.91	7455.46

Part (a)

Part (b)

Part (c)
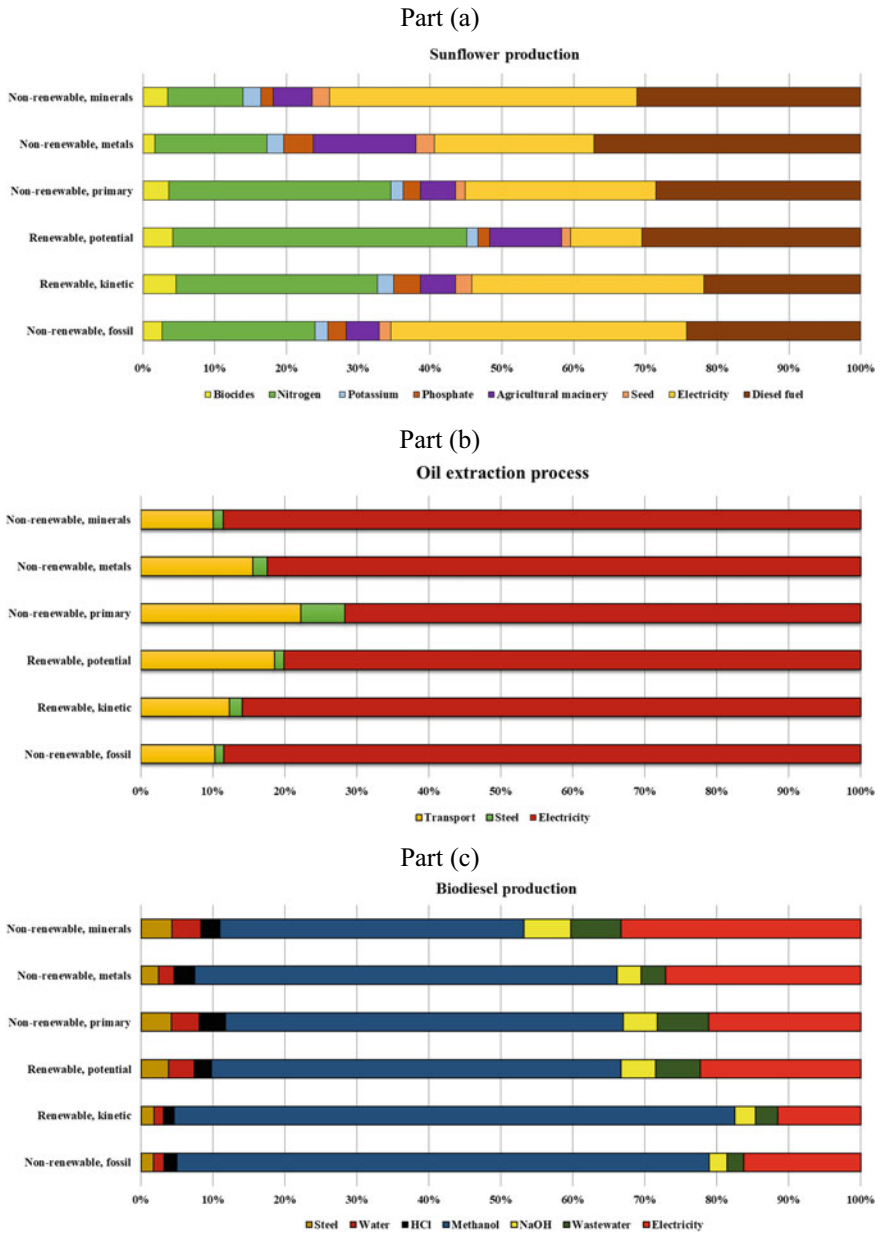
Fig. 6.12 The share of each inputs to form energy forms of CExD for farming system, oil extraction and biodiesel production

6.5.3   *Exergoenvironmental Damages of Power Generation*

In the last section of comprehensive studies, environmental assessment and exergy analysis of combusted blends should be investigated. Actually, this step shows exergoenvironmental damages from farm-to-combustion since all steps except combustion has been offered in previous steps and the results has been focused on combustion and consequently power generation in this step. In this stage, the results should be offered in two tables. The first table shows the environmental impact assessment of combusted blends and the second table shows the situation of blends from exergy categories viewpoint. The following example can be shown to avoid any ambiguity for presenting this step.

Table 6.7 exhibits environmental consequences for 20 fuel samples with farm to combustion approach based on FU as an example. Each environmental consequence result is a comprehensive LCA, which includes sunflower production, oil extraction,

Table 6.7 An example of the results of damages categories for 20 fuel samples with farm to combustion approach

Blend number	Fuel sample	Engine load (%)	Damage categories			Total weighted damage (Pt)
			Human health (DALY)	Ecosystems (species.yr)	Resources (USSD2013)	
1	Diesel	25	0.0163	452.61	3.69	3.11
2	Diesel	50	0.0042	247.71	2.06	1.05
3	Diesel	75	0.0020	190.19	1.63	0.64
4	Diesel	100	0.0014	171.35	1.51	0.53
5	B5	25	0.0125	602.21	3.68	2.58
6	B5	50	0.0030	339.72	2.11	0.89
7	B5	75	0.0016	271.83	1.73	0.60
8	B5	100	0.0014	258.34	1.66	0.56
9	B5A3	25	0.0123	578.84	3.53	2.53
10	B5A3	50	0.0029	322.83	2.00	0.86
11	B5A3	75	0.0014	243.46	1.53	0.54
12	**B5A3**	**100**	**0.0012**	**221.99**	**1.42**	**0.49**
13	B20	25	0.0191	1111.19	4.01	3.63
14	B20	50	0.0047	637.31	2.31	1.19
15	B20	75	0.0025	516.71	1.88	0.79
16	B20	100	0.0018	500.47	1.82	0.68
17	B20A3	25	0.0137	1042.44	3.79	2.82
18	B20A3	50	0.0033	588.85	2.14	0.97
19	B20A3	75	0.0017	455.75	1.66	0.62
20	B20A3	100	0.0016	502.83	1.84	0.66

biodiesel production, glycerol production, diesel, engine body and exhaust emissions (cradle to grave). They are computed in three damage categories (human heath, ecosystems, and resources). The results are summarized in the same unit (Pt) for better comparison, with the help of a weighting. As indicated in Table 6.7, the blend number 20 is nominated as the best blend in terms of total environmental consequences. This blend (B5A3), with the maximum engine load of 0.49 Pt, has the lowest total damage.

Table 6.8 indicates energy forms of CExD for 20 combusted blends as an example. Similar to the previous condition for environmental damages, results are illustrated for comprehensive farm-to-combustion. In the last column of Table 6.8, total CExD is also inserted to compare blends from exergy point of view. Based on the results, blend number 20 (B5A3 with 100% engine load) with 667.19 MJ is the best fuel in CExD.

Finally, it can be said the fuel B5A3 with 100% engine load has the lowest environmental damages and total CExD. In other words, this blend can be selected as exergoenvironmental friendly biodiesel blends among all.

6.6   Conclusion

Although biodiesel is the first generation of alternative biofuels to fossil resources, it is still one of the most important alternatives to other biofuels due to the high potential of oilseeds in the world. Most studies in the field of biodiesel environmental assessment focus only on exhaust emissions and do not cover the entire production process, including farm production and oil extraction process. However, the implementation of a macro policy to replace biofuels requires a comprehensive approach in the entire production process from farm-to-combustion and ultimately power generation. However, it is clear that there are no clear guidelines for achieving this comprehensive review. Accordingly, in addition to determining a specific principle for estimating exergoenvironmental damages in the entire biodiesel production chain from farm-to-combustion, the present study also shows a correct analysis by providing case allegories in each section.

Table 6.8 An example of the results of damages categories for 20 fuel samples with farm to combustion approach

Blend number	Fuel sample	Engine load (%)	Energy forms (MJ)						Total CExD (MJ)
			Non-renewable, fossil	Renewable, kinetic	Renewable, potential	Non-renewable, primary	Non-renewable, metals	Non-renewable, minerals	
1	Diesel	25	3777.31	14.44	82.69	96.51	118.60	145.03	4234.58
2	Diesel	50	1275.30	4.88	27.92	32.58	40.04	48.97	1429.68
3	Diesel	75	777.32	2.97	17.02	19.86	24.41	29.85	871.43
4	Diesel	100	643.72	2.46	14.09	16.45	20.21	24.72	721.65
5	B5	25	3133.59	11.98	68.60	80.06	98.39	120.31	3512.93
6	B5	50	1080.97	4.13	23.66	27.62	33.94	41.50	1211.83
7	B5	75	728.74	2.79	15.95	18.62	22.88	27.98	816.96
8	B5	100	680.16	2.60	14.89	17.38	21.36	26.11	762.50
9	B5A3	25	3072.86	11.75	67.27	78.51	96.48	117.98	3444.85
10	B5A3	50	1044.53	3.99	22.87	26.69	32.80	40.10	1170.98
11	B5A3	75	655.87	2.51	14.36	16.76	20.59	25.18	735.27
12	**B5A3**	**100**	**595.14**	**2.28**	**13.03**	**15.21**	**18.69**	**22.85**	**667.19**
13	B20	25	4408.88	16.86	96.52	112.65	138.43	169.28	4942.62
14	B20	50	1445.34	5.53	31.64	36.93	45.38	55.49	1620.31
15	B20	75	959.51	3.67	21.01	24.52	30.13	36.84	1075.67
16	B20	100	825.91	3.16	18.08	21.10	25.93	31.71	925.89
17	B20A3	25	3425.08	13.10	74.98	87.51	107.54	131.51	3839.72
18	B20A3	50	1178.13	4.50	25.79	30.10	36.99	45.23	1320.75
19	B20A3	75	753.03	2.88	16.49	19.24	23.64	28.91	844.19
20	B20A3	100	801.62	3.06	17.55	20.48	25.17	30.78	898.66

References

1. L. Lardon, A. Hélias, B. Sialve, J.P. Steyer, O. Bernard, Life-cycle assessment of biodiesel production from microalgae. Environ. Sci. Technol. **43**, 6475–6481 (2009)
2. K.F. Yee, K.T. Tan, A.Z. Abdullah, K.T. Lee, Life cycle assessment of palm biodiesel: Revealing facts and benefits for sustainability. Appl. Energy **86**, 189–196 (2009)
3. P.S. Nigam, A. Singh, Production of liquid biofuels from renewable resources. Prog. Energy Combust. Sci. **37**, 52–68 (2011)
4. FAO, Food and Agricultural Organization Statistical Yearbook (2018). http://www.fao.org
5. T. Eryilmaz, M.K. Yesilyurt, C. Cesur, O. Gokdogan, Biodiesel production potential from oil seeds in Turkey. Renew. Sustain. Energy Rev. **58**, 842–885 (2016)
6. A. Demirbas, New bio renewable fuels from vegetable oils. Energy Sources, Part A Recover Util Environ. Eff. **32**, 628–636 (2010)
7. A. Demirbas, Comparison of transesterification methods for production of biodiesel from vegetable oils and fats. Energy Convers. Manag. **49**, 125–130 (2008)
8. N. Kumar, J. Mudgal, V.K. Parihar, P.G. Nayak, N.G. Kutty, C.M. Rao, Sesamol treatment reduces plasma cholesterol and triacylglycerol levels in mouse models of acute and chronic hyperlipidemia. Lipids **48**, 633–638 (2013)
9. B. Dhinesh, I. JoshuaRamesh, J. Lalvani, M. Parthasarathy, K. Annamalai, An assessment on performance, emission and combustion characteristics of single cylinder diesel engine powered by Cymbopogon flexuosus biofuel. Energy Convers. Manag. **117**, 466–474 (2016)
10. R. Vigneswaran, K. Annamalai, B. Dhinesh, R. Krishnamoorthy, Experimental investigation of unmodified diesel engine performance, combustion and emission with multipurpose additive along with water-in-diesel emulsion fuel. Energy Convers. Manag. **172**, 370–380 (2018)
11. A. Atmanlı, B. Yüksel, E. Ileri, A. Atmanlı, B. Yüksel, Experimental investigation of the effect of diesel-cotton oil-n-butanol ternary blends on phase stability, engine performance and exhaust emission parameters in a diesel engine. Fuel **109**, 503–511 (2013)
12. N. Yilmaz, B. Morton, Effects of preheating vegetable oils on performance and emission characteristics of two diesel engines. Biomass Bioenerg. **35**, 2028–2033 (2011)
13. F. Bär, H. Hopf, M. Knorr, J. Krahl, Synthesis, characterization and antioxidant properties of 2, 4, 6-tris-isopropylbenzoic acid hydrazide in biodiesel. Fuel **215**, 249–257 (2018)
14. E.M. Shahid, Y. Jamal, Performance evaluation of a diesel engine using biodiesel. Pakistan J. Eng. Appl. Sci. (2016)
15. E. Jiaqiang, M. Pham, D. Zhao, Y. Deng, D.H. Le, W. Zuo, H. Zhu, T. Liu, Q. Peng, Z. Zhang, Effect of different technologies on combustion and emissions of the diesel engine fueled with biodiesel: A review. Renew. Sustain. Energy Rev. **80**, 620–647 (2017)
16. C. Swaminathan, J. Sarangan, Performance and exhaust emission characteristics of a CI engine fueled with biodiesel (fish oil) with DEE as additive. Biomass Bioenerg. **39**, 168–174 (2012)
17. G. Saranya, T.V. Ramachandra, Life cycle assessment of biodiesel from estuarine microalgae. Energy Convers. Manag. X **8**, 100065 (2020)
18. E.G. Smith, H.H. Janzen, N.K. Newlands, Energy balances of biodiesel production from soybean and canola in Canada. Can. J. Plant Sci. **87**, 793–801 (2007)
19. T.E. McKone, W.W. Nazaroff, P. Berck, M. Auffhammer, T. Lipman, MS. Torn, E. Masanet, A. Lobscheid, N. Santero, U. Mishra, A. Barrett, M. Bomberg, K. Fingerman, C. Scown, B. Strogen, A. Horvath, Grand challenges for life-cycle assessment of biofuels. Environ. Sci. Technol. **45**, 1751–1756 (2011)
20. R.R. Bora, M. Lei, J.W. Tester, J. Lehmann, F. You, Life cycle assessment and technoeconomic analysis of thermochemical conversion technologies applied to poultry litter with energy and nutrient recovery. ACS Sustain. Chem. Eng. **8**, 8436–8447 (2020)
21. F. Cherubini, GHG balances of bioenergy systems - Overview of key steps in the production chain and methodological concerns. Renew. Energy **35**, 1565–1573 (2010)

22. M. Hiloidhari, D.C. Baruah, A. Singh, S. Kataki, K. Medhi, S. Kumari, T.V. Ramachandra, B.M. Jenkins, I.S. Thakur, Emerging role of Geographical Information System (GIS), Life Cycle Assessment (LCA) and spatial LCA (GIS-LCA) in sustainable bioenergy planning. Bioresour. Technol. **242**, 218–226 (2017)
23. ISO 14040 International standard. Environmental Management–Life Cycle Assessment–Principles and Framework, International Organisation for Standardization, Geneva, Switzerland (2006)
24. B. Milanovic, B. Agarski, D. Vukelic, I. Budak, F. Kiss, Comparative exergy-based life cycle assessment of conventional and hybrid base transmitter stations. J. Clean Prod. **167**, 610–618 (2017)
25. M.V. Rocco, G. Cassetti, F. Gardumi, E. Colombo, Exergy Life Cycle Assessment of soil erosion remediation technologies: An Italian case study. J. Clean Prod. **112**, 3007–3017 (2016)
26. A. Ghannadzadeh, Exergy-aided environmental sustainability assessment of an ethylene dichloride–vinyl chloride production process. Chem. Eng. Res. Des. **130**, 109–128 (2018)
27. S. Kim, B.E. Dale, Life cycle assessment of various cropping systems utilized for producing biofuels: Bioethanol and biodiesel. Biomass Bioenerg. **29**, 426–439 (2005)
28. L.T. Peiró, L. Lombardi, G.V. Méndez, X.G. i Durany, Life cycle assessment (LCA) and exergetic life cycle assessment (ELCA) of the production of biodiesel from used cooking oil (UCO). Energy **35**, 889–893 (2010)
29. P. Collet, A. Hélias, L. Lardon, M. Ras, R. Goy, J. Steyer, Life-cycle assessment of microalgae culture coupled to biogas production. Bioresour. Technol. **102**, 207–214 (2011)
30. E.-E. Oprescu, R.E. Dragomir, E. Radu, A. Radu, S. Velea, I. Bolocan, E. Stepan, P. Rosca, Performance and emission characteristics of diesel engine powered with diesel–glycerol derivatives blends. Fuel Process Technol. **126**, 460–468 (2014)
31. L. Tarabet, K. Loubar, M.S. Lounici, K. Khiari, T. Belmrabet, M. Tazerout, Experimental investigation of DI diesel engine operating with eucalyptus biodiesel/natural gas under dual fuel mode. Fuel **133**, 129–138 (2014)
32. M.S. Lounici, K. Loubar, L. Tarabet, M. Balistrou, D-C. Niculescu, M. Tazerout, Towards improvement of natural gas-diesel dual fuel mode: An experimental investigation on performance and exhaust emissions. Energy **64**, 200–211 (2014)
33. M. Lapuerta, J. Rodríguez-Fernández, R. García-Contreras, Effect of a glycerol-derived advanced biofuel –FAGE (fatty acid formal glycerol ester)– on the emissions of a diesel engine tested under the New European Driving Cycle. Energy **93**, 568–579 (2015)
34. S. Imtenan, H.H. Masjuki, M. Varman, I.M. Rizwanul Fattah, H. Sajjad, M.I. Arbab, Effect of n-butanol and diethyl ether as oxygenated additives on combustion–emission-performance characteristics of a multiple cylinder diesel engine fuelled with diesel–jatropha biodiesel blend. Energy Convers. Manag. **94**, 84–94 (2015)
35. E. Moecke, R. Feller, H. Santos, M. Machado, A. Cubas, A. Dutra, L. Santos, S. Soares, Biodiesel production from waste cooking oil for use as fuel in artisanal fishing boats: Integrating environmental, economic and social aspects. J. Clean Prod. **135**, 679–688 (2016)
36. A. Zare, M.N. Nabi, T.A. Bodisco, F.M. Hossain, M.M. Rahman, Z.D. Ristovski, RJ. Brown, M.N. Nabi, H.M. Farhad, D. Stuart, The effect of triacetin as a fuel additive to waste cooking biodiesel on engine performance and exhaust emissions. Fuel **182**, 640–649 (2016)
37. M. Srinivasa Rao, R.B.B. Anand, Performance and emission characteristics improvement studies on a biodiesel fuelled DICI engine using water and AlO(OH) nanoparticles. Appl. Therm. Eng. **98**, 636–645 (2016)
38. S.H. Hosseini, A. Taghizadeh-Alisaraei, B. Ghobadian, A. Abbaszadeh-Mayvan, Effect of added alumina as nano-catalyst to diesel-biodiesel blends on performance and emission characteristics of CI engine. Energy **124**, 543–552 (2017)
39. A. Sharma, S. Murugan, Effect of blending waste tyre derived fuel on oxidation stability of biodiesel and performance and emission studies of a diesel engine. Appl. Therm. Eng. **118**, 365–374 (2017)
40. P. Zareh, A.A. Zare, B. Ghobadian, Comparative assessment of performance and emission characteristics of castor, coconut and waste cooking based biodiesel as fuel in a diesel engine. Energy **139**, 883–894 (2017)

41. A. Paul, R. Panua, D. Debroy, An experimental study of combustion, performance, exergy and emission characteristics of a CI engine fueled by Diesel-ethanol-biodiesel blends. Energy **141**, 839–852 (2017)

42. M.B. Forleo, N. Palmieri, A. Suardi, D. Coaloa, L. Pari, The eco-efficiency of rapeseed and sunflower cultivation in Italy. Joining environmental and economic assessment. J. Clean Prod. **172**, 3138–3153 (2018)

43. M.N. Nabi, M.G. Rasul, Influence of second generation biodiesel on engine performance, emissions, energy and exergy parameters. Energy Convers. Manag. **169**, 326–333 (2018)

44. M.S. Sidhu, M.M. Roy, W. Wang, Glycerine emulsions of diesel-biodiesel blends and their performance and emissions in a diesel engine. Appl. Energy **230**, 148–159 (2018)

45. Ş Yıldızhan, Hydrogen *addition to tea seed oil biodiesel: Performance and emission characteristics.* Int. J. Hydrogen Energy **43**, 18020–18027 (2018)

46. K.A. Abed, A.K. El Morsi, M.M. Sayed, A.A. El Shaib, M.S. Gad, Effect of waste cooking-oil biodiesel on performance and exhaust emissions of a diesel engine. Egypt J. Pet. **27**, 985–989 (2018)

47. S. Thangaraj, N. Govindan, Evaluating combustion, performance and emission characteristics of diesel engine using karanja oil methyl ester biodiesel blends enriched with HHO gas. Int. J. Hydrogen Energy **43**, 6443–6455 (2018)

48. R. Alloune, M. Balistrou, S. Awad, K. Loubar, M. Tazerout, Performance, combustion and exhaust emissions characteristics investigation using Citrullus colocynthis L. biodiesel in DI diesel engine. J. Energy Inst. **91**, 434–444 (2018)

49. P. Dinesha, S. Kumar, M.A. Rosen Combined effects of water emulsion and diethyl ether additive on combustion performance and emissions of a compression ignition engine using biodiesel blends. Energy (2019). https://doi.org/10.1016/J.ENERGY.2019.05.071

50. M.A. Asokan, S. Senthur Prabu, P.K.K. Bade, V.M. Nekkanti, S.S.G. Gutta, Performance combustion and emission characteristics of juliflora biodiesel fuelled DI diesel engine. Energy **173**, 883–892 (2019)

51. S.M. Krishna, P. Abdul Salam, M. Tongroon, N. Chollacoop, Performance and emission assessment of optimally blended biodiesel-diesel-ethanol in diesel engine generator. Appl. Therm. Eng. **155**, 525–533 (2019)

52. L.A. Raman, B. Deepanraj, S. Rajakumar, V. Sivasubramanian, Experimental investigation on performance, combustion and emission analysis of a direct injection diesel engine fuelled with rapeseed oil biodiesel. Fuel **246**, 69–74 (2019)

53. Y. Devarajan, Experimental evaluation of combustion, emission and performance of research diesel engine fuelled di-methyl- carbonate and biodiesel blends. Atmos. Pollut. Res. **10**, 795–801 (2019)

54. E. Akbarian, B. Najafi, A novel fuel containing glycerol triacetate additive, biodiesel and diesel blends to improve dual-fuelled diesel engines performance and exhaust emissions. Fuel **236**, 666–676 (2019)

55. E.J.C. Cavalcanti, M. Carvalho, A.AV. Ochoa, Exergoeconomic and exergoenvironmental comparison of diesel-biodiesel blends in a direct injection engine at variable loads. Energy Convers. Manag. **183**, 450–461 (2019)

56. H. Ghasemi-Mobtaker, F. Mostashari-Rad, Z. Saber, K.W. Chau, A. Nabavi-Pelesaraei, Application of photovoltaic system to modify energy use, environmental damages and cumulative exergy demand of two irrigation systems-A case study: Barley production of Iran. Renew. Energy **160**, 1316–1334 (2020)

57. M. Khanali, A. Akram, J. Behzadi, F. Mostashari-Rad, Z. Saber, K. Chau, A. Nabavi-Pelesaraei, Multi-objective optimization of energy use and environmental emissions for walnut production using imperialist competitive algorithm. Appl. Energy. **284**, 116342 (2021)

58. A. Nabavi-Pelesaraei, H. Azadi, S. Van Passel, Z. Saber, F. Hosseini-Fashami, F. Mostashari-Rad, H. Ghasemi-Mobtaker, Prospects of solar systems in production chain of sunflower oil using cold press method with concentrating energy and life cycle assessment. Energy **223**, 120117 (2021)

59. Ministry of Agriculture of Brazil, Annual Agricultural Statistics (2020)

60. L.I. Malinovski, A.F. Brighenti, M. Borghezan, M.P. Guerra, A.L. Silva, D. Porro, M. Stefanini, H.J. Vieira, Viticultural performance of Italian grapevines in high altitude regions of Santa Catarina State. Brazil. Acta Hortic. **1115**, 203–209 (2016)

61. A. Nabavi-Pelesaraei, S. Rafiee, F. Hosseini-Fashami, K.W. Chau, Artificial neural networks and adaptive neuro-fuzzy inference system in energy modeling of agricultural products, in *Predictive Modelling for Energy Management and Power Systems Engineering* (Elsevier, 2021), pp. 299–334

62. W.G. Cochran, The estimation of sample size. Sampl. Tech. **3**, 72–90 (1977)

63. P.D. Patil, S. Deng, Optimization of biodiesel production from edible and non-edible vegetable oils. Fuel **88**, 1302–1306 (2009)

64. G. Fontaras, V. Skoulou, G. Zanakis, A. Zabaniotou, Z. Samaras, Integrated environmental assessment of energy crops for biofuel and energy production in Greece. Renew. Energy **43**, 201–209 (2012)

65. G. Koçar, N. Civaş, An overview of biofuels from energy crops: Current status and future prospects. Renew. Sustain. Energy Rev. **28**, 900–916 (2013)

66. T.M. Harris, T.A. Hottle, K. Soratana, J. Klane, AE. Landis, Life cycle assessment of sunflower cultivation on abandoned mine land for biodiesel production. J. Clean Prod. **112**, 182–195 (2016)

67. S.H. Mousavi-Avval, S. Rafiee, M. Sharifi, S. Hosseinpour, B. Notarnicola, G. Tassielli, P.A. Renzulli, M. Khanali, Use of LCA indicators to assess Iranian rapeseed production systems with different residue management practices. Ecol. Indic. **80**, 31–39 (2017)

68. C. Dueso, M. Muñoz, F. Moreno, J. Arroyo, N. Gil-Lalaguna, A. Bautista, A. Gonzalo, J.L. Sánchez, Performance and emissions of a diesel engine using sunflower biodiesel with a renewable antioxidant additive from bio-oil. Fuel **234**, 276–285 (2018)

69. A.K. Yusuf, A review of methods used for seed oil extraction. Int. J. Sci. Res. **8**, 1854–1861 (2017)

70. V.R.S. Vadiraj.J.Hattimattur, P.S. Zade M.B.M, S. Walke, Review: Epoxidation of vegetable oils. Int. J. Trend Res. Dev. **5**, 542–548 (2018)

71. R. Dutta, U. Sarkar, A. Mukherjee, Soxhlet extraction of Crotalaria juncea oil using cylindrical and annular packed beds. Int. J. Chem. Eng. Appl. **6**, 130–133 (2015)

72. L.K. Sinha, S. Haldar, G.C. Majumdar, Effect of operating parameters on mechanical expression of solvent-soaked soybean-grits. J. Food Sci. Technol. **52**, 2942–2949 (2015)

73. M.M.K. Bhuiya, M.G. Rasul, M.M.K. Khan, N. Ashwath, A.K. Azad, M. Mofijur, Optimisation of oil extraction process from Australian native beauty leaf seed (Calophyllum inophyllum), in *Energy Procedia* (Elsevier Ltd., 2015), pp. 56–61

74. D.S. Ogunniyi, Castor oil: A vital industrial raw material. Bioresour. Technol. **97**, 1086–1091 (2006)

75. S. Azadmard-Damirchi, K. Alirezalu, B.F. Achachlouei, Microwave pretreatment of seeds to extract high quality vegetable oil. World Acad. Sci. Eng. Technol. **81**, 513–516 (2011)

76. H.H. Rassem, A. Nour, R. Yunus, Techniques for extraction of essential oils from plants: A review. Aust. J. Basic Appl. Sci. **10**, 117–127 (2016)

77. F. Takadas, O. Doker, Extraction method and solvent effect on safflower seed oil production. **51**, 9–17 (2017)

78. S.M.B. Hashemi, J. Michiels, S.H. Asadi Yousefabad, M. Hosseini, Kolkhoung (Pistacia khinjuk) kernel oil quality is affected by different parameters in pulsed ultrasound-assisted solvent extraction. Ind. Crops Prod. **70**, 28–33 (2015)

79. E.M. Shahid, Y. Jamal, A review of biodiesel as vehicular fuel. Renew. Sustain. Energy Rev. **12**, 2484–2494 (2008)

80. S. Jain, M.P. Sharma, Prospects of biodiesel from Jatropha in India: A review. Renew. Sustain. Energy Rev. **14**, 763–771 (2010)

81. S.P. Singh, D. Singh, Biodiesel production through the use of different sources and characterization of oils and their esters as the substitute of diesel: A review. Renew. Sustain. Energy Rev. **14**, 200–216 (2010)

82. M.Y. Koh, T.I. Tinia, A review of biodiesel production from Jatropha curcas L. oil. Renew. Sustain. Energy Rev. **15**, 2240–2251 (2011)

83. C. Goering, *Final Report for Project on Effect of Non Petroleum Fuels on Durability of Direct-Injection Diesel Engines Under Contract 59–2171–1–6–057–0. Peoria IL* (USDA, ARS, 1984)

84. J. Marchetti, V. Miguel, A. Errazu, Possible methods for biodiesel production. Renew. Sustain. Energy Rev. **11**, 1300–1311 (2007)

85. D.N. Thoai, C. Tongurai, K. Prasertsit, A. Kumar, Review on biodiesel production by two-step catalytic conversion. Biocatal. Agric. Biotechnol. **18**, 101023 (2019)

86. R. Senthil, R. Silambarasan, Environmental effect of antioxidant additives on exhaust emission reduction in compression ignition engine fuelled with Annona methyl ester. Environ. Technol. **36**, 2079–2085 (2015)

87. H.K. Rashedul, H.H. Masjuki, M.A. Kalam, A.M. Ashraful, S.M.A. Rahman, S.A. Shahir, The effect of additives on properties, performance and emission of biodiesel fuelled compression ignition engine. Energy Convers. Manag. **88**, 348–364 (2014)

88. R. Prasad, V.R. Bella, A review on diesel soot emission, its effect and control. Bull. Chem. React. Eng. Catal. **5**, 69–86 (2010)

89. A. Ito lu brahim, K. Altini ik, A. Keskin, İ.A. Reşitoğlu, K. Altinişik, A. Keskin, I.A. Reşitoʒlu, The pollutant emissions from diesel-engine vehicles and exhaust aftertreatment systems. Clean Technol. Environ. Policy **17**, 15–27 (2015)

90. A. Kumar, S.K. Tyagi, Benzene and toluene profiles in ambient air of Delhi as determined by active sampling and GC analysis. J. Sci. Ind. Res. (India) **65**, 252–257 (2006)

91. V.O. Adesanya, E. Cadena, S.A. Scott, A.G. Smith, Life cycle assessment on microalgal biodiesel production using a hybrid cultivation system. Bioresour. Technol. **163**, 343–355 (2014)

92. D. Pant, A. Singh, G. Van Bogaert, Y.A. Gallego, L. Diels, K. Vanbroekhoven, An introduction to the life cycle assessment (LCA) of bioelectrochemical systems (BES) for sustainable energy and product generation: relevance and key aspects. Renew. Sustain. Energy Rev. **15**, 1305–1313 (2011)

93. M.K. Lam, K.T. Lee, A.R. Mohamed, Life cycle assessment for the production of biodiesel: A case study in Malaysia for palm oil versus jatropha oil. Biofuels, Bioprod. Biorefining **3**, 601–612 (2009)

94. I. Zabalza Bribián, A. Valero Capilla, A. Aranda Usón, Life cycle assessment of building materials: Comparative analysis of energy and environmental impacts and evaluation of the eco-efficiency improvement potential. Build Environ. **46**, 1133–1140 (2011)

95. S.C. Davis, K.J. Anderson-Teixeira, E.H. DeLucia, Life-cycle analysis and the ecology of biofuels. Trends Plant Sci. **14**, 140–146 (2009)

96. A. Sabzevari, M. Yousefinejad-Ostadkelayeh, A. Nabavi-Pelesaraei, Modeling and sensitivity analysis of environmental impacts for eggplant production using artificial neural networks. Biol. Forum **7**, 375–381 (2015)

97. A. Nabavi-Pelesaraei, A. Kaab, F. Hosseini-Fashami, F. Mostashari-Rad, K.W. Chau, *Life Cycle Assessment (LCA) Approach to Evaluate Different Waste Management Opportunities. Advances in Waste-to-Energy Technologies* (CRC Press, 2019), pp. 195–216

98. EcoInvent. (n.d.), System Models in Ecoinvent 3.6. Retrieved 12 September 2019, from https://www.ecoinvent.org/database/ecoinvent-36/ecoinvent-36, 2019.

99. Z. Saber, M. Esmaeili, H. Pirdashti, A. Motevali, A. Nabavi-Pelesaraei, Exergoenvironmental-Life cycle cost analysis for conventional, low external input and organic systems of rice paddy production. J. Clean Prod. **263**, 121529 (2020)

100. F. Mostashari-Rad, H. Ghasemi-Mobtaker, M. Taki, M. Ghahderijani, A. Kaab, KW. Chau, A. Nabavi-Pelesaraei, Exergoenvironmental damages assessment of horticultural crops using ReCiPe2016 and cumulative exergy demand frameworks. J. Clean Prod. **278**, 123788 (2021)

101. M. Margni, D. Rossier, P. Crettaz, O. Jolliet, Life cycle impact assessment of pesticides on human health and ecosystems. Agric. Ecosyst. Environ. **93**, 379–392 (2002)

102. C. Gentil, C. Basset-Mens, S. Manteaux, C. Mottes, E. Maillard, Y. Biard, P. Fantke, *Coupling pesticide emission and toxicity characterization models for LCA: Application to open-field tomato production in Martinique*. J. Clean Prod. **277**, 124099 (2020)
103. J.B. Heywood, *Internal Combustion Engine Fundamentals* (McGraw-Hill Education, 1988)
104. M. Kapusuz, A. Cakmak, H. Ozcan, Emissions analysis of an SI engine with humidified air induction. Energy Procedia **147**, 235–241 (2018)
105. D. Lovarelli, M. Fiala, G. Larsson, Fuel consumption and exhaust emissions during on-field tractor activity: A possible improving strategy for the environmental load of agricultural mechanisation. Comput. Electron. Agric. **151**, 238–248 (2018)
106. Z. Saber, R. van Zelm, H. Pirdashti, A.M. Schipper, M. Esmaeili, A. Motevali, A. Nabavi-Pelesaraei, M.A. Huijbregts, Understanding farm-level differences in environmental impact and eco-efficiency: The case of rice production in Iran. Sustain. Prod. Consum. **27**, 1021–1029 (2021)
107. F. Hosseini-Fashami, A. Motevali, A. Nabavi-Pelesaraei, S.J. Hashemi, K.W. Chau, Energy-Life cycle assessment on applying solar technologies for greenhouse strawberry production. Renew. Sustain. Energy Rev.**116**, 109411 (2019)
108. A. Sabzevari, H. Kouchaki-Penchah, A. Nabavi-Pelesaraei, Investigation of life cycle assessment of hazelnut production in Guilan province of IR Iran based on orchards size levels. Biol Forum **7**, 807–813 (2015)
109. A. Nabavi-Pelesaraei, R. Bayat, H. Hosseinzadeh-Bandbafha, H. Afrasyabi, K.W. Chau, Modeling of energy consumption and environmental life cycle assessment for incineration and landfill systems of municipal solid waste management-A case study in Tehran Metropolis of Iran. J. Clean Prod. **148**, 427–440 (2017)
110. A. Chamkalani, S. Zendehboudi, N. Rezaei, K. Hawboldt, A critical review on life cycle analysis of algae biodiesel: current challenges and future prospects. Renew. Sustain. Energy Rev. **134**, 110143 (2020)
111. T. Bradley, D. Maga, S. Antón, Unified approach to life cycle assessment between three unique algae biofuel facilities. Appl. Energy **154**, 1052–1061 (2015)
112. H. Kouchaki-Penchah, A. Nabavi-Pelesaraei, J. O'Dwyer, M. Sharifi, Environmental management of tea production using joint of life cycle assessment and data envelopment analysis approaches. Environ. Prog. Sustain. Energy **36**, 1116–1122 (2017)
113. H. Peng, B.F. Wang, F.L. Yang, F.Q. Cheng, Study on the environmental effects of heavy metals in coal gangue and coal combustion by ReCiPe2016 for life cycle impact assessment. Ranliao Huaxue Xuebao/J. Fuel Chem. Technol. **48**, 1402–1408 (2020)
114. F. Mostashari-Rad, H. Ghasemi-Mobtaker, M. Taki, M. Ghahderijani, Z. Saber, K.W. Chau, A. Nabavi-Pelesaraei, Data supporting midpoint-weighting life cycle assessment and energy forms of cumulative exergy demand for horticultural crops. Data Br. **33**, 106490 (2020)
115. M. Goedkoop, R. Heijungs, M.A.J. Huijbregts, A. De Schryver, J. Struijs, R. Van Zelm, *ReCiPe 2008: A Life Cycle Impact Assessment Method Which Comprises Harmonised Category Indicators at the Midpoint and The Endpoint Level.* 1st edn. Report I: characterization (2009)
116. M.Z. Hauschild, A. Bonou, S.I. Olsen, *Life Cycle Interpretation* (Theory and Practice. Springer International Publishing, Life Cycle Assessment, 2017), pp. 323–334
117. A. Kaab, M. Sharifi, H. Mobli, A. Nabavi-Pelesaraei, K.W. Chau, Combined life cycle assessment and artificial intelligence for prediction of output energy and environmental impacts of sugarcane production. Sci. Total Environ. **664**, 1005–1019 (2016)
118. Szargut, J., Exergy analysis. Mag. Polish Acad. Sci. **3**, 31–33 (2005)
119. J. Szargut, D. Morris, F. Steward, *Exergy Analysis of Thermal, Chemical, and Metallurgical Processes* (Hemisphere Publishing Corporation, New York, 1988)
120. Power Ministry of Iran, *Iran's Power Industry Statistics For Strategic Management* (2018)

Chapter 7
Multi-generation System Optimization Compromising Water-Energy-Environment Nexus

Mohammad Tajik Mansouri, Zahra Ghaffarpour, Majid Amidpour, and José María Ponce-Ortega

Abstract Production of bioenergy and water by applying waste heat recovery system, capturing of CO_2, cultivating of microalgae and RO-MD unit are examined in this chapter. In the first step of recovery, the flue gas output of gas turbine is fed into an Organic Rankine Cycle (ORC) and the produced electricity is sent to reverse osmose (RO) unit of and then to desalinate outlet brine of RO system, the membrane distillation (MD) is launched. In the next step to prevent releasing the CO_2 of flue gas, the captured CO_2 is used as a main agent to growth microalgae which including of three steps named as cultivation, harvesting and anaerobic digestion. Converting of cultivated algae to methane by anaerobic digestion process, biogas as a sustainable bioenergy source is produced and sent into combustion chamber to provide part of gas turbine system fuel. Energy, environment and economic analysis are carried out for proposed integrated ORC with RO and MD as well CO_2 capture plant system and the effect of amount of flue gas fed to the algae production, ORC working fluid and seawater concentration on energy efficiency, levelized cost of freshwater and biogas production are investigated. Also, multi-objective optimization and sensitivity analysis are implemented from the economic and environmental points of views. Maximization of the annual profit and minimization the carbon dioxide emission per desalinated water production is defined as first and second objective functions of optimization process, respectively based on the environmental index.

Keywords Algal cultivation system · Membrane distillation · Optimization · Organic rankine cycle · Power and desalination plant · Water–energy-environmental nexus

M. Tajik Mansouri · Z. Ghaffarpour · M. Amidpour (✉)
Department of Mechanical Engineering, Energy Systems Division, Toosi University of Technology, Tehran, KN, Iran
e-mail: amidpour@kntu.ac.ir

Z. Ghaffarpour
e-mail: z.ghaffarpour@email.kntu.ac.ir

J. María Ponce-Ortega
Chemical Engineering Department, Universidad Michoacana de San Nicolás de Hidalgo, 58060 Morelia, Michoacán, Mexico
e-mail: jose.ponce@umich.mx

Nomenclature

A_{MD}	MD membrane area (m^2)
C	Concentration (ppm)
C_w	Salt concentration on the membrane wall in the feed water side (ppm)
CRF	Capital Recovery Factor
D_{MD}	MD permeate flowrate (kg/s)
i	Interest rate
J_w	Local permeate flux (kg/m^2 s)
J_s	Local solute flux (kg/m^2 s)
K_w	Membrane permeability (kg / m^2 Pa)
$\dot{m}$	Flow rate (kg/s)
n	Operation years of the system (year)
N	Operation hours in a year (Hour)
P	Pressure (kPa)
$p^o_{w,f}$	Water vapor pressure of the feed (Pa)
$p^o_{w,p}$	Vapor pressure of the permeate (Pa)
Q	Flow rate (m^3/h)
R	Recovery factor
T	Temperature
V_w	Average permeate velocity inside the membrane (m/s)
$\dot{W}$	Power (kw)
$x_{w,f}$	Mole fraction of the water in the feed
$year$	System service life (year)

Greek Symbols

γ	Activity coefficient
ΔP_f	Membrane pressure drop (kPa)
η_{th}	Thermal efficiency
π	Local osmotic pressures of the solutions [MPa]
ρ	Density (kg/m^3)
ρ^*	Non-dimensional density
Φ_η	First law efficiency correction factor

Subscripts

AH	Algal Harvesting
app	Approach
b	Brine

b, *p*	Permeate property in the bulk
bp	Booster pump
CW	Cooling water
eco	Economizer
eva	Evaporator
f	Feed stream
hpp	High pressure pump
IHE	Internal heat exchanger
P	Pump
p	Permeate
s	Salt
SWIP	Seawater Intake and Pre-Treatment
T	Turbine
w	Membrane wall

Abbreviations

AC	Annual Cost
AH	Algal Harvesting
AI	Annual Income
B	Benefit
BD	Biodiesel
CCHP	Combined cooling heating and power
CHP	Combine heat and power
CRF	Capital recovery factor
DCMD	Direct Contact Membrane Distillation
ERD	Energy Recovery Device
F	Fraction of the Flue gas to microalgae cultures
FLOC	Flocculation
FO	Forward Osmosis
GCC	Grand Composite Curve
GT	Gas Turbine
GWP	Greenhouse Warming Potential
HPP	High Pressure Pump
I	Income
ICE	Internal combustion engine
IDA	International Desalination Association
MD	Membrane Distillation
MED	Multi-effect desalination
MENA	Middle East and North Africa
MI	Mixing Index
MSF	Multi-stage flash distillation
MT	Microturbine

OC	Operating cost
ODP	Ozone Depleting Potential
ORC	Organic Rankine Cycle
PRO	Pressure retarded osmosis
PV	Pressure vessel
RO	Reverse Osmosis
RORC	Regenerative Organic Rankine Cycle
TMD	Thermal membrane distillation
TAI	Total annual income
TAC	Total annualized cost
TCF	Temperature correction Factor
TCI	Total capital investment
TCEORC	Two-Stage Evaporation Organic Rankine Cycle
WHO	World Health Organization

7.1 Introduction

Global warming and climate change are the most challengeable concerns in the recent years. Greenhouse gas emissions from the fossil fuel energy base systems are the main reason for creation and increasing these challenges [1]. Combustion of fossil fuels such as diesel, coal and petrol cause extreme air pollution by emitting of main greenhouse gas substances such as carbon dioxide to atmosphere. According to Karn Vohra et al. research study in the examination of effect of particular matter on mortality and health, it is estimated that 8.7 million were deaden in 2018 [2]. Energy efficiency, energy source and pollutant capture are the three important factors for managing of pollution which can be achieved through development of integrated energy systems. A new critical published report from International Energy Agency (IEA) shows that to reach the net-zero emission by 2050, the coal, oil and natural gas demands should be declined 90%, 75% and 55% respectively [3]. Definitive solutions for reduction of fossil fuel energy demands produce and apply renewable based energy systems and also improving the demand for energy-intensive processes in industries in the coming years. Among the high consumption energy process, power production and water desalination systems have more priority [4]. As can be seen in Fig. 7.1, for both advanced and developing economies share of renewable energy will be increased dramatically in comparison with common energy sources.

Pay special attention to develop new efficient and sustainable methods to produce clean electricity and water quality is necessary for researchers and governments. First of all, achieving to a proper knowledge of water desalination technologies and energy demands for related processes and sustainable energy sources is a critical point to reach a new effective design or optimize them. Based on the statistical data and energy supply and demand prediction algorithms, share of renewables in generation in 2020, 2030 and 2050 is 29, 61 and 88%, respectively. In the industry sector, bioenergy is
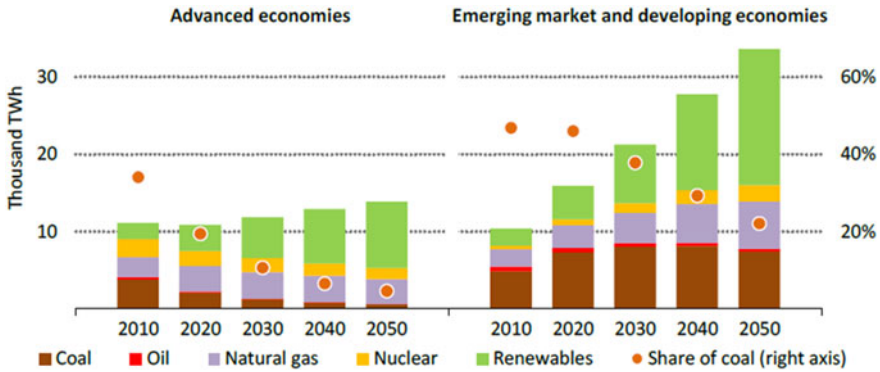
Fig. 7.1 Electricity generation from different sources by 2050 [3]

the most considerable renewable energy source since low and medium temperature applications. Geothermal and solar thermal in compared with bioenergy have low temperature operation and therefore they can be used in non-energy intensive systems and downstream processes of industry [3].

Microalgae is an important and sustainable resource to produce biofuels as a bioenergy like biodiesel, biomass and biogas. Short period cultivation process, high biomass yield in allover year by using integrated modes and utilization of domestic and industrial waste water as source of nutrients are the advantages of using microalgae for biofuel production [5]. Also, carbon dioxide is the main substance for microalgae production through different technologies and providing CO_2 is a critical subject from the environmental point of view. Carbon dioxide is a greenhouse gas that effects on global warming challenge so capturing of emitted CO_2 using energy efficient methods that lead to conserve the environment and produce valuable materials like microalgae, is a suitable solution [6]. Therefore, biogas production as a kind of modern bioenergy through microalgae not only give a good opportunity to prevent CO_2 emission also supply a sustainable energy source for power production.

The flue gas streams in electricity production plants have considerable CO_2 content that should be recovered efficiently and prevented to release to atmosphere. After energy recovery of flue gas its temperature usually fall down to acid dew point temperature which is suitable condition for microalgae cultivation. Power plants such as gas turbine with coal or natural gas fuel has more pollutant emissions through flue gas so, integration of gas turbine, heat and energy recovery system and biofuel production can provide a sustainable, friendly environment and efficient system. In this area, Tajik Mansouri et al. [7] proposed and optimized an integrated power and desalination system to cultivate algae. Minimum CO_2 emission is one of the main objective functions of optimization which is determined by defining an environmental index. They concluded that CO_2 bio-capturing by growing algae in the downstream of plant can improve the efficiency, economic and environmental factors considerably. Also, López et al. developed an integrated system consist of chemical looping combustion, power plant and CO_2 biological capturing system in order to

produce biodiesel from algae. The environmental and economic analysis showed that by using 1,049,874 tons/year coal as power plant fuel, 326 MW electricity annually was produced and with carbon bonus of 130 \$/tons, 71% CO_2 emission was reduced. From the environmental point of view, large scale microalgae cultivation implementation in different condition with injection of flue gas are evaluated by Yadav et al. [8]. Their evaluations show that in semi-continues condition cultivation, carbon footprint is less than batch cultivation especially when raceway ponds are located near to source of flue gas emission from power plant. Life cycle assessment as a feasibility study tool helps to recognize main effective hotspots in algae cultivation. In this regard many studies are carried out that represent environment impacts of biofuel production through microalgae [9, 10]. Porcelli et al. [11] perform a comprehensive life cycle assessment for a microalgae cultivation system based on different CO_2 source such as synthetic CO_2 and flue gas. Environmental benefits for cultivating of microalgae through using CO_2 content of flue gas (recovered and direct injection) and commercial liquid CO_2 are investigated experimentally in Kingston. Based on the results, the good environmental impact will be significant when direct injection of flue gas and wastewater into the algal pond is used [12].

Among applied technologies for harvesting biofuel from algae, anaerobic digestion (AD) is a prominence method which is used to generate sustainable energy source by reducing greenhouse gas emission from waste storage. A detail explanation of opportunities and challenges anaerobic digestion of microalgae is available in [13] Also, biofuel production potential from AD process with microalgae feed is demonstrated by Stiles et al. [14] and environmental and economic evaluations are carried out in [15].

Flue gas which is used for microalgae cultivation can be origin from different sources such as power plant, biomass Gasification, cement factory and industrial downstream process. Gas turbine system with natural gas as input fuel is one of the common methods to power production in many countries. They usually operate in open state and produce flue gas with high heat value and pollutant substances that should not be released to atmosphere without heat and material recovery. In previous paragraph, microalgae yield is presented as a material recovery technology in medium temperature. But before the flue gas is sent to the algae growth system, it needs to be thermally recovered. According to the temperature range of flue gas, high, medium and low energy demand technologies can be applied as recovery system. By recovering the thermal energy of flue gas, it can be used to generate electricity [16], produce cooling and desalinate seawater. Power generation through Organic Rankine Cycle (ORC), which is known as an efficient solution, has high flexibility in selecting the working fluid for low to high temperature applications [17], and therefore its use is of special interest to engineers and researchers. Supply of steam required for biomass gasification process and electricity generation by rankine cycle is one of the applications of flue gas recovery from gas turbine and its thermodynamic modeling and economic analysis has been done by Ghaffarpour et al. [18]. For flue gas temperature from 200 to 300 °C, conventional ORC and two stage serries ORC (TSORC) are evaluated and compared from the economic and performance point of view [19]. Thermodynamic analysis show that TSORC can enhance electricity

output and exergy efficiency at same flue gas temperature but with increasing the temperature, ORC can produce more power and improve energy efficiency. When cyclohexane is selected as working fluid for TSORC, the unit cost production of power is in the range of 0.077–0.133 $/kWh depend on flue gas temperature. Using of ORC and heat pump integrated system for production of power and hot water by recovering flue gas, is presented by Liang et al. [20]. In their combined system the power output of ORC is sent to run vapor compression and cold domestic water is heated 55 °C through heat pump. In other applications, the generated power through flue gas heat recovery can be used to drive reverse osmose (RO) desalination system or waste heat can be directly sent to thermal based desalination technologies such as multi-stage flash distillation (MSF), multi effect desalination (MED) and membrane distillation (MD). Due to importance of water shortage challenge and environmental issues of waste water in worldwide [21], in this paper the mentioned desalination systems are reviewed briefly and suitable systems are investigated in detail.

High demand for water consumption, increasing population growth (9.74 billion in 2050) and shortage of drinking water resources have made the use of water desalination methods very common in recent years [4]. However, water desalination processes are very energy intensive and most desalination plants in the world use fossil fuel sources for energy. For instance, Energy required for desalination in a year is 72 TWh which is approximately 0.4 of total world electricity [22], in detail energy demand for treatment of a cubic meter of industrial waste water, seawater, brackish and river water are 2–8.5, 0.62–8.5, 0.48 and 0.37 kW, respectively [23]. In order to prevent the harmful effects of environmental pollution, the use of polluting energy sources and adjusting the amount of energy consumed by desalination processes should be directed towards the use of recycled heat sources and renewable energy sources to be economically and energy justifiable. This undeniable dependence of water and energy resources on each other has led to the concept of Nexus, which accurately defines the relationship between energy and water consumption per unit of water and energy production through different modeling tools [24, 25]. Considering the environmental effects of each of the water and energy sectors in the Nexus concept is an inseparable part of the modeling and design of cogeneration and multi-generation systems [26]. Therefore, in this study for proposed multigeneration system energy, water and environment Nexus analysis are considered and proper results are obtained.

Presently, the feed water of desalination systems includes 59% seawater, 23% brakish water, 7% river water, 5% waste water and 6% other water which about 67% of them are treated by membrane method such as RO and 33% by thermal method such as MSF and MED [27]. In this regard, CO_2 emission of fossil fuel base energy desalination processes is calculated 76 million ton per year which should be controlled through switch to renewable energy source [28, 29].

From the economic point of view, unit cost of RO clean water production has the lowest value (0.26–0.54 $/m3) in compared with MSF (0.56–1.75 $/m3), MED (0.52–1.01 $/m^3) and MD (1.17–2 $/m^3) [30]. Also, Also, the environmental analysis shows that for conventional desalination technologies other than RO [31], the average CO_2 emission per treated water produced is 16 kg / m^3, but in the RO method this emission is reduced to 2 kg/m^3 [32]. Currently, RO is the most common system

in the world and in terms of energy consumption, total price and carbon dioxide emissions are more justifiable, but to achieve better results, this system must be combined with power generation units like ORC which is worked based on new energy sources and recovered heat. In this area, a low temperature solar driven ORC power production unit supplies the electricity demand of brakish and seawater RO desalination in Torres and Rodríguez work [33]. In their integrated system, four ORC working fluids including butane, isopentane, R245fa and R245ca are examined and R245fa is selected for detail design. Also, a comprehensive study about determination of important parameters in solar ORC with RO system is carried out in [34]. the other clean energy base ORC-RO system which electricity of components such as circulation and working fluid pumps are provided by Photovoltaic panels and produced ORC power is sent to RO unit, is proposed by Karellas et al. [35]. Financial feasibility study of the hybrid system shows that in the in the less subsided scenario, levelized cost of water production reaches to 8.35 Euro/m3 which can be competitive in Greek energy market. Water, Energy and Environmental nexus analysis through energy, exergy, economic and environment calculations are the main investigations in the ORC-RO systems [36]. A multi-objective optimization based on economic and environment variables is implemented for an ORC-RO-MD cogeneration system with consideration of energy-water-environment nexus by Tajik Mansouri et al. [37]. Their investigations resulted that adding MD desalination system in the output of RO brine stream can improve performance of system especially from economic and environment points of view.

Recovered energy of flue gas as an alternative source for ORC-RO and other combination systems can be applied to water, power and cooling generation [38]. The obtained heat of flue gas can be sent to different thermal desalination technologies such as MED. In a configuration the flue gas heat is fed directly to run the MED and after that RO is placed, and in another configuration flue gas is sent to a HRSG to produce high pressure steam and then power is generated through steam turbine and is fed to RO. Also, to gain cooling energy, a single effect LiBr-water absorption cycle can run by energy of extracted steam from turbine [39]. Energy, exergy and economic evaluation of a waste heat-based ORC-MED poly-generation cycle to electricity, water and cooling production is introduced by Mohammed et al. [40]. They obtained that 8.055 MW electricity with value of 1.035 ¢/kWh and 66.55 m^3/h freshwater with value of 0.4136 $/$m^3$ can be produced. By comparing the results of reviewed papers, it can be understood that the best scenario for power and water production of flue gas energy recovery is ORC-RO system but with considering the environment issue the outlet extreme brine water from RO should not be sent to ambient water directly. Therefore, in the downstream of OR system a MD desalination can be considered to prevent dangerous effects of rich saline water. A comparative study to examine the feasibility of using MD technology shows that the cost of producing water can be reduced to 0.57 $/$m^3$ when MD works in reverse osmose coupling and a cheap heat source is available [41]. Forward osmosis and reverse electrodialysis are the other technologies which can be applied for energy and water recovery of RO brine. However, the MD method is a more appropriate and attractive choice due to the use of low thermal energy levels for purification and insensitivity to the concentration

of input brine from the RO side [42]. An experiment to determine the economic and process conditions of using the MD system to recover energy and water of thermal power plant in Qatar was conducted by Summer Adam et al. [43].

As a result, reviewing previous articles shows that in order to solve the problems related to the energy supply of desalination units, they must seek to use renewable sources or use the waste heat sources of industries. Recovery of energy and materials from flue gas for use in water desalination and biofuel production are among the actual solutions to overcome the existing shortcomings. In this study, by considering the approach of water, energy and environment nexus, achieving clean and sustainable electricity, freshwater and biogas through heat recovery of flue gas exhaust from gas turbine system are the main objectives. By capturing the carbon dioxide in the flue gas stream in the final stages of recovery, the CO_2 needed for the algae growth unit is supplied. This can significantly reduce the amount of greenhouse gas emissions into the environment and make a valuable product. Next to the algal cultivation unit, an anaerobic digester is placed to produce biogas fuel, which is sent to the combustion chamber of the gas turbine as a modern and stable biofuel. The gas turbine power generated is sent to the grid, and the high-temperature exhaust flue gas is recovered thermally through triggering an organic Rankine cycle. The type of working fluid used in ORC is one of the main design parameters and an investigation has been done to select the appropriate fluid mixture. Subsequently, a RO water desalination unit has been set up after receiving the required power from the organic Rankin unit. Brine output from RO is sent to the MD system to recover and produce energy and water, and finally water in desire quality can be produced by RO and MD units. This new and novel proposed integrated system is fully conceptualized and used resources and produced values are clearly identified. Also, the effect of main operating parameters on the total performance are determined by modelling and analyzing from the energy, economic and environmental points of view. Since the fuel required for the gas turbine is supplied by the biogas produced in the algae cultivation unit, it is no longer dependent on an external energy source and thus reach to concept of zero fossil energy systems is the other valuable novelty of this study. Also, the flue gas is recovered in two stages, which leads to the production of the required power of the desalination unit and the supply of carbon dioxide to the algae growth unit. These recoveries have improved energy efficiency, increased the operational viability of the project economically and, most importantly, reduced the emission of pollutants into the air and water of the environment.

7.2 Methodology

In this research, the aim is to integrate the waste heat recovery system based on Organic Rankine Cycle with hybrid RO-MD desalination system. To reduce carbon footprint of the desalination plants, a biological CO_2 capture system based on the microalgae cultivation is considered. To take into account the environmental effect of the system in the plant optimization, an objective function is considered as the

minimization of the CO_2 emission to the water desalinated. For this purpose, the following procedure has been taken to achieve the optimum system configuration:

- Modeling of microturbine to determine flue gas temperature and mass flow.
- ORC system synthesis.
- RO system design and determining fresh water and brine produced in this system.
- Determining available waste heat for RO brine preheating in order to produce fresh water in MD system.
- Determining MD produced water and brine produced.
- Calculating levelized cost of produced water, annual profit of the system and also an environmental index as CO_2 emission per desalinated water production.

7.3 Modeling

A schematic diagram of the investigated cycle is presented in Fig. 7.2. As shown in the figure, in this system, air first enters the compressor and after compression, in the heat exchanger (recuperator), it exchanges heat with the combustion products from the gas turbine and exits at a higher temperature and enters the combustion chamber of the gas turbine. In this part, during the combustion process, the chemical energy in the fuel is released and increases the temperature of the combustion products. These combustion products then enter the turbine and generate power. The combustion products from the turbine then enter the recuperator and after heat transfer to the compressed air leaving the compressor, it enters the heat recovery boiler. The heat recovery boiler considered in this section consists of two main parts, the economizer and the evaporator. After heat exchange between the combustion products and the working fluid of the organic Rankin cycle in the heat recovery boiler, part of the flue gas enters the algae cultivation system and the rest is released into the environment.

After injecting the flue gas stream and required fertilizers into algae growth ponds, the concentrated algae are produced and fed into anaerobic digestion (AD) reactor.

The algal cultivation stage consists in raceway ponds in which nutrients (phosphorus and nitrogen), water, sunlight, carbon dioxide, and a culture inoculum (Chlorella vulgaris) are required. The modeling of this stage is based on the equations presented in [7]. By converting the algae to methane through AD process, biogas as a bioenergy source is generated and more part of it is sent into combustion chamber of gas turbine system and a small portion is used to supply the energy required by the anaerobic digestion process. The AD extracted biogas consists of 70% CH_4 and 30% of CO_2 with lower heat value of 6.958 kWh.m^3 which can be upgraded to pure biogas composed of 96% of CH_4 by pressurized water. Based on the life cycle assessment biogas production by algae plant [44], per one kg of algae, 1.172 kg CO_2 and 0.375 m^3 biogas consumed and produced in culture-harvesting and anaerobic digestion steps, respectively. Also, electricity consumption in all steps (algae to pure biogas) include culture and harvesting, natural settling, centrifugation, anaerobic digestion, and purification has been calculated 0.6173 kWh per kg of algae. Lower energy demand (electricity and water) and less effects on environment (ozone layer
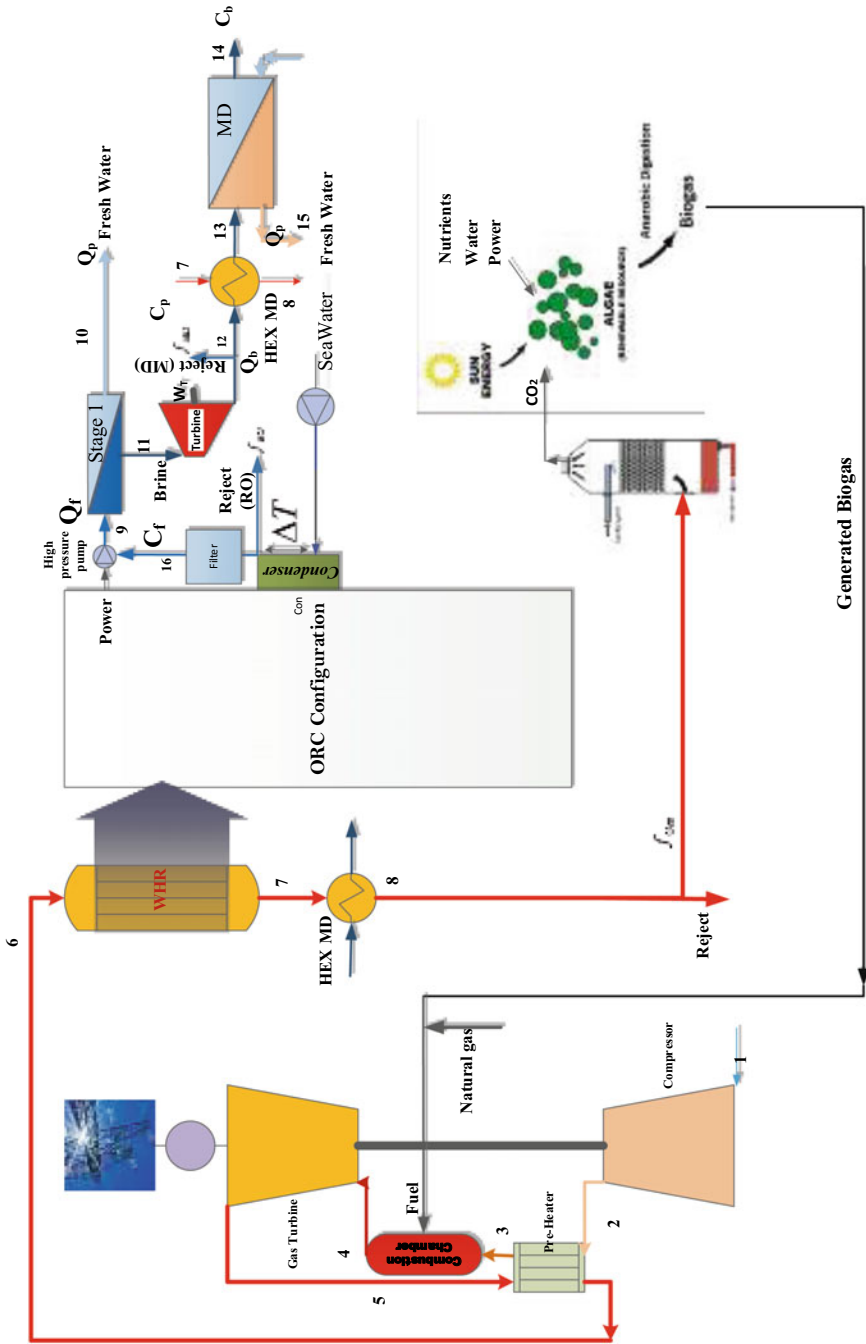
Fig. 7.2 Schematic diagram of the investigated system

depletion and photochemical oxidation) are the main advantages of production of biogas in comparison with biodiesel [45].

In the organic Rankin cycle, different configurations are considered as decision variables as shown in Fig. 7.3. For example, in the simple organic Rankin cycle, the working fluid pressure is increased by the pump and then the fluid enters the heat recovery boiler. In the first part, the fluid enters the economizer and its temperature increases by absorbing heat from the flue gas stream. Then the working fluid enters the evaporator. In this section, the working fluid exits the evaporator and enters the turbine by absorbing heat into saturated steam. After generating power in the turbine, the output fluid enters the condenser and transfers heat to the cooling fluid (seawater) and then enters the pump in saturated liquid phase [46–48].

For gas turbine modeling, the equations presented in [7] are applied. In addition, the governing equations for thermodynamic and economic modeling of the ORC and heat recovery system are presented in Table 7.1.
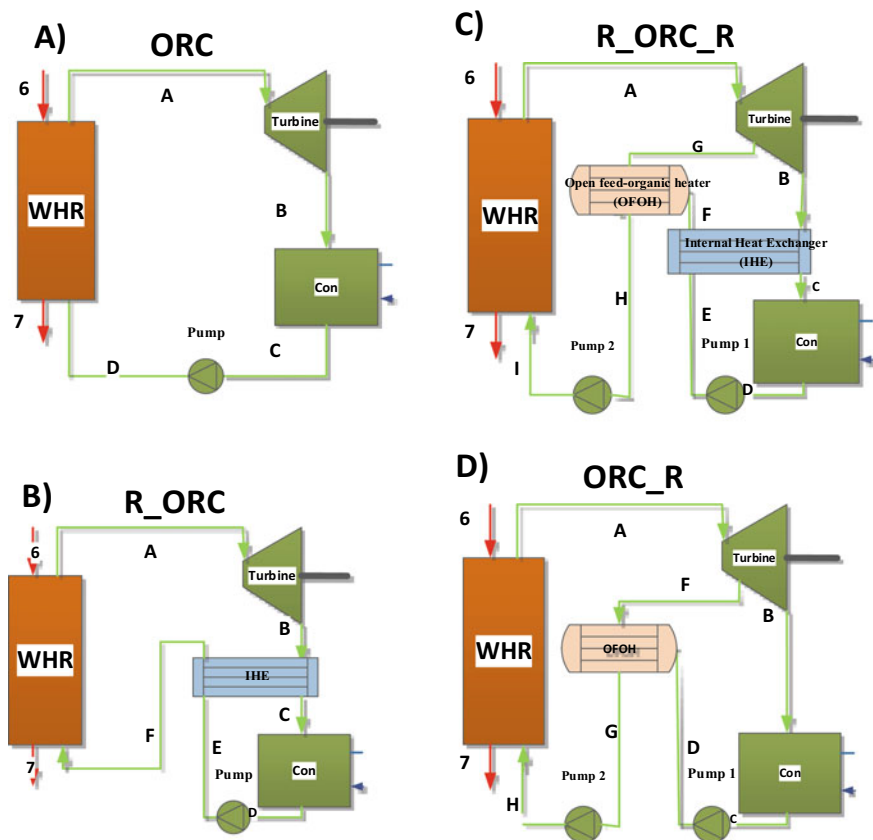

Fig. 7.3 Different configurations of the ORC considered in the present study

Table 7.1 Energy equations and cost functions of the components of ORC system [7]

Component	Input data	Energy Equation	Cost function
Turbine	η_T =80% P_A	$T_A \langle K \rangle = T_{sat}(P_A)$ $\eta_T = \dfrac{h_A - h_B}{h_A - h_{B,is}}$ $W \left\langle \dfrac{kJ}{kg} \right\rangle = (h_A - h_B)$ $W_T \langle kW \rangle = m_A(h_A - h_F) +$ $(m_A - m_F)(h_F - h_B)$	$CC_{Turbine} = 3880.5 W_T^{0.7} \phi_\eta \phi_T$ $\phi_\eta = \left[1 + \left(\dfrac{1-0.95}{1-\eta_\tau}\right)\right]^4$ $\phi_T = \left[1 + 5\left(\exp\left(\dfrac{T_A - 866}{10.42}\right)\right)\right]$
Condenser	T_D ΔT	$P_D = P_{sat}(T_{con})$ $Q_{cond} \langle W \rangle = m_C(h_C - h_D)$ $T_{cw,out} = T_{cw,in} + \Delta T$ $T_{cw,in} = T_{SeaWater}$ $m_{water} \left\langle \dfrac{kg}{s} \right\rangle = \dfrac{Q_{cond}}{Cp_{water} \Delta T}$	$CC_{cond} = \dfrac{280.74 Q_{cond}}{2200 \Delta T} + 746 m_{water}$ $+70.5 Q_{cond} \times$ $(-0.6936 \ln(T_{cw,out} - T_{cw,in}) + 2.1897)$
Pump	η_P =85% P_G	$h_I = h_H + W_p \left\langle \dfrac{kJ}{kg} \right\rangle$ $P_H = P_G + \rho g h / 100000$ $W_p \left\langle \dfrac{kJ}{kg} \right\rangle = \dfrac{(P_H - P_I)}{\eta_P \rho_I}$ $W_{p,2} \langle kW \rangle = m_H(h_H - h_I)$	$CC_p = a_1 (mV\Delta P)^{a_2} f_m \phi_\eta$ $\phi_\eta = 1 + \left(\dfrac{1-0.8}{1-\eta_\eta}\right)^3$ $f_m = \begin{cases} cast\,iron = 1 \\ Steel = 1.41 \end{cases}$ f_m: Material correction factor, here: $f_m = 1.41$

Table 7.1 (continued)

WHR (Eco+Eva)	$T_{p,p}$	$T_{app} = T_{sat} - T_{f,o,Eco}$ $T_{p,p} = T_{Gas,out,Eva} - T_{sat}$	$CC_{WHR} = c\left[\left(\dfrac{Q_{Eco}}{LMTD_{Eco}}\right)^{0.8} + \left(\dfrac{Q_{Eva}}{LMTD_{Eva}}\right)^{0.8}\right] =$
	T_{app}		
	$T_{gas,in}$	$Eco: m_{Gas}Cp_{Gas}\left(T_{Gas,o,Eco} - T_{Gas,i,Eco}\right)$ $m_f\left(h_{f,o,Eco} - h_{f,i,Eco}\right)$	$d \times m_{ORC} + e \times m_{Gas}^{1.2}$
	m_{gas}	$Eva: m_{Gas}Cp_{Gas}\left(T_{Gas,o,Eva} - T_{Gas,i,Eva}\right) =$ $m_f\left(h_g - h_{f,o}\right)$	$c = 6570 \ \$\big/(kW/K)^{0.8}$
	$\bar{X}_{gas}$	$Cp_{Gas} = f\left(y_{gas}, T_{Gas}\right)$	$d = 21276 \ \$\big/(kg/s)$
			$e = 1184.4 \ \$\big/(kg/s)^{1.2}$
Open feed-organic heater (OFOH)	P_G	$T_H = T_{sat}\left(P_G\right)$ $P_F = P_G$ $Q_{OFOH} = m_G h_G + m_F h_F$	$CC_{OFOH} = b\left(Q_{OFOH}\right)^{0.7}$ $b = 145.315 \ \dfrac{\$}{kW^{0.7}}$
Internal Heat Exchanger	η_{IHE} $=80\%$	$\eta_{IHE} = \dfrac{T_B - T_C}{T_B - T_E}$ $A_{IHE}\langle m^2 \rangle = \dfrac{Q_{IHE}}{U \times MTD}$	$CC_{IHE} = 8000 + 259.2 \times A_{IHE}^{0.91}$

$T_{f,o,Eco}$ (fluid temperature at the outlet of economizer), $T_{Gas,out,Eco}$ (gas temperature leaving the economizer), $T_{Gas,o,Eco}$ (gas temperature entering the economizer) and $\dot{m}_f$ (working fluid flow of ORC) are 4 unknown variables in the equations developed for waste hear recovery modeling. As the flow is obtained, the heat and power generation can be calculated.

To prevent acid corrosion in the heat exchanger of the membrane distillation system, a temperature constraint is considered for the flue gas entering the heat exchanger. The modeling of RO system is performed based on the element-by-element method described in [7]. In this method, each element is divided into small meshes and basic equations are implemented and solved for each mesh, then for each element, then for each pressure vessel, so finally, the whole stage is analyzed. The basic equations used in the modeling are presented in Table 7.4. The temperature correction coefficient for the DOW membrane is defined as follows [7].

$$
\begin{aligned}
TCF &= EXP\left[2640\left(\frac{1}{298} - \frac{1}{273 + T}\right)\right], \quad T \geq 25°C \\
TCF &= EXP\left[3020\left(\frac{1}{298} - \frac{1}{273 + T}\right)\right], \quad T \leq 25°C
\end{aligned}
\tag{7.1}
$$

Reverse osmosis plant investment cost can be determined based on [7]. MD system modeling is performed based on [7]. The driving force in this system is the partial pressure of water vapor on both sides of the membrane, which allows the water flux pass through the membrane to be determined. The partial pressure is also determined by Eqs. (7.14) and (7.15):

$$
J_w = B_w\left(p_{w,f}^0 \gamma_{w,f} x_{w,f} - p_{w,p}^0\right)
\tag{7.2}
$$

$$
p_{w,f}^0 = e^{\left(23.1964 - \frac{3816.44}{T_{m,f} - 46.13}\right)}
\tag{7.3}
$$

$$
p_{w,p}^0 = e^{\left(23.1964 - \frac{3816.44}{T_{m,p} - 46.13}\right)}
\tag{7.4}
$$

Then, based on the membrane type, feed and product temperatures are defined:

$$
\theta = \frac{T_{m,f} - T_{m,f}}{T_{b,f} - T_{b,p}}
\tag{7.5}
$$

Based on the experimental tests, it is assumed the following [7]:

$$
T_{b,f} - T_{m,f} \approx T_{m,p} - T_{bp}
\tag{7.6}
$$

Thermal efficiency of the MD system is calculated as follows:

$$\eta_{MD} = \frac{\frac{k_m}{\delta}\left(T_{m,f} - T_{m,p}\right)}{J_w H_{vw} + \frac{k_m}{\delta}\left(T_{m,f} - T_{m,p}\right)} = \frac{\dot{Q}_{abs}}{\dot{Q}_p H_{vw}} \tag{7.7}$$

In the above equations, J_w, $T_{m,f}$ and $T_{m,p}$ are unknown, which can be calculated by solving Eqs. (7.2), (7.5) and (7.6). In addition, based on Eq. (7.7) and the absorbed heat, the freshwater produced can be calculated. Finally, the required area for membrane can be calculated having desalinated water flow and flux. The capital cost of the membrane for MD system is calculated based on Eq. (7.9).

$$A_m = \frac{\dot{Q}_p}{J_w} \tag{7.8}$$

$$CC_{MD} = 58.5A_m + 1115\dot{Q}_f \tag{7.9}$$

7.4 Optimization

Economic advantage is necessary for the development of a multi-generation system. One of the objective functions that has been considered in this study is the annual profit of the investigated system. The annual profit of the system includes all the annual income of the system minus the total annual costs. System income consists of the income from freshwater produced in reverse osmosis and membrane distillation systems. In addition, the other part is the income from the sale of biogas to the gas turbine power plant. System costs also include costs associated with the organic Rankine cycle, reverse osmosis and membrane distillation, as well as the costs of the algae cultivation and biogas production system.

Another objective function considered is the amount of CO_2 emission per freshwater produced in the system. Since the amount of the flue gas outlet from the gas turbine and consequently the mass flow rate of carbon dioxide emitted through that is constant, so due to the dependence of the biological carbon dioxide capture system on the input carbon dioxide flowrate and also the defining the Flue gas fraction to algae system as one of the decision variables in optimization, it is necessary to consider the effects of changes in this parameter simultaneously with changes in the amount of fresh water produced in the integrated system. So, CO_2 emission flowrate per desalinated water production is considered as the objective function.

7.5   Results and Discussion

As mentioned before, the heat recovery of the flue gas from a gas turbine is considered in this study for cogeneration. The T-S diagram of the modeled gas turbine is shown in Fig. 7.4.

The main variables considered in the multi-objective optimization along with their bounds are shown in Table 7.2.

The optimization was performed using Genetic Algorithm through MATLAB optimization toolbox.

7.5.1   Optimization

In this case, the annual profit and CO_2 emissions of the plant per produced freshwater are considered as objective functions. The optimization was performed considering 12 variables with their associated constraints. We let the genetic algorithm to select between different mixtures of working fluids with different fractions to find the optimum one as one of the variables. Twenty mixture of fluids were selected (Table 7.3). Working fluid properties and their environmental impacts are shown in Table 7.4.
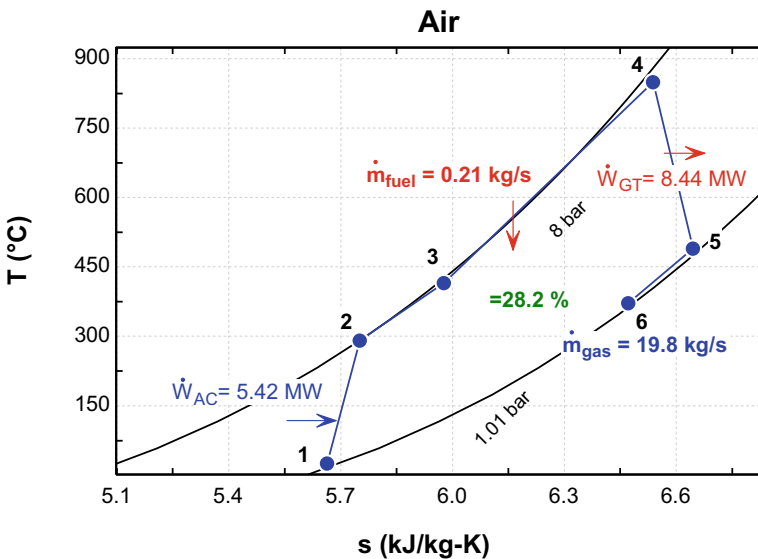

Fig. 7.4 T-S diagram of the modeled gas turbine

**Table 7.2** Main optimization variables of the investigated system with their associated bounds

No	Variable	Lower bound	Upper bound
1	Fraction of working fluid mixture	0.0	1.0
2	ORC turbine inlet pressure (kPa)	200	3000
3	ORC condenser Temp. (°C)	45.0	75.0
4	ORC evaporator approach Temp. (°C)	5	10
5	ORC evaporator pinch Temp. (°C)	5	270
6	MD system reject	0.0	1.0
7	Deaerator working pressure (kPa)	400	4500
8	RO system recovery factor	0.30	0.70
9	RO reject	0.0	1.0
10	Selected working fluid	1 (Table 7.3)	20 (Table 7.3)
11	Selected ORC configuration	1 → A in Fig. 7.3	4 → D in Fig. 7.3
12	Flue gas fraction to algae system	0.0	1.0

Table 7.3 Pair of working fluid in each considered mixtures

No	Working fluid 1	Working fluid 2	NO	Working fluid 1	Working fluid 2
1	R245ca	R141b	11	R245ca	R152a
2	R245ca	R123	12	R245ca	R134a
3	R245ca	R142b	13	R141b	R152a
4	R245ca	R236ea	14	R142b	R236ea
5	R141b	R123	15	R123	R142b
6	R141b	R142b	16	R123	R236ea
7	R141b	R236ea	17	R142b	R236ea
8	R123	R142b	18	R123	R142b
9	R123	R236ea	19	R236ea	R152a
10	R142b	R236ea	20	R236ea	R134a

Table 7.4 Properties of the selected working fluids

No	Working fluid	Molecular mass (kg/kmol)	T_b [K]	P_{cr} [MPa]	T_{cr} [K]
1	R245ca	134.05	298.28	3.925	447.57
2	R236ea	152.04	297.34	3.502	412.44
3	R141b	116.95	305.2	4.46	479.96
4	R123	152.93	300.97	3.662	456.83
5	R114	170.92	267.74	3.257	418.83
6	R113	187.38	320.74	3.392	487.21
7	R142b	100.5	264.03	4.055	410.26
8	R134a	102.03	247.08	4.0593	374.21
9	R152a	66.015	154.56	4.5168	386.41
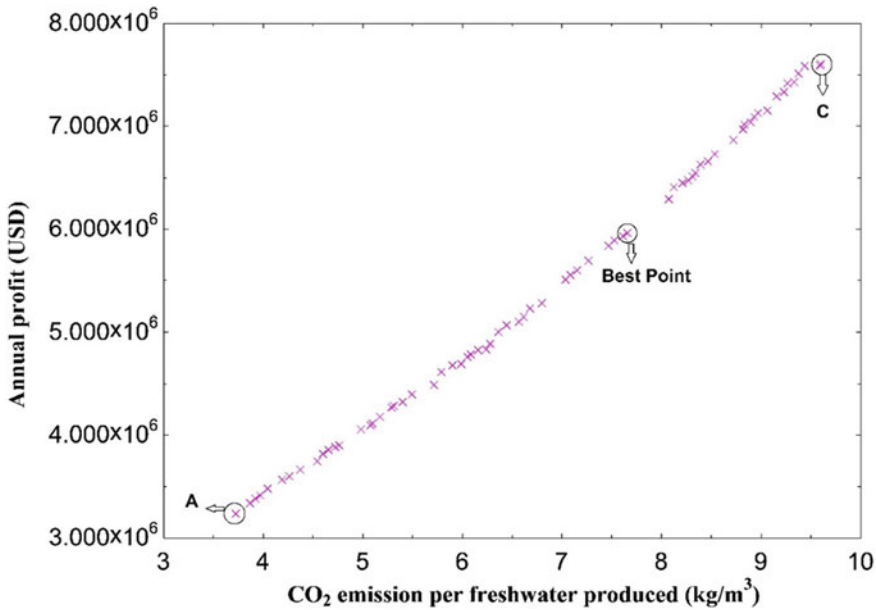
Fig. 7.5 Two-objective optimal Pareto-curve for the annual profit and CO_2 emissions of the plant per produced freshwater

Figure 7.5 shows two-objective optimal Pareto-curve for the total annual profit and the CO_2 emissions of the plant per produced freshwater.

Table 7.5 shows the optimization results for three investigated working point on Pareto curve. In addition, Table 7.6 shows the main techno-economic results of the two-objective optimization.

In this section, a sensitivity analysis of the main economic and technical parameters of the system to the main input variables is presented. Figure 7.6 shows the changes in the annual profit and CO_2 emission of the plant with flue gas fraction to the algae cultivation. As it can be seen, both optimization objectives decrease with the increase in the flue gas fraction to microalgae plant. As the fraction increases, the size of the biogas production system and consequently, the annual cost of the system increases. Also, due to the increase in the part of the exhaust gas that enters the algae production system and, consequently, increasing the biological capture of carbon dioxide, the amount of carbon dioxide emission per freshwater produced decreases.

One of the most important quality parameters in water desalination systems is the changes in the freshwater quality and also the concentration of the brine of the system. When the power delivered to the high-pressure pump of RO system decreases (due to the decrease in ORC generated power), feed pressure and thus, the quality of the desalinated water decreases. In addition, the concentration of the brine rejected from the system is one of the most important factors to be considered. Based on the

Table 7.5 Optimization results for three investigated working point on Pareto curve

No	Variable	Point A	Best point	Point C
1	Fraction of working fluid mixture	0.7	0.7	0.7
2	ORC turbine inlet pressure (kPa)	2931.2	2931.6	2932
3	ORC condenser Temp. (C)	49.6	49.6	49.7
4	ORC evaporator approach Temp. (C)	5.9	6.5	6.5
5	ORC evaporator pinch Temp. (C)	81.5	81.6	81.8
6	MD system reject	0.63	0.6	0.59
7	Deaerator working pressure (kPa)	–	–	–
8	RO system recovery factor	0.51	0.51	0.55
9	RO reject	0.32	0.21	0.2
10	Selected working fluid	R141b(0.7)/R236ea(0.3)	R141b(0.7)/R236ea(0.3)	R141b(0.7)/R236ea(0.3)
11	Selected ORC configuration	Basic cycle (configuration (a) in Fig. 7.3)	Basic cycle (configuration (a) in Fig. 7.3)	Basic cycle (configuration (a) in Fig. 7.3)
12	Flue gas fraction to algae system	1	0.4	0.03

RO equations, it is expected that the brine concentration increases with the decrease in the power delivered high pressure pump of RO, however, due to the utilization of MD system for RO brine treatment, the final concentration of the brine rejected from the hybrid desalination system is appropriately controlled (Fig. 7.7).

Another parameter investigated is the changes in the levelized cost of water with flue gas fraction to microalgae plant. As it is observed in Fig. 7.8, as the flue gas to microalgae plant increases, the levelized cost of produced freshwater increases. The reason for this is the increase in water consumption in the carbon dioxide biological

Table 7.6 The main techno-economic results of the two-objective optimization

Parameter	Unit	Optimum point	Point C	Point A
Unit production cost of water	$/m^3	0.54	0.5	0.58
Unit production cost of electricity in ORC system	Cent/kwh	3.1	3.14	3.16
RO system desalinated water production	Kg/s	54.88	59.35	46.95
MD system desalinated water production	Kg/s	0.85	0.1	0.1
Total desalinated water production	Kg/s	55.73	59.45	47.05
RO total annualized cost	$	586,090	594,790	511,260
MD total annualized cost	$	3215	3111	2656
ORC total annualized cost	$	266,420	265,370	268,770
Microalgae and biogas plant total annualized cost	$	1,108,000	90,171	2,779,200
Annual income	$	7,925,100	8,559,000	6,799,000
Annual cost	$	1,963,900	953,660	3,562,100
Annual profit	$	5,961,200	7,605,400	3,236,900
Percentage of GT fuel supplied by biogas		1.33	0.1	3.35
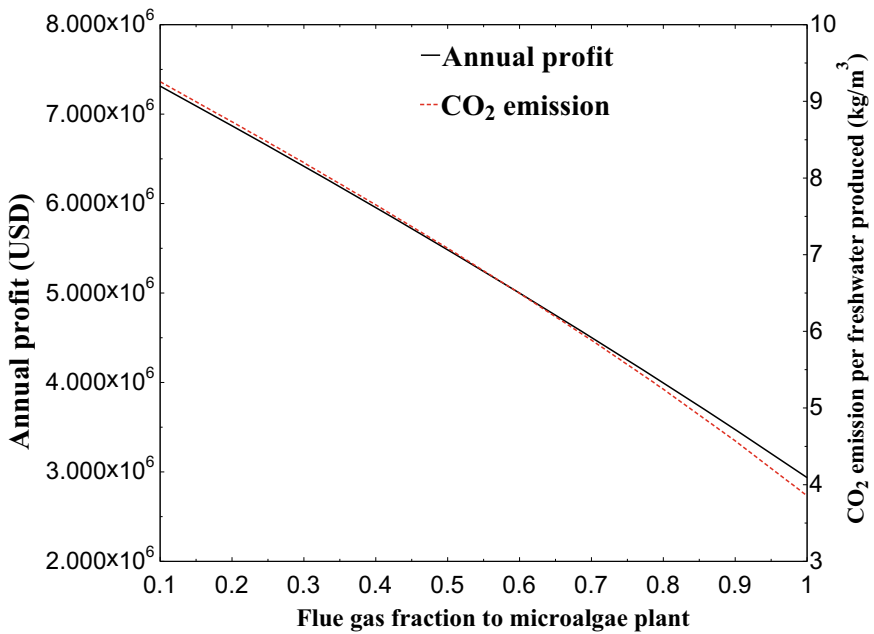
Fig. 7.6 Changes in the annual profit and CO_2 emission of the plant with flue gas fraction to the algae cultivation
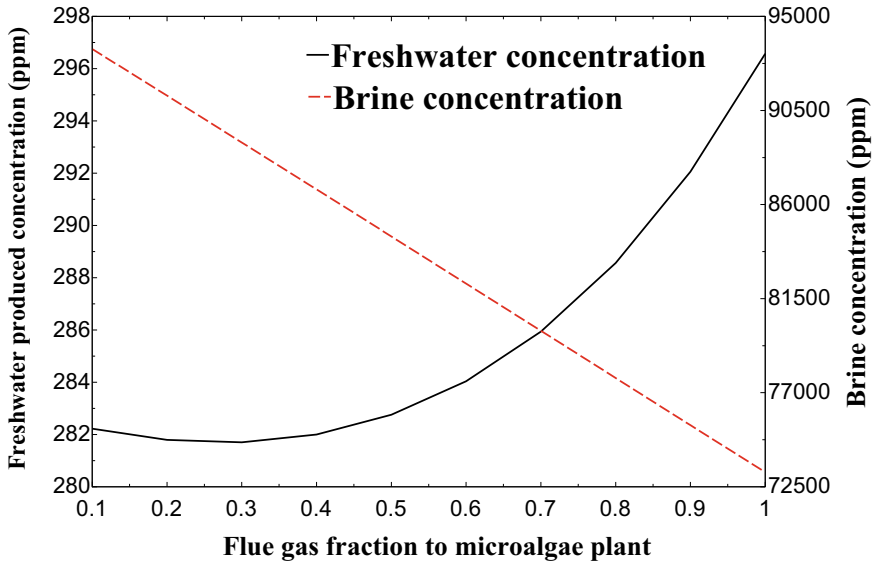
Fig. 7.7 Changes in brine and product concentration with flue gas fraction to the algae cultivation
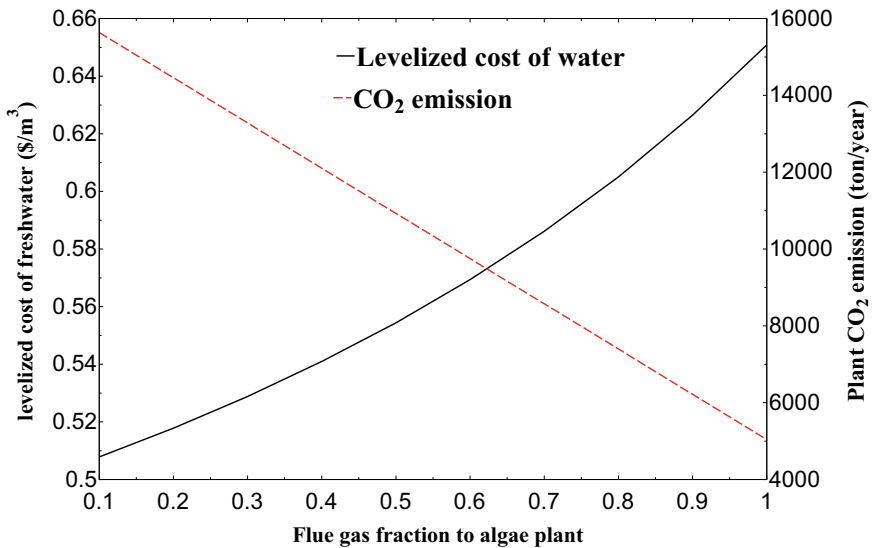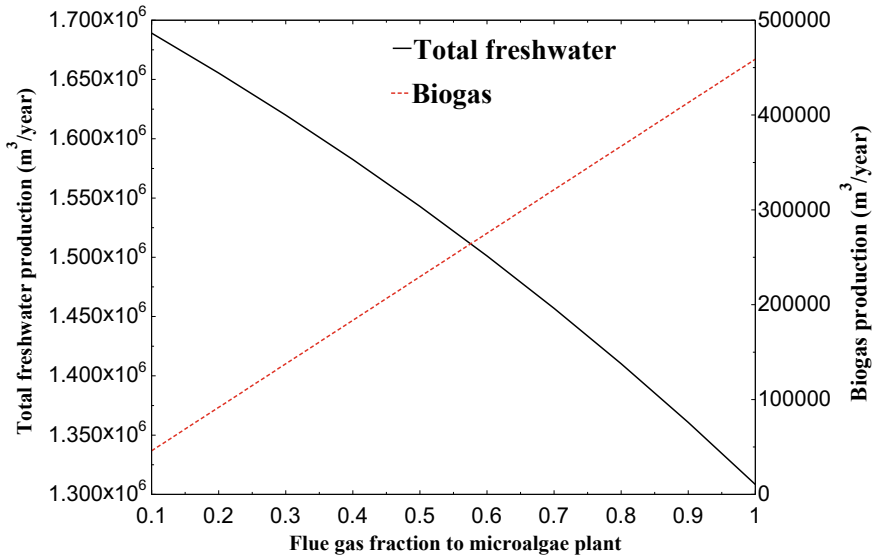

Fig. 7.8 Changes in brine and product concentration with flue gas fraction to the algae cultivation

Fig. 7.9   Changes in the system products with flue gas fraction to the algae cultivation

capture system and thus reduction in the amount of the total water production in the cogeneration system (amount of water which can be sold). Also, by the increase in the flue gas delivered to the microalgae system, total carbon dioxide emission of the system decreases, which is shown in Fig. 7.8.

As shown in Fig. 7.9, increasing the flue gas sent to the algae cultivation system, it is observed that the amount of freshwater production reduces and the amount of biogas produced increases.

One of the most important parameters in the modeling of the integrated system is the fraction of the working fluid in the working fluid mixture utilized in the ORC system. Sensitivity analysis of the main performance parameters of the system is investigated to the changes of this parameter. As it can be seen in Fig. 7.10, the annual profit of the system slightly decreases with the increase in the fraction of working fluid (R141b) in the mixture. It should be also noted that at a given pinch temperature, a change in fluid type leads to a change in critical temperature and pressure and saturation temperature, and as a result the second law of thermodynamics in the modeling of the heat exchanger is not satisfied. Therefore, at each pinch temperature, a sensitivity analysis was performed in the points with acceptable answers.
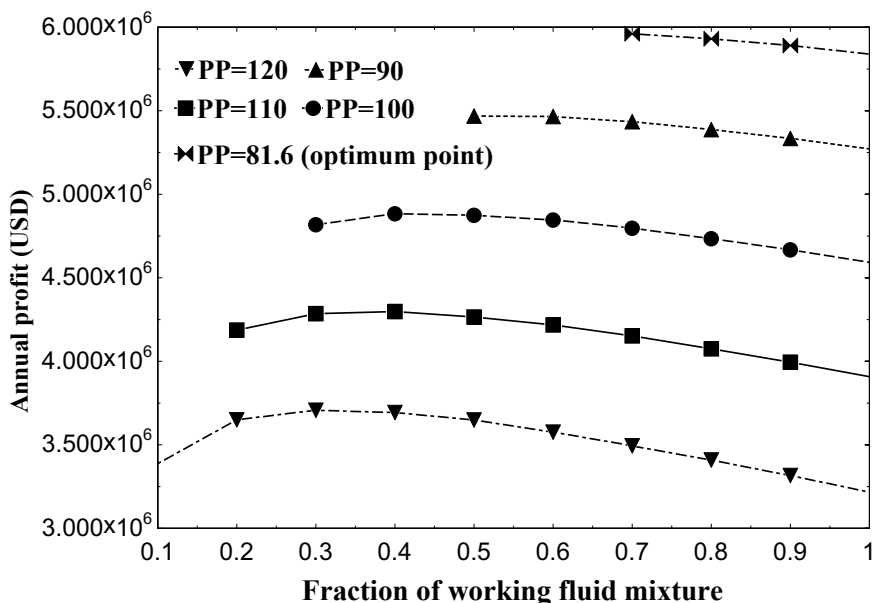
Fig. 7.10 Changes in the annual profit of the system with pinch point and fraction of working fluid mixture

Sensitivity analysis is performed at the optimum point and at this point, the optimal fluid is the mixture of R141b and R236ea. It can be seen in Table 4 that the critical temperature and saturation point of fluid R141b is higher than that of fluid R236ea. Therefore, in a fluid mixture with a higher percentage of R236ea, the mixed fluid has a lower saturation temperature and the condition of the second law of thermodynamics in modeling of the heat recovery system (in the evaporator section) is not satisfied.

On the other hand, since the working temperature of the ORC system using R236ea fluid is lower than the working temperature of the cycle using R141b, by increasing the percentage of R141b fluid in the working fluid mixture, the working temperature of the ORC system increases, and hence, the difference with flue gas temperature decreases. Therefore, the area of heat exchanger and as a result, the related costs increase which cause the reduction in the annual profit of the system.

The increase in pinch temperature, amount of waste heat recovery and hence power generation in the organic Rankine cycle decreases. Since the power generated in ORC is delivered to HPP of RO system to supply the required power, increase in the pinch point, assuming the other parameters are constant, decreases annual profit of the system due to the reduction in freshwater production (Figs. 7.10 and 7.11).

Figure 7.12 shows the changes in the amount of carbon dioxide emitted from the studied system per freshwater produced. As can be seen, with increasing the fraction of fluid R141b in the working fluid mixture and due to decreasing the amount of water produced in the system, the amount of CO_2 emission per freshwater produced increases. Also, with increasing pinch temperature and considering the decrease
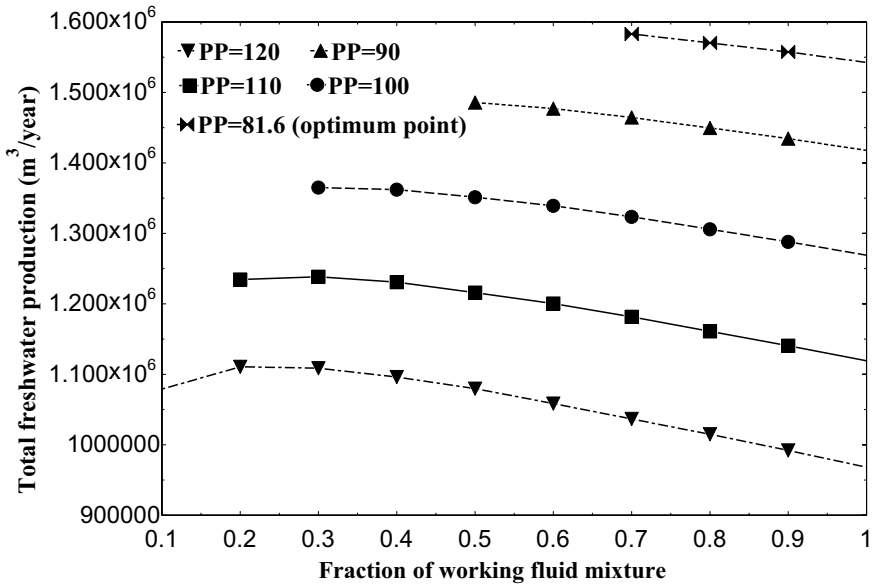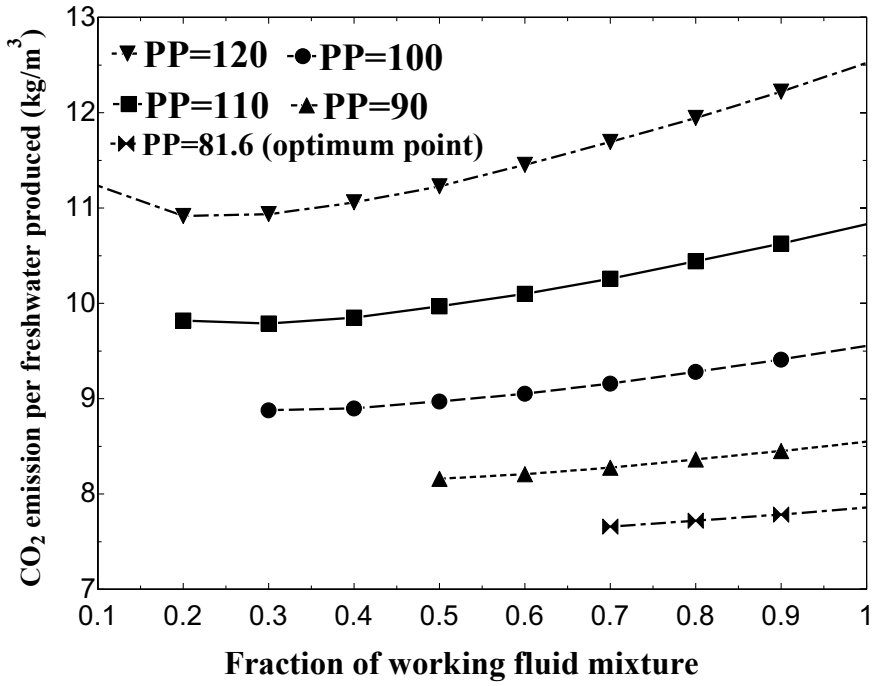
Fig. 7.11 Changes in the freshwater production in the system with pinch point and fraction of working fluid mixture

in power generation in organic Rankine cycle and thus reduction in the amount of produced water, assuming the other parameters of the system are constant, the amount of carbon dioxide emitted from the system increases.

Increasing the concentration of seawater entering the system reduces the annual profit of the system (assuming other model parameters remain constant). This can be related to the increase in osmotic pressure and thus the decrease in the potential of water to pass through the membrane. Given that the environmental objective function is inversely proportional to the amount of fresh water production, reducing the amount of water production increases the amount of carbon dioxide emissions per water produced (Fig. 7.13).

7.6   Conclusion

In this chapter, a conceptual design and energy, economic and environment analysis of an integrated ORC-RO-MD with algae cultivation to biogas production are carried out. Waste heat from gas turbine exhaust is used as to drive ORC then electricity of ORC unit is delivered to RO desalination system then the output brine to more purification is fed into MD unit. For more environmental and energetic recovery, the required CO_2 for algae production is given from flue gas stream and biogas is generated through anaerobic digestion. In ORC system, mixture of different working

Fig. 7.12 Changes in the CO_2 emission per freshwater of the system with pinch point and fraction of working fluid mixture

fluids with variable fractions are examined and their effect on annual profit, freshwater production and total CO_2 emission are investigated. Also, the effect of flue gas fraction to algae growth unit on levelized cost of produced freshwater and amount of biogas produced is sensitivity analyzed. Therefore, multi-objective optimization with considering the maximization of the economic benefit and minimization of the CO_2 emissions per desalinated water as objective functions is implemented and the obtained results shows that the proposed system with ORC, RO-MD and biogas production subsystems provide a good circumstance for multigeneration and cogeneration system developers to apply in practical scale.
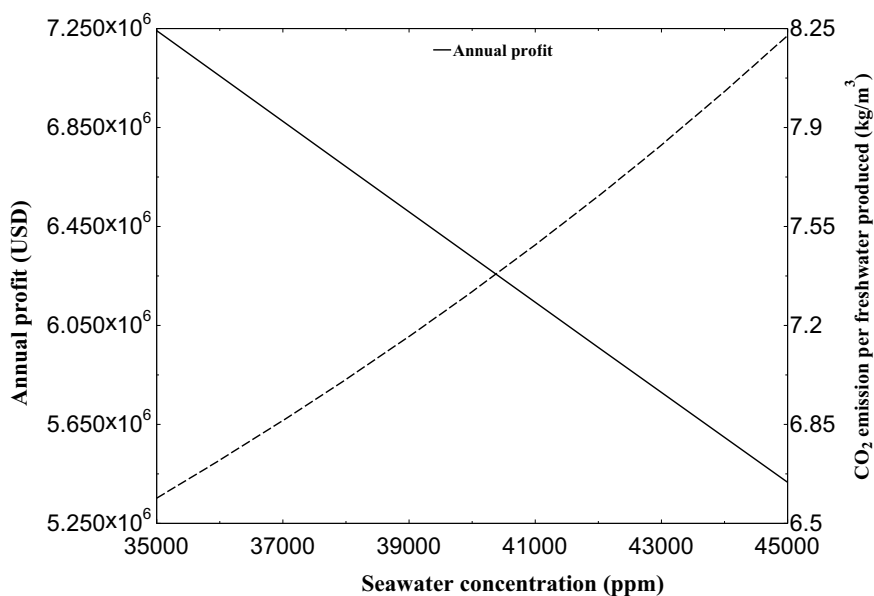
Fig. 7.13 Changes in the annual profit and CO_2 emission per freshwater produced of the system with seawater concentration

References

1. M.-R. Kolahi, M. Amidpour, M. Yari, Multi-objective metaheuristic optimization of combined flash-binary geothermal and humidification dehumidification desalination systems. Desalination **490**, 114456 (2020)
2. K. Vohra, A. Vodonos, J. Schwartz, E.A. Marais, M.P. Sulprizio, L.J. Mickley, Global mortality from outdoor fine particle pollution generated by fossil fuel combustion: results from GEOS-Chem. Environ. Res. **195**, 110754 (2021).https://doi.org/10.1016/j.envres.2021.110754.
3. IEA, Net zero by 2050 a roadmap for the global energy sector. Net Zero by 2050 Data%0Aiea.li/nzedata
4. J.J. Schmidt, The united nations world water development report 2021, valuing water (2021). https://doi.org/10.4324/9780429453571-2
5. P. Han, Q. Lu, L. Fan, W. Zhou, A review on the use of microalgae for sustainable aquaculture. Appl. Sci. **9**(11) (2019). https://doi.org/10.3390/app9112377
6. J. Pascual-González, L. Jiménez-Esteller, G. Guillén-Gosálbez, J.J. Siirola, I.E. Grossmann, Macro-economic multi-objective input–output model for minimizing CO2 emissions: Application to the U.S. economy. AIChE J. **62**(10), 3639–3656 (2016). https://doi.org/10.1002/aic.15376
7. M. Tajik Mansouri, M. Amidpour, J.M. Ponce-Ortega, Optimization of the integrated power and desalination plant with algal cultivation system compromising the energy-water-environment nexus, Sustain. Energy Technol. Assess. **42** (2020). https://doi.org/10.1016/j.seta.2020.100879
8. G. Yadav, B.K. Dubey, R. Sen, A comparative life cycle assessment of microalgae production by CO2 sequestration from flue gas in outdoor raceway ponds under batch and semi-continuous regime. J. Clean. Prod. **258**, 120703 (2020).https://doi.org/10.1016/j.jclepro.2020.120703
9. J.C. Quinn, R. Davis, The potentials and challenges of algae based biofuels: a review of the techno-economic, life cycle, and resource assessment modeling. Bioresour. Technol. **184**, 444–452 (2015). https://doi.org/10.1016/j.biortech.2014.10.075

10. L.Y. Batan, G.D. Graff, T.H. Bradley, Techno-economic and Monte Carlo probabilistic analysis of microalgae biofuel production system. Bioresour. Technol. **219**, 45–52 (2016). https://doi.org/10.1016/j.biortech.2016.07.085

11. R. Porcelli, F. Dotto, L. Pezzolesi, D. Marazza, N. Greggio, S. Righi, Comparative life cycle assessment of microalgae cultivation for non-energy purposes using different carbon dioxide sources. Sci. Total Environ. **721**, 137714 (2020). https://doi.org/10.1016/j.scitotenv.2020.137714

12. M. Collotta, P. Champagne, W. Mabee, G. Tomasoni, Wastewater and waste CO2 for sustainable biofuels from microalgae. Algal Res. **29**, 12–21 (2018). https://doi.org/10.1016/j.algal.2017.11.013

13. R. Ganesh Saratale, G. Kumar, R. Banu, A. Xia, S. Periyasamy, G. Dattatraya Saratale, A critical review on anaerobic digestion of microalgae and macroalgae and co-digestion of biomass for enhanced methane generation. Bioresour. Technol. **262**, 319–332 (2018). https://doi.org/10.1016/j.biortech.2018.03.030

14. W.A.V. Stiles et al., Using microalgae in the circular economy to valorise anaerobic digestate: challenges and opportunities. Bioresour. Technol. **267**, 732–742 (2018). https://doi.org/10.1016/j.biortech.2018.07.100

15. C. Zamalloa, E. Vulsteke, J. Albrecht, W. Verstraete, The techno-economic potential of renewable energy through the anaerobic digestion of microalgae. Bioresour. Technol. **102**(2), 1149–1158 (2011). https://doi.org/10.1016/j.biortech.2010.09.017

16. R. Loni, G. Najafi, E. Bellos, F. Rajaee, Z. Said, M. Mazlan, A review of industrial waste heat recovery system for power generation with organic rankine cycle: recent challenges and future outlook. J. Clean. Prod. **287**, 125070 (2021). https://doi.org/10.1016/j.jclepro.2020.125070

17. T. Zhang, L. Liu, J. Hao, T. Zhu, G. Cui, Correlation analysis based multi-parameter optimization of the organic Rankine cycle for medium- and high-temperature waste heat recovery. Appl. Therm. Eng. **188**, 116626 (2021). https://doi.org/10.1016/j.applthermaleng.2021.116626

18. Z. Ghaffarpour, M. Mahmoudi, A.H. Mosaffa, L. Garousi Farshi, Thermoeconomic assessment of a novel integrated biomass based power generation system including gas turbine cycle, solid oxide fuel cell and Rankine cycle. Energy Convers. Manag. **161**, 1–12 (2018). https://doi.org/10.1016/j.enconman.2018.01.071

19. T. Li, N. Meng, J. Liu, J. Zhu, X. Kong, Thermodynamic and economic evaluation of the organic Rankine cycle (ORC) and two-stage series organic Rankine cycle (TSORC) for flue gas heat recovery. Energy Convers. Manag. **183**, 816–829 (2019). https://doi.org/10.1016/j.enconman.2018.12.094

20. Y. Liang, M. Al-Tameemi, Z. Yu, Investigation of a gas-fuelled water heater based on combined power and heat pump cycles. Appl. Energy **212**, 1476–1488 (2018). https://doi.org/10.1016/j.apenergy.2017.12.117

21. E. Jones, M. Qadir, M.T.H. Van Vliet, V. Smakhtin, S. Kang, Science of the total environment the state of desalination and brine production: a global outlook. Sci. Total Environ. **657**, 1343–1356 (2019). https://doi.org/10.1016/j.scitotenv.2018.12.076

22. UN Water Report, The United Nations Inter-agency Mechanism on All Related Issues, Including Sanitation (2019)

23. M. Deymi-Dashtebayaz, E. Tayyeban, Multi objective optimization of using the surplus low pressure steam from natural gas refinery in the thermal desalination process. J. Clean. Prod. **238**, 117945 (2019). https://doi.org/10.1016/j.jclepro.2019.117945

24. R.H.E.M. Koppelaar, N. Shah, Energy-water nexus design and operation towards the sustainable development goals. Comput. Chem. Eng. (2019). https://doi.org/10.1016/j.compchemeng.2019.02.007

25. H. Nasrollahi, et al., The greenhouse technology in different climate conditions: a comprehensive energy-saving analysis. Sustain. Energy Technol. Assess. **47**, 101455 (2021)

26. H. Schlör, C. Märker, S. Venghaus, Developing a nexus systems thinking test –a qualitative multi- and mixed methods analysis. Renew. Sustain. Energy Rev. **138** (2021). https://doi.org/10.1016/j.rser.2020.110543

27. M. Eltawil, Renewable energy powered desalination systems: technologies and economics-state of the art. Recommendations **12**(1), 1–38 (2008). https://doi.org/10.1007/s12045-015-0272-6

28. Global Clean Water Desalination Alliance, "Global Clean Water Desalination Alliance - 'H2O minus CO2,'" no. December, pp. 1–25 (2015). http://www.diplomatie.gouv.fr/fr/IMG/pdf/global_water_desalination_alliance_1dec2015_cle8d61cb.pdf

29. S. Wu, Analysis of water production costs of a nuclear desalination plant with a nuclear heating reactor coupled with MED processes. Desalination **190**(1–3), 287–294 (2006). https://doi.org/10.1016/j.desal.2005.08.010

30. C. Sommariva, R. Borsani, M.I. Butt, A.H. Sultan, Reduction of power requirements for MSF desalination plants: the example of Al taweelah B. Desalination **108**(1–3), 37–42 (1997). https://doi.org/10.1016/S0011-9164(97)00006-4

31. C. Fritzmann, J. Löwenberg, T. Wintgens, T. Melin, State-of-the-art of reverse osmosis desalination. Desalination **216**(1–3), 1–76 (2007). https://doi.org/10.1016/j.desal.2006.12.009

32. T. Mezher, H. Fath, Z. Abbas, A. Khaled, Techno-economic assessment and environmental impacts of desalination technologies. Desalination **266**(1–3), 263–273 (2011). https://doi.org/10.1016/j.desal.2010.08.035

33. A.M. Delgado-Torres, L. García-Rodríguez, Preliminary design of seawater and brackish water reverse osmosis desalination systems driven by low-temperature solar organic Rankine cycles (ORC). Energy Convers. Manag. **51**(12), 2913–2920 (2010). https://doi.org/10.1016/j.enconman.2010.06.032

34. A.M. Delgado-Torres, L. García-Rodríguez, Design recommendations for solar organic Rankine cycle (ORC)-powered reverse osmosis (RO) desalination. Renew. Sustain. Energy Rev. **16**(1), 44–53 (2012). https://doi.org/10.1016/j.rser.2011.07.135

35. S. Karellas, K. Terzis, D. Manolakos, Investigation of an autonomous hybrid solar thermal ORC-PV RO desalination system. The Chalki island case. Renew. Energy **36**(2), 583–590 (2011). https://doi.org/10.1016/j.renene.2010.07.012

36. A.A. Shayesteh, O. Koohshekan, A. Ghasemi, M. Nemati, H. Mokhtari, Determination of the ORC-RO system optimum parameters based on 4E analysis; water–energy-environment nexus. Energy Convers. Manag. **183**, 772–790 (2019). https://doi.org/10.1016/j.enconman.2018.12.119

37. M. Tajik Mansouri, M. Amidpour, J.M. Ponce-Ortega, Optimal integration of organic Rankine cycle and desalination systems with industrial processes: energy-water-environment nexus. Appl. Therm. Eng. **158**, 113740 (2019). https://doi.org/10.1016/j.applthermaleng.2019.113740

38. M. Ebadollahi, et al., Close supercritical versus inverse Brayton cycles for power supply, using waste of a biogas-driven open Brayton cycle.. **143**(9), 092102 (2021)

39. K. Mohammadi, M.S.E. Khaledi, M. Saghafifar, K. Powell, Hybrid systems based on gas turbine combined cycle for trigeneration of power, cooling, and freshwater: a comparative techno-economic assessment. Sustain. Energy Technol. Assess **37**(September), 2020 (2019). https://doi.org/10.1016/j.seta.2020.100632

40. R.H. Mohammed, M.M. Ibrahim, A. Abu-Heiba, Exergoeconomic and multi-objective optimization analyses of an organic Rankine cycle integrated with multi-effect desalination for electricity, cooling, heating power, and freshwater production. Energy Convers. Manag. **231**, 113826 (2021). https://doi.org/10.1016/j.enconman.2021.113826

41. U.K. Kesieme, N. Milne, H. Aral, C.Y. Cheng, M. Duke, Economic analysis of desalination technologies in the context of carbon pricing, and opportunities for membrane distillation. Desalination **323**, 66–74 (2013). https://doi.org/10.1016/j.desal.2013.03.033

42. E. Drioli, A. Ali, F. Macedonio, Membrane distillation: recent developments and perspectives. Desalination **356**, 56–84 (2015). https://doi.org/10.1016/j.desal.2014.10.028

43. S. Adham, A. Hussain, J.M. Matar, R. Dores, A. Janson, Application of membrane distillation for desalting brines from thermal desalination plants. Desalination **314**, 101–108 (2013). https://doi.org/10.1016/j.desal.2013.01.003

44. P. Collet, A. Hélias Arnaud, L. Lardon, M. Ras, R.A. Goy, J.P. Steyer, Life-cycle assessment of microalgae culture coupled to biogas production. Bioresour. Technol. **102**(1), 207–214 (2011). https://doi.org/10.1016/j.biortech.2010.06.154

45. L. Clarens, A.F. Resurrection, E.P. White, M.A. Closi, Environmental life cycle comparison of algae to other bioenergy feedstock. Environ. Sci. Technol. **44**, 1813–1819 (2010)
46. H. Rostamzadeh et al., Energy and exergy analysis of novel combined cooling and power (CCP) cycles. Appl. Therm. Eng. **124**, 152–169 (2017)
47. M. Ebadollahi et al., Exergoeconomic analysis and optimization of innovative cascade bi-evaporator electricity/cooling cycles with two adjustable cooling temperatures. Appl. Therm. Eng. **152**, 890–906 (2019)
48. M. Kolahi et al., Thermodynamic and economic performance improvement of ORCs through using zeotropic mixtures: case of waste heat recovery in an offshore platform. Case Stud. Therm. Eng. **8**, 51–70 (2016)

Part II
Procedures for Storage and Carbon Capture in Energy System Set-Ups

Chapter 8
Primary Fuel Savings and CO₂ Emission Reduction in the Municipal Waste via Anaerobic Digestion

Mahdi Rezaei, Saghi Salehi, Mohammad Ebadollahi, Hadi Rostamzadeh, Zahra Ghaffarpour, Amir Farhang Sotoodeh, and Majid Amidpour

Abstract Galloping rate of environmental pollution and primary fuel growth has engendered engineers to devise alternative renewable energy-based processes for sustainable fuel supply of power plants. Anaerobic digestion (AD) process can be regarded as one of the main solutions to surmount this problem. With this regard, AD method is considered in this study for power generation and its main advantages in terms of CO_2 emission reduction and primary fuel savings are discussed versus two conventional waste management methods of incineration and landfill as well as different fossil fuel-based power plants. The comparison is carried out at two different scenarios of constant input waste and constant input electrical power under minimum and maximum capacities. It is found that the highest CO_2 emission reduction is calculated 14,739 tons per year when AD is used instead of gas oil in the diesel power plants (DPPs) under maximum power generation of 39.51 million kWh per year, and hence AD method is highly commendable for this scenario. Also, although using AD method instead of fossil fuel in the combined power plants (CPPs) increased CO_2 emission (which is not appealing), it saved equivalent primary fuel around 6.5 million m³ under minimum power capacity of 29.63 million kWh per year and 8.6 million m³ under maximum power capacity of 39.51 million kWh per year. Finally, fuel savings cost and payback time for different scenarios are estimated and the main advantages of using AD method instead of the conventional primary fuels in the screened power plants are pinpointed from economic vantage point. Also, under maximum power capacity of 39.51 million kWh/yr employing AD method instead of gas oil in the DPPs can save 8.22 million dollars in October with payback time of 1 year and 7.69 million dollars in November with payback time of 1.1 year.

M. Rezaei · S. Salehi
Renewable Energy Research Department, Energy & Environment Research Center, Niroo Research Institute (NRI), Tehran, Iran
e-mail: mahdirezaei@nri.ac.ir

M. Ebadollahi · H. Rostamzadeh · Z. Ghaffarpour · A. Farhang Sotoodeh · M. Amidpour (✉)
Energy & Environment Research Center, Niroo Research Institute (NRI), Tehran, Iran
e-mail: amidpour@kntu.ac.ir

M. Ebadollahi · Z. Ghaffarpour · M. Amidpour
Faculty of Mechanical Engineering, Department of Energy System Engineering, Toosi University of Technology, Tehran, KN, Iran

Nomenclature

Symbols

AD	Anaerobic digestion
CPP	Combined power plant
DC	Domestic consumption
DPP	Diesel power plant
FOB	Free-On-Board
GPP	Gas power plant
HV	Heat value
MOP	Ministry of Petroleum
MSW	Municipal solid waste
MWSM	Municipal solid waste management
N	Normal
NG	Natural gas
SPP	Steam power plant
TPD	Ton per day
$\dot{W}$	power (kW)

Subscripts and Superscripts

|	
Gen	Generation
N	Net

Greek Letters

η	Efficiency (%)

8.1 Introduction

In recent years, the supersedence of renewable energy sources such as biomass, solar and wind with oil and gas-based energy sources has been considered extremely controversial [1–3]. Fossil fuel-based energy sources, due to their limited and enduring potential and environmental pollution, have enforced researchers and decision-makers in the field of energy to look for cost-effective methods with low-emission factor [4–7]. Therefore, a comprehensive evaluation of the suggested approach in terms of energy, pollution production, and economic must be deliberated prior to the implementation of any new technology [8, 9]. A comparison between new and past technologies by considering the aforementioned factors is an efficient method to examine the performance of each technology [10, 11]. By employing such evaluation systems, decision-makers can choose the best and most suitable technology from the demanding criteria standpoint [12–14].

Municipal waste is known as one of the challengeable concern in cities (especially in urban areas) which is on the rise with population growth and community modernization. Municipal waste generation of the world is 2.01 billion tons per year and is 270 kg per person in average Also, it is estimated that in 2050 waste generation will reach 3.40 billion tons [15]. Generally speaking, the waste management hierarchies can be classified as follows: prevention, re-use, recycling, waste treatment, energy recovery, and disposal. Examining of three disposal methods is the main priority of the present study which can be accounted for to manage municipal wastes, and depends on waste material composition and economic and environmental conditions.

Anaerobic digestion (AD) method has the potential for controlling environmental pollution and recovering the energy lost [16, 17]. In this method, many industrial and agricultural wastes that have materials with biodegradable property can be converted to useful energy. More precisely, under anaerobic condition, organic material of municipal, industrial and agricultural wastes are degraded and stabilized through microbial organisms. This reaction produces methane and other inorganic species such as carbon dioxide, NH$_3$, and H$_2$S. The AD reaction is as follow:

$$Organic\ material + H_2O \rightarrow CH_4 + CO_2 + new\ biomass + NH_3 + H_2S + heat \qquad (8.1)$$
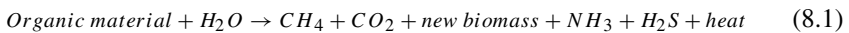
The instability of this process and low methane production are the main challenging problems in AD method [18]. Van Fan et al. [19] assessed steps of the anaerobic digestion process for municipal solid waste and different approaches for producing optimum biogas and other valuable products. Their assessment includes collection and transportation of waste material, pre-treatment, digestion reaction, and post-treatment. They concluded that thermal hybrid pre-treatment is less appropriate for MSW (municipal solid waste). Cheng et al. [20] investigated AD method by adding iron oxides and rusted iron shavings to the municipal and food wastes and found that the methane, biogas and volatile fatty acids productions can be

improved after such deliberation. Their results show that compared with the conventional methods (without adding any special materials) specific methane yield potential (SCH$_4$) and maximum daily methane production (DCH$_4$) are increased around 41.2% and 12.2%, respectively. Kumar et al. [21] examined single- and two-stage anaerobic processes in order to produce bio-hythane from the organic fraction of MSW (OFMSW). Their results confirmed that two-stage anaerobic digestion (AD) method is better than the single-stage one with two-run since it has blend of 56% CO2, 15% CH$_4$ and 6% H$_2$.

Landfilling is the other method for removing MSW which has been used widely because of its simplicity, low operating cost, large capacity and low investment [22]. Also, statistical data showed that around 95% of MSW of the world and more than 50% of MSW of European Union state members are being removing to landfills [23]. However, using landfills to dispose MSW has many negative effects on the safety of the surrounding environment, especially on the groundwater since it contains hazards toxic materials. Over the past years, many researchers have focused on improving and developing new methods and technologies to further reduce the destructive effects of landfills [24]. In this approach, when at least one pollutant exceeds the threshold concentration and reaches to groundwater, the energy barrier system lost its function and this pollutant can be considered as an indicator for identifying breakthrough from a landfill site [25]. For instance, four typical landfill systems, that have different leachate heads, are investigated by Shu et al. [26] via various numerical models. Their results underlined that chemical oxygen demand reaches the breakthrough threshold before the other pollutants. Also methane emission of landfill method, especially non-normative landfill sites and their potential for electricity generation should be examined. For this reason, in the Ghazipur, Delhi-Okhla and Bhalswa landfill sites of Delhi city, total emission of methane based on Default method (DM), First-order decay (FOD) and LandGEM (as methane estimation methods) are calculated 1,288.99, 311.18, 779.32 Gg, respectively. By evaluating these values of the produced methane, they computed the energy generation potential of 4.16×10^8 to 9.86×10^8 MJ for Ghazipur, 2.08×10^8 to 4.06×10^8 MJ for Okhla, and 3.42×10^8 to 8.11×10^8 MJ for Bhalswa.

The other common technology to dispose of MSW is incineration which is used widely in many countries. In comparison with landfills, incineration reduces the waste volumes which cannot be recycled [27]. Also, it is able to transfer the released combustion energy (heating value: approximately 10 MJ/kg) to useful energy in the form of flue gas which can be applied to generate steam and electricity in thermodynamic cycles such as organic Rankine cycle (ORC) [28]. However, this approach emits toxic pollutants such as heavy metals, nitrogen oxides, acid gases, and solid particles to the atmosphere, to name but a few [29]. One of the common MSW incineration technologies is grate-firing technology. The MSWs are mainly filled in a special bed on the grate where main heterogeneous conversion takes place [30]. Regarding that, Gu et al. [31] developed and simulated a comprehensive model based on a special calculation method for pyrolysis products, corrective boundary conditions, and homogeneous reactions. They examined the packed-bed transformation method to travel grates and accommodate different waste fractions in real MSW.

They also analyzed the effects of solid waste incineration in high-altitude areas and solid waste particle sizes.

Therefore, not only choosing a right method for disposing of MSW is important from cost, environment, and energy points of view, but also nowadays it is significantly important for sustainable municipal solid waste management (MSWM). A model based on two-objective optimization to minimize cost and CO_2 emission of the MSWM systems is proposed by Mohsenizadeh et al. [32]. The cost and emission of transportation activities of the Ankara city's MSWM system are the main research topic in this study. They examined the extended and hybrid systems (as extensions of a system). The results of analysis indicated that a little increase in cost can led to a considerable reduction of emissions. They also found that Ankara has 31.6 million tons of MSW and 1.14 kg municipal waste per capita per day in 2016 in average.

Another important point of view about the management of MSW is the assessment of electrical power generation potential. For instance, Rezaei et al. [33] investigated gasification and incineration systems of MSW in Iran based on sensitive analysis of different scenarios to choose the best method by considering the economic aspects. Their result showed that there is a substantial difference between incineration and gasification technologies, and the scenarios which include energy recovery from the gasification method have higher electricity conversion efficiency than the gasification process. According to their evaluation, the gasification technology has a payback period of 4.17 years in the gate fee of US$ 0.126 and 4.06 years in electricity power purchase agreement of US$ 0.276. Mesjasz-Lech [34] developed a zero-waste city concept through reverse logistic method in urban areas of Poland. The zero waste city concept is defined as the cities which have 100% of waste recirculation be converted to valuable resources that have social, economic, financial, environmental, and industrial benefits. In this study, the municipal waste trends in each city are measured separately which is the main necessity of reverse logistic. Also, they classified the polish provinces municipal wastes based on the treatment operations, fractions, mixed municipal waste, landfilling of municipal waste by urban areas, and degassing of landfill sites. They found that reverse logistic can help the regional government to design and use efficient management methods to remove wastes in cities. Also, the study showed that 25 percent of municipal waste is still being burring, where this amount in other developing countries is more than 50 percent.

One of the main aims of this study is qualification assessment of electricity production potential through anaerobic digestion method versus two conventional waste management methods, including incineration and landfill. The comparison is carried out at two different approaches. First, the input waste for each technology is fixed and the electrical power is calculated based on this assumption. In the second approach, the electrical power values for minimum and maximum capacities are fixed and the amount of waste required for the estimated capacities is obtained. Next, the main advantages of AD method versus incineration and landfill are discussed in terms of CO_2 emission reduction rate based on the calculated results. In the subsequent stage, the values of CO_2 emissions and primary fuel for four different power plants, namely steam power plant (SPP), gas power plant (GPP), combined power plant (CPP), and

diesel power plant (DPP) are calculated and the findings are compared with the scenario when AD is used instead of the conventional primary fuel of these power plants in terms of CO_2 emission and primary fuel consumption. Finally, fuel savings cost and payback time for different scenarios are estimated and the main advantages of using AD method instead of the conventional primary fuels in the screened power plants are pinpointed from economic vantage point.

8.2 Documents and Assumptions

Power generation from waste materials by anaerobic digestion (AD) process is the main target of this article. By calculating the energy savings and greenhouse emissions it can be proved that AD method has the highest priority to conventional technologies such as landfill or waste incinerator. To carry out AD analysis in the present study, the documents of the Strabag Company in Germany named "Learn Plug Flow" have been used. These documents report the waste materials of Isfahan (a central country in Iran) and help calculate the energy savings and greenhouse emissions. It should be noted that the greenhouse emission reduction is calculated based on reports issued by the Iran's Ministry of Petroleum (MOP) [35]. Some input data and assumptions associated with this report are given in Table 8.1.

8.3 Methodology

In this section, the AD is compared to other waste management technologies in terms of power production capacity and carbon dioxide emissions. In addition, the details of calculation process for these procedures (power plants, landfill, and waste incinerator) have been presented in separate subsections.

8.3.1 Anaerobic Dry Digestion

Electricity production in the AD process depends on potential of the biogas generation. Therefore, the amount of annual electricity production is calculated from Eq. (8.2) based on the Strabag Company available data given in Table 8.2.

$$\dot{W}_{gen}(kWh) = Solid\ Inputs(TPD) \times Biogas\ Yield\left(\frac{Nm^3}{ton}\right)$$
$$\times\ 0.55\frac{CH_4}{Biogas} \times \frac{10\text{kWh}}{1\text{m}^3 CH_4} \times 365 \tag{8.2}$$

Table 8.1 Assumptions and important data

Isfahan waste materials properties			
	Parameter	Unit	Amount
1	Input waste	ton/day (TPD)	300
2	Size of particles	Mm	60
3	Dry materials	%	28–35
4	Organic parts in dry material	%	68–75
Properties of dry digester and AD process			
5	Potential of biomass production from waste mass	m^3/ton	120–160
6	Methane percentage in produced biogas	%	55
7	Operation time in a year	hour	8760
Steam power plant characteristics in Iran			
8	Efficiency	Steam power plant (SPP)	%	36.6
		Gas power plant (GPP)		31.4
		Combined power plant (CPP)		45.8
		Diesel power plant (DPP)		34.6
9	Annual energy consumption	SPP	Equivalent to million cubic meter of natural gas	24,193
		GPP		25,243
		CPP		23,352
		DPP		13
10	Energy consumption compound	Energy carrier	Gas oil	NG	Fuel oil
		SPP	0.4%	78.4%	21.2
		GPP	11.8%	88.2%	–
		CPP	12%	88%	–
		DPP	100%	–	–
Carbon dioxide emission coefficients in power plant industries based on energy carrier			
11	Emission coefficient of natural gas	g CO_2/m^3 NG)	1991
12	Emission coefficient of gas oil	g CO_2/lit GO)	2979
13	Emission coefficient of fuel oil	g CO_2/lit FO)	3604

In Eq. (8.2), 0.55 indicates methane concentration in biogas, 10 is the amount of produced electricity in each cubic meter methane $\left(\frac{kWh}{m^3}\right)$, and 365 is the number of days in a year.

The electricity generation calculated by Eq. (8.2) is the overall gross electricity value in the digestion process, and hence must be modified by multiplying 0.41 as CHP efficiency in Iran to reach the net power. Since the net electricity is extracted

Table 8.2 Annual power generation and CO_2 emission in dry digester

Parameter	Unit	Generation/Emission amount	
		Minimum	Maximum
Biogas	Nm^3	13,140,000	17,520,000
Methane	Nm^3	7,227,000	9,636,000
Electricity	$MkWh$	29.36	39.51
Carbon dioxide	ton	14,389	19,185

from the methane through the AD process, the amount of carbon dioxide emissions can be calculated from MOP reports, too (Table 8.2).

8.3.2 Selected Power Plants

Generally speaking, one of the main benefits of dry digesters is their high superiority in terms of low energy consumption and greenhouse gas emissions to the conventional power plants for the same electricity capacity. To demonstrate this superiority, different power plants such as steam, gas, combined cycle, and diesel are selected to generate a same amount of electricity under possible hybrid primary energy consumption of gas oil, natural gas and fuel oil, and the total CO_2 emissions and the total primary energy consumptions are computed for each scenario. The results of this calculation in terms of the annual energy consumption and CO_2 emissions in different thermal power plants are listed in Table 8.3 under minimum and maximum electricity generation scenarios. According to Table 8.3a it can be seen that the CPP has the highest thermal efficiency of 45.8% under a minimum electricity of 29.63 M kWh/yr produced by the AD since the CPP consumes the least total equivalent energy of 6.5 Mm^3NG. By contrast, the GPP has the lowest thermal efficiency of 31.4% under the same condition since it has the highest total equivalent energy of 9.4 Mm^3NG. In terms of CO_2 equivalent emissions it can be conclude that the CPP emits the lowest CO_2 of 13,643 tons per year due to its low fossil fuel consumption rate, while the DPP emits the highest CO_2 of 25,443 tons per year since it predominantly consumes gas oil.

In the case when maximum electricity of 39.51 M kWh/yr is produced by the AD (Table 8.3b) under a constant thermal efficiency for each individual power plant, it can be found that the CPP evidently has the lowest total energy consumption and CO_2 emissions of 8.6 Mm^3NG and 18,190 tons per year, respectively. Conversely, the highest total energy consumption for maximum electricity generation of 39.51 M kWh/yr is attributed to the GPP by 12.6 Mm^3NG, while the highest CO_2 emissions for this scenario is attributed to the DPP by 33,924 tons per year.

A comparative study between results of Table 8.3a and b indicates that that under a constant thermal efficiency of each thermal power plants, increasing the electricity production from 29.63 $MkWh/yr$ to 39.51 $MkWh/yr$ (an increase of around 33.34%) leads to the increment of the total CO_2 emissions of 33.33% (for the SPP),

Table 8.3 Annual energy consumption and CO_2 equivalent emissions in the thermal power plants for the minimum and maximum electricity production (29.63 $MkWh/yr$ and 39.51 $MkWh/yr$) in the AD

Power plant	Efficiency (%)	Annual primary energy consumption				Equivalent emission amount ($\frac{tonCO2}{yr}$)			
		Gas oil ($Mlit$)	Natural gas (Mm^3)	Fuel oil ($Mlit$)	Total equivalent ($Mm^3\,NG$)	Gas oil	Natural gas	Fuel oil	Total
(a) Minimum state									
SPP	36.6	0.03	6.35	1.5	8.1	90	12,634	5,406	18,130
GPP	31.4	1.1	8.3	–	9.4	3,295	16,578	–	19,873
CPP	45.8	0.8	5.7	–	6.5	2,314	11,329	–	13,643
DPP	34.6	8.5	–	–	8.6	25,443	–	–	25,443
(b) Maximum state									
SPP	36.6	0.04	8.46	2	10.8	120	16,845	7208	24,173
GPP	31.4	1.5	11.1	–	12.6	4,393	22,104	–	26,497
CPP	45.8	1	7.6	–	8.6	3,085	15,105	–	18,190
DPP	34.6	11.4	–	–	11.4	33,924	–	–	33,924

34% (for the GPP), 32.3% (for the CPP), and 32.55% (for the DPP). Therefore, the total CO_2 emissions like the annual primary energy consumption vary linearly with the electricity value produced by the anaerobic digester.

8.3.3 Landfill Technology

Building landfills for landfill sanitation can be another alternative approach to anaerobic digestion for waste management. Two cases are defined through the computation process. In the first case, the electricity potential in landfills has been calculated under a specific amount of waste materials entered to digester, namely 300 ton per day (TPD). In the second scenario, however, the amount of waste required for the generation of the two constant amounts of electricity (29.63 M kWh and 39.51 M kWh) have been calculated.

8.3.3.1 First Approach: Calculation Based on Constant Input Waste

Practical electricity potential generated from waste materials can be calculated as follows [36]:

$$\dot{W}_{gen}(kWh) = \dot{M}_{total}(TPD) \times L_0 \times \eta_{gas} \times C_{methane} \times \eta_{engine} \times N_{operation} \quad (8.3)$$

where,

$\dot{M}_{total}$:   refers to total mass of dry and organic waste materials,

L_0:   refers to the equivalent potential of the biogas production from unit mass of the waste materials in which its average value in Iran is 150 $\left(\frac{m^3}{ton}\right)$,

η_{gas}:   stands for the gas extraction efficiency from landfill ($\eta_{gas} = 60\%$),

$C_{methane}$:   refers to the methane concentration in biogas ($C_{methane} = 0.55$),

η_{engine} :   refers to the conventional efficiency of the gas engine for electricity generation ($\eta_{engine} = 35\%$), and.

$N_{operation}$:   stands for the number of annual operating hour ($N_{operation} = 8760\,hr$).

Table 8.4 listed the value of annual electricity and CO_2 emissions under supply of the waste materials of 300 TPD. According to Table 8.4, the amount of electricity and CO_2 emissions are calculated 18.97 M kWh and 10,792 ton, respectively.

Table 8.4 Annual electricity generation and carbon dioxide emissions in landfill for the first approach

Parameters	Unit	Generation/Emission amount
Input waste materials	TPD	300
Biogas	Nm^3	9,855,000
Methane	Nm^3	5,420,250
Electricity	MkWh	18.97
Carbon dioxide	ton	10,792

8.3.3.2 Second Approach: Calculation Based on Constant Input Electricity

In the second approach, the value of input waste materials and CO_2 emissions under supply of two electricity powers of 29.63 M kWh and 39.51 M kWh are calculated and results are displayed in Table 8.5. According to Table 8.5, under a minimum electrical power of 29.63 M kWh, the value of waste materials required for biogas production of 15,329,571 Nm3 is calculated 469 TPD. In this case, the CO_2 emitted value is obtained 16,856 ton. On the other hand, when maximum electricity of 39.51 M kWh is the demand, the values of input waste materials and CO_2 emissions are computed 625 TPD and 22,474 ton, respectively.

8.3.4 Waste Incinerator

One of the proven methods to manage large amounts of municipal solid waste is the thermal treatment of the waste materials in the incinerator. The incineration method is known as an interesting approach since it reduces the amount of organic carbon of waste materials after combustion, while the residual waste materials may be consumed as a fuel instead of the conventional fuels. However, environmental pollution during the combustion process can be cited as a harmful factor of this technology [37]. The exact properties and the heat value of waste for the selected case study are categorized in Table 8.6 for two aforementioned approaches.

Table 8.5 Annual electricity generation and carbon dioxide emissions in landfill for the second approach

Parameters	Unit	Generation/Emission amount	
		Min	Max
Input waste materials	TPD	469	625
Biogas	Nm^3	15,329,571	20,523,429
Methane	Nm^3	8,465,914	11,287,886
Electricity	M kWh	29.63	39.51
Carbon dioxide	ton	16,856	22,474

Table 8.6 Compositions and heat value of Isfahan waste

Components	Composition percentage (%)	Humidity (%)		Heat value (kJ/kg)	
		Special value	Available value	Special value	Available value
Plastic	12.7	8	1.0	25,000	3,171
Plastic bottle	1.5	8	0.1	25,000	379
Glass	4.4	10	0.4	−290	−13
Textile	6.3	18	1.1	13,000	814
Ferrous metals	1.8	10	0.2	−290	−5
Non-ferrous metals	0.1	10	0.0	−290	0
Paper	3.2	20	0.6	12,000	385
Cardboard	3.2	20	0.6	12,000	383
Packing materials	0	20	0.0	20,000	0
Dangerous waste	0	10	0.0	1,500	0
Vegetables and organic substances	62.7	70	43.9	3,000	1,881
Stick and tree branch	2.5	20	0.5	15,000	368
Leather, horn, bone, and lactic	1.6	20	0.3	16,000	257
Baby diaper	0	60	0.0	18,000	0
Composite materials	0	10	0.0	10,000	0
Miniature waste (lower than 10 mm)	0	31	0.0	3,000	0
Construction block	0	10	0.0	−290	0
Grits	0	10	0.0	−290	0
Others	0	7	0.0	3,000	0
Total	100	–	48.9	–	7,600

8.3.4.1 First Approach: Calculation Based on Constant Input Waste

By specifying the Isfahan waste as the case study, the gross and net power potential in waste incinerator are calculated respectively as follows:

$$\dot{W}_{gross}(kWh) = [HV \times (1 - \eta_{loss})] \times \eta_{GT} \times TPD \times 365 \times 1000 \qquad (8.4)$$

$$\dot{W}_{net}(kWh) = \dot{W}_{gross} \times (1 - \eta_{DC}) \tag{8.5}$$

where,

HV: stands for the heat value of waste $\left(\frac{MWh}{ton}\right)$,

η_{loss}:   refers to the heat losses from the furnace, ash and gas stack ($\eta_{loss} = 10\%$),

η_{GT}:   refers to the thermal efficiency of the gas turbine ($\eta_{GT} = 28\%$), and.

η_{DC}:   refers to the domestic consumption of the gross power ($\eta_{DC} = 15\%$).

Therefore, assuming 300 tons of input waste per day, the potential of electricity generation through incineration of Isfahan municipal waste with the mentioned characteristics in the incinerator will be around 49.52 million kWh, which is more than maximum potential of electricity generation from AD technology (39.51 million kWh). It is noteworthy to note that information on the amount of pollution emitted by the waste incineration is not existed, but similar reports have underlined the significant amount of pollution emissions in the waste incineration. Moreover, also because of the high cost of waste incineration, AD is recommended for waste management compared to waste incineration [38, 39].

8.3.4.2 Second Approach: Calculation Based on Constant Input Electricity

In the second approach, the amount of waste required as input of incinerator to produce the same amount of electricity in both technologies (in the AD and waste incinerator) has been assessed. Given the maximum and minimum power generation amount in the anaerobic dry digester and waste incineration, the input waste required for each process is calculated and results can be discussed based on Tables 8.2 and 8.7. Accordingly, the minimum and maximum amounts of input waste to incinerator are calculated 180 and 239 TPD, respectively, which are lower than the same parameter in the AD (300 TPD).

Table 8.7 Annual electricity production and input waste for the waste incineration in Isfahan under the incinerator thermal efficiency of 28%

Electricity production ($\frac{MkWh}{yr}$)	Input waste (TPD)
49.52	300
29.63	180
39.51	239

8.4 Results and Discussions

8.4.1 Energy Saving and Emission Reduction

The main target of the present paper is to evaluate and prove the advantages of using AD compared to other technologies in converting waste to electrical power. These benefits are mainly addressed by saving energy and reducing greenhouse gas emissions. Table 8.8 contains value of the energy savings and emission gas reduction difference when AD is used instead of each discussed method. When the AD is compared with the SPP, GPP, CPP, and DPP, the value of input waste is assumed 300 TPD (base value given in Table 8.1) and the comparison is carried out under this assumption. But, when it comes to comparing landfills and AD, one of the factors to consider is the amount of input waste required to have an equal amount of electricity in both cases. Also, since both landfill and digestion methods are renewable technologies that use biogas from waste to generate electricity; thereby determining the amount of fossil fuels (including gas oil, furnace oil, and natural gas) saved during the use of AD process is meaningless and are excluded in the Table 8.8.

8.4.1.1 AD Versus SPP Under the Same Amount of Power Generation

The comparison between the AD and SPP is carried out in terms of two different electricity generation values of 29.63 M kWh/yr and 39.51 M kWh/yr. It is worth noting to mention that since the purpose of this study is to evaluate the benefits of dry digestion over some other technologies, the amount of electricity produced by the digester with the specifications stated by the Strabag Company has been considered as the basis of calculations. After determining the amount of electricity produced in the digester, the average amount of primary energy required in the Iran's SPPs to produce the same amount of electricity is calculated based on the available average thermal efficiency of the SPPs. Given that the primary energy of power generation in digester is prepared from the conversion of waste to biogas (which contains 55% methane), considering AD mechanism instead of direct use of fossil fuels in the SPPs can save primary energy up to 8.1 M m^3 gas for minimum power generation of 29.63 M kWh per year and 10.8 M m^3 gas for maximum power generation of 39.51 M kWh per year. Consequently, near 3,471 and 4,988 tons of CO_2 per year can be reduced of the environment when AD is used instead of SPP under the minimum and maximum power supply, respectively.

8.4.1.2 AD Versus GPP Under the Same Amount of Power Generation

A comparative study between results of employing AD method versus GPP is conducted and the findings are also displayed in Table 8.8. According to Table 8.8 it can be concluded that employing AD method instead of direct use of fossil fuels in

Table 8.8 A comparative study in terms of energy savings and greenhouse gas emissions between different methods

Methods	Electricity ($\frac{MkWh}{yr}$)	Input waste (TPD)	Annual primary energy consumption				Emission reduction difference* ($\frac{tonCO_2}{yr}$)
			Gas oil (M lit)	Natural gas (Mm^3)	Fuel oil (M lit)	Total equivalent (Mm^3 gas)	
AD versus SPP	29.63	AD: 300 —	0.03	6.35	1.5	8.1	3,471
AD versus SPP	39.51	AD: 300 —	0.04	8.46	2.0	10.8	4,988
AD versus GPP	29.63	AD: 300 —	1.1	8.3	–	9.4	5,484
AD versus GPP	39.51	AD: 300 —	1.5	11.1	–	12.6	7,312
AD versus CPP	29.63	AD: 300 —	0.8	5.7	–	6.5	−746
AD versus CPP	39.51	AD: 300 —	1.0	7.6	–	8.6	−995
AD versus DPP	29.63	AD: 300 —	8.5		–	8.6	11,054
AD versus DPP	39.51	AD: 300 —	11.4	–	–	11.4	14,739
AD versus Landfill	AD: 29.63 Landfill: 18.97	300	–	–	–	–	−3,597
AD versus Landfill	AD: 39.51 Landfill: 18.97	300	–	–	–	–	−8,394
AD versus Landfill	29.63	AD: 300 Landfill: 469	–	–	–	–	2,467
AD versus Landfill	39.51	AD: 300 Landfill: 625	–	–	–	–	3,289

* The positive value means AD in better than the compared method, while negative value means the compared method in better than AD

the GPPs can save primary energy up to 9.4 M m^3 gas for minimum power generation of 29.63 M kWh per year and 12.6 M m^3 gas for maximum power generation of 39.51 M kWh per year. As a result, applying AD method instead of direct use of fossil fuels in the GPPs can decrease CO_2 emissions approximately 5,484 and 7,312 tons per year under the minimum and maximum power supply scenarios, respectively.

8.4.1.3   AD Versus DPP Under the Same Amount of Power Generation

A comparative study between results of employing AD method versus DPP is conducted and the findings are also displayed in Table 8.8. According to Table 8.8, it can be concluded that employing AD method instead of direct use of gas oil in the GPPs can save energy up to 8.5 M m^3 gas oil for minimum power generation of 29.63 M kWh per year and 11.4 M m3 gas for maximum power generation of 39.51 M kWh per year. As a result, applying AD method instead of direct use of gas oil in the DPPs can decrease CO_2 emissions approximately 11,054 and 14,739 tons per year under the minimum and maximum power supply scenarios, respectively.

8.4.1.4   AD Versus CPP Under the Same Amount of Power Generation

The description in this section is similar to the above, except that the efficiency of the combined cycle power plant is more than the gas turbine (GT) cycle. Therefore, the amount of fuel required in the CPP is far less than the amount of biogas consumed in the digester of the GT cycle, thereby leading to CO_2 emission reduction. This augmentation in CO_2 emissions when AD is used instead of the CPP is shown in negative number in Table 8.8. Accordingly, a comparative study between results of employing AD method instead of CPP shows that the primary energy can be saved up to 6.5 M m^3 gas for minimum power generation scenario and 8.6 M m^3 gas for maximum power generation scenario. As a result, applying AD method instead of direct use of fossil fuels in the CPPs can increase CO_2 emissions approximately 746 and 995 tons per year under the minimum and maximum power supply scenarios, respectively.

8.4.1.5   AD Versus Landfill

Comparison of the AD and the landfill can be examined in terms of same input or output. In this section, regarding the same amount of waste, the main aim is to compare the calculated power between two technologies. According to the possibility of generating more electricity in digestion process with the same amounts of input waste, it is evident that the rate of biogas production, methane, and consequently carbon emissions, increases. According to Table 8.8, a comparative study between results of employing AD method versus landfill shows that applying AD method instead of landfill can increase CO_2 emissions approximately 3,597 and 8,394 tons

per year under supply of constant waste of 300 TPD to obtain minimum and maximum power supply scenarios, respectively. Meantime, under the second scenario (constant supply of input electricity) it is found that the supply of 300 TPD waste via AD method or 469 TPD waste via landfill method can result in 29.63 M kWh/yr power production and 2,467 tons of CO_2 reduction per year. Also, to supply maximum power of 39.51 M kWh/yr it is found that 325 TPD more waste is required if landfill is used instead of AD method, leading to increment of around 3,289 tons of CO_2 per year.

8.4.1.6   Comparison of Carbon Dioxide Emission Reduction in All Scenarios

To further illustrate results of this comparison in terms of CO_2 emissions, an illustrative diagram of CO_2 emission values for different methods is displayed in Fig. 8.1. As mentioned previously, this comparison is carried out to show the merits and demerits of AD versus other techniques. Accordingly, the highest emission reduction is calculated when AD is used instead of gas oil in the DPPs, and hence AD method is highly commendable from this vantage point. Meantime, the lowest emission reduction is calculated when AD method is used instead of landfill under the minimum supply of power. By contrast, the use of AD method instead of CPPs and landfill under 300 TPD input is not recommended since not only CO_2 emissions are not reduced, but they are also augmented (especially at high power supply).

8.4.2   *Energy Savings Cost and Payback Time*

The Euro cost announced by the German Strabag Company has been used to calculate payback time and energy savings cost with a simple method. The power generated in the digester is purchased based on the guaranteed renewable electricity purchase

Fig. 8.1 The amount of CO_2 emission reduction for different methods (1&2: AD vs. SPP; 3&4: AD vs. GPP; 5&6: AD vs. CPP; 7&8: AD vs. DPP; 9–12: AD vs. landfill)
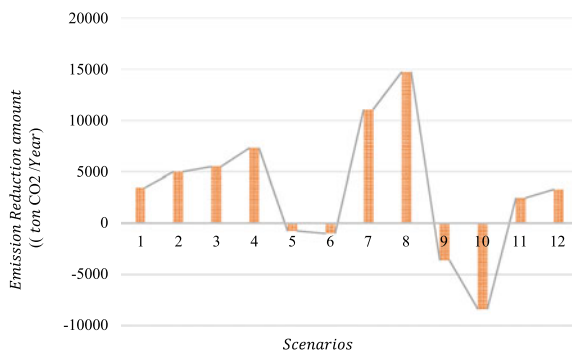
Table 8.9 Some input cost values based on FOB and guaranteed purchase contracts costs [35]

Energy type	Unit	Costs based on guaranteed purchase contracts	FOB cost (Oct 2018)	FOB cost (Nov 2018)
Electricity	Rial/kWh	3500	–	–
Fuel oil 180	cent/lit	–	47	45
Fuel oil 380	cent/lit	–	47	45
Gas oil	cent/lit	–	60	55

contract of 3,500 Rials[1] per kilowatt-hour by the state government of Iran [40]. The fossil fuel selling cost in each of the scenarios has been calculated based on Free On Board (FOB) cost (Table 8.9).

8.4.2.1 Capital Payback Time (Guaranteed Purchase of Electricity)

Given the cost of 3,500 Rials per kilowatt-hour of electricity produced in the digester, the annual repayment for the minimum and maximum amounts of annual electricity production have been calculated 1.04 million US $ with a payback period time of 8 years and 1.38 million US $ with a payback period time of 6 years, respectively.

8.4.2.2 Capital Payback Time (Fuel Saving Amount)

Table 8.10a and b indicate the annual fuel savings cost and capital payback time for Oct. and Nov. of 2018 FOB costs, respectively. According to the results of Table 8.10, the huge money associated with fuel supply can be saved when AD method is used instead of DPP, and hence payback time decreases considerably. Quantitatively speaking, using gas oil in the DPP under maximum power load of 39.51 M kWh can lead to the highest fuel savings cost of 6.84 M $ with payback time of 1.2 yr in Oct 2018 and 6.31 M $ with payback time of 1.3 yr in Nov. 2018. Meantime, under minimum power supply of 29.63 M kWh, the fuel savings cost of 5.13 M $ with payback time of 1.6 yr in Oct 2018 and 4.73 M $ with payback time of 1.8 yr in Nov. 2018 are obtained. In terms of worst scenario in terms of economic consideration of the methodologies, it can be stated that using gas oil in the SPP under maximum power load of 39.51 M kWh can lead to the lowest fuel savings cost of 0.02 M $ with payback time of 345.4 yr in Oct 2018 and 0.02 M $ with payback time of 374.4 yr in Nov. 2018. Also, under minimum power supply of 29.63 M kWh, the fuel savings cost of 0.02 M $ with payback time of 460.6 yr in Oct 2018 and 0.02 M $ with payback time of 499.2 yr in Nov. 2018 are calculated.

---

[1] In this article, each US dollar equals 100,000 Rials.

Table 8.10   Annual calculations of fuel savings cost and capital payback time (based on FOB costs)

(a) October 2018

Compared methods	Power (M kWh)	Gas oil		Fuel oil		Gas oil and Fuel oil	
		Saving cost of fuel (M $)	Capital payback time (yr)	Saving cost of fuel (M $)	Capital payback time (yr)	Saving cost of fuel (M $)	Capital payback time (yr)
AD versus SPP	29.63	0.02	460.6	0.71	11.8	0.72	11.5
AD versus SPP	39.51	0.02	345.4	0.94	8.8	0.96	8.6
AD versus GPP	29.63	0.66	12.5	–	–	0.66	12.5
AD versus GPP	39.51	0.89	9.4	–	–	0.89	9.4
AD versus CPP	29.63	0.47	17.9	–	–	0.47	17.9
AD versus CCP	39.51	0.62	13.4	–	–	0.62	13.4
AD versus DPP	29.63	5.13	1.6	–	–		
AD versus DPP	39.51	6.84	1.2	–	–		
(b) November 2018							
AD versus SPP	29.63	0.02	499.2	0.68	12.2	0.70	11.9
AD versus SPP	39.51	0.02	374.4	0.91	9.2	0.93	8.9
AD versus GPP	29.63	0.61	13.6	–	–	0.61	13.6
AD versus GPP	39.51	0.82	10.2	–	–	0.82	10.2
AD versus CPP	29.63	0.43	19.4	–	–	0.43	19.4
AD versus CCP	39.51	0.57	14.5	–	–	0.57	14.5
AD versus DPP	29.63	4.73	1.8	–	–		
AD versus DPP	39.51	6.31	1.3	–	–	–	–

8.4.2.3 Capital Payback Time (Combined State)

In this state, the calculations have been performed based on the sum of guaranteed electricity purchase costs and amount of fuel saved. The results of this calculation are presented in Table 8.11a and b based on October and November FOB costs. The results of fuel savings cost using AD method and payback time are reported in Table 8.11. According to government guaranteed electricity purchases in these scenarios, the amounts of fuel saving cost and payback time have been improved in all scenarios. Comparing AD to DPP under maximum power supply mode, it is found that around 8.22 million dollars (with payback time improvement of 1) and 7.69 million dollars (with payback time improvement of 1.1) are saved in terms of the combined gas oil and guaranteed electricity purchases in Oct. and Nov. 2018, respectively. The same values are also obtained for when combined gas oil, fuel oil, and guaranteed electricity purchases under the same power supply is considered. Also, under minimum power supply mode, employing AD instead of DPP can save around 6.16 million dollars and 5.77 million dollars (both with payback time improvement of 1.4) are saved in terms of the combined gas oil and guaranteed electricity purchases in Oct. and Nov. 2018, respectively. The same values are also obtained for when combined gas oil, fuel oil, and guaranteed electricity purchases under the same power supply is considered.

Figures 8.2 and 8.3 compare the annual fuel savings cost and payback time for each scenarios for different recorded months.

8.5 Conclusions

Anaerobic digestion (AD) method was introduced as an efficient alternative renewable energy-based waste management process to tackle the growth of the environmental pollution and fuel utility. The wastes of the Isfahan city were used as the case study through this calculation. The main advantages of AD method in terms of CO2 emission reduction and primary fuel savings were discussed in comparison with two conventional waste management methods of incineration and landfill as well as different fossil fuel-based power plants for two different approaches of constant input waste and constant input electrical power under minimum and maximum capacities. Also, fuel savings cost and payback time values for different scenarios were calculated and the main advantages of using AD method instead of the conventional primary fuels in the screened power plants were elaborated on in terms of the obtained economic results. Following concluding remarks can be drawn:

- AD method is highly recommended for the DPP scenario since the highest CO_2 emission reduction was calculated 14,739 tons per year was calculated for this scenario under maximum power generation of 39.51 million kWh per year.
- Although using AD method instead of fossil fuel in the CPPs increased CO_2 emission (which is not appealing), it saved equivalent primary fuel around 6.5

Table 8.11 Annual fuel savings cost and capital payback time with combined guaranteed electricity purchase and FOB costs

Compared methods	Power (M kWh)	Gas oil with guaranteed electricity purchase		Fuel oil with guaranteed electricity purchase		Gas oil & Fuel oil with guaranteed electricity purchase	
		Saving cost of fuel (M$)	Capital payback time (yr)	Saving cost of fuel (M$)	Capital payback time (yr)	Saving cost of fuel (M$)	Capital payback time (yr)
(a) October 2018							
AD versus SPP	29.63	1.06	7.9	1.74	4.8	1.76	4.7
AD versus SPP	39.51	1.41	5.9	2.32	3.6	2.35	3.5
AD versus GPP	29.63	1.70	4.9	1.04	8.0	1.70	4.9
AD versus GPP	39.51	2.27	3.7	1.38	6.0	2.27	3.7
AD versus CPP	29.63	1.50	5.5	1.04	8.0	1.50	5.5
AD versus CCP	39.51	2.00	4.2	1.38	6.0	2.00	4.2
AD versus DPP	29.63	6.16	1.4	1.04	8.0	6.16	1.4
AD versus DPP	39.51	8.22	1.0	1.38	6.0	8.22	1.0
(b) November 2018							
AD versus SPP	29.63	1.05	7.9	1.72	4.8	1.74	4.8
AD versus SPP	39.51	1.41	5.9	2.29	3.6	2.31	3.6
AD versus GPP	29.63	1.65	5.0	1.04	8.0	1.65	5.0
AD versus GPP	39.51	2.20	3.8	1.38	6.0	2.20	3.8
AD versus CPP	29.63	1.47	5.7	1.04	8.0	1.47	5.7
AD versus CCP	39.51	1.96	4.3	1.38	6.0	1.96	4.3
AD versus DPP	29.63	5.77	1.4	1.04	8.0	5.77	1.4
AD versus DPP	39.51	7.69	1.1	1.38	6.0	7.69	1.1
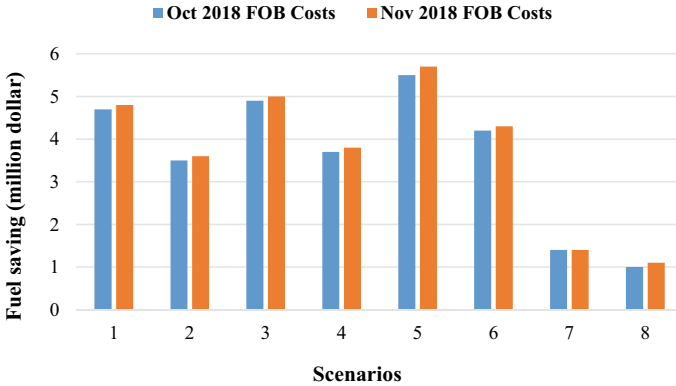
Fig. 8.2 Fuel saving cost values for different scenarios (1&2: AD vs. SPP; 3&4: AD vs. GPP; 5&6: AD vs. CPP; 7&8: AD vs. DPP)
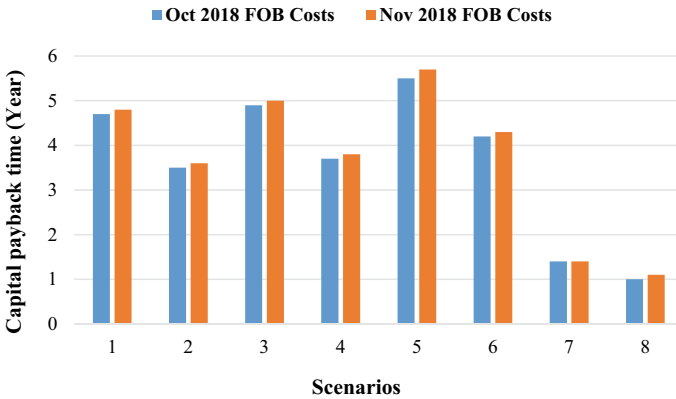
Fig. 8.3 Capital payback time for different scenarios (1&2: AD vs. SPP; 3&4: AD vs. GPP; 5&6: AD vs. CPP; 7&8: AD vs. DPP)

million m^3 under minimum power capacity of 29.63 million kWh per year and 8.6 million m^3 under maximum power capacity of 39.51 million kWh per year.

- Under maximum power capacity of 39.51 million kWh per year employing AD method instead of gas oil in the DPPs saved 8.22 million dollars in October with payback time of 1 year and 7.69 million dollars in November with payback time of 1.1 year.
- Comparing AD and landfill under the same electrical power capacity, it was found that AD method is superior to the landfill method since less CO_2 is emitted in AD method as less waste is required for that.
- Under guaranteed purchase of electricity scenario, the annual repayment for the minimum and maximum amounts of annual electricity production were calculated

1.04 million US $ with a payback period time of 8 years and 1.38 million US $ with a payback period time of 6 years.

- Under FOB cost evaluation scenario, using gas oil in the SPP under minimum power load of 29.63 M kWh was introduced as the worst scenario since it led to the lowest fuel savings cost of 0.02 M $ with payback time of 460.6 yr in Oct 2018 and 0.02 M $ with payback time of 499.2 yr in Nov. 2018.

References

1. H. Nasrollahi, F. Ahmadi, M. Ebadollahi, S. Najafi Nobar, M. Amidpour, The greenhouse technology in different climate conditions: a comprehensive energy-saving analysis. Sustain. Energy Technol. Assess. **47**, 101455 (2021)
2. M. Ebadollahi, H. Rostamzadeh, M.Z. Pedram, H. Ghaebi, M. Amidpour, Proposal and multi-criteria optimization of two new combined heating and power systems for the Sabalan geothermal source. J. Clean. Prod. **229**, 1065–1081 (2019)
3. M. Ebadollahi, H. Rostamzadeh, H. Ghaebi, M. Amidpour, Exergoeconomic analysis and optimization of innovative cascade bi-evaporator electricity/cooling cycles with two adjustable cooling temperatures. Appl. Therm. Eng. **152**, 890–906 (2019)
4. M.-R. Kolahi, M. Amidpour, M. Yari, Multi-objective metaheuristic optimization of combined flash-binary geothermal and humidification dehumidification desalination systems. Desalination **490**, 114456 (2020)
5. M.-R. Kolahi, A. Nemati, M. Yari, Performance optimization and improvement of a flash-binary geothermal power plant using zeotropic mixtures with PSO algorithm. Geothermics **74**, 45–56 (2018)
6. M. Kolahi, M. Yari, S.M.S. Mahmoudi, F. Mohammadkhani, Thermodynamic and economic performance improvement of ORCs through using zeotropic mixtures: case of waste heat recovery in an offshore platform. Case Stud. Therm. Eng. **8**, 51–70 (2016)
7. Z. Ghaffarpour, M. Mahmoudi, A.H. Mosaffa, L. Garousi Farshi, Thermoeconomic assessment of a novel integrated biomass based power generation system including gas turbine cycle, solid oxide fuel cell and Rankine cycle. Energy Convers. Manag. **161**, 1–12 (2018)
8. M. Tajik Mansouri, M. Amidpour, J.M. Ponce-Ortega, Optimal integration of organic Rankine cycle and desalination systems with industrial processes: Energy-water-environment nexus. Appl. Therm. Eng. **158**, 113740 (2019)
9. H. Rostamzadeh, M. Ebadollahi, H. Ghaebi, M. Amidpour, R. Kheiri, Energy and exergy analysis of novel combined cooling and power (CCP) cycles. Appl. Therm. Eng. **124**, 152–169 (2017)
10. M. Ebadollahi, H. Rostamzadeh, O. Pourali, H. Ghaebi, M. Amidpour, Inherently safety design of a dual-loop bi-evaporator combined cooling and power system: 4E and safety based optimization approach. Process Saf. Environ. Prot. (2021)
11. H. Rostamzadeh, M. Ebadollahi, H. Ghaebi, A. Shokri, Comparative study of two novel micro-CCHP systems based on organic Rankine cycle and Kalina cycle. Energy Convers. Manag. **183**, 210–229 (2019)
12. M. Ebadollahi, H. Rostamzadeh, P. Seyedmatin, H. Ghaebi, M. Amidpour, Thermal and exergetic performance enhancement of basic dual-loop combined cooling and power cycle driven by solar energy. Therm. Sci. Eng. Prog. **18**, 100556 (2020)
13. M. Bezaatpour, H. Rostamzadeh, J. Bezaatpour, M. Ebadollahi, Magnetic-induced nanoparticles and rotary tubes for energetic and exergetic performance improvement of compact heat exchangers. Powder Technol. **377**, 396–414 (2021)

14. A. Pirmohamadi, H. Ghaebi, B.M. Ziapour, M. Ebadollahi, Exergoeconomic analysis of a novel hybrid system by integrating the kalina and heat pump cycles with a nitrogen closed brayton system. Energy Rep. **7**, 546–564 (2021)
15. D. Hoornweg, P. Bhada-Tata, What a waste: a global review of solid waste management (2012)
16. Y. Chen, J.J. Cheng, K.S.J.B.t. Creamer, Inhibition of anaerobic digestion process: a review **99**(10), 4044–4064 (2008)
17. M. Ebadollahi, H. Rostamzadeh, O. Pourali, H. Ghaebi, M.J.J.o.E.R.T. Amidpour, Close super-critical versus inverse Brayton cycles for power supply, using waste of a biogas-driven open Brayton cycle **143**(9), 092102 (2021)
18. B. Kelleher, J. Leahy, A. Henihan, T. O'dwyer, D. Sutton, M.J.B.t. Leahy, Advances in poultry litter disposal technology–a review **83**(1), 27–36 (2002)
19. Y. Van Fan, J.J. Klemeš, C.T. Lee, S.J.J.o.e.m. Perry, Anaerobic digestion of municipal solid waste: Energy and carbon emission footprint **223**, 888–897 (2018)
20. J. Cheng, C. Zhu, J. Zhu, X. Jing, F. Kong, C.J.J.o.C.P. Zhang, Effects of waste rusted iron shavings on enhancing anaerobic digestion of food wastes and municipal sludge **242**, 118195 (2020)
21. C.P. Kumar et al., Bio-Hythane production from organic fraction of municipal solid waste in single and two stage anaerobic digestion processes **294**, 122220 (2019)
22. J. Li et al., Did municipal solid waste landfill have obvious influence on polychlorinated dibenzo-p-dioxins and polychlorinated dibenzofurans (PCDD/Fs) in ambient air: a case study in East China **62**, 169–176 (2017)
23. P. Ghosh, A. Gupta, I.S.J.E.S. Thakur, P. Research, Combined chemical and toxicological evaluation of leachate from municipal solid waste landfill sites of Delhi, India **22**(12), 9148–9158 (2015)
24. M.D. Vaverková et al., Impact of municipal solid waste landfill on environment–a case study **19**(4) (2018)
25. S. Shu, W. Zhu, S. Wang, C.W.W. Ng, Y. Chen, A.C.F.J.S.o.t.T.E. Chiu, Leachate break-through mechanism and key pollutant indicator of municipal solid waste landfill barrier systems: centrifuge and numerical modeling approach **612**, 1123–1131 (2018)
26. S. Shu et al., Effect of the leachate head on the key pollutant indicator in a municipal solid waste landfill barrier system **239**, 262–270 (2019)
27. M. Nadal, F. García, M. Schuhmacher, J.L.J.E.r. Domingo, Metals in biological tissues of the population living near a hazardous waste incinerator in Catalonia, Spain: Two decades of follow-up **176**, 108578 (2019)
28. H. Spliethoff, *Power generation from solid fuels.* Springer Science & Business Media (2010)
29. J. Van Caneghem et al., Fluidized bed waste incinerators: design, operational and environmental issues **38**(4), 551–582 (2012)
30. C. Yin, L.A. Rosendahl, S.K.J.P.i.E. Kær, Grate-firing of biomass for heat and power production. Science **34**(6), 725–754 (2008)
31. T. Gu, C. Yin, W. Ma, G.J.A.E. Chen, Municipal solid waste incineration in a packed bed: a comprehensive modeling study with experimental validation **247**, 127–139 (2019)
32. M. Mohsenizadeh, M.K. Tural, E.J.S.C. Kentel, Municipal solid waste management with cost minimization and emission control objectives: a case study of Ankara. Society **52**, 101807 (2020)
33. M. Rezaei, B. Ghobadian, S.H. Samadi, S.J.E. Karimi, Electric power generation from municipal solid waste: a techno-economical assessment under different scenarios in Iran **152**, 46–56 (2018)
34. A.J.T.R.P. Mesjasz-Lech, Reverse logistics of municipal solid waste–towards zero waste cities **39**, 320–332 (2019)
35. M.I.D. Portal (2016)
36. Renewable Energy and Energy Efficiency Organization (REEEO) (2018)
37. F. Alobaid et al., Dynamic simulation of a municipal solid waste incinerator **149**, 230–249 (2018)

38. F. Di Maria, C.J.T.I.J.o.L.C.A. Micale, Life cycle analysis of incineration compared to anaerobic digestion followed by composting for managing organic waste: the influence of system components for an Italian district **20**(3), 377–388 (2015)
39. https://anaerobic-digestion.com
40. Ministry of Energy (MOE) http://moe.gov.ir (2018)

Chapter 9
Carbon Capture and Utilization as an Alternative for Renewable Energy Storage

Nima Mohammadi and Behnam Mousazadeh

Abstract Globally increasing carbon dioxide emissions, as the result of increased anthropogenic activities, has been an environmental challenge for recent years, due to the significant contribution of CO_2 to global warming and air pollution. Therefore, proposing strategies to address this worldwide issue is of significant importance. The global move toward renewable energy sources and decreased greenhouse gas emissions has been commenced in recent years. The present chapter as well as broad insights into carbon capture and utilization (CCU) technology, explores CCU as a promising alternative for renewable energy storage. In addition, future objectives and research paths will be explored for the critical factors influencing CCU technology.

Keywords Carbon capture and utilization · CO_2 conversion · Air pollution · Renewable energy storage

9.1 Importance of CO_2 Capture

Carbon dioxide discharge into the environment leads to climate change, having detrimental influences on human health and other organisms [1]. Greenhouse gases are emitted as fossil fuels are burned [2]. These emissions lead to the trap of solar radiation in the atmosphere, which in turn increases the global temperature [3]. Global warming affects water sources and weather conditions, endangers coastal areas with rising sea levels, shifts the food crops growing conditions, and threatens human health [3].

According to the EPA, climate change would raise water demand while decreasing water supplies. Water is needed for either human and animal health or industrial and agricultural purposes. Climate change is projected to intensify precipitation in certain regions, increasing the amount of sediment and toxins washed into surface and groundwater [4]. As sea levels rise, saltwater can enter certain water networks, increasing water treatment demand. The agriculture sector is also impacted by changing weather patterns. Carbon emissions, on the other hand, can lead to rising

N. Mohammadi · B. Mousazadeh (✉)
Gas Engineering Department, Petroleum University of Technology, Ahwaz, Iran

temperatures and decreased rainfall, altering the farming practices for many food crops. As stated by the U.S. Global Change Research Program, for instance, greenhouse gas discharge has increased the temperature of the Central Valley in California. Consequently, the yield of some agricultural products such as rice, tomato, wheat, corn, and sunflower are fallen dramatically. Therefore, it is expected that food prices will increase across the world as crop yields shift.

According to NASA, wildfires, water shortages, and tropical storms would increase as the result of global warming. Hurricane Sandy in 2012 and Typhoon Haiyan in 2013 are examples of extreme weather conditions. The damage they create takes years to repair, even with international assistance. Infrastructure damage triggers several human health problems, including the spread of disease as water and sewage networks fail [5]. Storms and the disruption they cause to infrastructure also result in massive human suffering. Moreover, according to the Intergovernmental Panel on Climate Change, Earth will face a 1.5-degree Celsius increase in temperature over the next century. This slight shift in the temperature will cause ice sheets to melt and seas to expand. According to the EPA, in comparison with little discernible changes in sea levels during the last 2,000 years, Gulf Coast and mid-Atlantic regions have seen 20 cm increase in sea levels just over the last 50 years. Subsequently, rising sea levels may have drastic consequences for coastal areas, particularly areas with dense populations which are more vulnerable to storms, flooding of infrastructure, and shipping traffic disruption.

The threats caused by carbon emissions for human health are of urgent importance to be globally considered. Increased CO_2 concentrations further worsen ozone and other air pollution levels. As the result of increase in temperature, the loss of an extra 150,000 lives is projected [6]. Simultaneously, non-ozone air pollution associated with global warming can boost the prevalence of allergies, lung cancer, cardiovascular disease, and asthma [7]. The population of diseases carriers such as mosquitoes and ticks increase as the planet gets warmer, causing transmit of disease for longer durations before being shut down by cold climate conditions. There would be, of course, other threats to human health as the consequence of environmental alterations linked to the aggregation of atmospheric carbon dioxide.

Carbon dioxide is regarded as an economic drawback. The majority of today's global economic activity is based on energy derived from the combustion of fossil fuels, which release carbon dioxide as an unwanted product. While the prices of carbon-free energy sources such as solar and wind have dropped significantly in previous decades, significant obstacles remain to fully decarbonize our power grid and much larger barriers to fully decarbonizing the manufacturing and transportation industries [8]. The overall carbon emissions from anthropogenic activities are more than 35 billion tons per year [9]. The primary sources of CO_2 emissions include the burning of oil, gas, and coal. In 2018, carbon dioxide emissions from the oil and gas industry were as follows: 12.4 billion tons from oil combustion, 14.7 billion tons from coal burn, and 7.5 billion tons from gas burning [10].

The UN Environment Program suggests that in order to maintain a 2-degree Celsius temperature increase until 2100, a 25% decrease in emissions must occur before 2030. In order to maintain a temperature increase within 1.5°, a 55% decrease

must occur until 2030 [10]. CO_2 levels in the atmosphere have risen almost 50% from about 275 ppm in 1760 (the start of the industrial revolution) to about 410 ppm in 2020, as a result of human-caused CO_2 emissions [10]. The UN reports that greenhouse gas emissions are increasing much too fast to keep temperature rise within 1.5 °C. In 2019, the average temperature of the planet was observed to be 1.1 °C higher than that of pre-industrial times. Under existing patterns, limiting temperature increase within 2° will be challenging, even there is a small hope to maintain increases below 3° [10]. Accordingly, professor Strutton claims that "without large-scale carbon capture and storage, as well as major emissions reductions, there is no way for Earth to remain below 3 °C."

9.2   Strategies for Reducing Carbon Emissions

Most countries around the world today acknowledge that worldwide climate change creates a serious danger to the well-being of humans, and so it is necessary to decrease CO_2 levels in the environment by reducing CO_2 discharge. This agreement was reflected by the Kyoto Protocol (signed in 1997 and implemented in 2005), which established pollution mitigation goals for all governments (except for the US, South Sudan, Andorra, Canada, and Afghanistan). Then, it was up to the governments to find a way to achieve the emissions reduction target. So, the question is, how do countries resolve this problem?

A carbon tax or a cap-and-trade framework are two policies that a government might pursue. Carbon taxes would lower emissions by establishing a motivation to utilize renewable energy resources. The cap-and-trade policy, on the other hand, establishes an aggregate boundary on carbon emissions, the right to emit carbon is then allocated or auctioned off, and these emission shares will then be traded in an energy market. The benefit of this strategy is that the emissions have a defined level—they are easy to control and predict, while a basic "carbon tax" strategy would not ensure any precise overall emissions level, and if a government were to apply such a tax scenario to achieve individual objectives, the tax would have to be updated regularly, something that companies would find difficult to manage.

Developed countries, on the other hand, have been enthusiastic about using new technologies to reduce carbon dioxide emissions. They may make use of green energy sources [11–13]. Renewable energy is energy produced from non-finite or non-exhaustible natural sources on the planet like wind, geothermal, and solar energy that are less detrimental to the atmosphere than conventional energy sources that depend on fossil fuels [14–16]. These options, however, possess certain disadvantages that make them impossible to adopt on large scales.

Solar energy is green energy derived from the sun's light and heat. One of the many advantages of solar energy is that it can be used indefinitely. There is an infinite abundance of renewable energy with the infrastructure to harness it, which means fossil fuels will be made outdated. Solar technology has the potential to minimize energy prices in the long term while still lowering energy costs in the short term. While

there are many arguments to turn to an environmentally sustainable, green energy source, solar energy is not the right option for everyone. For instance, the capital cost of a solar energy system is quite high [17]. At night times, solar technology depends on the power grid to produce electricity [17]. If solar energy is not used immediately, batteries should be used to store the remaining energy, which will be expensive and take up a lot of space [18].

Wind farms use turbines to convert wind flow energy into electricity. Wind farms are often installed in remote regions, far from the busy cities where electricity is most required [19]. Wind energy must be transferred along transport lines, which increases costs [20]. Although wind turbines emit relatively little pollution, they are opposed by some cities because they obstruct skylines and create noise [21]. Wind farms even pose a threat to nearby wildlife, such as birds, which are harmed when they collide with the turbine's arms when flying [19].

Owing to the drawbacks mentioned earlier, renewable resources are insufficient to meet all human needs. As a result, researchers commenced investigating carbon capture and recycling strategy. This procedure has two significant benefits. First and foremost, the amount of carbon dioxide in the atmosphere would be decreased. Second, the captured gas may be recycled in manufacturing processes or converted back into value-added chemicals. There are several potential sources for carbon dioxide capture, such as the transportation sector [22], thermal power generation [23], and direct air capture [24]. However, fossil fuel-based power plants are essential contributors to anthropogenic CO_2 emissions. Of the 60% of the overall CO_2 emissions originate from coal or natural gas combustion in power plants for electricity generation [25]. Higher carbon dioxide levels render more cost-effective separation [26]. Therefore, the most promising sector for reducing emissions is the thermal power industry. Small-scale carbon capture from mobile transportation sources, directly capturing from the air, and from the residential sector, on the other hand, is projected to be more costly than large-scale capture sources. Using either green energy sources or electricity generated from thermal power plants equipped with carbon capture units would be promising alternatives to minimize emissions in small-scale CO_2 emitting points. As the carbon dioxide concentration in the atmosphere is lower than that of exhaust gas (approximately 380 ppm-around 1% of the concentration of exhaust gas), it is not discussed in this chapter [27].

9.3　CO_2 Capture Systems

Generally, there are four classifications for carbon dioxide capturing systems, including CO_2 removal from industrial streams, pre-combustion capture, oxy-fuel combustion capture, and post-combustion capture. However, post-combustion capture has been regarded as the most popular strategy in the industry. Post-combustion refers to the capture of carbon dioxide from a gas emitted by the combustion of fossil fuels. The carbon dioxide capturing systems are schematically shown in Fig. 9.1.
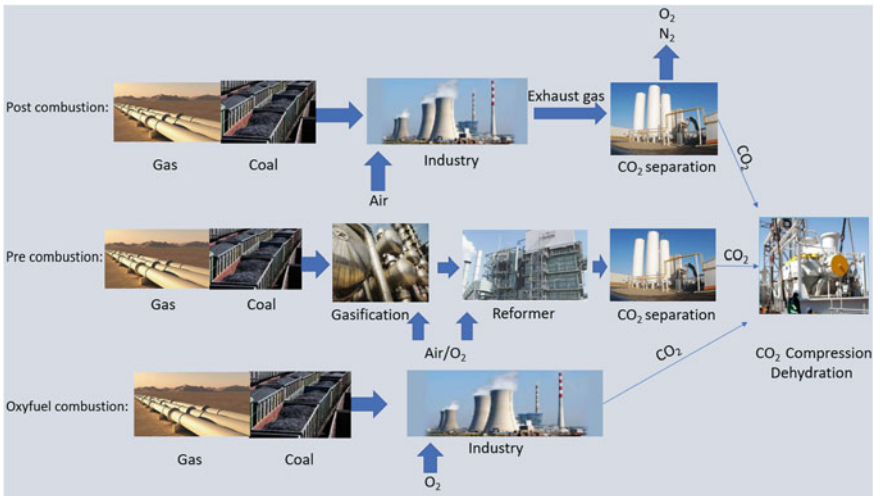
Fig. 9.1 Overview of carbon capture systems

9.3.1 Capture from Industrial Process Streams

It has been over 80 years that carbon dioxide is separated from streams of various industries such as the natural gas sweetening process, processing of hydrogen-containing syngas, and production of liquid fuels [28]. However, since there is no rationale or need to store CO_2, the majority of it is released into the environment. Cement and steel manufacturing, as well as food and beverage fermentation processes, are examples of industrial operations that release CO_2 that is not captured.

9.3.2 Post-combustion Capture

Post-combustion capture is the process of capturing CO_2 from exhaust gases emitted by the burning of fossil fuels and biomass in the atmosphere. Exhaust gas is passed into systems that filter the majority of the CO_2 before being released into the air [29]. The CO_2 is stored in a tank, and the residual exhaust stream is released into the atmosphere. For CO_2 separation, a chemical sorbent mechanism is often used [30]. Other strategies are being considered as well, but they are not as far along in their progress. Apart from industrial processes, the existing operating post-combustion capture capacity is 2261 GW_e of oil, coal, and natural gas power plants, including 155 GW_e of supercritical coal-based units and 339 GW_e of natural gas combined cycle (NGCC) units in particular [31, 32]. The latter systems are instances where carbon the capture process would be best implemented.

9.3.3 Oxy-Fuel Combustion Capture

Oxy-fuel combustion refers to the use of pure oxygen rather than air for fossil fuel combustion process. The resulting exhaust stream of this process mainly consists of water vapor and carbon dioxide gas [33]. When the combustion process is performed using pure oxygen the temperature of the flame becomes too high. However, recycling CO_2 and H_2O-containing exhaust stream to the combustion chamber can reduce the flame temperature [34]. In order to provide the required oxygen cryogenic air separation as well as innovative methods are often applied, including chemical looping processes and membrane systems [35, 36]. Similar to systems of reference for post-combustion capture, the power plants for oxy-fuel combustion capture are coal-based plants and natural gas combined cycle systems.

9.3.4 Pre-combustion Capture

In a pre-combustion capture configuration, CO_2 is feed with pure oxygen or air and/or steam to give mainly syngas. In a reactor system known as a shift converter, carbon monoxide is interacted with steam to produce CO_2 and additional hydrogen. CO_2 is subsequently isolated generally by a chemical or physical adsorption step, yielding a hydrogen-rich fuel that may be used in furnaces, boilers, engines, gas turbines, and fuel cells. Although the power plants capable of pre-combustion capture systems consist of 4 GWe accounting for both oil and coal-based plants (approximately 0.1% of the overall capacity worldwide (3719 GWe; IEA WEO, 2004)), the pre-combustion configuration is of significant importance.

9.4 Carbon Dioxide Utilization

There are two different strategies for CO_2 utilization, including mineral carbonation and industrial usages. Mineral carbonation is referred to the conversion of CO_2 gas to solid carbonates via specific chemical processes. Industrial utilization involves the use of CO_2 as raw material for the production of numerous chemicals.

9.4.1 Mineral Carbonation: Technology, Impacts and Costs

Mineral carbonation is the process of restoring CO_2 gas via chemical reactions using alkaline oxides found in natural sources like serpentine and olivine. Calcium carbonate ($CaCO_3$), known as limestone, and magnesium carbonate ($MgCO_3$) are major products of mineral carbonation reactions [37]. The amount of metal oxides

present in the Earth's natural sources like silicate rocks is greater than the amount required to restore all of the CO_2 released by the burning of all existing fossil fuel supplies [38]. Some industries such as stainless-steel produce wastes that contain trace amounts of metal oxides. Carbonates and silicates, the products of mineral carbonation, can be stored over long times in either silicate mines or can be re-used in the construction industry. CO_2 will not be emitted into the atmosphere after carbonation [39]. As a result, there will be no necessity to monitor landfill areas of disposal, and the threats associated with them would be minimal. The mechanism of mineral carbonation is defined as 'weathering' when it happens naturally. The mechanism happens quite slowly in the natural environment; as a result, it can only be speeded up to be a feasible storage system for CO_2 collected from anthropogenic activities. Researchers have focused on developing process pathways that can provide process rates that are suitable for industrial use while also reducing energy consumption [40]. Mineral carbonation via natural silicates is in the testing stage, although certain industrial waste-based technologies are in the demonstration stage. The mineral carbonation process is schematically shown in Fig. 9.2.

Mining, grinding, and milling of ores, as well as their transportation to a processing unit which has a concentrated CO_2 flow entering from a capture unit, would be needed for a commercial process. The energy needed for the carbonation plant would be approximately 30–50% of the energy output of a typical CO_2 capture plant [38]. When the extra energy needed for CO_2 capture is considered, a carbon capture and storage (CCS) process with a CO_2 fixation unit via mineral carbonation would consume about 60–180% more energy than that of a reference power plant without a CO_2 fixation unit [38]. As a result of these energy needs for CO_2 fixation units, the prices for the mineral carbonation process would increase dramatically.
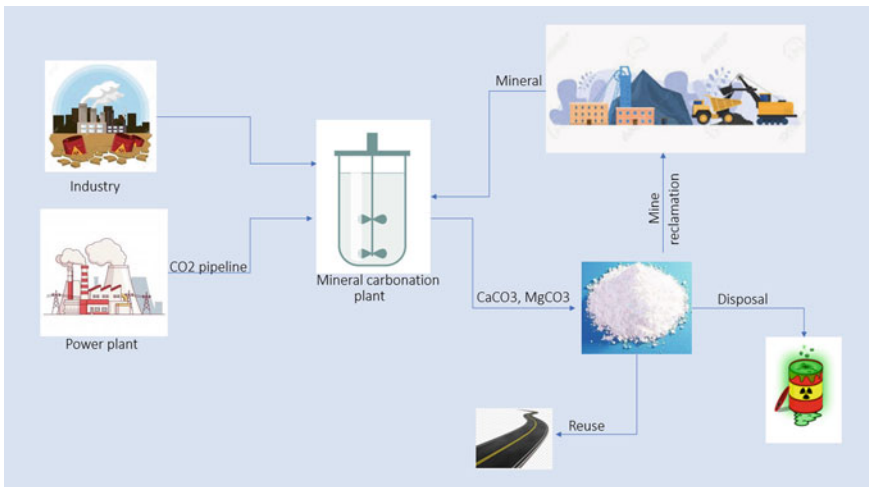

Fig. 9.2 Schematic presentation of mineral carbonation process

9.4.2 Industrial Uses

CO_2 potentially can be utilized through two strategies where either it is used as a reactant or is used directly. In chemical and biological processes such as methanol and urea production units, CO_2 is utilized as a reactant [41]. While, in industries such as refrigeration, welding, horticulture industry, fire extinguishers, and food packaging CO_2 is directly used as feedstock [42]. The annual global CO_2 utilization is currently 130 Mt [43]. Most of the overall CO_2 utilization is for urea production which is a raw material for fertilizers production and some other products [43]. The production of added-value chemicals from CO_2 contributes to eliminating it from the atmosphere and keeping it in chemicals. An overview of the industrial uses of carbon dioxide is shown in Fig. 9.3.

9.5 CO_2 Conversion

The global demand for energy storage has gained a lot of attention, particularly in European countries, United States, China and Japan [44, 45]. Basically, various classifications of energy storage systems include electric to heat, electric to chemicals, and electric to electric. Examples of energy storage technologies are liquid air storage systems, compressed air storage systems, and batteries. However, some energy storage systems direct the storage final product to the chemical market. Under the power to fuel concept, power to numerous chemicals such as methanol, hydrogen, natural gas, etc. are examples of electric to chemicals systems that eventually direct the storage final product to the transportation industry. In this context, energy storage
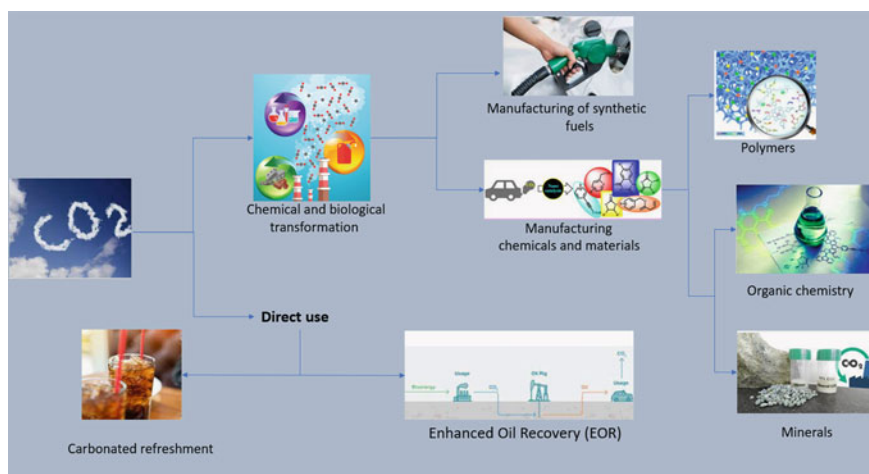
**Fig. 9.3** Overview of the industrial uses of carbon dioxide

can be combined with the concept of Carbon Capture and Utilization (CCU). Using renewable energy sources such as wind or solar energy as power supplies needed for carbon dioxide conversion can simultaneously provide solutions for both CO_2 emissions and energy storage challenges. Two major technological difficulties can be identified in this context. First, an efficient, cost-effective, and environmentally friendly technology for carbon dioxide capture. Next, an economically feasible practical approach for CO_2 conversion to various chemicals.

9.5.1 Modern Strategies for CO₂ Conversion

There is no doubt that today's chemists face a sign ificant challenge and an exciting potential in the effective conversion of CO_2 to functional molecules. Since conventional thermal methods have failed to solve the global CO_2 and energy challenges, a number of promising innovations are being developed.

9.5.2 Electrochemical Conversion

CO_2 electrochemical valorization is a novel technique that uses electrical energy to generate a potential between two electrodes, enabling CO_2 to be converted into value-added chemicals under moderate reaction conditions [46, 47]. There are different mechanisms where CO_2 can be transformed through gas, aqueous, and non-aqueous phases with various system configurations [46, 48]. The three common system
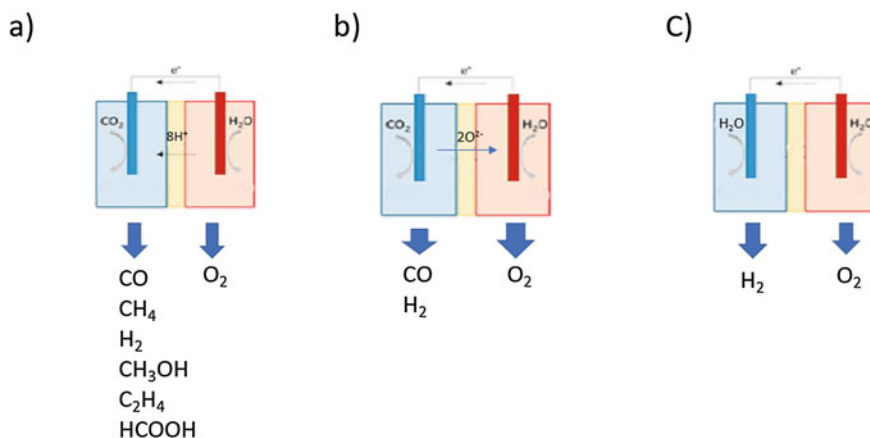
Fig. 9.4 Schematic demonstration of common electrochemical conversion systems, **a** solid state electrolysis system, **b** solid oxide electrolysis system, **c** water splitting system

configurations are schematically shown in Fig. 9.4. A typical solid-state electrolysis system for CO_2 and H_2O conversion is shown in Fig. 9.4a. The solid oxide electrolysis configuration for both pure and simultaneous conversion of CO_2 and H_2O is demonstrated in Fig. 9.4b. Also, a water splitting system in a typical alkaline electrolysis configuration is shown in Fig. 9.5c. There are numerous experimental variables that influence the final product components such as electrode materials, CO_2 concentration, the reaction medium, pH, buffer strength, the reaction temperature, etc. [48]. The most common product of the CO_2 conversion process includes CO (carbon monoxide), CH_2O (formaldehyde), HCOOH (formic acid) or $HCOO^-$ (formate in basic solutions), $H_2C_2O_4$ (oxalic acid), or $C_2O_4^{2-}$ (oxalate in basic solutions), CH_3OH (methanol), CH_4 (methane), C_2H_5OH (ethanol), and C_2H_4 (ethylene) [46, 48].

A number of advantages over other systems presents electrochemical process more promising for CO_2 conversion than other systems and configurations. The process output can be controlled via reaction variables such as temperature and electrode potential [49]. Also, a wide range of useful chemicals can be produced in mixtures or pure form. For instance, in the electrochemical process of CO_2 conversion to methanol, CO and H_2 with an approximately H_2/CO ratio of 2 can be produced at the cathode as well as pure oxygen being produced at the anode [50]. Moreover, besides solar energy, many other renewable energy supplies can be used for electrochemical conversion [48]. Eventually, for both small and large-scale applications, the electrochemical systems are ideal candidates as they are easy to use, compact and
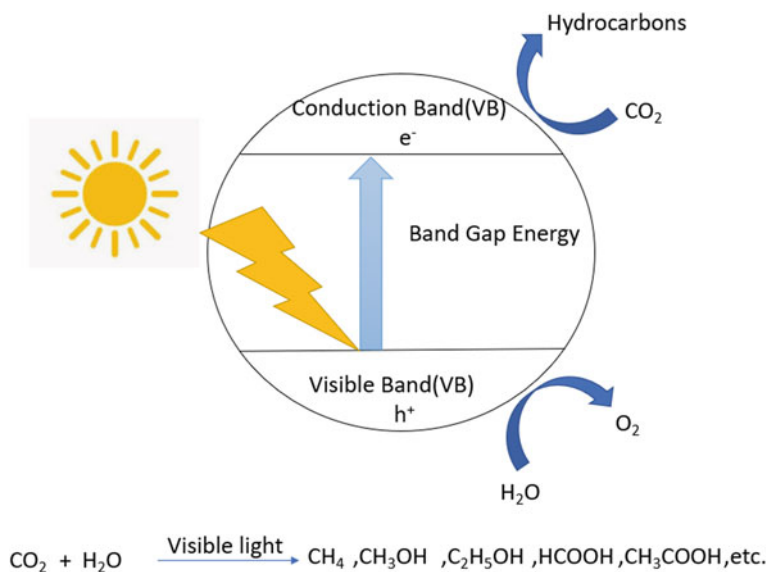
Fig. 9.5 Photocatalytic CO_2 conversion process

on-demand [48]. The single greatest difficulty, in general, is the low efficiency of electrocatalysts, which is caused by low activity and selectivity, and, most significantly, inadequate stability.

9.5.3 Solar Thermochemical Conversion

CO_2 conversion via the solar thermochemical conversion system is another method that has recently seen some significant advances. There are many options to minimize CO_2 amounts in the atmosphere with the help of clean solar technology, with direct irradiation of solar light being the most efficient approach since it requires no added energy and has no harmful environmental impact [51]. There are two types of immediate solar energy conversion: (i) thermal conversion, in which work is derived after sunlight is captured as thermal energy, and (ii) quantum conversion, in which work is derived immediately from the light absorbers such as a semiconductor, atom, or organic compound [52]. Intensely concentrated solar energy is utilized as the input energy supply required for the highly endothermic reactions.

The immediate utilization of solar radiation can be distinguished as the primary hallmark of CO_2 conversion via solar thermochemical systems. Integration of the currently commercially utilized concentrating solar systems for industrial scale power generation with the solar thermochemical CO_2 conversion systems can maximize the conversion efficiency levels. Therefore, the possibility of solar fuels generation at large scales and low costs can be increased [52].

Although significant advances have been made in the field of solar thermochemical CO_2 conversion technologies using metal oxides, a lack of fundamental research into the behavior of the metal oxides under the high-temperature conditions present in these cycles has hampered the development of materials.

Moreover, although the process thermodynamics is favorable, heat losses resulted from weak conductive and radiative heat transfer through the porous metal oxide structure will severely restrict the reactor's performance and cycling speeds [52].

Photochemical conversion:

In terms of how solar energy is utilized, photochemistry for photochemical CO_2 conversion varies from (solar) thermochemistry. In a photochemical system, photon energy is employed in chemical processes [53]. However, in thermochemical systems, the stored thermal energy is utilized to overcome activation energy needed for the chemical reaction [52].

Employing the semiconductors TiO_2, ZnO, CdS, GaP, SiC, and WO_3, the photoreduction of CO_2 to formaldehyde and methanol in pure water was first reported in 1979 [53]. The photoreduction of CO_2 is thought to occur when photoexcited electrons in the conduction band move to CO_2. This is based on a relationship between the conduction band energy potential and the methanol yield. Figure 9.5 depicts the primary process of selective photocatalysts under light irradiation.

The minimum energy here for the conduction band is larger compared to that of CO_2 photoreduction [53].

Also, the photocatalytic nature of materials is significantly important as it directly influences the efficiency of the CO_2 conversion reaction [54]. Several parameters, including catalyst dose, reactant concentration, duration, operating temperature, pressure distribution, pH, light intensity, and wavelength, impact this efficiency [51].

Similar to electrochemical systems, the reaction products of photocatalytic CO_2 conversion include CO (carbon monoxide), CH_2O (formaldehyde), CH_3OH (methanol), HCOOH (formic acid), CH_4 (methane), C_2H_6 (ethane), C_2H_4 (ethylene), and C_2H_5OH (ethanol) [54].

One of the benefits of photochemical systems is that photochemical systems are made of only a few pieces and are thus theoretically less likely to fail, provided the other elements are dependable [52]. TiO_2 has mostly been explored as the photoreduction catalyst for CO_2 conversion [55]. Numerous parameters have been investigated to improve the photocatalytic performance of TiO_2 such as dispersing active ions like Ti species, metal addition, and atomic dispersion of TiO_2 on porous structures like zeolites or SiO_2 [53].

CO_2 conversion to methane in the lack of an electrical power supply in a water-saturated environment using nitrogen-doped TiO_2 integrated with either Cu or Pt nanoparticles have been of significant importance [53, 54].

Although the current technology is not sufficient for the solar CO_2-to-fuel concept and further investigations are needed, photocatalytic CO_2 conversion using solar energy has been regarded as a promising approach [47, 49]. The ultimate objective of this process is to achieve photocatalytic CO_2 conversion at high rates under conditions where solar energy is the only power source. As a major proportion of the solar spectrum is composed of visible light, special consideration should be given to materials that are sensitive to sunlight [54]. The future research path could be either the development of co-catalysts in order to enhance the product selectivity or the investigation of co-catalyst sensitivity to improve CO_2 conversion rates [54].

9.5.4 Biochemical Conversion

The synthesis of biofuels via the natural photosynthesis process is a novel approach to convert CO_2 into added-value chemicals [56]. Microalgae might fulfill the criteria for producing technologically and commercially feasible biofuels. More precisely, effective biofuel production should be cost-competitive or less expensive than fossil fuel, involve little or no extra land usage, improve air quality, and use minimum water [56, 57]. The capture of CO_2 via microalgae can be performed from a variety of sources such as power plant emissions, CO_2 in the atmosphere, and soluble carbonates [57]. Microalgae are now regarded as one of the most potential biodiesel renewable resources; as a result, the majority of recent investigation and research activities are concentrated on microalgae, in particular because of their rapid expansion rate and oil content.

9.5.5 Catalytic Conversion

For catalytic conversion, two types of catalysis can be used: homogeneous and heterogeneous catalysts. Homogenous catalysts such as Rh-, Ru- and Ir-based materials have been investigated as efficient structures for the production of formats and formic acid, however, they possess difficulties when used at large scales. On the other hand, heterogeneous catalysts such as Cu-, Fe- and Ni-based materials are promising candidates for industrial applications, even though they have poor selectivity and low yield. Therefore, major advances in novel catalytic processes are required to make thermo-catalytic CO_2 conversion commercially viable [58].

The synthesis of catalysts using cheap metals, like iron and copper complexes, that are also active in moderate environments is a major issue from a scientific standpoint [58]. Unfortunately, the present pure thermocatalytic approaches can only provide a small net impact on CO_2 conversion because of their dependency on thermal energy—which is primarily supplied by burning fossil fuel sources. The heterogeneous (catalytic) reaction rate has been found to be aided by microwave radiation [59, 60]. In either CO_2 gasification or dry methane reforming processes, the integration of microwave heating with a carbon material functioning as both a catalyst and a microwave receiver leads to higher conversions than conventional heating [59, 60].

9.6 Adsorbent Materials for CO_2 Capture

This part scrutinizes the various types of adsorbents utilized for capturing CO_2 from flue gases. These materials comprise of carbon-based adsorbents, molecular sieves, zeolites, hydrotalcite-like compounds, metal–organic frameworks, and advanced adsorbents. The capability of each item has been discussed and described. Particularly, it has been proved that conventional adsorbent materials require more impregnation or functionalization with various nitrogen-containing species so as to become appropriate candidates for CO_2 capture.

9.6.1 Carbon-Based Adsorbents

Carbon dioxide might be recovered from flue gas utilizing non-reactive sorbents such as zeolites and carbonaceous materials. In addition, high porous materials such as activated carbons and charcoals reveal CO_2 capture capacities ranging between 10 and 15 wt%. Regarding all solid adsorbents, activated carbon demonstrates a couple of advantages including low consumption, easy-to-design pore structure, easy regeneration, and large surface area [61–63]. As a result, the pertinent costs of CO_2 capture are such that when the purity of CO_2 does not exceed 90%, the carbon-based systems can be appropriately utilized [64, 65].

A number of studies have been based on enhancing the adsorptive characteristics of porous adsorbents through surface modification, which normally boosts their basic properties. Such modifications comprise of cation exchange within the metal framework and surface chemical treatment or pores functionalization. It must be mentioned that although the modifications usually diminish the surface area, they enhance the adsorptive selectivity and capacity for CO_2. Regarding the adsorption applications, commercial activated carbons derived by physical activation normally exhibit low CO_2 adsorption capacity at ambient pressure. Thus, the introduction of micro-porosity in such materials with a considerable enhancement in the specific surface area is necessary. This is due to the fact that both chemical and physical activation together can lead to the production of activated carbons with considerably large values of surface areas [66, 67].

9.6.2 Zeolites

Zeolites, on their own, present better selectivity of CO_2 /N_2 compared to those of carbonaceous materials. Meanwhile, their CO_2 capacities are 2–3 times lower [68, 69]. In addition, the presence of water vapor precludes the performance of zeolites. To be competitive with liquid solvents, solid sorbents must show less sensitivity to steam and also should basically demonstrate more capacity and selectivity for CO_2 in comparison with currently existing physical sorbents.

Because of their high surface area as well as pore sizes variety, zeolites are regarded as excellent adsorbents. However, it must be noted that the thermal deterioration impacts their stability at raised temperatures and makes them impractical for high-temperature CO_2 capture operations. Therefore, to boost the capture capacity and selectivity, the utilization of chemically modified zeolites is regarded as an appropriate alternative which takes the benefits of high BET surface area and different pore sizes [70]. It is worth mentioning that introducing alkali metals or alkaline earth upon the adsorbent surface provides basic sites showing a strong affinity for acidic gases molecules, CO_2, for instance [71]. Many chemicals might be considered as modification materials on zeolites. Also, the hydrotalcite-like compounds are appropriate ones leading to optimistic results [72].

9.6.3 Advanced Adsorbents

Another approach to capture carbon dioxide is the introduction of various amines in the porous structure of adsorbents that are able to react with CO_2. To achieve this purpose, a myriad of amines, sorbent supports as well as immobilizing techniques have been examined.

9.6.4 Hydrotalcite-Like Compounds

Hydrotalcite-like compounds (HLC) have lately attracted considerable attention due to their CO_2 capture capabilities at raised temperatures. Also, HLC is known as layered double hydroxides which are among the bi-dimensional basic solids. Their structure comprises of positively charged brucite (magnesium hydroxide)-like layers with interlayer space containing charge-compensating anions and water molecules. It is alleged that these compounds can reveal high adsorption capacity at raised temperatures [73, 74]. On the opposite side, they reveal an anomalous adsorption pattern with temperature-related changes following a Q300 > Q20 > Q200 trend (where Q_T is the adsorption capacity at atmospheric pressure and temperature T in °C) [73].

The likely justification for such an unexpected behavior is recommended, on the one hand, through a decline of the interlayer spacing between room temperature and 473 K which leads to less available spacing for the target molecule that prevents the carbon dioxide adsorption, followed on the other hand, at 573 K, through decarbonization as well as dihydroxylation of the HLC, which would achieve by a structural modification to an enhanced porosity that could subsequently boost the CO_2 adsorption capacity [73].

9.6.5 Molecular Sieves

Carbon molecular sieves (CMS) are referred to as carbonaceous materials with a narrow distribution of pore size, granted with a selective adsorption capacity of specific components in a mixture. They are able to discriminate among molecules based on the size, shape, adsorption equilibrium differences, and adsorption rate. Therefore, microporous CMS demand the existence of a specific porous network comprising of pore throats of molecular dimensions, together with a noticeably high micro-pore volume. These properties will endow them with a high adsorption capacity and selectivity into a certain usage. As a result, a suitable molecular sieve must demonstrate high adsorption capacity as well as brisk adsorption kinetics of specific gas mixtures components which results in high selectivity [75]. Regarding the extensive range of CMS industrial usage, such adsorbent functions upon eliminating CO_2 from gas/air steams.

9.6.6 Metal Organic Framework

Similar to other newly developed functional materials, MOFs have seized the focus of many researchers' attention during the past two decades. These recent hybrid porous materials are synthesized through combining organic ligands and metal-containing

clusters or metal nodes [76]. Almost all metals and a noticeable variety of organic species might be utilized so as to develop MOFs. As a result, a considerable diversity of MOFs materials with various structures and features are then available. The major properties of the MOFs are their sturdy 3D structure, their permanent porosity as well as their modular nature. These perfect properties of MOFs contribute to preventing their structure from eliminating guest molecules like the solvents in their open channels and pores. Hence, the MOFs can successfully preserve their structures with subtle damage and can be used for another guest adsorption, too [77–79].

These attractive characteristics turn the MOFs into favorable porous materials with the capability of being utilized in various scopes including sensors, biomedical, catalysts as well as gas storage particularly for CO_2 adsorption [77]. Basically, the MOFs can be classified into two categories, rigid and flexible (dynamic) where the former has firm frameworks that make permanent pores like zeolites, whereas the latter owns soft (dynamic) frameworks whose structure alters through external stimuli like guest molecules, temperature, and pressure [80]. It must be noted that the majority of the MOFs have been employed as selective CO_2 adsorption and many of them are in the rigid classification. Meanwhile, nowadays the flexible MOF has been more scrutinized due to their astonishing capabilities.

9.7 Experimental Investigation of Activated Carbon Production

This part investigates activated carbon production for the CO_2 capture process and optimizing its preparation conditions with the objective of the highest CO_2 capture capacity. The activated carbons were produced from lotus nuts as a novel precursor via a one-step chemical activation process using KOH as the activating chemical reagent. The study was originally conducted by our team in the Gas Engineering laboratory at the Petroleum University of Technology, Ahvaz, Iran. This research project potentially shows that low-cost adsorbents from biomass waste materials exhibit promising capability for the carbon dioxide capture process.

During the last decade, organic precursors with high carbon content were mostly used for activated carbon production. A large number of research projects have been conducted regarding the activated carbon production from biomass derivatives such as bagasse, corn cob, nutshell, etc. These materials have a common characteristic of high lignin and carbon content making them resistant to high temperature and pressure conditions. Two methods of chemical and physical activation are widely used to convert biomass to activated carbon. However, as mentioned in the previous part the chemical activation approach has shown better results.

9.7.1 Experimental Process

Lotus nut is a biomass derivative produced in large quantities in the Khuzestan province of Iran. Each year a significant proportion of this waste material finds its way in grasslands or rivers with no specific usage. Therefore, producing added-value products using this waste material was of great attention. For this purpose, lotus nuts were collected from local regions in Khuzestan, subsequently washed, dried and stored for further use.

Firstly, lotus nuts were oven-dried at 110 °C for 24 h to ensure the removal of all moisture content. Dried nuts were sieved to obtain a homogenous precursor. 10 g of the precursor was initially impregnated with a saturated solution of KOH with a chemical to precursor mass ratio of 1. The mixture was stirred at room temperature for 24 h keeping the solution volume almost constant. The impregnated sample was then filtered and oven-dried for 2 h. Next, the sample was heat-treated under a flow of nitrogen gas in a tubular horizontal furnace up to the final temperature of 400–700 °C for different time intervals of 60–180 min. After carbonization, products were washed well with hot and cold water to remove the residual chemicals.

The CO_2 adsorption process was carried out using a manometric adsorption device, where the amount of CO_2 capture obtained via pressure difference before and after the process. The activated carbons were previously degassed at 180 °C in a vacuum oven overnight. Then, they were instantly transferred to the process cell to perform the experiment. The experiment conditions were the adsorbent dosage of 0.1 g, the temperature at 27 °C at a pressure range of 0–5 bar.

9.7.2 Experimental Design

According to the high cost of this research due to the extensive consumption of energy and chemical reagents, the number of tests is required to be minimized. For this aim, Response Surface Methodology (RSM) was used as a proper approach for modeling and optimization of the process. This methodology is used where a response of interest is affected by several independent variables. The design of experiments was performed under Central Composite Design (CCD) space. The variables investigated in this study were carbonization duration (A), and temperature (B). After employing the levels of variables and experimental domain, the experimental design was performed and 10 runs were obtained. The corresponding experimental domain, level of variables and the complete design of the experiment are shown in Table 9.1. The following quadratic model is the ultimate mathematical relationship between process variables and CO_2 capture capacity.

Table 9.1 Experimental design matrix, domain of variables, and response results

Run	Factor 1	Factor 2	Response
	A:Carbonization time	B:Temperature	Adsorption
	Min	°C	mmol/g
1	120	550	2.23
2	60	550	2.05
3	180	550	2.29
4	180	700	2.6
5	120	550	2.22
6	60	700	2.28
7	180	400	1.83
8	60	400	1.71
9	120	400	1.81
10	120	700	2.54

9.7.3 Model

9.7.3.1 Statistical Analysis

The analysis of variance (ANOVA) was performed to evaluate the results of obtained model, the corresponding parameters and calculations are presented in Table 9.2. F and P values were calculated to evaluate the significance of each term influencing the results. According to ANOVA, P-values less than 0.0500 indicates the significance of each term that exists in the model. Also, larger F-values identifies the most important variables. Therefore, A, B, AB, A^2, B^2 with low P-value are significant

Table 9.2 Analysis of variance (ANOVA)

Source	Sum of Squares	df	Mean Square	F-value	p-value	
Model	0.8221	5	0.1644	435.02	< 0.0001	Significant
A-Carbonization time	0.0771	1	0.0771	203.89	0.0001	
B-Temperature	0.7141	1	0.7141	1889.40	< 0.0001	
AB	0.0100	1	0.0100	26.46	0.0068	
A^2	0.0094	1	0.0094	24.95	0.0075	
B^2	0.0080	1	0.0080	21.18	0.0100	
Residual	0.0015	4	0.0004			
Lack of Fit	0.0015	3	0.0005	9.75	0.2303	Not significant
Pure Error	0.0000	1	0.0000			
Cor Total	0.8236	9				

model terms and temperature is the most important factor influencing the CO_2 capture capacity. The lack of fit value was not significant and was found to be 0.2303. Moreover, comparing predicted R^2 value ($R^2_{pre} = 0.9809$) and adjusted R^2 values ($R^2_{adj} = 0.9959$), as well as the coefficient of determination ($R^2 = 0.9982$), illustrated that the data predicted by the obtained model was in satisfactory agreement with the actual data. The corresponding parameters are recorded in Table 9.3.

Figure 9.6 shows the simultaneous effect of carbonization time and temperature on the CO_2 capture capacity at a chemical reagent to precursor ratio of 1. As can be seen in this figure, increased temperature results in the improvement of CO_2 capture capacity. This might be due to the release of volatile compounds from the botanical structure of lotus nuts leading to the development of pores which increases space for CO_2 immobilization on activated carbons [81]. Carbonization time also had a positive effect on the CO_2 uptake capacity. The prolonged carbonization leads to much more release of volatiles developing more pores in the activated carbon structure; although a long time may lead to a larger CO_2 uptake capacity, it is not economically suitable as the high carbonization temperature has to be maintained for a longer duration [82].

Table 9.3 Model summary statistics

Source	Sequential p-value	Lack of Fit p-value	Adjusted R^2	Predicted R^2	
Linear	< 0.0001	0.0736	0.9494	0.9023	
2FI	0.1530	0.0801	0.9592	0.8498	
Quadratic	*0.0045*	*0.2303*	*0.9959*	*0.9809*	*Suggested*
Cubic	0.1181	0.3550	0.9990	0.9779	*Aliased*
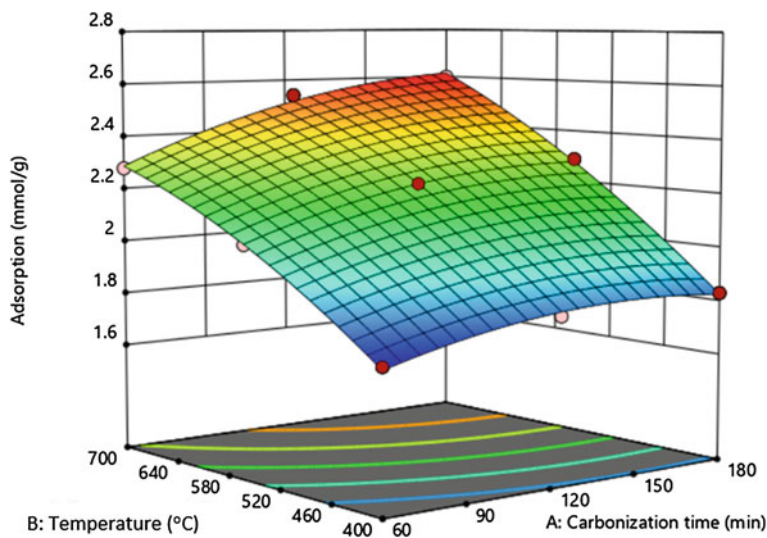
Fig. 9.6 The combined effect of temperature versus, time

This study shows the capability of lotus nuts to be used as a precursor for activated carbon production. These low-cost activated carbons exhibited large CO_2 capture capacity with the optimal value of 2.61 mmol/g activated carbon obtained from the optimization procedure under CCD space.

9.8 Cost Analysis of CO_2 Capture Process

The main components of a carbon dioxide capture and storage (CCS) system comprise of capture (separation as well as compression), transport, and storage (measurement, monitoring and verification altogether). These components, in one form or another, are commercially accessible. Meanwhile, there is relatively a trifle commercial experience regarding the configuration of all the mentioned components into entirely integrated CCS systems at the kinds of scales which would possibly characterize their future utilization. Based on the literature, a relatively extensive range of costs for deploying CCS systems with fossil-fired power production as well as different industrial procedures have been reported [83]. The range covered by this expenditure forecast is initially driven by site-specific considerations including the power plant technological characteristics or industrial equipment, the specific properties of the storage site, and the demanded transportation distance of carbon dioxide (CO_2) [84]. Moreover, the anticipation of the future functionality of components including capture, transport, storage, measurement and monitoring systems are ambiguous. An extensive established notion is reflected in the literature as the expenditure pertinent to developing and operating CO_2 capture systems will diminish over time due to technological advancements [85].

The cost of utilizing an entire CCS system for electricity generation from a fossil-fired power plant is overwhelmed by the cost of capture. The utilization of capture technology would add approximately 1.8 to 3.4 US\$ct kWh^{-1} to the cost of electricity from a pulverized coal power plant, 0.9 to 2.2 US\$ct kWh^{-1} to the cost for electricity from an integrated gasification combined cycle coal power plant, and 1.2 to 2.4 US\$ct kWh^{-1} from a natural gas combined-cycle power plant [83]. Transport and storage expenditures would add between –1 and 1 US\$ct kWh^{-1} to this range for coal plants, and about half as much for gas plants. The negative costs are associated with presumed offsetting profits from CO2 storage in enhanced oil recovery (EOR) or enhanced coal bed methane (ECBM) projects [83]. Routine expenditures for transportation and geological storage from coal plants would fluctuate between 0.05 and 0.6 US\$ct kWh^{-1}. Moreover, CCS technologies can be employed in other industrial procedures including hydrogen (H_2) production [86]. Regarding some of these non-power utilization, the capture cost is lower than for capturing from fossil-fired power plants, but the concentrations and partial pressures of CO_2 in the flue gases from these sources differ greatly, as do the costs. In addition to fossil-based energy conversion processes, CCS might be employed in biomass-fed energy systems so as to create useful energy (electricity or transportation fuels). The product cost of such systems is considerably affected by the potential price of the carbon permit and the relevant

credits earned by systems which leads to negative emissions. These systems can be merely fueled by biomass, or biomass can be co-fired in conventional coal-burning plants where the quantity is typically limited to nearly 10–15% of the input energy.

Economic and energy models are utilized to investigate more scenarios for CCS employment and considering the pertinent costs. Such models reveal that CCS systems are implausible to be applied on a large scale without a vivid policy that seriously inveighs against the emission of greenhouse gases into the atmosphere [87]. The literature as well as the current industrial experience prove that by ignoring the measurement of the permitted limitations of CO_2 emissions, there are negligible opportunities to utilize the CCS technologies. These primary opportunities for CCS utilization—that are possibly to involve CO_2 captured from high-purity, low-cost sources and utilized for value-added usages including EOR or ECBM production—could provide precious experience regarding CCS application, and brings the needed infrastructure and knowledge base required for the further employment of CCS systems in larger scales.

Considering the imposed limits of emitted greenhouse gases, many integrated appraisal analyses have proved that CCS systems will be more competitive with other large-scale mitigation alternatives including nuclear power and renewable energy technologies [88]. It must be noted that most energy and economic modeling carried out so far recommend that the utilization of CCS systems commences being important when carbon prices begin to reach approximately 25–30 US$/tCO$_2$ (90–110 US$/tC). Therefore, it is anticipated that the large-scale utilization of CCS systems will be viable through the following decades by the beginning of any considerable regime for ameliorating global warming. The literature proves that the utilization of CCS systems will soar in line with the stringency of the modeled emission reduction regime. Moreover, least-cost CO_2 concentration stabilization scenarios, which also prioritize the system's economic efficiency, demonstrate that emissions alleviation becomes progressively stricter over time [88]. Many investigations reveal that notwithstanding considerable progress of CCS systems by 2050, the major proportion of CCS utilization will befall in the second half of this century [85]. These investigations also demonstrate that early application of the CCS system will be in the industrialized countries and will become ubiquitous eventually. Although various scenarios demand a different quantitative mix of technologies required to achieve the modeled emissions limitation, the literature agrees on the issue that CCS could be a significant component of an extensive portfolio of energy technologies and emission reduction approaches. Moreover, CCS technologies show acceptable compatibility with the application of other potentially important long-term greenhouse gas alleviation technologies including H_2 production from biomass and fossil fuels [83].

The stated estimates (450–750 ppmv for CO_2 stabilization scenarios) of the global cumulative quantity of CO_2 that can be stored throughout this century in the ocean and different geological formations cover a wide spectrum ranging from very infinitesimal contributions to thousands of Giga-tones of CO_2. This extensive increment can majorly be justified by the uncertainty of long-term, socio-economic, demographic and technological change, the main drivers of future CO_2 emissions [89]. However, it must be remembered that the major proportion of stabilization scenarios from

450–750 ppmv have a propensity to cluster in the range of 220–2200 $GtCO_2$ (60–600 GtC). This demand for CO_2 storage proves to be within the global prediction of total CO_2 storage capacity. The actual utilization of CCS is possibly lower than the prediction for economic potential stated by energy and economic models. This is attributed to the fact that there are other hurdles to technology development which have not been sufficiently involved in such modeling frameworks.

Examples comprise of concerns regarding the environmental impact, unavailability of a vivid legal framework and uncertainty about how the achieved experience will diminish the costs.

Regarding the storage of CO_2 in different geological formations and the ocean, questions have been raised regarding the implications of steady release from these reservoirs. Considering the economic perspective, such release can be presumed as another potential source of CO_2 emissions in the future, with the cost of offsetting this leaked CO_2 being equivalent to the cost of emission impacts when the stored CO_2 leaks to the atmosphere. In such an economic framework, the few investigations that have looked at this subject reveal that some CO_2 leakage can be accommodated while proceeding towards the target of CO_2 concentration stabilization in the atmosphere.

References

1. N. Kundu, S. Sarkar, Porous organic frameworks for carbon dioxide capture and storage. J. Environ. Chem. Eng. 105090, 2021
2. M.-R. Kolahi, A. Nemati, M. Yari, Performance optimization and improvement of a flash-binary geothermal power plant using zeotropic mixtures with PSO algorithm. Geothermics **74**, 45–56 (2018)
3. T.F. Valone, Linear global temperature correlation to carbon dioxide level, sea level, and innovative solutions to a projected 6°C warming by 2100. J. Geosci. Environ. Prot. **9**(03), 84 (2021)
4. E. Lipczynska-Kochany, Effect of climate change on humic substances and associated impacts on the quality of surface water and groundwater: a review. Sci. Total Environ. **640**, 1548–1565 (2018)
5. K.D. Lafferty, The ecology of climate change and infectious diseases. Ecology **90**(4), 888–900 (2009)
6. J.A. Patz et al., Impact of regional climate change on human health. Nature **438**(7066), 310–317 (2005)
7. T. Islam et al., Relationship between air pollution, lung function and asthma in adolescents. Thorax **62**(11), 957–963 (2007)
8. J.D. Steven et al., Net-zero emissions energy systems. Science (New York, NY) **360**(6396), eaas9793 (2018)
9. M. Scott, R. Lindsey, Which emits more carbon dioxide: volcanoes or human activities **15** (2016)
10. F. Rouhani, A. Morsali, Goal-directed design of metal–organic frameworks for HgII and PbII adsorption from aqueous solutions. Chemistry–A Eur. J. **24**(65), 17170–17179 (2018)
11. M. Ebadollahi, et al., Close supercritical versus inverse brayton cycles for power supply, using waste of a biogas-driven open brayton cycle. J. Energy Resour. Technol. **143**(9) (2021)
12. M. Ebadollahi et al., Proposal and assessment of a new geothermal-based multigeneration system for cooling, heating, power, and hydrogen production, using LNG cold energy recovery. Renew. Energy **135**, 66–87 (2019)

13. M. Ebadollahi et al., Proposal and multi-criteria optimization of two new combined heating and power systems for the Sabalan geothermal source. J. Clean. Prod. **229**, 1065–1081 (2019)
14. M. Ebadollahi, et al., Thermal and exergetic performance enhancement of basic dual-loop combined cooling and power cycle driven by solar energy. Therm. Sci. Eng. Prog. **18**, 100556 (2020)
15. H. Rostamzadeh et al., Comparative study of two novel micro-CCHP systems based on organic Rankine cycle and Kalina cycle. Energy Convers. Manage. **183**, 210–229 (2019)
16. M.-R. Kolahi, M. Amidpour, M. Yari, Multi-objective metaheuristic optimization of combined flash-binary geothermal and humidification dehumidification desalination systems. Desalination **490**, 114456 (2020)
17. L. Lakatos, G. Hevessy, J. Kovács, Advantages and disadvantages of solar energy and wind-power utilization. World Futures **67**(6), 395–408 (2011)
18. F. Podjaski, J. Kröger, B.V. Lotsch, Toward an aqueous solar battery: direct electrochemical storage of solar energy in carbon nitrides. Adv. Mater. **30**(9), 1705477 (2018)
19. S. Jaber, Environmental impacts of wind energy. J. Clean Energy Technol. **1**(3), 251–254 (2013)
20. A. Mills, R. Wiser, K. Porter, The cost of transmission for wind energy in the United States: A review of transmission planning studies. Renew. Sustain. Energy Rev. **16**(1), 1–19 (2012)
21. P.A. Groothuis, J.D. Groothuis, J.C. Whitehead, Green vs. green: Measuring the compensation required to site electrical generation windmills in a viewshed. Energy Policy **36**(4), 1545–1550 (2008)
22. S. Sharma, F. Maréchal, Carbon dioxide capture from internal combustion engine exhaust using temperature swing adsorption. Front. Energy Res. **7**, 143 (2019)
23. M. Finkenrath, Cost and performance of carbon dioxide capture from power generation (2011)
24. A. Kumar et al., Direct air capture of CO2 by physisorbent materials. Angew. Chem. Int. Ed. **54**(48), 14372–14377 (2015)
25. D. Dunn, US energy information administration monthly energy review (2016)
26. M. Songolzadeh, et al., Carbon dioxide separation from flue gases: a technological review emphasizing reduction in greenhouse gas emissions. Sci. World J. (2014)
27. K.S. Lackner, A guide to CO2 sequestration. Science **300**(5626), 1677–1678 (2003)
28. A.L. Kohl, R. Nielsen, *Gas Purification.* Elsevier (1997)
29. T.-H. Bae et al., Evaluation of cation-exchanged zeolite adsorbents for post-combustion carbon dioxide capture. Energy Environ. Sci. **6**(1), 128–138 (2013)
30. A. Samanta et al., Post-combustion CO2 capture using solid sorbents: a review. Ind. Eng. Chem. Res. **51**(4), 1438–1463 (2012)
31. C. Mandil, *World Energy Outlook 2004* (International Energy Agency (IEA), Paris, 2004)
32. iEA, C., *IEA CCC (IEA Clean Coal Centre) The World Coalfired Power Plants Database.* Gemini House, Putney, London, United Kingdom (2005)
33. D. Kim, et al., Experimental analysis of CO/H2 syngas with NOx and SOx reactions in pressurized oxy-fuel combustion. Energy **219**, 119550 (2021)
34. T. Wall et al., An overview on oxyfuel coal combustion—state of the art research and technology development. Chem. Eng. Res. Des. **87**(8), 1003–1016 (2009)
35. C.-C. Cormos, Energy and cost efficient manganese chemical looping air separation cycle for decarbonized power generation based on oxy-fuel combustion and gasification. Energy **191**, 116579 (2020)
36. E. Portillo, et al., Oxygen transport membrane unit applied to oxy-combustion coal power plants: a thermodynamic assessment. J. Environ. Chem. Eng. **9**(4), 105266 (2021)
37. W. Ding, et al., Modified mineral carbonation of phosphogypsum for CO2 sequestration. J. CO2 Util.**34**, 507–515 (2019)
38. B. Metz, Special report on carbon dioxide capture and storage (2007). http://www.ipcc.ch/pub/reports.htm
39. E. Possan, et al., CO2 uptake potential due to concrete carbonation: a case study. Case Stud. Constr. Mater. **6**, 147–161 (2017)
40. H. Nasrollahi, et al., The greenhouse technology in different climate conditions: a comprehensive energy-saving analysis. Sustain. Energy Technol. Assess. **47**, 101455 (2021)

41. E. Koohestanian et al., A novel process for CO2 capture from the flue gases to produce urea and ammonia. Energy **144**, 279–285 (2018)
42. A.J. Hunt, et al., Generation, capture, and utilization of industrial carbon dioxide. ChemSusChem: Chem. Sustain. Energy Mater. **3**(3), 306–322 (2010)
43. E. Alper, O.Y. Orhan, CO2 utilization: developments in conversion processes. Petroleum **3**(1), 109–126 (2017)
44. L. Okobia, S. Hassan, A. Peter, Increase in outdoor carbon dioxide and its effects on the environment and human health in Kuje FCT Nigeria. Environ. Health Rev. **60**(4), 104–112 (2017)
45. H. Ritchie, M. Roser, CO$_2$ and greenhouse gas emissions. Our world in data (2020)
46. J. Albo et al., Towards the electrochemical conversion of carbon dioxide into methanol. Green Chem. **17**(4), 2304–2324 (2015)
47. I. Ganesh, Conversion of carbon dioxide into methanol–a potential liquid fuel: fundamental challenges and opportunities (a review). Renew. Sustain. Energy Rev. **31**, 221–257 (2014)
48. J. Qiao et al., A review of catalysts for the electroreduction of carbon dioxide to produce low-carbon fuels. Chem. Soc. Rev. **43**(2), 631–675 (2014)
49. B. Kumar et al., Photochemical and photoelectrochemical reduction of CO2. Annu. Rev. Phys. Chem. **63**, 541–569 (2012)
50. G.A. Olah, A. Goeppert, G.S. Prakash, Chemical recycling of carbon dioxide to methanol and dimethyl ether: from greenhouse gas to renewable, environmentally carbon neutral fuels and synthetic hydrocarbons. J. Org. Chem. **74**(2), 487–498 (2009)
51. S. Das, W.W. Daud, RETRACTED: Photocatalytic CO2 transformation into fuel: a review on advances in photocatalyst and photoreactor. Renew. Sustain. Energy Rev. **39**, 765–805 (2014)
52. G.P. Smestad, A. Steinfeld, photochemical and thermochemical production of solar fuels from H2O and CO2 using metal oxide catalysts. Ind. Eng. Chem. Res. **51**(37), 11828–11840 (2012)
53. Y. Izumi, Recent advances in the photocatalytic conversion of carbon dioxide to fuels with water and/or hydrogen using solar energy and beyond. Coord. Chem. Rev. **257**(1), 171–186 (2013)
54. S.C. Roy et al., Toward solar fuels: photocatalytic conversion of carbon dioxide to hydrocarbons. ACS Nano **4**(3), 1259–1278 (2010)
55. J.R. Scheffe, A. Steinfeld, Oxygen exchange materials for solar thermochemical splitting of H2O and CO2: a review. Mater. Today **17**(7), 341–348 (2014)
56. P.M. Schenk et al., Second generation biofuels: high-efficiency microalgae for biodiesel production. Bioenergy Res. **1**(1), 20–43 (2008)
57. L. Brennan, P. Owende, Biofuels from microalgae—a review of technologies for production, processing, and extractions of biofuels and co-products. Renew. Sustain. Energy Rev. **14**(2), 557–577 (2010)
58. W. Wang et al., Recent advances in catalytic hydrogenation of carbon dioxide. Chem. Soc. Rev. **40**(7), 3703–3727 (2011)
59. X. Zhang et al., Carbon dioxide reforming of methane with Pt catalysts using microwave dielectric heating. Catal. Lett. **88**(3), 129–139 (2003)
60. B. Fidalgo et al., Microwave-assisted dry reforming of methane. Int. J. Hydrogen Energy **33**(16), 4337–4344 (2008)
61. Z. Zhang et al., Sustainable and hierarchical porous enteromorpha prolifera based carbon for CO2 capture. J. Hazard. Mater. **229**, 183–191 (2012)
62. Z. Chen et al., Polyethylenimine-impregnated resin for high CO2 adsorption: an efficient adsorbent for CO2 capture from simulated flue gas and ambient air. ACS Appl. Mater. Interfaces **5**(15), 6937–6945 (2013)
63. H.-Y. Zhao et al., Evaluation of CO2 adsorption capacity of solid sorbents. J. Therm. Anal. Calorim. **106**(1), 199–205 (2011)
64. M. Radosz et al., Flue-gas carbon capture on carbonaceous sorbents: toward a low-cost multifunctional carbon filter for "green" energy producers. Ind. Eng. Chem. Res. **47**(10), 3783–3794 (2008)

65. D. Levesque, F.D. Lamari, Pore geometry and isosteric heat: an analysis of carbon dioxide adsorption on activated carbon. Mol. Phys. **107**(4–6), 591–597 (2009)
66. A. Wahby et al., High-surface-area carbon molecular sieves for selective CO2 adsorption. Chemsuschem **3**(8), 974–981 (2010)
67. N.P. Wickramaratne, M. Jaroniec, Activated carbon spheres for CO2 adsorption. ACS Appl. Mater. Interfaces. **5**(5), 1849–1855 (2013)
68. J. Merel, M. Clausse, F. Meunier, Experimental investigation on CO2 post− combustion capture by indirect thermal swing adsorption using 13X and 5A zeolites. Ind. Eng. Chem. Res. **47**(1), 209–215 (2008)
69. N. Konduru, P. Lindner, N.M. Assaf-Anid, Curbing the greenhouse effect by carbon dioxide adsorption with zeolite 13X. AIChE J. **53**(12), 3137–3143 (2007)
70. S. Beyaz Kayiran, F. Lamari Darkrim, Synthesis and ionic exchanges of zeolites for gas adsorption. Surface and Interface Analysis: An International Journal devoted to the development and application of techniques for the analysis of surfaces, interfaces and thin films **34**(1), 100–104 (2002)
71. J. Zhang, R. Singh, P.A. Webley, Alkali and alkaline-earth cation exchanged chabazite zeolites for adsorption based CO2 capture. Microporous Mesoporous Mater. **111**(1–3), 478–487 (2008)
72. M. Othman, N. Rasid, W. Fernando, Mg–Al hydrotalcite coating on zeolites for improved carbon dioxide adsorption. Chem. Eng. Sci. **61**(5), 1555–1560 (2006)
73. N.D. Hutson, S.A. Speakman, E.A. Payzant, Structural effects on the high temperature adsorption of CO2 on a synthetic hydrotalcite. Chem. Mater. **16**(21), 4135–4143 (2004)
74. Z. Yong, V. Mata, A.r.E. Rodrigues, Adsorption of carbon dioxide at high temperature—a review. Sep. Purif. Technol. **26**(2–3), 195–205 (2002)
75. W. Qiu, et al., Surprising olefin/paraffin separation performance recovery of highly aged carbon molecular sieve hollow fiber membranes by a super-hyperaging treatment. J. Membr. Sci. **620**, 118701 (2021)
76. N. Mohammadi, B. Mousazadeh, T. Hamoule, Synthesis and characterization of NH 2-SiO 2@ Cu-MOF as a high-performance adsorbent for Pb ion removal from water environment. Environ. Dev. Sustain. **23**(2), 1688–1705 (2021)
77. R.J. Kuppler et al., Potential applications of metal-organic frameworks. Coord. Chem. Rev. **253**(23–24), 3042–3066 (2009)
78. A.R. Millward, O.M. Yaghi, Metal− organic frameworks with exceptionally high capacity for storage of carbon dioxide at room temperature. J. Am. Chem. Soc. **127**(51), 17998–17999 (2005)
79. C.-H. Yu, C.-H. Huang, C.-S. Tan, A review of CO2 capture by absorption and adsorption. Aerosol Air Qual. Res. **12**(5), 745–769 (2012)
80. J.-R. Li et al., Carbon dioxide capture-related gas adsorption and separation in metal-organic frameworks. Coord. Chem. Rev. **255**(15–16), 1791–1823 (2011)
81. A. Ip, J. Barford, G. McKay, Production and comparison of high surface area bamboo derived active carbons. Biores. Technol. **99**(18), 8909–8916 (2008)
82. V. Manovic, E.J. Anthony, CO2 carrying behavior of calcium aluminate pellets under high-temperature/high-CO2 concentration calcination conditions. Ind. Eng. Chem. Res. **49**(15), 6916–6922 (2010)
83. H. Pilorgé et al., Cost analysis of carbon capture and sequestration of process emissions from the US Industrial Sector. Environ. Sci. Technol. **54**(12), 7524–7532 (2020)
84. J.-X. Guo, et al., Integrated operation for the planning of CO2 capture path in CCS–EOR project. J. Pet. Sci. Eng. **186**, 106720 (2020)
85. J.-X. Guo , C. Huang, Feasible roadmap for CCS retrofit of coal-based power plants to reduce Chinese carbon emissions by 2050. Appl. Energy **259**, 114112 (2020)
86. P. Gabrielli, M. Gazzani, M. Mazzotti, The role of carbon capture and utilization, carbon capture and storage, and biomass to enable a net-zero-CO2 emissions chemical industry. Ind. Eng. Chem. Res. **59**(15), 7033–7045 (2020)
87. J. Bae, et al., Knowledge spillover efficiency of carbon capture, utilization, and storage technology: a comparison among countries. J. Clean. Prod. **246**, 119003 (2020)

88. X. Chen, X. Wu, K.Y. Lee, The mutual benefits of renewables and carbon capture: achieved by an artificial intelligent scheduling strategy. Energy Convers. Manag. **233**, 113856 (2021)
89. S. Low, S. Schäfer, Is bio-energy carbon capture and storage (BECCS) feasible? The contested authority of integrated assessment modeling. Energy Res. Soc. Sci. **60**, 101326 (2020)

Chapter 10
A Critical Survey of Bioenergy with Carbon Capture and Storage (BECCS)

Christopher Sarkizi Shams Hajian and Mahsa Sedighi

Abstract Rising levels of carbon dioxide and other greenhouse gases are still a global concern. International organizations have indicated that to meet the 2 °C thresholds until 2100, carbon-negative technologies must be employed. Bioenergy with carbon capture and storage (BECCS) is one of the options to offer reduced fossil-based CO_2 emissions from a variety of industries and sectors. This promises the significant potential to remove atmospheric CO_2 at a comparable cost to conventional carbon capture and storage technologies while producing energy. From a technical standpoint, BECCS is referred to a group of technologies utilized to produce energy from biomass and storing CO_2 simultaneously. Substituting fossil fuels with biomass offers the possibility to utilize the carbon in the atmosphere for power generation. While BECCS might be a promising technology in theory, it has its own pros and cons which has made it one of the most controversial technologies to fight climate change. This chapter aims to investigate the advantages and the shortcomings of BECCS, from carbon removal efficiency and economic feasibility to scale-up issues associated with it. The urgency of the climate issues has created a political drive for environmental technologies like BECCS which might not be well-established. Also, the public perception of such technologies could promote or hinder their deployment in various parts of the globe. In addition, the deployment of BECCS cannot take place in isolation, and detailed investigations addressing the undeniable links within the food-water-energy-climate nexus will be required.

Keywords Carbon capture and storage (CCS) · Bioenergy · Biomass · Nexus

C. S. S. Hajian
Institute of Biochemical Engineering, University of Stuttgart, 70569 Stuttgart, Germany
e-mail: c.sarkizi@ibvt.uni-stuttgart.de

M. Sedighi (✉)
Energy and Environment Research Center, Niroo Research Institute, Tehran, Iran
e-mail: msedighi@nri.ac.ir

Abbreviations

BECCS	Bio-Energy with Carbon Capture and Storage/Sequestration
CCS	Carbon Capture and Storage/Sequestration
CCU	Carbon Capture and Utilization
CDR	Carbon Dioxide Removal
CHP	Combined Heat and Power
DACS	Direct Air Capture and Sequestration
EOR	Enhanced Oil Recovery
GHG	Greenhouse Gases
GMO	Genetically Modified Organism
IAM	Integrated Assessment Models
iLUC	Indirect Land Use Change
LCA	Life Cycle Assessment
IPCC	Intergovernmental Panel on Climate Change
LDC	Least Developed Countries
MSW	Municipal Solid Waste
NET	Negative Emission Technologies
SOC	Soil Organic Carbon
UNFCCC	United Nations Framework Convention on Climate Change

10.1   Introduction

Fossil energy production and other anthropogenic activities have led to an increase in the atmospheric concentration of CO_2 and other greenhouse gases (GHGs). The United Nations Framework Convention on Climate Change (UNFCCC) has targeted a 2 °C maximum increase in global average temperature as a "safe" threshold for climate change [1, 2]. The need for net CO_2 removal from the atmosphere to maintain this target value for 2100 is obvious. Significant changes in global and national energy systems is needed during decades ahead, for reducing the atmospheric CO_2 levels [3, 4]. Achieving CO_2 levels below 450 ppm by 2100 needs high advancement in energy efficiency as well as wide deployment of zero- or low- carbon energy supplies like renewable energy, nuclear power, carbon capture and storage from fossil energy (Fossil—CCS), and negative emission technologies (NETs) [3, 5].

NETs also referred to as carbon dioxide removal (CDR), cause net removal of CO_2 from the atmosphere including technologies like iron fertilization, large-scale afforestation, direct air capture and sequestration (DACS), and biomass in combination with CCS (BECCS or Bio-CCS) [3]. The latter is defined by the BECCS Joint Taskforce as [3, 6]:

> Processes in which CO_2 originating from biomass is captured and stored. These can be energy production processes or any other industrial processes with CO_2-rich process streams originating from biomass and feedstocks. The CO_2 is separated from these processes with technologies generally associated with CCS for fossil fuels. Biomass binds carbon from the atmosphere as it grows; but with the conversion of the biomass, this carbon is again released as CO_2. If instead, it is captured, transported to a storage site, and permanently stored deep underground, this would result in a net removal of CO_2 from the atmosphere.

According to this definition, BECCS will result in net negative emission, while Fossil-CCS usually results in near-zero emission at best [7, 8]. BECCS can be applied in different industries with varying amounts of CO_2 emissions such as co-firing biomass power plants, combined heat, and power plants (CHP), pulp and paper mills, ethanol plants, biogas refineries, and biomass gasification plants [9, 10]. BECCS is one the few technologies that can play a critical role in CO_2 removal from the atmosphere and can be considered as one of the most promising NETs. As a consequence, it is required to address the issues related to this technology like CCS technologies and their specific challenges, sustainability of feedstocks, the overall efficiency of bioenergy conversion systems, and the undeniable interconnection between food, water, energy, and the climate, as well as broader issues of socio-economic development and policy implementation [11–14].

This chapter aims is to critically investigate BECCS as a NET, considering its potentials and challenges, addressing its relation to the food-water-energy-climate nexus, and look at its prospects.

10.2 BECCS Overview

The core idea behind BECCS assumes that if a bioenergy plant can hypothetically achieve carbon neutrality by integrating a carbon capture and storage (CCS) unit downstream of the plant, it will be possible to reach carbon negativity.

Considering its constituting terms, BECCS refers to the combination of a bioenergy plant and a CCS unit. This means upgrading a net emission energy production (bioenergy) plant to a power plant with negative emissions.

As noted earlier, using NETs is inevitable to meet climate goals, and this urgency also forces policymakers to act quickly. To make informed decisions, policymakers rely on simulations predicting different scenarios, called integrated assessment models (IAMs). Although in most scenarios, BECCS is considered as one of the key NETs, this concept is highly case-specific and should be further evaluated.

From a technical point of view, it is required to ensure the necessary conditions such that this assumption holds true. To investigate this, one must thoroughly consider the impact of the BECCS plant and its supply chain for CO_2 sources and sinks [15].

Biomass production can be considered as the first phase of a BECCS process. The next phase can benefit from well-established knowledge in bioenergy. However, it is important to consider the fact that the commercialization of bioenergy power plants

is less common. The technical boundaries of such technologies compared to other highly efficient fossil fuel power plants are well recognized [16].

On the contrary, CCS is widely commercialized, and it will most probably not be the technological bottleneck. Nonetheless, further modifications of CCS are required to tailor it to meet the needs of bioenergy. Such modifications may involve the fluctuating composition of the gas and reconsidering the materials used for manufacturing the relevant equipment [17, 18].

As mentioned above, BECCS is considered an alternative for fossil fuel power plants. However, with growing power demand, BECCS cannot operate by only using by-products or agricultural residues; rather, this technology will require dedicated energy crop plantation on a substantial fraction of the available arable lands [19]. In addition to these complexities, previous unsuccessful bioenergy initiatives have also impacted public opinion, which will hinder BECCS development, especially in the least developed countries (LDCs) [20].

Eventually, to meet the climate goals, all available technologies need to be carefully evaluated; however, instead of waiting for a "one for all" solution to be deployed, globally-different opportunities should be considered in detail in a case-by-case manner. This is because the chosen approach must meet a minimum threshold of environmental, financial, and social requirements in each scenario which are unique to each case. In this section, the core concepts of BECCS will be discussed from a technical point of view along with its role in climate change goals and its potentials.

10.2.1 What is BECCS?

BECCS is categorized as one of the NETs in the geoengineering field. Although the concept of BECCS was introduced almost a decade ago, its development has faced numerous technical, socio-political, and financial challenges. The BECCS process can be divided into four stages as schematically illustrated in Fig. 10.1.

I. Biomass supply

Biomass supply and management is a key issue due to the availability limitations. This step is considered the most controversial stage of the process if one intends to achieve climate goals with large-scale BECCS implementation. Regarding the biomass sources considered so far, authors have not found any reports of first-generation biomass sources for BECCS because of the direct competition with food sources [13]. Some of the potential methods for biomass provision are shown In Fig. 10.1(i).

On the other hand, second-generation sources from by-products are already being considered in pilot and demonstration plants (e.g., ethanol projects); however, they are not well received by forest-based industries since their processes make use of any available by-products, using which for BECCS would decrease their revenues [16, 21]. It is worth mentioning that energy crops also fall into this category [22], and their application for BECCS has been the focus of attention in recent years [15].
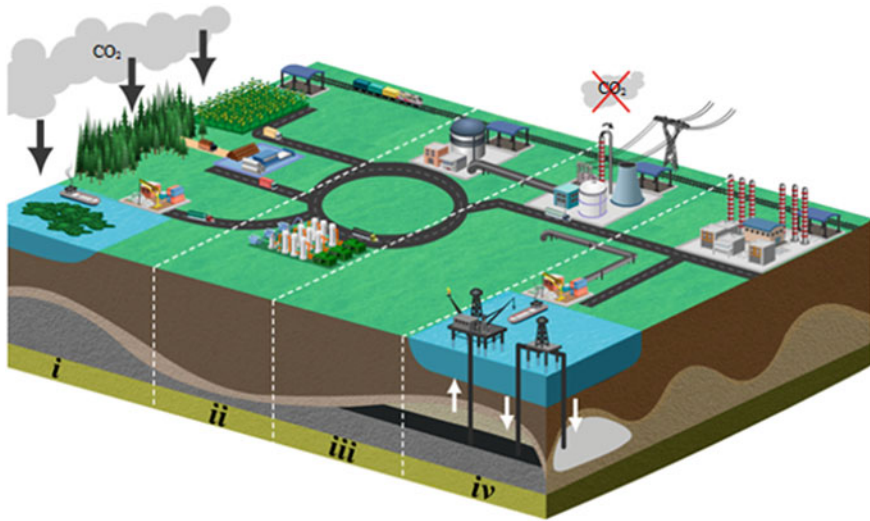
Fig. 10.1 BECCS overview: (i) biomass production from various sources, (ii) biomass processing or biofuel production, (iii) bioenergy power plant equipped with carbon capture unit, and (iv) sequestration or utilization of CO_2 (nonconversion: Enhanced Oil Recovery (EOR); conversion: biofuels, (bio)chemical manufacturing, food and beverage, algae cultivation,….)

In theory, such plantations will compete with arable lands for food production. In addition, flawed policies can encourage farmers to switch to energy crops if they are deemed lucrative, thus potentially disrupting the food supply chain. This, in turn, can increase the CO_2 emissions for food transportation [20] or threaten water security [23]. On the other hand, biomass logistics emissions need to be evaluated in short-term and long-term scenarios since in the latter, further expansion of plantations will also increase transport emissions. This aspect needs to be considered carefully since it can affect the carbon payback and the rate of negative emissions [14, 15].

It is worth mentioning that in some cases, municipal solid wastes (MSWs) are utilized in BECCS projects. Analyzing carbon emissions for such cases is complicated, and it is not possible to distinguish between biogenic and non-biogenic carbon types [24].

Furthermore, third-generation sources are algae-based which introduces another processing step to obtain biofuels. Similar to second-generation sources, algae need high land usage and depending on the facility, high rates of water evaporation occur (algae pond). To minimize these side effects, research has been carried out on offshore algae production sites [25–27].

Finally, fourth-generation sources are obtained from genetically modified organisms (GMOs). Such organisms can be engineered in such a way to proliferate with minimum land and nutrient requirements and on types of lands that are not favourable for agricultural purposes.

II.   Biomass upgrade or biofuel preparation

Depending on the design of the BECCS plant, a biomass upgrade or biofuel production unit can be implemented upstream of the power generation unit. This can range from anaerobic digestion and algal biodiesel production facilities to pyrolysis and gasification units [25, 28–32] (Fig. 10.1(ii)).

III.   Power generation and CO_2 capture

Bioenergy power plants (Fig. 10.1(iii)) can be designed specifically to operate with biofuels (gaseous or liquid) or to run in co-fire mode to replace the fossil carbon emissions with biogenic ones [33]. One case study investigating prospective BECCS projects in the UK suggested decentralized increments of the BECCS capacity to minimize the negative impacts of such projects [34]. CO_2 in the off-gas is captured mainly using oxy-fuel and pre-and post-combustion technologies. The applicable technologies are well-established, and different methods are found at the higher range of TRLs up to 9 (commercial scale) for pre-and post-combustion and 7 for oxy-fuel processes [18, 21, 26, 29]. In flue gas, impurities, such as water, are of importance for corrosion protection and non-condensable gases that can impact the vapour-liquid equilibrium [17, 18, 35]. It is worth noting that compression and liquefaction alone can take up to 12% of the power plant's output [18].
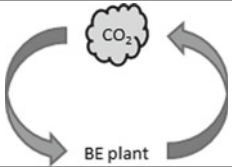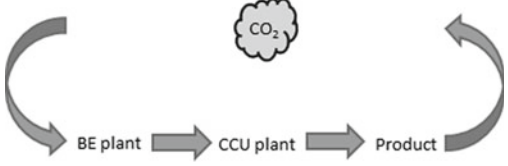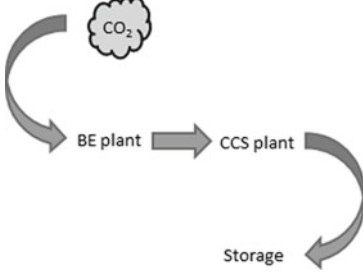
IV.   Storage or utilization

The final stage (Fig. 10.1(iv)) is to permanently store the captured CO_2, which is highly location-specific. Another common practice is to employ the captured CO_2 for enhanced oil recovery (EOR) purposes. In this way, the CO_2 injected into the oil well can have a positive contribution from an economic point of view. However, carbon balance needs to be assessed in the life cycle assessment (LCA) to balance the CO_2 stored against the carbon extracted from the oil well [17, 18].

While storing emissions can serve as a permanent solution, it might not be viable in terms of location and transportation. Utilizing CO_2 as a raw material is already at TRL 9 among various sectors from food and beverage industries to chemicals production [18]. In this case, carbon can be used for producing different products, prolonging its removal from the atmosphere. It is crucial to consider the scale at which utilization can contribute to negative emissions in the larger picture. This directly depends on the application of the product and it can be used for energy generation, which makes LCA more complicated in such scenarios and makes the carbon emissions relative to a timeframe. Another challenge is that global CO_2 demand as raw material can be met by the CO_2 emissions of a limited number of modern coal power plants [18], and the same is also true for country-wide scales [16]. This emphasizes the need to re-evaluate CO_2 as a productive chemical against a final product.

Table 10.1 illustrates modes of operation for a bioenergy plant equipped with different carbon capture units. As mentioned earlier, the capture process reduces the total power output capacity, thus decreasing the revenue. Permanently storing the captured CO_2 has two major limitations, i.e., requiring access to a suitable storage site and not being financially viable. In specific locations, CO_2 can be used for EOR

Table 10.1 Comparison of bioenergy plants with and without CO_2 capture units

Mode of operation		Location	Carbon isolation timescale
BE		Access to feed required	Days
BE+CCU		Access to feed required	Months-years [i]
BE+CCS		Access to feed and storage site required	Indefinitely

Depending on the product lifecycle

to improve the economic feasibility; however, this introduces more fossil carbon into the atmosphere as a result. On the other hand, utilization of the captured CO_2 using carbon capture and utilization technologies (CCU) may solve these issues and offer the possibility to convert it into valuable products, while removing the location constraint.

10.2.2 The Role of BECCS in Climate Change

According to Paris Climate Agreement, about 20 billion tonnes of CO_2 need to be removed from the atmosphere every year by 2100 to meet a global temperature rise of less than 2 °C. BECCS can be scaled up to store large amounts of carbon at the cost of 80€ per tonne. It is estimated that BECCs has the potential of removing 3–5 billion tonnes per year. Therefore, it may not be enough for climate change's impact. But, NETs –typically BECCS- are now included by climate scientists as the major modeled pathways showing how the world can avoid the limit of staying below 2 °C

of global warming. Therefore, it is required that the negative emission potential of BECCS, be strictly assessed.

In interesting research conducted by [36], a global spatially explicit analysis of life-cycle GHG emissions for lignocellulosic crop-based BECSS was performed. Their research showed that negative emission of BECCS is highly dependent on the biomass cultivation location, original vegetation treatment, the final produced energy carrier, and the time.

BECCS electricity deployment on abandoned agricultural lands, typically achieves lower emission factors, while the electricity supply potentials on such lands are also limited. Furthermore, by producing electricity at locations with high biomass yields and low carbon stocks such as subtropical and warmer temperature areas, negative emissions would be achieved [36, 37].

Bioenergy production by use of initial biomass increases overall energy potential and sequestration of BECCS and, decreases emission factors due to the allocated emissions over more energy produced. By utilizing the original vegetation for bioenergy or materials, the climate change mitigation potential of BECCS would be the most [36].

Long evaluation periods lead to higher BECCS energy potential at low emission factors. This could be to a high extent due to the decreases in land-use change emissions over longer periods, and to a lesser extent due to projected yield increases and decreased levels of former carbon sequestered. Biophysically, a large global electricity supply, and carbon sequestration potential of 28 EJ and 2.5 Gt per year could be achieved over 30 years, 220 EJ and 40 Gt CO_2 per year over 80 years, and 129 EJ and 11 Gt CO_2 per year over 30 years by utilizing initial biomass. This highlights that crop-based BECSS should be deployed early, as BECCs capacity installed late in the century may achieve negative emission just beyond the target year 2100 [36].

Among the energy carriers generated, the sequestration potential of liquid biofuels such as bioethanol with CCS is limited due to their low carbon capture rates (12 and 24% for lignocellulosic and sugarcane ethanol, respectively). However, lignocellulosic biodiesel with CCS has the highest potential of energy and sequestration of the investigated liquid biofuels pathways over a long evaluation period. Therefore, at long evaluation period, replacing fossil transport fuels highly reduces emissions. It is estimated that by replacing the entire current global consumption of diesel of 60 EJ per year, GHG emission savings of approximately 5.5 $GtCO_2$ per year, would be achieved theoretically [36].

It can be concluded that BECCS plays an important role in climate change mitigation along with other NETs or emission reductions. Deployment of BECCS on abandoned agricultural lands, use of residues and waste flows as feedstocks, and supply chain configurations would reduce the biodiversity and other environmental impacts of BECCS [36, 38]. Time is also an important factor and the earlier deployment of BECCS would greatly increase its potential for climate change mitigation. Therefore, complementing BECCS with other alternatives of GHG emission reductions and CO_2 removals should be considered by policymakers to approach

the BECCS sequestration projected in IPCC (Intergovernmental Panel on Climate Change) SR1.5 °C pathways.

10.2.3   The Potentials of BECCS

While use cases of BECCS are evaluated in different IAMs to reach the climate goal of 2 °C on a global scale, BECCS has to be deployed sustainably [15]. Efforts have been made to investigate BECCS' potential for ethanol manufacturers in the US, Brazil, and the Netherlands [31], while its main application is relying on EOR for financial gains. In Australia, the potential of BECCS was evaluated to reach the capturing capacity of 25 Mtpa (million tonnes per annum) [39]. The pulp and paper sector is also considered a potential benefactor of BECCS in Scandinavian countries and the US, while the latter has the capacity of capturing 150 Mtpa (~77% biogenic). The UK is also committed to its ambitious plans for BECCS and has already received feedback from the updated modeled scenarios on how to proceed with BECCS deployment [34]. After almost one decade, the expectations of BECCS have become more rational in terms of its technical, financial, and social impacts [3, 16]. At this point, well-informed decisions are expected to be made compared to the last decade. In the next section, an overview of BECCS projects during the last decade is presented.

10.3   BECCS Plants: Past, Present, and Future

Given the current financial, socio-political, technical, and environmental conditions, specific types of BECCS projects went into operation in the 2010s, with a few planned to be scaled up in this decade. With the current technology level, it is estimated that under given circumstances, the cost of CO_2 capture per tonne could reach 100€ [40]. This makes such projects economically challenging and far from feasible in most of the countries where the CO_2 tax is below such ranges [41, 42]. In addition, a sustainable inflow of biomass/biofuel is essential for BECCS operations. Considering these issues, pulp and paper production sites, ethanol manufacturers, and biomass-based combined heat and power facilities are among the most suitable candidates for integrating this technology [31].

All around the world, numerous point sources of the above-mentioned types could allow the cost of CO_2 capture to fall below 100 euros per tonne [31, 42]. Among these, the pulp industry is the largest CO_2 emitter per facility by emitting 750,000 tonnes per plant annually, while in some cases, an individual plant can emit as much as 2,000,000 tonnes per year.

Bioethanol production facilities provide another potential field for BECCS. These sources provide a high concentration of CO_2 in the fermentation off-gas, and this, in

turn, will reduce the cost of CCS. On average, a single plant can produce 50,000–300,000 tonnes of CO_2 per year, while in a few cases, annual numbers higher than 1,000,000 tonnes are reported [31].

Another potential for BECCS is its implementation in bioenergy facilities, especially combined heat, and power facilities or emerging biomass technologies, such as pyrolysis and gasification. However, here, the size also matters, and sources with minimal emissions close to 1,000,000 tonnes of biogenic CO_2 per year could benefit from BECCS.

It is worth mentioning that a large coal power plant has the potential to emit 10 million tonnes of CO_2 annually. For such cases, substituting the partial amount of coal with biomass could impact the CO_2 emissions.

In 2010, four projects were either canceled for financial/social reasons or switched to a CCS type. In this review, we will mainly focus on the status of the projects implemented within the last decade with only three cases before 2010 (Fig. 10.2).

The first case of documented BECCS application goes back to the early 2000s in Russel, Kansas, USA [31], i.e., a pilot plant that only managed to capture 7700 tonnes of CO_2 during its operation. This project was only concerned with investigating the potential use of CO_2 from a nearby ethanol plant for EOR and had nothing to do with BECCS; however, it served as the first operating BECCS facility.

In 2009, two projects went into operation. In Japan, Mikawa Thermal Power Plant in Omuta was equipped with a post-combustion demonstration plant that managed to capture 3,000 tonnes of CO_2 using coal and biomass [30]. Later in 2020, Toshiba announced the operation of its main BECCS facility [43]. The primary fuel source for this power plant came from palm kernel shells. In Liberal, Kansas, USA, Arkalon CO_2 Compression Facility was set up downstream of an ethanol plant. The CO_2 was then transferred via pipelines to a nearby oil field for EOR purposes, making it the
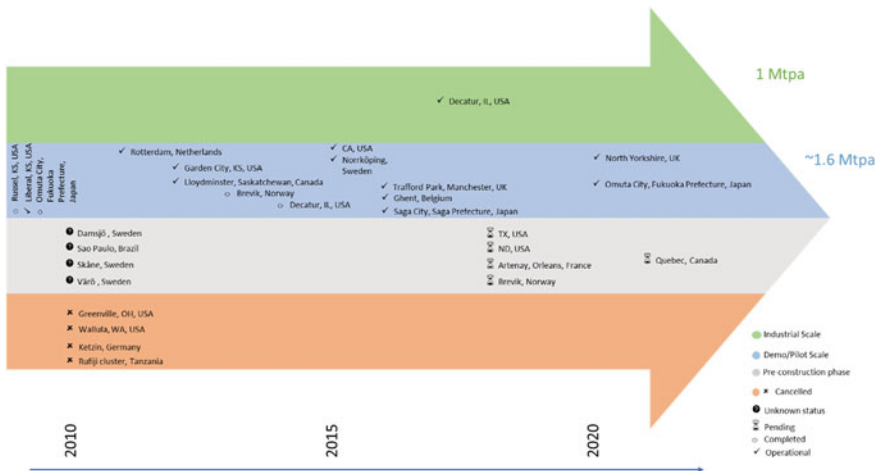

Fig. 10.2 BECCS projects timeline in the last decade

first project to use biogenic CO_2 for such operations. This unit is operational with a carbon capture capacity of 290,000 tpa (almost tripled since 2010) [30, 31].

In early 2010, three projects in Sweden and one in Brazil were announced. However, there is no evidence of their progress or termination in recent reports and literature [44, 45]. In addition, the literature focusing on these two potent countries for BECCS implementation is expanding. On the one hand, Sweden with sophisticated forestry management and its pulp and paper industry has the potential to implement BECCS sustainably [42]. Brazil, on the other hand, could integrate BECCS into its ethanol sector, which can result in a major cut back in CO_2 emissions [46].

In 2011, OCAP Facility started using the CO_2 emissions of an Abengoa's ethanol plant for the early purpose of utilizing greenhouses. Although the initial capture capacity was estimated to be around 330,000 tpa [31], it was able to capture 400,000 tpa. The project was intended to become a full BECCS plant once a suitable storage solution was decided upon.

Bonanza BioEnergy Group built a demonstration plant in Garden City, Kansas, USA, which started its operations in 2012. Similar to other plants in the USA, this plant was designed to make use of high purity CO_2 of an ethanol plant for EOR purposes. The plant is still in operation with a capture capacity of 100,000 tpa.

In the same year, Husky Energy managed to start up its capture plant close to an ethanol producer in Lloydminster Saskatchewan, Canada, with a capacity of 90,000 tpa to be used for EOR.

In the full-chain CCS project in Norway, a pilot facility was added to a cement manufacturer in Brevik. It is speculated that the facility will be equipped with a large-scale BECCS unit by 2023–2024 with the potential of capturing 800,000 tpa of CO_2.

In Decatur, Illinois, USA, a project consisting of a pilot/demonstration plant that started operations in 2011 came to an end in 2014 while capturing 300,000–350,000 tpa. It was estimated that for a plant to be financially independent of EOR, the capture capacity had to be increased to 1,000,000 tpa. This happened in 2017, making Decatur Project the largest operating BECCS plant so far.

Between 2015 and 2016, a few notable projects became operational all around the world across different industrial sectors from ethanol plants and pulp and paper manufacturers to waste-to-energy power plants.

For the near future, two BECCS projects are expected to start with the execution phase in the 2020s. In North Yorkshire, UK, Drax Power Plant has already announced the success of its pilot plant and its intention to achieve a carbon capture capacity of 4,000,000 tpa by 2027 [44]. Moreover, in Quebec, Canada, CO_2 Solutions Company is planning to carry out carbon capture for Saint Félicien Pulp Mill on a commercial scale, claiming that their enzyme technology is at TRL 8 [47].

Since BECCS has been implemented successfully in a handful of cases within a decade, this might be an indication of how delicately such decisions must be made for BECCS implementation to have a meaningful effect. Therefore, for BECCS deployment on a meaningful level, much attention should be focused on developing countries as well as policies that could encourage them to make effective initiatives

[20, 46]. It is also important to transfer the technical knowledge obtained in developed countries to speed up the deployment in developing countries.

10.4 BECCS Challenges

10.4.1 Technical Challenges

Worldwide large-scale implementation of BECCS could affect the environment, society, and biodiversity. BECCS could potentially increase the demand for land, water, and biomass at local and global scales. To identify the technical limitations related to BECCS, the comprising technologies and the methodologies should be investigated. In this section, the technical aspects will be discussed.

1. In-detail assessment of BECCS projects and their supply chain

One of the major challenges in NETs is to evaluate emissions throughout the supply chain, the power plant, and its downstream. A cradle-to-grave approach is required to reach carbon balance. For this purpose, LCAs and IAMs should include a large spectrum of factors from indirect effects of BECCS implementation, realistic market, and biodiversity to bioenergy regulations. Therefore, a set of standards are needed to certify the sustainability of a BECCS project under an international framework [48–51].

To predict the real net negative carbon emissions of a plant, it is necessary to calculate the carbon payback [22]. This is the point where the removed CO_2 becomes equal to the amount generated during the construction of the BECCS unit. While this is an important index, it does not consider the changes caused in CDR of the land before the project. In addition, bioenergy is less efficient than fossil fuel energy in terms of the unit energy produced [16]. Considering energy efficiency, previous land usage and the energy crop carbon payback can range from 10 to 100 years in different scenarios [15]. Moreover, the construction of a BECCS plant emits a significant amount of CO_2. A turning point for evaluating such plants is the point when it has reached the carbon payback, and its emissions will then be compared with the emissions of a coal power plant.

The logistics of the biomass also play an important role in carbon payback. It is worth mentioning that combustion efficiency depends on the type of biomass; however, it is considered to be only 70% efficient when compared to coal [15, 52]. In addition, energy loss for biomass processing is larger. For example, wood pellets from forest residuals perform approximately four times better than wood pellets from trees when offsetting the carbon emission of a coal-fired plant [15]. In an investigation, it was speculated that the financial payback for such a BECCS plant could be as short as seven years [48].

One of the core features of BECCS is carbon negativity. Nonetheless, this underlying assumption needs to be checked using detailed cradle-to-grave carbon balance analysis.

2.   Biomass and land requirements

With ever-rising power demand, it is expected for technologies such as BECCS to scale up to keep up with such demands. This means that more biomass/biofuel is required upstream. This has already been a talking point since it implicitly requires more dedicated bioenergy plantations to some extreme extents [12, 15], which could have an adverse impact on the food-water-energy-climate nexus [53].

An alternative approach is to employ marine biomass to avoid competition with the food supply chain [54]. While the concern for land-grown biomass is related to its competition with food crops and the disruption of biodiversity, the effects on marine biodiversity in the context of BECCS are not well documented.

As land use is one of the major concerns of BECCS deployment, ABECCS[1] has been proposed as an alternative to using offshore sites for algae cultivation. The biomass would later be converted to biogas or other biofuels [25]. In a case study, ABECCS was defined using algae as biomass (to be processed to biofuel) and the EOR process for storage. It was speculated that in an ideal case, an energy return investment of 50–60% could be expected when reaching carbon negativity. The production of the biofuel, the algae production yield and EOR were considered to be the bottlenecks [27].

GMOs can also be used as high yield biomass sources with less extensive land and water requirements compared to conventional sources [50].

Once the land is converted for energy crop production, two kinds of effects can be observed. The direct effects can be considered based on land-use change. The secondary effects consist of removing a piece of arable land, thus reducing the local food production, which, in turn, might result in increased emissions in the transportation sector. The secondary effects are quite difficult to measure and should be evaluated on a case-by-case basis. These are also referred to as indirect land use change (iLUC) emissions [15].

The crop itself plays a key role in CDR and energy production. Energy consumption per unit energy produced for second-generation biomass is almost 10% of the consumption for the first generation, i.e., in addition to less extensive water and nutrient requirements [55].

IAMs usually don't take into account the variable crop conditions. This could result in errors in estimating the energy production, even in local scenarios. In addition, it is recommended to limit the energy crop production to abandoned agricultural lands to avoid competition with food crops [15].

When choosing a crop, it is also important to consider the carbon directly stored by the plant in the form of soil organic carbon (SOC). For example, perennial crops are known to fix CO_2 in the form of SOC. On the other hand, second- generation biofuels and wood pellets reduce SOC [15].

---

[1] Aquatic BECCS or algae BECCS depending on the reference.

3.   BECCS optimization and alternative NETs

DACS is a more viable option when there is no need for energy generation. It has been noted that DACS could capture 650 Gt of CO_2 by 2100 with far fewer environmental consequences compared to BECCS [50]. Another alternative that has been the focus of attention is CCU. Converting CO_2 to a value-added product could be financially more lucrative, reducing transportation requirements compared to carbon storage solutions [29, 56, 57]. BECCS also shares some weaknesses of bioenergy production. Intermittent biomass availability could cause inconsistent energy production, especially at smaller scales. In a study, the integration of a biogas combined cycle plant and compressed air storage into a CCS unit was proposed for solving this problem. This was defined as a BECCS unit that could generate and store power. It was claimed that the project could replace a small-scale coal-fired plant for a remote location in terms of power generation. However, no specific details of verified locations for CCS were provided [58].

10.4.2   *Social and Political Challenges*

The sustainability of a BECCS process depends on many parameters. Some parameters of major concern include (1) having a disruptive impact on food crop production, (2) using arable land suitable for food crops, (3) endangering biodiversity, and (4) inefficient transportation and processing, leading to high emissions in the upstream of BECCS. To claim that a BECCS project is indeed sustainable, balancing the social, economic, and environmental aspects is required [15].

(1)   Governments

It has been pointed out that to achieve a sustainable BECCS deployment, governments are to encourage the companies by supporting the promotion of BECCS performance from biomass harvesting and energy generation to CO_2 capture and storage. This should also be accompanied by the development of international performance and good practice standards for BECCS [59]. The governmental policies are motivated by climate goals, and they are usually implemented in the form of financial incentives or supports in developed countries. Developing countries, on the other hand, would require international assistance in various forms in addition to domestic cooperation of the governments. For such synergy to exist, international standards for BECCS practices can pave the way for sustainable BECCS deployment. In such countries, the quickest way to deploy BECCS is to integrate it into a biofuel manufacturing plant. Furthermore, it is important to address the accounting aspects of negative emissions for developed and developing countries. For this purpose, many institutions, including the Global Environment Facility and Green Climate Fund, are proposed to mediate the financial flow [46]. The Least developed countries (LDC) are among the first to suffer the consequences of climate change, mainly because of the fragile infrastructures for food and water supplies. Therefore, in addition to

technological barriers, domestic policies and international incentives or lack thereof also contribute to the sluggish progress of BECCS. It is suggested that negative emissions of LDCs resulting from BECCS should not be included in the carbon budget. This is because including them will result in a slower transition for the countries that are large carbon emitters, while it could cause soil quality loss in LDCs due to the lack of close monitoring of land- use change in these countries. It is deemed more appropriate for LDCs to actively take part in fighting climate change; however, such efforts need to be evaluated in a very delicate case and context-specific manner [20].

(2)   Public image of BECCS

Regarding the public's view, BECCS faces less resistance compared to fossil CCS; however, environmental NGOs seem to be more skeptical about BECCS. While BECCS is gaining more attention lately, it is still among the least prioritized technologies [60].

As a politically-driven technology, BECCS needs to be introduced with special attention to ensure public support. In a survey, while the uninformed individuals were, in general, supportive of BECCS, they raised concerns similar to those associated with bioenergy and geoengineering. When asked about the policymaking aspect of BECCS, a high level of approval was observed for coercive and persuasive policies as opposed to supportive policies, such as a guaranteed purchase. The policies regulating BECCS can also have a significant impact on public perception [61].

One of the contributing factors for political decision making is the net welfare loss because of implementing BECCS. Two BECCS projects in the UK, i.e., Drax and Easington, were located ideally to benefit from the plantation for flood mitigation purposes. This, in turn, improved the net welfare impact of the project. It has also been shown that the loss of welfare index correlates with the plant size, and this can be prevented by constructing several 1GW plants instead of one 6 GW plant [34].

(3)   BECCS from the companies' view

Finland and Sweden are among the countries that aim for net negative emissions by 2050. Such an ambitious goal requires the implementation of technologies such as BECCS to be deployed at a large scale. Having numerous large-scale sources for biogenic CO_2 emission from energy and forestry facilities with a capacity over 100 ktpa (50–60%), these countries could benefit from such technologies. However, companies were found reluctant to implement BECCS. Their main arguments can be categorized as follows:

I.   Absence of reassuring policies for long-term decisions

In addition to the fact that CO_2 as a product does not have an attractive market for such companies, investing in technologies like BECCS is not feasible [16, 42, 62, 63]. Some companies mentioned that they would welcome governmental aid to construct a demo plant, while others claimed that investment in other methods of sustainability could have a more significant impact for the same amount of investment. It was also mentioned that an artificial spike in CO_2 capture price might cause productivity and efficiency loss, which might prevent any significant environmental impact [16].

II.   Higher responsibility for fossil-fuel industries against climate change

Facilities included in the survey, such as companies in the energy sector, cement industries, and pulp and paper manufactures, acknowledge the fact that such a transition is only a matter of time, and they are willing to contribute to achieving this goal in certain manners. However, the fact that fossil fuel industries are still large CO_2 emitters is a point that makes other emitters less likely to be the first to invest in technologies like BECCS [16].

III.   Less efficient power generation for the power sector, less profit for forestry

Energy companies have evolved to become highly efficient in terms of power supply, and integrating a BECCS plant will require consuming some of the generated power, reducing the total efficiency [16, 18]. On the other hand, forestry companies have evolved to utilize most of their by-products for purposes other than fuel consumption. Therefore, the integration of a BECCS facility would compete with the production of some valuable goods. Furthermore, a BECCS unit has specific land requirements. Assuming that all the conditions are met, BECCS has to be evaluated similar to any other investment, and while the technical aspect of the capturing process is well understood, transportation and storage are quite location-specific, preventing BECCS from becoming an attractive investment for now [16].

IV.   No demand, no investment

The social acceptability of negative emission methods differs based on location. While most end users might agree that such methods are important steps toward climate goals, marketing studies indicate that there is no significant demand in the market to encourage companies in that direction [16].

Social and political aspects are formed from the interactions among the government, the public, and the power producers. Governments must provide the infrastructure for the power plants to make the transition to technologies like BECCS. One of the important measures is to provide a transparent accounting system to incorporate in the business plans. Without such a system, it would not be possible to evaluate the potentials reasonably. On the other hand, governments need to introduce their climate goals clearly to the public to reach an agreeable outcome and avoid public resistance.

10.5 BECCS and the Food-Water-Energy-Climate Nexus

Although BECCS may has a significant effect on global climate change, its consequences on food security, clean energy, water resources, and other valuable traits of society are less clear [1]. These systems support human welfare and lifestyle and their increased interconnection has made them as a nexus_ the water-energy-food nexus_ for better identification of the cross-sector efficiencies and solving the resource challenges without indeliberate purposes [1]. BECCS approaches may be

technically feasible, but their consequences on regional economies may make them socially impractical. Therefore, the BECCS interaction with this nexus should be considered for approaching sustainability and protecting against potential risks of future water, energy, and food insecurity [1, 53].

10.5.1 Food Security

High deployment levels of BECCS require extensive use of 2nd generation biofuel crops and additional bioenergy crops which likely can occur adverse impacts on land use and food production [3, 64]. In an investigation, the combination of large-scale bioenergy deployment with forest conservation programs was evaluated [9, 65]. Under this scenario, a possible increase of food price indices until 2095 by 82% in Africa, 73% in Latin America, and 52% in the Asia Pacific is probable due to the intensified land competition. Rising food prices would also occur in the EU (22%) and the Former Soviet Union (16%). Another problem which is determined in an interesting study by [66] is that the large-scale lignocellulosic bioenergy deployment, i.e. 100 J/year, will not only increase food prices (5%) but also cause much larger climate change impacts (25%). On the other hand, numerous studies show positive environmental consequences under adequate management systems, e.g. by establishing bioenergy crops in already degraded ecosystems [9, 67–70]. Authors in [13] predict increasing the food gap by definition of wider bioenergy targets. The commitment to 20% in 2050 could correspond to twice the world's annual harvest of all plant materials and avoid the use of land resources for nutritional purposes, i.e., food and feed. In a research conducted by [71] for investigating the biomass availability status in the UK, they found available sufficient indigenous resources and concluded that energy crops, residues, and wastes, could supply up to 44% of the UK's energy demand by 2050 without food systems. In another study, the role of biofuel policy in Thailand was examined, which showed that food prices will only rise slightly and will not have a negative effect on food security in long term [9, 72]. According to what mentioned above, the large-scale use of bioenergy and drawing any universal conclusion about bioenergy's and BECCS' impact on food security remains controversial.

10.5.2 Water Issues

A significant amount of water is likely required by BECCS, especially for the production of biomass for bioenergy. Factors like the type of crop, location, irrigation requirements, agricultural practices, and biomass processing technologies certainly affect the reductions in water consumption [9]. Additional irrigation of energy crops may increase pressure on water resources due to the competition between bioenergy cropland and other agricultural applications for irrigation water. Under the scenario

of forests conservation, further effects on regional water price indices are reported by [65]. The increase could be as large as 460% in Latin America, 390% in Africa, and 330% in the Asia Pacific. However, the scenarios with no forest conservation will have somewhat smaller increases in water prices as 210%, 170%, and 130%, respectively. The water footprint for 12 different bioenergy crops has been presented by [14]. The water footprint of most crops uses as a biofuel is about two times higher than use in bioelectricity. This difference is due to the total biomass use for bioelectricity, including stems and leaves, in comparison with the use of sugar, starch, and/or oil fractions only for biofuel production. What is certain is that the production of bioenergy with low water footprint is mainly due to the careful selection of crops, the climate of location, and cultivation methods [9].

10.5.3   Energy

GHG reduction and decarbonization of the energy sector are mainly affected by reducing demand in the final energy consumption sector. Behavioral changes, lifestyle, and culture could have substantial effects on energy use and its related emissions [9]. In a study conducted by [73], comparable upstream energy requirements for coal, gas, and biomass production chains are reported which shows that no more than 10% of total energy production is required for the cultivation, pre-treatment biomass transfer. In other respects, in some other studies, no benefit in applying CCS has been reported even to extra biomass until all fossil fuel emissions have been removed or captured and stored [9, 13, 74]. They believe that producing 1 kWh of Bio-CCS using waste or extra biomass in one place and applying coal-CCS in another, results in the same amount of GHG benefit. Bioenergy expansion would require significant economic incentives under projected climate change, strong and sustained markets for food production, or advancement in new bioenergy crops (including biofuels). The adoption of bioenergy ultimately depends on economic viability interconnected with cultural values, which likewise influence decision-making.

10.5.4   Climate Change

National Energy Technology Laboratory of the US Department of Energy reports significantly more PM emissions for biomass co-firing compared with dedicated coal firing [9, 75] and higher PM emissions for both biomass co-firing and BECCS has also been reported by [76]. This increase could be due to the performed pretreatments of biomass for effective combustion. Besides biomass combustion which can affect global warming and climate change, the effects of climate change on future crop yields should also be concerned as a key problem [9, 66]. Climate change might play a price-forcing role for crops, led to no large-scale deployment of bioenergy. There are also feedbacks loops on fertilizer and irrigation water applications which both

can increase crop yields. Concerning climate change, large-scale use of bioenergy remains controversial due to the risk of reducing carbon stocks and emission of carbon to the atmosphere [9, 77]. Global warming rates show an unprecedented increase for the last 1000 years which can cause significant dangers like increasing the risk of reaching activation threshold values for tipping elements if global warming exceeds 2 °C. Although the NETs like BECCS seem to be the most promising route for the reduction of atmospheric CO_2, however, it should be concerned that some irreversible changes in system earth might happen even if the atmospheric CO_2 concentration reaches the previous level [9, 64, 78].

As mentioned above, BECCS has remarkable potential to reach the atmospheric CO_2 removal at a comparable cost to conventional CCS technologies, but its deployment cannot happen isolate. Thus, an approach addressing the undeniable interconnections within the food, water, energy, and climate nexus will be required.

10.6   Conclusion and Outlooks

BECCS, termed as a "negative carbon emission technology", has significant advantages over other CO_2 reduction methods. This priority is due to the biomass usage which removes atmospheric carbon through its growth and then storing the carbon emission resulting from bioenergy production permanently underground. BECCs can be applied to a wide range of biomass-related technologies, although its outlook is not fully recognized yet. The contribution of BECCS in the future of carbon reduction technologies is strongly dependent on the potential and societal acceptance of bioenergy on the one hand, and the development of CCS technologies on the other hand. Large-scale bioenergy deployment faces some major uncertainties including biophysical, technical, economic, and social challenges and CCS technologies are to be implemented widely yet [26].

Therefore, before we hope that BECCS will play a crucial role in reducing climate change, it is very important to clarify the values and challenges of each BECCS technology route and to understand what makes the value chain sustainable. This may lead us to relevant regional regulations concerning food, water, energy, and climate nexus to make sure that other societal and environmental objectives will not be compromised by this deployment and will encourage a regionally tailored mixed technologies deployment not limited to BECCS only [79].

Another critical factor affecting the future of BECCS for the international climate regime is the implementation of incentive and regulation policies which could be concerned as a regulatory framework to support the CCS business models than the societal and environmental implications [80]. This implies that governments will have to play a decisive role in projects and technology development investment to ensure that the expected goal of CO_2 reduction will be achieved by CCS technologies [52, 80]. So, it seems that the official guidelines and the role played by the states in this area would lead to better visibility and prediction of the future role of BECCS.

What is important is concerning that BECSS is expected to have necessary but not only limited contribution to meeting our climate change targets. Concerning BECCS as the only way to solve the climate change mitigation problem, detract us from paying attention to other low-carbon solutions which are already available today [79].

References

1. P.C. Stoy, S. Ahmed, M. Jarchow, B. Rashford, D. Swanson, S. Albeke et al., opportunities and trade-offs among BECCS and the food, water, energy, biodiversity, and social systems nexus at regional scales. Bioscience **68**(2), 100–111 (2018)
2. M. Meinshausen, N. Meinshausen, W. Hare, S.C.B. Raper, K. Frieler, R. Knutti et al., Greenhouse-gas emission targets for limiting global warming to 2°C. Nature **458**(7242), 1158–1162 (2009)
3. J. Kemper, Biomass and carbon dioxide capture and storage: A review. Int. J. Green Gas Control [Internet]. **40**, 401–30 (2015). https://doi.org/10.1016/j.ijggc.2015.06.012
4. Intergovernmental Panel on Climate Change. Climate Change 2014 Mitigation of Climate Change. Climate Change 2014 Mitigation of Climate Change (2014)
5. Intergovernmental Panel on Climate Change. Assessing Transformation Pathways. Clim. Chang. 2014 Mitig. Clim. Change 413–510 (2015)
6. EBTP/ZEP JTB-C. Biomass with CO_2 capture and storage (Bio-CCS): The way forward for europe [Internet] (2012). https://www.etipbioenergy.eu/images/bioccsjtf/EBTP-ZEP-Report-Bio-CCS-The-Way-Forward.pdf
7. IEA (International Energy Agency). Combining bioenergy with CCS—Reporting and accounting for negative emissions under UNFCCC and the Kyoto Protocol, 1–32 (2011)
8. J. Koornneef, P. can Breevoort, C. Hendricks, M. Hoogwijk, M.K. Klaas Koops, Potential for biomass and carbon dioxide capture and storage. IEAGHG [Internet]. **43**(4), 222 (2011). https://www.ieaghg.org
9. J. Kemper, Biomass and carbon dioxide capture and storage: A review. Int. J. Greenh. Gas Control. **40**, 401–430 (2015)
10. M. Junginger, C.S. Goh, A. Faaij, International bioenergy trade: History status & outlook on securing sustainable bioenergy supply, demand and markets. Lect. Notes Energy **17**, 233 p. (2014)
11. N. Bauer, D. Klein, F. Humpenöder, E. Kriegler, G. Luderer, A. Popp et al., Bio-energy and CO_2 emission reductions: An integrated land-use and energy sector perspective. Clim. Change **163**(3), 1675–1693 (2020)
12. F. Creutzig, K.H. Erb, H. Haberl, C. Hof, C. Hunsberger, S. Roe, Considering sustainability thresholds for BECCS in IPCC and biodiversity assessments. GCB Bioenergy **13**(4), 510–515 (2021)
13. T. Searchinger, R. Heimlich, Avoiding bioenergy competition for food crops and land. World Resour. Inst. Work Pap. [Internet] (9), 44 (2015). https://www.wri.org/publication/avoiding-bioenergy-competition-food-crops-and-land
14. W. Gerbens-Leenes, A.Y. Hoekstra, T.H. Van Der Meer, The water footprint of bioenergy. Proc. Natl. Acad. Sci. USA **106**(25), 10219–10223 (2009)
15. M.B. Jones, F. Albanito, Can biomass supply meet the demands of bioenergy with carbon capture and storage (BECCS)? Glob. Chang. Biol. **26**(10), 5358–5364 (2020)

16. E. Rodriguez, A. Lefvert, M. Fridahl, S. Grönkvist, S. Haikola, A. Hansson, Tensions in the energy transition: Swedish and Finnish company perspectives on bioenergy with carbon capture and storage. J. Clean. Prod. **280** (2021)

17. M.E. Boot-Handford, J.C. Abanades, E.J. Anthony, M.J. Blunt, S. Brandani, N. Mac Dowell et al., Carbon capture and storage update. Energy Environ. Sci. **7**(1), 130–189 (2014)

18. M. Bui, C.S. Adjiman, A. Bardow, E.J. Anthony, A. Boston, S. Brown et al., Carbon capture and storage (CCS): The way forward. Energy Environ. Sci. **11**(5), 1062–1176 (2018)

19. S.J. Smith, J. Edmonds, C.A. Hartin, A. Mundra, K. Calvin, Near-term acceleration in the rate of temperature change. Nat. Clim. Chang. **5**(4), 333–336 (2015)

20. A. Hansson, M. Fridahl, S. Haikola, P. Yanda, N. Pauline, E. Mabhuye, Preconditions for bioenergy with carbon capture and storage (BECCS) in sub-Saharan Africa: The case of Tanzania. Environ. Dev. Sustain. **22**(7), 6851–6875 (2020)

21. W.J. Sagues, H. Jameel, D.L. Sanchez, S. Park, Prospects for bioenergy with carbon capture & storage (BECCS) in the United States pulp and paper industry. Energy Environ. Sci. **13**(8), 2243–2261 (2020)

22. M. Fajardy, D.N. Mac, Can BECCS deliver sustainable and resource efficient negative emissions? Energy Environ. Sci. **10**(6), 1389–1426 (2017)

23. B. Hu, Y. Zhang, Y. Li, Y. Teng, W. Yue, Can bioenergy carbon capture and storage aggravate global water crisis? Sci. Total Environ. 714 (2020)

24. N. Pour, P.A. Webley, P.J. Cook, Potential for using municipal solid waste as a resource for bioenergy with carbon capture and storage (BECCS). Int. J. Greenh Gas Control [Internet] **68**, 1–15 (2018). https://doi.org/10.1016/j.ijggc.2017.11.007

25. C.M. Beal, I. Archibald, M.E. Huntley, C.H. Greene, Z.I. Johnson, Integrating algae with bioenergy carbon capture and storage (ABECCS) increases sustainability. Earth's Fut. **6**(3), 524–542 (2018)

26. M.A. Quader, S. Ahmed, Bioenergy with carbon capture and storage (BECCS): Future prospects of carbon-negative technologies [Internet]. Clean Energy Sustainable Development: Comparisons and Contrasts of New Approaches, 91–140 pp. Elsevier Inc. (2017). https://doi.org/10.1016/B978-0-12-805423-9.00004-1

27. A.J. Melara, U. Singh, L.M. Colosi, Is aquatic bioenergy with carbon capture and storage a sustainable negative emission technology? Insights from a spatially explicit environmental life-cycle assessment. Energy Convers. Manag. [Internet]. **224**, 113300 (2020). https://doi.org/10.1016/j.enconman.2020.113300

28. I. Ghiat, F. Mahmood, R. Govindan, T. Al-Ansari, CO_2 utilisation in agricultural greenhouses: A novel 'plant to plant' approach driven by bioenergy with carbon capture systems within the energy, water and food Nexus. Energy Convers. Manage. [Internet]. **228**, 113668 (2021). https://doi.org/10.1016/j.enconman.2020.113668

29. S. Restrepo-Valencia, A. Walter, BECCS opportunities in Brazil: Pre and post-combustion comparison in a typical sugarcane mill. SSRN Electron. J. (2021)

30. C. Consoli, Bioenergy and Carbon Capture and Storage (2019)

31. Global Status of BECCS Projects 2010 [Internet] (2010). http://cdn.globalccsinstitute.com/sites/default/files/publications/13516/gccsi-biorecro-global-status-beccs-110302-report.pdf

32. F. Levihn, L. Linde, K. Gustafsson, E. Dahlen, Introducing BECCS through HPC to the research agenda: The case of combined heat and power in Stockholm. Energy Rep. **5**, 1381–9 (2019). https://doi.org/10.1016/j.egyr.2019.09.018

33. L. Rosa, D.L. Sanchez, M. Mazzotti, Assessment of carbon dioxide removal potential via BECCS in a carbon-neutral Europe. Energy Environ. Sci. (2021)

34. C. Donnison, R.A. Holland, A. Hastings, L.M. Armstrong, F. Eigenbrod, G. Taylor, Bioenergy with carbon capture and storage (BECCS): Finding the win–wins for energy, negative emissions and ecosystem services—size matters. GCB Bioenergy **12**(8), 586–604 (2020)

35. N. MacDowell, N. Florin, A. Buchard, J. Hallett, A. Galindo, G. Jackson et al., An overview of CO2 capture technologies. Energy Environ. Sci. **3**(11), 1645–1669 (2010)

36. S.V. Hanssen, V. Daioglou, Z.J.N. Steinmann, J.C. Doelman, D.P. Van Vuuren, M.A.J. Huijbregts, The climate change mitigation potential of bioenergy with carbon capture and storage. Nat. Clim. Change **10**(11), 1023–9 (2020). https://doi.org/10.1038/s41558-020-0885-y

37. P.A. Turner, K.J. Mach, D.B. Lobell, S.M. Benson, E. Baik, D.L. Sanchez et al., The global overlap of bioenergy and carbon sequestration potential. Clim. Change **148**(1–2), 1–10 (2018)

38. S. Fuss, W.F. Lamb, M.W. Callaghan, J. Hilaire, F. Creutzig, T. Amann et al., Negative emissions—Part 2: Costs, potentials and side effects. Environ. Res. Lett. **13**(6) (2018)

39. N. Pour, P.A. Webley, P.J. Cook, Opportunities for application of BECCS in the Australian power sector. Appl. Energy **224**, 615–35 (2018). https://doi.org/10.1016/j.apenergy.2018.04.117

40. Zep Zero emissions platform. The Costs of CO 2 Capture, Transport and Storage. 50 (2011). http://www.zeroemissionsplatform.eu/library/publication/165-zep-cost-report-summary.html

41. OECD. Effective Carbon Rates: 2021: Pricing Carbon Emissions through Taxes and Emissions Trading. OECD Publishing. Paris (2021)

42. S. Fuss, F. Johnsson, The BECCS implementation gap—A Swedish case study. Front Energy Res. **8**(February), 1–18 (2021)

43. Corporation TES& S, Toshiba starts operation of large-scale carbon capture facility (2020). https://www.toshiba-energy.com/en/info/info2020_1031.htm

44. Global CCS Institute (GCI). Global status of CCS. Glob. CCS Inst. **40** (2020). https://www.globalccsinstitute.com/wp-content/uploads/2019/12/GCC_GLOBAL_STATUS_REPORT_2019.pdf

45. V. Stavrakas, N.A. Spyridaki, A. Flamos, Striving towards the deployment of bio-energy with carbon capture and storage (BECCS): A review of research priorities and assessment needs. Sustain. **10**(7) (2018)

46. D. Rassool, Financing BECCS in Developing Countries. Glob. CCS Inst. (2019)

47. C. Solutions, CO_2 Solutions provides update on Saint-Félicien pulp mill [Internet]. Pulp & Paper Canada (2017). https://www.pulpandpapercanada.com/co2-solutions-provides-update-on-saint-felicien-pulp-mill-1100000824/

48. H.B. Carminati, F.D. Milão R de, J.L. de Medeiros, Q.F. Araújo O de, Bioenergy and full carbon dioxide sinking in sugarcane-biorefinery with post-combustion capture and storage: Techno-economic feasibility. Appl. Energy **254**, 113633 (2019). https://doi.org/10.1016/j.apenergy.2019.113633

49. M. Muratori, N. Bauer, S.K. Rose, M. Wise, V. Daioglou, Y. Cui et al., EMF-33 insights on bioenergy with carbon capture and storage (BECCS). Clim. Change **163**(3), 1621–1637 (2020)

50. W. Burns, S. Nicholson, Bioenergy and carbon capture with storage (BECCS): the prospects and challenges of an emerging climate policy response. J. Environ. Stud. Sci. **7**(4), 527–534 (2017)

51. F.Y. Van, J.J. Klemeš, C.H. Ko, Bioenergy carbon emissions footprint considering the biogenic carbon and secondary effects. Int. J. Energy Res. **45**(1), 283–296 (2021)

52. Sustainable T, Energy U. IEA (2016), Energy Technology Perspectives 2016, IEA, Paris (2016). https://www.iea.org/reports/energy-technology-perspectives-2016

53. E.M. Biggs, E. Bruce, B. Boruff, J.M.A. Duncan, J. Horsley, N. Pauli, et al., Sustainable development and the water-energy-food nexus: A perspective on livelihoods. Environ. Sci. Policy [Internet]. **54**, 389–97 (2015). https://doi.org/10.1016/j.envsci.2015.08.002

54. M. Fridahl, A. Hansson, S. Haikola, Towards indicators for a negative emissions climate stabilisation index: Problems and prospects. Climate **8**(6), 1–22 (2020)

55. N. Pour, Status of bioenergy with carbon capture and storage-potential and challenges. Bioenergy Carbon Capt. Storage Using Nat. Resour. Sustain. Dev. 85–107 (2019)

56. A.W. Zimmermann, J. Wunderlich, L. Müller, G.A. Buchner, A. Marxen, S. Michailos et al., Techno-economic assessment guidelines for CO_2 utilization. Front Energy Res. **8**(January), 1–23 (2020)

57. T. Wich, W. Lueke, G. Deerberg, M. Oles, Carbon2Chem®-CCU as a step toward a circular economy. Front Energy Res. **7**(January), 1–14 (2020)

58. I.B.S. Poblete, Q.F. Araujo O de, J.L. de Medeiros, Dynamic analysis of sustainable biogas-combined-cycle plant: Time-varying demand and bioenergy with carbon capture and storage. Renew. Sustain. Energy Rev. **131** (2020)

59. A. Torvanger, Governance of bioenergy with carbon capture and storage (BECCS): Accounting, rewarding, and the Paris agreement. Clim. Policy [Internet]. **19**(3), 329–41 (2019). https://doi.org/10.1080/14693062.2018.1509044

60. M. Fridahl, Pre- and post-Paris views on bioenergy with carbon capture and storage. Bioenergy with Carbon Capture Storage Using Nat. Resour. Sustain. Dev. 47–62 (2019)

61. R. Bellamy, J. Lezaun, J. Palmer, Perceptions of bioenergy with carbon capture and storage in different policy scenarios. Nat. Commun. [Internet]. **10**(1), 1–9 (2019). https://doi.org/10.1038/s41467-019-08592-5

62. M. Fridahl, M. Lehtveer, Bioenergy with carbon capture and storage (BECCS): Global potential, investment preferences, and deployment barriers. Energy Res. Soc. Sci. [Internet] **42**, 155–65 (2018). https://doi.org/10.1016/j.erss.2018.03.019

63. R. Bellamy, M. Fridahl, J. Lezaun, J. Palmer, E. Rodriguez, A. Lefvert et al., Incentivising bioenergy with carbon capture and storage (BECCS) responsibly: Comparing stakeholder policy preferences in the United Kingdom and Sweden. Environ. Sci. Policy **2021**(116), 47–55 (2020)

64. Intergovernmental Panel on Climate Change. Agriculture, Forestry and Other Land Use (AFOLU). Clim. Chang. 2014 Mitig. Clim. Chang. 811–922 (2015)

65. A. Popp, J.P. Dietrich, H. Lotze-Campen, D. Klein, N. Bauer, M. Krause, et al., The economic potential of bioenergy for climate change mitigation with special attention given to implications for the land system. Environ. Res. Lett. **6**(3) (2011)

66. H. Lotze-Campen, M. von Lampe, P. Kyle, S. Fujimori, P. Havlik, H. van Meijl et al., Impacts of increased bioenergy demand on global food markets: An AgMIP economic model intercomparison. Agric. Econ. (UK) **45**(1), 103–116 (2014)

67. J. Hill, E. Nelson, D. Tilman, S. Polasky, D. Tiffany, Environmental, economic, and energetic costs and benefits of biodiesel and ethanol biofuels. Proc. Natl. Acad. Sci. USA **103**(30), 11206–11210 (2006)

68. T. Semere, F.M. Slater, Ground flora, small mammal and bird species diversity in miscanthus (Miscanthus×giganteus) and reed canary-grass (Phalaris arundinacea) fields. Biomass Bioenerg. **31**(1), 20–29 (2007)

69. J.E. Campbell, D.B. Lobell, R.C. Genova, C.B. Field, The global potential of bioenergy on abandoned agriculture lands. Environ. Sci. Technol. **42**(15), 5791–5794 (2008)

70. M. Nijsen, E. Smeets, E. Stehfest, D.P. van Vuuren, An evaluation of the global potential of bioenergy production on degraded lands. GCB Bioenergy **4**(2), 130–147 (2012)

71. A. Welfle, P. Gilbert, P. Thornley, Securing a bioenergy future without imports. Energy Policy **2014**(68), 1–14 (2014)

72. S. Wianwiwat, J. Asafu-Adjaye, Is there a role for biofuels in promoting energy self sufficiency and security? A CGE analysis of biofuel policy in Thailand. Energy Policy [Internet] **55**, 543–55 (2013). https://doi.org/10.1016/j.enpol.2012.12.054

73. J. Mastop, D. Best, M. Waldhober, C. Hendriks, A.R. Ramirez, Informed public opinions on CO 2 mitigation options in the Netherlands : deliberating expert information and lay beliefs (2014)

74. NRC. Climate intervention: Carbon dioxide removal and reliable sequestration. Climate Intervention: Carbon Dioxide Removal and Reliable Sequestration. 2015. 1–154 p.

75. Laboratory NET. Role of Alternative Energy Sources : Pulverized Coal and Biomass Co-firing Technology Assessment Report 2012/1537 (2012)

76. W. Schakel, H. Meerman, A. Talaei, A. Ramírez, A. Faaij, Comparative life cycle assessment of biomass co-firing plants with carbon capture and storage. Appl. Energy [Internet] **131**, 441–67 (2014). https://doi.org/10.1016/j.apenergy.2014.06.045

77. R. Bailis, H. Mccarthy, Carbon impacts of direct land use change in semiarid woodlands converted to biofuel plantations in India and Brazil. GCB Bioenergy **3**(6), 449–460 (2011)

78. B. Caldecott, G. Lomax, M. Workman, Stranded carbon assets and negative emissions technologies about the stranded assets programme (2015). https://ora.ox.ac.uk/objects/uuid: 258c4d8e-3ea7-4b72-a24e-44acd01405d1/download_file?file_format=pdf&safe_filename= 2015.02.03_NETs.pdf&type_of_work=Report
79. M. Fajardy, A. Koberle, N. Mac Dowell, A. Fantuzzi, BECCS deployment: a reality check (Grantham Institute, 2019), vol. 28
80. S. Selosse, Bioenergy with carbon capture and storage: How carbon storage and biomass resources potentials can impact the development of the BECCS. Bioenergy with Carbon Capture Storage Using Nat. Resour. Sustain. Dev. 237–56 (2019)

Chapter 11
Working, Modeling and Applications of Molten Salt TES Systems

Mumtaz A. Qaisrani, Naveed Ahmed, and Qiuwang Wang

Abstract   As the global energy mix transit towards renewables, it inherently leads to fluctuations in smooth energy supply. Natural constraints with unpredictable climatic fluctuations further exacerbate the issue. The challenge to a constant energy supply can be coped using energy storage methods. There are number of ways energy can be stored, i.e., electrical mechanical, chemical and thermal. Mechanical energy storage method has geographical constraints such as in the case of Compressed Air Energy Storage systems, whereas electrical and chemical are prone to high losses in large scale systems. Thermal energy storage, although has higher thermodynamic costs, however, it out performs other technologies in terms of cost benefits, further, not only it is a zero-emission technology but has excellent grid integrity, and dispatchability characteristics, as per demand, making it widely known as the "future of renewable energy". Thermal energy storage systems usually utilize latent heat storage material i.e., phase-change materials or sensible heat storage material i.e., solid medium or molten salts. This chapter will only focus on thermal energy storage using the molten salts. The molten salt is stored either in the form of Two-tank storage system or the direct single tank (thermocline) methods as "sensible heat". The two-tank system involves a simple mechanism whereas the single tank system reduces the cost by about 35%. The amount of energy stored is dependent upon the temperature gradient and the heat flow from higher temperature (hot) to lower temperature (cold) using the

M. A. Qaisrani
Mechanical Engineering Department, Khwaja Fareed University of Engineering and Information Technology, Rahim Yar Khan, Pakistan
e-mail: mumtaz.ahmed@kfueit.edu.pk

N. Ahmed (✉)
US Pakistan Centre for Advanced Studies in Energy (USPCAS-E), National University of Sciences and Technology, Islamabad, Pakistan
e-mail: Naveed.ahmed@uspcase.nust.edu.pk

Q. Wang
Key Laboratory of Thermo-Fluid Science and Engineering, Ministry of Education, School of Energy and Power Engineering, Xi'an Jiaotong University, Xi'an, Shaanxi 710049, PR China
e-mail: wangqw@mail.xjtu.edu.cn

mathematical expressions $Q = m\,C\,\Delta T$, where Q denotes the sensible heat, m represents the mass of the salt, C denotes the specific heat of the salt, whereas ΔT represents the difference in temperature. Later, the stored molten salt is utilized to heat the water/steam and run the turbines and the thermal to electricity conversion usually proceeds through different power cycles such as the Brayton and Rankine cycles. Whereas, the cold salt is sent for storage to heat it up and continue the cycle.

Keywords Thermal energy storage (TES) · Molten salt thermal energy storage · Applications of thermal energy storage

Nomenclature

Abbreviations

CSP	Concentrated solar power
GHG	Greenhouse gas emission
CO_2	Carbon dioxide
GW	Giga Watt
KWh	Kilowatt Hour
LCOE	Levelized cost of energy
MW	Mega Watt
Parabolic trough collector	PTC
Solar-PV	Solar Photovoltaic
ST	Solar tower
TES	Thermal Energy Storage

Variables

|	
C_p	Specific heat J/kg K
H	Enthalpy
Q	Heat rate
$\dot{m}$	Mass flow rate [t/h]
h	Convective heat transfer coefficient, $W/(m^2 K)$

11.1 Introduction

In recent years, the upsurge in energy demand and a rising wakefulness about the constraints of CO_2 emissions, has resulted into a substantial rise in the development

of innovative technologies with an aim to conserve energy along with its production through renewable sources [1]. The integration of sustainable energy systems and application processes create a multi-disciplinary research area with an intense motivation for researchers to address urgent global climate change [2]. The utilization of green energy resources and to enhance overall energy efficiency are the key approaches which needs to adopt in order to lessen the reliance on depleting fossil fuels and reduce greenhouse effects [3]. However, the erratic behavior of potential green energy resources such as wind energy, solar energy or industrial waste heat recovery [4], its internment nature due to its availability and usage, makes it unpredictable [5].

In this global energy scenario, the integration of thermal energy storage units is essential to provide a variety of solutions and combinations of different new technologies for better synergy from already existing energy systems [6]. Moreover, thermal energy storage (TES) systems have a crucial contribution in this regard to enhance the applicability, durability and field performance using novel technologies [7]. The impact of thermal energy storage is improved by adopting the strategy of large-scale switching. of the TES units [8]. Thermal energy storage systems moderate the imbalance between seasonal energy supply and demand and contributes to enhance the efficiency and consistency of whole energy system. Thus TES units play a pivotal in the conservation of heat energy [9]. Moreover, the innovative energy storage units can also be utilized to ensure the expected level of demand during peak hours, thus helping minimize the temporary decline of production from conventional energy resources. This results in improving the overall plant performance with added advantage of fuel savings [10]. In recent years, the importance and wide scope of energy storages in high temperature applications has motivated the scientists to focus their research directions towards molten salt thermal energy storage systems [11]. They are of the opinion that it is an effective technique to make the available energy resource more efficient and sustainable [12].

To overcome the seasonal energy demand and supply imbalance is a core focus of the researchers in the current energy scenario [13]. Molten salt based thermal energy storage systems with desired integration characteristics can play an important role in such situations [2]. The integration of TES units allows the development and implementation of renewable energy resources in a wide temperature range for different applications [14]. A practical example is the application of high temperature molten salt TES in concentrated solar power (CSP) plants, where surplus sunshine during day time can be stored for further utilization later on when the energy from sun the solar energy is not available, for instance during cloudy weather or at night time [15]. Another example is integration of medium to high temperature thermal storage system in heat recovery processes, where the excess heat energy is available in exhaust gases [16]. An efficient energy storage needs to be integrated, due to different timings of thermal energy availability and demand in industrial process [4]. TES systems not only lessen the mismatch between energy demand and supply but also enhances the reliability and performance of the overall systems [17]. Thus the thermal energy storage systems perform a main role in the energy conservation and carbon emissions reduction [18] (Fig. 11.1).
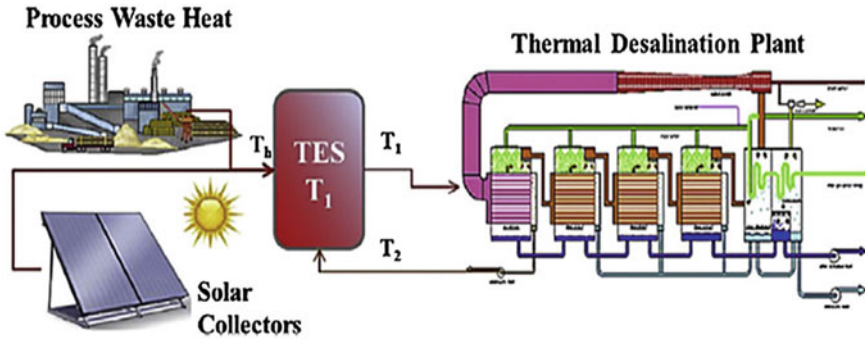
Fig. 11.1 An application of TES system making use of industrial waste heat and solar energy [4]

Following are different requirements [17] which needs to be considered to ensure optimized performance and durability, depending on type of TES system:

1. High storage density per unit volume of storage filler media.
2. Enhanced heat transfer characteristics between thermal storage media and HTF.
3. Stable thermos-physical characteristics of storage media and the HTF.
4. Storage media must be chemically compatible with fluid, type of heat exchanger and the tank walls.
5. Reversible during charge/discharge cycles.
6. Minimal thermal losses.
7. Cost effective.
8. Environment friendly.

TES systems find their applications in various sectors depending upon the temperature range. The applicability of TES systems in various applications with a wide range of temperature led researchers to look for innovative energy storage solutions [19–22]. In recent decade, due to this great interest for the researchers and scientists, many studies are reported in the literature dealing with TES system for high temperature applications [23, 24].

In recent years the application of TES for high temperature has risen considerably. The potential and transition of thermal energy storage systems in CSP Power plants depends on the design of individual components e.g., heliostat field, internal/external receivers, heat exchanger etc. and material constraints [25–29]. Gasia et al. presented an extensive review for high temperature thermal energy storage systems in two parts, highlighting preliminary system designs and materials requirements. First part focused on general requirements for high temperature TES units [8] and the second part gave a detailed review on thermal conductivity enhancement techniques [30]. The study reported by Liu et al. [31] focused on phase change materials used in TES at a temperature higher than 300 °C and discussed thermal performance enhancement techniques. The studies investigated by Fernandes et al. [32] and Cárdenas et al. [33] discussed material selection criteria of a TES system for different defined applications. They also reviewed performance enhancement techniques of TES systems

based on variable thermos-physical properties. The literature review reveals CSP based thermal power plants integrated with TES systems are evolving as a promising energy generation technology in the next generation renewable power system as the capability to supply abundantly dispatchable and cheap electricity. However, this technology faces the issue of intermittent solar energy. To meaningfully minimize the levelized cost of energy (LCOE) of the currently developed concentrated solar power plants, the next generation concentrated thermal power plants for higher temperature range and unenhanced energy efficiency is being improved. The media used to store thermal energy and heat transfer fluid (HTF) being used in the next generation CSP plants operates at higher temperatures (>550 °C) and thus making molten salt thermal energy storage (MSTES) system an ideal candidate to be used in such applications. The advancement and maturity in the development of the next generation thermal power generation technology can be addressed more efficiently by engaging MSTES systems utilizing nitrate/chloride salt mixtures such as $MgCl_2$/ KCl/$NaNO_3$/KNO_3/$NaCl$ possessing stable thermo-physical properties, reduced levelized costs of energy (<0.35 USD/kg), and improved thermal stability properties (>800 °C) [34]. The most commonly used mixtures of molten salt fluid known as solar salt has a composition of 40% KNO_3 and 60% $NaNO_3$. The mixtures of these salts have been widely used CSP power plants for decades with a detailed information and proven techno economic feasibilities available both at pilot and commercial level. The development progress in selecting and optimizing of different molten salt mixtures as potential storage media/fluid for high temperature applications has excelled but the optimization of charging/discharging performance under variable load conditions, control strategy for energy mixing, material formulation, and corrosion mitigation of materials (such as alloys) remains a challenge.

The receiver is mounted on the top of the tower is placed toward the heliostat field. The external receiver as shown in above Fig. 11.2 absorbs the solar radiation from the heliostat and transfer the energy to the HTF.

HTF carries the thermal energy from the receiver through the hot storage tank or to the steam generator. HTF is a key to CSP success because it serves the key responsibility of transferring the solar radiation collected form the receiver to the steam generator to produce electricity. There are many types of HTF in practice, such as.

1. Water
2. Water-Glycol mixtures
3. Synthetic thermal fluids
4. Molten salts.

Among all these fluid molten salts are mostly used owing to their high temperature energy storage capabilities (above 400 °C). Molten salt storage is employed at many solar thermal power plants however the freezing of molten salt presents a challenging issue and it must be overcome by using appropriate salt mixture with freezing point lying within the operational range. The application of molten salt TES systems offer economical solution for CSP plants and it rarely needs maintenance for a duration of more than thirty years of the power generation plant. Also, molten salts have the
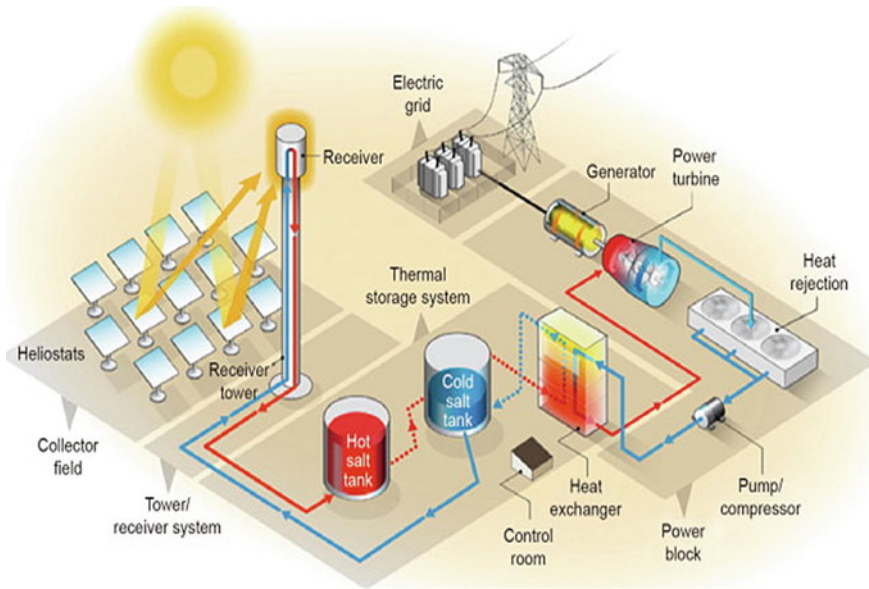
Fig. 11.2 Second generation CSP plant integrated with molten salt TES [30]

advantage of being non-toxic, as these are environmentally friendly salt mixtures and can also be used as high-quality fertilizer when needs to be discarded.

11.2 Integration Requirements of TES Systems for an Application

The incorporation of a thermal storage system into a specific application is dominated by various influencing factors [9]. Therefore, the incorporation requirements for MSTES unit vary vastly depending upon the desired application. This is because the process systems have variable capabilities based on their working principles [35]. The work of Gibb et al. is focused on more in-depth study on methodology to characterize and evaluate TES systems in a variety of applications [14].

The methodology includes guidelines for process analysis and defining explicitly the thermal storage boundaries. Then techno-economic parameters of the system need to be addressed while evaluating benefits gained by integrating TES system to an application specific process. This is indicated by analyzing key performance indicators by considering the perspective of different stakeholders. Figure 11.3 shows interaction between application specific process analysis and the techno-economic requirements of a TES system for successful integration. It highlights three main features: the application, the TES system and the advantages of incorporating a TES system to an application specific process.
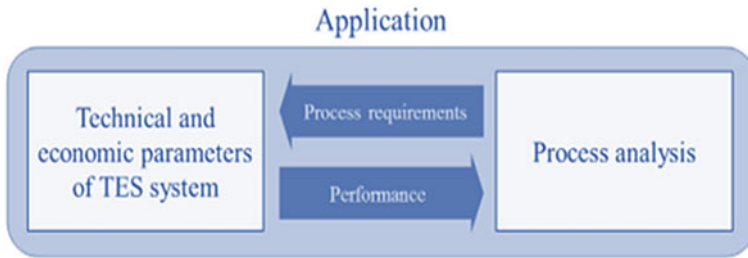
Fig. 11.3 Integration interatction between application, specific process and TES system

11.3 Economic Requirements of TES Systems

There exists a common and pertinent issue in the research related of molten salt TES systems, i.e., economic feasibility of the system. The researchers mainly focused their work on investigating molten salt material properties and its performance enhancement for high temperature applications [8]. An important aspect of TES requirements has usually been ignored hitherto i.e., economic feasibility and system integration of MSTES for an application specific process. The economics of a TES unit is addressed by considering different aspects and parameters e.g., availability of TES media, its per unit costing, operational life time of components, management costs and recurring costs etc.

The development of a novel and cost effective MSTES faces the main concern of erratic nature of the potential renewable energy sources and it should overcome this mismatch of energy demand and supply [14]. To date, techno-economic feasibilities of molten salt based TES system focused on the hybridization of thermal technologies [36]. Presently the cost of storing unit thermal energy is comparatively higher as the expensive individual components increase the total system cost [37]. The main components of a TES which primarily contribute to the cost HTF costs, storage material, container of tank, encapsulation cost in case of PCMs, pump energy cost and miscellaneous costs [38]. The use of suitable storage materials and smart system integration schemes enables controlled operation with greater temperature swings and it also helps to improve overall efficiency of a CSP generation plant while optimizing levelized cost of energy [39]. However, the two major issues faced by MSTES technologies to gain the market attention are, i.e., performance stability of TES unit while integrated in a process and the economic feasibility [14].

11.4 Economic Requirements of TES Systems

11.4.1 General Classification of TES Systems

TES units can generally fall into two categories depending upon the type of mechanical assistance for heat transfer; passive type thermal storage system and active type TES system. Active type thermal energy storage units are assisted mechanically to empower the heat transfer between source of energy and the storage filler media. Therefore, in such systems the dominant mean of heat transfer is forced convection which occurs between the filler media and the HTF via a heat exchanger. Whereas, in a passive type TES unit, the heat transfer mechanism between the HTF and the thermal storage media occurs due natural convection mode or is driven by buoyancy forces. No mechanical assistance of external source is involved in this system [40]. Active type TES systems are further divided into direct type and indirect TES systems. In direct type thermal storage systems, the circulating heat transfer fluid is also utilized as a thermal storage material omitting the need of heat exchanger. Whereas, in the indirect TES systems, HTF circulates separately from storage material and requires heat exchanger for heat transfer[33]. Figure 11.4 shows classification of TES types as active and passive TES.

Moreover, the classification of TES units can also be made based on how heat energy is stored in the filler material, i.e., sensible heat energy, latent heat energy or chemical energy [41]. The classification flowchart is shown in Fig. 11.5.

In sensible heat storage media (usually solid or liquid) no phase change is involved over the operating range of temperature and heat energy is stored as increase in internal energy of the storage material. In this category of storage materials, the thermal energy storage is influenced by its heat capacity which predicts its storage capacity and the thermal diffusivity, which regulates the rate of energy extraction or released [42]. Sensible heat storage is given by the following formula.
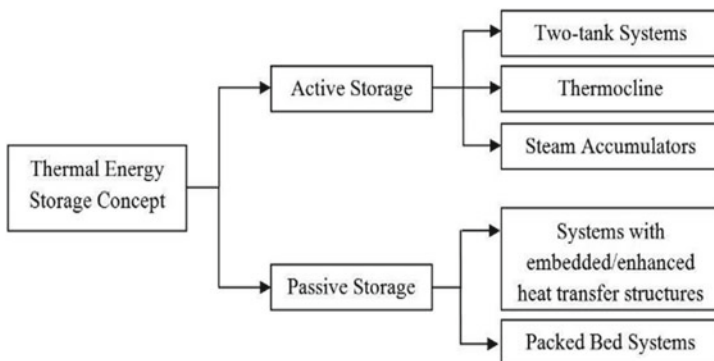

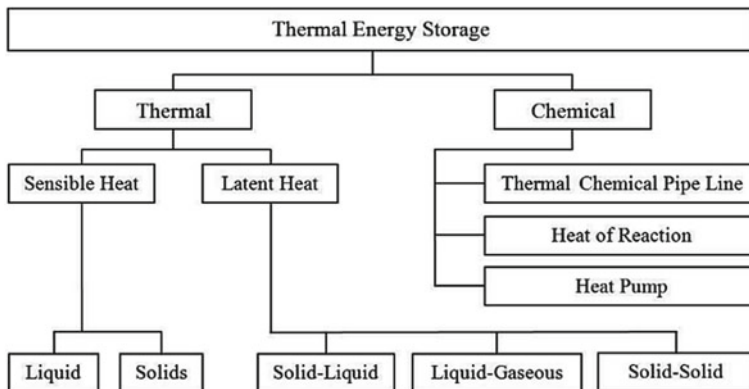**Fig. 11.4** Classification of TES systems as active and passive types [4]

Fig. 11.5 Classification of TES systems based on methods of heat [41]

$$Qs = mcp(Tf - Ti) \tag{11.1}$$

where Q_s represents the quantity of heat stored in Joule, m represents the mass of heat storage medium, c_p denotes the specific heat in J/kg.k, T_f and T_i represent initial and final values of temperature in degrees [43].

Molten salt TES systems fall in the category of sensible heat TES systems. The use of molten salt as sensible heat storage material refers to a liquid fluid formulated by melting mixtures of inorganic salts and also it maintains its molten state during the operation. To meet different requirements as per nature of applications a variety of salt mixtures have been developed such as nitrates, fluorides, carbonates etc. For instance, to avoid hard freeze of molten salt in the tubing of CSP thermal power plants, molten salt HTFs should having lower freezing point are preferred (Fig. 11.6).

11.5   Working Principal of Molten Salt with TES

The working principle of MSTES involves heating of molten salt by means of solar radiations in an insulated container, this phenomenon is called charging of TES system. During heat recovery cycles where a need arises to operate load during peak hours, molten salt is then passed into the steam generator, here it heats the water and the steam is then passed through the turbine for the power production.

There are two main TES configurations.

- Two-Tank type TES Configuration.
- Single Thermocline TES Configuration.
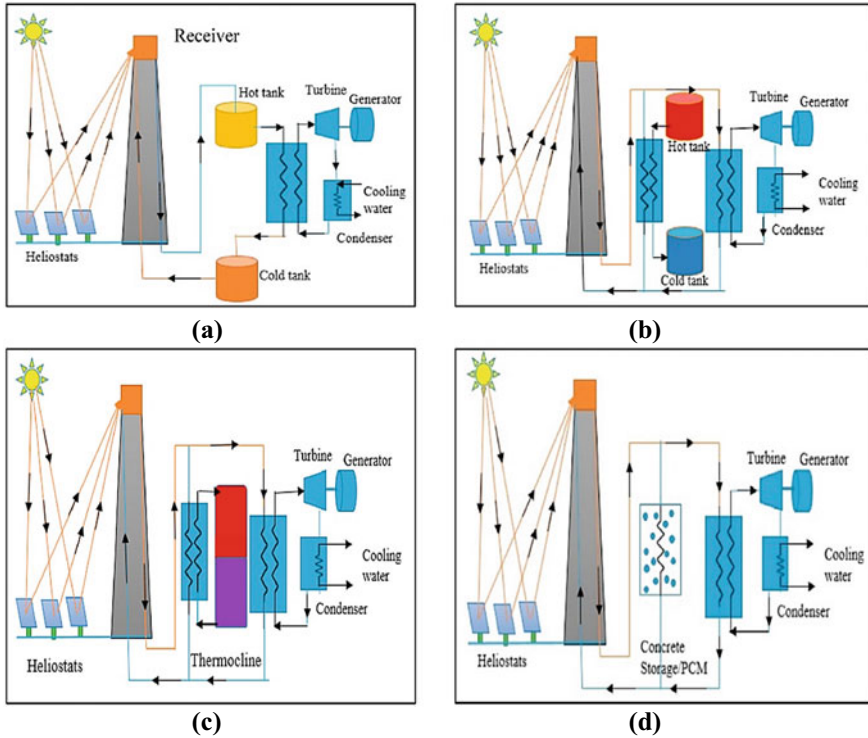
Fig. 11.6 Schematics of heating modes for thermal energy storage. **a** Schematic of direct active. **b** Active indirect single tank (thermocline). **c** Active indirect single tank (thermocline). **d** Passive concept

11.5.1 Two-Tank Type Configuration

The two-tank type MSTES configuration works by pumping HTF from the solar plant field to charge hot thermal storage tank via heat exchanger containing molten salt as storage media and is then pumped from cold molten salt tank. The hot storage tank is discharged by pumping salt from the hot storage tank to cold storage tank via steam generator. The superheated steam is transferred to the power generation block and the cold salt gets back to the cold storage tank [44] (Fig. 11.7).

11.5.2 Single Thermocline TES Configuration

Single tank type molten salt TES systems are 20–37% cheaper as compared to the two-tank type MSTES systems [45]. The thermal gradient formed due to the separation of high heat energy areas and low heat energy areas in single energy storage.
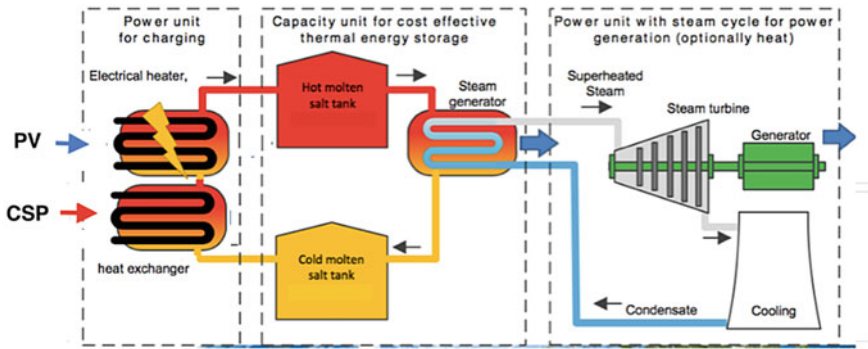
Fig. 11.7 Schematic flow illustration of a parabolic trough (CSP) plant having two-tank molten salt storage system [44]

tank is called thermocline thickness. Moreover, the characteristics associated with stratification behavior of molten salt in thermocline TES tank makes it more advantageous to utilize cheap naturally occurring filler material [46]. The thermal gradient formed inside single storage tank due to buoyancy effects maintains a clear separation between cold fluid at the bottom section and high heat fluid at the top section [47]. In charging cycles as the high heated molten salt is pumped from the top into the tank, it displaces the low heated fluid at lower sections while remains hot at the top. Whereas, the discharging process occurs by pumping cold HTF from the lower section of the TES tank and exchanges thermal energy with storage material as it moves to the top. The rate of heat transfers between molten salt HTF and the storage material depends on heat transfer coefficient that can be correlated to the temperature difference between them [48] (Fig. 11.8).

The performance of molten salt TES tank best be visualized by studying thermocline thickness profiles of HTF formed during charging or discharging process [50]. A thick thermocline profile means poor stratification behavior and lower thermocline characteristics. So usually a thin profile is desired [51]. Thermocline thickness is evaluated using temperature distribution profile of HTF inside the tank as shown Fig. 11.9. Thermocline characteristics depends on many factors which may move either in upward or downward direction depending upon charging or discharging process.

The amount of energy charged/discharged, utilization factor effective discharging time and effective discharging efficiency depends on the type of filler material used and its thermocline characteristics [52]. Molten salt can efficiently be used as HTF and storage material. To make TES cost effective, a low-cost filler material (such as rocks, concrete, brick manganese etc.) compatible with molten can be used as primary filler occupying major volume of the thermocline tank. However, using only sensible filler material may make the system economically more feasible but not performance effective [53]. Therefore, researchers tried different combinations of
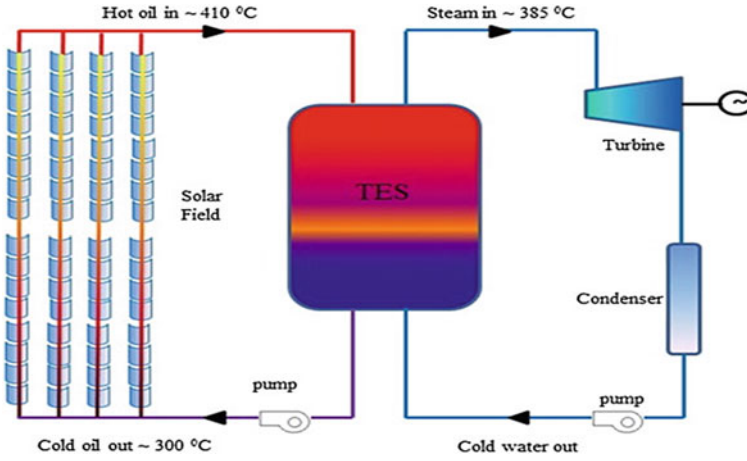
Fig. 11.8 Schematic flow diagram of a parabolic trough power plant with thermocline molten salt storage [49]
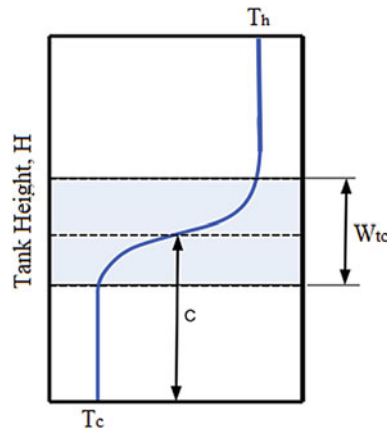

Fig. 11.9 Visualization of thermocline profile of HTF along tank height

filler material to enhance the performance of thermocline TES system while keeping it cost effective.

11.6 Potential and Applications of Molten Salt Thermal Energy Storage

Molten salts exhibiting high specific heat capacity, wide operational temperature range and little corrosive, are considered as very promising HTF and thermal storage media in solar thermal power plants, fuel cell, and nuclear fuel reprocessing etc. For effective utilization of high-temperature sensible heat, thermodynamic and transport properties of molten salts should be evaluated accurately over the entire operating temperature range for system design in relevant industry. Higher demand of molten salt in a number of high temperature applications has led the researchers to look for suitable molten salts mixtures which could be used as HTF as well as thermal energy storage media. Molten salt to be used as a potential candidate as storage media, the thermal stability together with its thermos physical properties play a dominant role.

Applications of the molten salt thermal energy storage are of wide range in engineering field, involving in the industrial, residential heating application and to meet the electricity power supply. Table 11.1 enlists some of the most commonly utilized molten salts and their applications.

Thermal stability of solar salt serves as a practical criteria and guideline for other types of molten nitrate salts for the investigation of their thermal stability and is indispensable. Its melting point is 220 °C and possess the thermal stability around a temperature of 600 °C, particularly when it is operated in an enclosed thermal storage system the thermal stability increases significantly. Figure 11.10 shows stability limits and melting point of different molten salts.

Table 11.1 Some commonly used molten salt mixtures and their applications [54]

| Molten salt	Eutectics mixture	Type of application
Carbonates	K_2CO_3–Na_2CO_3	High temperature fuel cells, molten salt oxidation
	Li_2CO_3–Na_2CO_3	
Fluorides	LiF–BeF_2 ("FLiBe")	Heat transfer fluid (HTF), Molten salt reactors (MSR), Thermal energy storage (TES)
	LiF-NaF-KF("FLiNaK")	
	LiF–BeF_2–ThF_2–UF_4	
	$NaBF_4$–NaF	
Nitrates	$NaNO_3$–KNO_3–$NaNO_2$ (hitec salt)	Thermal energy storage (TES), Heat transfer fluid (HTF)
	KNO_3–$NaNO_3$ (solar salt)	
Chlorides	KCl–$MgCl_2$–NaCl	Alloy heat treatment molten salt reactors (MSR), thermal energy storage (TES), heat transfer fluid (HTF)
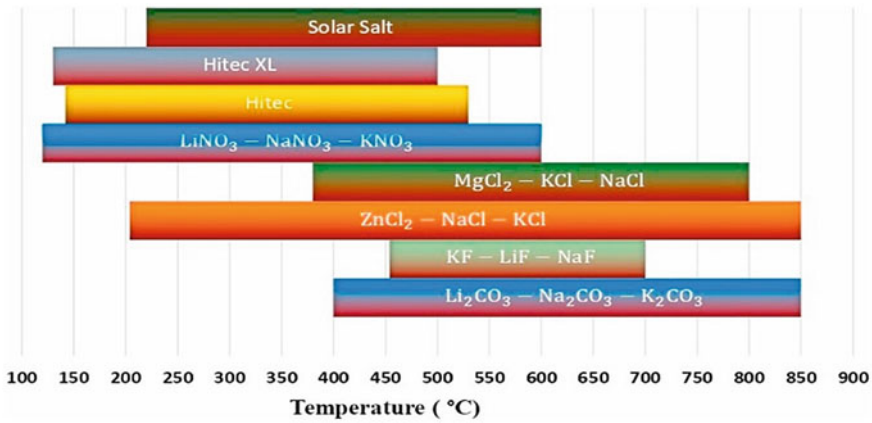
Fig. 11.10 Stability limits and Melting point of different molten salts [55]

11.6.1 Molten Salt Thermal Energy Storage in CSP System—Transition from Coal to Renewables Energy Resources

The coal-based power plants have adverse effect on the environment and it remains a challenge to integrate such power plants together with renewable energy systems to the national grid due to their complex structure and other infrastructural and technical issues with the most prominent one as the intermittent nature of renewable resources. Therefore, the key issue remains maintaining the stability of renewables into the national power grid. Along the same lines for coal fed power plant combined with renewables the contribution of coal fueled plants during the "dark cold doldrums", (refers to cold spells concurring along the meteorological situation and resulting in an inadequate power production from wind and solar plants). Researchers studied the model for Germany and opined that role of electricity from renewables for energy production is required to provide "mid-term" flexibility, becomes immensely important with gradual and steady increase in shares of renewables in the national energy mix. That can be boosted with the aid of storage systems added to renewable energy systems. Among the renewables the CSP offers large scale power plants with large scale energy storage systems courtesy molten salts. The conventional storage systems for PV systems and wind energy storage systems mostly in practice are limited to electrochemical batteries at for medium scale plants and the hydro-pumped technology. The primary issue with former lies in its cost whereas the issue with the latter technology lies in its sitting factors involving complex geographical constraints make it a difficult choice.

CSP Concentrating solar power are best known for the production of electricity from the solar energy. The working principle of a CSP system is already explained in the above section. It is found that the integration of molten salt TES in CSP system

meets the electricity demand and overcome the base and peak load. The different type of high temperature thermal energy storage media that contains solid media.

11.6.2 Molten Salt Storage for Residential Heating Applications

Molten salt thermal energy storage coupled with thermal for heating purpose plays a significant role in areas where resident pays a significant amount in energy bills particularly for space/floor heating. For heating applications, among the CSP types, parabolic trough collector is most commonly used as well as the most matured and adopted technology for such applications. For direct heating usually synthetic salts are used operating in the range of 200 to 400 ^{0}C. For indirect heating molten salts are used. PTC are used for direct and indirectly heating [56, 57]. For residential application mostly Nitrate salts are used for floor heating due to their suitable temperature range for operation [58, 59]. A case study comprising of two different models for temperature conditions in Australia was proposed in a study by [56]. A two-tank direct system was utilized in the model owing to its higher efficiency which in turn is because of less heat loss in heat exchange compared to indirect systems. Conclusions of their mathematical state that the system to be feasible under heat losses with changing solar radiation. For more in-depth study please refer to their work [56]. for example, pressurized water, molten salt, latent heat, and thermo-chemical. Mostly CSP system use sensible heat storage with molten salts. For example, to the hot water to the residential sector, the storage tank the molten salt can be used for the storage of hot water up to 550 °C. Efficient storage systems like molten salt storage systems are essential to stabilize the grid, aid enhance the base-load capabilities and produce dependable and consistent electricity as per the with the demand (Fig. 11.11).
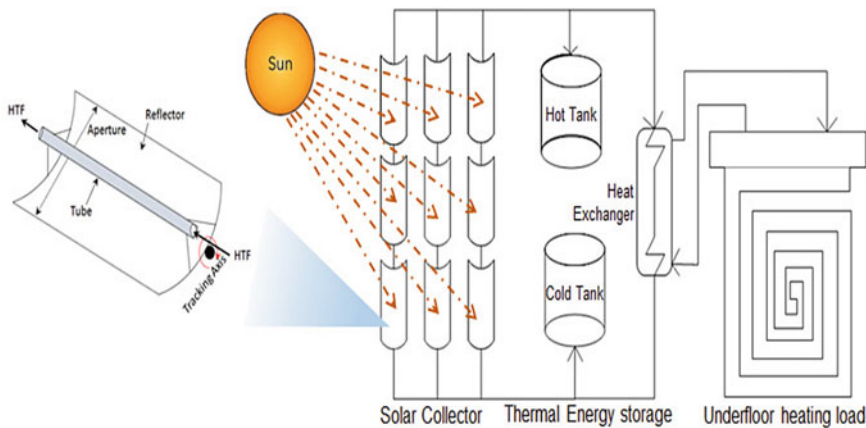

Fig. 11.11 Residential heating system using PTC

11.6.3 Molten Salt Storage for Industrial Processes

An application of the molten salt thermal energy storage is to improve the energy efficiency of the industries. Particularly the industries that operates on very high temperature and thermal losses are common and significant. Wasted heat can be recovered and used as needed, however, such applications are not yet common and research is needed for such applications for process optimization in such industries for examples the waste heat recovery in flue gas, better heat integration of batch processes, backup heat, cushioning of instable waste heat streams and stabilizing the supply of steam along with improved electrical load management with power-to-heat and TES as shown in Fig. 11.12.

11.7 Numerical Modeling and Simulation Techniques

The key aspects of design, operation, and performances of MSTES system and its model formulation depends upon the use of molten salt either as only HTF or in combination with types of storage material. Molten salt mixtures are a suitable choice as heat transfer fluid and as storage material with other materials such as sensible heat, latent heat or combined sensible-latent heat storage media in a variety of ways. The purpose of choosing different storage in combination with molten salt is to enhance to effective charge/discharge efficiency and storage capacity. It is important to analyze and compare the numerical models which enable to quantify the main physical phenomena involved in molten salt thermal energy storage operation. The model formation of molten salt TES systems based on mass, momentum and energy conservation laws enable us to calculate the Temperature, Pressure and Velocity variables as a function of time and location. Moreover, the developed correlations based different experimental and numerical data enable to calculate HTF/solid and HTF/wall effective thermal conductivity, heat transfer coefficients and pressure drop in MSTES tanks.
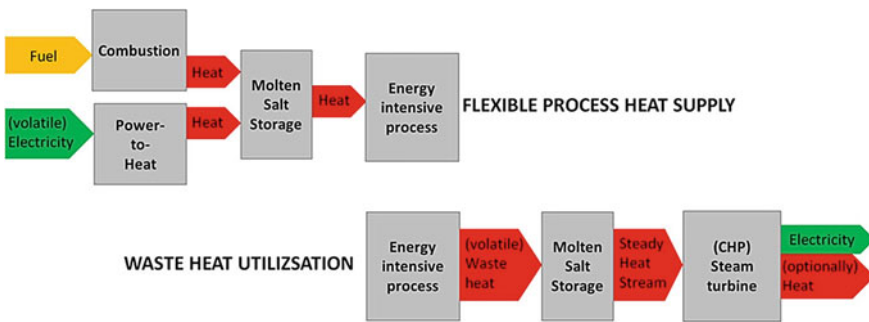

Fig. 11.12 Molten salt storage technology in industrial processes

The working methodology for modeling of MSTES system has following main steps.

(1) Selection of storage material with properties suiting high temperature applications while keeping it cost effective.

  (a) Structured filler material is used to avoid the issue of thermal ratcheting
  (b) Sensible heat storage material having stable thermos-physical properties and cheap easily available.
  (c) Latent heat material is selected having combination of melting point and heat of fusion suiting high temperature in combination with molten salt.
  (d) Molten salt as HTF should be chemically compatible with the storage media

(2) To develop numerical model and validate it using experimental data.
(3) Develop the cost model for economic analysis of the proposed MSTES system.
(4) Thermal and economic performance comparison of the proposed TES unit with existing TES systems.
(5) Then perform parametric sensitivity analysis using validated numerical model.
(6) Performance optimization.

To evaluate the temperatures of fluid and storage material at a particular location and time in the storage tank; the mathematical models for MSTES systems involves the derivation of proper governing equations following energy conservation laws for the selected control volumes in a storage tank during charge or heat recovery cycles; identification of the boundary condition requirements to be applied on the governing equations; and realizing the most suitable mathematical method based on the physics of storage material involved to solve the governing equations with greater accuracy. The researchers have reported a number models which can be used to address different configurations of molten salt thermal storage systems, including only one fluid (molten salt only) TES system, dual media (molten salt and solid storage) sensible heat TES system, and dual-media (molten salt and PCM) latent heat thermal storage systems.

11.7.1 Mathematical Models

The most common energy balance model for modeling packed thermal storage systems is two phase Schumann's model, comprised of two separate equations for fluid and storage material [60]. It is a one dimensional two-phase energy balance model assuming ideal plug flow of the HTF through storage tank and neglecting resistance due to conduction in the solid particles [61]. The heat transfer model can be expressed using the following set of governing equations for solid and fluid phases, respectively.

$$\frac{\partial}{\partial t}(\rho_f \varepsilon T_f) + \frac{\partial}{\partial x}(\rho_f u A_f T_f) = \frac{h_v A}{C_{p,f}}(T_s - T_f) \tag{11.2}$$

$$\frac{\partial}{\partial t}\Big(\rho_S(1-\varepsilon)C_{p,S}A_f T_S\Big) = h_v A(T_f - T_S) \tag{11.3}$$

Where f and s denote the fluid and solid phase, respectively with x as the *axial coordinate* along flow direction. The governing equations are coupled by a heat transfer coefficient [60] quantifying the amount of heat transferred through convection mode between the HTF and solid surface of particles. u is the superficial velocity of fluid in the packed bed, ε is the porosity; T, ρ and C_p, denotes Temperature, density and specific heat, respectively.

11.7.2 Single Phase Models

Vortmeyer and Schaefer [62] using two-phase continuous solid (C-S) model derived a single equation correlation for energy balances in a packed-bed and it was based on interaction of fluid–solid phases without considering thermal equilibrium between the phases. The model assumed that fluid phase can be neglected owing to the condition that the value of thermal capacity for HTF is very less than that of the solid phase. assuming that $\partial^2 T_f/\partial z^2 = \partial^2 T_s/\partial z^2$, holds the following expression:

$$(1-\varepsilon)\rho_s C_{p_s}\frac{\partial T_s}{\partial t} = \left(k_0 + \frac{G^2 C_{p_f}^2}{h_p a}\right)\frac{\partial^2 T_s}{\partial z^2} - GC_{p_f}\frac{\partial T_s}{\partial z} \tag{11.4}$$

where the axial effective thermal conductivity k_o, is defined as mass flux rate of fluid and was proposed by Yagi et al. [63]. The ratio of specific heat capacity between fluid-solid phases was indicated by Vortmeyer and Schaefer in their investigation.

For the TES systems wherein property of the fluid thermal capacity cannot be ignored, an assumption is made thermal boundary layer moves across the storage tank with constant velocity and is expressed as

$$w = \frac{GC_{p_f}}{\varepsilon \rho_f C_{p_f} + (1-\varepsilon)\rho_s C_{p_s}} \tag{11.5}$$

The single phase model proposed by Vortmeyer and Schaefer [62] can be expressed as

$$\begin{aligned}
\left(\varepsilon \rho_f C_{p_f} + (1-\varepsilon)\rho_s C_{p_s}\right)\frac{\partial T_f}{\partial t} = &-GC_{p_f}\frac{\partial T_f}{\partial z} \\
&+ \left(k_0 + \frac{(w(1-\varepsilon)\rho_s C_{ps})^2}{h_p a}\right)\frac{\partial^2 T_f}{\partial z^2}
\end{aligned}$$

$$+ \frac{w(1-\varepsilon)^2 \rho_s C_{p_s} k_s}{h_p a} \frac{\partial^3 T_s}{\partial z^3} \tag{11.6}$$

The last term of order three term in this equation is relatively insignificant. Thermal losses accruing from the walls of tank can be assessed for by evaluating the overall heat transfer coefficient and it involves the internal convection between the wall of the tank and hot fluid flow, Thermal conduction resistance offered due to insulation on the tank wall and the heat losses to ambient air due to convection on outer side of the tank.

11.7.2.1 Two-Phase Continuous Solid Phase Model (C-S)

The Schumann's model introduced earlier [60] can be applied to flow regimes with high Reynolds numbers. However, for flows involving low Reynolds numbers, a new correlation is added to include the effect of axial conduction for solid phase should be included in Eqs. (11.1) and (11.2). The thermal diffusion effect for fluid phase is also included [64]; nevertheless, this effect might be neglected with assumption that the value of thermal conductivity for fluid phase has smaller value as compared to that in the solid phase [65, 66]. Recently, Littman et al. proposed that bed cross sectional should be considered while evaluating the thermal conductivity for both fluid and solid phases. Accordingly, the set of governing equations for C-S model becomes:

$$\frac{\partial T_f}{\partial t} = \frac{k_{f_{eff}}}{\varepsilon \rho_f C_{p_f}} \frac{\partial^2 T_f}{\partial z^2} - u \frac{\partial T_f}{\partial z} + \frac{h_p a}{\varepsilon \rho_f C_{p_f}} \left(T_s - T_f \right) \tag{11.7}$$

$$\frac{\partial T_s}{\partial t} = \frac{k_{s_{eff}}}{(1-\varepsilon)\rho_s C_{p_s}} \frac{\partial^2 T_s}{\partial z^2} - \frac{h_p a}{(1-\varepsilon)\rho_s C_{p_s}} \left(T_s - T_f \right) \tag{11.8}$$

where k_{se} and k_{fe} denote the value of effective thermal conductivity in solid and fluid phases, respectively.

C-S model can also be expanded to include the effect of radial thermal conduction in fluid and solid phases, yet to simplify the complex calculations this effect is ignored for fluid phase by some authors [64]. This model is preferred when heat transfer through walls of the tank is significant and inducing large thermal losses.

11.7.2.2 Two Phase Continuous Solid Phase Model (C-S)

More precise approach should be adopted for characterizing the thermal performance of a thermal storage system and it is proposed by the two phase *Dispersed Concentric* model. The two phase D-C model proposed by the researchers [67], presented a numerical model governed by set of partial differential equations using appropriate initial and boundary conditions. The developed numerical model considers intra

particle heat conduction with radial symmetry and assumes dispersed plug fluid flow regime. Few years later, Gunn and De Souza [68], proposed an investigation regarding the response of thermal frequency for the evaluation of dispersion coefficients in a packed bed of particles and this was proposed with the assumption that there exists a radial symmetry of the thermal gradients within the elements. Accordingly, the governing equations for D-C model proposed by Handley and Heggs [67] is written as:

$$\frac{\partial T_f}{\partial t} = \kappa_{f_{ax}} \frac{\partial^2 T_f}{\partial z^2} - u \frac{\partial T_f}{\partial z} + \frac{h_p a}{\varepsilon \rho_f C_{p_f}} \left(T_s|_{r=R} - T_f \right) \tag{11.9}$$

$$\frac{\partial T_s}{\partial t} = \kappa_s \frac{1}{r^2} \frac{\partial}{\partial r} \left(r^2 \frac{\partial T_s}{\partial r} \right) \tag{11.10}$$

where, K_s denotes thermal diffusivity constant for solids and is expressed as

$$\kappa_s = \frac{k_s}{\rho_s C_{p_s} (1 - \varepsilon)} \tag{11.11}$$

And K_{fa} denotes dispersion coefficient. Wakao [69] developed following correlation for fluid flow regimes with low Reynolds number and predicted results with good accuracy.

$$k_{fax} = \frac{k_{eff_{ax}}}{\varepsilon C_{p_f} \rho_f} \tag{11.12}$$

The unknown temperature variable for the solid particle is evaluated by using convection boundary conditions and is governed by heat transfer coefficient as expressed below

$$k_s \left(\frac{\partial T_s}{\partial r} \right) = -h_p (T_s - T_f) \text{ at } r = R \tag{11.13}$$

where r and R represents the radial coordinates and sphere radius, respectively.

11.7.3 Performance Parameters

11.7.3.1 Exergy

Exergy efficiency (ψ_{ex}) is used to calculate overall exergy balance and the energy recovery potential of the sensible heat MSTES system and can be defined the ratio of total exergy utilized ($Ex_{rec,d}$) during discharge operation to the overall exergy provided during charge operation ($Ex_{rec,c}$).

$$\psi_{ex} = \frac{Ex_{\text{rec,d}}}{Ex_{\text{sup,c}}} \tag{11.14}$$

where

$$Ex_{\text{rec,d}} = \int_{t_{0,d}}^{t_{\text{final,d}}} \dot{m}_f \, c_{p,f} \left(T_{f,\text{out}} - T_{f,\text{inlet}} - T_{\text{amb}} \ln \frac{T_{f,\text{out}}}{T_{f,\text{inlet}}} \right) dt \tag{11.15}$$

$$Ex_{\text{sup,c}} = \int_{t_{0,c}}^{t_{\text{final,c}}} \dot{m}_f \, c_{p,f} \left(T_{f,\text{out}} - T_{f,\text{inlet}} - T_{\text{amb}} \ln \frac{T_{f,\text{out}}}{T_{f,\text{inlet}}} \right) dt \tag{11.16}$$

The subsequent exergy flow is quantified as the exergy difference at entrance the storage tank and exit with the HTF.

The overall impact of the thermal energy that is recovered from the MSTES system during the discharge operation evaluated by quantifying the discharge efficiency. It is the ratio useful heat energy extracted from the thermal storage system during discharge period to the maximum quantity of thermal energy stored before the start of discharging operation [70]. It is given by the correlation as

$$\eta_d = \frac{\int_0^{t_c} \dot{m} C_p \left(T_{f,\text{out}} - T_{f,\text{inlet}} \right) dt}{Q_i} \tag{11.17}$$

where t_c is the time duration after which it is cutoff time in discharging process when the temperature of molten salt working as HTF at outlet falls below the threshold temperature value. This threshold value is dependent upon on process and application type of process or application to which thermal energy storage is integrated. To prevent freezing of molten salt during the whole operating cycles minimum temperature must be maintained above the solidification temperature and usually it is above 250 °C. It is noteworthy that practical effectiveness of the TES system is significantly influenced by the threshold temperature of the process or application [71].

11.7.3.2   Thermocline Thickness

Thermocline thickness is amongst the most critical parameters used to quantify the thermal performance of single tank molten salt thermal energy storage system during discharge process and can be defined as the length covered by thermocline region [11].

$$W_{\text{tc}} = \begin{cases} H(T_h) - H(T_c) & (T_{f,\text{inlet}} \le T_c) \& (T_{f,\text{out}} \ge T_h) \\ H(T_h) - 0 & (T_{f,\text{inlet}} > T_c) \\ H - H(T_c) & (T_{f,\text{out}} < T_h) \end{cases} \tag{11.18}$$

Where Tc, is the critical cold temperature and Th, is the critical hot temperature.

11.7.3.3 Pumping Energy

The amount of energy required to propel the molten salt as heat transfer fluid is calculated from the correlation [65]

$$E_{\text{pump}} = \int\limits_0^{t_d} \frac{A\Delta p G}{\rho_f} dt \tag{11.19}$$

To quantify the pressure drop across a thermal storage tank following relation is used [67]

$$\Delta P = \frac{2(1-\varepsilon)HG^2}{r\,\varepsilon^3\rho}\left(1.75 + 300\frac{\mu}{Gr}\right)^c \tag{11.20}$$

11.7.3.4 Overall Efficiency

Overall efficiency of the TES system is evaluated by including pumping work during charging and discharging cycles. It is the ratio of amount of heat energy extracted from the thermal storage tank for a single charging/discharging cycle to the sum of heat energy stored initially during charging and pumping power needed [64].

$$\eta_{Overall} = \frac{E_{\text{rec}}}{E_{\text{stored}} + E_{\text{pump,c}} + E_{\text{pump,d}}} \tag{11.21}$$

Where the charge efficiency is the ratio of the amount of heat energy stored in storage media as the charging process is completed (E_{stored}) to the sum of overall heat input (E_{overall}) and pumping energy used ($E_{\text{pump,c}}$) [64]:

$$\eta_C = \frac{E_{\text{stored}}}{E_{\text{overall}} + E_{\text{pump,C}}} \tag{11.22}$$

And the discharging efficiency can be defined as the amount of energy extracted or recovered (E_{rec}) during discharge process to the summation of thermal energy stored initially and pumping work ($E_{\text{pump,d}}$):

$$\eta_d = \frac{E_{\text{rec}}}{E_{\text{stored}} + E_{\text{pump,d}}} \tag{11.23}$$

The charging and discharging process has no fixed operational time but it is controlled by setting a threshold temperature value of heat transfer fluid exiting the molten salt thermal energy storage system.

11.8 Numerical Modeling Using CFD Tools

Computational fluid dynamic (CFD) software (Like Fluent, CFX, COMSOL Multiphysics etc.) and self-developed programming using coding (Like, C++, MATLAB, FORTRON etc.) to investigate the fluid flow phenomenon and heat transfer mechanisms is a powerful computer aided engineering tool. These commercially available CFD software are efficient tested tool used to simulate the different fluid dynamics and engineering applications, e.g., heating, ventilation, air conditioning (HVAC), building thermal management, cooling technology etc. These tools to test and efficiently design molten salt thermal energy storage system is believed to be an effective method to save time and money.

The numerical model of MSTES systems based on local thermal non-equilibrium (LTNE) Schumann model equations, are formulated using energy balance equations as discussed in the previous section. The governing equations are solved using a set initial and boundary conditions. The geometrical configuration of computational domain consists of 2-D/3-D control volume divided into small cells called meshing. In some CFD software like Ansys FLUENT we also have to option to input customized parameters to the built-in model as User Defined Equations (UDF) or User Defined Scalar (UDS). With a set of different discretization schemes available. The formulated energy balance equations are coded in C++ language and compiled using C compiler. Depending upon the order of equation, first order or higher order implicit/explicit schemes are employed for the transient formulation of temporal terms. Usually, the numerical model of MSTES system assumes fluid flow as laminar/turbulent, Newtonian incompressible and its thermo-physical properties are set constant/variable for the considered temperature range. Consequently, the governing equations for molten salt thermal energy system are solved.

For instance, we can model the fluid flow and heat transfer problem of molten salt TES is modeled in FLUENT. In FLUENT software there are two main solvers for numerical computations, one is density-based coupled solver and the other is pressure-based solver [14, 15]. It employs the computational algorithm that is classified as projection method which belongs to the general class of these methods [16, 72]. This method fulfills the conditions of continuity equation (conservation of mass) for the velocity field by introducing pressure correction, i.e., the pressure equation is solved. Here the formulated pressure equation (derived from continuity and momentum equation) is solved along such lines that the corrected velocity field from the pressure satisfies the continuity equation. The formulated nonlinear and coupled governing equations are solved repeatedly involving a number of iterations until solution is converged. The overview of this solution procedure is illustrated in Fig. 11.13. Moreover, the figure shows the algorithm of two types of pressure-based solvers, i.e., segregated algorithm and the coupled algorithm.

The interpolation scheme of the face pressure for the momentum conservation may use the semi-implicit pressure-linked equation (SIMPLE) or options available in the numerical tool. The numerical model is usually considered as converged as the residuals for the flow variables (Temperature, Velocity) approach well defined
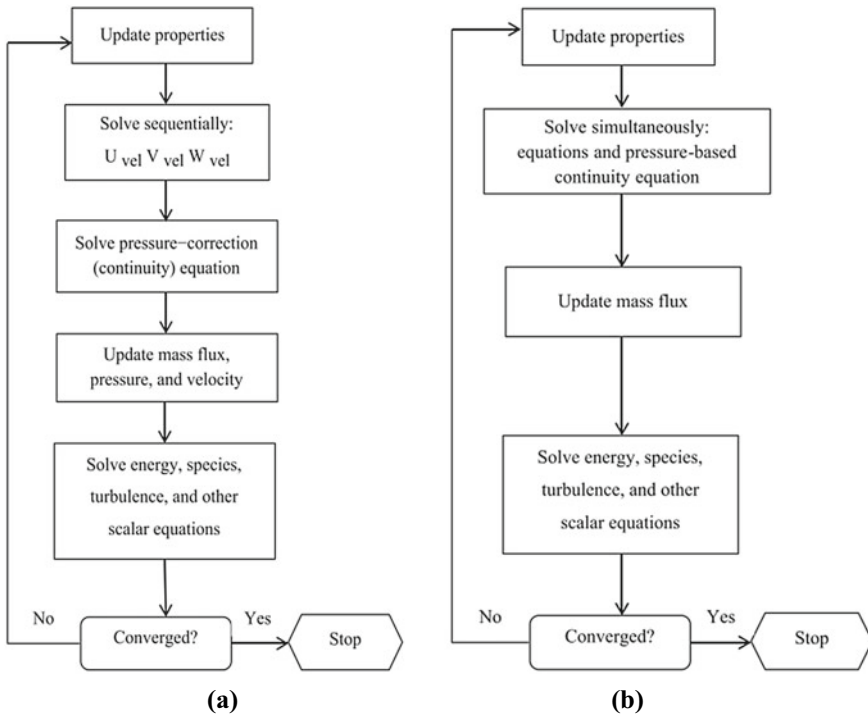
Fig. 11.13 Overview of pressure based solution methods. **a** Pressure-based segregated algorithm. **b** Pressure based coupled algorithm [12]

values less than 10^6 and 10^3, respectively. An overview of this solution procedure is illustrated in Fig. 11.14.

11.8.1 Setting up the Problem and Models Validation

Before setting up the heat transfer and fluid flow problem of thermal energy storage in a CFD tool for numerical simulations, first the physical computational domain is sketched and then it is meshed in a specific grid generation tool which is compatible with the selected software like ICEM CFD, GAMBIT, Ansys workbench. The grid generation software has the capability to import and process files of other programs like Solidworks or Auto CAD. After grid generation of the computational domain, the names selections of boundary layers and type of zones are defined. The file containing mesh is then imported in the FLUENT software to setup the numerical problem.

To ensure that the accuracy of the developed model is right, it is necessary to validate that the performance results are independent of the influence of mesh size.

Fig. 11.14 Overview of the solution procedure using numerical methods [73, 74]
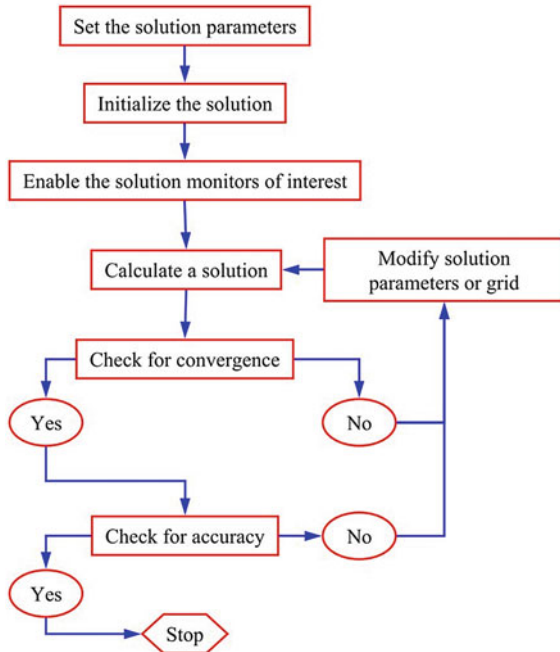
It is carried out by applying different mesh sizes and time-steps in the developed numerical model and then check the accuracy of numerical results. It is a general practice that smaller mesh sizes and time steps are favored in computers to improve the accuracy of simulation results. But it can be applied for simple problems and for complex problems right size of grid size must be used in order to reduce the computational time and at the same time maintain the calculation accuracy. It is done by performing grid independence tests. It is also very important to validate the developed numerical model before performing detailed analysis. The numerical energy model established is then validated against experimental data from previously published research or by developing a prototype.

11.9 Recent Trends and Challenges in TES

Molten salts as a heat transfer fluid or storage material are utilized in a variety of engineering fields, with specialized role involving high-temperature thermo-fluid applications. A large number of molten salt based thermal energy storage technologies has been explored, demonstrated and/or deployed in a variety of applications but there is need to investigate MSTES units with a specific emphasis on thermal storage materials perspective. A thorough analysis on the state-of-the-art developed technologies will help highlight the issues involved in the commercialization and innovation

of these technologies. The major penetration of molten salt thermal energy storage system for commercial scale applications is in CSP power plants. The development path of CSP technology has been driven by the deployment of the storage media and heat transfer fluid. Molten salts are utilized as working fluids in different high temperature industrial processing units, such as for production of fuel, for manufacturing of exotic ceramics, and for the processing of waste materials in pyrolysis. The deployment of molten salt as a storage media and HTF finds its applications in in the fields of Concentrated Solar Power, modern nuclear reactors, fuel cycles in nuclear applications and enhancement of oil recovery operations. For a wide range of industrial applications molten salt can be used as a storage media and HTF to provide flexibility in operation for grid using CSP technology to meet peak load demand. The use of molten salts as thermal energy storage system has gained the attention of researchers for next generation CSP power plants because of following favorable characteristics

- Salts possess low vapor pressure
- Large temperature ranges of application
- It is safe to operate and handle
- Environmental footprint offered by salt-based TES systems is minimal
- Offers moderate levelized cost of energy when integrated with other renewable source of energy in comparison to traditional HTF (thermal oils and ionic liquids).

The use of solar Salt mixture (40% KNO_3–60% $NaNO_3$) mixture as heat transfer fluid or heat storage filler is considered as vital in CSP power plants as being technologically most mature and abundantly used molten salt. However, it has been facing critical problems of lower specific heat capacities and penetrating corrosion. To overcome these drawbacks more investigations should be carried out to come up with alternate unconventional options. Different mixtures of nitrate salts, fluorides, carbonates and chlorides should be explored with a focus on enhancing thermos physical properties, improve thermal stability range, and to minimize the issues of corrosion during its operational life time.

The use of different eutectic salt mixtures in thermal storage systems is very advantageous due its favored thermophysical properties. However, the presence of impurities such O_2, H^+ and OH^-, adversely the thermal performance of MSTES systems and also accelerate corrosion processing metallic storage containers. Researchers need to develop new techniques which will be able to quantify, characterize, and, most importantly, the vindication and control of these impurities.

The use of Molten Salt based TES systems in the next generation concentrated solar thermal power plants are being used with new formulated thermal storage materials at higher temperature (>570 °C) and with more stable thermophysical properties. However, high levelized cost of electricity (LCOE) of the existing CSP plants with these newly developed molten salts presents crucial challenge for the researchers.

11.10 Chapter Summary

Molten salt TES systems provides with the flexibility to make intermittent resources of energy dispatchable, more reliable and more competitive on demand. The applications of molten salts/eutectics mixtures as engineering thermo-fluids and heat storage fillers have gained noteworthy attention in the last few years. However, for the deployment of molten salts in high temperature engineering applications especially as thermal storage system, it is crucial to characterize stable thermo-physical properties for a wide range of operating conditions. Moreover, thermal performance of MSTES systems is characterized by longer effective charging/discharging time, utilization factor, lower pumping energy and reduced thermocline thickness. Heat transfer and fluid flow the problems of any type of molten salt TES system can be modeled efficiency by selecting appropriate energy balance model. The use of CFD tool for numerical modeling of MSTES tank is a cost-effective method to predict thermal performance and pressure drop over extended number of charge/discharge cycles, and is essential for assisting in the design and dimensioning of different thermal storage components. The development progress of MSTES system can be made at a quicker pace by addressing the issues of selection/optimization salt mixtures, properties characterization, introducing novel corrosion control techniques for construction materials, and lowering LCOE.

References

1. J. Rockström, O. Gaffney, J. Rogelj, M. Meinshausen, N. Nakicenovic, H.J. Schellnhuber, A roadmap for rapid decarbonization. Science **80**, 355–1269 LP–1271 (2017). https://doi.org/10.1126/science.aah3443
2. Ş Kılkış, G. Krajačić, N. Duić, M.A. Rosen, M.A. Al-Nimr, Advancements in sustainable development of energy, water and environment systems. Energy Convers. Manage. **176**, 164–183 (2018). https://doi.org/10.1016/j.enconman.2018.09.015
3. Energy Technology Perspectives 2017. OECD (2017). https://doi.org/10.1787/energy_tech-2017-en
4. L. Miró, J. Gasia, L.F. Cabeza, Thermal energy storage (TES) for industrial waste heat (IWH) recovery: A review. Appl. Energy **179**, 284–301 (2016). https://doi.org/10.1016/J.APENERGY.2016.06.147
5. P. Murray, K. Orehounig, D. Grosspietsch, J. Carmeliet, A comparison of storage systems in neighbourhood decentralized energy system applications from 2015 to 2050. Appl. Energy **231**, 1285–1306 (2018). https://doi.org/10.1016/J.APENERGY.2018.08.106
6. A. Gil, M. Medrano, I. Martorell, A. Lázaro, P. Dolado, B. Zalba, et al., State of the art on high temperature thermal energy storage for power generation. Part 1-Concepts, materials and modellization. Renew. Sustain. Energy Rev. **14**, 31–55 (2010). https://doi.org/10.1016/j.rser.2009.07.035
7. I. Dincer, M. Rosen, *Thermal Energy Storage: Systems and Applications* (John Wiley & Sons, 2002)
8. J. Gasia, L. Miró, L.F. Cabeza, Review on system and materials requirements for high temperature thermal energy storage. Part 1: General requirements. Renew. Sustain. Energy Rev. **75**, 1320–38 (2017). https://doi.org/10.1016/j.rser.2016.11.119

9. R. Jacob, M. Belusko, M. Liu, W. Saman, F. Bruno, Using renewables coupled with thermal energy storage to reduce natural gas consumption in higher temperature commercial/industrial applications. Renew. Energy **131**, 1035–1046 (2019). https://doi.org/10.1016/J.RENENE.2018.07.085

10. Inc B. Waste Heat Recovery: Technology Opportunities in the US Industry. Waste Heat Recover Technol Oppor US Ind 1–112 (2008). https://doi.org/10.1017/CBO9781107415324.004

11. Y. Lin, G. Alva, G. Fang, Review on thermal performances and applications of thermal energy storage systems with inorganic phase change materials. Energy **165**, 685–708 (2018). https://doi.org/10.1016/J.ENERGY.2018.09.128

12. A.A. Al-Abidi, S. Bin Mat, K. Sopian, M.Y. Sulaiman, A.T. Mohammed, CFD applications for latent heat thermal energy storage: A review. Renew. Sustain. Energy Rev. **20**, 353–363 (2013). https://doi.org/10.1016/j.rser.2012.11.079

13. S. Kapila, A.O. Oni, A. Kumar, The development of techno-economic models for large-scale energy storage systems. Energy **140**, 656–672 (2017). https://doi.org/10.1016/j.energy.2017.08.117

14. D. Gibb, M. Johnson, J. Romaní, J. Gasia, L.F. Cabeza, A. Seitz, Process integration of thermal energy storage systems—Evaluation methodology and case studies. Appl. Energy **230**, 750–760 (2018). https://doi.org/10.1016/j.apenergy.2018.09.001

15. S. Kuravi, J. Trahan, D.Y. Goswami, M.M. Rahman, E.K. Stefanakos, Thermal energy storage technologies and systems for concentrating solar power plants. Prog. Energy Combust. Sci. **39**, 285–319 (2013). https://doi.org/10.1016/j.pecs.2013.02.001

16. M. Jiménez-Arreola, R. Pili, F. Dal Magro, C. Wieland, S. Rajoo, A. Romagnoli, Thermal power fluctuations in waste heat to power systems: An overview on the challenges and current solutions. Appl. Therm. Eng. **134**, 576–584 (2018). https://doi.org/10.1016/j.applthermaleng.2018.02.033

17. B. Nienborg, S. Gschwander, G. Munz, D. Fröhlich, T. Helling, R. Horn et al., Life Cycle Assessment of thermal energy storage materials and components. Energy Proc. **155**, 111–120 (2018). https://doi.org/10.1016/J.EGYPRO.2018.11.063

18. A. Kylili, P.A. Fokaides, A. Ioannides, S. Kalogirou, Environmental assessment of solar thermal systems for the industrial sector. J. Clean. Prod. **176**, 99–109 (2018). https://doi.org/10.1016/J.JCLEPRO.2017.12.150

19. N. Ahmed, K.E. Elfeky, L. Lu, Q.W. Wang, Thermal and economic evaluation of thermocline combined sensible-latent heat thermal energy storage system for medium temperature applications ☆. Energy Convers. Manage. **189**, 14–23 (2019). https://doi.org/10.1016/j.enconman.2019.03.040

20. A. Crespo, C. Barreneche, M. Ibarra, W. Platzer, Latent thermal energy storage for solar process heat applications at medium-high temperatures—A review. Sol. Energy (2018). https://doi.org/10.1016/J.SOLENER.2018.06.101

21. N. Ahmed, K.E. Elfeky, L. Lu, Q.W. Wang, Thermal performance analysis of thermocline combined sensible-latent heat storage system using cascaded-layered PCM designs for medium temperature applications. Renew. Energy **152**, 684–697 (2020). https://doi.org/10.1016/j.renene.2020.01.073

22. N. Ahmed, K.E. Elfeky, M.A. Qaisrani, Q.W. Wang, Numerical characterization of thermocline behaviour of combined sensible- latent heat storage tank using brick manganese rod structure impregnated with PCM capsules. Sol. Energy **180**, 243–256 (2019). https://doi.org/10.1016/j.solener.2019.01.001

23. K.E. Elfeky, A.G. Mohammed, N. Ahmed, L. Lu, Q. Wang, Thermal and economic evaluation of phase change material volume fraction for thermocline tank used in concentrating solar power plants. Appl. Energy **267**(2020). https://doi.org/10.1016/j.apenergy.2020.115054

24. K.E. Elfeky, X. Li, N. Ahmed, L. Lu, Q. Wang, Optimization of thermal performance in thermocline tank thermal energy storage system with the multilayered PCM (s) for CSP tower plants ☆. Appl. Energy **243**, 175–190 (2019). https://doi.org/10.1016/j.apenergy.2019.03.182

25. Z. Wan, J. Wei, M.A. Qaisrani, J. Fang, N. Tu, Evaluation on thermal and mechanical performance of the hot tank in the two-tank molten salt heat storage system. Appl. Therm. Eng. **167**, 114775 (2020)

26. M.A. Qaisrani, J. Wei, J. Fang, Y. Jin, Z. Wan, M. Khalid, Heat losses and thermal stresses of an external cylindrical water/steam solar tower receiver. Appl. Therm. Eng. **163**, 114241 (2019)
27. Z. Wan, J. Fang, N. Tu, J. Wei, M.A. Qaisrani, Numerical study on thermal stress and cold startup induced thermal fatigue of a water/steam cavity receiver in concentrated solar power (CSP) plants. Sol. Energy **1**(170), 430–441 (2018 Aug)
28. M.A. Qaisrani, J. Fang, Y. Jin, Z. Wan, N. Tu, M. Khalid, M.U. Rahman, J. Wei, Thermal losses evaluation of an external rectangular receiver in a windy environment. Sol. Energy **15**(184), 281–291 (2019 May)
29. M.A. Qaisrani, J. Wei, L.A. Khan, Potential and transition of concentrated solar power: A case study of China. Sustain. Energy Tech. **44**, 101052 (2021)
30. J. Gasia, L. Miró, L.F. Cabeza, Materials and system requirements of high temperature thermal energy storage systems : A review. Part 2 : Thermal conductivity enhancement techniques. Renew. Sustain. Energy Rev. **60**, 1584–601 (2016). https://doi.org/10.1016/j.rser.2016.03.019
31. M. Liu, W. Saman, F. Bruno, Review on storage materials and thermal performance enhancement techniques for high temperature phase change thermal storage systems. Renew. Sustain. Energy Rev. **16**, 2118–2132 (2012). https://doi.org/10.1016/j.rser.2012.01.020
32. D. Fernandes, F. Pitié, G. Cáceres, J. Baeyens, Thermal energy storage: "How previous findings determine current research priorities." Energy **39**, 246–257 (2012). https://doi.org/10.1016/j.energy.2012.01.024
33. B. Cárdenas, N. León, Latent heat based high temperature solar thermal energy storage for power generation. Energy Proc. **57**, 580–589 (2014). https://doi.org/10.1016/j.egypro.2014.10.212
34. W. Ding, T. Bauer, Progress in research and development of molten chloride salt technology for next generation concentrated solar power plants. Engineering **7**, 334–47 (2021). https://doi.org/10.1016/j.eng.2020.06.027
35. S.M. Flueckiger, Z. Yang, S.V. Garimella, Review of molten-salt thermocline tank modeling for solar thermal energy storage. Heat Transf. Eng. **34**, 787–800 (2013)
36. R.G. Reddy, Molten salts: Thermal energy storage and heat transfer media. J. Phase Equilibria Diffus. **32**, 269–270 (2011). https://doi.org/10.1007/s11669-011-9904-z
37. F. Carducci, A. Giovannelli, M. Renzi, G. Comodi, Improving flexibility of industrial microgrids through thermal storage and HVAC management strategies. Energy Proc. **142**, 2728–2733 (2017). https://doi.org/10.1016/J.EGYPRO.2017.12.217
38. Lazard. Lazard's levelised cost of storage v2.0. Clim. Policy **6**, 600–6 (2016). https://doi.org/10.1080/14693062.2006.9685626
39. D. Zhou, C.Y. Zhao, Y. Tian, M.C. Lott, S.-I. Kim, P. Eames et al., Technology Roadmap. Springer Reference **92**, 24 (2013). https://doi.org/10.1007/SpringerReference_7300
40. K. Nithyanandam, R. Pitchumani, Cost and performance analysis of concentrating solar power systems with integrated latent thermal energy storage. Energy **64**, 793–810 (2014). https://doi.org/10.1016/j.energy.2013.10.095
41. S. Thaker, A. Olufemi Oni, A. Kumar, Techno-economic evaluation of solar-based thermal energy storage systems. Energy Convers. Manage. **153**, 423–434 (2017). https://doi.org/10.1016/j.enconman.2017.10.004
42. S. Kalaiselvam, R. Parameshwaran, Thermal energy storage technologies for sustainability : Systems design, assessment, and applications. n.d
43. L.F. Cabeza, Advances in thermal energy storage systems : Methods and applications. n.d
44. G. Alva, L. Liu, X. Huang, G. Fang, Thermal energy storage materials and systems for solar energy applications. Renew. Sustain. Energy Rev. **68**, 693–706 (2017). https://doi.org/10.1016/j.rser.2016.10.021
45. A.L. Nash, A. Badithela, N. Jain, Dynamic modeling of a sensible thermal energy storage tank with an immersed coil heat exchanger under three operation modes. Appl. Energy **195**, 877–889 (2017). https://doi.org/10.1016/J.APENERGY.2017.03.092
46. L.G. Socaciu, Seasonal sensible thermal energy storage solutions. Leonardo Electron. J. Pract. Technol. **10**, 49–68 (2011)

47. U. Herrmann, Two-tank molten salt storage for parabolic trough solar power plants two-tank molten salt storage for parabolic trough solar power plants. 5442 (2017). https://doi.org/10.1016/S0360-5442(03)00193-2

48. C. Libby, Solar thermocline storage systems: Preliminary design study. Electr. Power Res. Inst. Palo Alto, CA (2010)

49. Y. Grosu, I. Ortega-Fernández, L. González-Fernández, U. Nithiyanantham, Y.F. Baba, A. Al Mers et al., Natural and by-product materials for thermocline-based thermal energy storage system at CSP plant: Structural and thermophysical properties. Appl. Therm. Eng. **136**, 185–193 (2018). https://doi.org/10.1016/J.APPLTHERMALENG.2018.02.087

50. H. Yin, J. Ding, R. Jiang, X. Yang, Thermocline characteristics of molten-salt thermal energy storage in porous packed-bed tank. Appl. Therm. Eng. **110**, 855–863 (2017). https://doi.org/10.1016/J.APPLTHERMALENG.2016.08.214

51. J. Gasia, A. de Gracia, G. Zsembinszki, L.F. Cabeza, Influence of the storage period between charge and discharge in a latent heat thermal energy storage system working under partial load operating conditions. Appl. Energy **235**, 1389–1399 (2019). https://doi.org/10.1016/J.APENERGY.2018.11.041

52. T. Configuration, G. Angelini, A. Lucchini, G. Manzolini, Comparison of thermocline molten salt storage performances to commercial science. Direct comparison of thermocline molten salt storage performances to commercial two-tank configuration (2015). https://doi.org/10.1016/j.egypro.2014.03.075

53. B. Zhao, M. Cheng, C. Liu, Z. Dai, Cyclic thermal characterization of a molten-salt packed-bed thermal energy storage for concentrating solar power. Appl. Energy **195**, 761–773 (2017). https://doi.org/10.1016/J.APENERGY.2017.03.110

54. H.A. Aljaerani, M. Samykano, A.K. Pandey, K. Kadirgama, R. Saidur, Thermo-physical properties and corrosivity improvement of molten salts by use of nanoparticles for concentrated solar power applications: A critical review. J. Mol. Liq. **314**(2020). https://doi.org/10.1016/j.molliq.2020.113807

55. A. Ibrahim, H. Peng, A. Riaz, M. Abdul Basit, U. Rashid, A. Basit, Molten salts in the light of corrosion mitigation strategies and embedded with nanoparticles to enhance the thermophysical properties for CSP plants. Sol. Energy Mater. Sol. Cells **219**, 110768 (2021). https://doi.org/10.1016/j.solmat.2020.110768

56. Z. Zhao, M.T. Arif, A.M.T. Oo, Solar thermal energy with molten-salt storage for residential heating application. Energy Proc. **110**, 243–249 (2017). https://doi.org/10.1016/j.egypro.2017.03.134

57. D. Barlev, R. Vidu, P. Stroeve, Innovation in concentrated solar power. Sol. Energy Mater. Sol. Cells **95**(10), 2703–2725 (2011)

58.] S. Kuravi, J. Trahan, D. Yogi Goswami, M.M. Rahman, E.K. Stefanakos, Thermal energy storage technologies and systems for concentrating solar power plants. Progr. Energy Combust. Sci. **39**(4), 285–319 (2013)

59. M. Diesendorf, *Sustainable Energy Solutions for Climate Change* (UNSW Press, 2013)

60. T.E.W. Schumann, Heat transfer: a liquid flowing through a porous prism. J. Franklin. Inst. **208**, 405–416 (1929)

61. N. Wakao, S. Kaguei, T. Funazkri, Effect of fluid dispersion coefficients on particle-to-fluid heat transfer coefficients in packed beds. Correlation of nusselt numbers. Chem. Eng. Sci. **34**, 325–36 (1979). https://doi.org/10.1016/0009-2509(79)85064-2

62. D. Vortmeyer, R.J. Schaefer, Equivalence of one- and two-phase models for heat transfer processes in packed beds: one dimensional theory. Chem. Eng. Sci. **29**, 485–91 (1974). https://doi.org/10.1016/0009-2509(74)80059-X

63. S. Yagi, D. Kunii, N. Wakao, Studies on axial effective thermal conductivities in packed beds. AIChE J. **6**, 543–6 (1960). https://doi.org/10.1002/aic.690060407

64. I. Calderón-Vásquez, E. Cortés, J. García, V. Segovia, A. Caroca, C. Sarmiento et al., Review on modeling approaches for packed-bed thermal storage systems. Renew. Sustain. Energy Rev. **143**(2021). https://doi.org/10.1016/j.rser.2021.110902

65. M. Hänchen, S. Brückner, A. Steinfeld, High-temperature thermal storage using a packed bed of rocks—.Heat transfer analysis and experimental validation. Appl. Therm. Eng. **31**, 1798–1806 (2011). https://doi.org/10.1016/j.applthermaleng.2010.10.034

66. J.E. Crider, A.S. Foss, Effective wall heat transfer coefficients and thermal resistances in mathematical models of packed beds. AIChE J. **11**, 1012–9 (1965). https://doi.org/10.1002/aic.690 110613

67. D. Handley, P.J. Heggs, The effect of thermal conductivity of the packing material on transient heat transfer in a fixed bed. Int. J. Heat Mass Transf. **12**, 549–70 (1969). https://doi.org/10. 1016/0017-9310(69)90038-6

68. D.J. Gunn, J.F.C. De Souza, Heat transfer and axial dispersion in packed beds. Chem. Eng. Sci. **29**, 1363–71 (1974). https://doi.org/10.1016/0009-2509(74)80160-0

69. N. Wakao, Particle-to-fluid transfer coefficients and fluid diffusivities at low flow rate in packed beds. Chem. Eng. Sci. **31**, 1115–22 (1976). https://doi.org/10.1016/0009-2509(76)85021-X

70. C. Xu, Z. Wang, Y. He, X. Li, F. Bai, Sensitivity analysis of the numerical study on the thermal performance of a packed-bed molten salt thermocline thermal storage system. Appl. Energy **92**, 65–75 (2012). https://doi.org/10.1016/j.apenergy.2011.11.002

71. K. Merlin, J. Soto, D. Delaunay, L. Traonvouez, Industrial waste heat recovery using an enhanced conductivity latent heat thermal energy storage. Appl. Energy **183**, 491–503 (2016). https://doi.org/10.1016/j.apenergy.2016.09.007

72. P. Chandra, D.H. Willits, Pressure drop and heat transfer characteristics of air-rockbed thermal storage systems. Sol. Energy **27**, 547–53 (1981). https://doi.org/10.1016/0038-092X(81)900 50-5

73. Ansys Inc. ANSYS Fluent UDF Manual **15317**, 724–46 (2013)

74. A.J. Chorin, Numerical solution of the Navier-Stokes equations. Math. Comput. **22**, 745–745 (1968). https://doi.org/10.1090/S0025-5718-1968-0242392-2

Chapter 12
Optimization of Multi-stage Cooling System's Performance for Hydrogen Fueled Scramjet

Check for updates

Pourya Seyedmatin, Mohammad Ebadollahi, Mojtaba Bezaatpour, and Majid Amidpour

Abstract Hydrogen fueled scramjet is an interesting choice to be used as engine of aerospace vehicles because of its high specific impulse. The most important challenge in scramjet engine technology is the thermal management of them. Due to high temperature of combustion, a competent cooling system which is able to recover the waste energy is needed. The multi-stage open cooling cycle was proposed as appropriate choice by many recent studies. In the present study, the optimization of a novel multi-stage cooling system for hydrogen fueled scramjets is conducted in which the waste heat of scramjet is recovered to produce power and electricity. The optimization process has been done through a thermodynamic zero dimensional analysis. The waste heat of scramjet is used as main heat source of the system. The present study results declare that the energy and exergy efficiencies of the system is improved by 49.24% and 45.98% by optimizing the M-OCC, respectively. In both performance criterion of the system a huge sensible improvement is observed by accomplished optimization.

Keywords Optimization · Scramjet · Hydrogen production · Thermodynamic analysis · Mach number

Nomenclature

Symbols

c_p Special heat magnitude ($kJ \cdot kg^{-1} \cdot K^{-1}$)

P. Seyedmatin
Tarbiat Modares University of Tehran, Tehran, Iran

M. Ebadollahi · M. Amidpour (✉)
Khajeh Nasir Toosi University of Technology, Tehran, Iran
e-mail: amidpour@kntu.ac.ir

M. Bezaatpour
Sahand University of Technology, Tabriz, Iran

D	Thickness of memberane (μm)
E	Electrical energy (kJ)
ex	The exergy rate (kW/kg)
$\dot{Ex}$	The energy rate (kW)
F	Faraday constant (C/mol)
G	Gibbs free energy (kJ $\cdot$ kmol^{-1})
H	Molar specific enthalpy (kJ $\cdot$ kmol^{-1})
h	Mass specific enthalpy (kJ $\cdot$ kg^{-1})
J	Density of current (A.m^{-2})
J_a^{ref}	Anode pre-exponential factor (A $\cdot$ m^{-2})
J_c^{ref}	Cathode pre-exponential factor (A $\cdot$ m^{-2})
J_i^{ref}	Pre-exponential factor (A $\cdot$ m^{-2})
LHV	Lower heating value (kJ $\cdot$ kg^{-1})
$\dot{m}$	Mass flow rate (kg $\cdot$ s^{-1})
Ma	Mach number
$\dot{N}$	Molar mass flow rate (kmol $\cdot$ s^{-1})
P	Pressure (MPa)
Q	Heat energy (kJ)
$\dot{Q}$	The rate of heat transfer (kW)
R	Ohmic resistance of PEM (Ω)
Re	Reynolds number
T	Temperature (K)
V_0	Reversible potential (V)
$V_{act,a}$	Anode activation over-potential (V)
$V_{act,c}$	Cathode activation over-potential (V)
V_0	Reversible potential (V)
V	Electrical potential (V)
w	Specific power per mass unit (MW/kg)
$\dot{W}$	Electricity rate (kW)
x	Membrane distance (m

Greek Symbols

η	Efficiency (%)
$\varnothing$	Fuel equivalence ratio
δ	Ratio of multiplication
ϕ	Ratio of reduction
ρ	Density (kg.m^{-3})
γ	Heat capacity ratio
K	Air heat capacity ratio
π	Pressure ratio

Acronyms

EES	Engineering Equation Solver
HE	Heat exchanger
OCC	Open cooling cycle
PEM	Proton exchange membrane
RCC	Regenerative cooling cycle

Superscripts and Subscripts

a	Anode
act,a	Anode activation
act,c	Cathode activation
ave	Average
c	Cathode
CP	Cooling passage
cr	Critical
D	Destruction
en	Energy
ex	Exergy
F	Fuel
int	Intermediate
in	Inlet
is	Isentropic
j	Jth stage
KN	Kinetic
net	Net value
out	Outlet
P	Product
p	Pump
scr	Scramjet
t	Turbine
v	Vapor
1,2,…	Cycle locations
0	Dead state
A,B,..	Scramjet states

12.1   Introduction

Aerospace scientists have noticed the air-breathing propulsion vehicles, since several decades ago. Supersonic combustion chambers (scramjets) have great ability in high speed hence have acquired high level of recent research interest in all over the world [1, 2]. Due to high fuel impulse, scramjets can be considered as one of economic choice in long-distance flights [3]. However, scramjets are not very appropriate for accelerating missions since their net thrust is lower than a rocket [4]. Whereas, scramjet technology face up to many challenges such cooling management of high working temperature, onboard fuel storage restriction, flight condition sustainability etc. Accordingly, prevailing over these challenges can be purpose of developed research centers.

High heat flux level in scramjet combustion chambers demands a reliable cooling system. Heat flux range of 0.5–2.5 MW per unit of area in working temperature of 500–2000 K for Mach number of 8 flight condition is reported [5]. Due to such high temperature, even the most developed composite materials cannot withstand a work properly [6]. Regenerative cooling systems (RCC) especially open cooling cycle (OCC) is introduced as one of the most efficient and feasible solution encountering heat management challenge. Utilizing the high heat absorption of hydrogen to cool down the scramjet is the innovative point of this method. Over-temperature of the wall in the scramjet systems is a crucial phenomenon through the cooling process which can be avoided by preheating of the fuel before entering the cooling channel [7]. Thus, an appropriate cooling treatment prevents the heat transfer deterioration at the entrance region. This process may be repeated in various times that is called multi-OCC (M-OCC). OCC is also applicable to both hydrocarbon and hydrogen-fueled scramjet engines.

The ancillary set-ups, including circuit measuring, fuel injection, and tracking controller set-ups on aircrafts and aerospace vehicles need a definite deal of electrical energy. Thus, for such a high speed enormous vehicles, it is completely important to provide an energy recovery set-up to address its surplus electricity need [8]. In recent years, recovering energy and implementing energy-saving methods for producing power, useful products and other required commodities have been utilized in numerous energy conversion systems [9]. Consequently, co-production systems are introduced as the most efficient and pragmatic solutions for energy recovery purposes when low-quality heat resources (such as waste heat) are pondered [10, 11]. Using co-production systems render the feasibility of producing other useful forms of energies such as heating, cooling, purified water and hydrogen alongside the power production [12–14]. Co-production (also known as co-generation) systems have higher energy efficiency and low exergy destruction than the single-production systems under a same condition, as shown by Onovwiona and Ugursl [15]. Dincer et al. [16] carried out a thermodynamic study of a high degree set-up electrolysis (HDSE) for cogeneration of H_2 and electricity, including a solar tower, a Brayton system, a Rankine system, and an organic Rankine system. Based on the results, the total efficiencies. Ghaebi et al. [17] recommended two novel combined cycles for

electricity and H_2 co-production using huge value of wasted heat of the city gas post (CGP) regulators in which the high pressure NG is decreased to an acceptable pressure for consumption. These set-ups are integrated by a combination of a Rankine system (RS) and CGP system as well as an absorption power system (APS) as an alternative electricity unit. In both systems, PEM electrolyzer is utilized to generate hydrogen. The power sub-cycle is actuated by waste heat of CGP and PEM is operated by a fair segment of net output electricity. An executive and comparative 4E (energy, exergy, economy and environment) analysis of both systems have been fulfilled. The outcomes of assessment have demonstrated 6.868 and 6.351 kg/h hydrogen production as well as 8.571 and 7.618 MW electricity generation for the CGP-RS and CGP-APS set-ups, correspondingly. The exergy destruction study has demonstrated that the generator of system has introduced as the highest exergy destructive component (in both systems). Li and Wang [5] have performed a theoretical study on producing power from the waste energy of scramjet. In their study, a thermoelectrical generator (TEG) is assimilated with a regenerative cooling cycle of scramjet engine for power production. The results of this study revealed power production of 61.69 kW and exergy efficiency of about 22% for fuel flow rate of 0.4 kg/s. And a parametric analysis which has been accomplished in their investigation denoted that the pressure ratio of turbine has a significant effect on the exergy efficiency.

Hydrogen has higher-ranking properties compared to all kinds of carbon based fuels such as substantial flame stability for combustion and high ignitability. These intrinsic profits nowadays have captured a great attention in recent studies of H_2-fueled scramjet engines [7, 10, 18]. H_2 production process c is performed by biomass conversion water splitting or steam methane reforming. Splitting water is a thermochemical process which is called electrolysis. There are three conventional forms for electrolyzing process, consist of the alkaline, oxidation of solid, and proton exchange membrane (PEM) electrolysis. Hydrogen generation by PEM electrolysis has several benefits especially in renewable-based procedures, including: being compact, low environmental effect, zero hazardous chemicals and extremely pure hydrogen [19]. PEM is the most widespread procedure of hydrogen production in energy set-ups with low grade energy sources because of its high compatibility with these systems and is introduced as the commendable hydrogen production method for future utilities accordingly [20, 21]. Marangio et al. [22] presented a model for theoretical study of the PEM cells in which a complicated pattern of Ohmic losses in electrodes and membrane. They have validated the presented model using available experimental data. In the other study presented by Ahmadi et al. [23], a PEM electrolyzer which is actuated by solar energy, has been assimilated with an OHEC (ocean heat energy conversion) system to extract H_2. Energy and exergy assessment have been performed in the recommended model and it is concluded that the extracted hydrogen rate is 1.2 kg/h with exergy and thermodynamic efficiencies of 23% and 3.6%, respectively.

The importance of thermal management of the scramjet and its effects on operation of this hypersonic vehicle has drawn attention of many researches about it in more recent years. The M-OCC is known as one of the most feasible system for cooling of scramjet engines. On the other hand, some studies have tried to examine the exergy aspect of utilizing this kind of cooling system for co-production aims such

as a limited exergy based study conducted by Li and Wang. Despite all efforts to study and outstrip these cooling systems and conducting thermodynamic analysis of these systems, the lack of an exclusive thermodynamic and exergy analysis of the M-OCC and investigating the effects of multi-expansion process is also indispensable. Moreover, no thoroughgoing investigation for producing electricity and hydrogen from waste heat of scramjet via PEM electrolyzer is presented up to yet.

The aim of present work is to advance a novel multi-stage OCC in order to produce electricity and hydrogen and cooling the scramjet engine as well. Additionally, a thoroughgoing study on multi-expansion effects is accomplished from thermodynamic standpoint. In the proposed set-up, the PEM is driven by a portion of net output power the cooling cycle, whilst the waste heat of scramjet is pondered as the heat source of the multi cooling cycle.

12.2 System Expression

Figure 12.1 shows a comprehensive illustration of system layout. Two prominent systems, Power and PEM electrolyzer cycles, are operating in this system. Hydrogen as working flow, is streamed through scramjet cooling pass entry by pump (state 2). Coolant absorbs the combustion chamber heat and changes to superhot gas quickly. Afterwards, the superhot hydrogen gets on the turbine number 1 (state 3). By entering to the turbine the hydrogen as working fluid not only produce electric power but also the temperature decreases to T_4. Hydrogen produced power, by circulating in turbine, and now is cooled down. Thus it is again ready to absorb the heat and cool down through the second cooling passage and turbine number 2, respectively. This
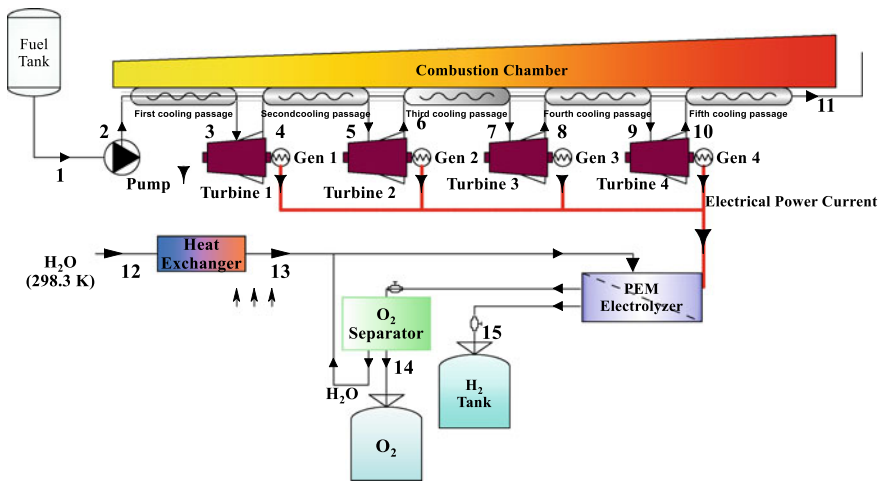

Fig. 12.1 Simple schematics of proposed system

process of chilling the scramjet wall down and expanding through turbine to extract electricity from the heated coolant continues two times again in order to attain a high performance. Finally hydrogen enters to the combustion chamber of scramjet as fuel after streaming into last cooling passage to close the power sub-cycle.

Electricity and heat energy are two main inputs of PEM electrolyzer to produce hydrogen. Some portion of produced electricity in the power sub-cycle supplies the electricity need of PEM and high heat flux of scramjet meets heat needs of PEM. A simple electrolyzing process of water separation occurs in the PEM. Electric voltage difference make to anode and cathode sides. Hydrogen is produced in cathode side then is storied in a special tank (state 15). In the anode side the separated oxygen is accumulated and transferred to a storage tank (state 16). The surplus water is recirculated to the PEM and closes the PEM sub-cycle.

12.3 Methodology and Assumptions

12.3.1 Considered Suppositions

Some of the main assumptions of the suggested system are made as following [24–28]:

- Mathematical modeling is zero dimensional steady state
- Specific heat is considered constant.
- After the first cooling passage, the coolant is assumed perfect gas.
- Any energy and pressure drops are not considered through joints and transfer lines.
- Any losses is not considered by heat transfer process in the turbine.
- 298 K and 0.101 MPa are reference temperature and presure, respectively.
- Any energy losses is not considered through PEM electrolyzer.

12.3.2 The Mathematic Simulation of Scramjet

The thermodynamic analysis based modeling of scramjet is conducted in present modeling. Therefore, two main parameters consisting of the scramjet's entry pressure ratio (π_{in}) and fuel equivalence ratio are needed to evaluate the average temperature of scramjet combustion chamber wall. The mean wall combustor temperature is calculated by averaging TD and TC, which means the outlet and inlet combustor temperatures (Fig. 12.2):
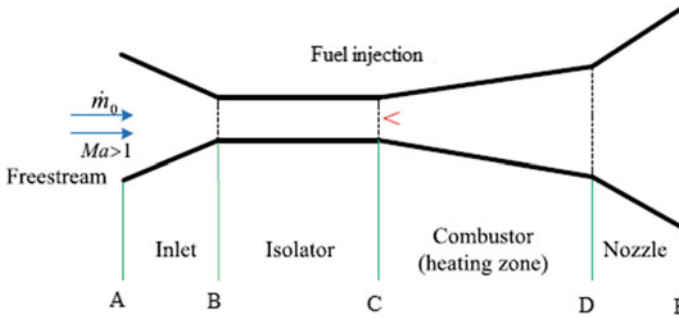
$$T_{ave} = \frac{T_c + T_D}{2} \tag{12.1}$$

Fig. 12.2 Ideal scramjet Schematic condition

Figure 12.2 indicates a schematic plot of an ideal scramjet, which includes four prominent zones of inlet, nozzle, isolator, and combustor. The combustor is supplied by hydrogen.

12.3.3 Cycle Analysis for the Scramjet Engine Modeling

As demonstrated in Fig. 12.3, the ideal scramjet system is drawn on a T-s plot. A-C process indicates the adiabatic compression from the static temperature to the combustor inlet temperature. A-B and B-C indicate air compression in the enter section and isolator. C-D shows the energy receiving operation in to combustor, performing at a consistent static pressure. Process D-E occurs isentropically in the nozzle. Also, process E-A is only an unreal constant static pressure event. Based on

Fig. 12.3 T-s diagram of an ideal scramjet system
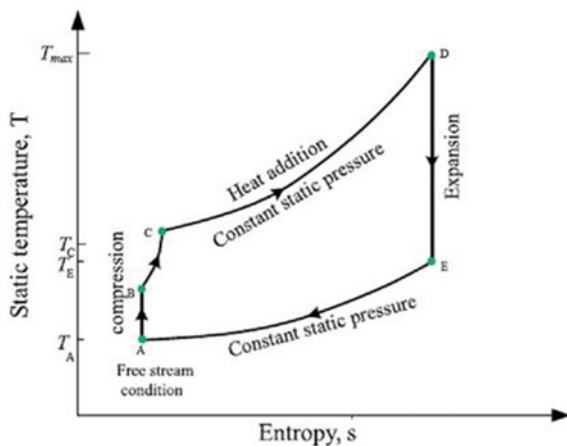
energy conversion principle, heat is wasted from nozzle outlet to the atmosphere at D-A process. The Three main sectors in scramjet modeling are described extensively.

12.3.3.1 Compression Process

The amount of compression in the scramjet inlet section defines as inlet pressure ratio (π_{in}). At cruise situations, the freestream circumstances (P_{tA}, T_{tA} and Ma_A) are expressed. However, the steady flow through the inlet compression part may be written as below [29, 30]:

$$P_{tB} = P_{tA} \tag{12.2}$$

$$T_{tB} = T_{tA} \tag{12.3}$$

$$Ma_B = \sqrt{\left[\left(\frac{P_{tA}}{\pi_{in} P_A}\right)^{(k-1/k)}\right] \Big/ \left(\frac{k-1}{2}\right)} \tag{12.4}$$

Also, k is the specific heat capacity ratio of air.

The isolator compression is followed by a shock train. The empirical relations are described by Billig et al. [31, 32]:

$$\frac{L}{H} = \frac{\left[50\left(\frac{P_C}{P_B} - 1\right)^2 + 170\left(\frac{P_C}{P_B} - 1\right)^2\right]}{\left(Ma_1^2 - 1\right)} \cdot \frac{\sqrt{\theta/H}}{\sqrt[4]{Re_\theta}} \tag{12.5}$$

where, Re_θ is the inlet Reynolds number, θ is the thickness of boundary layer momentum, and L/H is the of shock train length to isolator height ratio. The consistent coefficient (C) is defined for brevity targets. The amounts of L/H, θ/H and Re_θ are estimated 10, 0.02 and 10,000, respectively [30].

$$C = \frac{L}{H} \Big/ \frac{\sqrt{\theta/H}}{\sqrt[4]{Re_\theta}} \tag{12.6}$$

The isolator exit pressure is defined by manipulating Eqs. (12.5) and (12.6) [30]:

$$P_C = P_B \cdot \frac{\sqrt{680.C.\left(Ma_B^2 - 1\right) + 2500} + 290}{340} \tag{12.7}$$

The whole pressure and temperature at the isolator outlet are given as [29]:

$$T_{tC} = T_{tB} = T_{tA} \tag{12.8}$$

$$P_{tC} = P_C \cdot \left(1 + (k-1) \cdot \frac{Ma_C^2}{2}\right)^{(k/k-1)} \tag{12.9}$$

$$\frac{P_{tC}}{P_{tB}} = \left[\left(\frac{1 + \frac{(k-1)}{2} \cdot Ma_C^2}{1 + \frac{(k-1)}{2} \cdot Ma_B^2}\right)^{(k/k-1)}\right] \cdot \left[\frac{1 + k \cdot Ma_B^2}{1 + k \cdot Ma_C^2}\right] \tag{12.10}$$

The static temperature at C is obtained from [29]:

$$T_C = T_{tC} / \left(1 + (k-1) \cdot \frac{Ma_C^2}{2}\right) \tag{12.11}$$

12.3.3.2   Heat Addition Process

Based on the energy conversation relation at steady state condition for the combustor, the Eq. (12.12) is written [30]:

$$\left(\dot{m}_A + \dot{m}_f\right)h_{tD} = \dot{m}_A h_{tC} + \dot{m}_f LHV_{H_2} \tag{12.12}$$

where, LHV_{H_2} is the hydrogen combustion low heat value and is reported 120.11 MJ/kg.

The Eq. (12.12) can be expressed in the other way as below:

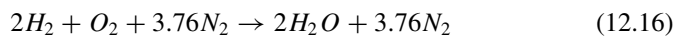$$\dot{m}_0 C_p T_{tC} + \dot{m}_f LHV_{H_2} = \dot{m}_0 C_p T_{tD} \tag{12.13}$$

or

$$\dot{m}_f LHV_{H_2} = \dot{m}_A C_p T_{tD}\left(T_{tC}/T_{tD} - 1\right) = \dot{m}_A C_p(T_{tD} - T_{tC}) \tag{12.14}$$

The whole temperature ratio is introduced as:

$$\tau = T_{tC}/T_{tD} \tag{12.15}$$

The stoichiometric hydrogen-air reaction is described as [33]:

$$2H_2 + O_2 + 3.76N_2 \rightarrow 2H_2O + 3.76N_2 \tag{12.16}$$

The highest demand of hydrogen $\dot{m}_{fs}$, takes place in the stoichiometric situation with Eq. (12.17):

$$\dot{m}_{fs} = \frac{\dot{m}_A \times 4 \times 0.21}{1 \times 32} \cong \dot{m}_A/40 \tag{12.17}$$

Also, the fuel equivalence ratio ($\varnothing$) is introduced as below:

$$\varnothing = \frac{\dot{m}_f}{\dot{m}_{fs}} \tag{12.18}$$

Moreover, the total temperature ratio may be described as below:

$$\tau = 1 + \frac{\varnothing LHV_{H_2}}{40 C_p T_{tA}} \tag{12.19}$$

In the constant pressure process:

$$P_D = P_C \tag{12.20}$$

Then, whole pressure P_{tD} is denoted as [29]:

$$P_{tD} = P_D.\left((k-1).\frac{Ma_D^2}{2} + 1\right)^{(k/k-1)} \tag{12.21}$$

$$\tau = \left[\frac{1 + k.Ma_C^2}{1 + k.Ma_D^2}\right].\left[\frac{Ma_D^2}{Ma_C^2}\right].\left[\left(\frac{1 + \frac{(k-1)}{2}.Ma_D^2}{1 + \frac{(k-1)}{2}.Ma_C^2}\right)^{(k/k-1)}\right] \tag{12.22}$$

By simultaneous solving of Eq. (12.21) and (12.22), the Mach number) and after that static temperature at the pint D are calculated.

$$T_D = T_{tD}/\left(1 + (k-1).\frac{Ma_D^2}{2}\right) \tag{12.23}$$

12.3.3.3 Expansion Process

Expansion process has been occurred isentropically in the nozzle as the followed relations [29]:

$$P_E = P_A \tag{12.24}$$

$$P_{tE} = P_{tD} \tag{12.25}$$

$$Ma_E = \sqrt{\left[\left(\frac{P_{tE}}{P_E}\right)^{(k-1/k)} - 1\right] \Bigg/ \left(\frac{k-1}{2}\right)} \qquad (12.26)$$

12.3.4 Performance Criteria of Open Cooling Cycle

Decreasing in the fuel flow rate for refrigeration by rising the heat absorption of fuel is the prominent target of the OCC.

One of the main parameters is the multiplication ratio of the fuel heat absorption (δ), which is obtained from the first passage cooling per second passage cooling amounts as Eq. (12.27) [34].

$$\delta_1 = \frac{Q_2}{Q_1} \qquad (12.27)$$

By the similar definition, δ_2, δ_3, and δ_4 are introduced for the third, fourth and fifth cooling passages, correspondingly:

$$\delta_2 = \frac{Q_3}{Q_1 + Q_2} \qquad (12.28)$$

$$\delta_3 = \frac{Q_4}{Q_1 + Q_2 + Q_3} \qquad (12.29)$$

$$\delta_4 = \frac{Q_5}{Q_1 + Q_2 + Q_3 + Q_4} \qquad (12.30)$$

The other main parameter is introduced as reduction ratio of mass flow rate (ϕ). The increasing of the fuel heat absorption load is explained as decreasing in the mass flow rate of fuel. Particularly, direct effect of utilizing OCC in performance of the scramjet cooling unit is decreasing of the essential fuel flow rate. Moreover, the reduction ratio of the second cooling passage is described as below [34]:

$$\phi_1 = \frac{Q_2}{Q_1 + Q_2} \qquad (12.31)$$

Similarly, ϕ_2, ϕ_3, and ϕ_4 are introduced for the third, fourth and fifth cooling passages, as written:

$$\phi_2 = \frac{Q_3}{Q_1 + Q_2 + Q_3} \qquad (12.32)$$

$$\phi_3 = \frac{Q_4}{Q_1 + Q_2 + Q_3 + Q_4} \tag{12.33}$$

$$\phi_4 = \frac{Q_5}{Q_1 + Q_2 + Q_3 + Q_4 + Q_5} \tag{12.34}$$

12.3.5 PEM Electrolyzer Equations

The structure of PEM electrolyzer is drawn in the bottom section of Fig. 12.1. The main relations of the PEM set-up are described comprehensively in our other works [24, 35].

12.3.6 Thermodynamic Assessment

The governing format of the energy and mass balance at steady state condition may be explained as below [28, 36–38]:

$$\sum \dot{m}_{in} = \sum \dot{m}_{out} \tag{12.35}$$

$$\dot{Q} - \dot{W} = \sum \dot{m}_{out} h_{out} - \sum \dot{m}_{in} h_{in} \tag{12.36}$$

The energy performance of the suggested set-up is calculated from the summing the net generated power and produced hydrogen as products of the system divided by input heat as below:

$$\eta_{en} = \frac{(1 - \eta_G) \cdot \dot{W}_{net} + LHV_{H_2} \cdot \dot{m}_{15}}{\dot{Q}_{totla}} \tag{12.37}$$

where, $\dot{Q}_{total}$ is the scramjet's whole cooling utilized as the system heat source.

Some of the important thermodynamic relations which extracted from energy balance are tabulated in Table 12.1.

Total exergy rate ($\dot{Ex}_{total}$) has four major part: physical exergy ($\dot{Ex}_{PH}$), potential exergy ($\dot{Ex}_{PT}$), kinetic exergy ($\dot{Ex}_{KN}$), and chemical exergy rate ($\dot{Ex}_{CH}$) [38, 39]:

$$\dot{Ex}_{total} = \dot{Ex}_{PH} + \dot{Ex}_{PT} + \dot{Ex}_{KN} + \dot{Ex}_{CH} \tag{12.38}$$

Also, potential and kinetic exergies can be assumed negligible. The physical and chemical exergies are given as below [40]:

Table 12.1 Energy balance relations for each constituents of the recommended unit

Parameters	Relation
Power of turbine 1	$w_t = \eta_t c_p T_3 \left[1 - \pi_1^{(1-\gamma)/\gamma} \right]$
Power of pump	$w_p = \frac{P_2 - P_1}{\eta_p \rho_1}$
Whole net power	$w_{net} = w_{t1} + w_{t2} + w_{t3} + w_{t4} - w_p$
Net electricity	$\dot{W}_{net} = \dot{m}_0 w_{net}$
Cooling capacity of passage 1	$\dot{Q}_1 = \dot{m}_1 c_p (T_3 - T_2)$
Capacity of heat exchanger	$\dot{Q}_{HE} = \dot{m}_w (h_{13} - h_{12})$
Total cooling	$\dot{Q}_{total} = \dot{Q}_1 + \dot{Q}_2 + \dot{Q}_3 + \dot{Q}_4 + \dot{Q}_5 + \dot{Q}_{HE}$

$$\dot{Ex}_{PH} = \dot{m}(h - h_0 - T_0(s - s_0)) \tag{12.39}$$

$$\dot{Ex}_{CH} = \dot{m} \left[\sum_{i=1}^{n} y_i ex_{CH,i}^0 + RT_0 \sum_{i=1}^{n} y_i \ln y_i \right] \tag{12.40}$$

For each constituent, the exergy balance relation is denoted as [39, 41]:

$$\dot{Ex}_F^i = \dot{Ex}_P^i + \dot{Ex}_D^i \tag{12.41}$$

In the above equation, $\dot{Ex}_D^i$ is the exergy destruction, $\dot{Ex}_P^i$ and $\dot{Ex}_F^i$ are product and fuel exergies, respectively.

Exergetic efficiency of the constituents is written as:

$$\eta_{ex}^i = \dot{Ex}_P^i / \dot{Ex}_F^i \tag{12.42}$$

Destruction rate of each component can be expressed by exergy destruction ratio as below [39]:

$$Y_{D,i} = \dot{Ex}_{D,i} / \dot{Ex}_{D,total} \tag{12.43}$$

The overall exergetic efficiency of the set-up can be written as following

$$\eta_{ex}^{total} = \dot{Ex}_P^{total} / \dot{Ex}_F^{total} \tag{12.44}$$

Some of the necessary exergy relations of the recommended set-up is tabulated in Table 12.2

Table 12.2 Exergy equations of the main components of the simulated system

Component	Product exergy	Fuel exergy	Exergetic efficiency	Exergy destruction ratio
Turbine 1	$\dot{Ex}_{P,t1} = \dot{W}_{t1}$	$\dot{Ex}_{F,t1} = \dot{Ex}_3 - \dot{Ex}_4$	$\eta_{ex,t1} = \frac{\dot{Ex}_{P,t1}}{\dot{Ex}_{F,t1}}$	$Y_{D,t1} = \frac{\dot{Ex}_{D,t1}}{\dot{Ex}_{D,total}}$
Turbine 2	$\dot{Ex}_{P,t2} = \dot{W}_{t2}$	$\dot{Ex}_{F,t2} = \dot{Ex}_5 - \dot{Ex}_6$	$\eta_{ex,t2} = \frac{\dot{Ex}_{P,t2}}{\dot{Ex}_{F,t2}}$	$Y_{D,t2} = \frac{\dot{Ex}_{D,t2}}{\dot{Ex}_{D,total}}$
Turbine 3	$\dot{Ex}_{P,t3} = \dot{W}_{t3}$	$\dot{Ex}_{F,t3} = \dot{Ex}_7 - \dot{Ex}_8$	$\eta_{ex,t3} = \frac{\dot{Ex}_{P,t3}}{\dot{Ex}_{F,t3}}$	$Y_{D,t3} = \frac{\dot{Ex}_{D,t3}}{\dot{Ex}_{D,total}}$
Turbine 4	$\dot{Ex}_{P,t4} = \dot{W}_{t4}$	$\dot{Ex}_{F,t4} = \dot{Ex}_9 - \dot{Ex}_{10}$	$\eta_{ex,t4} = \frac{\dot{Ex}_{P,t4}}{\dot{Ex}_{F,t4}}$	$Y_{D,t4} = \frac{\dot{Ex}_{D,t4}}{\dot{Ex}_{D,total}}$
Cooling passage 1	$\dot{Ex}_{P,CP1} = \dot{Ex}_3 - \dot{Ex}_2$	$\dot{Ex}_{F,CP1} = \dot{Q}_1\left(1 - \frac{T_0}{T_{scr}}\right)$	$\eta_{ex,CP1} = \frac{\dot{Ex}_{P,CP1}}{\dot{Ex}_{F,CP1}}$	$Y_{D,CP1} = \frac{\dot{Ex}_{D,CP1}}{\dot{Ex}_{D,total}}$
Cooling passage 2	$\dot{Ex}_{P,CP2} = \dot{Ex}_5 - \dot{Ex}_4$	$\dot{Ex}_{F,CP2} = \dot{Q}_2\left(1 - \frac{T_0}{T_{scr}}\right)$	$\eta_{ex,CP2} = \frac{\dot{Ex}_{P,CP2}}{\dot{Ex}_{F,CP2}}$	$Y_{DCP2} = \frac{\dot{Ex}_{D,CP2}}{\dot{Ex}_{D,total}}$
Cooling passage 3	$\dot{Ex}_{P,CP3} = \dot{Ex}_7 - \dot{Ex}_6$	$\dot{Ex}_{F,CP3} = \dot{Q}_3\left(1 - \frac{T_0}{T_{scr}}\right)$	$\eta_{ex,CP3} = \frac{\dot{Ex}_{P,CP3}}{\dot{Ex}_{F,CP3}}$	$Y_{D,CP3} = \frac{\dot{Ex}_{D,CP3}}{\dot{Ex}_{D,total}}$
Cooling passage 4	$\dot{Ex}_{P,CP4} = \dot{Ex}_9 - \dot{Ex}_8$	$\dot{Ex}_{F,CP4} = \dot{Q}_4\left(1 - \frac{T_0}{T_{scr}}\right)$	$\eta_{ex,CP4} = \frac{\dot{Ex}_{P,CP4}}{\dot{Ex}_{F,CP4}}$	$Y_{D,CP4} = \frac{\dot{Ex}_{D,CP4}}{\dot{Ex}_{D,total}}$
Cooling passage 5	$\dot{Ex}_{P,CP5} = \dot{Ex}_{11} - \dot{Ex}_{10}$	$\dot{Ex}_{F,CP5} = \dot{Q}_5\left(1 - \frac{T_0}{T_{scr}}\right)$	$\eta_{ex,CP5} = \frac{\dot{Ex}_{P,CP5}}{\dot{Ex}_{F,CP5}}$	$Y_{D,CP5} = \frac{\dot{Ex}_{D,CP5}}{\dot{Ex}_{D,total}}$
PEM	$\dot{Ex}_{P,PEM} = \dot{Ex}_{14} + \dot{Ex}_{15}$	$\dot{Ex}_{F,PEM} = (1 - \eta_G)\dot{W}_{net}$	$\eta_{ex,PEM} = \frac{\dot{Ex}_{P,PEM}}{\dot{Ex}_{F,PEM}}$	$Y_{D,PEM} = \frac{\dot{Ex}_{D,PEM}}{\dot{Ex}_{D,total}}$
Pump	$\dot{Ex}_{P,p} = \dot{Ex}_2 - \dot{Ex}_1$	$\dot{Ex}_{F,p} = \dot{W}_p$	$\eta_{ex,p} = \frac{\dot{Ex}_{P,p}}{\dot{Ex}_{F,p}}$	$Y_{D,p} = \frac{\dot{Ex}_{D,p}}{\dot{Ex}_{D,total}}$
Heat exchanger	$\dot{Ex}_{P,HE} = \dot{Ex}_{13} - \dot{Ex}_{12}$	$\dot{Ex}_{F,HE} = \dot{Q}_{HE}\left(1 - \frac{T_0}{T_{scr}}\right)$	$\eta_{ex,HE} = \frac{\dot{Ex}_{P,HE}}{\dot{Ex}_{F,HE}}$	$Y_{D,HE} = \frac{\dot{Ex}_{D,HE}}{\dot{Ex}_{D,total}}$

12.3.7 Multi-criteria Optimization

In this investigation, optimization procedure is applied to maximize the energy and exergy efficiencies simultaneously. The multi-criteria optimization procedure is utilized via genetic algorithm (GA) which is a strong approach compared to other methods [42].

Two Thermodynamics factor, consisting of the energy and exergy efficiencies have been determined as objective functions, while the six parameters are presented as the prominent decision variables. The multi-criteria function is presented in Eq. (12.45), and the major target of optimization is maximizing the suggested function.

$$Max(MCF = w_1 \times \eta_{en} + w_2 \times \eta_{ex}), \tag{12.45}$$

$$w_1 + w_2 = 1, 0 \le w_1, w_2 \le 1$$

$$200 \le T_1(K) \le 250$$

$$200 \le T_{15}(K) \le 250$$

$$0.1 \le P_1(MPa) \le 0.4 \tag{12.46}$$

$$15 \le P_2(MPa) \le 25$$

$$5 \le Mach_A \le 7$$

$$0.5 \le \eta_G \le 0.7$$

Moreover, Table 12.3 shows some main accountable parameters applied in the GA.

Table 12.3 Some main accountable parameters applied in the GA [43–46]

Parameter	Value
Individuals population number	32
Generation number	64
Highest mutation rate	0.25
Lowest mutation rate	0.0005
Crossover probability	0.85
Primary mutation rate	0.25

12.4   Result and Arguments

Based on coding in EES software, the recommended set-up is analyzed from energy and exergy standpoint. Table 12.4 expressed the initial parameters for modeling the set-up. The calculated outcomes regarding to prominent thermodynamic flow properties are written in Table 12.5. The properties consist of pressure, temperature, mass flow rate, enthalpy, entropy, and exergy rate at each state.

12.4.1   Results of Thermodynamic Simulation

This section reveals the results of simulation, in which 4840 kW and 59.45 kg/h power and hydrogen are produced and 13.87% total energy efficiency is achieved for uniform condition of $m = 0.4$ kg/s, $Ma_A = 6$, $T_A = 223$ K, $P_A = 2.56$ kPa when 65% of the generated electricity is consumed in the PEM electrolyzer. The quantity of hydrogen production is satisfying compared to that of other similar systems, which can be widely used in aerospace industry (Table 12.6).

Table 12.7 and Fig. 12.4 demonstrate the results of exergy analysis. Accordingly, the overall exergy efficiency is 17.48%, and the PEM electrolyzer and the first cooling pas-sage account for the highest exergy destruction, with 72.47% and 10.67%

Table 12.4 Input data for simulation of the set-up

Parameter	Value
Efficiency of Generator power, η_G	0.65
Efficiency of pump, η_p	0.7
Efficiency of turbine, η_t	0.8
Temperature of PEM, T_{PEM} (K)	353
Temperature of PEM entrance water, T_{12} (K)	298
PEM entrance water mass flow rate, $\dot{m}_{12}$ (kg/s)	0.0311
Fuel mass flow rate, $\dot{m}_0$ (kg/s)	0.4
Pressure of fuel tank, P_1 (MPa)	0.24
Temperature of fuel tank, T_1 (K)	225
Pressure of Scramjet combustion chamber, P_{11} (MPa)	1
Pump's back pressure, P_2 (MPa)	22
Ratio of inlet pressure, π_{in}	300
Ratio of fuel equivalence, $\varnothing$	0.6
Temperature of Freestream, TA (K)	223
Pressure of Freestream, P_A (MPa)	0.00256
Mach number of Freestream, Ma_A	6

Table 12.5 Thermodynamic properties in each state of the set-up

State	Fluid	T (K)	P (MPa)	$\dot{m}$ (kg/s)	h (kJ/kg)	s (kJ/kg.K)	$\dot{Ex}$ (kW)
1	H_2	225	0.24	0.4	617.1	57.22	509.3
2	H_2	254.9	22	0.4	1037	57.22	677.3
3	H_2	1408	22	0.4	16,555	65.46	6590
4	H_2	1006	4.69	0.4	10,349	66.66	3969
5	H_2	1408	4.69	0.4	16,555	71.84	5850
6	H_2	1185	2.166	0.4	13,073	72.33	4400
7	H_2	1408	2.166	0.4	16,555	75.02	5481
8	H_2	1291	1.472	0.4	14,706	75.25	4715
9	H_2	1408	1.471	0.4	16,555	76.62	5296
10	H_2	1291	1	0.4	14,706	76.84	4530
11	H_2	1408	1	0.4	16,555	78.21	5111
12	H_2O	290	0.101	0.0321	70.75	0.251	83.53
13	H_2O	353	0.101	0.0321	334.3	1.073	84.33
14	O_2	353	0.101	0.0929	50.36	0.156	31.27
15	H_2	353	0.101	0.01171	789.3	67.21	3.357

proportional exergy destruction ratio caused by chemical reaction and high temperature difference, respectively [47]. There is a direct relation between the temperature difference and exergy destruction [39]. Also, the highest exergy efficiency belongs to the pump in the system.

12.4.2　Optimization Results

In this section, optimized outcomes are reported and the comparison be-tween base scenario and multi-criteria optimizing scenario (MCO) have been presented in the Fig. 12.5. Accordingly, the energy efficiency increases from 13.87% to 20.7% (49.24% improvement) and exergy efficiency rises from 17.87% to 26.09% (45.98% improvement). Also. The last column of the results shows the optimized amounts of decision variables.

12.5　Noteworthy Conclusions

In our previous work [19] a novel M-OCC system is proposed and its analytic modeling developed. The previous study showed that the proposed system not only is able to aid scramjet in managing the heat properly but also has great potential in producing other variant useful energy forms such as electric power and hydrogen as

**Table 12.6** The outcomes of the energy assessment

Parameter	Amount
Pump power, w_p (MJ/kg)	0.4353
Net electricity output, $\dot{W}_{net}$ (kW)	4840
Power of turbine 1, w_{t1} (MJ/kg)	5.856
power of turbine 2, w_{t2} (MJ/kg)	3.25
power of turbine 3, w_{t3} (MJ/kg)	1.715
power turbine 4, w_{t4} (MJ/kg)	1.715
Total cooling, $\dot{Q}_{total}$ (kW)	12,231
PEM power entrance, $\dot{W}_G$ (kW)	3146
PEM heat exchanger load, $\dot{Q}_{HE}$ (kW)	8.461
Hydrogen production, $\dot{m}_{H_2}$ (kg/h)	59.45
heat load in cooling passage I, $\dot{Q}_1$ (kW)	6869
heat load in cooling passage II, $\dot{Q}_2$ (kW)	2482
heat load in cooling passage III, $\dot{Q}_3$ (kW)	1393
heat load in cooling passage IV, $\dot{Q}_4$ (kW)	739.6
heat load in cooling passage V, $\dot{Q}_5$ (kW)	739.6
Reduction ratio II, ϕ_1	0.2585
Reduction ratio III, ϕ_2	0.08025
Reduction ratio IV, ϕ_3	0.03107
Reduction ratio V, ϕ_4	0.03106
Energy efficiency overall system, η_{en} (%)	13.87
Multiplication ratio II, δ_1	0.3487
Multiplication ratio III, δ_2	0.1189
Multiplication ratio IV, δ_3	0.04234
Multiplication ratio V, δ_4	0.04232
Average temperature of scramjet combustion chamber, T_{ave} (K)	1408
Reduction ratio II, ϕ_1	0.2585
Reduction ratio III, ϕ_2	0.08025
Reduction ratio IV, ϕ_3	0.03107
Reduction ratio V, ϕ_4	0.03106

fuel, by recovering a useless waste heat. Accordingly, the necessity of conducting a research work to improve the performance of the proposed system is comprehensible. Thus the present study focused on the optimization of novel M-OCC system. The present study had been accomplished to have a better understanding from the system's operation. The following outlines can be expressed as brief:

- The energy efficiency of the system have been increased from 13.87 to 20.7%.
- The exergy efficiency of the system have been increased from 17.87 to 26.09%.

Table 12.7 Exergy results of the equipment

Sector	$\dot{E}x_F$(kW)	$\dot{E}x_P$(kW)	$\dot{E}x_D$(kW)	η_{ex}(%)	Y_D(%)
Cooling passage I	5912	5485.4	458.2	92.25	10.67
Cooling passage II	1971	1881	89.91	95.43	2.094
Cooling passage III	1106	1081	25.33	97.6	0.59
Cooling passage IV	587.3	580.6	6.729	98.85	0.1567
Cooling passage V	587.3	580.6	6.729	98.85	0.1567
Pump	174.1	168	6.172	96.46	0.1438
Turbine 1	2620	2342	278.1	87	6.47
Turbine 2	1450	1300	150.3	89.39	3.5
Turbine 3	765.4	685.8	79.59	89.63	1.85
Turbine 4	765.4	685.8	79.59	89.6	1.85
PEM heat exchanger	1.883	0.8046	1.078	42.74	0.0251
PEM	3146	34.63	3111	1.101	72.47
Total	9708	1697	4293	17.87	–
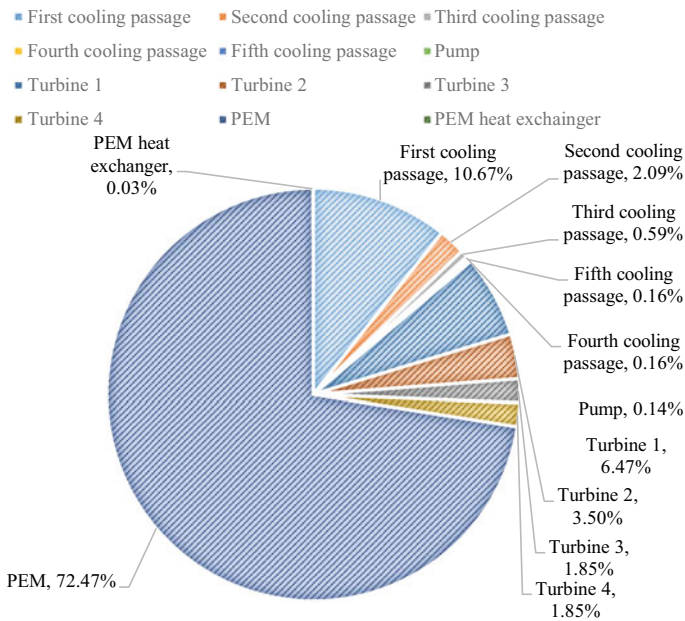
Fig. 12.4 Diagram of exergy destruction in different fixtures of the system
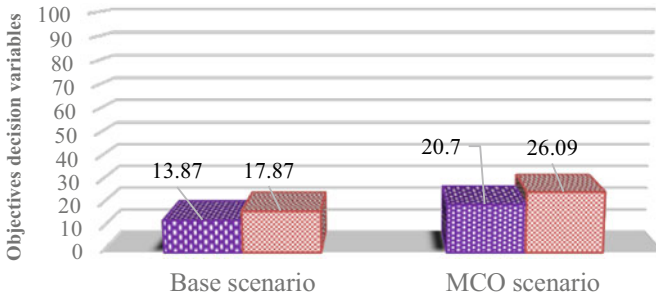
	Base scenario	MCO scenario
w_1	-	1/2
w_2	-	1/2
$T_1(K)$	225	249.7
$T_{15}(K)$	353	355.1
$P_1(MPa)$	0.24	0.201
$P_2(MPa)$	22	25
$Mach_A$	6	5.797
η_G	0.65	0.512

Fig. 12.5 Comparison of major parameters for base and optimum scenarios

- The overall improvement of the system performance is more than 45% which is really considerable.

References

1. W.H. Heiser, D.T. Pratt, *Hypersonic airbreathing propulsion* (Aiaa, 1994.), vol. 1
2. E.T. Curran, Scramjet engines: The first forty years. J. Propul. Power **17**(6), 1138–1148 (2001)
3. P.L. Moses et al., NASA hypersonic flight demonstrators—Overview, status, and future plans. Acta Astronaut. **55**(3–9), 619–630 (2004)
4. R. Varvill, A. Bond, A comparison of propulsion concepts for SSTO reusable launchers. J. Br. Interplanet. Soc. **56**(3/4), 108–117 (2003)
5. X. Li, Z. Wang, Exergy analysis of integrated TEG and regenerative cooling system for power generation from the scramjet cooling heat. Aerosp. Sci. Technol. **66**, 12–19 (2017)
6. E. Daniau, et al., Fuel reforming for scramjet thermal management and combustion optimization, in *AIAA/CIRA 13th International Space Planes and Hypersonics Systems and Technologies Conference*, 2005
7. W. Bao et al., Effect of cooling channel geometry on re-cooled cycle performance for hydrogen fueled scramjet. Int. J. Hydrogen Energy **35**(13), 7002–7011 (2010)
8. W. Bao et al., Power generation and heat sink improvement characteristics of recooling cycle for thermal cracked hydrocarbon fueled scramjet. Sci. China Technol. Sci. **54**(4), 955–963 (2011)

9. H. Nasrollahi, et al., The greenhouse technology in different climate conditions: A comprehensive energy-saving analysis. Sustain. Energy Technol. Assessm. **47**, 101455 (2021)
10. H. Cho, A.D. Smith, P. Mago, Combined cooling, heating and power: A review of performance improvement and optimization. Appl. Energy **136**, 168–185 (2014)
11. M. Mohsenipour et al., Investigation of a geothermal-based CCHP system from energetic, water usage and CO_2 emission viewpoints. Gas Process. J. **7**(1), 41–52 (2019)
12. L. Jiang et al., Experimental study on a resorption system for power and refrigeration cogeneration. Energy **97**, 182–190 (2016)
13. T. Ratlamwala, I. Dincer, Comparative efficiency assessment of novel multi-flash integrated geothermal systems for power and hydrogen production. Appl. Therm. Eng. **48**, 359–366 (2012)
14. F. Sun et al., New waste heat district heating system with combined heat and power based on absorption heat exchange cycle in China. Appl. Therm. Eng. **37**, 136–144 (2012)
15. H. Onovwiona, V.I. Ugursal, Residential cogeneration systems: Review of the current technology. Renew. Sustain. Energy Rev. **10**(5), 389–431 (2006)
16. M.S. Azhar, G. Rizvi, I. Dincer, Integration of renewable energy based multigeneration system with desalination. Desalination **404**, 72–78 (2017)
17. H. Ghaebi, H. Rostamzadeh, P.S. Matin, Performance evaluation of ejector expansion combined cooling and power cycles. Heat Mass Transf. **53**(9), 2915–2931 (2017)
18. A.R. Choudhuri, S. Gollahalli, Combustion characteristics of hydrogen–hydrocarbon hybrid fuels. Int. J. Hydrogen Energy **25**(5), 451–462 (2000)
19. P. Seyedmatin, et al., Electricity and hydrogen co-production via scramjet multi-expansion open cooling cycle coupled with a PEM electrolyzer. Energy **199**, 117364 (2020)
20. M. Carmo et al., A comprehensive review on PEM water electrolysis. Int. J. Hydrogen Energy **38**(12), 4901–4934 (2013)
21. M. Lebbal, S. Lecœuche, Identification and monitoring of a PEM electrolyser based on dynamical modelling. Int. J. Hydrogen Energy **34**(14), 5992–5999 (2009)
22. F. Marangio, M. Santarelli, M. Calì, Theoretical model and experimental analysis of a high pressure PEM water electrolyser for hydrogen production. Int. J. Hydrogen Energy **34**(3), 1143–1158 (2009)
23. P. Ahmadi, I. Dincer, M.A. Rosen, Energy and exergy analyses of hydrogen production via solar-boosted ocean thermal energy conversion and PEM electrolysis. Int. J. Hydrogen Energy **38**(4), 1795–1805 (2013)
24. M. Ebadollahi et al., Proposal and assessment of a new geothermal-based multigeneration system for cooling, heating, power, and hydrogen production, using LNG cold energy recovery. Renew. Energy **135**, 66–87 (2019)
25. A. Pirmohamadi et al., Exergoeconomic analysis of a novel hybrid system by integrating the kalina and heat pump cycles with a nitrogen closed brayton system. Energy Rep. **7**, 546–564 (2021)
26. M. Ebadollahi, et al., Thermal and exergetic performance enhancement of basic dual-loop combined cooling and power cycle driven by solar energy. Therm. Sci. Eng. Progress **18**, 100556 (2020)
27. M. Mohsenipour, et al., Design and evaluation of a solar-based trigeneration system for a nearly zero energy greenhouse in arid region. J. Clean. Prod. **254**, 119990 (2020)
28. H. Rostamzadeh et al., Energy and exergy analysis of novel combined cooling and power (CCP) cycles. Appl. Therm. Eng. **124**, 152–169 (2017)
29. J.D. Anderson, *Modern Compressible Flow: With Historical Perspective* (McGraw-Hill, New York, 1990), vol. 2
30. Q. Yang, J. Chang, W. Bao, Thermodynamic analysis on specific thrust of the hydrocarbon fueled scramjet. Energy **76**, 552–558 (2014)
31. F.S. Billig, Research on supersonic combustion. J. Propul. Power **9**(4), 499–514 (1993)
32. P. Waltrup, F.S. Billig, Prediction of precombustion wall pressure distributions in scramjet engines. J. Spacecr. Rocket. **10**(9), 620–622 (1973)
33. J.W. Heffel, NOx emission and performance data for a hydrogen fueled internal combustion engine at 1500rpm using exhaust gas recirculation. Int. J. Hydrogen Energy **28**(8), 901–908 (2003)

34. J. Qin et al., Performance cycle analysis of an open cooling cycle for a scramjet. Proc. Inst. Mech. Eng. Part G J. Aerosp. Eng. **223**(6), 599–607 (2009)
35. M. Ebadollahi et al., Energy and Exergy Analysis of a Geothermal-Based Multi-generation System, in *Integration of Clean and Sustainable Energy Resources and Storage in Multi-Generation Systems.* (Springer, 2020), pp. 121–140
36. Y.A. Cengel, M.A. Boles, Thermodynamics: An engineering approach. Sea **1000**, 8862 (2002)
37. M. Bezaatpour et al., Magnetic-induced nanoparticles and rotary tubes for energetic and exergetic performance improvement of compact heat exchangers. Powder Technol. **377**, 396–414 (2021)
38. M.-R. Kolahi, M. Amidpour, M. Yari, Multi-objective metaheuristic optimization of combined flash-binary geothermal and humidification dehumidification desalination systems. Desalination **490**, 114456 (2020)
39. A. Bejan, G. Tsatsaronis, *Thermal Design and Optimization* (John Wiley & Sons, 1996)
40. R. Kheiri et al., Thermodynamic modeling and performance analysis of four new integrated organic Rankine cycles (A comparative study). Appl. Therm. Eng. **122**, 103–117 (2017)
41. M. Kolahi et al., Thermodynamic and economic performance improvement of ORCs through using zeotropic mixtures: Case of waste heat recovery in an offshore platform. Case Stud. Therm. Eng. **8**, 51–70 (2016)
42. H. Rostamzadeh, et al., Exergoeconomic optimisation of basic and regenerative triple-evaporator combined power and refrigeration cycles. **26**(1–2), 186–225 (2018)
43. M. Ebadollahi, et al., Close supercritical versus inverse brayton cycles for power supply, using waste of a biogas-driven open brayton cycle. J. Energy Resour. Technol. **143**(9) (2021)
44. M. Ebadollahi et al., Proposal and multi-criteria optimization of two new combined heating and power systems for the Sabalan geothermal source. J. Clean. Prod. **229**, 1065–1081 (2019)
45. M. Ebadollahi et al., Exergoeconomic analysis and optimization of innovative cascade bi-evaporator electricity/cooling cycles with two adjustable cooling temperatures. Appl. Therm. Eng. **152**, 890–906 (2019)
46. H. Rostamzadeh et al., Comparative study of two novel micro-CCHP systems based on organic Rankine cycle and Kalina cycle. Energy Convers. Manage. **183**, 210–229 (2019)
47. T.J. Kotas, *The Exergy Method of Thermal Plant Analysis* (Elsevier, 2013)

Part III
Energy Procurement in Sensitive Places and Remote Areas

Chapter 13
Abandoned Wells and Geothermal Energy: A Survey on the Utilization of Geothermal Heat from Abandoned Wells in Energy Systems

Mohammad-Reza Kolahi, Mohammad Ebadollahi, Hossein Nami, Mortaza Yari, Majid Amidpour, and Davar Ebrahimi

Abstract Every year many oil and gas wells in the oilfields get depleted and abandoned all over the world. Notwithstanding the costs and risks of the petroleum wells depletion, they contain sufficient amounts of geothermal energy that can be used for different purposes. Utilizing the geothermal heat of the abandoned oil and gas wells, besides saving drilling costs and managing the residual oil pollution, can relieve the energy problems. This chapter will focus on the plausibility of geothermal heat extraction from the abandoned wells, their associated advantages and challenges, the methods of heat extraction, and the utilized energy systems. Finally, a new approach in the application of energy systems in the abandoned wells will be analyzed and optimized.

M.-R. Kolahi
Energy and Environment Research Center, Niroo Research Institute, Tehran, Iran
e-mail: mcolahi@nri.ac.ir

M. Ebadollahi · M. Amidpour (✉)
Faculty of Mechanical Engineering, Department of Energy System Engineering, K.N. Toosi University of Technology, Tehran, Iran
e-mail: amidpour@kntu.ac.ir

H. Nami
Department of Energy Conversion and Storage, Technical University of Denmark, Kongens Lyngby, Denmark
e-mail: hona@dtu.dk

M. Yari
Faculty of Mechanical Engineering, University of Tabriz, Tabriz, Iran
e-mail: myari@tabrizu.ac.ir

D. Ebrahimi
Renewable Energy Research Department, Energy and Environment Research Center, Niroo Research Institute, Tehran, Iran
e-mail: debrahimi@nri.ac.ir

Nomenclature

Abbreviations

ORC	Organic Rankine Cycle
ODP	Ozone Depletion Potential
HDH	Humidification Dehumidification
GWP	Global Warming Potential (year)
PSO	Particle Swarm Optimization
GOR	Gained Output Ratio

Symbols

T	Temperature (K)
h	Specific enthalpy (kJ/kg)
$\dot{m}$	Mass flow rate (kg/s)
mf_{ORC}	Mass fraction of zeotropic mixtures
mf_{HDH}	Mass flow rate of the HDH unit
$\dot{Q}$	Heat (kW)
$\dot{W}$	Work (kW)

Greek letters

ε	Effectiveness (%)
φ	Relative humidity
ω	Absolute humidity (kg/kg)

Subscripts

cr	critical point
pp	pinch point
in	Inlet
out	Outlet
Turbine	ORC's Turbine
Pump	Pump
Hu	Humidifier
DH	Dehumidifier
tot	Total

da   dry air
pw   pure water
fg   vaporization latent heat

13.1   Introduction

Geothermal energy is sustainable and renewable energy with some advantages such as reliability, stability, independence, and environmentally friendly feature [1, 2]. It has also been widely investigated for climate change mitigation, air pollution reduction, and energy demand solution [3]. The continuous availability and reliability of geothermal energy make geothermal resources more attractive for the power industry than other energy sources [4]. However, despite the positive potential of geothermal energy, it is not without drawbacks: boreholes' exploration and drilling high costs and technical problems are the main barriers to the commerciality of geothermal systems worldwide [5]. Although the expensive cost of drilling restricts geothermal energy developments, many oil wells are abandoned all around the world that have previously been explored, drilled, exploit, and depleted and now they can be used as geothermal resources for energy generation. If the abandoned wells can be utilized for generating geothermal energy, it not only would decrease the cost of drilling wells but also give more renewable energy [6].

In the petroleum industry, the final step of developing an oil field has been usually considered abandonment [7]. It is estimated that there are about 20–30 million abandoned oil and gas wells worldwide [8], and with continuous petroleum exploitation, more and more oil and gas wells have been abandoned without economic feasibility, which contain abundant geothermal energy and have the potential of severe pollution by the leak of the residue oil [9]. These wells, which are dry holes that never strike oil [10], are normally considered as permanent liabilities that require high costs to plug and abandon; but, their existing wellbore is a way to the geothermal energy resources. Consequently, an abandoned oil or gas well can give an opportunity for the extraction of geothermal heat [3]. In geothermal heat extraction, although the flow rate of active wells, in which the produced water is dominated by oil production, are usually higher, the abandoned wells, because of their more flexibility for modifications (e.g., selection of the injection fluid and its temperature and rate), are more manageable than the producing wells [3]. In this chapter, the possibility of geothermal heat extraction from abandoned oil and gas wells, their utilization advantages and challenges, the methods of heat extraction, and the utilized energy systems are discussed. Also, a new approach in applied energy systems will be analyzed.

13.2   Advantages and Challenges

The utilization of the abandoned oil and gas wells for geothermal energy generation can save drilling costs, reduce energy problems, and manage the pollution of wells' residual oil [8]. One of the advantages of utilizing abandoned wells for geothermal heat harnessing is the positive environmental aspect that creates the opportunity of utilizing heat resources locally, and gives partial independence of cost trends for conventional fuels [11]. Compared to traditional geothermal fields, abandoned oil wells can provide some advantages to develop geothermal energy through existing wellbores and facilities in a low-cost and low-risk manner [3, 4, 12]:

1. Cost-effectiveness: No drilling investment is required because the wellbore with established integrity is previously there, and the design of the recharge well can be neglected completely. Furthermore, existing surface infrastructures in the oilfield (e.g., installed well site facilities, service roads to well sites, and pipes) could further lower the initial costs.
2. Data Availability: From the long-term petroleum exploration and production, adequate information has been gathered and investigated. Therefore, the geological and thermal properties of wells are known and available.
3. Risk reduction: The risk of drilling is decreased during a long time, and the reservoir uncertainties' risk also can be more reduced based on the information for the reservoir characterizations.
4. Sufficient well candidates: In an oilfield, especially in a mature oilfield, there is a sufficient number of wells for geothermal utilization, and among those candidates, the wells with high bottom hole temperature and reliable wellbore integrity can be picked.
5. No groundwater extraction: Abandoned oil wells are dry holes, and groundwater recession, corrosion, and scaling issues can be neglected.
6. Existing technology: Retrofitting wellbore with equipping the inner pipe is a proven technology. Also, the working fluid selection with acceptable thermodynamic properties can be easy with the developed principles.
7. Company support: A sufficient amount of geothermal energy can be produced continuously from the abandoned oil wells. With the utilization of this energy in the oilfield itself, the overall operation cost can be compensated.

Despite the advantages of abandoned oil wells geothermal applications and its successful projects, there are still some challenges for the large-scale developments of geothermal resources: low efficiency of energy conversion, unsound policies, insufficient planning and assessment, insufficient involvement, and some other problems [3].

13.3   Heat Extraction from the Abandoned Wells

Geothermal heat has been traditionally extracted in locations characterized by hydrogeological anomalies [13]. But, the risk of induced earthquakes and groundwater pollution caused by new geothermal sites substantially impact the population living in the places near to the sites. Therefore, it is crucial to search some solutions to prevent these risks, which can lead to a low social acceptance for the geothermal projects [14]. Recent geothermal engineering advances, however, have enabled some alternative approaches; for instance, heat extraction without geothermal fluid production by Borehole Heat Exchangers (BHE) or the application of Enhanced Geothermal Sources (EGS). Both the technologies harvest the earth's heat without the location constraints of hydrothermal systems [13]. A deep borehole heat exchanger (wellbore heat exchanger) is a closed-loop in which a heat carrier fluid circulates and extracts the geothermal heat from the surrounding rock [14].

Between oil extraction operations and geothermal projects has apparent similarities that lead to the possibility of applying the experiences and advanced technologies from the petroleum industry in geothermal plans [5]. For the heat extraction from an abandoned oil well, a wellbore heat exchanger is suggested [15]. In the heat exchanger, the heat carrier fluid at the surface is injected into the well, and then it is gradually heated up with the surrounding formation by its descent. The cement and casing are usually used as the shield preventing fluid from touching with the formation [9]. When the injected fluid arrives at the bottom of the well, when it is at the top temperature, it reverses its direction and ascends to the wellhead. Then the fluid's heat is taken and consumed for different purposes, and after that, the cooled fluid flows out from the consumer system and returns into the heat exchanger, which forms a closed-loop.

There are two common types of abandoned wells heat exchangers: double pipe and U-tube heat exchangers that are presented in Fig. 13.1. Although the u-tube heat exchanger was the most common form of heat extraction method, the double pipe one attracts more attention due to its advantages [3]: (1) it has a larger heat transfer area and contains more volume of fluid for exchanging the heat, (2) because of the lower flow velocity, it needs less hydraulic pressure, and thus lower pumping energy consumption, to circulate the fluid, (3) because of the coaxial geometry it reduces the thermal resistance between the wellbore and the fluid, and (4) since the outer pipe (casing) is previously existed in the cased abandoned wells, creating a double pipe heat exchanger is more suitable option than a U-tube one, saving money and time.
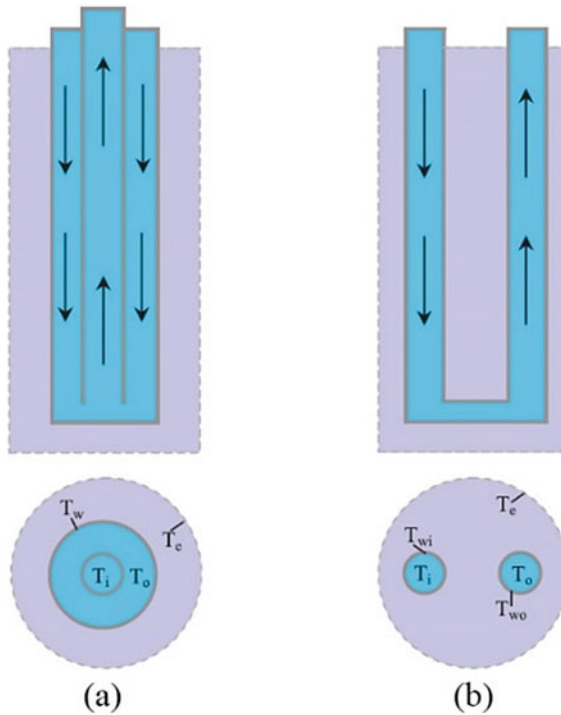
Fig. 13.1 The schematic presentation of **a** double pipe and **b** U-tube heat exchangers [4]

13.4 The Utilized Micro Energy Systems in the Abandoned Wells

A significant amount of heat, because of the thermal properties of reservoir rock, is accumulated within it during thermal processes, and this trapped heat can be exploited as geothermal energy potential [16]. The geothermal energy potential from the abandoned oil wells not only would add more renewable energy to the grid, but it would also help avert environmental problems and drilling costs [12]. Besides getting rid of the drilling cost of the boreholes, using oil wells means that all the required information for the geothermal plants are available [5]. Hence, many researchers have begun to study geothermal energy potential from the abandoned oil wells for heat extraction and power generation.

Since the petroleum wells, in many cases, go to a high depth below the surface, the temperatures of the wells' bottom holes are high enough to generate geothermal power. Geothermal resources generally are categorized into three classes: low-temperature (<90 °C), medium-temperature (90–150 °C), and high-temperature resources (>150 °C). Abandoned oil wells geothermal energy is classified as medium to low-temperature sources [10]. The abandoned oil wells' geothermal resources have
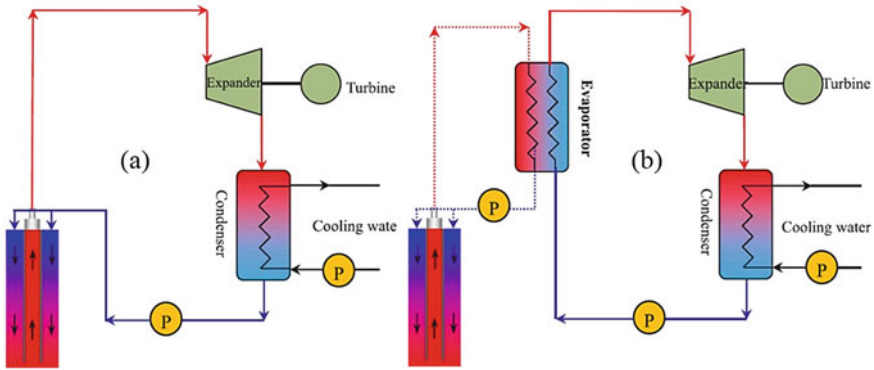
Fig. 13.2 The schematic of **a** direct and **b** indirect utilization of the abandoned wells [4]

been utilized in different applications, and the heat extracted from the wells: either direct use (in which the heat directly enters the system) or indirect use (in binary systems). The direct and indirect utilization of the abandoned wells is shown in Fig. 13.2. By reviewing the literature, for heating applications, most of the works are about the simulation of the borehole heat exchangers, and for power generation, many of them have analyzed binary power systems like organic Rankine cycles.

Bu et al. [6], studied the feasibility of obtaining geothermal energy from China's abandoned oil and gas wells and showed that both heat and power could be produced from the wells. Their results also indicated that geothermal energy depends mainly on the flow rate of fluid and the geothermal gradient. Śliwa and Kotyza [11], conducted a preliminary calculation and economic analysis of the energy resource and the possible heat exchange from depleted oil wells of Poland. They showed that the borehole heat exchangers were rarely affected by geological situations, and well parameters were significantly affected by the cost of conventional energy carriers. Caulk and Tomac [13], studied the suitability of abandoned wells for Enhanced Geothermal Systems (EGS) and low-temperature deep Borehole Heat Exchanger (BHE) utilization for aquaculture, district heating, and greenhouse heating in California, USA. They pointed that the deep coaxial BHE was a reasonable low-risk and low-cost alternative to EGS, and deep BHE was proper for the low and high heat flows. Limpasurat and Falcone [16], used a thermal and compositional simulator to investigate the overall heat transfer efficiency in an abandoned oil well. Then, they performed sensitivity analyses to recognize essential parameters that may influence the harnessing geothermal energy potential. Their study revealed that it can be possible to beneficially increase the heavy oil fields life through a heat-recovery phase after the oil-recovery phase. Nian and Cheng [9], conducted the energy and economic analysis to assess the thermo-economic performance of a geothermal heating system utilizing abandoned oil wells, and they confirmed that the system could keep a building (with the maximum heating area of 11,000 m^2) at around 26 °C with water flow rate 20 m^3/h. Also, their system's maximum annualized cost was 1.72$/$m^2$ (about half of that of the formal heating method). Macenić and Kurevija [17], considered an

abandoned oil well in Croatia for the geothermal heat production through the coaxial heat exchanger, and from their results, the extraction of heat for possible industrial direct heating was 400 kW in 20 years, while maximum potential heat extraction in a variable system was 1750 MWh/year.

Davis and Michaelides [12], performed a simulation for the determination of geothermal power production from abandoned oil wells with double-pipe heat exchanger by injecting and retrieving a secondary fluid (Isobutane), and they can produce 2–3 MW of electric power from the wells of the South Texas region. Zhang et al. [7], evaluated the possible power and income that can be produced from an abandoned oil reservoir in China that has been transferred into an enhanced geothermal reservoir by oxidization of crude oil with air (or oxygen) injection; and they concluded that the utilization of the binary geothermal cycles for electricity generation is more suitable than the other power generation technologies in their cases. Ebrahimi and Moussavi Torshizi [15], investigated and optimized an Organic Rankine Cycle (ORC) to produce power from a set of low-temperature abandoned gas wells in Iran, and they could generate 135 kW from each well by direct injection of working fluid into the wells. Kharseh et al. [5], presented an analysis of two binary ORC geothermal systems (air-cooled and water-cooled cycles) for electricity production in Qatar. They showed that the utilization of the oil wells as the heat source for the proposed ORCs has an economic potential in which the payback period was less than eight years, and the levelized cost of electricity was 3.6 US$/kWh. Cheng et al. [10], investigated theoretical analysis of geothermal power production from abandoned wells utilizing isobutane as the cycle fluid. They used an ORC with a double-pipe heat exchanger and achieved the maximum net power of 154 kW. Cheng et al. [18], also studied the geothermal power generation performances applying various organic fluids in some power systems, and they concluded that R134a and R245fa are more suitable than R600a, R600, propylene, R290, and R143a for the geothermal power production in the abandoned oil wells. Wight and Bennett [19], adopted an abandoned well as a heat exchanger for a binary ORC in which water was the wellbore circulating fluid. They could produce 109 kW power using a wellbore depth of 4200 m with a mass flow rate of 2.5 kg/s. Mayer et al. [20], inserted two electricity generation cycles (single and double loop ORC systems) to the abandoned hydrocarbon wells in Hungary, and they found that the single-loop system was able to operate at higher efficiency, and the payback period for the systems could be less than ten years. Yang et al. [21], designed and manufactured a 500 kW geothermal ORC system from the abandoned oil wells of Huabei oilfield, China. Their experimental results showed that the turbine efficiency and the ORC efficiency could be 78.52% and 5.33%, respectively, using R245fa as the system's working fluid. Alimonti et al. [14], analyzed the power production of the wellbore heat exchanger with two different systems (an ORC plant and a Stirling motor) in the abandoned oil wells of Villafortuna Trecate oilfield, Italy. The results revealed that the ORC plant, whose working fluid was R-C318, generated 121 kW power, while the net electrical power of Stirling motor was 152 kW.

Besides the abandoned wells, there are many active production wells in the oilfields whose liquid medium contains a large amount of water. During petroleum

extraction projects, water is produced over the lifetime of a production well that generally comprises vast concentrations of Total Dissolved Solids (TDS), requiring desalination [22]. Conventional water desalination systems, however, generally consume lots of energy, such as electricity or fossil fuels. Also, these desalination technologies are not entirely environmentally friendly and release a lot of greenhouse gasses. Therefore, a combination of renewable energy systems (e.g., wind, waste heat, solar, wave, and geothermal) with desalination units would be helpful [22, 23]. In this regard, some researchers have also utilized the geothermal energy of abandoned wells to desalinate seawater and produced water from petroleum fields. Kiaghadi et al. [22], combined heat transfer modelling with water desalination relations to study the utilization of abandoned oil and gas wells geothermal resources, in order to turn brackish water into freshwater. They showed that in a 4000 m deep well with a geothermal gradient of 0.05 °C/m, almost 600,000 L of clean water per day could be reduced. Noorollahi et al. [24], carried out a numerical study of an abandoned oil well in Iran for a multi-effect seawater desalination process, and they can purify about 565 m^3/day of freshwater.

The presented literature review outlines an obvious absence of studies on the combined or multigeneration systems in geothermal resources of abandoned oil wells. Also, notwithstanding the outstanding efforts on this subject, no research can be seen on the use of zeotropic mixtures in their binary ORC systems. Therefore, a new approach has been presented in the next section for the use of abandoned wells' geothermal heat by a multigeneration energy system.

13.5 A New Approach

The proposed new approach in this study is illustrated in Fig. 13.3. As shown in the figure, the system is a combined power generation and water purification system whose energy is obtained from an abandoned oil well geothermal resource. The system comprises two parts: a cascade ORC unit and a Humidification Dehumidification Desalination unit (HDH). The geothermal energy from the heat carrier fluid first moves into the evaporator of the cascade ORC unit then continues to the HDH unit's heater. Cascade ORC unit actually includes two ORCs in which the condenser of the upper one is the evaporator of the other cycle. Also, the ORC units' working fluids are zeotropic mixtures. Each of the mixtures is a combination of two organic fluids. Besides, in the desalination unit, salty water moves through the dehumidifier, in which the streaming airflow between the dehumidifier and the humidifier will cool and condense. After that, salty water is heated up in the heater, and then it warms up and humidifies the airflow into the humidifier. Eventually, with the repetition of this process, freshwater is collected from the dehumidifier, and the remaining water is discharged as brine [25].

In this system, the heat carrier fluid is water, and its mass flow rate and top temperature are considered 5 kg/s and 393.15 K. The selection of organic fluid, however, is an essential step in which many conditions have to be considered: (1)
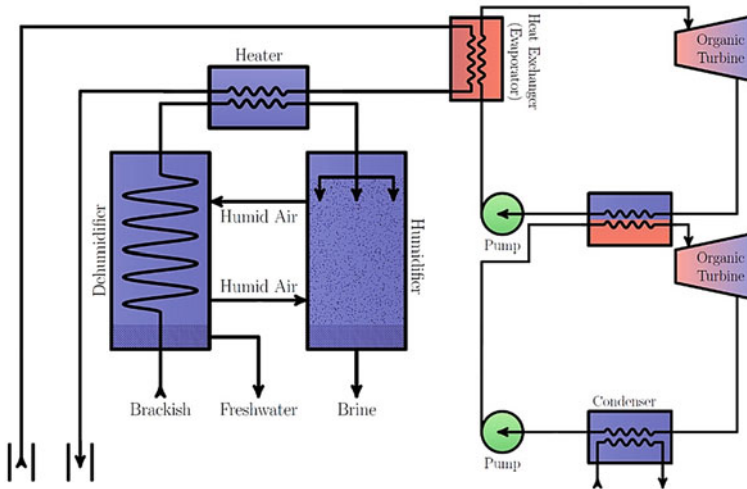
Fig. 13.3 The schematic illustration of the proposed system

positive/isentropic saturation vapor curve (ds/dT), (2) good thermodynamic performance, (3) low viscosity, (4) high conductivity, (5) fine safety level, (6) high vapour density, (7) less Ozone Depleting Potential (ODP), (8) small Global Warming Potential (GWP), (9) suitable availability, and (10) low cost. Obviously, it is impossible to gather all of the named features in just one fluid; consequently, employing zeotropic mixtures instead of single fluids is another solution that overcomes this problem. Besides, the zeotropic mixture has other advantage: the glide in temperature profile of the two phase process that makes the temperature profiles of the working fluids match better together and improves the system's efficiency [26]. After considering the mentioned conditions, 17 most used organic fluids in the literature which have low ODP and GWP were examined here: ISOHEXANE, CYCLOPENTANE, CYCLOHEXANE, HEXANE, TOLUENE, BUTANE, DECANE, NEOPENTANE, HEPTANE, BENZENE, ISOBUTAN, OCTANE, BUTENE2C, ISOBUTENE, ISOPENTANE, R1233ZD, and PENTANE. Two of them have to be mixed together for the upper ORC, and two others should be selected for the lower ORC. The selection procedure among these fluids and optimizing each related system were a bit challenging and time-consuming; but, finally, 4 cases were chosen: (case 1) ISOHEXANE—CYCLOPENTANE (for upper ORC)/ISOPENTANE—PENTANE (for lower ORC), (case 2) ISOHEXANE—HEXANE (for upper ORC)/ISOPENTANE—PENTANE (for lower ORC), (case 3) CYCLOPENTANE—HEXANE (for upper ORC)/ISOPENTANE—PENTANE (for lower ORC), and (case 4) CYCLOHEXANE—HEXANE (for upper ORC)/ISOPENTANE—PENTANE (for lower ORC).

The performance of the system is analyzed by the laws of thermodynamics; then, a metaheuristic optimization will be conducted on the indicators. In this regard, some assumptions should be considered: the system is in the steady state condition

[27], pressure drops and heat losses are negligible [28], and kinetic and potential energies changes are insignificant [29]. Also, during the operation of the systems, the composition of the zeotropic mixtures will not change [30]. Thermodynamic modelling and optimization code of the systems have been written in MATLAB, and thermodynamic properties of the working fluids (e.g., heat carrier fluid, humid air, zeotropic mixtures, and salty water) are obtained from CoolProp [31] and REFPROP 8.0. [32] libraries, and Sharqawy et al. correlations [33].

Energy and mass balances equations for each component of the system are as follows [34, 35]:

$$\dot{Q} - \dot{W} = \sum \dot{m}_{out} h_{out} - \sum \dot{m}_{in} h_{in} \tag{13.1}$$

$$\sum \dot{m}_{out} = \sum \dot{m}_{in} \tag{13.2}$$

where $\dot{m}$ is the mass flow rate, $\dot{W}$ is the net output work, $\dot{Q}$ is the net input heat, and h is the specific enthalpy. Also, $\dot{W}_{tot}$ is achieved by [36]:

$$\dot{W}_{tot} = \dot{W}_{ORC1} + \dot{W}_{ORC2} \tag{13.3}$$

$$\dot{W}_{ORC} = \dot{W}_{Turbine} - \dot{W}_{Pump} \tag{13.4}$$

The mass flow rate produce freshwater is:

$$\dot{m}_{pw} = \dot{m}_{da} \Delta \omega_{humidair} \tag{13.5}$$

where da and pw subscripts refer to dry air and pure water. The effectiveness of water production in an HDH system, is determined as the ratio of evaporation latent heat of freshwater ($\dot{m}_{pw} h_{fg}$) to input heat of the system ($\dot{Q}_{He}$), that is named Gained Output Ratio (GOR) [37]:

$$GOR = \frac{\dot{m}_{pw} h_{fg}}{\dot{Q}_{He}} \tag{13.6}$$

where h_{fg} is the evaporation latent heat of freshwater, which is obtained at the water vapor's average partial pressure.

Here Particle Swarm Optimization (PSO) has been used for the optimization. PSO is introduced by Kennedy and Eberhart [38], and inspired by the natural swarm behaviours such as the birds' choreography [25, 39]. The goal of optimization in this work is to get the optimal total output power, $\dot{W}_{tot}$, and obtained freshwater, $\dot{m}_{pw}$. The two objectives of the optimization should be optimized separately. As the HDH unit is placed after the cascade ORC unit, optimization should first be conducted on the ORCs. Also, the optimization variables are the mass flow rate of the HDH unit

($mf_{HDH} = m\dot{H}DH_{in}/\dot{m}_{da}$) and the ORCs' top and low temperatures (T_{top}, T_{mid}, and T_{low}). The other parameters (e.g., air relative humidity (ϕ_{air}), the zeotropic mixtures' mass fraction (mf_{ORC}), and effectiveness of the humidifier and the dehumidifier (ε_{Hu} and ε_{DH})) are supposed to be constant or as design variables. Mathematically, the optimization problem can be shown as:

$$\begin{cases} \dot{W}_{tot} = f_1(T_{top}, T_{low}) \\ \dot{m}_{pw} = f_2(mf_{HDH}) \end{cases} \tag{13.7}$$

and the constraints and the bounds of the variables are:

$$\begin{cases} \Delta T_{pp} \geq 5K \\ T_{mid} < T_{top} < T_{cr} \\ T_{low} < T_{mid} < T_{top} \\ T_0 < T_{low} < T_{mid} \\ 1 \leq mf_{HDH} \leq 3 \end{cases} \tag{13.8}$$

where ΔT_{pp} is the pinch points temperature difference.

Figure 13.4 gives the T-s diagram of the cascade ORC unit. As the figure shows, there are apparent temperature glides in the two-phase regions, making the temperature profiles match better together. For the HDH unit, Fig. 13.5 shows its $GOR - mf_{HDH}$ diagram, which is the performance of the desalination system in relative humidity of 0.95. Here, the HDH unit's maximum temperature is considered 60 °C. As Fig. 13.5 shows, with rising the effectiveness of the dehumidifier and humidifier (ε_{DH} and ε_{Hu}), the desalination system gives better performance (GOR). Furthermore, by raising the HDH unit's mass flow rate, GOR increases to a maximum value then reduces [25].
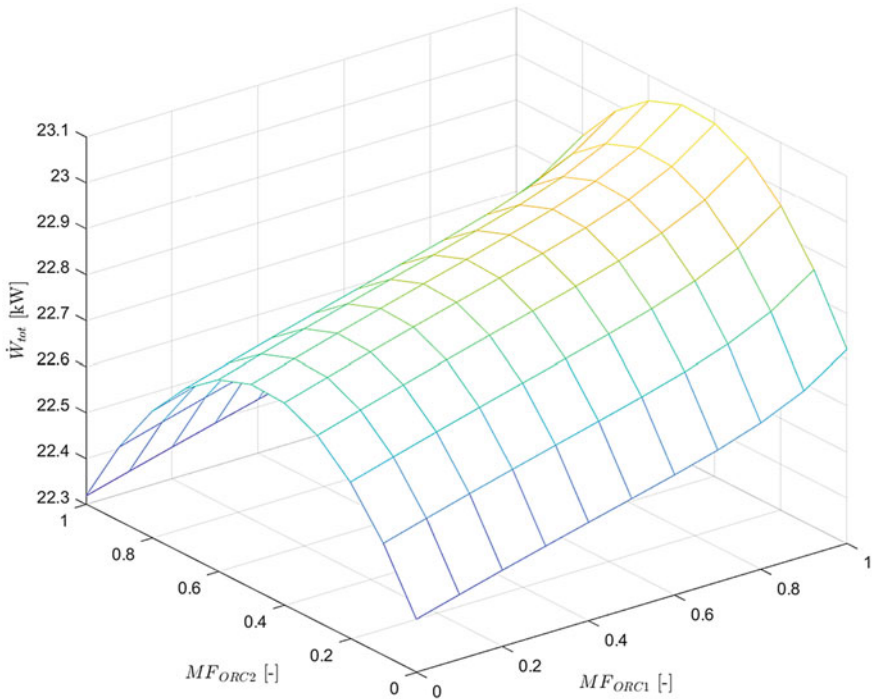
**Fig. 13.4** The T-s diagram of the cascade ORC unit
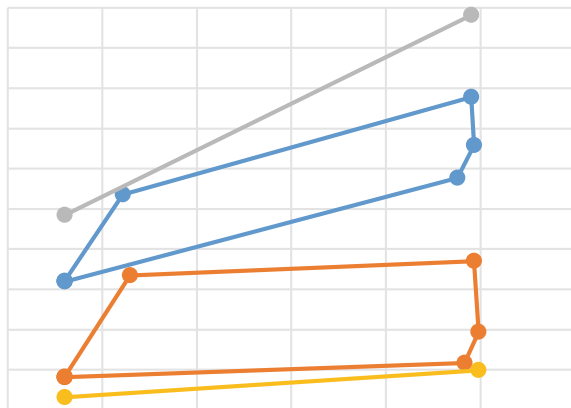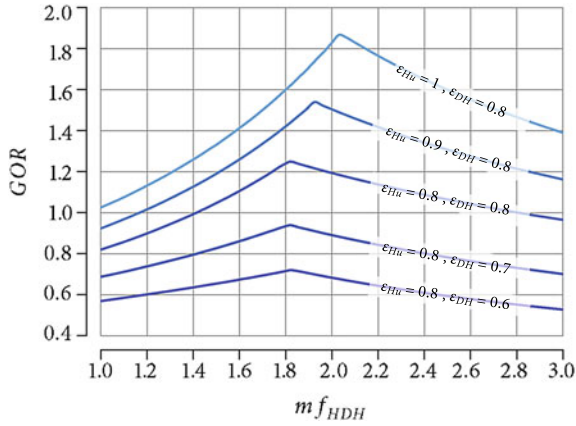
Fig. 13.5 The $GOR - mf_{HDH}$ diagram of the HDH unit

If the medium temperature (T_{mid}) of the cascade ORC unit is considered as the average of the top and low temperatures, the total output works of the system (for the 4 cases of mixtures) are presented in Figs. 13.6, 13.7, 13.8, and 13.9. As the figures

Fig. 13.6 The system's total output work in the 1st case of the mixtures
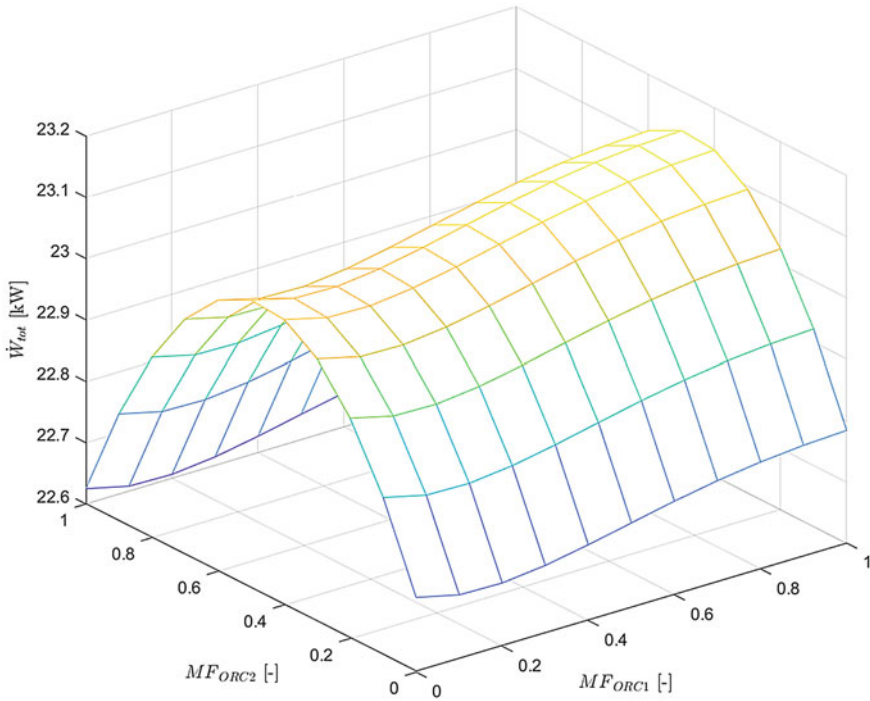
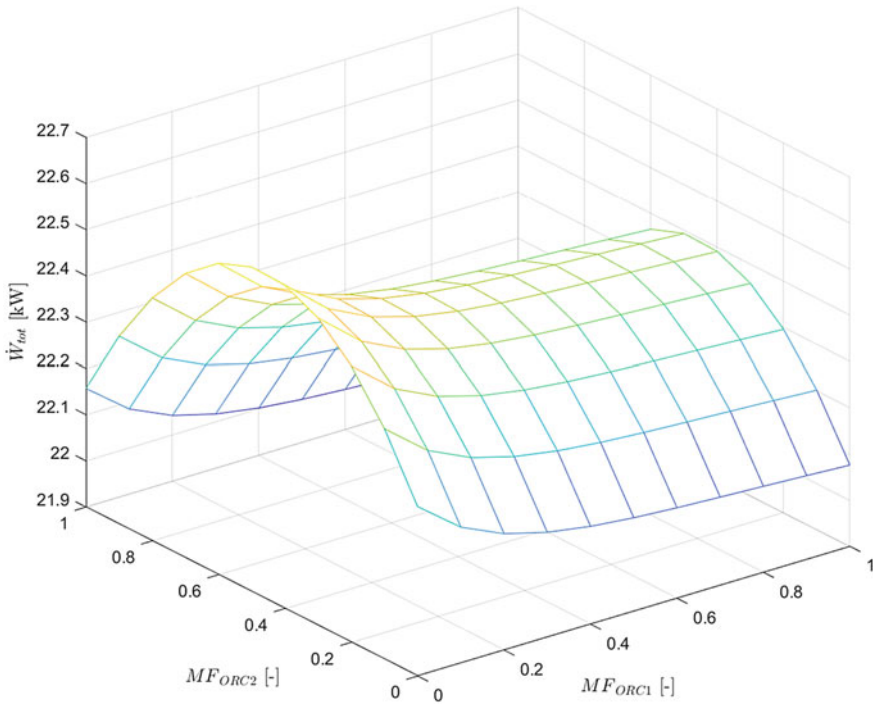**Fig. 13.7** The system's total output work in the 2nd case of the mixtures

show, in some cases, with the variations of the mass fractions, the total output work gets an optimum value; and it is because of the better match in temperature profiles.

In the mass fractions of 0.5 for the cascade ORC unit and in operating conditions of $\varepsilon_{Hu} = 80\%$, $\varepsilon_{DH} = 80\%$, and $\phi_a = 0.95$ for the HDH unit, the amount of produced freshwater (in L/day) for each case is illustrated in Fig. 13.10.

As Fig. 13.10 indicates, it is clear that in the cases with higher output work, the amount of produced freshwater is lower; since, in these cases, most of the geothermal energy are consumed for power generation. Also, from the figures, for all of the selected mixtures cases, the total output works are about 22–23 kW, and the produced freshwater is in the range of 532,750–533,042 L/day.

13.6   Conclusion

This chapter investigated the possibility of geothermal heat extraction from the abandoned oil and gas wells. Besides, it discussed the advantages and challenges of the utilization of the wells. Borehole heat exchangers were also compared and shown

Fig. 13.8 The system's total output work in the 3rd case of the mixtures

that although the u-tube heat exchanger was the most common form of heat extraction method, the double pipe ones attract more attention due to their benefits. Then almost all kinds of the utilized energy systems in the abandoned wells were reviewed. The literature review outlined that there was an obvious absence of the combined or multigeneration systems in geothermal resources of abandoned oil wells. Therefore, a new approach was presented to use the abandoned wells' geothermal heat by a multigeneration energy system that simultaneously produced power and water with a cascade ORC unit and an HDH unit. For the working fluids of the ORCs, four sets of zeotropic mixtures were chosen, and the results showed that the total output works were about 22–23 kW, and the produced freshwater was in the range of 532,750–533,042 L/day.
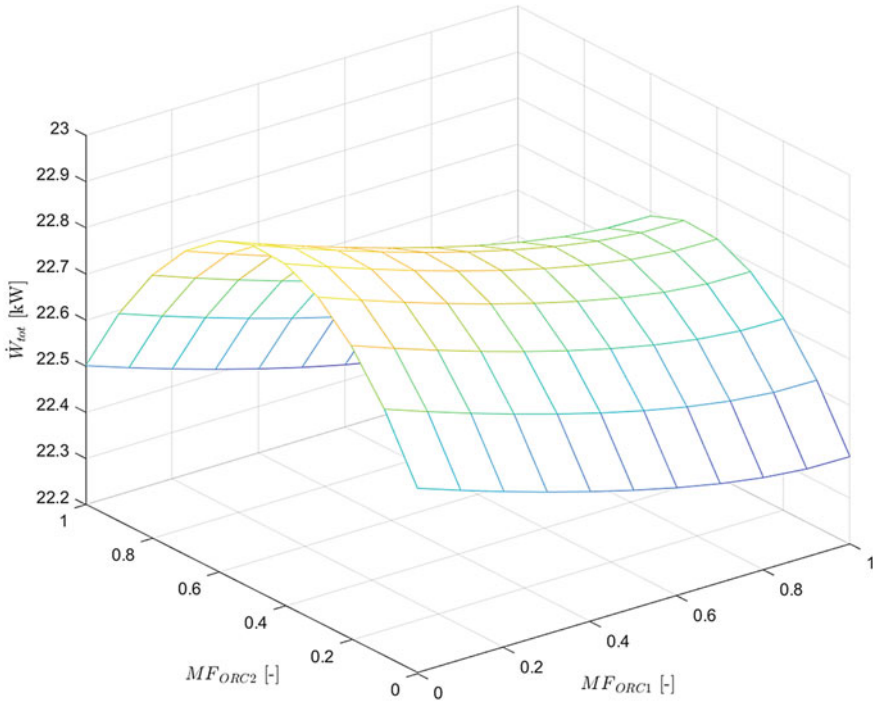
Fig. 13.9 The system's total output work in the 4th case of the mixtures
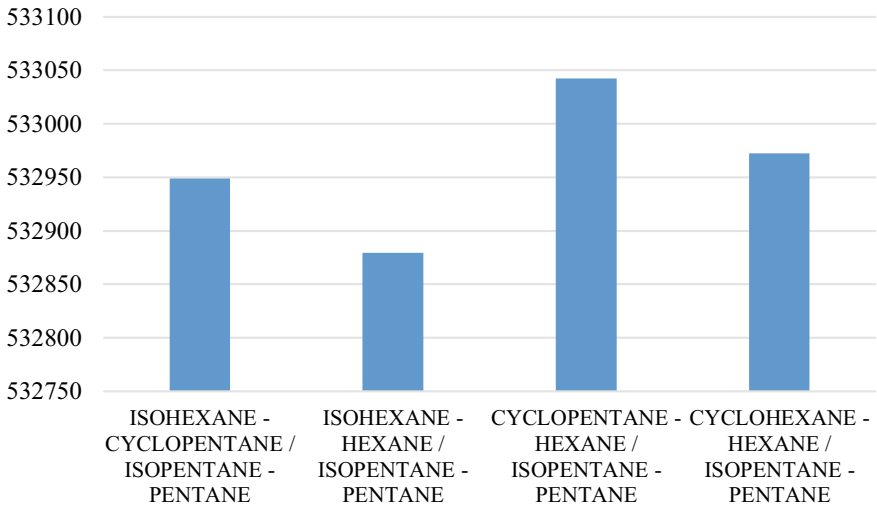
Fig. 13.10 The amount of produced freshwater (in L/day) for each case

References

1. M.R. Kolahi, A. Nemati, M. Yari, Performance optimization and improvement of a flash-binary geothermal power plant using zeotropic mixtures with PSO algorithm. Geothermics **74**, 45–56 (2018). https://doi.org/10.1016/j.geothermics.2018.02.004
2. M. Mohsenipour, F. Ahmadi, A. Mohammadi, M. Ebadollahi, M. Amidpour, Investigation of a geothermal-based CCHP system from energetic, water usage and CO_2 emission viewpoints. Gas Process. J. **7**(1), 41–52 (2019). https://doi.org/10.22108/GPJ.2019.118131.1058
3. K. Wang, B. Yuan, G. Ji, and X. Wu, A comprehensive review of geothermal energy extraction and utilization in oilfields. J. Petrol. Sci. Eng. **168**. Elsevier B.V., 465–477 (2018). https://doi.org/10.1016/j.petrol.2018.05.012
4. Y. le Nian, W. L. Cheng, Insights into geothermal utilization of abandoned oil and gas wells. Renewable Sustainable Energy Rev. **87**. Elsevier Ltd, 44–60 (2018). https://doi.org/10.1016/j.rser.2018.02.004
5. M. Kharseh, F. Hassani, and M. Alkhawaja, Potential of geothermal energy for electricity generation in Qatar, in *ISARC 2013 - 30th International Symposium on Automation and Robotics in Construction and Mining, Held in Conjunction with the 23rd World Mining Congress* (2013), pp. 1350–1358. https://doi.org/10.22260/isarc2013/0152
6. X. Bu, W. Ma, H. Li, Geothermal energy production utilizing abandoned oil and gas wells. Renewable Energy **41**, 80–85 (2012). https://doi.org/10.1016/j.renene.2011.10.009
7. L. Zhang, J. Yuan, H. Liang, and K. Li, Energy from abandoned oil and gas reservoirs, in *SPE Asia Pacific Oil and Gas Conference and Exhibition 2008 - "Gas Now: Delivering on Expectations,"* vol. 1 (2008), pp. 495–503. https://doi.org/10.2118/115055-ms
8. W.L. Cheng, J. Liu, Y. le Nian, C.L. Wang, Enhancing geothermal power generation from abandoned oil wells with thermal reservoirs. Energy **109**, 537–545 (2016). https://doi.org/10.1016/j.energy.2016.05.009
9. Y. le Nian, W.L. Cheng, Evaluation of geothermal heating from abandoned oil wells. Energy **142**, 592–607 (2018). https://doi.org/10.1016/j.energy.2017.10.062
10. W.L. Cheng, T.T. Li, Y. le Nian, C.L. Wang, Studies on geothermal power generation using abandoned oil wells. Energy **59**, 248–254 (2013). https://doi.org/10.1016/j.energy.2013.07.008
11. T. Śliwa, J. Kotyza, Application of existing wells as ground heat source for heat pumps in Poland. Appl. Energy **74**(1–2), 3–8 (2003). https://doi.org/10.1016/S0306-2619(02)00125-3
12. A.P. Davis, E.E. Michaelides, Geothermal power production from abandoned oil wells. Energy **34**(7), 866–872 (2009). https://doi.org/10.1016/j.energy.2009.03.017
13. R.A. Caulk, I. Tomac, Reuse of abandoned oil and gas wells for geothermal energy production. Renewable Energy **112**, 388–397 (2017). https://doi.org/10.1016/j.renene.2017.05.042
14. C. Alimonti, D. Berardi, D. Bocchetti, E. Soldo, Coupling of energy conversion systems and wellbore heat exchanger in a depleted oil well. Geothermal Energy **4**(1), 1–17 (2016). https://doi.org/10.1186/s40517-016-0053-9
15. M. Ebrahimi, S.E.M. Torshizi, Optimization of power generation from a set of low-temperature abandoned gas wells, using organic Rankine cycle. J. Renewable Sustainable Energy **4**(6), 063133 (2012). https://doi.org/10.1063/1.4768812
16. A. Limpasurat, G. Falcone, C. Teodoriu, M.A. Barrufet, Unconventional heavy oil exploitation for waste energy recovery, in *SPE Latin American and Caribbean Petroleum Engineering Conference Proceedings*, vol. 2 (2010), pp. 953–964. https://doi.org/10.2118/139054-ms
17. M. Macenić, T. Kurevija, Revitalization of abandoned oil and gas wells for a geothermal heat exploitation by means of closed circulation: Case study of the deep dry well Pčelić-1. Interpretation **6**(1), SB1–SB9 (2018). https://doi.org/10.1190/INT-2017-0079.1
18. W.L. Cheng, T.T. Li, Y. le Nian, K. Xie, Evaluation of working fluids for geothermal power generation from abandoned oil wells. Appl. Energy **118**, 238–245 (2014). https://doi.org/10.1016/j.apenergy.2013.12.039
19. N.M. Wight, N.S. Bennett, Geothermal energy from abandoned oil and gas wells using water in combination with a closed wellbore. Appl. Therm. Eng. **89**, 908–915 (2015). https://doi.org/10.1016/j.applthermaleng.2015.06.030

20. M.J. Mayer, V. Nyerges, A. Schroth, Investigation of geothermal power generation on abandoned hydrocarbon wells (2015). https://doi.org/10.1109/IYCE.2015.7180820

21. Y. Yang, Y. Huo, W. Xia, X. Wang, P. Zhao, Y. Dai, Construction and preliminary test of a geothermal ORC system using geothermal resource from abandoned oil wells in the Huabei oilfield of China. Energy **140**, 633–645 (2017). https://doi.org/10.1016/j.energy.2017.09.013

22. A. Kiaghadi, R.S. Sobel, H.S. Rifai, Modeling geothermal energy efficiency from abandoned oil and gas wells to desalinate produced water. Desalination **414**, 51–62 (2017). https://doi.org/10.1016/j.desal.2017.03.024

23. M.D. Madvar, F. Ahmadi, R. Shirmohammadi, A. Aslani, Forecasting of wind energy technology domains based on the technology life cycle approach. Energy Rep. **5**, 1236–1248 (2019). https://doi.org/10.1016/J.EGYR.2019.08.069

24. Y. Noorollahi, S. Taghipoor, B. Sajadi, Geothermal sea water desalination system (GSWDS) using abandoned oil/gas wells. Geothermics **67**, 66–75 (2017). https://doi.org/10.1016/j.geothermics.2017.01.008

25. M.-R. Kolahi, M. Amidpour, M. Yari, Multi-objective metaheuristic optimization of combined flash-binary geothermal and humidification dehumidification desalination systems. Desalination **490**, 114456 (2020). https://doi.org/10.1016/j.desal.2020.114456

26. M. Kolahi, M. Yari, S.M.S. Mahmoudi, F. Mohammadkhani, Thermodynamic and economic performance improvement of ORCs through using zeotropic mixtures: case of waste heat recovery in an offshore platform. Case Stud. Therm. Eng. **8**, 51–70 (2016). https://doi.org/10.1016/j.csite.2016.05.001

27. M. Ebadollahi, H. Rostamzadeh, O. Pourali, H. Ghaebi, M. Amidpour, Inherently safety design of a dual-loop bi-evaporator combined cooling and power system: 4E and safety based optimization approach. Process Saf. Environ. Prot. **154**, 393–409 (2021). https://doi.org/10.1016/J.PSEP.2021.08.036

28. M. Ebadollahi, H. Rostamzadeh, M.Z. Pedram, H. Ghaebi, M. Amidpour, Proposal and assessment of a new geothermal-based multigeneration system for cooling, heating, power, and hydrogen production, using LNG cold energy recovery. Renewable Energy **135**, 66–87 (2019). https://doi.org/10.1016/J.RENENE.2018.11.108

29. M. Ebadollahi, H. Rostamzadeh, P. Seyedmatin, H. Ghaebi, M. Amidpour, Thermal and exergetic performance enhancement of basic dual-loop combined cooling and power cycle driven by solar energy. Therm. Sci. Eng. Progr. **18**, 100556 (2020). https://doi.org/10.1016/J.TSEP.2020.100556

30. S.F. Ranjbar, A. Nemati, M.R. Kolahi, Thermodynamic analysis and improvement of a flash/ORC geothermal plant using zeotropicmixtures as working fluids in ORC. J. Mech. Eng. **48** 2 (83), #f00993, 131–138 (2018) Available: https://www.sid.ir/en/journal/ViewPaper.aspx?id=734778

31. I.H. Bell, J. Wronski, S. Quoilin, V. Lemort, Pure and pseudo-pure fluid thermophysical property evaluation and the open-source thermophysical property library coolprop. Ind. Eng. Chem. Res. **53**(6), 2498–2508 (2014). https://doi.org/10.1021/ie4033999

32. E.W. Lemmon, M.L. Huber, M.O. Mclinden, NIST standard reference database 23: reference fluid thermodynamic and transport properties-REFPROP, version 8.0. (2007). Available: https://nist.gov/publications/nist-standard-reference-database-23-reference-fluid-thermodynamic-and-transport-0

33. M.H. Sharqawy, J.H. Lienhard V, S.M. Zubair, Thermophysical properties of seawater: A review of existing correlations and data. Desalin. Water Treat. **16**(1–3), 354–380 (2010). https://doi.org/10.5004/dwt.2010.1079

34. M. Ebadollahi, H. Rostamzadeh, O. Pourali, H. Ghaebi, M. Amidpour, Close supercritical versus inverse Brayton cycles for power supply, using waste of a biogas-driven open Brayton cycle. J. Energy Resour. Technol. **143**(9) (2021). https://doi.org/10.1115/1.4050780

35. A. Pirmohamadi, H. Ghaebi, B.M. Ziapour, M. Ebadollahi, Exergoeconomic analysis of a novel hybrid system by integrating the Kalina and heat pump cycles with a nitrogen closed Brayton system. Energy Rep. **7**, 546–564 (2021). https://doi.org/10.1016/J.EGYR.2021.01.009

36. H. Nasrollahi, F. Ahmadi, M. Ebadollahi, S. Najafi Nobar, M. Amidpour, The greenhouse technology in different climate conditions: A comprehensive energy-saving analysis. Sustainable Energy Technol. Assess. **47**, 101455 (2021). https://doi.org/10.1016/J.SETA.2021.101455
37. G.P. Narayan, M.H. Sharqawy, J.H. Lienhard V, S.M. Zubair, Thermodynamic analysis of humidification dehumidification desalination cycles. Desalin. Water Treat. **16**(1–3), 339–353 (2010). https://doi.org/10.5004/dwt.2010.1078
38. J. Kennedy, R. Eberhart, Particle swarm optimization, in *Proceedings of ICNN'95-International Conference on Neural Networks*, vol. 4 (1995), pp. 1942–1948. https://doi.org/10.1007/978-3-642-37846-1_3
39. C. Coello, G. Lamont, D. van Veldhuizen, Evolutionary Algorithms for Solving Multi-Objective Problems (2007). https://doi.org/10.1007/978-0-387-36797-2

Chapter 14
Introducing a New System for Energy Recovery of High and Mid-Temperature Renewable Energy Sources: Free Piston Stirling Engine Combined with a Permanent Magnet Linear Synchronous Machine

Check for updates

Mahdi Majidniya, Benjamin Remy, and Thierry Boileau

Abstract Some of the main issues concerning the future of the world energy supply can be outlined as reduction of fossil fuel resources, energy demand increment, climate issues due to conventional power production methods, and the cost of the energy. To solve these problems, many methods are developed, including renewable and non-renewable energy ones, and also discrete and centralized power production systems. One of these methods, which focuses on improving the existed system instead of developing a new one, is based on the fact that most energy production methods and industries are dealing with thermal energy and, as a result, waste heat that should be recovered. Here, a new waste heat recovery system for mid and high-temperature energy sources is introduced. In the present chapter a Free Piston Stirling Engine (FPSE) combined with a Permanent Magnet Linear Synchronous Machine (PMLSM) is studied due to its many advantages including high efficiency, compactness, lightweight, quiet operation, reliability, the ability for overall cost reduction, and the ability to work with all thermal energy sources due to its external combustion nature, is a key to recover the waste heat from all kinds of thermal sources. This system is analyzed in detail from thermodynamic and electro-control points of view, and its feasibility to work as a waste heat recovery option for a tri-generation Internal Reforming Solid Oxide Fuel Cell (IRSOFC) based system is also studied.

M. Majidniya (✉) · B. Remy · T. Boileau
Université de Lorraine, CNRS, LEMTA, 54000 Nancy, France
e-mail: mahdi.majidniya@univ-lorraine.fr

B. Remy
e-mail: benjamin.remy@univ-lorraine.fr

T. Boileau
e-mail: thierry.boileau@univ-lorraine.fr

Nomenclature

Variables

A	Area, m^2
B_v	Friction coefficient
C	Clearance, m
C_f	Darcy friction factor
C_p	Heat transfer coefficient at constant pressure, J/(kg.K)
C_v	Heat transfer coefficient at constant volume, J/(kg.K)
d	Diameter, m
$\dot{W}$	Force, N
Faraday constant, 96,487 C/mol	Specific exergy, kJ/kg
h	Convective heat transfer coefficient, W/(m^2.K)
i	Current, A
i_{limit}	Limiting current density, A/m^2
L	Inductance, mH
LHV	Lower Heating Value, J/kg
l	Length, m
$M; m$	Mass, kg
$\dot{m}$	Mass flow rate, kg/s
n_e	Number of electrons
P	Pressure, Pa
Pr	Prandtl number
$\dot{Q}$	Heat transfer rate, W
R	Gas constant
Re	Reynolds number
r	Resistance, Ω
T	Temperature, K
u	Velocity, m/s
V	Volume, m^3
$\dot{V}$	Volumetric rate, m^3/s
v	Voltage, V
x	Displacement, m
$\dot{x}$	Velocity, m/s
$\ddot{x}$	Acceleration, m/s^2

Greek Symbols

λ	Specific heat ratio

μ	Dynamic viscosity, Pa.s
η	Efficiency
θ	Angle
ρ	Density, kg/m^3
ψ_f	Flux linkage, Wb
ω	Frequency, rad/s

Index and Exponent

a; b; c; d; q; α; β	Axis
Act	Activation
b	Buffer
c	Compression
$Conc$	Concentration
D	Displacer
e	Expansion
el	Electric
em	Electromagnetic
gs	Gas spring
h	Heater
k	Cooler
Ohm	Ohmic
P	Poer piston
R	Regenerator

Abbreviations

FPSE	Free Piston Stirling Engine
PMLSM	Permanent Magnet Linear Synchronous Machine
IRSOFC	Internal Reforming Solid Oxide Fuel Cell
DEACH	Double Effect Absorption Chiller

14.1   Introduction

Nowadays, many industries and power plants, including renewable and nonrenewable ones, deal with thermal energy. Such systems, less or more, are always accompanied by heat loss. Recovering this waste heat is important from energy efficiency, economic, and environmental points of view. Thus, choosing the right waste heat

recovery system is very critical. Here, a new waste heat recovery system will be introduced to meet all these aspects.

In the research of such a heat recovery system, many vital parameters should be considered, including efficiency, cost, environmental effect, and reliability. Stirling engine, which was invented by Stirling in 1816 [1], and has the highest possible theoretical efficiency [2], is one of these heat recovery systems that can match all these criteria. This system, due to its external combustion, can be used beside different systems, including solar energy systems [3], high-temperature fuel cells [4, 5], gasification systems [6], combustion systems [7], and also many industries that directly or indirectly deal with thermal energy like steel or chemistry industries [8]. Thus, the Stirling engine can be used as a master key to recover heat energy from all kinds of thermal energy sources. Furthermore, it has a high potential to reduce the overall costs [9], and also has a silent operation [5]. Thus, Stirling engines, based on the defined criteria, are one of the best candidates for waste heat recovery.

There are different types of Stirling engines that the best one for the heat recovery purpose should be chosen. In Stirling engines, there are two pistons: displacer and power pistons. Based on the transmission mechanism point of view, which is the synchronization method between these pistons, Stirling engines can be classified into kinematic and dynamic ones. In kinematic Stirling engines, which is also called standard Stirling engines, this synchronization is through a rigid connection. In dynamic Stirling engines two pistons are synchronized by their dynamic behavior. Free Piston Stirling Engine (FPSE) are dynamic ones [10, 11]. The FPSE was invented by W.T. Beale in 1964 [12]. In both types of Stirling engines, the power piston has a linear movement, which is generally connected to a generator for power production. This linear movement in a standard Stirling engine is generally transformed by a crankshaft to a rotary one. This crankshaft is always connected to an electric rotary generator. Besides, with an FPSE connected to a linear generator, the linear movement can be directly used to produce electricity. By transforming a standard Stirling engine to a free piston one, the crankshaft will be eliminated, which results in a system with fewer moving parts, better sealing, more reliability, more compact, and more lightweight, which also needs less maintenance [13–15]. Furthermore, from another point of view, Stirling engines can be classified into three main types: alpha, beta, and gamma. Since the beta one has a higher power density, it was selected [16]. Now, based on the advantages of beta-type FPSE compared to the other Stirling engine types, this system is chosen.

As it was already mentioned, in order to transfer the FPSE linear movement to electricity, a linear generator is required. There are different types of linear generators. The linear generator can be a three-phase or a one-phase one. Also, it can be an induction or a permanent magnet one. Since a three-phase generator needs less wire than the equivalent one-phase one, a three-phase generator is chosen [17]. Also, between induction and permanent magnet linear generators, due to the higher efficiency of the permanent magnet one, this type of generator is selected [18]. Thus, a three-phase Permanent Magnet Linear Synchronous Machine (PMLSM) is chosen as the linear generator to be coupled with the FPSE.

As a result, by considering all the advantages and criteria, the final proposed waste heat recovery system for high and mid-temperature renewable or nonrenewable energy sources will be a Free Piston Stirling Engine (FPSE) combined with a three-phase Permanent Magnet Linear Synchronous Machine (PMLSM). To have a comprehensive analysis of such a system, a precise model that considers all the dynamic, thermic, electric, and control aspects are required. The goal of the presented chapter is to introduce a precise model that can accurately predict the behavior of an FPSE-PMLSM system and then optimizes its performance. Finally, to study an application of such a system and its impact when it combines with other systems, the FPSE-PMLSM system will be used as a heat recovery option for an Internal Reforming Solid Oxide Fuel Cell (IRSOFC), which is the power source of a tri-generation system. This tri-generation system consists of an IRSOFC, a Double Effect Absorption Chiller (DEACH), a combustion chamber, and a heat exchanger.

14.2 Thermodynamic Modeling of the Free Piston Stirling Engine

In order to study the FPSE system in detail and have an appropriate estimation of the system stability and control parameters, its precise model should be developed. There are dynamic and thermic models and also linear and non-linear ones [2, 8, 19, 20]. Since the FPSE works as a heat recovery system and is mechanically connected to a linear generator, both dynamic and thermic models are required. Also, between linear and nonlinear models, since the linear model cannot predict the realistic behavior of the system [2], the nonlinear model should be used. Here, first, the nonlinear dynamic model of the FPSE will be developed and then will be coupled with the thermic one. Then the results of the nonlinear thermodynamic model will be analyzed.

14.2.1 Dynamic Analysis

The schematic of the Free Piston Stirling Engine system is shown in Fig. 14.1.

As it is shown in Fig. 14.1, the power piston and displacer piston are two moving pistons of the FPSE. The dynamic equations of the system come from the pistons ones. The spaces around these pistons are buffer space, compression space, gas spring space, and expansion space. Through pressure balances between pistons and spaces around them, the dynamic equations of the system can be written as:

$$m_P \ddot{x}_P = A_P (P_c - P_b) - F_{Load} \tag{14.1}$$

$$m_D \ddot{x}_D = A_D P_e - (A_D - A_{rod}) P_c - A_{rod} (P_{gs}) = A_D (P_e - P_c) + A_{rod} (P_c - P_{gs}) \tag{14.2}$$

Fig. 14.1 Free Piston
Stirling Engine (FPSE)
schematic

Fig. 14.1 Free Piston Stirling Engine (FPSE) schematic
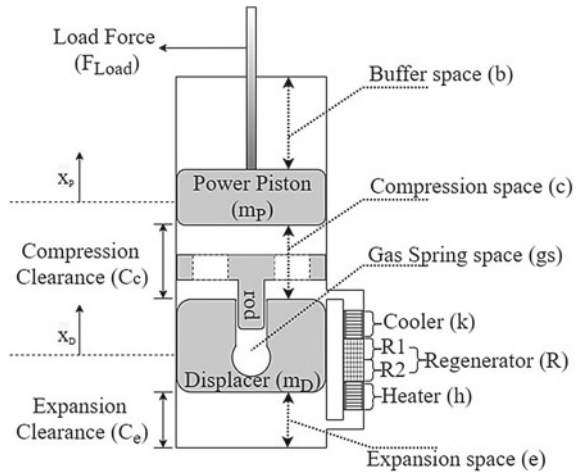
The compression space pressure can be calculated based on the mass conservation in the system (constant total mass of the gas inside the system M_{tot} without leakage) and ideal gas law considering the instantaneous volumes and temperatures of the gas at each space [21]:

$$P_c = M_{tot} R \left(\frac{V_c}{T_c} + \frac{V_e}{T_e} + \frac{V_h}{T_h} + \frac{V_k}{T_k} + \frac{V_{R1}}{T_{R1}} + \frac{V_{R2}}{T_{R2}} \right)^{-1} \qquad (14.3)$$

The reason that the regenerator is divided into two parts is to have a more precise model of it. For heater, cooler, and regenerator, the volumes are constant, but for the compression and expansion spaces, their instantaneous volumes can be calculated as:

$$V_c = A_P(x_P + C_c) - (A_D - A_{rod})x_D \qquad (14.4)$$

$$V_e = A_D(x_D + C_e) \qquad (14.5)$$

The instantaneous temperature calculations will be discussed in the next section.

Other parameters required to solve Eqs. (14.1) and (14.2) are buffer and gas spring spaces' pressures. For buffer and gas spring, the adiabatic assumption can be applied, and their pressures can be calculated as [21]:

$$P_i = P^{mean} \left(V_i^{mean} / V_i^{instantaneous} \right)^{\lambda}; i : b, gs \qquad (14.6)$$

Instantaneous volumes of the buffer and the gas spring are as:

$$V_b^{instantaneous} = V_b^{mean} - A_P x_P \qquad (14.7)$$

$$V_{gs}^{\text{instantaneous}} = V_{gs}^{mean} - A_{rod}x_D \qquad (14.8)$$

The last required parameter to solve equations Eqs. (14.1) and (14.2) is the pressure difference between expansion and compression spaces which is equal to the pressure drop between these two spaces:

$$P_e - P_c = \Delta P \qquad (14.9)$$

This pressure drop is due to the gas flow through cooler, regenerator, and heater that can be calculated as follow [2, 21]:

$$\Delta P_i = \frac{1}{2}\rho_i \left(\frac{C_{f_i}l_i}{d_{hydraulici}} \right) u_i|u_i|; \, i : h, k, R1, R2 \qquad (14.10)$$

The hydraulic diameter for the heater and the cooler can be defined as:

$$d_{hydraulici} = \frac{4A_i}{Wetted\,perimeter_i}; \, i : h, k \qquad (14.11)$$

For the wire mesh porous media of the regenerator, the hydraulic diameter can be calculated as [2]:

$$d_{hydraulicR} = \frac{d_{wire} \times Porosity}{1 - Porosity} \qquad (14.12)$$

Darcy friction factors based on the Reynolds number are presented in Table 14.1. Reynolds number can be calculated as:

$$Re_i = \frac{\rho_i u_i d_{hydraulici}}{\mu_i}; \, i : h, k, R1, R2 \qquad (14.13)$$

Dynamic viscosity and gas density based on its temperature and pressure at each space can also be calculated as [8]:

$$\mu_i = 3.674 \times 10^{-7}T_i^{0.7}; \, i : h, k, R1, R2, e, c \qquad (14.14)$$

Table 14.1 Darcy friction factor [2]

For heater and cooler:	Re< 2000	$C_f = 64/Re$
	Re> 2000	$C_f = 0.316Re^{-0.25}$
For regenerator:	Re< 60	$C_f = 4 \times 10^{(1.73 - 0.93\log Re)}$
	60 < Re < 1000	$C_f = 4 \times 10^{(0.714 - 0.365\log Re)}$
	Re> 1000	$C_f = 4 \times 10^{(0.015 - 0.125\log Re)}$

$$\rho_i = \frac{48.14 P_i \times 10^{-5}}{T_i \left(1 + 0.4446 P_i \times 10^{-5} / T_i^{1.2}\right)}; i : h, k, R1, R2, e, c \qquad (14.15)$$

The pressure of the gas at each space, based on the calculated pressure drops (Eq. (14.10)) also can be calculated as [8, 21]:

$$P_k = P_c + \frac{\Delta P_k}{2} \qquad (14.16)$$

$$P_{R1} = P_k + \frac{\Delta P_k}{2} + \frac{\Delta P_{R1}}{2} \qquad (14.17)$$

$$P_{R2} = P_{R1} + \frac{\Delta P_{R1}}{2} + \frac{\Delta P_{R2}}{2} \qquad (14.18)$$

$$P_h = P_{R2} + \frac{\Delta P_{R2}}{2} + \frac{\Delta P_h}{2} \qquad (14.19)$$

$$P_e = P_h + \frac{\Delta P_h}{2} \qquad (14.20)$$

Finally, instant gas velocity in the heater, cooler, and regenerator should be calculated. It is assumed that the variation of the total volume of the gas inside the system causes gas to pass through the heater, cooler, and regenerator at the same time, and based on that, the instantaneous gas velocity can be calculated as [8, 21]:

$$u_i = \frac{\dot{V}_{tot}}{A_i}; i : h, k, R1, R2 \qquad (14.21)$$

The total gas volume variation is due to the volume variations of the gas in compression and expansion spaces that can be calculated as:

$$\dot{V}_c = A_P \dot{x}_P - (A_D - A_{rod})\dot{x}_D \qquad (14.22)$$

$$\dot{V}_e = A_D \dot{x}_D \qquad (14.23)$$

$$\dot{V}_{tot} = \dot{V}_c - \dot{V}_e = A_P \dot{x}_P - (2A_D - A_{rod})\dot{x}_D \qquad (14.24)$$

Now, to solve Eqs. (14.1) and (14.2), since some of the dynamic parameters are temperature dependent, the thermic model of the system should be developed to be coupled with the presented dynamic one. Also, the isothermal assumption with the constant temperature in all the spaces can be used. This method is an easy method to apply but not a precise one and does not provide all the required information concerning the FPSE operating condition.

14.2.2 Thermic Analysis

In order to have a precise estimation of the FPSE behavior, its thermic model is developed here to be coupled with the dynamic one. For the thermic model, the following conservation of energy equation should be solved for each space [8, 21]:

$$\dot{Q}_{in} + \left(\dot{m}C_pT\right)_{in} - \left(\dot{m}C_pT\right)_{out} - Power_{out} = C_v\frac{d}{dt}(mT) \tag{14.25}$$

By this equation, the gas temperature in each space can be calculated. Expansion and compression spaces are assumed to be isolated and the only heat transfers with the environment happen through the heater, cooler, and regenerator. These heat transfers which are through the walls, can be calculated as [8, 21]:

$$\dot{Q}_{ini} = h_i A_{wettedi}(T_{walli} - T_i); i : h, k, R1, R2 \tag{14.26}$$

$$h_i = \frac{C_{fi}}{4} \times \frac{Re_i\mu_iC_p}{2d_{hydraulici}Pr_i}; i : h, k, R1, R2 \tag{14.27}$$

$$Pr_i = \frac{0.7117 \times T_i^{-(0.01-1.42\times10^{-4}\times P_i\times10^{-5})}}{1 + 1.123 \times 10^{-3} \times P_i \times 10^{-5}}; i : h, k, R1, R2 \tag{14.28}$$

Now, based on Fig. 14.1, the conservation of energy equation for each space is reformulated as follow to be used for each space temperature calculation [8, 21]:

$$\dot{T}_c = \left(\frac{\dot{m}_{ktoc}CpT_{kc} - \dot{W}_P}{Cv} - \dot{m}_cT_c\right)/m_c \tag{14.29}$$

$$\dot{T}_k = \left(\frac{\dot{Q}_{ink} + \dot{m}_{ctok}CpT_{ck} + \dot{m}_{R1tok}CpT_{R1k}}{Cv} - \dot{m}_kT_k\right)/m_k \tag{14.30}$$

$$\dot{T}_{R1} = \left(\frac{\dot{Q}_{inR1} + \dot{m}_{ktoR1}CpT_{kR1} + \dot{m}_{R2toR1}CpT_{R2R1}}{Cv} - \dot{m}_{R1}T_{R1}\right)/m_{R1} \tag{14.31}$$

$$\dot{T}_{R2} = \left(\frac{\dot{Q}_{inR2} + \dot{m}_{R1toR2}CpT_{R1R2} + \dot{m}_{htoR2}CpT_{hR2}}{Cv} - \dot{m}_{R2}T_{R2}\right)/m_{R2} \tag{14.32}$$

$$\dot{T}_h = \left(\frac{\dot{Q}_{inh} + \dot{m}_{R2toh}CpT_{R2h} + \dot{m}_{etoh}CpT_{eh}}{Cv} - \dot{m}_hT_h\right)/m_h \tag{14.33}$$

$$\dot{T}_e = \left(\frac{\dot{m}_{htoe}CpT_{he} - \dot{W}_D}{Cv} - \dot{m}_eT_e\right)/m_e \tag{14.34}$$

In these equations, $\dot{m}_{itoj}$ is the gas mass flowrate from space i to space j. This mass flow, based on the conservation of mass equation between spaces, and according

to Fig. 14.1, can be written as [8, 21]:

$$\dot{m}_{ktoc} = -\dot{m}_{ctok} = \dot{m}_c \qquad (14.35)$$

$$\dot{m}_{R1tok} = -\dot{m}_{ktoR1} = \dot{m}_c + \dot{m}_k \qquad (14.36)$$

$$\dot{m}_{R2toR1} = \dot{m}_c + \dot{m}_k + \dot{m}_{R1} \qquad (14.37)$$

$$\dot{m}_{htoe} = -\dot{m}_{etoh} = \dot{m}_e \qquad (14.38)$$

$$\dot{m}_{R2toh} = -\dot{m}_{htoR2} = \dot{m}_e + \dot{m}_h \qquad (14.39)$$

$$\dot{m}_{R1toR2} = \dot{m}_e + \dot{m}_h + \dot{m}_{R2} \qquad (14.40)$$

Based on these equations, the relation between the gas flowrate passes through boundaries and gas mass variations in each space is known. Also, the instantaneous mass of gas in each space can be calculated as:

$$m_i = \rho_i V_i; \; i : h, k, R1, R2, e, c \qquad (14.41)$$

Furthermore, T_{ij} which is the temperature of the gas passing through the boundary, can be identified based on the gas flow direction. It means if the gas flows from space i to space j, $\dot{m}_{itoj}$ will be positive and $T_{ij} = T_{ji} = T_i$, otherwise, $T_{ij} = T_{ji} = T_j$.

14.2.3 Thermodynamic Analysis

After developing dynamic and thermic models of the FPSE, they should be coupled to develop the thermodynamic one. With the thermodynamic model, it would be possible to study the FPSE behavior in detail. The thermodynamic model provides information about the pistons' movements, gas temperatures in different spaces, the thermal balance of the system, and the FPSE output power.

There are two important points that should be considered while developing a model. The first is about knowing the equations and the relations between them, and the second is the order in which the equations must be solved. The first point was already presented in Sects. 14.2.1 and 14.2.2. Here the second point, which is about linking the equations of each section, will be discussed. This linking will help to use the equations in an appropriate order to get to the requested results.

The first things that should be clarified are the inputs and outputs of the system as it is shown in Fig. 14.2.

Fig. 14.2 FPSE inputs and outputs
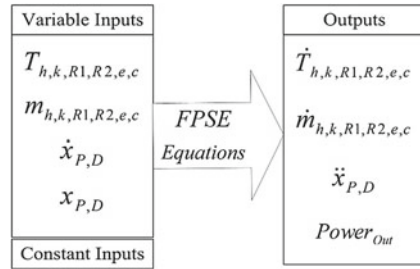
As can be seen in Fig. 14.2, two sets of inputs are defined: variable and constant inputs. Variable inputs are the inputs calculated by integration or derivation of the outputs at each time step. Constant inputs are initial values and the parameters that are shown in Table 14.2.

Now, to link the equations, the suggested order to use the equations and develop the FPSE model is presented in Table 14.3.

Table 14.2 FPSE input data [2]

T_h^{wall}	814.3 K	d_P	5.718 cm	A_h	1.4898 cm^2
T_k^{wall}	322.8 K	d_D	5.67 cm	A_k	2.6163 cm^2
T_{R1}^{wall}	418.4 K	d_{rod}	1.663 cm	$A_{R1,R2}$	8.745 cm^2
T_{R2}^{wall}	662.7 K	d_h	0.2362 cm	$Wetted perimeter_k$	115.2 cm^2
P^{mean}	71 bars	d_{wire}	0.00889 cm	C_c	1.83 cm
$Porosity$	75.9%	l_k	7.92 cm	C_e	1.861 cm
m_D	0.426 kg	l_h	18.34 cm	V_b^{mean}	2615 cm^3
m_P	6.2 kg	l_{R1}	3.22 cm	V_{gs}^{mean}	37.97 cm^3
		l_{R2}	3.22 cm	$V_{R1,R2}$	28.185 cm^3

Table 14.3 FPSE modeling steps

1	Equation (14.24)	12	Equation (14.6)
2	Equation (14.21)	13	$\Delta P = \sum \Delta P_i$
3	Equation (14.14)	14	Equation (14.1)
4	Equation (14.13)	15	Equation (14.2)
5	Equation (14.4)	16	Equation (14.41)
6	Equation (14.5)	17	Equation (14.35)–(14.40)
7	Equation (14.3)	18	Equation (14.28)
8	Equation (14.10)	19	Equation (14.27)
9	Equation (14.16)–(14.20)	20	Equation (14.26)
10	Equation (14.15)	21	Equation (14.29)–(14.34)
11	Repeat 4–10 with new ρ		
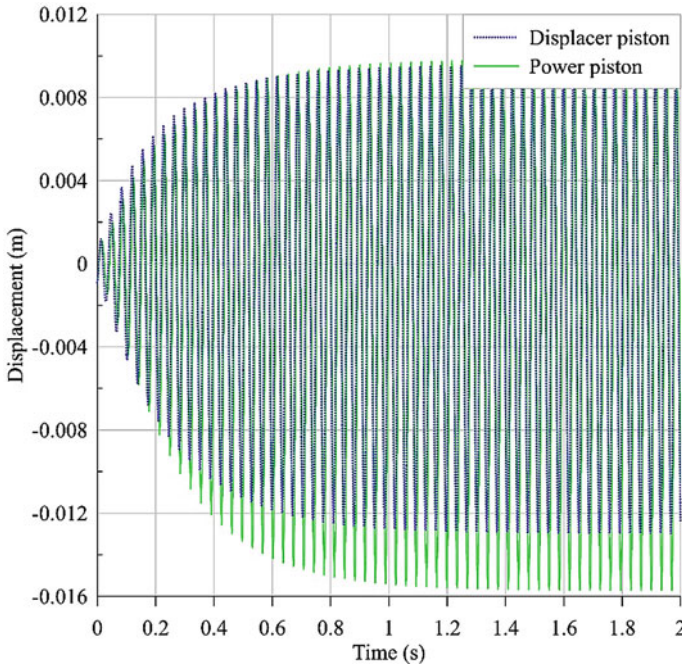
**Fig. 14.3** FPSE pistons' displacement-from transient to steady state

To start the procedure of Table 14.3, since the pressure in each space is unknown, an initial value of ρ (function of P_i) was used. Then after recalculating ρ in step 11 with calculated P_i values from step 9, steps 4–11 were repeated a few times to correct ρ and the dependent variables.

The results of the FPSE thermodynamic model based on the input data of Table 14.2 are presented in Figs. 14.3, 14.4, 14.5, 14.6, 14.7 and 14.8. The FPSE power production is equal to 1 kW with an efficiency of 29.63% in the present simulation. In Figs. 14.3 and 14.4, the transition from transient to the steady-state of the pistons' movement (position and speed) is shown.

As shown in Figs. 14.3 and 14.4, it takes around 1 s to get to the steady-state condition. Furthermore, the behavior of the system, as it is expected, is almost sinusoidal. To have a closer look at the behavior of the pistons, their speed and displacement in one steady-state cycle are shown in Figs. 14.5 and 14.6.

Figures 14.5 and 14.6 show the results for one period. Based on Fig. 14.5, the stroke ratio, which is the ratio of the displacer stroke to the power piston stroke, is equal to 0.88. The phase shift between two pistons' displacements is equal to 34°. The frequency of the pistons' displacement is equal to 28.57 Hz.

For the same period of time, which correspond to the steady-state condition, the pressure drop concerning each space and the temperature variation of each space are shown in Figs. 14.7 and 14.8.
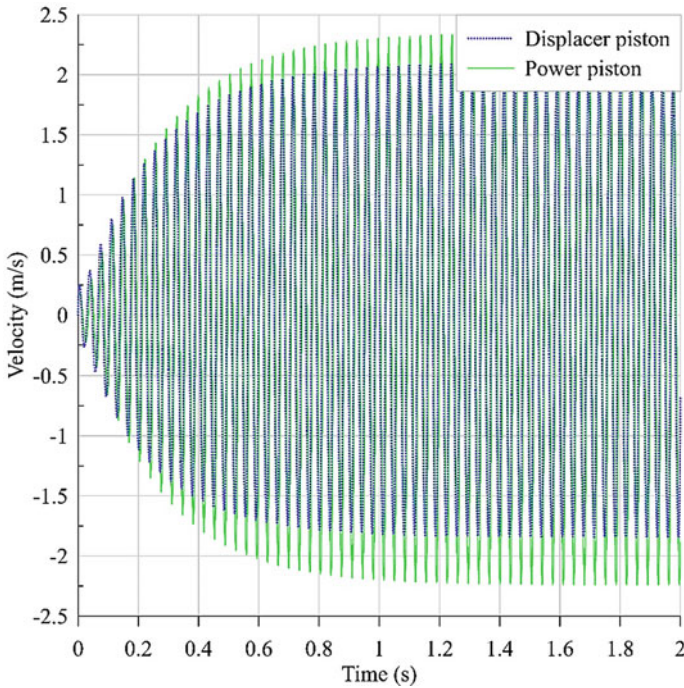
Fig. 14.4 FPSE pistons' velocity-from transient to steady-state

As can be seen in Fig. 14.7, the regenerator has the highest pressure drop, which is due to its porous media. The pressure drop in the heater and cooler are at the same order of magnitude and small compared to the pressure drop of the regenerator. Due to the porous media of the regenerator, and its thermal storage characteristic, its temperature, as it is shown in Fig. 14.8, is almost constant. Also, expansion space has the maximum variation of the temperature. This variation directly affects the heater temperature, which causes it to have a higher variation than the cooler temperature. In general, temperature variation in the heater and cooler compared to the expansion and compression spaces are smaller due to the constant wall temperature assumption that was made and also the constant volumes of these spaces.

14.3   Electrodynamic Modeling of the Permanent Magnet Linear Synchronous Machine

As it was already discussed, the FPSE system is coupled to a three-phase Permanent Magnet Linear Synchronous Machine (PMLSM) to produce electricity. Here in the first part, the electro-dynamic model of the PMLSM is developed. Then, a controller for this system is introduced. In the coupled FPSE-PMLSM model, this controller
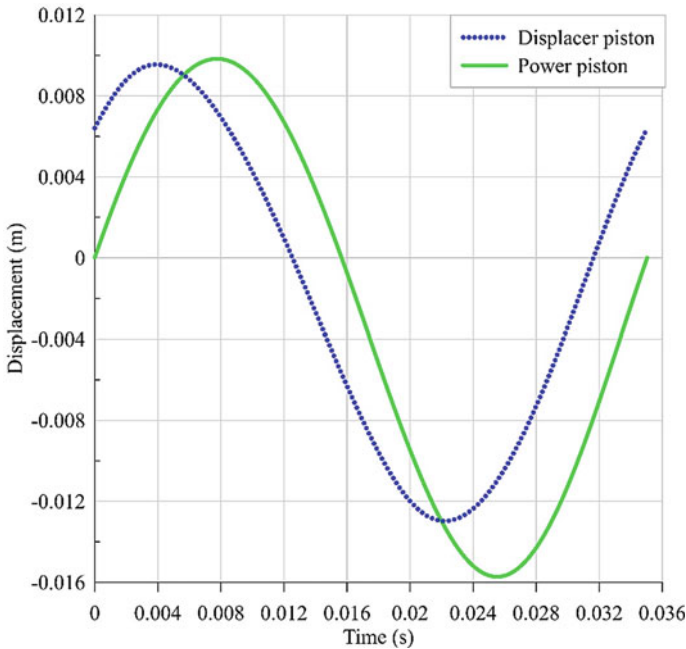
**Fig. 14.5** FPSE pistons' displacement in a cycle

will be modified to match the system requirements. The schematic of the PMLSM system combined with its control system is shown in Fig. 14.9.

As can be seen in Fig. 14.9, there is an inverter which is a power electronic system constructed by power transistors and diodes. This system absorbs the sinusoidal currents ($i_a - i_b - i_c$) from the PMLSM side using the information received by the controller. On the other side, the power is received by a DC voltage source. In the present system with the current setting, the inverter can be modeled as a unit gain. The control system is formed of two current controllers and one position controller.

14.3.1 Electro-Dynamic Analysis

The link between the PMLSM and the FPSE is through a rigid rod that connects the PMLSM mover to the power piston. Thus, the dynamic model is needed to study this connection. Also, the electrical model of the PMLSM is needed to calculate the output power.

In general, due to the hard controlling of the PMLSM in the three-phase ($a - b - c$) frame directly, the mathematical model is written in $d - q$ frame using Park and Concordia transformations. These transformations convert the stationary phase coordinate system ($a - b - c$) to the rotary one ($d - q$) that by assuming Y as current
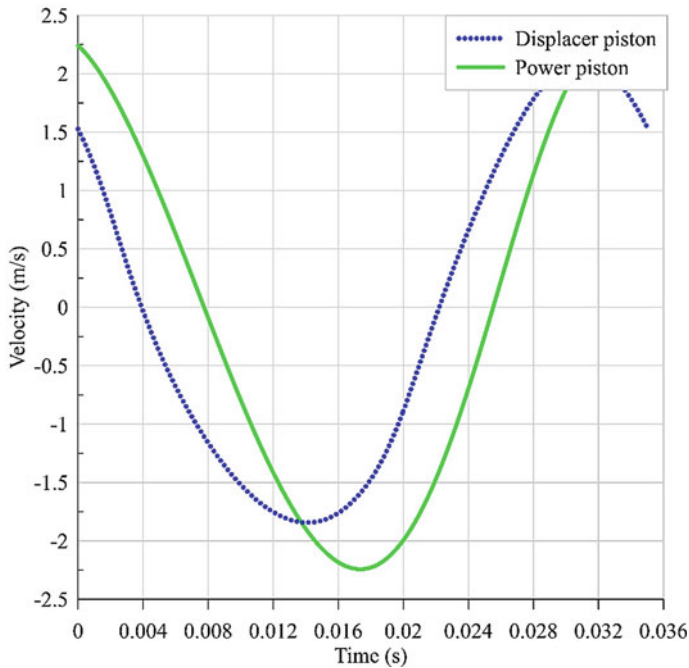
Fig. 14.6 FPSE pistons' velocity in a cycle

or voltage, can be expressed as [2]:

$$\begin{bmatrix} Y_\alpha \\ Y_\beta \end{bmatrix} = \sqrt{\frac{2}{3}} \begin{bmatrix} 1 & -1/2 & -1/2 \\ 0 & \sqrt{3}/2 & -\sqrt{3}/2 \end{bmatrix} \begin{bmatrix} Y_a \\ Y_b \\ Y_c \end{bmatrix} \tag{14.42}$$

$$\begin{bmatrix} Y_d \\ Y_q \end{bmatrix} = \begin{bmatrix} \cos\theta & \sin\theta \\ -\sin\theta & \cos\theta \end{bmatrix} \begin{bmatrix} Y_\alpha \\ Y_\beta \end{bmatrix} \tag{14.43}$$

$$\begin{bmatrix} Y_\alpha \\ Y_\beta \end{bmatrix} = \begin{bmatrix} \cos\theta & -\sin\theta \\ \sin\theta & \cos\theta \end{bmatrix} \begin{bmatrix} Y_d \\ Y_q \end{bmatrix} \tag{14.44}$$

$$\begin{bmatrix} Y_a \\ Y_b \\ Y_c \end{bmatrix} = \sqrt{\frac{2}{3}} \begin{bmatrix} 1 & 0 \\ -1/2 & \sqrt{3}/2 \\ -1/2 & -\sqrt{3}/2 \end{bmatrix} \begin{bmatrix} Y_\alpha \\ Y_\beta \end{bmatrix} \tag{14.45}$$

With Eqs. (14.42)–(14.45), the transformation from $(a - b - c)$ frame to $(d - q)$ frame and vice versa, is possible. The value of θ for these equations can be calculated as [2]:
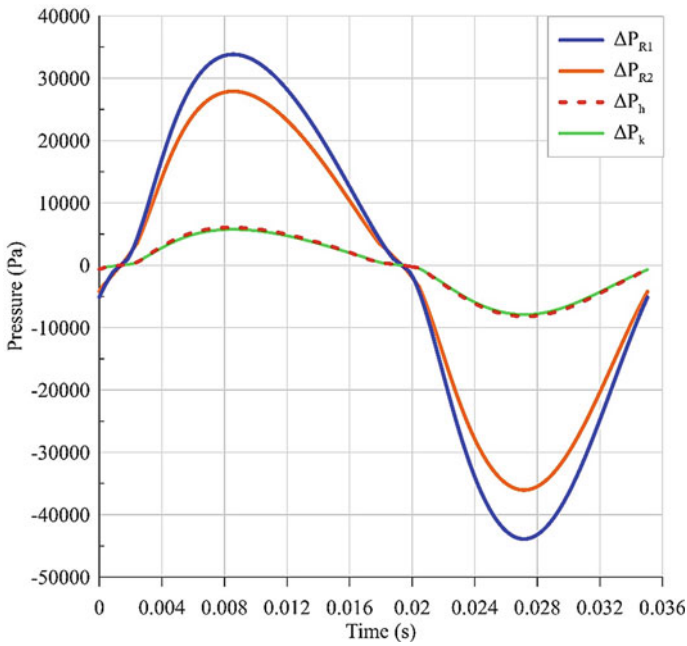
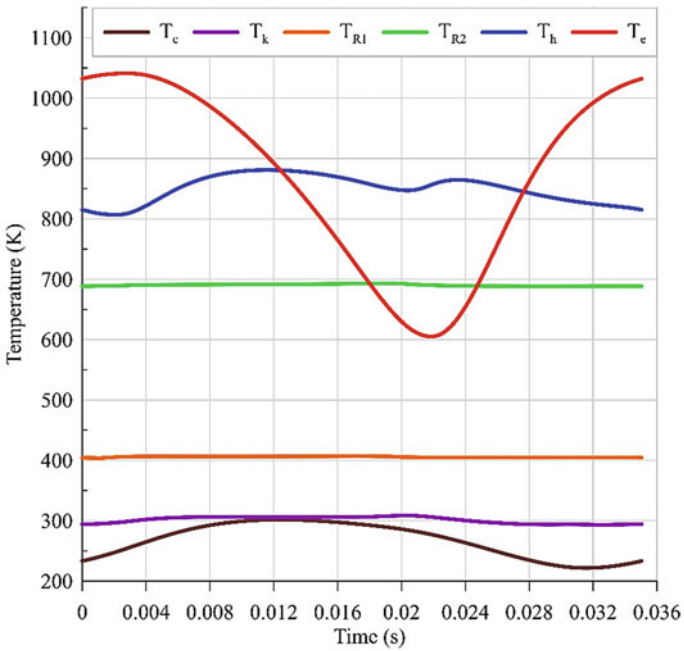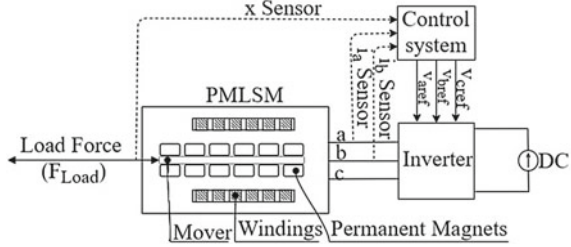**Fig. 14.7** Pressure drops in different spaces of the FPSE

Fig. 14.8 Temperatures in different spaces of the FPSE

Fig. 14.9 PMLSM
schematic

$$\theta = \int \frac{\pi}{\tau} \dot{x}_{mover} dt = \frac{\pi}{\tau} x_{mover} \qquad (14.46)$$

Finally, based on the developed transformation, the PMLSM system can be modeled in $d - q$ frame, in motor convention, as following [2]:

$$v_d = L_d \frac{di_d}{dt} + r i_d - \frac{\pi}{\tau} \dot{x}_{mover} L_q i_q \qquad (14.47)$$

$$v_q = L_q \frac{di_q}{dt} + r i_q + \frac{\pi}{\tau} \dot{x}_{mover} \left(L_d i_d + \sqrt{3/2} \psi_f \right) \qquad (14.48)$$

$$F_{em} = \frac{\pi}{\tau} \left(\sqrt{3/2} \psi_f i_q + \left(L_d - L_q \right) i_d i_q \right) \qquad (14.49)$$

$$m_{mover} \ddot{x}_{mover} = F_{em} - B_v \dot{x}_{mover} - F_{load} \qquad (14.50)$$

$$Power_{em} = F_{em} \dot{x}_{mover} \qquad (14.51)$$

$$Power_{el} = v_q i_q + v_d i_d \qquad (14.52)$$

Equation (14.50) will be used to identify the dynamic link between the FPSE and the PMLSM. Figure 14.10 shows how to use the PMLSM equations through a block diagram.

F_{load} is the input and v_a, v_b, and v_c voltages are the results of the system control which are applied by the inverter and will be identified in the next section. Also, i_a, i_b, and i_c will be used in the control model. Now to have the required behavior of the system, it should be controlled, which is described in the next section.

14.3.2 Control System

In this section, the control of the PMLSM system is developed. Here, for the linear machine, the same idea of controlling the rotor flux and motor torque of the rotary
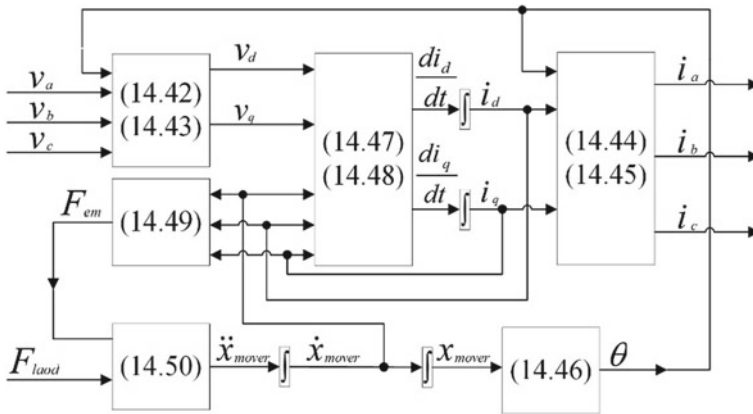
Fig. 14.10 PMLSM block diagram

machine can be applied. Thus, $i_{dreference} = 0$ and $i_{qreference}$ will be deduced from speed controlling. So, a reference velocity for the mover as $\dot{x}_{moverreference}$ will be defined. In defining this reference velocity, the limited reciprocating motion of the mover should be considered. Since the nature of the speed is sinusoidal, a Proportional Resonance (PR) controller is more adapted for speed controlling.

The PMLSM currents are controlled with two Proportional Integral (PI) controllers and one Proportional Resonance (PR) controller that can be defined as:

$$PI = K_{p_{PI}} + K_{i_{PI}} \frac{1}{s} \tag{14.53}$$

$$PR = K_{p_{PR}} + K_{i_{PR}} \frac{s}{s^2 + \omega_0^2} \tag{14.54}$$

The K_p and K_i are the controller gains and ω_0 is the resonance frequency. The block diagram of Fig. 14.11 describes the control system which is used beside the PMLSM model.

As can be seen in Fig. 14.11, one PR and two PI controllers are used. One controller for the velocity ($\dot{x}_{mover}$) and two controllers for the currents (i_d and i_q). $\dot{x}_{moverreference}$ and $i_{dreference}$ are the inputs. For the present study, $\dot{x}_{moverreference}$ is assumed to be a sinusoidal wave and $i_{dreference} = 0$. i_a, i_b, and i_c are the results of the PMLSM modeling and v_a, v_b, and v_c are the results of the system control that were already shown in Fig. 14.10.

To identify the PI controllers' gains, the MATLAB Simulink® tuning method is used (PID tuner app) and their values are given in Table 14.4. The decoupling method allows to control the currents separately [22]. Figure 14.12 is the schematic of the decoupled model that can be simplified as the cross hatched part of Fig. 14.13.

In Figs. 14.12 and 14.13 the Gain which is equal to 1 is the inverter model. The goal of Fig. 14.13 is to identify PR gains. It should be noted that to identify the PR
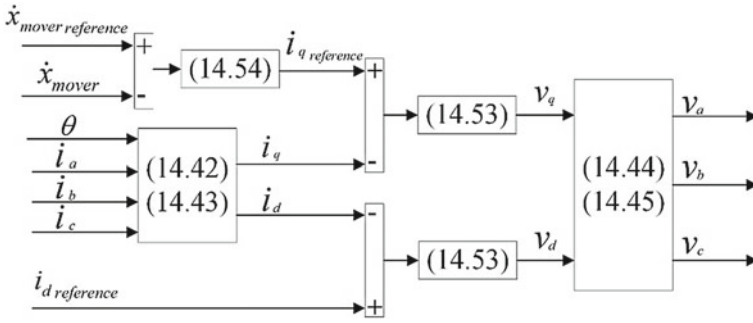
Fig. 14.11 PMLSM control block diagram

Table 14.4 Controller gains

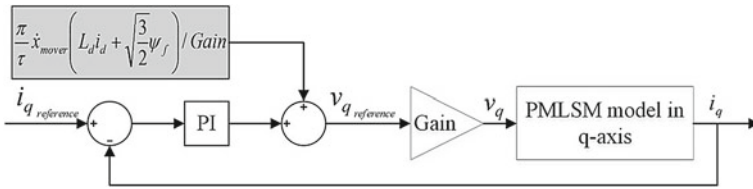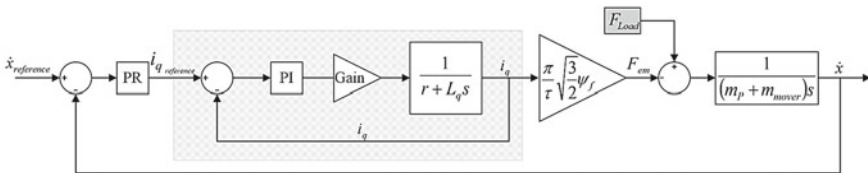| $K_{pPI} - i_d$	4×10^4	$K_{pPI} - i_q$	554.1	$K_{pPR} - \dot{x}$	10^3
$K_{iPI} - i_d$	1×10^8	$K_{iPI} - i_q$	47,062,993.6	$K_{iPR} - \dot{x}$	10^4

Fig. 14.12 Decoupled PMLSM model

Fig. 14.13 Schematic of the control system

gains that match the FPSE-PMLSM combined system, the dynamic FPSE force is considered in F_{Load} besides the friction force, and the piston mass is also considered besides the mover mass. Anyway, the F_{Load} will be treated as perturbation that will be rejected by the controller.

The frequency response of the open loop system of Fig. 14.13, by ignoring the perturbations and assuming $\dot{x}_{reference}$ as the open loop input and $\dot{x}$ as the open loop output, is studied. Then, the effect of the setting of the PR coefficients (K_{pPR} and K_{iPR}) on the gain and phase margins is evaluated. The results show that there is a

Bode Diagram
From: Reference speed To: Speed
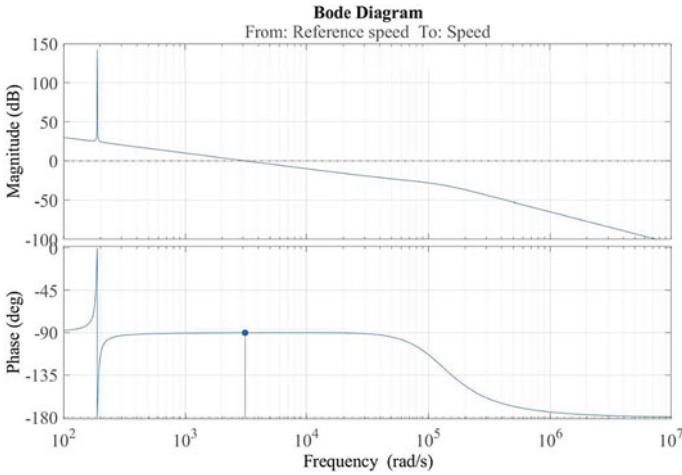
Fig. 14.14 Bode diagram of Fig. 14.13

Table 14.5 PMLSM input data [2]

r	0.1 (Ω)	L_q	3.01 (mH)	L_d	1.77 (mH)
ψ_f	0.0513 (Wb)	B_v	10	m_{mover}	0.824 (kg)

zone in the bode diagram that the phase margin in this zone has its maximum value and the system is stable. Since these PR gains will be used later in the combined system, and the FPSE system behavior is treated as perturbation, it is proposed to be in the safest place in this zone which is the middle of the zone. The bode diagram of Fig. 14.13 with $K_{p_{PR}}$ and $K_{i_{PR}}$ gains given in Table 14.4 is shown in Fig. 14.14.

As can be seen in Fig. 14.14, with the defined values of PR gains, the system phase margin is almost in the middle of the zone with the maximum phase values.

Furthermore, the input data of the PMLSM that will be used in the coupled system are presented in Table 14.5.

14.4 FPSE-PMLSM Combined System

In the last two previous sections, the thermodynamic model of the FPSE and electrodynamic model of the PMLSM and the control system were developed. Now, these two models will be coupled to study the combined FPSE-PMLSM system. The schematic of the combined FPSE-PMLSM system with the control system is shown in Fig. 14.15.
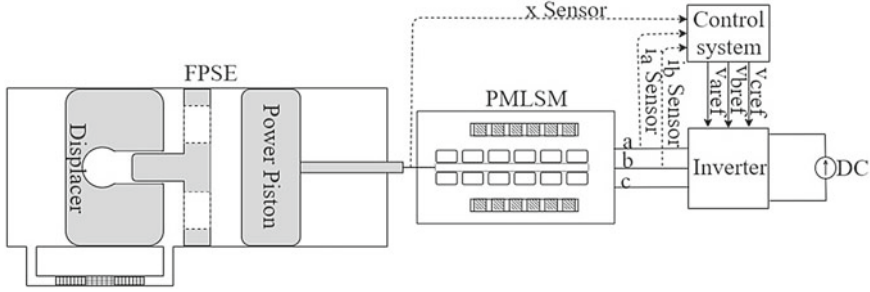
Fig. 14.15 FPSE-PMLSM schematic

14.4.1 *Thermo-Electro-Dynamic Analysis*

As it was already discussed, the coupling between the FPSE and the PMLSM is due to the rigid rode that connects the power piston to the mover. Thus, in order to couple these two systems, their dynamic equations related to the power piston and the mover should be combined. After combining these two equations ((14.1) and (14.50)) that results in the Eq. (14.55), the set of combined system equations will be as:

$$(m_P + m_{mover})\ddot{x}_P = A_P(P_c - P_b) + F_{em} - B_v\dot{x}_P \tag{14.55}$$

$$m_D\ddot{x}_D = A_D(P_e - P_c) + A_{rod}\left(P_c - P_{gs}\right) \tag{14.56}$$

$$v_d = L_d\frac{di_d}{dt} + ri_d - \frac{\pi}{\tau}\dot{x}_P L_q i_q \tag{14.57}$$

$$v_q = L_q\frac{di_q}{dt} + ri_q + \frac{\pi}{\tau}\dot{x}_P\left(L_d i_d + \sqrt{3/2}\psi_f\right) \tag{14.58}$$
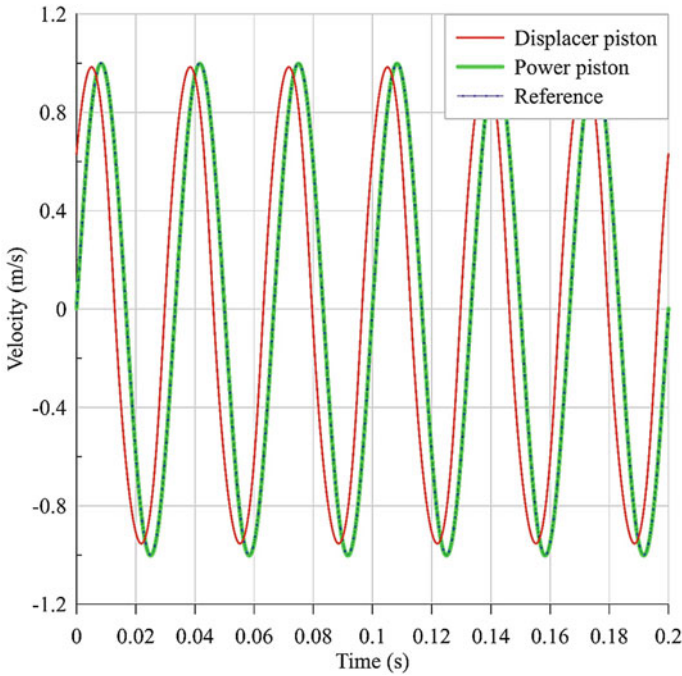
$$F_{em} = \frac{\pi}{\tau}\left(\sqrt{3/2}\psi_f i_q + (L_d - L_q)i_d i_q\right) \tag{14.59}$$

$$Power_{em} = F_{em}\dot{x}_P \tag{14.60}$$

$$Power_{el} = v_q i_q + v_d i_d \tag{14.61}$$

$$\eta = \frac{Power_{el}}{\dot{Q}_{in}} \tag{14.62}$$

As can be seen, the only equation which is different compared to the previous set of equations is Eq. (14.55) (Fig. 14.16).

Fig. 14.16 Pistons' velocity

14.4.2 Control System

In order to show that the setting of the control system already developed in Sect. 14.3.2 is reliable for the combined FPSE-PMLSM, the results of the simulation for an operating point in steady-state with $\dot{x}_{Preference} = 1 \times \sin(30 \times 2\pi \times t)$ are shown. The results based on the input data of Tables 14.2 and 14.5 are presented in Figs. 14.17, 14.18 and 14.19.

As can be seen, first, the dynamic results of the coupled FPSE-PMLSM system are presented in Figs. 14.17 and 14.16. Then, the thermic results are presented in Fig. 14.18, and at the end, the electric results are presented in Figs. 14.19 and 14.20. Since the developed model is a thermo-electro-dynamic model, all these results are connected and are not independent. For example, the results of the system control directly affect the electric results (Fig. 14.19) and dynamic results (Fig. 14.16). It is the same for other results, and directly or indirectly, they are connected.
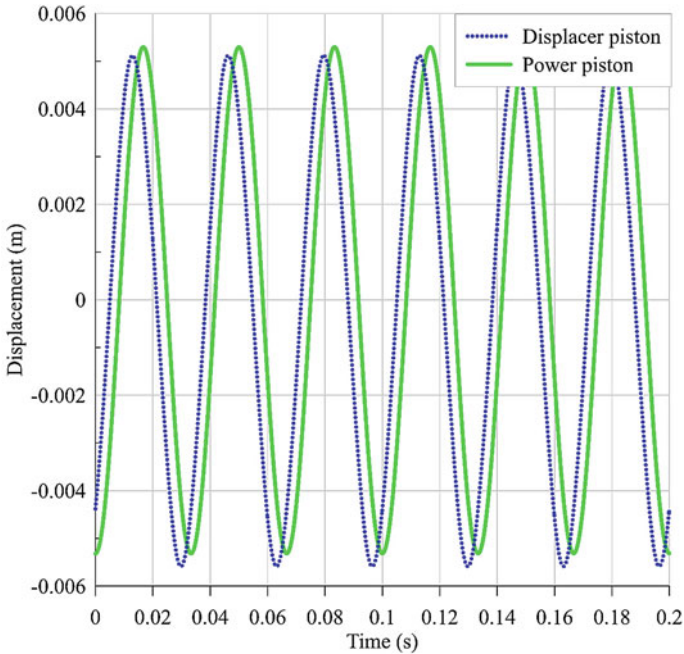
Fig. 14.17 Pistons' displacement

14.4.3 Optimization

In the previous section, the results of the combined FPSE-PMLSM system based on the constant amplitude and frequency for the sinusoidal reference value of the power piston velocity were shown. Since both velocity amplitude and frequency can have different values, the goal of the present section is to find the best frequency-amplitude pair to have the maximum efficiency of the system. In these variations, the physical limitations of the system, which are the maximum possible strokes of two pistons, should be considered. To do the performance optimization, it is assumed that the maximum strokes for power and displacer pistons are 0.014 m and 0.0154 m, respectively. Based on these limitations, the effect of the reference velocity amplitude and frequency on the system efficiency, will be studied separately. To achieve this goal, one of the velocity amplitude or frequency will be fixed, and the other one will be changed considering the physical limitations to see its effect on the system performance.

Figures 14.21 and 14.22 are the results of the reference velocity parameter variations. In Fig. 14.21, the reference velocity amplitude is constant while its frequency is varying, and in Fig. 14.22, the velocity frequency is constant while its amplitude is varying.
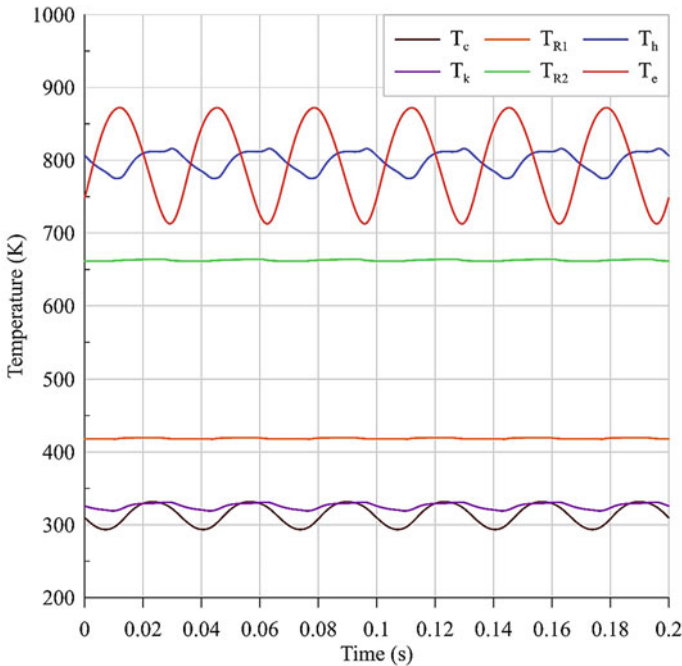
Fig. 14.18 Spaces' temperature

As shown in Figs. 14.21 and 14.22, the frequency decrement at constant amplitude and the amplitude increment at constant frequency improve the system performance. This increment or decrement continues until one of the pistons gets to its maximum stroke. In these conditions, since the system meets its physical limitation, more amplitude increment or frequency decrement is not possible.

The first important result of Figs. 14.21 and 14.22 is that to have the best performance of the system at the defined physical conditions, the reference velocity amplitude should be maximized, and its frequency should be minimized. The second important point is that there is a direct link between pistons' strokes and the system performance. Thus, the frequency and amplitude pairs of the reference velocity should be defined in a way that at least one of the pistons gets to its maximum possible stroke. There are many frequency-amplitude pairs for the reference velocity that can meet these conditions, which obviously all of them are not the optimum points, and the best pair should be identified. Thus, at each frequency, the maximum possible amplitude of the reference velocity to meet the physical limitations is found to identify all the pairs. Then, the efficiency is calculated for each pair. Finally, the results of the system modeling for all pairs are shown in Fig. 14.23.

Based on Fig. 14.23, the amplitude-frequency pair of the reference velocity that gives the maximum efficiency is 1.075 m/s - 25 Hz. All the amplitude-frequency pairs of Fig. 14.23 are concerned with the physical limitations of the system. To
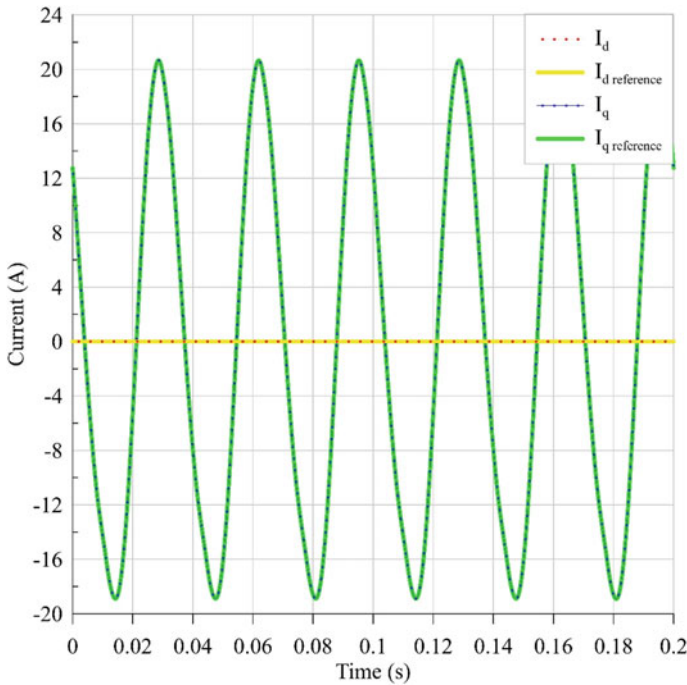
Fig. 14.19 Controlled currents and their references

show which piston's stroke identifies the physical limit of the system of each pair, Fig. 14.24 is presented.

As can be seen in Fig. 14.24, at each frequency-amplitude pair of the reference velocity, at least one of the pistons gets to its maximum possible stroke. At high frequencies, the physical limit is applied by the displacer piston, and at the small frequencies, this limit is applied by the power piston. As can be seen in Fig. 14.24, the maximum of the summation of pistons' strokes divided by their physical limit value happens at the same point that was already found in Fig. 14.23 as the optimum point (1.075 m/s - 25 Hz). An interesting and important result that can be obtained here is that in the FPSE-PMLSM combined system, the both piston strokes are important. It means, since the power piston is connected to the PMLSM mover, it should not be concluded that the power piston stroke should be increased regardless of the displacer piston stroke.
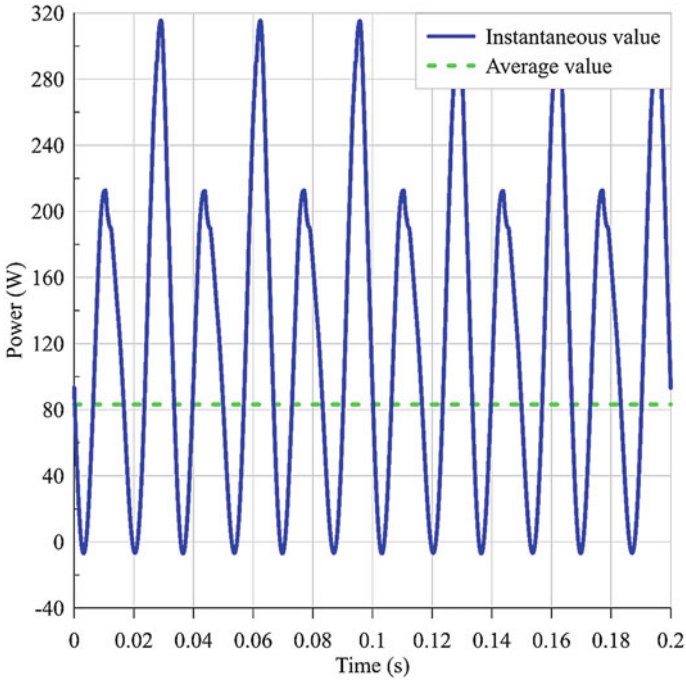
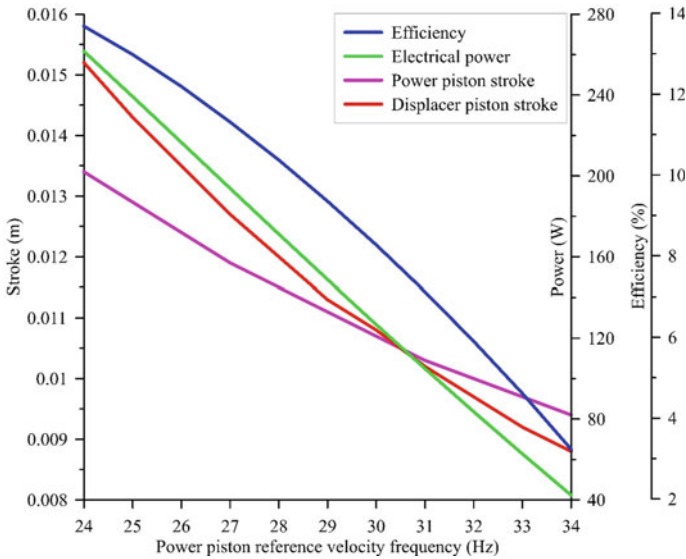**Fig. 14.20** Output electrical power and its average value

Fig. 14.21 FPSE-PMLSM results at constant reference amplitude and variable frequency
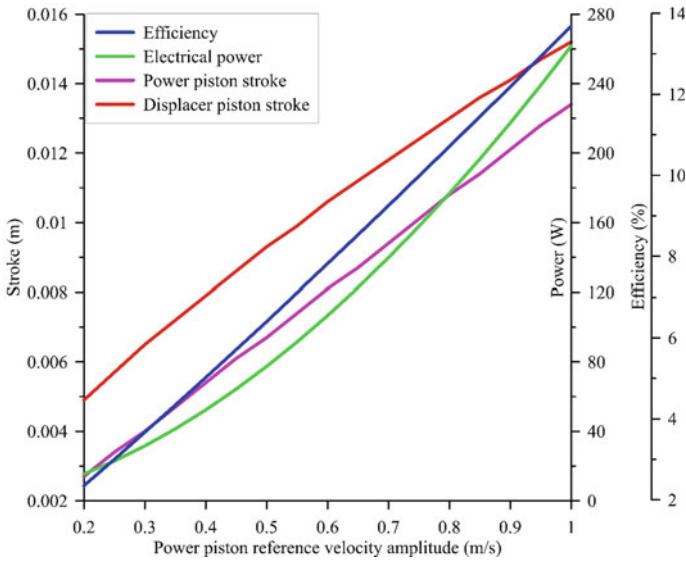
Fig. 14.22 FPSE-PMLSM results at constant reference frequency and variable amplitude

14.5 Applications (in a Tri-Generation IRSOFC Based System)

In the previous sections, the FPSE-PMLSM model was introduced, modeled, and based on the control parameters, its efficiency was maximized. In the present section, the application of this system as a heat recovery option for a tri-generation system is presented, and its effect on the general system performance is studied.

The proposed tri-generation system produces electricity by an Internal Reforming Solid Oxide Fuel Cell (IRSOFC), cooling by a Double Effect Absorption Chiller (DEACH), and hot water through a heat exchanger. The FPSE-PMLSM system is added after IRSOFC to recover the high-quality thermal energy of it as electricity which is the main product of this tri-generation system. Since the focus of the present chapter is on the FPSE-PMLSM system, for IRSOFC and DEACH systems, the general equations are presented, and a more detailed model can be found in Majidniya et al. [5] study.

The schematic of the tri-generation system after adding the FPSE-PMLSM system to it is shown in Fig. 14.25.

The schematic of the DEACH using lithium bromide as absorbent and water as refrigerant is shown in Fig. 14.26.

The DEACH system has three pressure levels and five temperature levels which are presented in Table 14.6.

By calculating the temperature and the enthalpy of the lithium bromide-water solution at each point [5], and some simplifying assumptions, the DEACH chiller
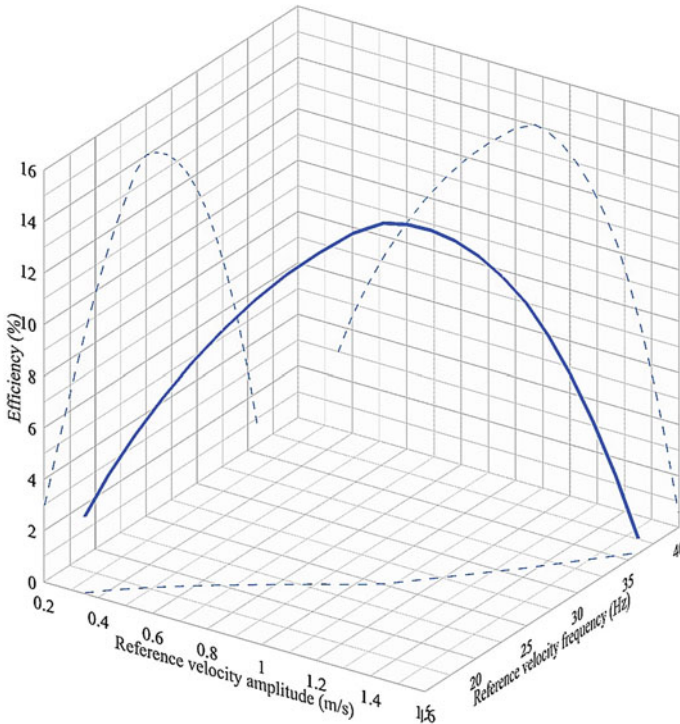
Fig. 14.23 FPSE-PMLSM efficiency at different amplitude-frequency pairs of the reference velocity

model, can be developed. It is assumed that the refrigerant leaves the condenser and evaporator at the saturated state and the expansion valve procedure is enthalpy constant. The system is well isolated and is working at steady-state [5]. The DEACH chiller model gives a COP equal to 1.6.

The modeling of the IRSOFC, which is a tubular one and works at 1 bar in a steady-state condition, and is assumed to be isolated, should be developed in three parts. In the first part, the internal reformer model should be developed based on the reforming, shifting, and electrochemical reactions that can be shown in order as:

$$CH_4 + H_2O \rightarrow CO + 3H_2 \tag{14.63}$$

$$CO + H_2O \rightarrow CO_2 + H_2 \tag{14.64}$$

$$H_2 + 1/2O_2 \rightarrow H_2O \tag{14.65}$$
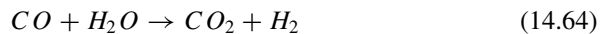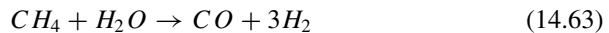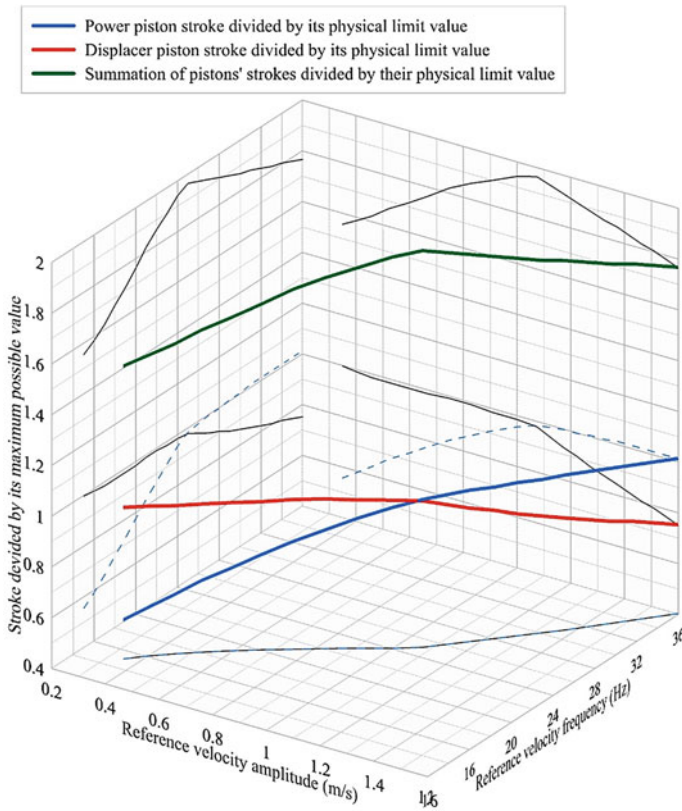
Fig. 14.24 System physical limitation at each frequency-amplitude reference value pair

Fig. 14.25 Tri-generation schematic
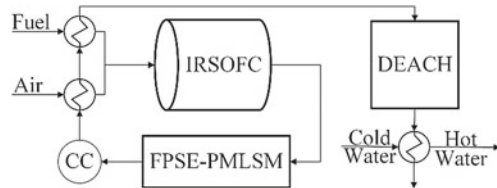
By using the molar balance of the reactions and their related equilibrium constants, considering the flow channels of Fig. 14.27, it is possible to calculate the molar flow rate of gasses.

In the second part, the IRSOFC voltage should be calculated. The cell voltage can be calculated as:

$$v_{cell} = v_{reversible} - (v_{Act} + v_{Ohm} + v_{Conc}) \qquad (14.66)$$

Fig. 14.26 Double effect absorption chiller schematic
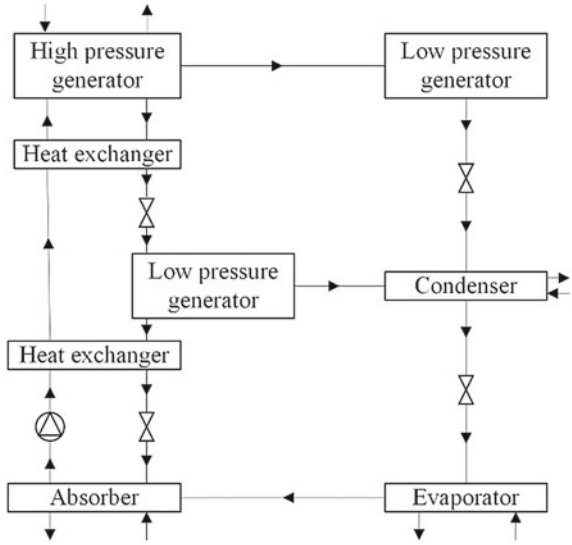
Table 14.6 DEACH temperature levels

Evaporator	280.15 K
Absorber	305.15 K
Low-pressure generator	340.95 K
High-pressure generator	381.05 K
Condenser	305.35 K

Fig. 14.27 IRSOFC flow channels
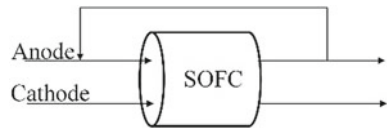
The reversible voltage of the cell can be calculated based on the Nernst equation. As can be seen, three polarizations (v_{Act}, v_{Ohm}, and v_{Conc}) should be calculated beside the reversible voltage to calculate the real cell voltage. These polarizations can be calculated as [5]:

$$v_{Act} = \frac{2RT}{n_e Fr} \sinh^{-1}\left(\frac{i_{cell}}{2A_{cell}i_0}\right) \tag{14.67}$$

$$v_{Ohm} = \sum \frac{i_{cell}}{A_{cell}} r \tag{14.68}$$

$$v_{Conc} = \frac{RT}{n_e Fr}\left(1 - \frac{i_{cell}}{i_{limit}}\right) \tag{14.69}$$

n_e, which is the number of electrons, is equal to 2. The method of i_0 calculation for v_{Act} and r calculation for v_{Ohm} was described in detail in Majidniya et al. study [5, 23]. The limiting current density is also assumed to be equal to 9000 $\frac{A}{m^2}$. After these calculations, the power of each IRSOFC cell can be calculated as:

$$Power_{cell} = i_{cell} v_{cell} \tag{14.70}$$

To calculate the total IRSOFC power, its cell power is multiplied by the number of cells that here is equal to 26.

The last part of the IRSOFC modeling is the thermal balance inside the system that, through a trial and error method, can provide the cell temperature. For the present study, the calculated cell temperature is 1000 K.

The results of the IRSOFC modeling are shown in Figs. 14.28 and 14.29.

As can be seen, by increasing the cell current density, the cell power increases until around 7000 A/m^2 and then decreases, while the cell voltage is decreasing. For the present study, a cell current density equal to 2000 A/m^2 with a cell area equal to 0.0834 m^2 is considered.

Finally, the results of the tri-generation system are shown in Table 14.7.

In Table 14.7, $\dot{Q}_{intri-generation}$ is the input thermal energy to the system that can be calculated based on the fuel flow rate, which is methane, and its Lower Heating
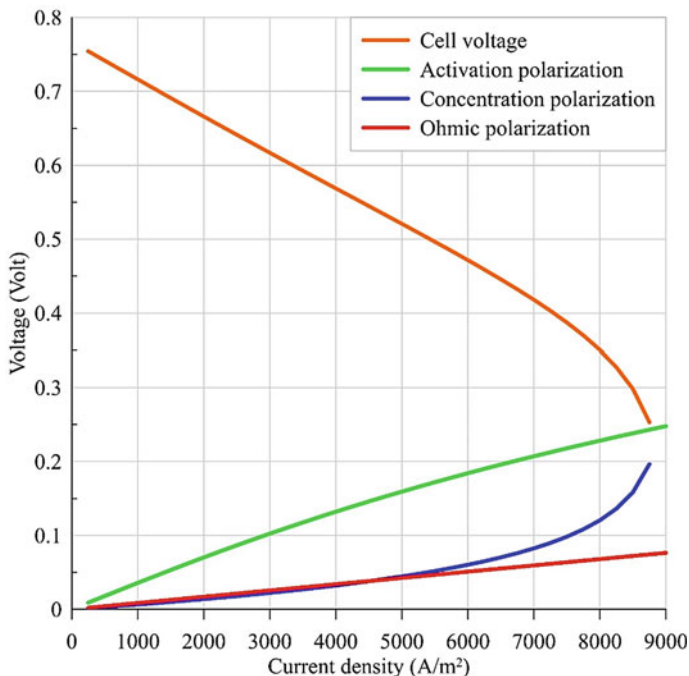
Fig. 14.28 IRSOFC cell voltage and polarizations
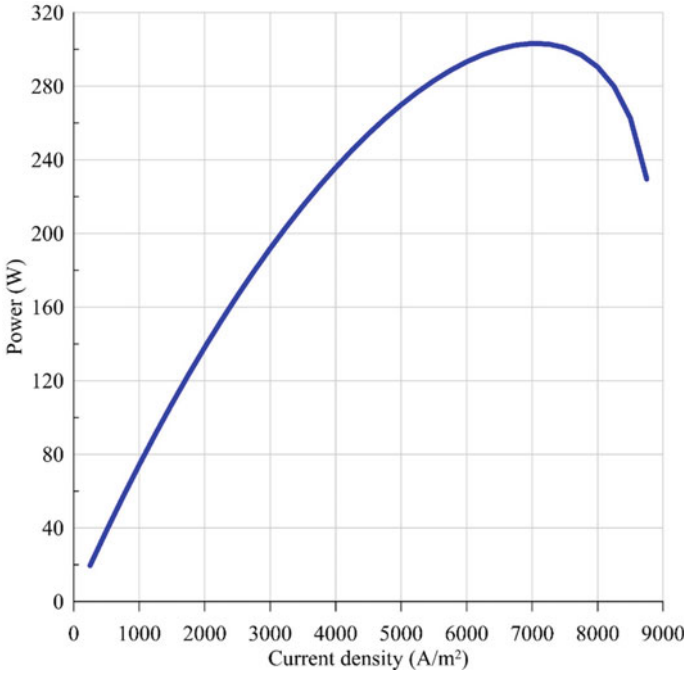
Fig. 14.29 IRSOFC cell power

Table 14.7 Tri-generation results

$Power_{IRSOFC}$	1981 W
$Power_{FPSE-PMLSM}$	279.4 W
DEACH cooling production	1366.6 W
$\dot{Q}_{Hotwater}$	0.27 kg/s
$\dot{Q}_{intri-generation}$	6165.4 W

Value (LHV) as:

$$\dot{Q}_{intri-generation} = \dot{m}_{CH_4}LHV \tag{14.71}$$

$\dot{Q}_{Hotwater}$ is the thermal energy while heating the water from 25 °C to 60 °C. Then, the tri-generation efficiency can be defined as:

$$\eta = \frac{Power_{IRSOFC} + Power_{FPSE-PMLSM} + \dot{Q}_{DEACH} + \dot{Q}_{Hotwater}}{\dot{Q}_{intri-generation}} \tag{14.72}$$

Here, two methods of efficiency calculations based on the $\dot{Q}_{DEACH}$ value are defined. In the first method, $\dot{Q}_{DEACH}$ is assumed to be the same value of Table 14.7,

Fig. 14.30 Methods of $\dot{Q}_{DEACH}$ calculation
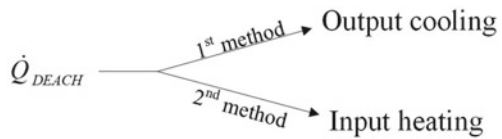
which is the produced cooling, and in the second method, it is assumed to be the consumed heat by the DEACH. These two methods are shown in Fig. 14.30. The reason for defining these two methods is that, in general, for refrigeration systems like DEACH, the output (cooling) is higher than the input energy. Thus, for such systems, instead of efficiency, COP is defined, which is always bigger than 1.

Based on these two methods, the efficiency of the tri-generation system is equal to 72.4% and 63.82%, respectively. The efficiency of the standalone IRSOFC is also equal to 32.13%. This means that the tri-generation system improves the IRSOFC standalone efficiency by 40% considering the first method of efficiency calculation or 31.7% based on the second method. Also, by adding the FPSE-PMLSM system to the IRSOFC, the electrical power increases from 1981 W to 2260.4 W, which is around a 14.1% increment in electrical power production. This means around 4.5% of electrical efficiency improvement.

All these results show how the FPSE-PMLSM system can play an essential role in a thermal-based system as a heat recovery option. Here through a tri-generation fuel cell based system, this fact is clarified, and the FPSE-PMLSM proves itself as a new efficient waste heat recovery system.

References

1. R. Stirling, Stirling air engine and the heat regenerator, US Pat. 4081 (1816)
2. M. Majidniya, T. Boileau, B. Remy, M. Zandi, Nonlinear modeling of a Free Piston Stirling Engine combined with a Permanent Magnet Linear Synchronous Machine, Appl. Therm. Eng. 165 (2020) 114544. https://doi.org/10.1016/j.applthermaleng.2019.114544
3. M.A. Al-Nimr, W.A. Al-Ammari, A novel hybrid and interactive solar system consists of Stirling engine /vacuum evaporator /thermoelectric cooler for electricity generation and water distillation. Renew. Energy. **153**, 1053–1066 (2020). https://doi.org/10.1016/j.renene.2020.02.072
4. M. Rokni, Thermodynamic and thermoeconomic analysis of a system with biomass gasification, solid oxide fuel cell (SOFC) and Stirling engine. Energy **76**, 19–31 (2014). https://doi.org/10.1016/j.energy.2014.01.106
5. M. Majidniya, B. Remy, T. Boileau, M. Zandi, Free Piston Stirling Engine as a new heat recovery option for an Internal Reforming Solid Oxide Fuel Cell, Renew. Energy. 171 (2021) 1188–1201. https://doi.org/10.1016/j.renene.2021.02.082.
6. Ł Bartela, J. Kotowicz, L. Remiorz, A. Skorek-Osikowska, K. Dubiel, Assessment of the economic appropriateness of the use of Stirling engine as additional part of a cogeneration system based on biomass gasification. Renew. Energy. **112**, 425–443 (2017). https://doi.org/10.1016/j.renene.2017.05.028
7. M. Marion, H. Louahlia, H. Gualous, Performances of a CHP Stirling system fuelled with glycerol. Renew. Energy. **86**, 182–191 (2016). https://doi.org/10.1016/j.renene.2015.08.012

8. M. Majidniya, T. Boileau, B. Remy, M. Zandi, Performance simulation by a nonlinear thermo-dynamic model for a Free Piston Stirling Engine with a linear generator, Appl. Therm. Eng. 184 (2021) 116128. https://doi.org/10.1016/j.applthermaleng.2020.116128

9. A.C. Ferreira, J. Silva, S. Teixeira, J.C. Teixeira, S.A. Nebra, Assessment of the Stirling engine performance comparing two renewable energy sources: Solar energy and biomass. Renew. Energy. **154**, 581–597 (2020). https://doi.org/10.1016/j.renene.2020.03.020

10. S. Zare, A.R. Tavakolpour-Saleh, Frequency-based design of a free piston Stirling engine using genetic algorithm. Energy **109**, 466–480 (2016). https://doi.org/10.1016/j.energy.2016.04.119

11. K. Wang, S.R. Sanders, S. Dubey, F.H. Choo, F. Duan, Stirling cycle engines for recovering low and moderate temperature heat: A review. Renew. Sustain. Energy Rev. **62**, 89–108 (2016). https://doi.org/10.1016/j.rser.2016.04.031

12. G. Walker, Stirling engines, (1980).

13. J. Subramanian, G. Heiskell, F. Mahmudzadeh, P. Famouri, Study of radial and axial magnets for linear alternator - Free piston engine system, in, North Am. Power Symp. NAPS 2017. IEEE **2017**, 1–6 (2017). https://doi.org/10.1109/NAPS.2017.8107293

14. R. Redlich, A summary of twenty years experience with linear motors and alternators, Sunpower Inc. (1995) 1–9

15. E.Y. Loktionov, A.A. Martirosyan, M.D. Shcherbina, Solar powered free-piston stirling-Linear alternator module for the lunar base, in, 2nd Int. Conf. Ind. Eng. Appl. Manuf. ICIEAM 2016 - Proc. IEEE **2016**, 1–6 (2016). https://doi.org/10.1109/ICIEAM.2016.7910983

16. W. Ye, P. Yang, Y. Liu, Multi-objective thermodynamic optimization of a free piston Stirling engine using response surface methodology. Energy Convers. Manag. **176**, 147–163 (2018). https://doi.org/10.1016/j.enconman.2018.09.011

17. C.K. Alexander, M.N.O. Sadiku, e-Text Fundamentals of Electric Circuits, McGraw-Hill Higher Education, 2001. https://books.google.fr/books?id=SBdigDfQB5cC

18. T.T. Dang, M. Ruellan, L. Prévond, H. Ben Ahmed, B. Multon, Sizing Optimization of Tubular Linear Induction Generator and Its Possible Application in High Acceleration Free-Piston Stirling Microcogeneration, IEEE Trans. Ind. Appl. 51 (2015) 3716–3733. https://doi.org/10.1109/TIA.2015.2427284

19. M. Majidniya, T. Boileau, R. Benjamin, M. Zandi, Thermoelectric modeling of a Free Piston Stirling Engine (FPSE) combined with a Permanent Magnet Linear Synchronous Machine (PMLSM) with its control system, in: Int. Conf. Renew. Energy Distrib. Gener. Iran (2019)

20. M. Majidniya, T. Boileau, R. Benjamin, M. Zandi, Modélisation thermo-électrique d'un moteur Stirling à piston libre et d'une machine synchrone linéaire à aimant permanent avec sa commande, in: Congrès Annu. La Société Française Therm. (2019)

21. I. Urieli, D. Berchowitz, Stirling Cycle Engine Analysis, A. Hilger Bristol (1984)

22. J. Zheng, J. Chen, P. Zheng, H. Wu, C. Tong, Research on control strategy of free-piston Stirling power generating system. Energies **10**, 1609 (2017)

23. M. Majidniya, K. Gharali, K. Raahemifar, A Comparison of Off-Grid-Pumped Hydro Storage and Grid-Tied Options for an IRSOFC-HAWT Power Generator, Int. J. Rotating Mach. 2017 (2017). https://doi.org/10.1155/2017/4384187.

Chapter 15
Detailed 3E Exploration of a Sugar Industry Using Its Experimental Data

Hamed Ghiasirad, Rahim Khoshbakhti Saray, Bahman Abdi, and Keyvan Bahlouli

Abstract Sugar beet production is low in Iran, and about 50% of sugar demand is imported from other countries. Meanwhile, the factories are old in Iran, and novel technologies are not employed, and consequently, the sugar production unit cost is high. Sugar production is one of the most important industries. An increase in energy usage and cost of sugar production has forced the researchers to concentrate on cost analysis while considering the thermodynamics analysis of sugar production systems. In the present study, using experimental data of Urmia Sugar Factory in northwestern Iran, first, the energetic and exergetic analyses are done on different parts of the plant. Then, the most inefficient parts of the system under study are identified, and a thermo-economic analysis is performed for that unit. The results show that cogeneration, purification, and crystallization units have the highest exergy destruction, respectively. Also, the cogeneration unit with 20.17%, the purification unit with 89.25%, and the condensation unit with 91.31% have the lowest second law efficiency, respectively. The total exergy efficiency of the plant is found to be 56.44%. In the cogeneration unit, the 5th and 3rd economizers have the lowest exergy efficiency, and the 2nd and 3rd combustion chambers have the highest exergy destruction. Also, the 2nd HRSG and 4th combustion chamber have the highest values of the summation of investment cost and exergy destruction, and exergy loss costs.

H. Ghiasirad · R. K. Saray (✉)
Faculty of Mechanical Engineering, Sahand University of Technology, Sahand New Town, Tabriz, Iran
e-mail: khoshbakhti@sut.ac.ir

H. Ghiasirad
e-mail: h_ghiasirad@sut.ac.ir

B. Abdi
Department of Mechanical Engineering, Faculty of Engineering, Khoy Branch, Islamic Azad University, Khoy, Iran

K. Bahlouli
Mechanical Engineering Department, Faculty of Engineering, Girne American University, Via Mersin 10, Girne, N. Cyprus, Turkey
e-mail: keyvanbahlouli@gau.edu.tr

Nomenclature

Symbols

A/F	Mass-based air-fuel ratio
APTD	Approach point temperature difference,(°C)
$\dot{C}$	Cost rate, ($/h)
C	Unit cost, ($/GJ)
CRF	Capital recovery factor
Ex	Specific exergy, (kJ/kg)
$\dot{E}$	Exergy rate, (kW)
F	Exergo-economic factor
φ	Equivalence ratio
H	Specific enthalpy, (kJ/kg)
HFO	Heavy Fuel Oil
$\dot{I}$	Irreversibility rate, (kW)
K	Interest rate, (%)
LHV	Lower heating value, (kJ/kg)
LMTD	Logarithmic mean temperature difference,(°C)
$\dot{m}$	Mass flow rate, (kg/s)
MW	Molecular weight, (kg/kmol)
N	Number of moles
$\dot{n}$	Molar flow rate, (kmol/s)
n_r	System lifetime, (Year)
P	Pressure, (kPa)
PEC	Purchased equipment cost, ($)
PPTD	Pinch point temperature difference, (°C)
Q	Quality of juice, (%)
$\dot{Q}$	Heat transfer rate, (kW)
R	The relative cost difference, (%)
S	Specific entropy, (kJ/kg.K)
St	Steam
Sup	Superheater
T	Temperature, (°C)
τ	Annual operating hours, (h)
treat	Treatment unit
$\dot{W}$	Power, (kW)
X	Mass fraction
Y	Mole fraction

Subscripts and Superscripts

CC	Combustion chamber
CI	Capital investment
Cogen	Cogeneration
Conc	Concentration unit
cond	Condensation unit
crys	Crystallization unit
Dest	Destruction
Desup	Desuperheater
DS	Dry Substance
eco	Economizer
eva	Evaporator
exp	Expansion of steam
ext	Extraction unit
F	Fuel
f	Formation
Fb	Fiber
Fr	Fructose
gen	Generator
heat	Heating unit
L	Liquid
L	Loss
mix	Mixer
OM	Operating and maintenance cost
R	Reactants
r	Reference
S	Sucrose
sto	Stoichiometric
Turb	Turbine
w	Water
W	Work
water	Water distribution unit

Greek Letters

η	Efficiency, (%)
φ	Operating and maintenance factor

15.1 Introduction

Increasing energy costs, satisfying environmental regulations, and finding more profitable and sustainable solutions within the process industries have been driving forces for exploring energy integration opportunities for reducing energy costs over the last several decades. This is especially important in processes (e.g., evaporation, crystallization, and drying) that consume large amounts of energy and present potentials for energy savings [1]. An increase in energy usage and cost of sugar production has forced the researchers to concentrate on cost analysis while considering the thermodynamics analysis of sugar production systems. Tekin and Bayramoglu [2] employed an exergy analysis of the industrial process of the production of white refined sugar beets. They found that the main source for exergy losses in a steam-power system occurs as a result of combustion and also using waste exergies of stack gases. The work also suggested that the old liming-carbonation method for the raw juice clarification could be replaced by new technologies that do not involve any chemical reaction, like a suitable membrane separation process. In the juice concentration unit, the vapor recompression method and membrane separation process could be used to reduce losses. Grabowski et al. [3] did a thermodynamic study on a sugar manufacturing process. They found that vapor recompression could reduce the energy consumption of the system. The work demonstrated that between steam turbines, gas turbines, and diesel engines, using the gas turbine in the power plant could save up to 30% energy compared to the traditional system. Tekin and Bayramoglu [4] performed an exergetic analysis of raw juice production and the steam-power units of the sugar production plant from sugar beet. It was found that the exergy efficiency of raw juice production and steam-power units is 32.3% and 22.6%, respectively. Their study showed that by increasing the production of juice, the exergy losses of the raw juice production would be decreased however it inversely affects the exergy losses of the plant. It was concluded that an optimum range would be 110–125 kg juice production from 100 kg of sugar beet. For sugar production stages, through an energetic and exergetic analysis, Bayrak et al. [5] found that the highest amount of exergy losses happened at the sherbet production process. Results of the work revealed that the lowest exergy efficiency took place at the Sherbet production stage. Also, the Sherbet thickening had the highest exergy efficiency. Furthermore, based on the exergy inflow, the Sherbet crystallization stage involved the highest irreversibility rate. As a result, the work suggested that to have a more efficient sugar production process, the irreversibility, mostly arising from the finite temperature differences at the sugar production stages, should be reduced. Krajnc et al. [6] carried out a detailed investigation of the possibility of improving the economic and environmental performances of the beet sugar industry in Slovenia. To approach zero-waste from beet sugar processing, the feasibility of using waste and by-products from sugar processing was conducted. The work also revealed that the energy consumption of the plant could be reduced through the simultaneous optimization of evaporation and crystallization processes. For the case of fuel type, from an economic point of view, the use of heavy fuel oil was reasonable. However, taking to account the environmental impact, the

use of natural gas in the optimized sugar production process results in the lowest total cost. In 2015, Taner and Sivrioglu used laboratory data from a sugar factory in Turkey and, after selecting input data and applying assumptions, evaluated the plant from the energy and exergy points of view. The study showed that the energy efficiency and exergy efficiency of the whole plant are 72.2% and 37.4%, respectively. The authors did not include the 1st process, which was the cutting sugar beets process in their calculations and found that the highest and lowest values of the energy efficiency took place in the raw juice production process and the factory energy generation process, respectively. The work also revealed that the highest and lowest values of exergy efficiency are for the raw juice purification process and the factory energy generation process, respectively. The reason for these results is that there is a high exergy loss in the factory energy generation process. Also, a 48.6% exergy efficiency for the thick juice refining process was reported, which suggested that this process was also not favorable. In 2015, Sahin et al. [7] analyzed the Ergli sugar plant in Turkey from energetic and exergetic points of view. They found that the sherbet production process and crystalization process with 30.4% and 89.5% had the lowest and highest exergy efficiency, respectively. They also recommended that to improve the performance of the system, the heat exchanger efficiency and its insulation should be improved in the sherbet production process. In 2017, Taner and Sivrioglu [8], by using data from a real plant, developed a general model for sugar production processes and provided an exergy analysis. The authors then performed thermoeconomic analysis of a steam turbine power plant. It was found that by increasing the turbine power capacity from 8 to 14 MW, energy efficiency increases from 46.4% to 48.7% and exergy efficiency enhances 4%. Also, it was claimed that by increasing the turbine power capacity from 8 to 14 MW, the payback period would be reduced from 5.33 to 4.32 years. In 2018, Dogbe et al. [9] simulated a typical sugar mill using Aspen Plus simulation software and conducted an exergetic analysis to identify inefficient processes. The overall irreversibility of 217.3 MJ per ton of cane crushed was found for the sugar mill, and the exergetic efficiency of the sugar mill was calculated as 9.7%. The highest irreversibility took place at the evaporation unit with a value of 100 MJ/ton of cane. Also, the lowest functional exergy efficiency of 9.6% was related to the crystallization unit with the greatest possibility for improvement of 47.0 MJ/ton of cane. It is suggested that, by adopting a single-stage crystallization with an integrated biorefinery, the exergetic performance of the mill could be improved. The sugar industry is the second-largest agro-industry in the world, with more than 80% of sugar produced from sugar cane. Sugar mills may be energy self-sufficient, but they are energy-intensive, designed inefficiently [9].

Based on available researches in the literature on sugar factories, it can be concluded that optimizing energy consumption, increasing the productivity of energy sources, recovering waste heat, reducing fuel consumption, increasing the efficiency of different parts of the plant, performance of the whole system can be improved. In this work, an Urmia sugar factory case study is analyzed in which beet converts to pulp and raw juice in the juice extraction process. After that, in the purification process, the juice color becomes clear using lime and carbon dioxide. Factory steam

demand is supplied from a cogeneration unit. The system is modeled from a thermo-dynamic viewpoint. More attention is paid to the second law and exergo-economic behavior of the most irreversible part of the plant. Finally, a parametric analysis is conducted to evaluate the effects of some critical parameters on the performance of the cycle.

15.2   System Description

In the present study, using experimental data of Urmia Sugar Factory in northwestern Iran, the energetic and exergetic analyses will be done on different parts of the plant to recognize how various factory units perform. Finally, the most inefficient parts of the system under study are identified, and a thermo-economic analysis is performed for that unit.

A schematic diagram of the system is shown in Fig. 15.1. As can be seen, the system has eight distinct components, including extraction, purification, heating, evaporation, crystallization, condensing, water distribution, and cogeneration. The rate of beet input to the process is about 150 $\frac{ton}{h}$. The total electricity consumption of the plant is about 7400 kWh, in which 5400 kWh of this amount is supplied by the power plant and about 2000 kW is purchased from the grid. As shown in Fig. 15.2,
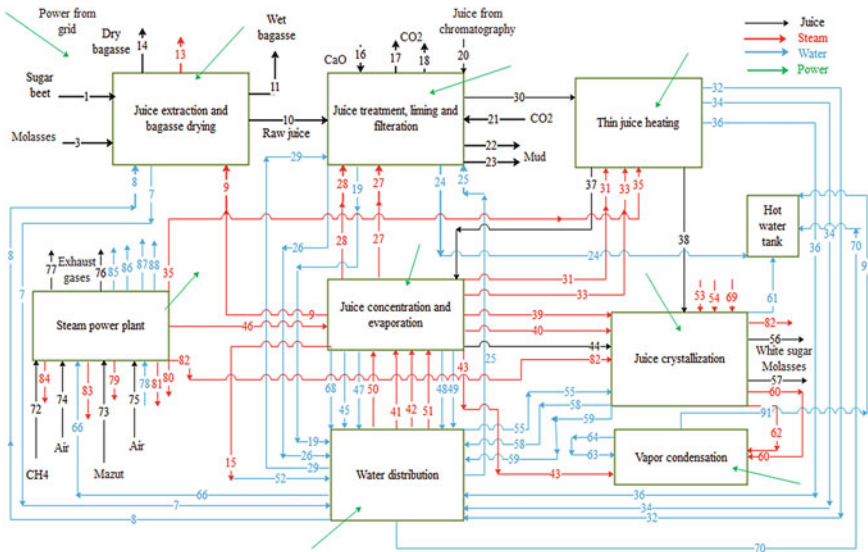
Fig. 15.1 Schematic diagram of the Urmia sugar factory
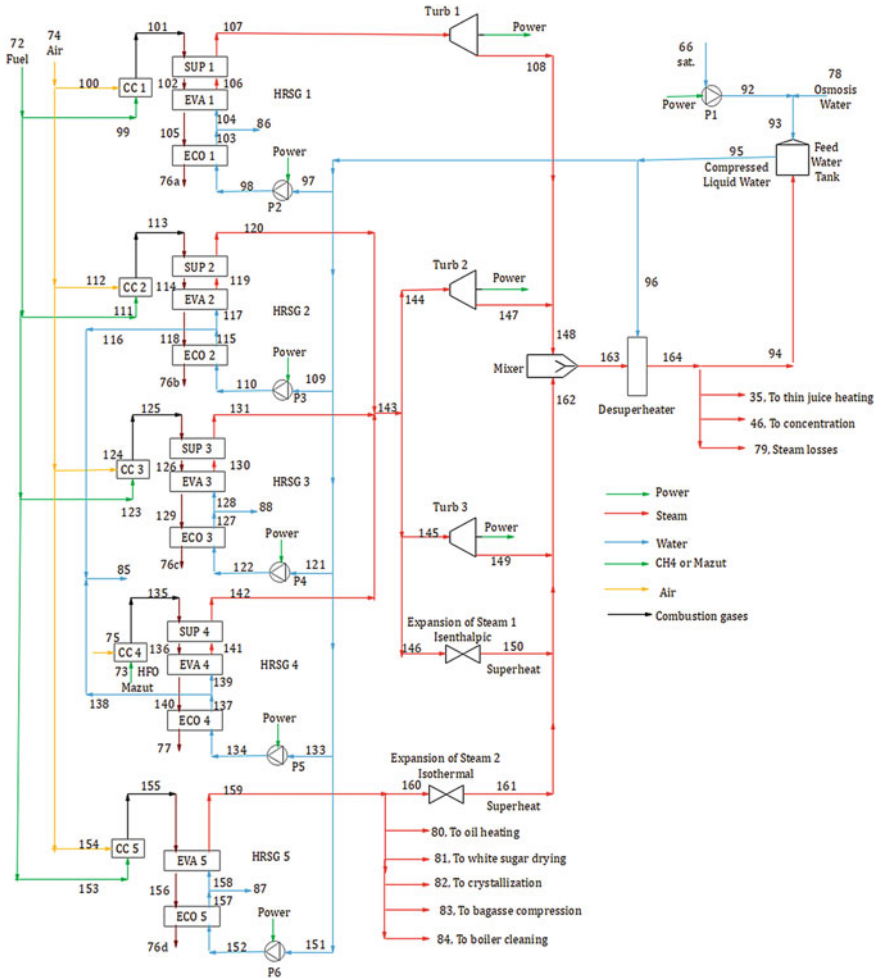
Fig. 15.2 Schematic diagram of the cogeneration unit

the sugar plant has five boilers and three steam turbines. All boilers have been fueled by fuel oil in the past, but in recent years 4 of them have been converted to use natural gas to reduce the environmental impacts. Total natural gas consumed by 4 boilers is approximately equal to 8500 $\frac{Nm^3}{h}$. Also, the heavy fuel oil consumption of a boiler is 1220 $\frac{kg}{h}$. The lime consumption of the raw juice purification process is also 2.9 $\frac{ton}{h}$. Plant units receive approximately 161 $\frac{ton}{h}$ of the saturated steam at 141 °C from the power plant. The plant sugar production is approximately at a rate of 21 $\frac{ton}{h}$.

Due to the importance of the power and steam generation system in the plant, this section will be discussed in more detail below. At the sugar plant investigated, the total power consumption is about 7400 kWh, of which 2000 kWh is provided

through the grid and the rest is powered by the plant. The sugar production process requires about 65 $\frac{ton}{h}$ saturated vapor at about 140 °C, which must be met by the plant. The saturated liquid water at 126.1 °C at point 66 is transferred from the water distribution system to the steam power plant and enters pump 1 and its pressure is raised to 370 kPa at point 92. Also, the treated water of the reverse osmosis process is introduced at point 78, with a mass flow rate of 12.74 kg/s, a temperature of 15 °C, and the same pressure of point 92. Then, in the feed water tank, a portion of the saturated steam output from the turbines at point 94 mixes with water coming from point 93 and becomes liquid water at point 95. Then, some parts of the water at point 95 flows to point 96 to convert superheated steam coming from the turbines to the saturated steam, and the rest is directed to pump inlets at points 97, 109, 121, 133, and 151. On the other hand, methane and heavy fuel oil, at ambient temperature and pressure, enter the combustion chambers at points 72 and 73 with a mass flow rate of 1.63 kg/s and 0.34 kg/s, respectively, along with 40% excess air at points 74 and 75. Then, the combustion is done and the products are formed at high temperatures.

The pinch point temperature difference and the approach point temperature difference in the boilers are about 450 and 50 degrees, respectively. The output pressure of the turbines and expansion valves is 370 kPa. The turbine inlet pressure and temperature are also about 4,000 kPa and 400 °C. Some of the saturated steam of the fifth boiler is used in various plant units. The superheated vapors are also converted to saturated vapor at 140.8 °C by compressed liquid water of point 96. Then, some of it dissipates at point 79 and, through points 35 and 46, are transferred to the heating and condensing sections. Also, some of the steam at point 94 returns to the starting point of the cycle.

The main part of the sugar production process is the extraction step, as the sucrose in the sugar beet is extracted at this stage, and the rest of the process is carried out to purify the sucrose as much as possible. Therefore, if the extraction stage is carried out efficiently, then the whole plant efficiency will be optimal. As shown in Fig. 15.1, the beet slices enter the extraction system at point 1 with a rate of 41.49 kg/s, which contains 23% dry substance. The extraction process in the investigated plant has two diffusion towers in which hot water and beet are mixed in the opposite direction. The main components of the extraction system are the diffuser tower and the counterflow mixer. After extracting the raw juice in the extraction system, the slices that have already lost about 98% of their sucrose are compressed by the press device to remove the remaining sucrose and are returned to the extraction tower. In the juice treatment, the raw juice is processed to remove any impurities. Calcium carbonate is first decomposed in the lime furnace, according to Eq. (15.1), which is an endothermic reaction to lime (calcium oxide) and carbon dioxide. Subsequently, the produced lime mixes with the injected water to the system, and a reaction happens according to Eq. (15.2). The solution absorbs the impurities in the juice. Subsequently, the impurities absorbed in the mixture are heated and transferred to the clarifier, and its sedimentary material is removed. This will remove any impurities in the raw juice.

$$CaCO_3(s) \rightarrow CaO(s) + CO_2(g) \qquad (15.1)$$

$$CaO(g) + H_2O(l) \rightarrow Ca(OH)_2(aq) \tag{15.2}$$
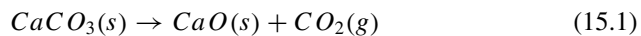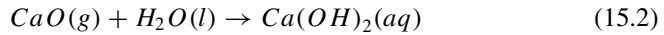
Then, the diluted juice at point 30 enters the thin juice heating stage. At this stage, the temperature of the diluted juice is increased by several heat exchangers and heat transfer between the diluted juice and the incoming water vapor. The primary purpose of this step is to decrease the temperature difference between the juice and the steam entering the juice concentration and evaporation stage. This will reduce the exergy loss in the juice concentration and evaporation stage. The diluted juice with high temperature is then entered into the juice concentration and evaporation section. The system uses multistage evaporators to reduce sucrose degradation, prevent the color change of the juice, and save energy. In general, the arrangement is forward feed. Initially, the dilute juice exits from the heating stage at point 37 at 124 °C enters the first stage of the multistage concentration process. On the other hand, at point 46, the saturated steam from the power plant enters the first body, and after condensation, at point 47, it is transferred to the water distribution system. The temperature and pressure of the saturated vapor and the juice separated from point 37 decreases, but the juice exits the first body. Finally, the concentrated juice at point 44 is directed to the juice crystallization stage at a temperature of 80 °C, and about 65% concentrated Brix with 7.8 PH. Following the juice, crystallization is explained.

The purpose of this section is to increase the purity of the juice to about 100%. For this purpose, the concentrated juice at 80 °C at point 44 is introduced from the juice concentration and evaporation section to the juice crystallization section. On the other hand, the heated juice at 90 °C at point 38 is transferred from the thin juice heating section to the juice crystallization section, then two flows of points 44 and 38 are mixed and boiled after being heated in the heat exchanger. At the end of this step, a product containing sugar crystals, a small amount of juice, and impurities (waste syrup) is obtained. The product is then transferred to a centrifuge to separate the sugar and impurities. Finally, sugar with 100% Brix is dried and stored and waste syrup of higher purity is reused in subsequent vacuum pans.

As shown in Fig. 15.1, several other subsystems are considered in the investigated system. The vapor condensation system converts the saturated steam, from the boiling process obtained from the juice concentration and evaporation section and the juice crystallization section to the saturated liquid water. The water distribution system is responsible for the distribution of water to different parts of the plant. The combined power and steam generation system provides part of the power required at the plant as well as the saturation steam required by the systems. The hot water tank stores the distilled hot water from different parts of the system to be used in the other parts.

15.3 System Modeling and Simulation

In the present study, the Engineering equation Solver (EES) [10] is used to simulate the plant. The following assumptions are considered:

- The pressure drop in pipes, fittings, and heat exchangers is ignored [11].
- All processes are considered a steady-state [11].
- Changes in kinetic and potential energies are ignored [12].
- Natural gas is considered to contain only methane [1].
- The density of natural gas is set to be 0.7064 $\left(\frac{kg}{m^3}\right)$ [1].
- Isentropic efficiencies of pumps and turbines are assumed to be 80% and 85%, respectively [11].
- Electricity purchased from the grid is not consumed in the power plant and is transferred to the other systems [13].
- The power consumption of the power plant is equal to the total power consumption of the pumps fed by the turbines [11].

In addition to the assumptions mentioned above, the assumed input parameters are reported in Table 15.1.

To study the system, each unit such as extraction, purification, heating, evaporation, crystallization, condensing, water distribution, and cogeneration is considered as the general control volume and each of the equipment of the power plant is in a steady-state condition. Then the equations of mass, concentration, energy, and exergy are applied.

The first law of thermodynamics for the control volumes is given by Eq. (15.3):

$$\dot{Q}_{CV} + \sum_{in} \dot{m}_i(h_i + \frac{v_i{}^2}{2} + gz_i) = \dot{W}_{CV} + \sum_{out} \dot{m}_e(h_e + \frac{v_e{}^2}{2} + gz_e) \qquad (15.3)$$

In the above Equation, variations in kinetic and potential energies are ignored.

In the system studied, beet enters the extraction system at point 1, the mass fraction of dry matter (x_{DS}), the degree of purity (q) and the cellulose mass fraction (x_{FB}) are known, and it is possible to calculate the mass fraction of sucrose (x_S), water (x_W) and fructose (x_{FR}) by Eqs. (15.4)–(15.6):

$$x_S = x_{DS} \bullet q \qquad (15.4)$$

$$x_W = 1 - x_{DS} \qquad (15.5)$$

$$x_{FR} = 1 - x_S - x_W - x_{FB} \qquad (15.6)$$

Table 15.1 Input parameters for energy analysis

Assumption	Value	References
Ambient temperature	$T_0 = 0(°C)$	[14]
Ambient pressure	$P_0 = 100(kPa)$	[15]
Reference temperature for properties calculation	$T_r = 0(°C)$	[14]
Chemical formula of heavy fuel oil	$C_{11.6}H_{17}$	[16]
Chemical formula of sucrose Chemical formula of fructose Chemical formula of cellulose (fiber)	$C_{12}H_{22}O_{11}$ $C_6H_{12}O_6$ $C_6H_{10}O_5$	[9]
Approach point temperature difference of boilers	$APTD = 50(°C)$	[13]
Pinch point temperature difference of 1st boiler	$PPTD_1 = 421(°C)$	[13]
Pinch point temperature difference of 2nd boiler	$PPTD_2 = 417(°C)$	[13]
Pinch point temperature difference of 3rd boiler	$PPTD_3 = 638.5(°C)$	[13]
Pinch point temperature difference of 4th boiler	$PPTD_4 = 674.6(°C)$	[13]
Pinch point temperature difference of 5th boiler	$PPTD_5 = 332.7(°C)$	[13]
The efficiency of 1st electrical generator	$\eta_{Gen1} = 60(\%)$	[13]
The efficiency of the 2nd and 3rd electrical generator	$\eta_{Gen2,3} = 90(\%)$	[13]
Power consumption of the extraction unit	$\dot{W}_{Ext} = 1800(kW)$	[13]
Power consumption of the treatment unit	$\dot{W}_{Puri} = 1500(kW)$	[13]
Power consumption of the heating unit	$\dot{W}_{Heat} = 400(kW)$	[13]
Power consumption of concentration unit	$\dot{W}_{Evap} = 1350(kW)$	[13]
Power consumption of crystallization unit	$\dot{W}_{Crys} = 2040(kW)$	[13]
Power consumption of water distribution unit	$\dot{W}_{Water} = 200(kW)$	[13]
Power consumption of condensation unit	$\dot{W}_{Cond} = 80(kW)$	[13]
Lower heating value of methane	$LHV_{CH_4} = 802661(\frac{kJ}{kmol})$	[13]

In the current study, the following equations are used to determine the specific heat capacity of water and fiber ($C_{P,FB}, C_{P,W}$) [14], sucrose ($C_{P,S}$) [17], and fructose ($C_{P,FR}$) [18]:

$$C_{P,W} = 4.1762 - 9.0864 \times 10^{-5}T + 5.4731 \times 10^{-6}T^2 \qquad (15.7)$$

$$C_{P,FB} = 1.8459 + 1.8306 \times 10^{-3}T - 4.6509 \times 10^{-6}T^2 \qquad (15.8)$$

$$C_{P,S} = 1.161837 + 0.0035587T \qquad (15.9)$$

$$C_{P,FR} = 1.2 + 48.4 \times 10^{-4}T - 3 \times 10^{-5}T^2 + 16.6 \times 10^{-8}T^3 \qquad (15.10)$$

The heat capacity, specific enthalpy, and entropy can be driven from the Eqs. (15.11)–(15.13) [14]:

$$C_{P,tot.} = \sum x_i C_{P,i} \tag{15.11}$$

$$h = C_{P,tot.}(T - T_r) \tag{15.12}$$

$$s = C_{P,tot.} Ln\left(\frac{T + 273.15}{T_r + 273.15}\right) \tag{15.13}$$

In the above equations, $T_r = 0(°C)$ and to calculate the properties of the dead state, T should be replaced by $T_0 = 0(°C)$.

Also, by neglecting changes in the potential and kinetic energies, the physical exergy is obtained from the following relation [19]:

$$e_{ph} = h - h_0 - (T_0 + 273.15)(s - s_0) \tag{15.14}$$

The specific molar chemical exergy of liquid water can be obtained from the following equation [19]:

$$\overline{e}_W^{Ch} = \overline{R}T_0 ln\left(\frac{P_{g@T_0}}{X_v^0 P_0}\right) \tag{15.15}$$

where $P_{g@T_0}$ and P_0 are saturated pressure of water at T_0 and pressure at dead state conditions, respectively. X_v^0 is the reference standard mole fraction of water vapor in the air at dead state conditions. The chemical exergy of water is assumed to be 900 $kJ/kmol$ [19].

The specific molar chemical exergy of a mixture of ideal gases is defined as below [1]:

$$\overline{e}_{Mixture}^{Ch} = \sum_i X_i \overline{e}_i^{Ch} + \overline{R}T_0 \sum_i X_i ln X_i \tag{15.16}$$

In which, X_i and $\overline{e}_i^{Ch}$ define the mole fraction and the standard chemical exergy of a mixture component, respectively. The standard chemical exergy of some substances is given in Ref. [19].

The specific molar chemical exergy of feedstock biomass can be derived from the following equations [20]:

$$\overline{e}_{Biomass}^{Ch} = \beta \overline{LHV}_{Biomass} \tag{15.17}$$

where $\overline{LHV}_{Biomass}$ defines the molar heating value of feedstock biomass and β is calculated for solid fuels as follows:

$$\beta = \frac{1.044 + 0.016\frac{M_H}{M_C} - 0.34493\frac{M_O}{M_C}\left(1 + 0.0531\frac{M_H}{M_C}\right)}{1 - 0.4124\frac{M_O}{M_C}} \tag{15.18}$$

And M_H, M_C and M_O are the weight fractions of hydrogen, carbon, and oxygen in the biomass, respectively.

The chemical exergy of solids and liquids such as juice, sugar, beet, molasses, pulp, water, steam, lime, calcium carbonate, and heavy fuel oil is calculated from the following equation [12].

$$e_{ch} = \sum x_i e^0_{ch,i} \tag{15.19}$$

Also, the total exergy at each stream is obtained from the following relation.

$$\dot{E} = \dot{m}(e_{ph} + e_{ch}) \tag{15.20}$$

It is noteworthy to mention that all of the standard molar chemical exergies are reported in Ref. [9, 19].

In the present work, the mass and concentration balance equations are calculated using Eqs. (15.21) and (15.22) [21].

$$\sum_{in} \dot{m}_k = \sum_{out} \dot{m}_k \tag{15.21}$$

$$\sum_{in} \dot{m}_k x_k = \sum_{out} \dot{m}_k x_k \tag{15.22}$$

Besides, the specific heat capacity of lime and calcium carbonate are calculated from Eqs. (15.23) and (15.24) [16, 22]:

$$C_{P,CaO} = \left(\frac{\overline{R}}{MW}\right)(6.104 + 0.443 \times 10^{-3}T - 1.047 \times 10^5 T^{-2}), \; T(K) \tag{15.23}$$

$$C_{P,CaCO_3} = \left(\frac{\overline{R}}{MW}\right)(12.572 + 2.637 \times 10^{-3}T - 3.12 \times 10^5 T^{-2}), \; T(K) \tag{15.24}$$

The system under study has 5 HRSGs. Their structure is similar, and in the first to fourth steam generators, gas heat is used to produce superheated steam, and in the fifth steam generator, gas heat is used to produce saturated steam. For example, in the first steam generator, as shown in Fig. 15.3, there is an economizer unit for preheating the input water to the steam generator, an evaporator for producing saturated vapor, and a superheater unit for producing high-temperature superheated steam.
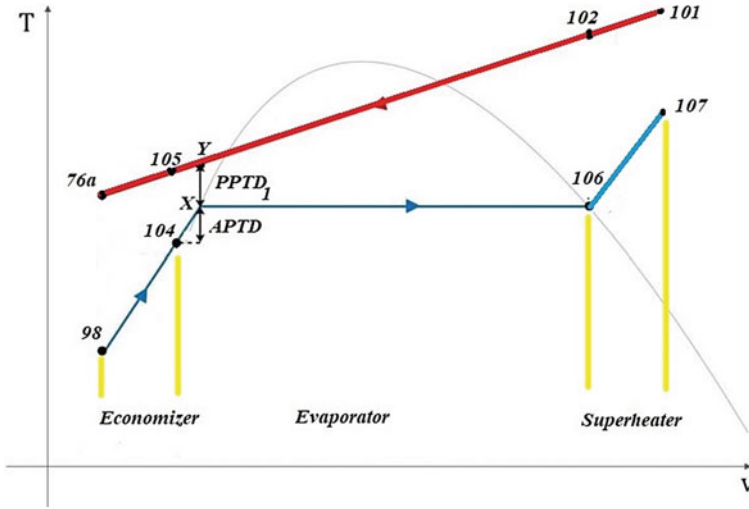
Fig. 15.3 Heat transfer diagram between hot and cold fluids in the HRSG1

The standard chemical exergy of heavy fuel oil is also calculated from the following equations [23].

$$A = \frac{N_C M W_C}{10} \tag{15.25}$$

$$B = \frac{N_H M W_H}{10} \tag{15.26}$$

$$X_C = \frac{100A}{A + B} \tag{15.27}$$

$$X_H = \frac{100B}{A + B} \tag{15.28}$$

$$e^0_{ch,HFO}(\frac{kJ}{kg}) = 363.439X_C + 1075.633X_H + 190.798X_S - 86.308X_O$$
$$+ 4.147X_N - 21.1X_{Ash} \tag{15.29}$$

Given the power consumption of each section and the turbines' generation capacity, the electricity purchased from the grid is calculated from the following equation:

$$\dot{W}_{Grid} = \dot{W}_{Ext} + \dot{W}_{Puri} + \dot{W}_{Heat} + \dot{W}_{Evap} + \dot{W}_{Crys} + \dot{W}_{Water} + \dot{W}_{Cond}$$
$$+ \dot{W}_{Cogen} - \dot{W}_{Turbs} \tag{15.30}$$

15.3.1 Simulation of the Combustion Process

The equivalence ratio is an effective parameter in the combustion process and has an important effect on the composition of exhaust gases. All of the combustion chambers operate with 40% excess air and an equivalence ratio of 0.71, but it should be analyzed in a parametric study to find its effect on system performance. For this reason, a chemical reaction should be considered to change the equivalence ratio from 0 to 2 to find the composition of exhaust gases. As shown in Fig. 15.4, owing
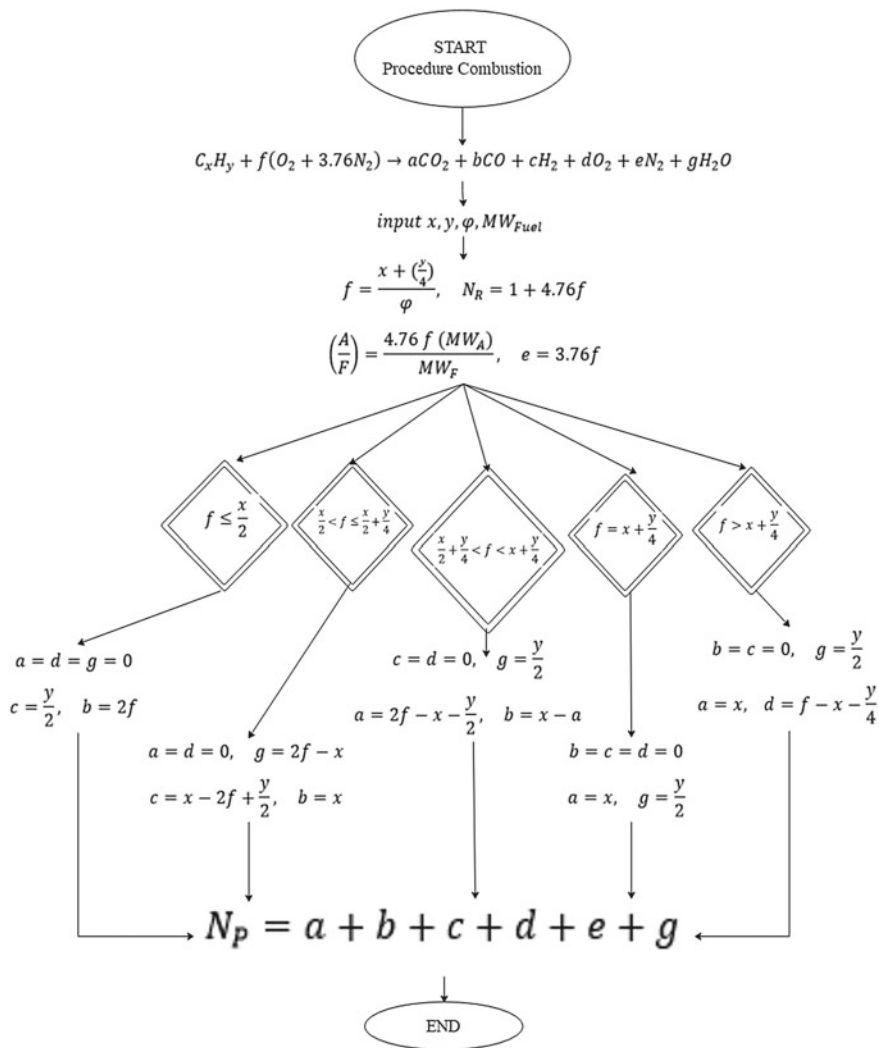
Fig. 15.4 The calculation flowchart of molar constants in combustion processes

to constant values of fuel composition, any changes in the equivalence ratio lead to the variation of parameter f and combustion product composition [24].

After calculation of the molar concentration of combustion products (a, b, c, d, e, g), the mole fraction of each species (y_i), the molecular weight of the mixture (MW_{mix}) and mass fraction of each species (x_i) can be found as follows [24]:

$$y_i = (a, b, c, d, e, g)/N_P \tag{15.31}$$

$$MW_{mix} = \sum y_i MW_i \tag{15.32}$$

$$y_i MW_i = x_i MW_{mix} \tag{15.33}$$

After that, by equalization of reactants' and products' enthalpies, the adiabatic flame temperature is calculated as follows [24]:

$$h_{mix} = \sum x_i (h_{f,i}^0 + \Delta h_i) \tag{15.34}$$

$$h_R = h_P \tag{15.35}$$

In the above equations, $h_{f,i}^0$ is species' enthalpy of formation at ambient temperature and Δh_i is the sensible enthalpy.

15.3.2 Definition Parameters in Exergy Balance

An exergy rate balance for the system or components can be written as [12]:

$$\dot{E}_F = \dot{E}_P + \dot{E}_L + \dot{E}_D \tag{15.36}$$

Here, $\dot{E}_F$ refers to the fuel exergy that represents the resources spent to generate the products. $\dot{E}_P$ indicates the exergy rate of the products, and $\dot{E}_L$ displays the rate of exergy loss associated with heat losses to the environment [12]:

$$\dot{E}_L = \sum_i \dot{Q}_L (1 - \frac{T_0}{T_{C.V}}) \tag{15.37}$$

where $\dot{Q}_L$ is the rate of heat losses across the control surfaces at $T_{C.V}$.

Moreover, $\dot{E}_D$ accounts for the exergy destruction rate due to irreversibilities within the system and can be calculated by the following equation [19]:

$$\dot{E}_D = T_0 \dot{S}_{gen} \tag{15.38}$$

In which, $\dot{S}_{gen}$ is entropy generation within the system.

Furthermore, the exergetic efficiency of a component is defined as the ratio of the product exergy to the fuel one [19]:

$$\varepsilon = \frac{\dot{E}_P}{\dot{E}_F} \tag{15.39}$$

Tables 15.2 and 15.3 provide the exergy of the fuel, the exergy of the product, and exergy loss for each component of the system.

Table 15.2 Relations for exergy of the fuel, the exergy of the product, and exergy loss for each system component

System	$\left(\dot{E}_{Fuel}\right)$	$\left(\dot{E}_{Product}\right)$	$\left(\dot{E}_{Loss}\right)$
Extraction	$\dot{E}_1 + \dot{E}_3 + \dot{E}_8 + \dot{E}_9 + \dot{W}_{Ext}$	$\dot{E}_{11} + \dot{E}_{14} + \dot{E}_7 + \dot{E}_{10}$	$\dot{E}_{13}$
Treatment	$\dot{E}_{10} + \dot{E}_{25} + \dot{E}_{27} + \dot{E}_{28} + \dot{E}_{20} + \dot{E}_{16} + \dot{E}_{21} + \dot{E}_{29} + \dot{W}_{Puri}$	$\dot{E}_{26} + \dot{E}_{19} + \dot{E}_{24} + \dot{E}_{30}$	$\dot{E}_{17} + \dot{E}_{18} + \dot{E}_{22} + \dot{E}_{23}$
Thin Juice heating	$\dot{E}_{30} + \dot{E}_{31} + \dot{E}_{33} + \dot{E}_{35} + \dot{W}_{Heat}$	$\dot{E}_{32} + \dot{E}_{34} + \dot{E}_{36} + \dot{E}_{37} + \dot{E}_{38}$	−
Concentration	$\dot{E}_{46} + \dot{E}_{50} + \dot{E}_{41} + \dot{E}_{42} + \dot{E}_{51} + \dot{E}_{37} + \dot{W}_{Evap}$	$\dot{E}_9 + \dot{E}_{15} + \dot{E}_{68} + \dot{E}_{45} + \dot{E}_{47} + \dot{E}_{48} + \dot{E}_{49} + \dot{E}_{43} + \dot{E}_{44} + \dot{E}_{40} + \dot{E}_{39} + \dot{E}_{31} + \dot{E}_{33} + \dot{E}_{27} + \dot{E}_{28}$	−
Crystallization	$\dot{E}_{44} + \dot{E}_{40} + \dot{E}_{39} + \dot{E}_{82} + \dot{E}_{55} + \dot{E}_{38} + \dot{E}_{53} + \dot{E}_{54} + \dot{E}_{69} + \dot{W}_{Crys}$	$\dot{E}_{56} + \dot{E}_{57} + \dot{E}_{58} + \dot{E}_{59} + \dot{E}_{60} + \dot{E}_{61} + \dot{E}_{62}$	$\dot{E}_{82}$
Condensation	$\dot{E}_{43} + \dot{E}_{60} + \dot{E}_{62} + \dot{E}_{63} + \dot{W}_{Cond}$	$\dot{E}_{64} + \dot{E}_{91}$	−
Water distribution	$\dot{E}_{19} + \dot{E}_{26} + \dot{E}_{52} + \dot{E}_7 + \dot{E}_{32} + \dot{E}_{34} + \dot{E}_{36} + \dot{E}_{58} + \dot{E}_{59} + \dot{E}_{48} + \dot{E}_{49} + \dot{E}_{45} + \dot{E}_{47} + \dot{E}_{68} + \dot{W}_{Water}$	$\dot{E}_{66} + \dot{E}_8 + \dot{E}_{70} + \dot{E}_{25} + \dot{E}_{55} + \dot{E}_{50} + \dot{E}_{51} + \dot{E}_{41} + \dot{E}_{42} + \dot{E}_{29}$	−
Power plant	$\dot{E}_{66} + \dot{E}_{78} + \dot{E}_{72} + \dot{E}_{73} + \dot{E}_{74} + \dot{E}_{75} + \dot{W}_{Cogen}$	$\dot{E}_{35} + \dot{E}_{46} + \dot{E}_{80} + \dot{E}_{81} + \dot{E}_{82} + \dot{E}_{83} + \dot{E}_{84} + \dot{W}_{Turbs}$	$\dot{E}_{76} + \dot{E}_{77} + \dot{E}_{79} + \dot{E}_{85} + \dot{E}_{86} + \dot{E}_{87} + \dot{E}_{88}$
Total factory	$\dot{W}_{Grid} + \dot{E}_1 + \dot{E}_3 + \dot{E}_{16} + \dot{E}_{20} + \dot{E}_{21} + \dot{E}_{53} + \dot{E}_{54} + \dot{E}_{69} + \dot{E}_{72} + \dot{E}_{74} + \dot{E}_{73} + \dot{E}_{75} + \dot{E}_{78}$	$\dot{E}_{11} + \dot{E}_{14} + \dot{E}_{56} + \dot{E}_{57} + \dot{E}_{61} + \dot{E}_{24} + \dot{E}_{70} + \dot{E}_{91} + \dot{E}_{80} + \dot{E}_{81} + \dot{E}_{83} + \dot{E}_{84}$	$\dot{E}_{13} + \dot{E}_{17} + \dot{E}_{18} + \dot{E}_{22} + \dot{E}_{23} + \dot{E}_{82} + \dot{E}_{85} + \dot{E}_{86} + \dot{E}_{87} + \dot{E}_{88} + \dot{E}_{76} + \dot{E}_{77} + \dot{E}_{79}$

Table 15.3 Relations for exergy of the fuel, the exergy of the product, and exergy loss for each component of the cogeneration unit

Pump 1	$\dot{W}_{P1}$	$\dot{E}_{92} - \dot{E}_{66}$	–
Pump 2	$\dot{W}_{P2}$	$\dot{E}_{98} - \dot{E}_{97}$	–
Economizer 1	$\dot{E}_{105}$	$\dot{E}_{104} - \dot{E}_{98}$	$\dot{E}_{76a} + \dot{E}_{86}$
Evaporator 1	$\dot{E}_{102} - \dot{E}_{105}$	$\dot{E}_{106} - \dot{E}_{104}$	–
Superheater 1	$\dot{E}_{101} - \dot{E}_{102}$	$\dot{E}_{107} - \dot{E}_{106}$	–
Combustion chamber 1	$\dot{E}_{99} + \dot{E}_{100}$	$\dot{E}_{101}$	–
Turbine 1	$\dot{E}_{107} - \dot{E}_{108}$	$\dot{W}_{T1}$	–
Pump 3	$\dot{W}_{P3}$	$\dot{E}_{110} - \dot{E}_{109}$	–
Economizer 2	$\dot{E}_{118}$	$\dot{E}_{117} - \dot{E}_{110}$	$\dot{E}_{76b} + \dot{E}_{116}$
Evaporator 2	$\dot{E}_{114} - \dot{E}_{118}$	$\dot{E}_{119} - \dot{E}_{117}$	–
Superheater 2	$\dot{E}_{113} - \dot{E}_{114}$	$\dot{E}_{120} - \dot{E}_{119}$	–
Combustion chamber 2	$\dot{E}_{111} + \dot{E}_{112}$	$\dot{E}_{113}$	–
Turbine 2	$\dot{E}_{144} - \dot{E}_{147}$	$\dot{W}_{T2}$	–
Pump 4	$\dot{W}_{P4}$	$\dot{E}_{122} - \dot{E}_{121}$	–
Economizer 3	$\dot{E}_{129}$	$\dot{E}_{128} - \dot{E}_{122}$	$\dot{E}_{76c} + \dot{E}_{88}$
Evaporator 3	$\dot{E}_{126} - \dot{E}_{129}$	$\dot{E}_{130} - \dot{E}_{128}$	–
Superheater 3	$\dot{E}_{125} - \dot{E}_{126}$	$\dot{E}_{131} - \dot{E}_{130}$	–
Combustion chamber 3	$\dot{E}_{123} + \dot{E}_{124}$	$\dot{E}_{125}$	–
Turbine 3	$\dot{E}_{145} - \dot{E}_{149}$	$\dot{W}_{T3}$	–
Mixer	$\dot{E}_{148} + \dot{E}_{162}$	$\dot{E}_{163}$	–
Desuperheater	$\dot{E}_{163} + \dot{E}_{96}$	$\dot{E}_{35} + \dot{E}_{46} + \dot{E}_{94}$	$\dot{E}_{79}$
Pump 5	$\dot{W}_{P5}$	$\dot{E}_{134} - \dot{E}_{133}$	–
Economizer 4	$\dot{E}_{140}$	$\dot{E}_{139} - \dot{E}_{134}$	$\dot{E}_{138} + \dot{E}_{77}$
Evaporator 4	$\dot{E}_{136} - \dot{E}_{140}$	$\dot{E}_{141} - \dot{E}_{139}$	–
Superheater 4	$\dot{E}_{135} - \dot{E}_{136}$	$\dot{E}_{142} - \dot{E}_{141}$	–
Combustion chamber 4	$\dot{E}_{73} + \dot{E}_{75}$	$\dot{E}_{135}$	–
Expansion of steam 1	$\dot{E}_{146}$	$\dot{E}_{150}$	–
Expansion of steam 2	$\dot{E}_{160}$	$\dot{E}_{161}$	–
Pump 6	$\dot{W}_{P6}$	$\dot{E}_{152} - \dot{E}_{151}$	–
Economizer 5	$\dot{E}_{156}$	$\dot{E}_{158} - \dot{E}_{152}$	$\dot{E}_{76d} + \dot{E}_{87}$
Economizer 5	$\dot{E}_{155} - \dot{E}_{156}$	$\dot{E}_{159} - \dot{E}_{158}$	–
Combustion chamber 5	$\dot{E}_{153} + \dot{E}_{154}$	$\dot{E}_{155}$	–

15.3.3   Exergo-Economic Analysis of the System

The most common exergo-economic analysis method in the literature is the specific exergy cost method. To perform an exergy-economic analysis using the specific exergy costing method, cost balance equations should be written along with appropriate auxiliary equations for each component of the system [25].

In the specific exergy costing method, the general cost balance equation is based on the concept of fuel exergy and product exergy. All exergy additions to a component are considered as the fuel and all exergy removals from it are counted as the product [25].

$$\sum_e \dot{C}_{e,k} + \dot{C}_{w,k} = \dot{C}_{q,k} + \sum_i \dot{C}_{i,k} + \dot{Z}_K \tag{15.40}$$

where $\dot{C}$ is the cost rate ($/h), e and i stand for entering and leaving flow rate of the equipment k. $\dot{C}_{w,k}$ and $\dot{C}_{q,k}$ are the cost rates associated with the work and heat transfer, respectively and $\dot{Z}$ is the entire cost rate, including investment, operation, and maintenance costs [25].

In Eq. (15.40), all cost rates can be expressed as a function of cost per unit exergy or exergy flow [25]:

$$\dot{C}_i\left(\frac{\$}{h}\right) = c_i\left(\frac{\$}{GJ}\right) \times \dot{E}_i(kW) \times \frac{3600}{1000000} \tag{15.41}$$

Also, the term $\dot{Z}_k$ of the Component k can be written as [25]:

$$\dot{Z}_k = \dot{Z}_k^{CI} + \dot{Z}_k^{OM} \tag{15.42}$$

$$\dot{Z}_k\left(\frac{\$}{h}\right) = \frac{PEC_k(\$) \times \varphi \times CRF}{\tau(h)} \tag{15.43}$$

The term $\dot{Z}_k^{CI}$ represents the investment cost rate and the term $\dot{Z}_k^{OM}$ is the operating and maintenance cost. Here, PEC_K is the purchase cost of kth equipment, N is the annual operating hours of the system, and φ is the maintenance factor.

The capital recovery factor is calculated from the following equation [25]:

$$CRF = \frac{k(1+k)^{n_r}}{(1+k)^{n_r} - 1} \tag{15.44}$$

In the above Equation, k is the interest rate and n_r is the useful life of the system. The values in the exergo-economic analysis can be considered as 15% interest rate, 20 years for the system's lifetime, 1.06 for Operating and maintenance factor, and 4000 h for annual operation [26].

The equation for calculating the purchase cost of a component in different references is presented based on the reference year cost fits. The following formula is used to convert the cost of purchasing equipment from the original year to the reference year [25]:

$$PEC_{2018}(\$) = PEC_{Ref}(\$) \times \frac{CEPCI_{2018}}{CEPCI_{Ref}} \qquad (15.45)$$

In the above Equation, subscripts 2018 and Ref are the study's year and the reference year, respectively. Also, the CEPCI is a chemical engineering cost index for the power plant in the reference year. The purchase costs of equipment are presented in Table A.1.

Regarding the purchase cost of steam generators, $\dot{Q}$ is the heat transfer rate of the heat exchangers such as economizer, evaporator, and superheater. The term LMTD is the logarithmic mean temperature difference of the heat exchanger based on Ref. [27].

If a component has n exergy outputs, then there are n unknowns while there is only one cost balance equation. Therefore, it is necessary to have n-1 auxiliary equations. These auxiliary equations are derived based on the concept of fuel and product [28]. In Table 15.4, the cost balance and auxiliary equations for each component of the studied system are presented. It is necessary to mention that the exergo-economic analysis is done only on the power plant, as will be discussed in the next section.

$\dot{Z}_k$ has already been obtained independently from Table A.1. According to Table 15.4, one of the cost rate ($\dot{C}_k$) or unit cost (c_k) parameter for all inputs and outputs in the system is solved simultaneously, with 82 equations and 82 unknowns, and then the other parameter is obtained.

It is worth noting that the cost balance equation for each piece of equipment is not similar to the exergy balance equation as in the cost balance equation, there is no exergy destruction cost rate. This cost rate is a high hidden cost that is applied automatically in the equation. It is calculated using Eq. (15.46). In this equation, it is assumed that the exergy of the products is constant, and the unit cost of the fuel is independent of the exergy degradation [28]:

$$\dot{C}_{Dest,k} = c_{Fuel,k} \times \dot{E}_{Dest,k}, \dot{E}_{Product,k} = const. \qquad (15.46)$$

$$r_k = \frac{c_{Product,k} - c_{Fuel,k}}{c_{Fuel,k}} \qquad (15.47)$$

$$f_k = \frac{\dot{Z}_k}{\dot{Z}_k + \dot{C}_{Dest,k} + \dot{C}_{Loss,k}} \qquad (15.48)$$

In Eq. (15.47), r_k is the relative cost difference, which represents the relative increase in the average unit cost between fuel and product and is a useful parameter in evaluating and optimizing system components. In the exergo-economic analysis of thermodynamic systems, particular attention must be paid to components of the

Table 15.4 Exergy balance and auxiliary equations for the system components

Equipment	Cost balance	Auxiliary equation
Pump 1 Feed water tank	$\dot{C}_{66} + \dot{C}_{W,P1} + \dot{Z}_{P1} = \dot{C}_{92}$ $\dot{C}_{93} = \dot{C}_{78} + \dot{C}_{92}$ $\dot{C}_{95} = \dot{C}_{93} + \dot{C}_{94} + \dot{Z}_{tank}$	$7 \times \dot{C}_{66} = (\dot{C}_{35} + \dot{C}_{46} + \dot{C}_{80} + \dot{C}_{81} + \dot{C}_{82} + \dot{C}_{83} + \dot{C}_{84})$ $c_{w,P1} = c_{w,T1}, c_{78} = 0$
Pump 2	$\dot{C}_{97} + \dot{C}_{W,P2} + \dot{Z}_{P2} = \dot{C}_{98}$	$c_{w,P2} = c_{w,T1}, c_{97} = c_{95}$
Pump 3	$\dot{C}_{109} + \dot{C}_{W,P3} + \dot{Z}_{P3} = \dot{C}_{110}$	$c_{w,P3} = c_{w,T2}, c_{109} = c_{95}$
Pump 4	$\dot{C}_{121} + \dot{C}_{W,P4} + \dot{Z}_{P4} = \dot{C}_{122}$	$c_{w,P4} = c_{w,T2}, c_{121} = c_{95}$
Pump 5	$\dot{C}_{133} + \dot{C}_{W,P5} + \dot{Z}_{P5} = \dot{C}_{134}$	$c_{w,P5} = c_{w,T3}, c_{133} = c_{95}$
Pump 6	$\dot{C}_{151} + \dot{C}_{W,P6} + \dot{Z}_{P6} = \dot{C}_{152}$	$c_{w,P6} = c_{w,T3}, c_{151} = c_{95}$
CC 1	$\dot{C}_{99} + \dot{C}_{100} + \dot{Z}_{CC1} = \dot{C}_{101}$ $c_{72,CH_4} = 3.365\left(\frac{\$}{GJ}\right)$ [29]	$c_{74,Air} = 0$ $c_{99} = c_{72}, c_{100} = c_{74}$
CC 2	$\dot{C}_{111} + \dot{C}_{112} + \dot{Z}_{CC2} = \dot{C}_{113}$	$c_{111} = c_{72}, c_{112} = c_{74}$
CC 3	$\dot{C}_{123} + \dot{C}_{124} + \dot{Z}_{CC3} = \dot{C}_{125}$	$c_{123} = c_{72}, c_{124} = c_{74}$
CC 4	$\dot{C}_{73} + \dot{C}_{75} + \dot{Z}_{CC4} = \dot{C}_{135}$	$c_{75} = c_{74}, c_{73,HFO} = 0.436\left(\frac{\$}{kg}\right)$ [30]
CC 5	$\dot{C}_{153} + \dot{C}_{154} + \dot{Z}_{CC5} = \dot{C}_{155}$	$c_{153} = c_{72}, c_{154} = c_{74}$
HRSG 1	$\dot{C}_{98} + \dot{C}_{101} + \dot{Z}_{HRSG1} = \dot{C}_{107} + \dot{C}_{76a} + \dot{C}_{86}$	$c_{86} = c_{98}, c_{101} = c_{76a}$
Turbine 1	$\dot{C}_{107} + \dot{Z}_{T1} = \dot{C}_{108} + \dot{C}_{W,T1}$	$c_{108} = c_{107}$
HRSG 2	$\dot{C}_{110} + \dot{C}_{113} + \dot{Z}_{HRSG2} = \dot{C}_{120} + \dot{C}_{76b} + \dot{C}_{116}$	$c_{116} = c_{110}, c_{113} = c_{76b}$
HRSG 3	$\dot{C}_{122} + \dot{C}_{125} + \dot{Z}_{HRSG3} = \dot{C}_{131} + \dot{C}_{76c} + \dot{C}_{88}$	$c_{88} = c_{122}, c_{125} = c_{76c}$
HRSG 4	$\dot{C}_{134} + \dot{C}_{135} + \dot{Z}_{HRSG4} = \dot{C}_{142} + \dot{C}_{77} + \dot{C}_{138}$	$c_{138} = c_{134}, c_{135} = c_{77}$ $\dot{C}_{85} = \dot{C}_{116} + \dot{C}_{138}$
HRSG 5	$\dot{C}_{152} + \dot{C}_{155} + \dot{Z}_{HRSG5} = \dot{C}_{159} + \dot{C}_{76d} + \dot{C}_{87}$ $\dot{C}_{143} = \dot{C}_{120} + \dot{C}_{131} + \dot{C}_{142}$ $c_{80} = c_{159}, c_{81} = c_{159}$ $c_{82} = c_{159}, c_{83} = c_{159}$	$c_{87} = c_{157}, c_{155} = c_{76d}$ $c_{144} = c_{143}, c_{145} = c_{143}$ $c_{146} = c_{143}, c_{160} = c_{159}$ $c_{84} = c_{159}$
Turbine 2	$\dot{C}_{144} + \dot{Z}_{T2} = \dot{C}_{147} + \dot{C}_{W,T2}$ $\dot{C}_{148} = \dot{C}_{147} + \dot{C}_{108}$	$c_{147} = c_{144}$
Turbine 3	$\dot{C}_{145} + \dot{Z}_{T3} = \dot{C}_{149} + \dot{C}_{W,T3}$	$c_{149} = c_{145}$
Expansions of steam	$\dot{C}_{146} + \dot{Z}_{exp1} = \dot{C}_{150}$ $\dot{C}_{160} + \dot{Z}_{exp2} = \dot{C}_{161}$	$\dot{C}_{162} = \dot{C}_{161} + \dot{C}_{150} + \dot{C}_{149}$
Mixer	$\dot{C}_{148} + \dot{C}_{162} + \dot{Z}_{Mixer} = \dot{C}_{163}$	
Desuperheater	$\dot{C}_{163} + \dot{C}_{96} + \dot{Z}_{Desup} = \dot{C}_{164}$ $c_{96} = c_{95}$	$c_{94} = c_{164}, c_{35} = c_{164}$ $c_{46} = c_{164}, c_{79} = c_{164}$

(continued)

Table 15.4 (continued)

Equipment	Cost balance	Auxiliary equation
HRSGs	$\dot{C}_{76} = \dot{C}_{76a} + \dot{C}_{76b} + \dot{C}_{76c} + \dot{C}_{76d}$	

system that have a high relative cost difference. Cost resources in one component can be divided into two groups. The first group includes investment costs that have nothing to do with exergy. The second group includes the costs of exergy loss and exergy destruction. The decision of whether the costs of a component is related to its investment costs or low exergy efficiency is determined by f_k, exergo-economic factor.

Finally, the rate of input costs to the power plant is calculated from relation (15.49):

$$\dot{C}_{in,Cogen} = \dot{Z}_{Cogen} + \dot{C}_{Fuel,Cogen} \tag{15.49}$$

Here, $\dot{Z}_{Cogen}$ is the sum of investment and operating and maintenance costs of the power plant and $\dot{C}_{Fuel,Cogen}$ represents the fuel cost rates of the power plant.

15.4 Results and Discussion

Results of energetic and exergetic analysis of the whole system and also, the results of energy, exergy, and exergo-economic study of the combined power and steam generation system are presented in Table A.2. Also, the mass percentages of different materials for flows are reported in Table A.3. It is worth noting that in these tables, the numbers marked with an asterisk (*) are used as input data and factory information in the analysis.

Figure 15.5 shows the percentage of exergy destruction in a different part of the whole plant. As can be seen from Fig. 15.5, the cogeneration system has the highest exergy destruction in about 72% of the total exergy destruction. The main source of irreversibilities in this unit is the presence of 5 combustion chambers and 5 steam generators in the power plant in which the steam generators have a high-temperature difference temperature.

Figure 15.6 presents the thermal losses of different parts of the plant. Thermal losses are obtained from the energy balance of each section and are the cause of the exergy losses. As can be seen from this figure, the condensation section has the highest thermal losses.

The second law efficiencies for different sections of the plant are given in Fig. 15.7. The figure shows that the CHP system with 20.17% exergy efficiency is the most inefficient. This is expected as this section has much higher exergy destruction than the other parts.
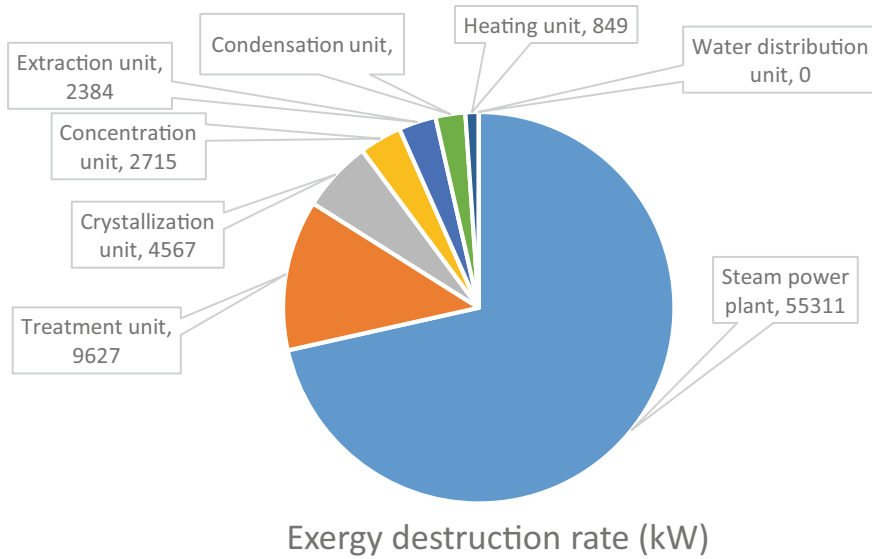
Fig. 15.5 The percentage of exergy destruction in different parts of the whole plant
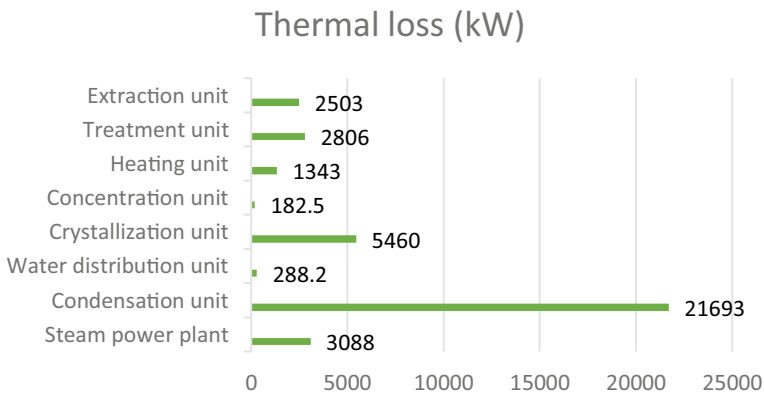
Fig. 15.6 Thermal losses of different parts of the plant

Table 15.5 gives the results of the exergy analysis for the system. From these tables can be seen that the highest exergy destruction happens in the second and third combustion chambers. This can be explained by the increased fuel mass flow rate of these combustion chambers. Also, pumps have the lowest amounts of exergy destruction $(Y^*_{Dest,k})$ since they consume less power and have no heat loss.

Important parameters of thermo-economic analysis are presented in Table 15.6. From this table, the HRSG 4 has the highest value of $(\dot{Z} + \dot{C}_{Dest} + \dot{C}_{Loss})_k$; therefore, economically, it is of significant importance. The low value of the exergo-economic
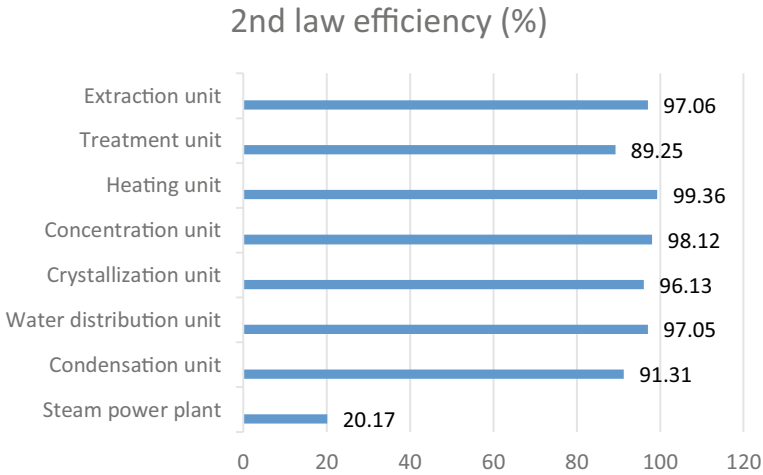
2nd law efficiency (%)

Fig. 15.7 Second law efficiencies for different sections of the plant

factor, f_k HRSG 4 suggests that the cost of exergy destruction is higher than the investment cost. Also, higher values of exergo-economic factor and relative cost difference in pumps 1 and 6 indicate that these equipment are more important in terms of investment costs than the cost of exergy destruction.

15.4.1 Parametric Study

In this section, the effects of variation in different parameters on the cogeneration plant performance are presented.

15.4.1.1 Equivalence Ratio

The equivalence ratio is one of the important parameters that will affect the combustion product compositions and adiabatic flame temperature and consequently the system performance. Figure 15.8 indicates the effect of this parameter on the adiabatic flame temperature of the methane and heavy fuel oil is investigated. It can be seen that complete combustion takes place at the stoichiometric equivalence ratio, and the highest adiabatic flame temperature is achieved. Also, this figure reveals that the adiabatic flame temperature of the heavy fuel oil combustion is greater than that of methane. The reason is that in stoichiometric combustion, the mass fraction of carbon dioxide is higher in the combustion of heavy fuel oil and air, and the mass fraction of the diluents is lower than that of methane and air combustion. Thus the heat of combustion is higher, which results in greater flame temperature.

Table 15.5 Results of exergy analysis for the cogeneration unit

Systems	$\dot{E}_{Fuel,k}$ (kW)	$\dot{E}_{Prod,k}$ (kW)	$\dot{E}_{Loss,k}$ (kW)	$\dot{E}_{Dest,k}$ (kW)	$\eta_{II,k}$ (%)
Comb. chamber 1	27288	21290	–	5998	78.02
Comb. chamber 2	29533	23042	–	6492	78.02
Comb. chamber 3	29533	23042	–	6492	78.02
Comb. chamber 4	14971	11170	–	3801	74.61
Comb. chamber 5	5872	4581	–	1291	78.02
Desuperheater	26388	16980	8918	489.7	64.35
Economizer 1	7159	1084	5260	815	15.15
Economizer 2	7703	1171	5502	1030	15.2
Economizer 3	10961	854.7	9150	956.1	7.798
Economizer 4	4344	480.9	3349	567	11.07
Economizer 5	1156	58.26	1039	58.87	5.04
Evaporater 1	11481	7021	–	4460	61.15
Evaporater 2	12363	7575	–	4789	61.27
Evaporater 3	9332	5536	–	3796	59.32
Evaporater 4	5263	3119	–	2144	59.27
Evaporater 5	3426	1758	–	1667	51.32
Steam expansion 1	12907	10556	–	2351	81.78
Steam expansion 2	1005	903.4	–	101.1	89.93
Mixer	26096	25932	–	163.8	99.37
Pump 1	3.074	2.654	–	0.4207	86.32
Pump 2	37.16	31.78	–	5.374	85.54
Pump 3	29.03	24.83	–	4.2	85.53
Pump 4	21.25	18.18	–	3.074	85.53
Pump 5	11.99	10.26	–	1.735	85.53
Pump 6	1.7	1.454	–	0.246	85.53
Superheater 1	2650	1688	–	961.8	63.7
Superheater 2	2975	1621	–	1354	54.48
Superheater 3	2749	1597	–	1152	58.09
Superheater 4	1563	900	–	662.7	57.59
Turbine 1	3905	2099	–	1806	53.75
Turbine 2	1357	1103	–	254.2	81.27
Turbine 3	2796	2272	–	523.7	81.27
Feed water tank	4002	3734	–	268.4	93.29

Table 15.6 Important parameters of thermo-economic analysis

Systems	$\dot{C}_{Dest,k}$ ($\frac{\$}{h}$)	$\dot{C}_{Fuel,k}$ ($\frac{\$}{h}$)	$\dot{Z}_k$ ($\frac{\$}{h}$)	$\dot{C}_{Prod,k}$ ($\frac{\$}{h}$)	$\dot{C}_{Loss,k}$ ($\frac{\$}{h}$)	$c_{F,k}$ ($\frac{\$}{GJ}$)	$c_{P,k}$ ($\frac{\$}{GJ}$)	r_k (%)	f_k (%)
Combustor 1	19481	319	85.17	404.2	0	3.25	5.27	62.39	0.44
Combustor 2	21084	345.3	89.8	435.1	0	3.25	5.25	61.51	0.42
Combustor 3	21084	345.3	89.8	435.1	0	3.25	5.25	61.51	0.42
Combustor 4	37527	532.1	55.53	587.6	0	9.87	14.61	48.02	0.15
Combustor 5	4192	68.66	30.43	99.08	0	3.25	6.01	84.98	0.72
Desuperheater	6810	1321	0	866.1	454.9	13.91	14.17	1.89	0
Expansion 1	31289	618.3	0.02	618.4	0	13.31	16.27	22.28	0
Expansion 2	1387	49.61	0.02	49.63	0	13.72	15.26	11.24	0.001
HRSG 1	32893	404.2	32.55	334.4	102.4	5.27	9.48	79.83	0.1
HRSG 2	37625	435.1	33.4	361.9	106.6	5.25	9.7	84.89	0.09
HRSG 3	30970	435.1	16.21	276.3	175	5.25	9.61	83.29	0.05
HRSG 4	48524	587.6	17.57	428.6	176.6	14.61	26.45	81.01	0.04
HRSG 5	10371	99.08	8.52	84.69	22.91	6.01	12.95	115.6	0.08
Mixer	2262	1298	0	1298	0	13.82	13.9	0.63	0
Pump 1	9.897	0.2604	4.63	4.89	0	23.53	511.5	2074	31.86
Pump 2	126.4	3.15	6.52	9.67	0	23.53	84.5	259.2	4.9
Pump 3	90	2.24	6.52	8.76	0	21.43	97.99	357.3	6.75
Pump 4	65.88	1.64	6.52	8.16	0	21.43	124.7	481.7	9
Pump 5	36.57	0.91	6.52	7.43	0	21.08	201.1	853.9	15.12
Pump 6	5.186	0.13	4.63	4.76	0	21.08	908.7	4211	47.15
Turbine 1	18236	142	35.82	177.8	0	10.1	23.53	1.33	0.2
Turbine 2	3383	65.01	20.07	85.09	0	13.31	21.43	61.04	0.59
Turbine 3	6969	133.9	38.47	172.4	0	13.31	21.08	58.39	0.55
Water tank	3526	189.3	0	189.3	0	13.14	14.08	7.19	0

Fig. 15.8 Effect of equivalence ratio on the adiabatic flame temperature of the methane and heavy fuel oil
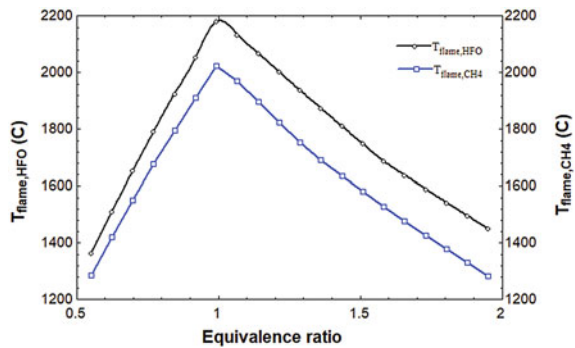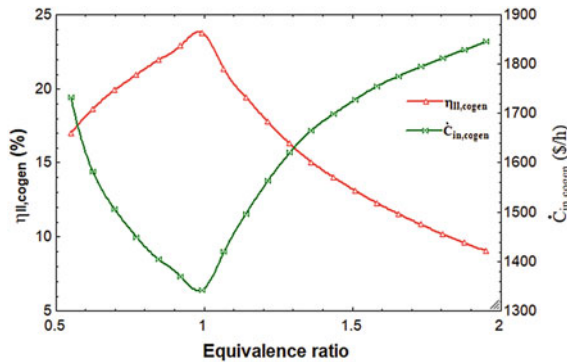
Fig. 15.9 Effect of variation in equivalence ratio on the second law efficiency and total cost rate of the cogeneration system

Figure 15.9 shows the effect of variation in equivalence ratio on the second law efficiency and total cost rate of the system. Because of the abovementioned reasons, the second law efficiency of the power plant behaves similarly to the adiabatic flame temperature curve, and the input cost rate of the power plant shows the inverse behavior. So, it can be concluded that the stoichiometric mode in Fig. 15.9 is the best choice because the exergy efficiency is maximum and the cost rate is minimum.

15.4.1.2 Pinch Point Temperature Difference of the HRSGs

Due to the similar behavior of HRSGs, only the pinch point temperature difference (PPTD) of the third steam generator is investigated. The influence of the PPTD on the second law efficiency and the total cost rate of the system is illustrated in Fig. 15.10. According to Fig. 15.10, the second law efficiency decreases, and the
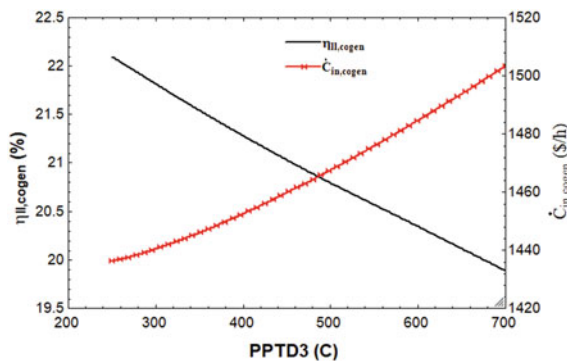
Fig. 15.10 Influence of the pinch point temperature difference on the second law efficiency and the total cost of the system
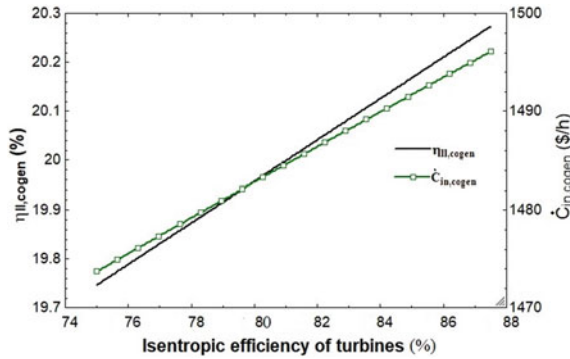
Fig. 15.11 Effect of isentropic efficiency of the turbine on the second law efficiency and the total cost rate of the system

cost rate increases as PPTD increases. By increasing the PPTD, the mass flow rate of the pumps and turbines declines, and consequently, the net power of the plant is reduced. Also, an increase in the PPTD increases the temperature of the exhaust gases from the evaporator, which results in a higher exergy loss. Therefore, exergy efficiency will decrease with increasing PPTD. A higher PPTD leads to a reduction in the investment cost of HRSGs. It should be mentioned that, in the design of heat exchangers, the heat transfer area will be decreased as PPTD increases, which slightly reduces the investment cost rate for the heat exchangers. However, the cost rate of exergy destruction also increases substantially. Reduction in the investment cost rate does not make up for the increase in the cost rate of exergy destruction. Thereby, the total cost of the system will be increased.

15.4.1.3 Isentropic Efficiency of Turbine

Figure 15.11 shows the effect of the isentropic efficiency of the turbine on the second law efficiency and the total cost rate of the system. As expected in Fig. 15.11, as the isentropic efficiency of the turbine increases, the net power of the system enhances, which results in an improvement in the second law efficiency. Also, the turbine purchase and maintenance costs are increased by increasing the isentropic efficiency of the turbine which leads to an increase in the total cost rate of the system.

15.5 Conclusions

In the present work, an exergy-economic investigation was carried out to study a sugar beet plant. The beet feed rate of the Urmia sugar factory is 150 $\frac{ton}{h}$ beet. Meanwhile, this factory consumes 2000 kWh grid power, 2.9 $\frac{ton}{h}$ lime, 8.85 $\frac{ton}{h}$ carbon dioxide

gas, 6.4 $\frac{ton}{h}$ methane gas, 1.22 $\frac{ton}{h}$ heavy fuel oil. Also, it produces 20.74 $\frac{ton}{h}$ of sugar, 15.26 $\frac{ton}{h}$ of dry and wet pulp and 5.55 $\frac{ton}{h}$ of molasses. The system, by developing a thermodynamic model, is analyzed from the thermodynamic viewpoint. The main section of the plant with the most exergy destruction is recognized. Then, an exergo-economic analysis and a parametric study have been performed to identify the parameters affecting the target functions, the second law efficiency, and the total cost rate of the power plant. The main results are as follows:

The cogeneration system, purification, and crystallization units have the highest exergy loss, respectively. Also, the cogeneration system with 20.17% and the condensation unit with 91.31% have the lowest and highest exergy efficiency, respectively. Also, the exergy efficiency of the whole plant is 56.44%.

In the cogeneration system, the third and fifth economizers have the lowest second law efficiency and the combustion chambers 2 and 3 have the highest exergy losses.

To maximize the exergy efficiency and minimize the total cost rate of the cogeneration unit, the combustion processes should be done at stoichiometric conditions.

To maximize the exergy efficiency of the cogeneration unit, it is better to decline the pinch point temperature differences and enhance the turbines' isentropic efficiency.

Appendix

See Tables A.1, A.2 and A.3.

Table A.1 Considered relations for calculation of the PEC (purchase of equipment cost)

Component	CEPCI [25]	Reference year	PEC	References
Pump 1, 6	357.6	1990	$PEC_{Pump} = -2.9(\dot{W}_P)^2 + 3228(\dot{W}_P) + 61233$ $\dot{W}_P[MW]$, $for \dot{W}_P < 0.3(MW) \& P_{out} \sim 5(bar)$	[27]
Pump 2, 3, 4, 5	357.6	1990	$PEC_{Pump} = -4.05(\dot{W}_P)^2 + 3277(\dot{W}_P) + 86205$ $\dot{W}_P[MW]$, $for \dot{W}_P < 0.3(MW) \& P_{out} \sim 25(bar)$	[27]
Combustion chamber	521.9	2009	$PEC_{CC} = (\frac{\dot{m}_{gases}}{628.5})^{0.67} \times 21.9 \times 10^6$	[27]
Steam turbine	521.9	2009	$PEC_{Turb} = (\frac{\dot{W}_T}{120})^{0.9} \times 26.4 \times 10^6, \dot{W}_T in[MW]$	[27]
HRSG	381.1	1995	$PEC_{HRSG} =$ $6570\left[\left(\frac{\dot{Q}_{eco}}{LMTD_{eco}}\right)^{0.8} + \left(\frac{\dot{Q}_{eva}}{LMTD_{eva}}\right)^{0.8} + \left(\frac{\dot{Q}_{sup}}{LMTD_{sup}}\right)^{0.8}\right] + 21276\dot{m}_{st} + 1184.4\dot{m}_{gases}^{1.2}$	[27]
Expansion of steam	394.1	2000	$PEC_{exp} = 300$	[25]
Mixer		–	$PEC_{Mixer} = 0$	[25]
Feedwater tank		–	$PEC_{Tank} = 0$	[25]
Desuperheater		–	$PEC_{Desup} = 0$	[25]

Table A.2 Thermodynamics and thermo-economic results (* refers to input data)

State	Working fluid	$\dot{m}$ $(\frac{kg}{s})$	P (kPa)	T $(°C)$	h $(\frac{kJ}{kg})$	s $(\frac{kJ}{kg.K})$	$\dot{E}$ (kW)	c $(\frac{\$}{GJ})$	$\dot{C}$ $(\frac{\$}{h})$
1	Sugar beet	41.49*	–	25*	88.51	0.31	166,967	–	–
3	Molasses	0.02*	–	70	115	0.37	348.4	–	–
7	Saturated water	2.49	–	105.8	443.6	1.37	296.3	–	–
8	Saturated water	17.05*	–	115.2*	483.4	1.47	2220	–	–
9	Saturated steam	2.49*	–	105.8*	2685	7.28	1859	–	–
10	Raw juice	50.28	–	30*	112.5	0.39	132,188	–	–
11	Wet pulp	2.57*	–	30*	107.9	0.37	11,025	–	–
13	Saturated steam	4.05*	–	90*	2660	7.47	2700	–	–
14	Dry pulp	1.67*	–	30*	64.41	0.22	24,601	–	–
15	Saturated steam	5.68*	–	126.1*	2715	7.06	4748	–	–
16	$CaO(s)$	0.80*	100*	70*	55.7	0.18	1593	–	–
17	$CO_2(g)$	2.90*	100*	83.9*	−8889	0.22	1339	–	–
18	$CO_2(g)$	0.11	100*	91*	−8883	0.24	54.56	–	–
19	Saturated water	1.27	–	115.2	483.4	1.47	165.6	–	–
20	Raw juice	0.91*	–	60*	177	0.58	7096	–	–
21	CO_2	2.46*	100*	40*	−8928	0.11	1117	–	–
22	Mud	1.57*	–	89.5*	194	0.61	2810	–	–
23	Mud	1.44*	–	89.7*	242.6	0.76	2077	–	–
24	Comp. liq. water	13.75	200*	88*	368.6	1.16	1363	–	–
25	Comp. liq. water	13.75*	300*	105.8*	443.7	1.37	1634	–	–
26	Saturated water	2.17	–	105.8*	443.6	1.37	258.5	–	–
27	Saturated steam	2.17*	–	105.8*	2685	7.28	1621	–	–
28	Saturated steam	1.27*	–	115.2*	2699	7.18	1002	–	–
29	Comp. liq. water	2.13*	600*	105.8*	443.9	1.37	253.9	–	–
30	Treated juice	50.55	–	95.4*	365.6	1.14	130,311	–	–

(continued)

Table A.2 (continued)

State	Working fluid	$\dot{m}$ ($\frac{kg}{s}$)	P (kPa)	T (°C)	h ($\frac{kJ}{kg}$)	s ($\frac{kJ}{kg.K}$)	$\dot{E}$ (kW)	c ($\frac{\$}{GJ}$)	$\dot{C}$ ($\frac{\$}{h}$)
31	Saturated steam	1.56*	–	115.2*	2699	7.18	1228	–	–
32	Saturated water	1.56	–	115.2	483.4	1.47	203.1	–	–
33	Saturated steam	0.87*	–	126.1*	2715	7.06	732.8	–	–
34	Saturated water	0.87	–	126.1	529.8	1.59	126.8	–	–
35	Saturated steam	0.53*	370*	140.9	2644	6.70	465.1	14.17	23.72
36	Saturated water	0.53	–	140.9	592.9	1.74	89.05	–	–
37	Heated juice	48.61	–	124*	480.3	1.45	126,878	–	–
38	Heated juice	1.94*	–	90*	344.2	1.08	4991	–	–
39	Saturated steam	2.41*	–	115.2*	2699	7.18	1901	–	–
40	Saturated steam	0.73*	–	105.8*	2685	7.28	544.2	–	–
41	Saturated steam	0.29*	–	105.8*	2685	7.28	221.1	–	–
42	Saturated steam	0.13*	–	85.9*	2653	7.53	89.72	–	–
43	Saturated steam	2.20*	–	85.9*	2653	7.53	1422	–	–
44	Concentrated juice	10.85	–	80*	196	0.62	121,156	–	–
45	Saturated water	1.7*	–	105.8*	443.6	1.37	201.7	–	–
46	Saturated steam	17.73	370*	140.9	2644	6.70	15,297	14.17	780.3
47	Saturated water	17.73	–	140.9	592.9	1.74	2929	–	–
48	Saturated water	11.11*	–	126.1*	529.8	1.59	1604	–	–
49	Saturated water	0.25*	–	115.2*	483.4	1.47	33.58	–	–
50	Saturated steam	0.36*	–	115.2*	2699	7.18	286.6	–	–
51	Saturated steam	0.51*	–	126.1*	2715	7.06	431.5	–	–

(continued)

Table A.2 (continued)

State	Working fluid	$\dot{m}$ $(\frac{kg}{s})$	P (kPa)	T $(°C)$	h $(\frac{kJ}{kg})$	s $(\frac{kJ}{kg.K})$	$\dot{E}$ (kW)	c $(\frac{\$}{GJ})$	$\dot{C}$ $(\frac{\$}{h})$
52	Saturated water	5.68	–	126.1	529.8	1.59	821.6	–	–
53	Saturated steam	4.80*	–	115.2*	2699	7.18	3784	–	–
54	Saturated steam	0.11*	–	115.2*	2699	7.18	87.41	–	–
55	Saturated water	4.02*	–	105.8*	443.6	1.37	478	–	–
56	White sugar	5.76*	–	50*	66.99	0.22	101,145	–	–
57	Molasses	1.54	–	70*	115	0.37	24,427	–	–
58	Comp. liq. water	7.33	300*	115.2*	483.5	1.47	955.2	–	–
59	Comp. liq. water	0.74	300*	105.8*	443.7	1.37	88.89	–	–
60	Saturated steam	5.17*	–	65*	2617	7.83	2734	–	–
61	Comp. liq. water	2.85*	270*	90*	377.1	1.19	288.5	–	–
62	Saturated steam	1.49*	–	65*	2617	7.83	788.8	–	–
63	Comp. liq. water	303.7*	100*	28*	117.4	0.40	16,880	–	–
64	Comp. liq. water	303.7	100*	45.08	188.8	0.63	19,435	–	–
66	Saturated water	17.75*	–	126.1*	529.8	1.59	2563	13.25	122.3
68	Saturated water	6.58	–	115.2*	483.4	1.47	857.3	–	–
69	Saturated steam	0.01*	–	105.8*	2685	7.28	12.65	–	–
70	Comp. liq. water	4.04*	270*	85.9*	359.9	1.14	392.4	–	–
72	CH_4	1.77*	100*	0*	−4705	11.4	92,227	3.365*	1078
73	HFO $(C_{11.6}H_{17}(L))$	0.33*	430*	81*	103.5*	0.31*	14,971	9.873*	532.1
74	Air	42.82	100*	0*	0	0.16	0	0	0
75	Air	6.63	100*	0*	0	0.16	0	0	0
76	Comb. gases	44.6	100*	457	−1699	1.35	20,465	5.36	395.3
77	Comb. gases	6.96	100*	596.1	−1430	1.49	3318	14.61	174.5

(continued)

Table A.2 (continued)

State	Working fluid	$\dot{m}$ $(\frac{kg}{s})$	P (kPa)	T $(°C)$	h $(\frac{kJ}{kg})$	s $(\frac{kJ}{kg.K})$	$\dot{E}$ (kW)	c $(\frac{\$}{GJ})$	$\dot{C}$ $(\frac{\$}{h})$
78	Comp. liq. water	12.74*	370*	15*	63.27	0.22	661.2	0	0
79	Saturated steam	10.33*	370*	140.9	2644	6.70	8918	14.17	454.9
80	Saturated steam	0.03*	–	180	2778	6.58	31.44	13.72	1.55
81	Saturated steam	0.15*	–	180	2778	6.58	154.3	13.72	7.62
82	Saturated steam	0.66*	–	180	2778	6.58	688.8	13.72	34.01
83	Saturated steam	0.09*	–	180	2778	6.58	100	13.72	4.94
84	Saturated steam	0.08*	–	180	2778	6.58	80.02	13.72	3.95
85	Comp. liq. water	0.37	3000*	200	853	2.32	99.31	16.93	6.05
86	Comp. liq. water	0.23*	4000*	200*	853.4	2.32	63.19	16.44	3.74
87	Comp. liq. water	0.06*	1000*	130*	546.9	1.63	9.194	19.44	0.64
88	Comp. liq. water	0.19*	3000*	200*	853	2.32	52.62	16.79	3.18
91	Saturated water	8.86	–	45.08	188.7	0.63	566.6	–	–
92	Comp. liq. water	17.75	370*	126.1	529.9	1.59	2566	13.77	127.2
93	Comp. liq. water	30.49	370*	79.93	334.9	1.07	2784	12.69	127.2
94	Saturated steam	1.41*	370*	140.9	2644	6.70	1218	14.17	62.12
95	Comp. liq. water	31.9	370*	104.2	437	1.35	3734	14.08	189.3
96	Comp. liq. water	3.89	370*	104.2	437	1.35	456.2	14.08	23.13
97	Comp. liq. water	7.83	370*	104.2	437	1.35	916.5	14.08	46.47
98	Comp. liq. water	7.83	4000*	104.7	441.8	1.35	948.3	16.44	56.14
99	CH_4	0.52*	100*	0*	−4705	11.4	27,288	3.365	319
100	Air	12.67	100*	0*	0	0.16	0	0	0

(continued)

Table A.2 (continued)

State	Working fluid	$\dot{m}$ $(\frac{kg}{s})$	P (kPa)	T $(°C)$	h $(\frac{kJ}{kg})$	s $(\frac{kJ}{kg.K})$	$\dot{E}$ (kW)	c $(\frac{\$}{GJ})$	$\dot{C}$ $(\frac{\$}{h})$
101	Comb. gases	13.2	100*	1580	−212.6	2.57	21,290	5.27	404.2
102	Comb. gases	13.2	100*	1411	−450.1	2.43	18,640	–	–
103	Comp. liq. water	7.83	4000*	200	853.4	2.32	2096	–	–
104	Comp. liq. water	7.59	4000*	200	853.4	2.32	2033	–	–
105	Comb. gases	13.2	100*	563.3	−1571	1.52	7159	–	–
106	Saturated steam	7.59	4000*	250	2801	6.07	9053	–	–
107	Sup. steam	7.59	4000*	400*	3213	6.76	10,741	10.1	390.5
108	Sup. steam	7.59	370*	148.9	2753	6.96	6836	10.1	248.5
109	Comp. liq. water	8.44	370*	104.2	437	1.35	988	14.08	50.1
110	Comp. liq. water	8.44	3000*	104.6	440.5	1.35	1013	16.14	58.86
111	CH_4	0.56*	100*	0*	−4705	11.4	29,533	3.365	345.3
112	Air	13.71	100*	0*	0	0.16	0	0	0
113	Comb. gases	14.28	100*	1580	−212.6	2.57	23,042	5.25	435.1
114	Comb. gases	14.28	100*	1405	−459.1	2.43	20,067	–	–
115	Comp. liq. water	8.44	3000	200	853	2.32	2252	–	–
116	Comp. liq. water	0.25*	3000*	200*	853	2.32	68.18	16.14	3.96
117	Comp. liq. water	8.18	3000*	200*	853	2.32	2184	–	–
118	Comb. gases	14.28	100*	559.5	−1576	1.51	7703	–	–
119	Saturated steam	8.18	3000*	250	2801	6.07	9759	–	–
120	Sup. steam	8.18	3000*	400*	3231	6.92	11,380	10.27	420.8
121	Comp. liq. water	6.18	370*	104.2	437	1.35	723.3	14.08	36.67
122	Comp. liq. water	6.18	3000*	104.6	440.5	1.35	741.5	16.79	44.83
123	CH_4	0.56	100*	0*	−4705	11.4	29,533	3.365	345.3
124	Air	13.71	100*	0*	0	0.16	0	0	0
125	Comb. gases	14.28	100*	1580	−212.6	2.6	23,042	5.25	435.1
126	Comb. gases	14.28	100*	1418	−440.2	2.44	20,292	–	–

(continued)

Table A.2 (continued)

State	Working fluid	$\dot{m}$ ($\frac{kg}{s}$)	P (kPa)	T (°C)	h ($\frac{kJ}{kg}$)	s ($\frac{kJ}{kg.K}$)	$\dot{E}$ (kW)	c ($\frac{\$}{GJ}$)	$\dot{C}$ ($\frac{\$}{h}$)
127	Comp. liq. water	6.18	3000*	200	853	2.32	1649	–	–
128	Comp. liq. water	5.983	3000*	200	853	2.32	1596	–	–
129	Comb. gases	14.28	100*	813.5	−1256	1.84	10,961	–	–
130	Saturated steam	5.98	3000*	250	2801	6.07	7132	–	–
131	Sup. steam	5.98	3000*	450*	3344	7.08	8729	10.22	321.2
133	Comp. liq. water	3.48	370*	104.2	437	1.35	408.2	14.08	20.7
134	Comp. liq. water	3.48	3000*	104.6	440.5	1.35	418.5	18.67	28.12
135	Comb. gases	6.96	100*	1685	−18.92	2.54	11,170	14.61	587.6
136	Comb. gases	6.96	100*	1492	−281.8	2.39	9607	–	–
137	Comp. liq. water	3.48	3000*	200	853	2.32	930.5	–	–
138	Comp. liq. water	0.11*	3000*	200*	853	2.32	31.13	18.67	2.09
139	Comp. liq. water	3.37	3000*	200	853	2.32	899.4	–	–
140	Comb. gases	6.96	100*	766.3	−1224	1.71	4344	–	–
141	Saturated steam	3.37	3000*	250	2801	6.07	4019	–	–
142	Sup. steam	3.37	3000*	450*	3344	7.08	4919	25.79	456.7
143	Sup. steam	17.54	3000*	426.6	3291	7.01	25,021	13.31	1199
144	Sup. steam	2.77*	3000*	426.6	3291	7.01	3959	13.31	189.6
145	Sup. steam	5.71*	3000*	426.6	3291	7.01	8155	13.31	390.7
146	Sup. steam	9.04	3000*	426.6	3291	7.01	12,907	13.31	618.3
147	Sup. steam	2.77	370*	194.2	2850	7.18	2601	13.31	124.6
148	Sup. steam	10.37	370*	160.8	2779	7.02	9432	10.99	373.2
149	Sup. steam	5.71	370*	194.2	2850	7.18	5359	13.31	256.7
150	Sup. steam	9.04	370*	408.3	3291	7.96	10,556	16.27	618.4
151	Comp. liq. water	2.06	370*	104.2	437	1.35	241.4	14.08	12.24
152	Comp. liq. water	2.06	1000*	104.3	437.9	1.35	242.8	19.44	16.99
153	CH_4	0.11*	100*	0*	−4705	11.4	5872	3.365	68.66
154	Air	2.72	100*	0*	0	0.16	0	0	0

(continued)

Table A.2   (continued)

State	Working fluid	$\dot{m}$ $(\frac{kg}{s})$	P (kPa)	T $(°C)$	h $(\frac{kJ}{kg})$	s $(\frac{kJ}{kg.K})$	$\dot{E}$ (kW)	c $(\frac{\$}{GJ})$	$\dot{C}$ $(\frac{\$}{h})$
155	Comb. gases	2.84	100*	1580	−212.6	2.6	4581	6.01	99.08
156	Comb. gases	2.84	100*	384.8	−1785	1.23	1156	–	–
157	Comp. liq. water	2.06	1000*	130	546.9	1.63	310.3	–	–
158	Comp. liq. water	2	1000*	130	546.9	1.63	301.1	–	–
159	Saturated steam	2	–	180	2778	6.58	2059	13.72	101.7
160	Saturated steam	0.97	–	180	2778	6.58	1005	13.72	49.61
161	Sup. steam	0.97	370*	180	2820	7.11	903.4	15.26	49.63
162	Sup. steam	15.74	370*	316.8	3102	7.66	16,664	15.41	924.7
163	Sup. steam	26.11	370*	254.2	2973	7.43	25,932	13.9	1298
164	Saturated steam	30.01	370*	140.9	2644	6.70	25,898	14.17	1321
76a	Comb. gases	13.2	100*	365.4	−1808	1.19	5197	5.274	98.67
76b	Comb. gases	14.28	100*	345	−1831	1.15	5434	5.245	102.6
76c	Comb. gases	14.28	100*	673.2	−1835	1.67	9097	5.245	171.8
76d	Comb. gases	2.84	100*	316.8	−1864	1.11	1030	6.01	22.27

Table A.3   Mass percentages of different materials for composite flows (* refers to input data)

State	x_{CO_2}	x_{H_2O}	x_{O_2}	x_{N_2}	x_{CaCO_3}	x_{Fr}	x_S	x_W	x_{Ds}	q	x_{Fb}
1	–	–	–	–	–	1.07	16.35	77	23*	71.1*	5.58*
3	–	–	–	–	–	14.61	77.24	8.15	91.85	84.09	0
10	–	–	–	–	–	1.26	13.17	85.13	14.87	88.6	0.44*
11	–	–	–	–	–	0.27	1.81	75	25*	7.23*	22.92*
14	–	–	–	–	–	0.93	7.98	13.4	86.6*	9.22*	77.69*
20	–	–	–	–	–	3.22	39.74	55.6	44.4*	89.5*	1.44*
22	–	–	–	–	55.3*	1.43	0.9	35	65*	1.38*	7.4*
23	–	–	–	–	40.3*	0.98	1.31	52	48*	2.73*	5.4*
30	–	–	–	–	–	0.45	13.75	85.8	14.2*	96.86	0*
37	–	–	–	–	–	0.45	13.75	85.8	14.2	96.86	0
38	–	–	–	–	–	0.45	13.75	85.8	14.2	96.86	0
44	–	–	–	–	–	2	61.62	36.38	63.62	96.86	0*
56	–	–	–	–	–	0	100	0	100*	100*	0*
57	–	–	–	–	–	14.61	77.24	8.15	91.85	84.09	0*

(continued)

Table A.3 (continued)

State	x_{CO_2}	x_{H_2O}	x_{O_2}	x_{N_2}	x_{CaCO_3}	x_{Fr}	x_S	x_W	x_{Ds}	q	x_{Fb}
74	–	–	21.59	78.41	–	–	–	–	–	–	–
75	–	–	22.99	77.01	–	–	–	–	–	–	–
76	10.99	8.99	6.39	73.63	–	–	–	–	–	–	–
77	15.93	4.78	6.33	72.95	–	–	–	–	–	–	–

References

1. H. Ghiasirad, R. Khoshbakhti Saray, B. Abdi, and K. Bahlouli, "Energy, exergy, and exergo-economic analyses of Urmia sugar factory: a case study of Iran," in *The 11th International Chemical Engineering Congress & Exhibition (IChEC)*, 2020, p. 6.
2. T. Tekin, M. Bayramoğlu, Exergy analysis of the sugar production process from sugar beets. Int. J. Energy Res. **22**(7), 591–601 (1998). https://doi.org/10.1002/(SICI)1099-114X(199806 10)22:7%3c591::AID-ER360%3e3.0.CO;2-D
3. M. Grabowski, J. Klemeš, K. Urbaniec, G. Vaccari, X.X. Zhu, Minimum energy consumption in sugar production by cooling crystallisation of concentrated raw juice. Appl. Therm. Eng. **21**(13), 1319–1329 (2001). https://doi.org/10.1016/S1359-4311(01)00020-5
4. T. Tekin, M. Bayramoğlu, Exergy and structural analysis of raw juice production and steam-power units of a sugar production plant. Energy **26**(3), 287–297 (2001). https://doi.org/10. 1016/S0360-5442(00)00068-2
5. M. Bayrak, A. Midilli, K. Nurveren, Energy and exergy analyses of sugar production stages. Int. J. Energy Res. **27**(11), 989–1001 (2003). https://doi.org/10.1002/er.916
6. D. Krajnc, M. Mele, P. Glavič, Improving the economic and environmental performances of the beet sugar industry in Slovenia: increasing fuel efficiency and using by-products for ethanol. J. Clean. Prod. **15**(13), 1240–1252 (2007). https://doi.org/10.1016/j.jclepro.2006.07.037
7. I. Faruk Yaka, A. Gungor, N. Sahin, E. Kaplan, M. Bayrak, and I. Faruk Yaka, "Exergy analysis of Eregli sugar factory," *Artic. World J. Eng.*, vol. 12, no. 5, pp. 463–470, 2015, doi: https:// doi.org/10.1260/1708-5284.12.5.463.
8. T. Taner, M. Sivrioglu, Energy–exergy analysis and optimisation of a model sugar factory in Turkey. Energy **93**, 641–654 (2015). https://doi.org/10.1016/j.energy.2015.09.007
9. E.S. Dogbe, M.A. Mandegari, J.F. Görgens, Exergetic diagnosis and performance analysis of a typical sugar mill based on Aspen Plus® simulation of the process. Energy **145**, 614–625 (2018). https://doi.org/10.1016/j.energy.2017.12.134
10. S. Klein and S. Alvarda, "Engineering equation solver (EES)." 2007.
11. H. Ghiasirad, N. Asgari, R. Khoshbakhti Saray, and S. Mirmasoumi, "Thermoeconomic assessment of a geothermal based combined cooling, heating, and power system, integrated with a humidification-dehumidification desalination unit and an absorption heat transformer," *Energy Convers. Manag.*, vol. 235, p. 113969, 2021, doi: https://doi.org/10.1016/j.enconman.2021. 113969.
12. H. Ghiasirad, N. Asgari, R. Khoshbakhti Saray, and S. Mirmasoumi, "Geothermal-based freshwater production by humidification-dehumidification and evaporating desalination units integrated with a CCHP system: Energy and exergy analysis," in *International Conference on Desalination and Water Purification*, 2021, p. 8, doi: ICDWP01_017.
13. "Exprimental data of Urmia sugar beet factory," 2016. https://ipsb.fr/.
14. F. Balkan, N. Colak, A. Hepbasli, Performance evaluation of a triple-effect evaporator with forward feed using exergy analysis. Int. J. Energy Res. **29**(5), 455–470 (2005). https://doi.org/ 10.1002/er.1074
15. H. Ghiasirad, H. Rostamzadeh, S. Nasri, *"Design and Evaluation of a New Solar Tower-Based Multi-Generation System: Part I, Thermal Modeling", in Integration of Clean and Sustainable*

Energy Resources and Storage in Multi-Generation Systems (Springer International Publishing, Cham, 2020), pp. 83–102

16. J.M. Smith, Introduction to chemical engineering thermodynamics. J. Chem. Educ. **27**(10), 584 (1950). https://doi.org/10.1021/ed027p584.3

17. S. A. Nebra and M. I. Fernandez Parra, "THE EXERGY OF SUCROSE-WATER SOLUTIONS: PROPOSAL OF A CALCULATION METHOD," 2005, Accessed: Mar. 07, 2020. [Online]. Available: https://www.researchgate.net/publication/283730424.

18. P.A. Sopade, P.J. Halley, B.R. D'Arcy, Specific heat capacity of Australian honeys from 35 to 165c as a function of composition using differential scanning calorimetry. J. Food Process. Preserv. **30**(2), 99–109 (2006). https://doi.org/10.1111/j.1745-4549.2006.00051.x

19. H. Ghiasirad, H. Rostamzadeh, S. Nasri, *"Design and Evaluation of a New Solar Tower-Based Multi-Generation System: Part II, Exergy and Exergoeconomic Modeling", in Integration of Clean and Sustainable Energy Resources and Storage in Multi-Generation Systems* (Springer International Publishing, Cham, 2020), pp. 103–120

20. A. Darabadi Zareh, R. Khoshbakhti Saray, S. Mirmasoumi, and K. Bahlouli, "Extensive thermodynamic and economic analysis of the cogeneration of heat and power system fueled by the blend of natural gas and biogas," *Energy Convers. Manag.*, vol. 164, pp. 329–343, 2018, doi: https://doi.org/10.1016/j.enconman.2018.03.003.

21. H. Nasrollahi, F. Ahmadi, M. Ebadollahi, S. Najafi Nobar, and M. Amidpour, "The greenhouse technology in different climate conditions: A comprehensive energy-saving analysis," *Sustain. Energy Technol. Assessments*, vol. 47, p. 101455, 2021, doi: https://doi.org/10.1016/j.seta.2021.101455.

22. H. P. Robert, W. G. Don, O. M. J.-M. G.-H. N. York, and U. 1997, *Perry's chemical engineers' handbook*. .

23. G. Song, J. Xiao, H. Zhao, L. Shen, A unified correlation for estimating specific chemical exergy of solid and liquid fuels. Energy **40**(1), 164–173 (2012). https://doi.org/10.1016/j.energy.2012.02.016

24. S. Turns, *An introduction to combustion.* 1996.

25. H. Rostamzadeh, H. Ghiasirad, M. Amidpour, and Y. Amidpour, "Performance enhancement of a conventional multi-effect desalination (MED) system by heat pump cycles," *Desalination*, vol. 477, p. 114261, 2020, doi: https://doi.org/10.1016/j.desal.2019.114261

26. A.V. Ensinas, M. Modesto, S.A. Nebra, L. Serra, Reduction of irreversibility generation in sugar and ethanol production from sugarcane. Energy **34**(5), 680–688 (2009). https://doi.org/10.1016/j.energy.2008.06.001

27. F. Petrakopoulou, "Comparative Evaluation of Power Plants with CO 2 Capture: Thermodynamic, Economic and Environmental Performance," TU-Berlin, 2011.

28. A. Bejan, G. Tsatsaronis, M. Maran, *Thermal Design and Optimization* (Wiley, John, 1996)

29. M. Khaljani, R.K. Saray, K. Bahlouli, Comprehensive analysis of energy, exergy and exergoeconomic of cogeneration of heat and power in a combined gas turbine and organic Rankine cycle. Energy Convers. Manag. **97**, 154–165 (2015). https://doi.org/10.1016/j.enconman.2015.02.067

30. B.-Y. Yoo, Economic assessment of liquefied natural gas (LNG) as a marine fuel for CO2 carriers compared to marine gas oil (MGO). Energy **121**, 772–780 (2017). https://doi.org/10.1016/j.energy.2017.01.061

Chapter 16
Energy-Efficient Humidity Pump System for Poultry Houses

Muhammad Sultan, Muhammad Aleem, and Takahiko Miyazaki

Abstract The poultry industry is a major contributor to worldwide food production. Poultry birds are fatally sensitive to humidity and temperature. Therefore, a temperature/humidity control system is principally required for optimum growth of the birds. Conventionally, to regulate temperature/humidity in control sheds, vapor compression air-conditioning systems are used which are not only costly but also consume an enormous amount of primary energy. Alternatively, evaporative cooling pads are also used which increase humidity level inside control sheds results in various fungal diseases. In this regard, this study explores desiccant air-conditioning (DAC) options for climatic conditions of Multan (Pakistan). These systems are operated with thermal energy that could be available via low-grade waste heat and renewable energy options. Such systems would allow the development of poultry houses in off-grid remote areas which eventually support the green smart grid's philosophy. Two DAC options are studied which are involved in standalone DAC and evaporative cooling (EC) assisted DAC concepts. Psychrometric and thermodynamic analysis with two types of desiccant materials is used in the study (i.e., silica-gel and hydrophilic polymeric-sorbent). The study determined body-weight-gain, feed-conversion-ratio, sensible/latent heat, and temperature-humidity-index of birds. As such, the performance of the proposed

M. Sultan (✉)
Faculty of Agricultural Sciences & Technology, Department of Agricultural Engineering, Bahauddin Zakariya University, Bosan Road, Multan 60800, Pakistan
e-mail: muhammadsultan@bzu.edu.pk

M. Aleem
Department of Agricultural Engineering, Bahauddin Zakariya University, Bosan Road, Multan 60800, Pakistan

T. Miyazaki
Department of Advanced Environmental Science and Engineering, Faculty of Engineering Sciences, Kyushu University, Fukuoka 816-8580, Japan
e-mail: miyazaki.takahiko.735@m.kyushu-u.ac.jp

431

systems is investigated for cooling capacity and COP. According to results, the EC-assisted polymeric-sorbent system has resulted feasible in terms of maximum cooling capacity and COP. This system could achieve thermal comfort of birds at THI of less than 30 °C.

Nomenclature

AC	Air-conditioning
BWG	Body-weight-gain (g)
COP	Coefficient of performance ($-$)
DAC	Desiccant air-conditioning
DEC	Direct evaporative cooling
EC	Evaporative cooling
FCR	Feed-conversion-ratio ($-$)
FI	Feed intake (g/day/bird)
h	Enthalpy of air (kJ/kg)
HP	Heat production (kJ/day/bird)
HS	Heat source
HX	Heat exchanger
IEC	Indirect evaporative cooling
LBW	Live body weight (g)
LH	Latent heat (J/s/bird)
M-DAC	Maisotsenko cycle assisted desiccant air-conditioning
ME	Metabolizable energy
MEC	Maisotsenko cycle evaporative cooling
MEI	Metabolizable energy intake (kJ/day/bird)
RE	Retained energy (kJ/day/bird)
SH	Sensible heat (J/s/bird)
THI	Temperature-humidity-index (°C)
VCAC	Vapor-compression air-conditioning
WI	Water intake (ml/day/bird)
T	Temperature (°C)
X	Humidity ratio (gw/kgDA)
h_{fg}	Latent heat of vaporization of water (J/kg)
ME_{diet}	Metabolizable energy content of diet (kJ/g)
Q_c	Cooling capacity (kJ/kg)
ϕ^*	Slope of dehumidification line ($-$)
ε	Effectiveness ($-$)
$\dot{m}$	Mass flow rate (kg/s)

Subscripts

dB	Dry-bulb
HX	Heat exchanger
in	Inlet
out	Outlet
PA	Process air
RA	Regeneration air
wB	Wet-bulb

16.1 Introduction

In the recent decade, the food-energy nexus has become a global concern due to rapid population growth, economic development, and urbanization that exert pressure on available resources to meet the socioeconomic demand [1]. It is expected that in 2050, the world population will reach up to 9.8 billion that would cause a 70% increase in food production (i.e. agricultural products) and consequently a 30% increase in energy demand [2–4]. In this regard, the livestock sector has emerged as the largest subsector in agriculture and a major contributor to food production (i.e., meat production). In Pakistan, poultry meat contributes 35% (1,647 thousand tons) to the overall country's meat production (i.e. 4,708 thousand tons) [5]. The worldwide poultry meat production is shown in Fig. 16.1 which shows the significance of the problem statement of this study. As poultry birds are highly sensitive to
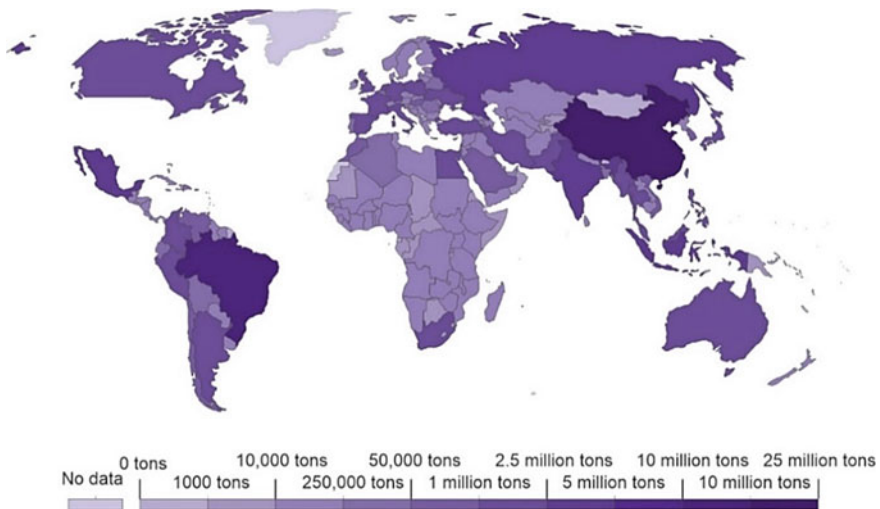
Fig. 16.1 Poultry meat production all over the world reproduced from [15]
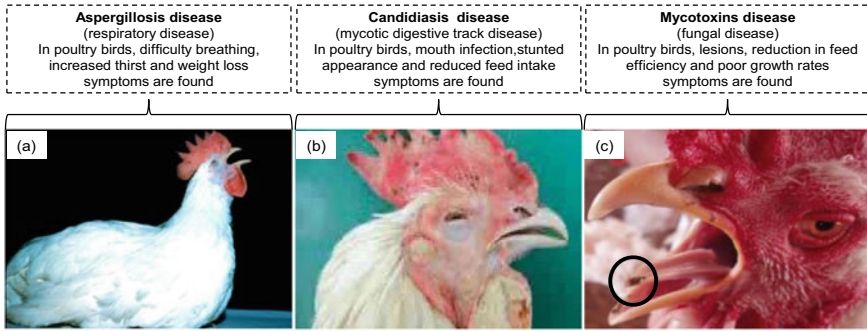
Fig. 16.2 Effects of **a** aspergillosis, **b** candidiasis, and **c** mycotoxins disease on the poultry birds

temperature and humidity fluctuations, ideal temperature and humidity conditions in poultry sheds are essential for their long-term growth [6]. In addition, high humidity in poultry houses causes fungal diseases including aspergillosis, candidiasis, and mycotoxins [7]. The effect and symptoms of fungal diseases on the birds are shown in Fig. 16.2. Aspergillosis is an infectious disease in which the birds struggle to take a breath [8]. Candidiasis is a mycotic digestive tract disease produced by fungal yeast that disturbs the crop (i.e., part of the digestive system) and result in mouth infection [9]. Mycotoxins is a disease caused by a natural toxin (i.e., fungus) and produces oral lesions in the poultry [10]. In addition, high temperatures have a considerable effect on the anatomy and immune system of birds [11]. Thus, an optimum temperature-humidity-index (THI) is needed for the birds up to the meat harvest stage. As the ambient air is conditioned to obtain the optimal THI, a variety of air-conditioning (AC) systems are utilized to ensure the birds' thermal comfort, i.e., THI < 30 °C [12].

Typically, vapor-compression AC (VCAC) systems have been used which leads to high energy consumption. In addition, the VCAC systems are involved in environmental degradation due to the use of environmentally harmful refrigerants [13]. In addition, the VCAC systems are unable to operate in remote areas where grids energy is not available. Alternatively, evaporative cooling (EC) systems are used in poultry houses to attain required thermal comfort [14], however, these systems achieve the cooling effect by employing an increase in humidity while keeping the enthalpy constant. The most prevalent types of EC systems are direct EC (DEC), indirect EC (IEC), and Maisotsenko cycle EC (MEC) systems [14]. In humid regions, the EC systems are not efficient because the moisture content in the air is relatively high which limits its applicability in humid regions [12]. In addition, the inside environment of poultry sheds became humid due to the continuous mass transfer from the birds' bodies to the surrounding air. To overcome this limitation, desiccant heat pump systems could be employed with and without the aid of EC options.

Desiccant is a material that adsorbs moisture from surrounding air because of its hygroscopic nature. The desiccant AC (DAC) systems are operated with thermal energy that could be available via low-grade waste heat as well as renewable energy

options e.g., solar thermal heat and biogas/biomass, etc. Such systems would allow the development of poultry houses in the off-grid remote areas in Pakistan particularly in the region of Sindh and Baluchistan. In literature, the DAC systems has shown promising results for various applications which include building [16–18], greenhouse AC [19, 20], agriculture product storage, and livestock AC [16, 21–26], automobiles [27], drying grains [28], marine ships [29, 30], museums [31, 32] and wet markets [33]. The Maisotsenko cycle (M-cycle) assisted desiccant AC (M-DAC) deals with latent and sensible load through desiccant dehumidification, and EC, respectively [34–36]. The M-DAC systems showed promising results in the literature for humid climates [37–40].

Therefore, from the above viewpoint, the present study explores two DAC options that are involved in standalone DAC and EC assisted DAC concepts. The research methodology is based on the slope of the dehumidification line and thermodynamic analyses using two types of desiccant materials which are, (i) silica-gel, (ii) hydrophilic polymeric-sorbent. The study explores body-weight-gain, feed-conversion-ratio, sensible heat, latent heat, and temperature-humidity-index (THI) of the birds. The feasibility of the proposed systems is investigated from viewpoint of cooling capacity and coefficient of performance (COP).

16.2 Proposed Humidity Pump Systems

The current study explores two types of humidity pump systems which involve standalone DAC system and M-cycle based DAC system. The thermodynamic evaluation of silica-gel and hydrophilic polymeric-sorbent (i.e., desiccant material) have been explored and the applicability of these systems is investigated for poultry houses against the climatic condition of Multan (Pakistan). Below is a quick description of the suggested systems.

16.2.1 Standalone Desiccant Air-Conditioning (DAC) System

Referring to Fig. 16.3a, the standalone desiccant air-conditioning (DAC) system comprises of dehumidification component (i.e., desiccant block), a sensible heat exchanger (HX), and a heating source (HS). The DAC system is being used to dehumidify the ambient/process air and increases temperature (i.e., air condition 1–2). The sensible (HX) receives this dehumidified and hot air and the temperature gets decreased, ideally as air condition 3. The desiccant material is regenerated by ambient/process air which is condition 4. Therefore, the ambient/process air is passed as a return air through sensible HX which increases the temperature (i.e., air condition 5). The hot air is then passed via a heat source (HS) to increase temperature to the desired regeneration temperature of air (i.e., air condition 6). Consequently, the regeneration air is passed over desiccant material to regenerate the desiccant material
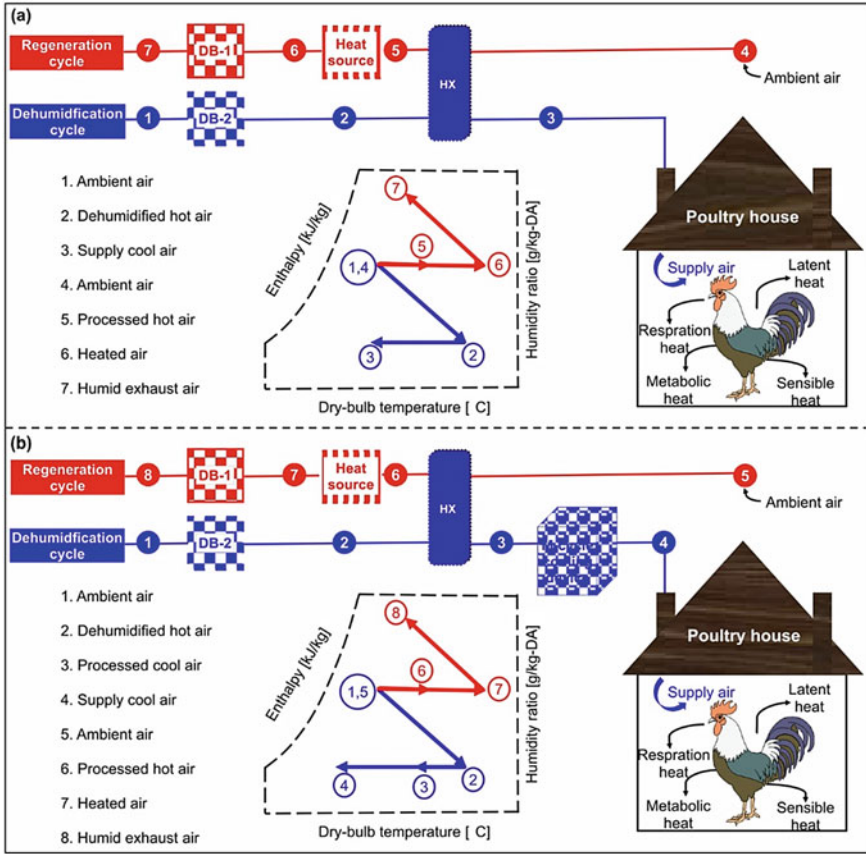
Fig. 16.3 Schematic and psychrometric representations of **a** standalone DAC, and **b** M-cycle assisted DAC systems

(i.e., air condition 7) causes a decrease in temperature because of the addition of moisture from desiccant material. The air condition 1–7 are presented in Fig. 16.3a.

16.2.2 M-Cycle Assisted DAC System

Referring to Fig. 16.3b, the M-cycle-based DAC system comprises of dehumidification component (i.e., desiccant block) in combination with a sensible heat exchanger (HX), M-cycle cooling device, and heating source (HS). The DAC system is utilized to dehumidify the ambient/process air that causes an increase in temperature of the air (i.e., air condition 1–2). Sensible (HX) gets hot dehumidified air which reduces the temperature up to the ambient/process air temperature, ideally (i.e., condition 3). As a result, the product air of sensible (HX) is passed via an evaporative

cooling device (i.e., M-Cycle) which decreases the temperature (i.e., condition 4). The ambient/process air is utilized for regeneration of desiccant material (i.e., air condition 5). The ambient/process air is passed through sensible HX as a return air which increases the temperature (i.e., air condition 6). Temperature is increased up to the desired regeneration temperature as this hot air is passed via a heating source (HS) (i.e., air condition 7). This sensibly heated air is passed through the desiccant material (i.e., air condition 8) and causes a decrease in temperature because of the addition of moisture from the desiccant material. The air condition 1–8 are shown in Fig. 16.3b.

16.3   Materials and Methods

For the thermal comfort of both human and non-human, temperature and humidity control is important [12]. Likewise, poultry birds also need optimum temperature and relative humidity conditions that vary with age for healthy growth. The optimum temperature for one, two, three, four, five-week poultry birds ranges from 34–32 °C, 32–28 °C, 28–26 °C, 26–24 °C, 24–20 °C, respectively [41, 42]. In the same period, the relative humidity fluctuates between 50 and 70% [41, 42]. The poultry birds consume feed and water for body-weight-gain (BWG), the building of tissues, and for their growth as well. The BWG and feed-conversion-ratio (FCR) is a function of the environmental temperature of the poultry house. FCR is a measure of how well a flock (i.e., poultry birds) converts feed intake into live weight. Moreover, the BWG and FCR also depend on the amount of feed intake (FI) by poultry birds that vary with age [43, 44]. The BWG by poultry birds as a function of temperature and live body weight (LBW) is calculated by Eq. (16.1) [45]. Consequently, Eq. (16.2) is used to determine the FCR as a function of LBW and temperature [45].

$$
\begin{aligned}
\text{BWG} = {} & 98.838 + 4.2822 \times 10^{-2}\text{LBW} - 1.1662 \times 10^{-5}\text{LBW}^2 \\
& - 13.167 T_{\text{dB}} + 0.72569 T_{\text{dB}}^2 - 1.1155 \times 10^{-2} T_{\text{dB}}^3 + 2.3823 \times 10^{-3}\text{LBWT}_{\text{dB}} \\
& - 9.3517 \times 10^{-5}\text{LBWT}_{\text{dB}}^2
\end{aligned}
\tag{16.1}
$$

$$
\begin{aligned}
\text{FCR} = {} & -0.30582 + 1.8099 \times 10^{-4}\text{LBW} + 1.3633 \times 10^{-7}\text{LBW}^2 \\
& + 0.38552 T_{\text{dB}} - 1.9945 \times 10^{-2} T_{\text{dB}}^2 + 2.9056 \times 10^{-4} T_{\text{dB}}^3 \\
& - 6.9059 \times 10^{-5}\text{LBWT}_{\text{dB}} + 2.45998 \times 10^{-6}\text{LBWT}_{\text{dB}}^2
\end{aligned}
\tag{16.2}
$$

where, BWG is body-weight-gain by poultry bird [g/day]; LBW is the live body weight of poultry birds (g); T_{dB} is dry-bulb temperature (°C) and FCR is feed-conversion-ratio in a gram of feed consumed per gram of body-weight-gain, respectively.

The feed has metabolizable energy (ME) content because it contains carbohydrates, fat, or protein. In this study, ME content has been taken as 3383 kcal/kg. The ME is transformed into sensible heat (SH) production in the bird's body because of the digestion of constituents of feed. The poultry birds retained a fair portion of the heat (i.e., retained energy) for building their body weight, tissues, muscles and to maintain their relatively constant body temperature (i.e., 41 °C). Water intake (WI) by the birds leads to latent heat (LH) production. The sensible and latent heat production creates heat stress on the birds. THI is the key parameter to evaluate the thermal comfort (i.e., THI < 30 °C) of poultry birds and it is a relative measurement of dry-bulb and wet-bulb temperature [46]. The SH production by the birds is determined by Eq. (16.3) [47]. In addition, Eq. (16.4) is used to determine the energy retained by poultry birds for their maintenance as a function of metabolizable energy intake (MEI) [48]. The latent heat (LH) produced by poultry birds is calculated by Eq. (16.5). The THI is calculated by Eq. (16.6).

$$HP = FI \times ME_{diet} - RE \tag{16.3}$$

$$RE = -404 + 0.63 \times MEI \tag{16.4}$$

$$LH = WI \times h_{fg} \tag{16.5}$$

$$THI = 0.85 T_{dB} + 0.15 T_{wB} \tag{16.6}$$

where, HP is the heat production (kJ/day/bird); FI is the feed intake by the bird (g/day/bird); ME_{diet} is the metabolizable energy content of the diet (kJ/g); RE is the retained energy (kJ/day/bird); LH is latent heat produced by poultry bird (J/s/bird); WI is water intake by poultry bird (kg/s/bird) and h_{fg} is the latent heat of vaporization of water (J/kg); THI is temperature-humidity-index (°C); T_{dB} is the dry-bulb temperature (°C) and T_{wB} is the wet-bulb temperature (°C), respectively.

The desiccant material adsorbs water vapor because of the pressure gradient between the ambient air and the desiccant material surface. When the ambient air is passed via a desiccant unit, it gets dehumidified, and the temperature of the air relatively increases. The heat exchanger (HX) is used for both cooling and heating of process/ambient air sensibly. In addition, the Maisotsenko-cycle (M-cycle) device is used for further cooling of the sensibly cooled air. The air condition that passes through sensible HX and M-cycle cooling devices is calculated from Eqs. (16.7–16.8), respectively [21].

$$T_{3,dB} = T_{2,dB} - \varepsilon_{HX}\left(T_{2,dB} - T_{1,dB}\right) \tag{16.7}$$

$$T_{4,dB} = T_{3,dB} - \varepsilon_{wB}\left(T_{3,dB} - T_{1,wB}\right) \tag{16.8}$$

$$T_{6,\mathrm{dB}} = T_{5,\mathrm{dB}} - \varepsilon_{\mathrm{HX}}\left(T_{2,\mathrm{dB}} - T_{5,\mathrm{dB}}\right) \tag{16.9}$$

where in the subscripts 1–6 represented in Fig. 16.3 are the air states. T_{dB}, refers to dry-bulb temperature (°C); $\varepsilon_{\mathrm{HX}}$ is sensible heat exchanger (HX) effectiveness and has been taken as 0.9 [21], $\varepsilon_{\mathrm{wB}}$ is wet-bulb effectiveness of M-cycle cooling device and has been considered as 0.6 [21], T_{wB} is wet-bulb temperature (°C).

After some time, the desiccant material gets saturated, and its capacity to dehumidify the air decreases. Therefore, hot air is supplied to desorb moisture from desiccant material. The process/ambient air is passed through the sensible HX to increase its temperature. The air condition that passed through sensible HX is calculated from Eq. (16.9) [21]. In addition, the sensibly hot air is further heated by a heat source (i.e., thermal heat source, biogas/biomass) to increase its temperature to the desired regeneration temperature. This regenerated air is supplied through the desiccant unit that takes away the moisture from the desiccant material and gets regenerated.

The desiccant dehumidification process has a unique relationship with the slope of the dehumidification line on a psychrometric chart. Ideally, the slope of the dehumidification line follows an isenthalpic behavior. But experimentally, the behavior of the dehumidification line's slope differs from isenthalpic behavior due to adsorption mechanism and adsorbent pair interactions [49–51]. The study utilized two kinds of desiccant material's slope (i.e., $\phi^* = 0.22$ for silica-gel and $\phi^* = 0.31$ for hydrophilic polymeric-sorbent) for the dehumidification practice. The slope of dehumidification line for both materials is shown in Fig. 16.4 [52]. Equation (16.10) determined the slope of the dehumidification line. Enthalpy of air is determined by Eq. (16.11) [53].
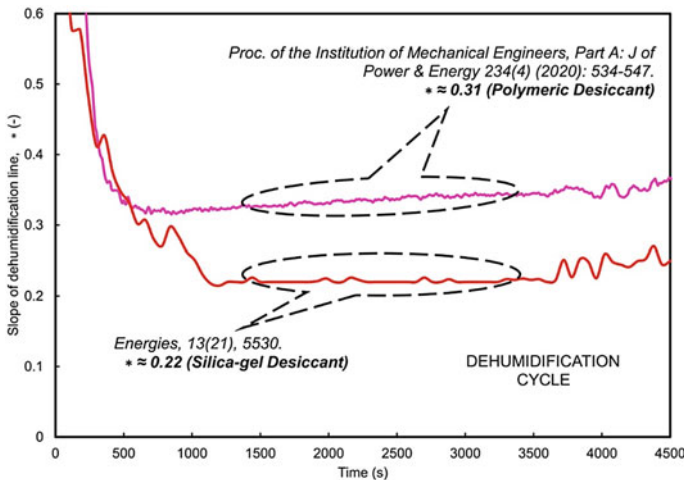
Fig. 16.4 The slope of the dehumidification line for silica-gel desiccant and polymeric-desiccant was reproduced from [52]

$$\phi^* = \frac{X_{\text{in}} - X_{\text{out}}}{T_{\text{dB,out}} - T_{\text{dB,in}}} \qquad (16.10)$$

$$h = 1.006 T_{\text{dB}} + X(2501 + 1.86 T_{\text{dB}}) \qquad (16.11)$$

where ϕ^* is the slope of dehumidification line (−); X_{in} is humidity ratio of process/ambient air at an inlet side of the desiccant system (gw/kgDA); X_{out} is humidity ratio of dehumidified air at an outlet side of the desiccant system (gw/kgDA); h is the enthalpy of air (kJ/kg); T_{dB} is the dry-bulb temperature (°C); and X is humidity ratio [gw/kgDA], respectively.

The cooling capacity and coefficient of performance (COP) for both DAC (i.e. standalone DAC, M-cycle assisted DAC) systems are calculated from Eqs. (16.12–16.15), respectively [52, 54].

$$Q_{c,\text{DAC}} = h_1 - h_3 \qquad (16.12)$$

$$Q_{c,M-\text{DAC}} = h_1 - h_4 \qquad (16.13)$$

$$COP_{\text{DAC}} = \frac{\dot{m}_{\text{PA}}}{\dot{m}_{\text{RA}}} \left(\frac{h_1 - h_3}{h_5 - h_6} \right) \qquad (16.14)$$

$$COP_{M-\text{DAC}} = \frac{\dot{m}_{\text{PA}}}{\dot{m}_{\text{RA}}} \left(\frac{h_1 - h_4}{h_6 - h_7} \right) \qquad (16.15)$$

where the subscripts 1, 3, 5–7 are the air states shown in Fig. 16.3. h is air enthalpy (kJ/kg); $Q_{c,\text{DAC}}$ is the cooling capacity of the standalone desiccant system (kJ/kg); $Q_{c,M-\text{DAC}}$ is cooling capacity of M-cycle based desiccant system (kJ/kg); COP_{DAC} is coefficient of performance of the standalone desiccant system (−); $COP_{M-\text{DAC}}$ is the coefficient of performance of M-cycle based desiccant system (−); $\dot{m}_{\text{PA}}$ is the mass flow rate of process air (kg/s) and $\dot{m}_{\text{RA}}$ is the mass flow rate of regeneration air (kg/s), respectively.

16.4 Results and Discussion

Temperature-humidity-index (THI) is a relative measurement of dry-bulb temperature as well as wet-bulb temperature and one of the key parameters to evaluate the thermal comfort of the poultry birds. Figure 16.5 shows the effect of THI on the thermal comfort of the birds. The THI > 30 °C indicates that the birds are in danger zone and THI between 20 and 30 °C indicates the bird's comfort zone. THI below 20 °C indicates too low temperature-humidity conditions for the birds to survive.
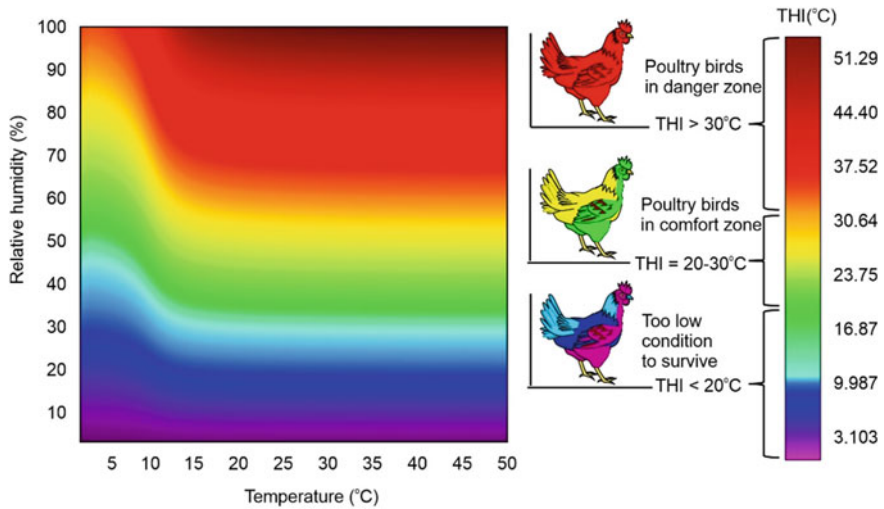
Fig. 16.5   Effect of the temperature-humidity-index (THI) on poultry bird's thermal comfort

The birds need an optimum amount of energy for their body-wight-gain and body maintenance that depends on temperature.

Figure 16.6 shows the optimum performance temperature zone for the birds. An increase in temperature creates energy deficit and heat stress that affect the performance of poultry birds. In contrast, a decrease in temperature also creates energy deficit and cold stress that decreases the performance of the birds to gain their body
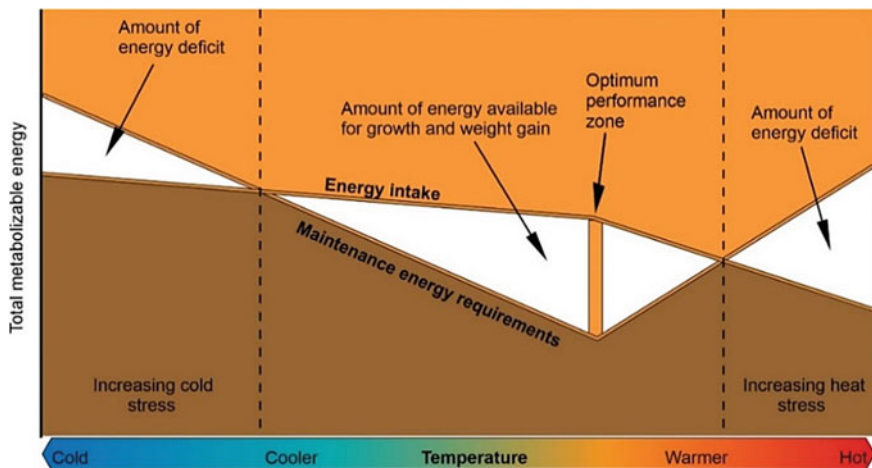
Fig. 16.6   Optimum performance temperature zone for the poultry birds [55]

weight. Therefore, the optimum temperature and relative humidity zones are mandatory for the optimum growth of the birds. Figure 16.7 shows a psychrometric representation of the optimum temperature and relative humidity zones for poultry birds and an hourly climatic condition of Multan.

The efficient BWG by the birds depends on the temperature of the poultry house. Figure 16.8a shows the effect of temperature on the BWG by poultry birds. At 26 °C, 30 °C, and 34 °C the poultry birds of 1500 g gain their body weight of 84 g, 74 g, and 49 g, respectively. The BWG decreases with an increase in temperature that leads to poor production. The effect of temperature on FCR by the birds is shown in Fig. 16.8b. FCR by the birds increases with temperature. The FCR by the birds
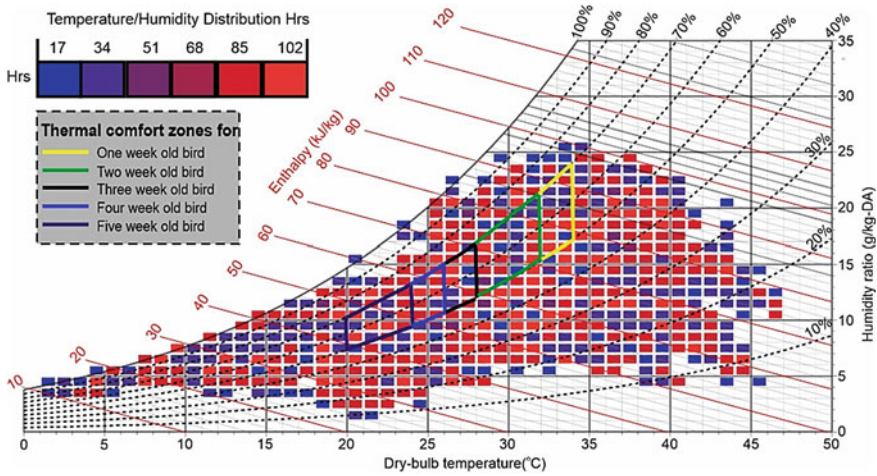
Fig. 16.7 Psychrometric description of the ideal temperature and relative humidity zones for poultry birds and an hourly climatic condition of Multan (Pakistan)
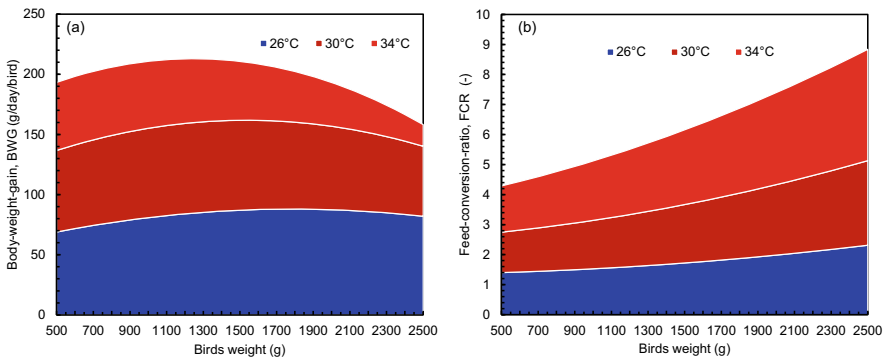
Fig. 16.8 Effect of temperature on **a** body-weight-gain (BWG) and **b** feed conversion ratio (FCR) of the poultry bird
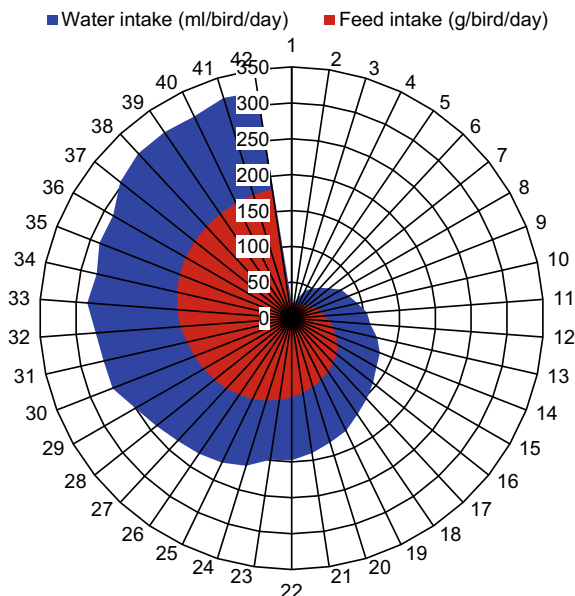
Fig. 16.9 Daily feed and water intake behavior of poultry birds concerning age, reproduced from [43, 44]

of 1500 g at 26 °C, 30 °C, 34 °C is 1.72, 1.94, and 2.48, respectively. The high temperature caused relatively more feed consumption but less BWG.

The bird's intake of feed and water for their growth/development varies concerning age. Figure 16.9 shows the feed intake (FI) and water intake (WI) by the birds concerning age.

The feed contains metabolizable energy (ME) content that produces sensible heat in the bird's body because of the digestion of feed. Some amount of the sensible heat production consumes by the birds (i.e., retained energy) for their growth. Likewise, water intake (WI) by the birds causes latent heat production because of continuous mass transfer from the bird's body. Figure 16.10 represents metabolizable energy intake (MEI) and retained energy (RE) by the birds for building their tissues and muscles with respect to age. The metabolizable energy intake (MEI) by the birds on the 21st day of their production is 1486 kJ, while the energy retained for their growth or maintenance is 532 kJ. MEI and RE by the birds increase with age.

Figure 16.11 shows the sensible, latent, and total heat production as a result of feed and water intake by poultry birds with respect to age. On the 21st day of the bird production, the sensible, latent, and total heat production is 11.1 J/s, 2.2 J/s, and 13.3 J/s, respectively. The sensible, latent, and total heat production by the birds increases with respect to the age of their production.

The results from proposed AC systems are obtained on daily basis for selected months (i.e., June–September) and climatic conditions. Figure 16.12 displays the
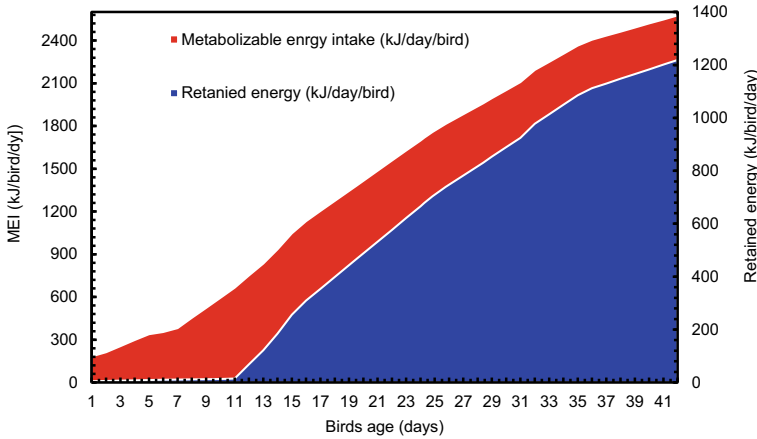
Fig. 16.10 Metabolizable energy intake (MEI) and retained energy (RE) by poultry birds with respect to age
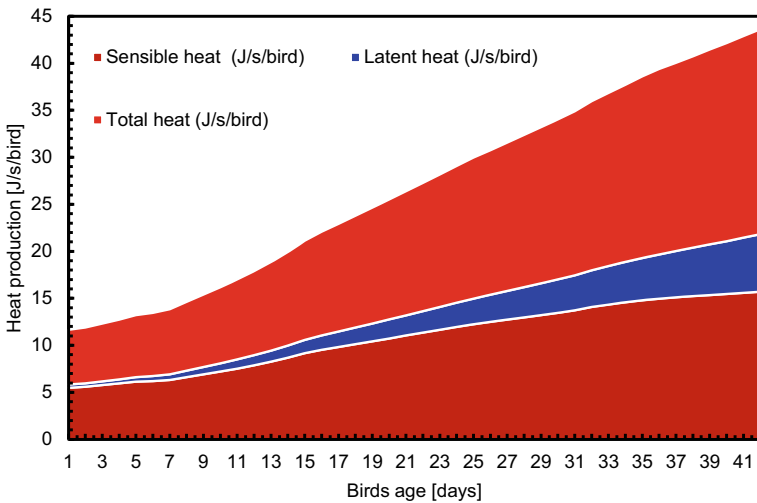
Fig. 16.11 Sensible, latent, and total heat production by poultry birds with respect to age

temperature and relative humidity profiles on daily basis of the standalone silica-gel integrated DAC system for the selected months. The inlet process/ambient air temperature, and relative humidity for June–September ranges from 22–31 °C; 41–73%, 27–36 °C; 56–85%, 26–33 °C; 62–88% and 25–32 °C; 59–88%, respectively. The outlet air temperature and relative humidity for June–September ranges from 29–38 °C; 32–62%, 29–39 °C; 43–72%, 28–35 °C; 45–71% and 28–34 °C; 43–70%, respectively.
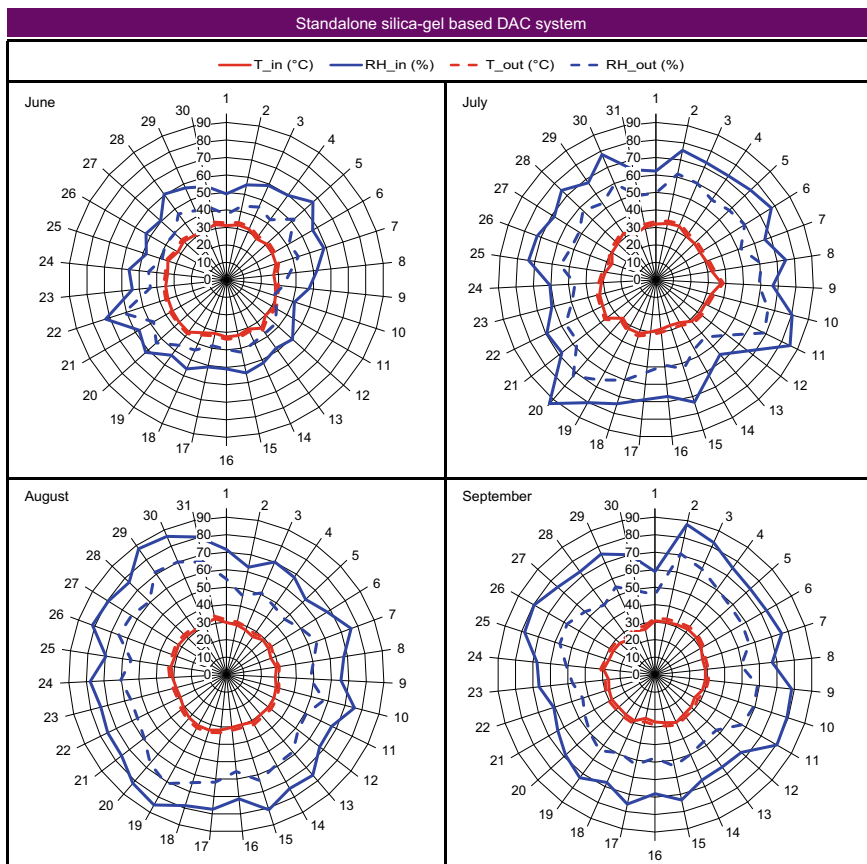
Fig. 16.12 Temperature and relative humidity profiles on daily basis of standalone silica-gel based DAC system for June–September

The temperature and relative humidity profiles of standalone polymer-based DAC system on daily basis for the selected months are represented in Fig. 16.13. The outlet air temperature ranges from 28–38 °C; 29–59%, 28–39 °C; 40–68%, 28–35 °C; 42–68% and 27–33 °C; 42–67% for June–September, respectively.
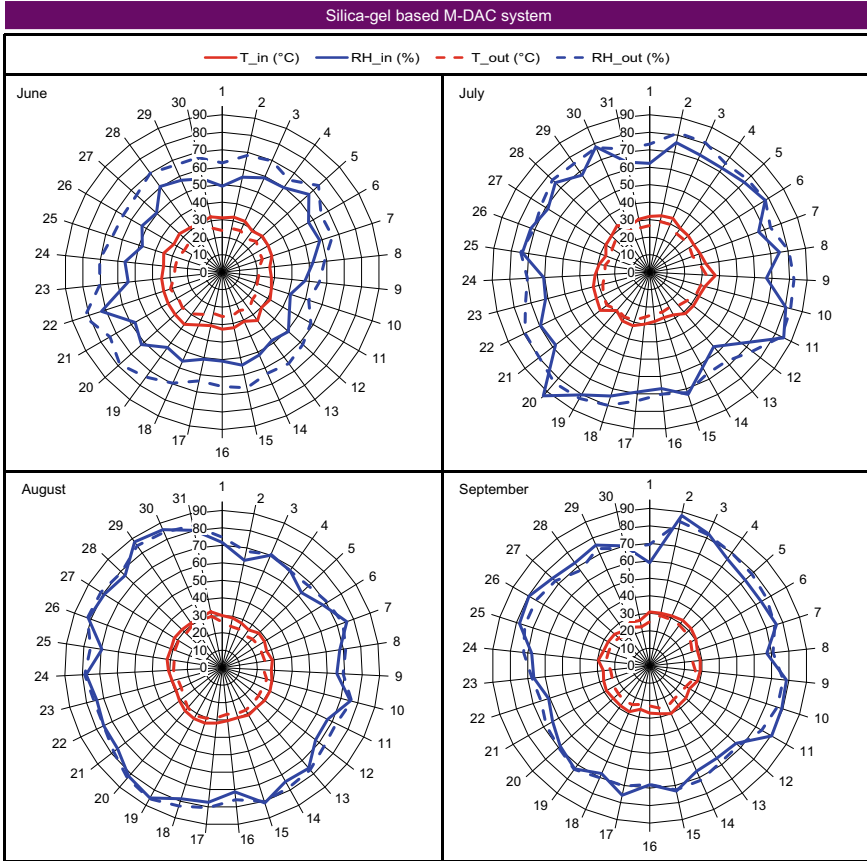
Figure 16.14 shows temperature and relative humidity profiles of silica-gel based M-DAC system on daily basis for the selected months. The outlet air temperature and relative humidity from the M-DAC system range from 20–31 °C; 52–82%, 23–33 °C; 66–84%, 22–32 °C; 67–86% and 22–29 °C; 65–84% for June–September, respectively. The temperature and relative humidity profiles of polymer-based M-DAC system on daily basis for the selected months are represented in Fig. 16.15. The outlet air temperature and relative humidity of polymer-based M-DAC system range from 21–31 °C; 46–79%, 23–32 °C; 60–80%, 22–31 °C; 60–82% and 22–29 °C; 58–80% for June–September, respectively.
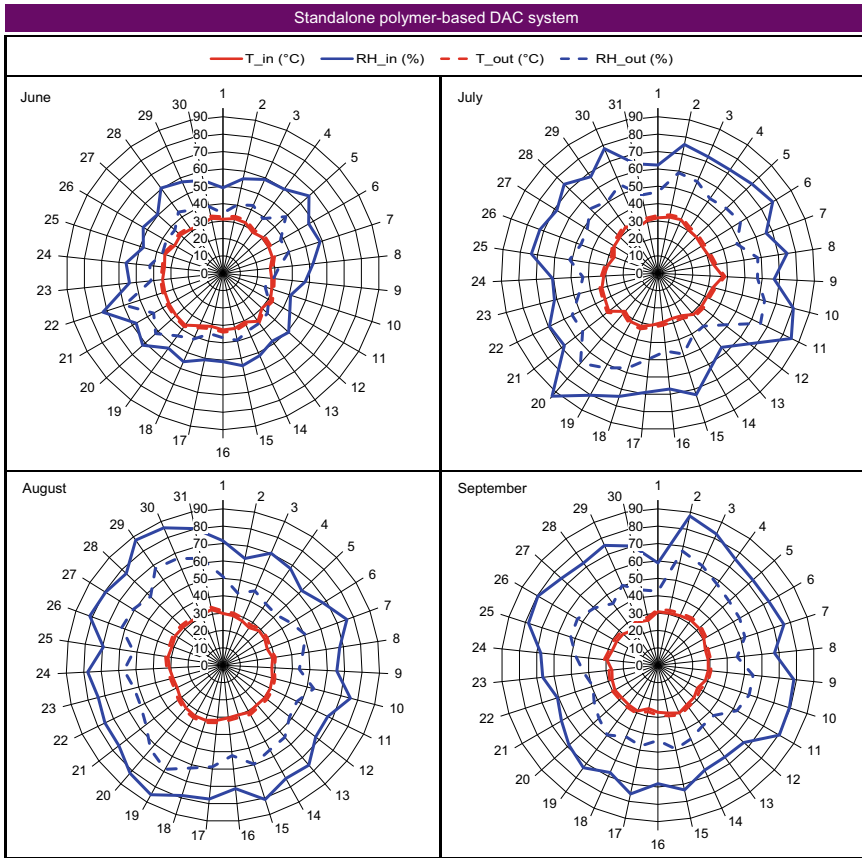
Fig. 16.13 Temperature and relative humidity profiles on daily basis of standalone polymer-based DAC system for June–September

Figure 16.16 shows the Temperature-humidity-index (THI) values against the climatic condition of Multan (Pakistan) on daily basis for the selected months. The THI was greater than 30 °C causes heat stress, mortality, and poor production of the birds. Red color boxes show the THI values greater than 32 °C that indicates the heat stress for the birds. Orange color boxes show the THI values between 30 and 32 °C that indicate the moderate heat stress on the birds. Green color boxes show the THI values less than 30 °C that indicates the bird's thermal comfort. Figure 16.17 shows the THI values of silica-gel based standalone DAC system for the selected months. The THI values of the standalone polymer-based DAC system for the selected months are represented in Fig. 16.18. The THI values of standalone silica-gel as well as polymer-based DAC systems are mostly greater than 30 °C.

Figure 16.19 shows the THI values of the silica-gel integrated M-DAC system for the selected months. Mostly the THI values of silica-gel integrated M-DAC system

Fig. 16.14 Temperature and relative humidity profiles of on daily basis of silica-gel based M-DAC system for June–September

are less than 30 °C and some are greater than 30 °C. Figure 16.20 shows the THI values of the polymer-based M-DAC system for the selected months. In the case of polymer-based M-DAC system, almost all the THI values are less than 30 °C. Therefore, the polymer-based M-DAC system could be a viable option for poultry houses.

The psychrometric representation on daily basis of investigated desiccant AC system's performance for the selected months is shown in Fig. 16.21. The performance of the polymer-based M-DAC system is maximum for the selected months as compared to other proposed desiccant AC systems. Conventional vapor-compression based AC systems could not achieve effectively optimum temperature and relative humidity conditions. Also, the cooling pads used in control sheds increases the humidity level which increases fungal attacks on the birds. Because of its ability
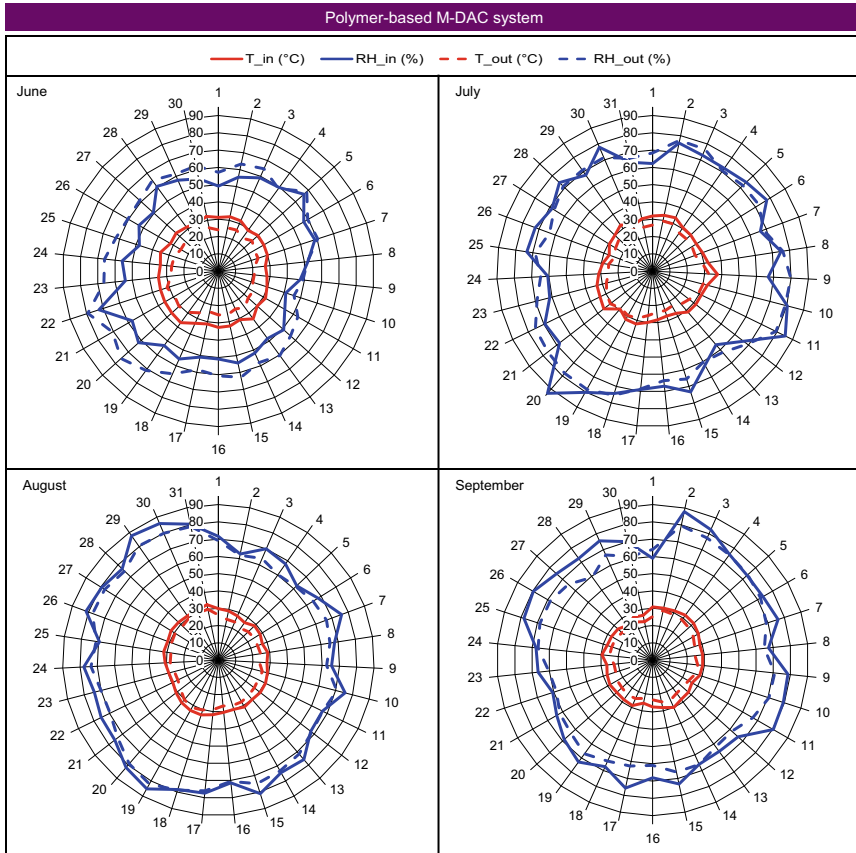
Fig. 16.15 Temperature and relative humidity profiles on daily basis of polymer-based M-DAC system for June–September

to deal with both sensible and latent load, the polymer-based M-DAC system was able to keep the birds at their ideal temperature and relative humidity.

Figure 16.22 shows the air enthalpy required by the proposed AC systems on daily basis for June–September. Maximum air enthalpy required by the polymer-based M-DAC is 90 kJ/kg, 96 kJ/kg, 93 kJ/kg, 82 kJ/kg for June–September respectively. Conventional vapor-compression based AC systems consume a huge amount of energy for their operation. The polymer-based M-DAC system required less amount of energy per kilogram of air (i.e. enthalpy) for its operation which can be easily obtained via low-grade heat sources as well as renewable energy options.

Figure 16.23 shows the cooling capacity profile on daily basis of the investigated AC systems for the selected months. The polymer-based M-DAC system has achieved a maximum cooling capacity of 17.1 kJ/kg, 15.8 kJ/kg, 15.6 kJ/kg, 15.7 kJ/kg for June–September respectively. Figure 16.24 shows the coefficient of performance
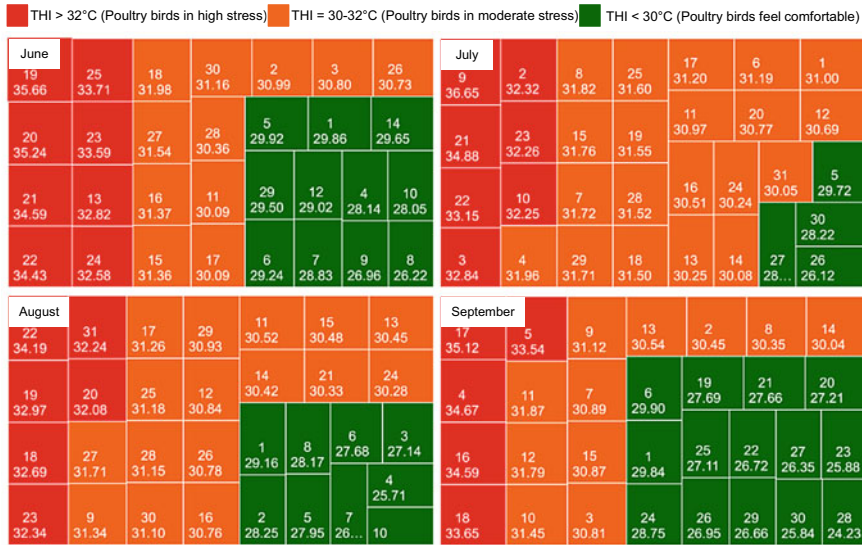
Fig. 16.16 Temperature-humidity-index (THI) values against climatic conditions of Multan (Pakistan) on daily basis for June–September
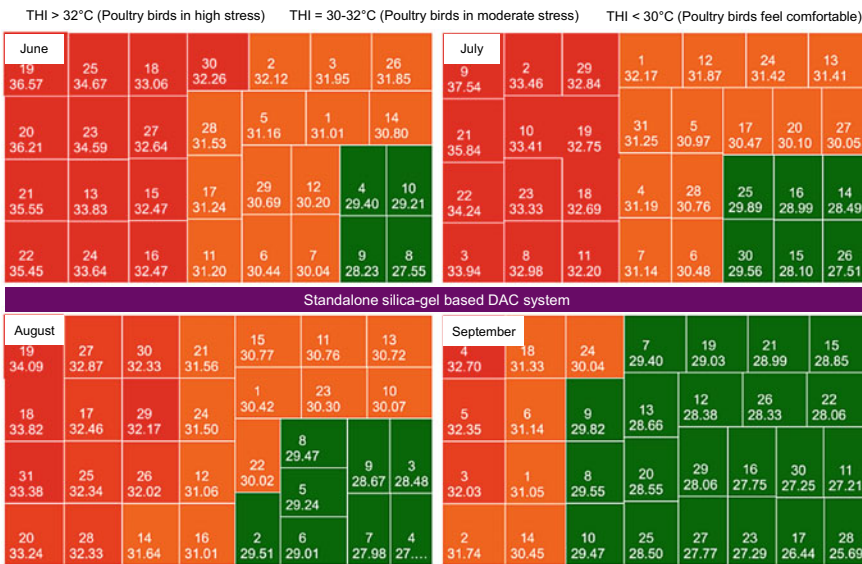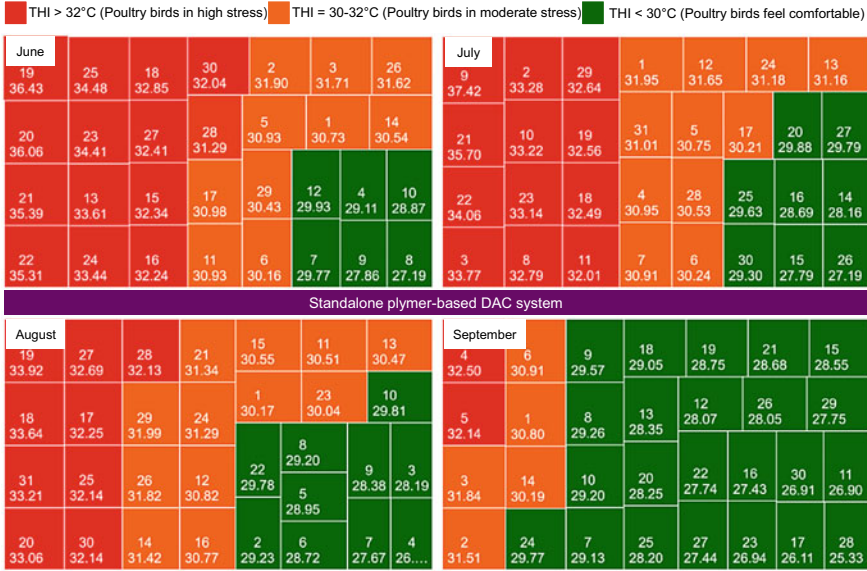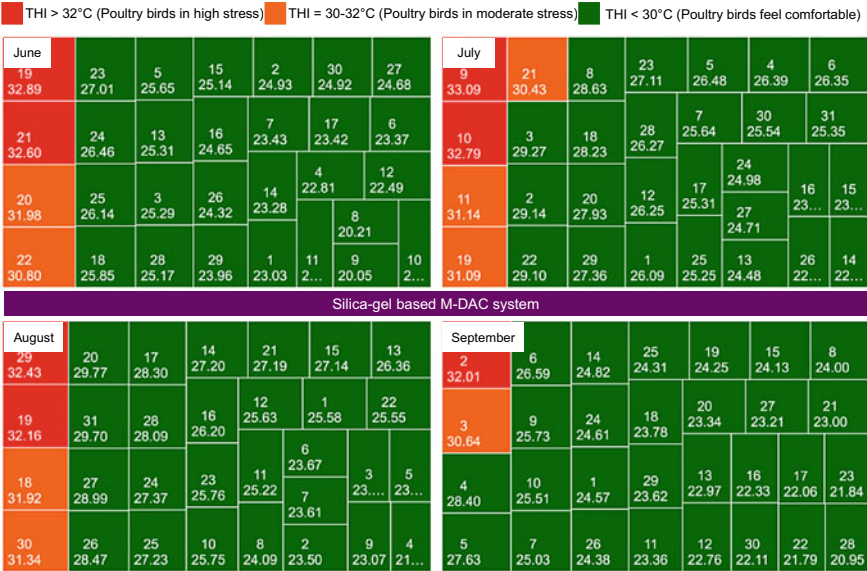

Fig. 16.17 Temperature-humidity-index (THI) values on daily basis of standalone silica-gel based DAC system for June–September

Fig. 16.18 Temperature-humidity-index (THI) values of standalone polymer-based DAC system on daily basis for June–September

Fig. 16.19 Temperature-humidity-index (THI) values of silica-gel based M-DAC system on daily basis for June–September
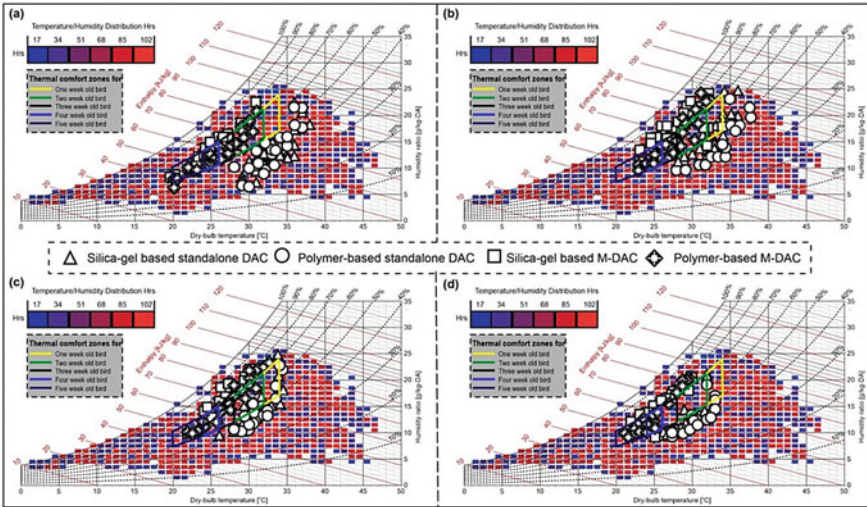
Fig. 16.20 Temperature-humidity-index (THI) values on daily basis of polymer-based M-DAC system for June–September

Fig. 16.21 Psychrometric representation of the daily based performance of proposed AC systems for month of **a** June, **b** July, **c** August, and **d** September
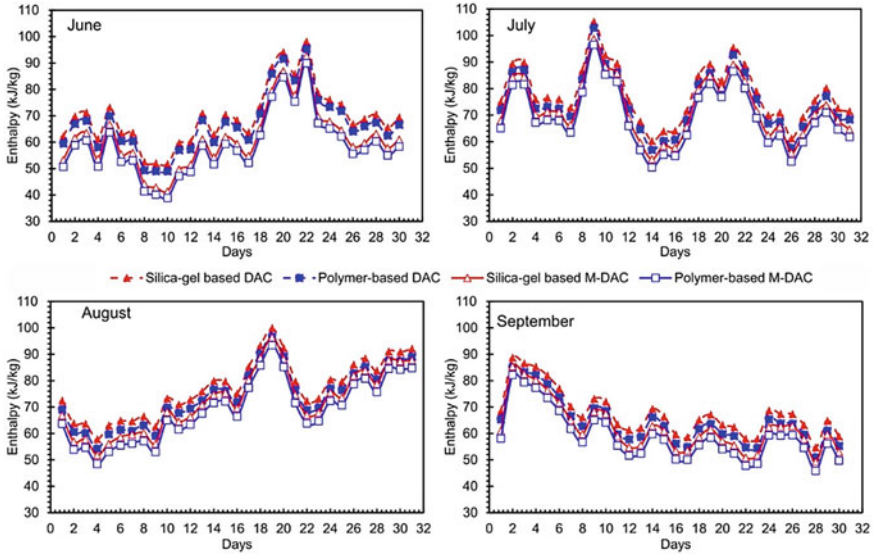
Fig. 16.22 Air enthalpy required on daily basis by the investigated AC systems for the month of June–September
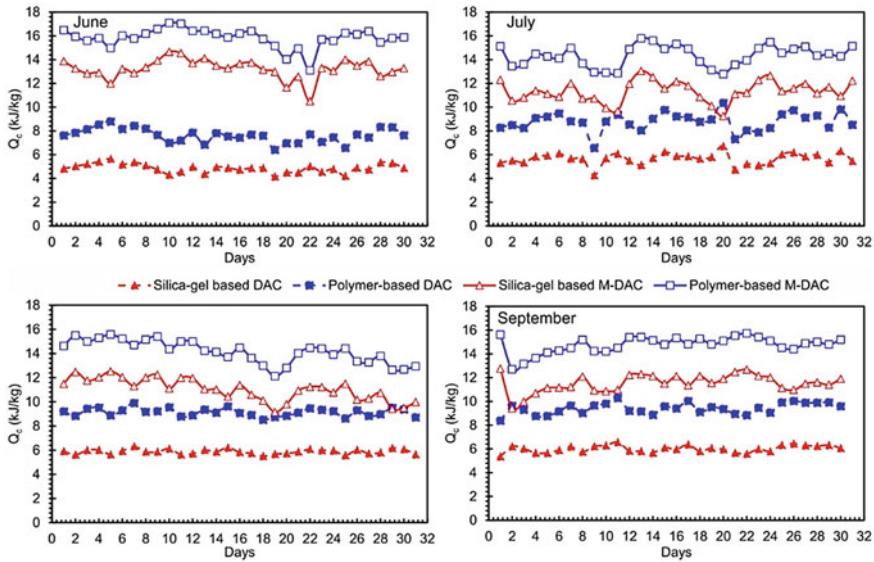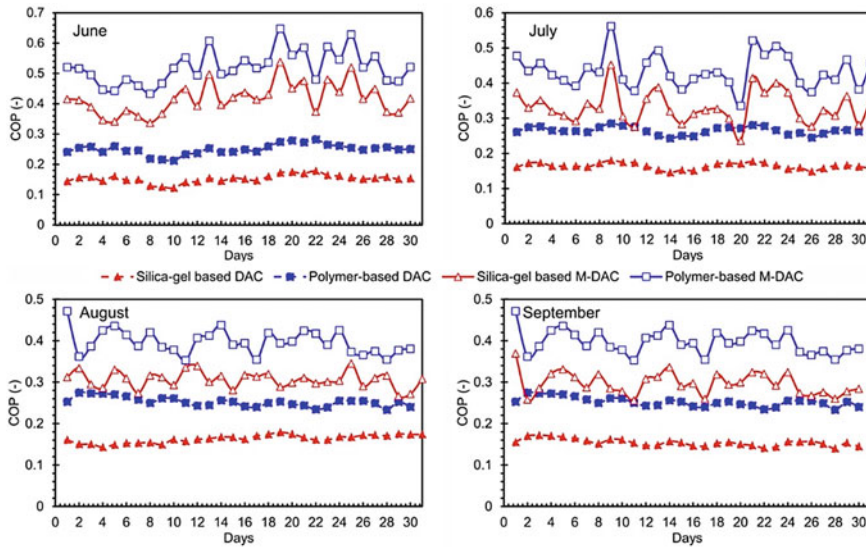

Fig. 16.23 Cooling capacity profile on daily basis of the investigated AC systems for June–September

Fig. 16.24 Coefficient of performance (COP) profile of investigated AC systems on daily basis for June–September

(COP) profile of the proposed AC systems for the selected months. The maximum COP of the polymer-based M-DAC system is 0.64, 0.52, 0.45, 0.47 for the selected months.

16.5 Conclusion

In the last few decades, the demand for energy and food production has been increasing due to rapid increase in population, economic development, and urbanization. The poultry industry is a major contributor to worldwide food production. However, poultry birds require optimum temperature and humidity conditions for their growth and maintenance. Usually, conventional AC systems are used for controlled poultry houses to regulate the temperature and humidity which are costly and cause high primary-energy consumption. In addition, EC pads are also used in control sheds which increase the fungal attacks e.g., aspergillosis, candidiasis, and mycotoxins on the birds because of continuous mass transfer (i.e., water vapors).

In this regard, the present study investigates energy-efficient desiccant AC (DAC) options for the climatic conditions of Multan (Pakistan). Such systems can operate with thermal energy (low-grade waste heat source) as well as renewable energy (solar thermal heat, biogas). These systems would allow the development of the poultry houses in off-grid remote areas (particularly for Sindh and Baluchistan). The study investigates the standalone DAC system and EC coupled DAC system

using silica-gel and hydrophilic polymeric-sorbent materials from the viewpoints of psychrometric and thermodynamic analysis. Moreover, the study determined body-weight-gain (BWG), feed-conversion-ratio (FCR), sensible heat (SH), latent heat (LH), and THI of the birds. The feasibility of the proposed AC systems is investigated from perceptions of cooling capacity, and coefficient of performance (COP). The results show that the polymer DAC assisted EC system was feasible in terms of maximum cooling capacity, COP (i.e., 17 kJ/kg and 0.64, respectively) and achieved the thermal comfort of THI < 30°C for the birds. Thus, this system could be an alternate option for conventional AC systems as well as cooling pads and thereby contributing towards the green smart grids philosophy.

Conflicts of Interest The authors declare no conflict of interest.

References

1. A. Karabulut, B.N. Egoh, D. Lanzanova, B. Grizzetti, G. Bidoglio, L. Pagliero et al., Mapping water provisioning services to support the ecosystem-water-food-energy nexus in the Danube river basin. Ecosyst. Serv. **17**, 278–292 (2016). https://doi.org/10.1016/j.ecoser.2015.08.002
2. UNDESA, World population prospects: the 2017 revision, key findings and advance tables (2017). https://esa.un.org/unpd/wpp/Publications/Files/WPP2017_KeyFindings.pdf. Accessed 30 Nov 2020
3. FAO, The water–energy–food nexus: a new approach in support of food security and sustainable agriculture (Food and Agriculture Organization, Rome, 2014). http://www.fao.org/3/I9553EN/i9553en.pdf. Accessed 30 Nov 2020
4. WEF, World energy focus, in World Energy Council (2017)
5. GoP, Pakistan economic survey (2014), pp. 23–41. http://finance.gov.pk/survey/chapters_14/02_Agriculture.pdf. Accessed 30 Oct 2020
6. H. Xin, I.L. Berry, G.T. Tabler, T.L. Barton, Temperature and humidity profiles of broiler houses with experimental conventional and tunnel ventilation systems. Appl. Eng. Agric. **10**, 535–542 (1994). https://doi.org/10.13031/2013.25883
7. K. Dhama, S. Chakraborty, A.K. Verma, R. Tiwari, R. Barathidasan, A. Kumar et al., Fungal/mycotic diseases of poultry-diagnosis, treatment and control: a review. Pakistan J. Biol. Sci. **16**, 1626–1640 (2013). https://doi.org/10.3923/pjbs.2013.1626.1640
8. P. Arné, S. Thierry, D. Wang, M. Deville, G. Le Loch, A. Desoutter, et al., Aspergillus fumigatus, Poultry. Int. J. Microbiol. 746356 (2011). https://doi.org/10.1155/2011/746356
9. Z.Y. Ibrahim, B.H. Ali, R.K. Ali, A.S. Jarad, W.H. Farhan, M.S. Hasan, Avian candidiasis: a review. Int. J. Pharm. Res. **12**, 1088–1091 (2020). https://doi.org/10.31838/ijpr/2020.12.01.199
10. B. Zunic, S. Peter, World' s largest science. Technol. Med. (Open Access book publisher) 267–322 (2018)
11. L.J. Lara, M.H. Rostagno, Impact of heat stress on poultry production. Animals **3**, 356–369 (2013). https://doi.org/10.3390/ani3020356
12. M. Sultan, T. Miyazaki, Energy-efficient air-conditioning systems for nonhuman applications. Refrigeration (2017). https://doi.org/10.5772/intechopen.68865

13. M. Sultan, I.I. El-Sharkawy, T. Miyazaki, B.B. Saha, S. Koyama, An overview of solid desiccant dehumidification and air conditioning systems. Renew. Sustain. Energy Rev. **46**, 16–29 (2015). https://doi.org/10.1016/j.rser.2015.02.038

14. H.M.U. Raza, H. Ashraf, K. Shahzad, M. Sultan, T. Miyazaki, M. Usman et al., Investigating applicability of evaporative cooling systems for thermal comfort of poultry birds in Pakistan. Appl. Sci. **10** (2020). https://doi.org/10.3390/app10134445

15. FAO, UN food and agriculture organization (FAO) (2018). http://www.fao.org/faostat/en/?#data/

16. M.H. Mahmood, M. Sultan, T. Miyazaki, S. Koyama, V.S. Maisotsenko, Overview of the Maisotsenko cycle—A way towards dew point evaporative cooling. Renew. Sustain. Energy Rev. **66**, 537–555 (2016). https://doi.org/10.1016/j.rser.2016.08.022

17. M.F. Habib, M. Ali, N.A. Sheikh, A.W. Badar AW, Mehmood S. Building thermal load management through integration of solar assisted absorption and desiccant air conditioning systems: a model-based simulation-optimization approach. J. Build. Eng. **30**, 101279 (2020). https://doi.org/10.1016/j.jobe.2020.101279

18. J.-H. Lee, J.-Y. Ko, J.-W. Jeong, Design of heat pump-driven liquid desiccant air conditioning systems for residential building. Appl. Therm. Eng. **183**, 116207 (2021). https://doi.org/10.1016/j.applthermaleng.2020.116207

19. M. Sultan, T. Miyazaki, B.B. Saha, S. Koyama, V.S. Maisotsenko, Steady-state analysis on thermally driven adsorption air-conditioning system for agricultural greenhouses. Procedia Eng. **118**, 185–192 (2015). https://doi.org/10.1016/j.proeng.2015.08.417

20. M. Sultan, T. Miyazaki, B.B. Saha, S. Koyama, Steady-state investigation of water vapor adsorption for thermally driven adsorption based greenhouse air-conditioning system. Renew. Energy **86**, 785–795 (2016). https://doi.org/10.1016/j.renene.2015.09.015

21. M. Sultan, T. Miyazaki, S. Koyama, Z.M. Khan, Performance evaluation of hydrophilic organic polymer sorbents for desiccant air-conditioning applications. Adsorpt. Sci. Technol. **36**, 311–326 (2018). https://doi.org/10.1177/0263617417692338

22. M. Sultan, T. Miyazaki, S. Koyama, Optimization of adsorption isotherm types for desiccant air-conditioning applications. Renew. Energy **121**, 441–450 (2018). https://doi.org/10.1016/j.renene.2018.01.045

23. M.H. Mahmood, M. Sultan, T. Miyazaki, Experimental evaluation of desiccant dehumidification and air-conditioning system for energy-efficient storage of dried fruits. Build Serv. Eng. Res. Technol. **41**, 454–465 (2020). https://doi.org/10.1177/0143624419893660

24. M. Sultan, T. Miyazaki, M.H. Mahmood, Z.M. Khan, Solar assisted evaporative cooling based passive air-conditioning system for agricultural and livestock applications. J. Eng. Sci. Technol. **13**, 693–703 (2018)

25. H. Niaz, M. Sultan, A.A. Khan, T. Miyazaki, Y. Feng, Z.M. Khan et al., Study on evaporative cooling assisted desiccant air conditioning system for livestock application in Pakistan. Fresenius Environ. Bull. **28**, 8623–8633 (2019)

26. M. Kashif, H. Niaz, M. Sultan, T. Miyazaki, Y. Feng, M. Usman et al., Study on desiccant and evaporative cooling systems for livestock thermal comfort: theory and experiments. Energies **13** (2020). https://doi.org/10.3390/en13112675

27. K. Nagaya, T. Senbongi, Y. Li, J. Zheng, I. Murakami, High energy efficiency desiccant assisted automobile air-conditioner and its temperature and humidity control system. Appl. Therm. Eng. **26**, 1545–1551 (2006). https://doi.org/10.1016/j.applthermaleng.2005.12.005

28. M.Z. Ismail, D.E. Angus, G.R. Thorpe, The performance of a solar-regenerated open-cycle desiccant bed grain cooling system. Sol. Energy **46**, 63–70 (1991). https://doi.org/10.1016/0038-092X(91)90017-Q

29. G. Zheng, C. Zheng, G. Yang, W. Chen, Development of a new marine rotary desiccant airconditioning system and its energy consumption analysis. Energy Procedia **16**, 1095–1101 (2011). https://doi.org/10.1016/j.egypro.2012.01.175

30. J. Zhu, W. Chen, Energy and exergy performance analysis of a marine rotary desiccant air-conditioning system based on orthogonal experiment. Energy **77**, 953–962 (2014). https://doi.org/10.1016/j.energy.2014.10.014

31. F. Ascione, L. Bellia, A. Capozzoli, F. Minichiello, Energy saving strategies in air-conditioning for museums. Appl. Therm. Eng. **29**, 676–686 (2009). https://doi.org/10.1016/j.applthermaleng.2008.03.040

32. F. Ascione, L. Bellia, A. Capozzoli, A coupled numerical approach on museum air conditioning: energy and fluid-dynamic analysis. Appl. Energy **103**, 416–427 (2013). https://doi.org/10.1016/j.apenergy.2012.10.007

33. S.H. Lee, W.L. Lee, Site verification and modeling of desiccant-based system as an alternative to conventional air-conditioning systems for wet markets. Energy **55**, 1076–1083 (2013). https://doi.org/10.1016/j.energy.2013.04.029

34. K. Daou, R.Z. Wang, Z.Z. Xia, Desiccant cooling air conditioning: a review. Renew. Sustain. Energy Rev. **10**, 55–77 (2006). https://doi.org/10.1016/j.rser.2004.09.010

35. D. La, Y.J. Dai, Y. Li, R.Z. Wang, T.S. Ge, Technical development of rotary desiccant dehumidification and air conditioning: a review. Renew. Sustain. Energy Rev. **14**, 130–147 (2010). https://doi.org/10.1016/j.rser.2009.07.016

36. L. Mei, Y.J. Dai, A technical review on use of liquid-desiccant dehumidification for air-conditioning application. Renew. Sustain. Energy Rev. **12**, 662–689 (2008). https://doi.org/10.1016/j.rser.2006.10.006

37. M. Saghafifar, M. Gadalla, Innovative inlet air cooling technology for gas turbine power plants using integrated solid desiccant and Maisotsenko cooler. Energy **87**, 663–677 (2015). https://doi.org/10.1016/j.energy.2015.05.035

38. O. Amer, R. Boukhanouf, H.G. Ibrahim, A review of evaporative cooling technologies. Int. J. Environ. Sci. Dev. **6**, 111–117 (2015). https://doi.org/10.7763/ijesd.2015.v6.571

39. W.Z. Gao, Y.P. Cheng, A.G. Jiang, T. Liu, K. Anderson, Experimental investigation on integrated liquid desiccant—Indirect evaporative air cooling system utilizing the Maisotesenko—Cycle. Appl. Therm. Eng. **88**, 288–296 (2015). https://doi.org/10.1016/j.applthermaleng.2014.08.066

40. T. Miyazaki, I. Nikai, A. Akisawa, Simulation analysis of an open-cycle adsorption air conditioning system-numeral modeling of a fixed bed dehumidification unit and the maisotsenko cycle cooling unit. Int. J. Energy Clean Environ. **12**, 341–354 (2011). https://doi.org/10.1615/InterJEnerCleanEnv.2012005977

41. D.C. Cassuce, S. Zolnier, P.R. Cecon, M.D.E.F.A. Vieira, Atualização da temperaturas de conforto térmico para frangos de corte de até 21 dias de idade. Eng Agrícola **33**, 28–36 (2013). https://doi.org/10.1590/S0100-69162013000100004

42. M.G.L. Cândido, F.F. Tinôco I de, C. Pinto F de A d, N.T. Santos, R.P. Roberti, Determination of thermal comfort zone for early-stage broilers. Eng. Agric. **36**, 760–767 (2016). https://doi.org/10.1590/1809-4430-Eng.Agric.v36n5p760-767/2016

43. S. Leeson, J.D. Summers, *Commercial Poultry Nutrition* (Nottingham University Press, Nottingham, UNITED STATES, 2009)

44. C.L. Williams, G.T. Tabler, S.E. Watkins, Comparison of broiler flock daily water consumption and water-to-feed ratios for flocks grown in 1991, 2000–2001, and 2010–2011. J. Appl. Poult. Res. **22**, 934–941 (2013). https://doi.org/10.3382/japr.2013-00767

45. J.D. May, B.D. Lott, Relating weight gain and feed : gain of male and female broilers to rearing temperature **1**, 1–4 (n.d.)

46. J.L. Purswell, W.A. Dozier, H.A. Olanrewaju, J.D. Davis, H. Xin, R.S. Gates, Effect of temperature-humidity index on live performance in broiler chickens grown from 49 to 63 days of age, in *ASABE—9th International Livestock Environment Symposium 2012, ILES 2012*, pp. 41–49

47. S.A.S. van der Klein, J.A. More-Bayona, D.R. Barreda, L.F. Romero, M.J. Zuidhof, Comparison of mathematical and comparative slaughter methodologies for determination of heat production and energy retention in broilers. Poult. Sci. **99**, 3237–3250 (2020). https://doi.org/10.1016/j.psj.2020.02.005

48. W. Liu, C.H. Lin, Z.K. Wu, G.H. Liu, H.J. Yan, H.M. Yang et al., Estimation of the net energy requirement for maintenance in broilers. Asian-Austr. J. Anim. Sci. **30**, 849–856 (2017). https://doi.org/10.5713/ajas.16.0484

49. M. Sultan, I.I. El-Sharkawy, T. Miyazaki, B.B. Saha, S. Koyama, T. Maruyama et al., Water vapor sorption kinetics of polymer based sorbents: theory and experiments. Appl. Therm. Eng. **106**, 192–202 (2016). https://doi.org/10.1016/j.applthermaleng.2016.05.192

50. M. Sultan, T. Miyazaki, B.B. Saha, S. Koyama, H.S. Kil, K. Nakabayashi et al., Adsorption of difluoromethane (HFC-32) onto phenol resin based adsorbent: theory and experiments. Int. J. Heat Mass. Transf. **127**, 348–356 (2018). https://doi.org/10.1016/j.ijheatmasstransfer.2018.07.097

51. F. Shabir, M. Sultan, T. Miyazaki, B.B. Saha, A. Askalany, I. Ali, et al., Recent updates on the adsorption capacities of adsorbent-adsorbate pairs for heat transformation applications. Renew. Sustain. Energy Rev. **119**, 109630 (2020). https://doi.org/10.1016/j.rser.2019.109630

52. M. Aleem, G. Hussain, M. M. Sultan, T. Miyazaki, M.H. Mahmood, M.I. Sabir et al., Experimental investigation of desiccant dehumidification cooling system for climatic conditions of multan (pakistan). Energies **13** (2020). https://doi.org/10.3390/en13215530

53. ASHRAE, Handbook of fundsamentals, in *American Society of Heating, Refrigerating and Air-Conditioning Engineers.* Inc., Atlanta, GA, USA (2013)

54. M.H. Mahmood, M. Sultan, T. Miyazaki, Solid desiccant dehumidification-based air-conditioning system for agricultural storage application: theory and experiments. Proc. Inst. Mech. Eng. Part A J Power Energy **234**, 534–547 (2020). https://doi.org/10.1177/0957650919869503

55. J.P. Donald, How poultry housing can reduce stress and optimize performance (2018). https://www2.biomin.net/hr/articles/how-poultry-housing-can-reduce-stress-and-optimize-performance/. Accessed 15 Nov 2020

Part IV
Deterministic and Risk-Aware Short-Term Scheduling of Smart Grids

Chapter 17
Emerging Business Models for IoT-Based Smart Distribution Systems

**Farid Moazzen, Omid Shahhoseini, Hamidreza Arasteh,
Seyed Masoud Mirsadeghi, and Farkhondeh Jabari**

Abstract Recently, Internet of Things (IoT) has been developing in several social areas such as energy, transportation, health, etc., through the physical and virtual connection of objects using the communication and information technologies. In the IoT technology, it is possible to provide different services with high reliability and security levels based on data identification, recording, storing, and processing as well as communication of objects. Meanwhile, traditional power systems are changing towards smart grids to overcome problems regarding the one-way data transmission, energy losses, security and reliability of the system, demand increases, Distributed Generations (DGs) penetration, changing nature of electricity consumers, etc. Moreover, the smart grids use several equipment for monitoring and control of the network. The IoT development as the reliable, accurate, and fast communication and information infrastructure, has led to the belief that the architecture of the future smart distribution networks would be based on this technology. It will make a huge difference in distribution networks due to the use of various equipment such as sensors, actuators, and smart meters. Not only it will cause some technical changes, but also cause structural changes such as stakeholders and their role and relationships, as well as their economic issues. Considering these technical and structural concepts, the existing businesses in distribution networks will be changed. Therefore, new business model canvases should be developed to satisfy the upcoming requirements based on the new business environment. Although several remarkable studies have been conducted to investigate the IoT technology and its applications, its business models have not been developed. This chapter aims to investigate the IoT-based smart distribution grids, and also identify the emerging players and their roles, as well

F. Moazzen
Faculty of Electrical & Computer Engineering, Tarbiat Modares University, Tehran, Iran

O. Shahhoseini (✉) · H. Arasteh · F. Jabari
Power Systems Operation and Planning Research Department, Niroo Research Institute, Tehran, Iran
e-mail: oshahhoseini@nri.ac.ir

S. M. Mirsadeghi
Jundi-Shapur University of Technology, Dezful, Iran

461

as their communications in the new environment. Finally, the appropriate business model canvases will be proposed for the future IoT-based smart distribution grids.

Keywords Internet of things (IoT) · Business model canvas · Smart distribution systems

17.1 Introduction

Nowadays, technological advances and subsequent changes in various aspects of life have been accelerated as a result of information technology. The growing desire for globalization necessitates a better understanding of "change" and the "future" for governments, businesses, organizations, and people. It is clear that choosing the right path, which ultimately leads to maximizing opportunities and minimizing risks and challenges, depends on better understanding the current situation and examining future trends.

In the recent years, different definitions have been provided for the business model, in which the model components have been identified and extracted according to each definition. In general, the business model shows how to gain profit and maintain revenue stream in a period of time. For example, identifying and evaluating a business model alongside a business plan gives the investor and lender a sufficient power to be secure against the uncertainties. By presenting a business model, business plans can be better justified. In this way, issues such as identifying the business model components as well as the types of classifications and patterns available to create a business model, evaluating the business models, and examining the impact of innovation on the structure of business models are important and should be studied.

Nowadays, the increase in electricity demand has caused the power companies to face many problems such as electricity losses, energy shortages, and environmental pollutants [1]. One of the most effective ways to overcome these challenges is to use smart grids, bringing very high profits and efficiency [2]. Smart technologies consisting of subscribers, equipment and communications, modernize distribution networks aiming to supply demand in a reliable manner with less emission footprints. Smart technologies have the potential to bring about fundamental changes in the generation, transmission, distribution, and use of electricity along with economic and environmental benefits that ultimately lead to meeting customer needs and the availability of reliable and sustainable electricity. On the other hand, due to the capabilities of smart grids, the network operator can use the gathered information to make decisions in critical situations and prevent unwanted outages.

In smart grids, IoT has recently emerged as a new communication platform. In fact, smart grids with IoT capabilities make it possible to monitor and control their status. It should be noted that the future smart distribution networks will be based on IoTs that follow their own business models. More precisely, the Internet of Things can be defined by the interaction and cooperation of objects in different environments in order to achieve a common goal by which the physical world becomes a large

information system. Therefore, objects can be intelligently identified based on their unique identification and specific internet protocol (IP), and also send and receive data. In this case, they also have access to information collected by other objects. The information will be visible by various smart devices such as mobile phones, computers and tablets. The design of various devices with the ability to communicate wirelessly to track and control via internet and applications, expresses the concept of IoT.

The connection of objects not only changes their nature but also changes their relationships, positions and the way in which the interconnected objects are affected, and creates a new space with new dimensions. This space will bring about structural changes in any area of expertise and thus drastically transform traditional businesses and related models, meaning that the development of new business models will be crucial. The IoT capabilities in sending, receiving and processing data have convinced almost all researchers and experts that this technology will be a dominant and reliable communication platform.

In this chapter, definitions of business models, their components and types of existing models are presented. Further, IoT topics, applications, and key concepts, such as architecture, operating systems, platforms, data processing, storage, and security, are discussed in detail. Finally, related businesses are identified. Overall, identifying and explaining the emergence of new technologies and their effects on the business environment for application in smart distribution networks has been discussed.

17.2 Definition of Business Models

Researchers have considered several approaches to define a business model, including resource-based, activity-oriented, economic, strategy-oriented and networked approaches. It should be noted that a combination of the aforementioned approaches has been considered by many researchers.

(A) Resource-based approach

Some believe that this business model is based on the internal resources of the company and these resources create the capabilities and competencies of an organization. Ref. [3] considers this model as a company's approach for creating and using its resources to provide better value for its customers than competitors.

(B) Activity-based approach

The activity-based business model is based on a set of activities in the form of a process. Betz stated the business model as a summary of how an organization's inputs are converted into value-added outputs. In this category, some researchers have referred to value chain, mainstream production or activities such as marketing [4].

(C) Economic approach

In this approach, the business model is defined based on company's profit and economic justification.

(D)   Network approach

Because in today's world, the value creation process takes place across corporate boundaries and as a network, the organization interacts with multiple actors in its business. Ref. [5] considers the business model as the structure and content of transactions between the central company and the trading partners.

(E)   Strategy-oriented approach

In this approach, in addition to the internal environment of the company, the competitive environment and strategic options of the organization are emphasized according to the opportunities in the market.

In fact, although the concept of business model has been studied by several researchers over the years, no single definition has been provided. However, based on the literature review, definitions of the business model are provided in Table 17.1.

Organizations need to know more about the factors affecting business models and provide a framework for such models. The benefits of using these models can be mentioned as follows:

1. Determining the exact target markets and identifying the characteristics and needs of customers
2. Providing products and services tailored to the needs of customers to satisfy them
3. Finding suitable communication methods with customers and using appropriate communication channels
4. Creating a balance between the cost and revenue of organization
5. Determining the degree of success in achieving financial and non-financial goals
6. Identifying the main capabilities and competencies of the organization and focusing more on them
7. Determining the structure of the value chain for the company
8. Determining the best business partners.

17.3   The Components of the Business Model

The business models that have been presented so far, from different perspectives and based on their intended goals, have considered different factors. That is why the main framework and a wide variety of components for business models have been proposed. Among these, the most frequent components of business models are as follows:

1. Proposed Value
2. Profitability Model
3. Customer Relationship

Table 17.1 Different definitions of business model from the perspective of researchers in this field

Refs.	Researcher	Business model definition
Timmers [6]	Timmers	An architectural business model for product, service, and information flow includes a description of the various business actors and their rules, a description of the potential benefits to business actors, and a description of revenue sources
Weill and Vitale [7]	Weill and Vitale	The business model introduces a description of the plans and relationships between customers and suppliers that represent the mainstream of production, information, money and key beneficiaries
Amit and Zott [5]	Amit and Zott	Business model is the design of the relationship between the content, structure and governance of the organization that creates value through the use of business opportunities. In fact, the business model is a system of interconnected activities that goes beyond the main environment of the company and shows the relationship between its boundaries and the external environment
Chesbrugh and Rosenbaum [8]	Chesbrugh and Rosenbaum	Business models relate technical capabilities to real economic values by creating innovative zones. In fact, the business model shows how a company creates value by identifying where it is in the value chain
Betz [4]	Betz	Business models are a summary of how an organization's inputs are converted into value-added outputs

<div align="right">(continued)</div>

4. Partner Network
5. Main Activities
6. Market Sections.

Table 17.1 (continued)

Refs.	Researcher	Business model definition
Faber et al. [9]	Faber et al.	The business model of a network of companies aims to create value through the establishment of technology opportunities. These companies need to adapt and balance in technical areas, users, organization and financial requirements
Rappa [10]	Rappa	A business model is a way of doing business that is done by a company for its own survival. In other words, it is the same way of generating income
Afuah [3]	Afuah	A business model is a set that shows what activities a company should do, how and when to use its resources to create surplus value for the customer and gain a good position
Shafer et al. [11]	Shafer et al.	The business model is a picture of the basic logic and strategic choices in order to create and gain value by a company in a network
Nordlund and Teece [12]	Nordlund and Teece	The business model reflects the management assumption about what customers want, how they want it and how the company meets these needs and the amount of payment
Osterwalder and Pigneur [13]	Osterwalder and Pigneur	The business model describes a company's logic in how value is created, presented, and acquired
Demil and Lecocq [14]	Demil and Lecocq	Business model is the method of using activities and resources to ensure the continuity of activity and growth of the company
Meier et al. [15]	Meier et al.	The business model describes the practical model for value creation, revenue generation, and communication between customers and suppliers

Table 17.1 (continued)

Refs.	Researcher	Business model definition
Gao et al. [16]	Gao et al.	Business model is a way of showing how partners work together
Lin et al. [17]	Lin et al.	The business model is a set of organizational strategies for creating and managing an organization that includes different items such as revenue model, high level of business processes and alliance
Leitao et al. [18]	Leitao et al.	Business models are formed in response to specific competitive conditions and describe how companies generate revenue according to its value chain and its interaction with suppliers, customers and other partners who have complementary competencies
DaSilva [19]	DaSilva	The business model is the logic of creating value for the company and includes identifying opportunities, gaining competitive advantage and creating more value in the market and dynamic environment

Among the models offered, the Osterwalder and Pigneur model is a general, flexible and practical model for most industries [13]. The nine components of this model reflect how an organization gains profit. In fact, these components cover the four main areas of business: customer, value, infrastructure and financial sustainability. The components of this model are described below and the dimensions of the problem will be clarified by providing an example.

17.3.1 Customer Section

Each organization serves one or more customer sections. In fact, this component defines the different groups of individuals or organizations that the company intends to reach and serve. Customers are the key component of the business model. The organization must intelligently decide which parts it wants to serve or ignore.

Table 17.2 Classification of business model channels

Channels			Channel phases				
Owned by the company	Direct	Web sales	Awareness	Assessment	Purchase	delivery	After sales
Owned by partner	Indirect	Company stores	Increase the level of customer awareness	Help evaluate the value proposition	How to buy products/services	Value delivery	Provide after-sales service

17.3.2 Proposed Value

The organization seeks to solve customer problems and meet their needs through Proposed Value. The Proposed Value component describes a package of products and services that are value to a particular customer. Value is the reason why a company is preferred by the customers. Each Proposed Value consists of a selected package of products or services that meet the needs of a specific section of customers. Some of the Proposed Value are innovative and distinctive. However, some may be similar to current market offers but have additional features and distinctions. Values may be either quantitative, such as price, speed of service, reliability or loss reduction in electricity distribution sector, or qualitative, such as customer experience.

17.3.3 Channels

This component describes how the company communicates and accesses its target customer sections in order to deliver the desired Proposed Value. Distribution and sales communication channels are the interface between a company and its customers. Channels are the point of contact with the customer and play an important role in the customer experience. The business model channel classification is summarized in Table 17.2.

17.3.4 Customer Relationship

The customer relationship component describes the types of relationships that the company establishes with specific sections of customers. These relationships can range from face-to-face communications to automated support services. The customer relationship part of the business model has a profound impact on the overall customer experience.

17.3.5   Revenue Stream

The revenue stream component represents the revenue that the company earns from each customer section. In fact, Proposed Value that are successfully delivered to customers lead to revenue streams. The company should know what value each part of the customer is really willing to pay for. Each revenue stream may have different pricing mechanisms, such as fixed prices, bargaining, auctions, market-based, quantity-based, or return management.

The business model can include two different types of transactional or repeatable revenue streams. Transactional revenue is the result of a single customer payment, and recurring revenue is the result of repeated payments by customers for a Proposed Value.

17.3.6   Key Resources

Every business model needs key resources. These resources enable the company to create and deliver Proposed Value, reach the market, maintain relationships with customer sections, and ultimately obtain revenue. Depending on the business model, different key resources are required. Key resources can be human resources or physical, financial, and spiritual. These resources can be owned or leased by the company or provided by partners.

17.3.7   Key Activities

Every business model requires a number of key activities. These activities are the most important steps that a company must take to have a successful operation. Like key resources, key activities vary depending on the business type.

17.3.8   Key Contributions

Companies choose partners for a variety of reasons, which means partnerships are the basis of many business models. Companies form alliances to optimize the business models, reduce risks, or gain resources. There are four different types of partnerships:

- Strategic alliances between competing companies
- Strategic partnerships and competitors' cooperation
- Joint ventures to create new businesses
- Buyer–supplier relationships to ensure supplies are met.

Table 17.3 Overview of the business model of Osterwalder and Pigneur [13]

Key partners	Key activities	Proposed value	Communication with clients	Customer section
	Key resources		Channels	
Cost structure			Revenue stream	

17.3.9   Cost Structure

The cost structure describes all the costs that the business model components entail. This component describes the most important costs incurred during the implementation of a business model. Creating and delivering value, maintaining customer relationships, and generating revenue result in expenses. After defining key resources, key activities and key contributions, such costs can be easily calculated. Cost structure can have fixed cost characteristics or variable cost. Of course, it is necessary to determine the business model type in terms of cost-oriented or value-oriented. Cost-oriented business models focus on minimizing costs. The goal of this approach is to create and maintain the most agile cost structure possible by maximizing activity automation and extensive outsourcing. But in a value-based structure, the company pays less attention to the cost aspect and its main focus is on value creation. High Proposed Value and dedicated services are the hallmarks of value-driven business models.

The nine components of a business model form the basis for an easy-to-use tool, which its general outline is presented in Table 17.3.

In order to identify the classifications presented in the business model literature, business models based on the classification presented by Osterwalder and Pigneur in the form of five categories of business models including "segregated", "Follow-up", "multidimensional platforms", "Free" and "Open" are discussed [13].

17.4   A Variety of Business Models

17.4.1   Segregated Business Model

According to this view, a company's businesses fall into three completely different categories: customer relationship businesses, product innovation businesses, and infrastructure businesses. Each one has its own economic, competitive and cultural principles and requirements. It is possible for all three types of businesses to exist together in the same company. But in order to avoid conflicts or adverse interactions, it is ideal to separate them into independent institutions. The economic, competitive and cultural pros and cons of each item are listed in Table 17.4.

Table 17.4   Three main types of business models

	Product innovation	Customer relation management	Infrastructure management
Economy	Early market entry, higher pricing and gaining more market share. Speed is the key factor	High customer acquisition costs, trying to make money from customers. Economic savings due to range are a key factor	High production costs, high production volume. Economic savings from scale are a key factor
Culture	Admissions are low. Many small actors flourish and grow	A few big actors come in	A few big actors come in
Competition	Focus on employees, creative elites	Highly service-oriented, customer-focused	Focus on cost, standardization and efficiency

17.4.2   Follow-Up Business Model

The subject of follow-up business models is the low sales of a large number of items. The focus of this business model type is on offering a large number of products, that are sold from time to time, with a specific and limited audience. The utilization of a follow-up business model requires strong platforms to make products easily accessible to a specific and limited audience and interested buyers. Common examples of this business model are YouTube and Facebook.

17.4.3   Free Business Model

In a free business model, at least a significant portion of the company's customers benefit from a free offer. Customers who pay no money are covered by another part of the business model or customer. Getting something for free has always been an attractive Proposed Value. Demand generated at zero price is more than that provided at other prices. In recent years, the number of free offers, especially on the Internet, has increased significantly. There are several templates that allow you to integrate free products and services with your business model. Some of these free templates, such as ads based on the template discussed in the multidimensional platforms, are well known. The second model is the Freemium (free and premium) model, which provides basic and introductory services for free and charges for additional services. This pattern has become increasingly popular with the increasing digitization of products and services offered through the web. The third model is the prey and hunting model, in which a free or low-cost offer is offered to encourage customers to repeat the purchase.

17.4.4   Open Business Model

Companies can use open business models to create and acquire value through systematic partnerships with partners outside the organization. Creating and gaining value in this way is possible in two ways:

- Exploitation of external ideas within the company during the "Outside-to-Inside" process.

Outside-to-Inside innovation occurs when an organization incorporates ideas, technology, and intellectual property outside the organization into its development and commercialization processes. Starting companies with strong brands, distribution channels and customer relationships are well-suited to the open Outside-to-Inside business model. They can dramatically improve the quality of current customer relationships by relying on external sources of innovation. On the other hand, acquiring innovation from external sources requires the financial sources. Therefore, the company must increase the internal productivity of research and development by reducing the time required to supply the market.

- Presenting ideas or unused assets inside the company to outside during the "Inside-to-Outside" process

In Inside-to-Outside innovation, organizations transfer or sell ownership of their unused technologies and assets. Some R&D outputs that remain unused within the company for strategic or operational reasons may be of great value to organizations in other industries. Usually organizations with significant domestic R&D operations have a lot of unused knowledge, technology and intellectual property. These companies do not use some of their assets to focus on their core business, and as a result these assets, which can be valuable for other applications, remain unused. Such businesses are good candidates for an open Inside-to-Outside business model.

17.5   IoT Ecosystems

17.5.1   The Concept of the Internet of Things and Its Application

The International Telecommunication Union defines IoT as follows: There is a connection for anyone or anything at any time and place. Figure 17.1 shows the different dimensions of IoT [20].

The information flow required for IoT can be discussed in four steps, which are:

1.   Data collection
2.   Transfer of selected data through communication networks
3.   Data Evaluation and estimation
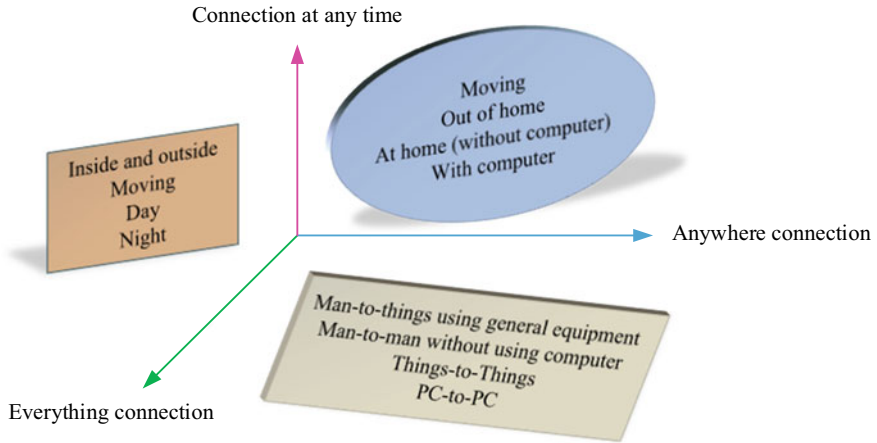
Fig. 17.1 The concept of IoT
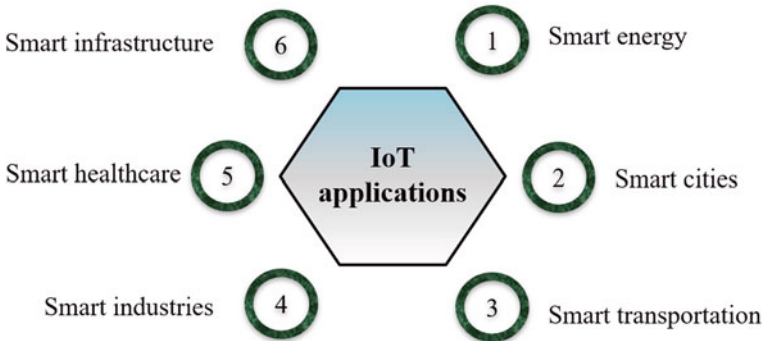
Fig. 17.2 The IoT applications [23]

4. Response to the created needs.

IoT applications are very broad and not only include the medical, health and transportation fields, but also encompass smartness in various areas. The use of IoT in smartness is very diverse and can appear in different industries. Some researchers believe that the application areas for IoT are very wide, as shown in Fig. 17.2. [21, 22] (Fig. 17.3).

17.5.2 Different Types of IoT

The three main types of IoT are as follows [20]:

Fig. 17.3 Smart grid architecture [24]
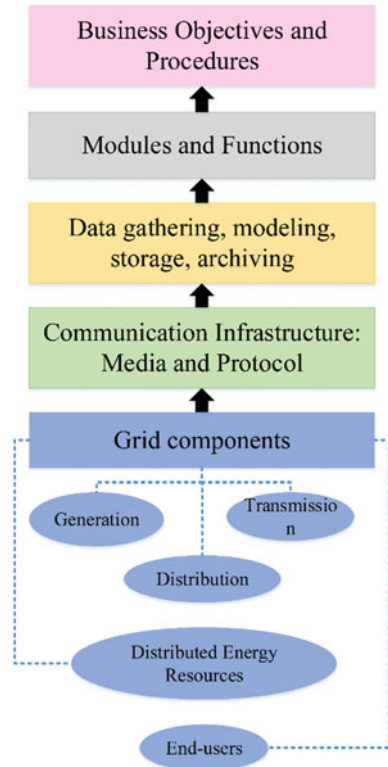
- Industrial IoT: It means the application of this technology in industrial fields and its use as an smart industrial network.
- IoT for Consumers: Unlike industrial environments, the consumer IoT does not need to be real-time. At the same time, the certainty of the answer is not important and its structure is based on the interaction of the device with humans. In this type of IoT, the connection is usually client/server and the data is in a continuous flow with high volume.
- Machine-to-machine (M2M) connection: In M2M systems, the devices are connected to each other one by one. Practically, in this type devivices do not exchange a lot of data and consequently there is no place to store the data.

17.5.3 IoT Architectures

The wide applications of IoT has a tremendous impact on human life. For this purpose, IoT needs a coherent and coordinated structure and architecture. It should be mentioned that, from the viewpoint of researchers, experts, and large corporations, IoT architecture and infrastructure are more important than its implication.

IoT helps to develop new businesses that are driven by technological solutions. Putting aside some business considerations, it is obvious that current solutions cannot meet all the IoT needs. In the field of communication and management, existing devices do not have the necessary functionality for IoT. Lack of coordination and compatibility between existing governance models creates problems in the field of privacy, security of individuals and companies, and creates legal consequences in terms of legal vacuum. But if there is a coherent architecture, it can provide a solution for existing designs. In fact, IoT has the concept of providing services and creating communication levels and is expected to be applicable in various fields. As a result, an IoT reference model is needed at first to implement such a view (A model that can create a common understanding and language between all devices equipped with IoT). The most populare architectures are:

1. IoT-A architecture
2. MGC[1] architecture
3. Five-layer SOA and compose architectures
4. WOA[2] architecture
5. Architecture proposed by ITU
6. Architecture proposed by Cisco [24]
7. Four-layer SOA architecture [25]
8. Ericsson proposed architecture
9. Architecture proposed by Harbinger
10. WSO2 architecture
11. Korean architecture [26]
12. CCSA[3] architecture.

17.5.4 Operating Systems on IoT

In general, IoT devices are divided into two categories in terms of efficiency and capability. The first category is unlimited devices that can run normal operating systems such as Linux and Windows (High-end) such as RaspberryPi due to sufficient resources and appropriate specifications. The second category include devices with limitations in Processing power (limited amount of RAM and ROM) and limited power, can not run normal operating systems (Low-end) such as Arduino, Econota, Zolertia.

---

[1] Embedded Devices Gateways Cloud.

[2] Web Oriented Architecture.

[3] China Communications Standards Association.

17.5.5   Data Storage

An important part of IoT is data processing when needed (not always). For this possible processing, the data must be stored somewhere. Due to conditions such as the existence of various data from different sources, huge data volumes, low-level data with poor semantic relevance and inaccurate data, measures should be taken to store them. Due to the above issues, various data modules have been developed and used in IoT. In general, IoT data modules include the following [27]:

- Data collection and integration module
- Data storage module
- Data management module
- Data processing module
- Data mining module
- Application optimization module.

17.5.6   IoT Platform

In addition to nodes and networks of IoT, data needs to be processed before it reaches the user or another node. Thus, an interface between IoT elements is required to perform these tasks. This interface is called a platform. In general, there is no clear definition for a platform. The IoT platform is divided into two parts: the software and the hardware platforms. The hardware platform includes the hardware part of the nodes and related items. The data received from the nodes is transmitted by the network to the software platform. This data is transmitted to the user or another node after processing by the software platform. Usually wherever the term IoT platform is mentioned, it mostly refers to a software platform. In fact, anything between two nodes or nodes with the user that is not performed by neither the node nor the user, is the responsibility of the IoT software platform. Therefore, the other layers are part of the software platform.

17.5.7   IoT Data Processing

One of the issues that needs to be addressed in some IoT applications is big data processing or IoT data processing. In the future, a large number of devices, including High-End and Low-End, will connect to the Internet and generate big data. This data can be categorized into three dimensions: volume, variety and velocity. In applications such as smart city control, health, etc., that it is necessary to extract results from data and allowed to do so in terms of privacy, the issue of dealing with big data and processing it to get results is important.

17.5.8 Internet Network

One of the most important parts of IoT is the connection of objects with an independent identity to the Internet. To do this, solutions should be created to connect all devices, both Low-End and High-End. The next issue is the number of devices connected to the Internet. As the number of devices connected to the Internet is increasing, this imposes a large volume of data transmismitted via the Internet. Hence, the infrastructure network should be able to ensure the secure data transfer. Data received from some IoT devices, such as sensors, should be processed if necessary. This requires servers with special capabilities to be able to process data volumes quickly and, if necessary, as soon as data is entered. Thus, servers should use methods such as distributing their various components and connecting these components over the network.

According to the explanations, the network used in IoT can be divided into the following three parts [28]:

- Network of nodes connecting to the internet or sensing network
- Internet infrastructure network or delivery network
- The network used between the components of the data processing system or analytics network.

17.5.9 IoT Security

One of the main problems in IoT security is malicious activities or cyber attacks. In fact, many reasons including the limitations of objects used in IoT (such as the lack of enough space for saving data, their programmabilities, etc.), the presence of numerous sensors, operators, and physically accessible objects, the wireless connections of objects in IoT, and the openness of the system, make IoT-based systems the target of security attacks. Backdoors that are entered into the system by vendors and through object updates are one of the most important concerns in IoT. Identifying and naming things is also a crucial issue. Moreover, the use of wireless sensor networks in IoT can also cause security problems. The important challenges and main research areas in the field of IoT security are listed below:

- Identifing and locating objects on IoT
- Authentication and access permission
- Privacy
- Existence of trust
- Security protocols and lightweight encryption systems
- Software vulnerabilities
- Vulnerability to malware.

17.5.10   IoT Technologies

In IoT, various technologies have been proposed so far in order to communicate between objects and the Internet. The separation of IoT technologies seems difficult due to the interdependence and complexity of technologies and tools. However, fog and 5G computing technology can be mentioned as the new technologies of IoT. After that, we can refer to fiber optic and satellite technologies that are used for data transfering. Communication technologies are divided into short and long-range communications, sensor-related technologies, location technologies, detection technologies, wireless sensor network technologies, and finally virtualization technologies as complementary to IoT.

17.5.11   Suggested IoT Ecosystems

The Internet of Things, known as the new industrial revolution, has also transformed the interactions between governments and the world around them with the virtual and technological worlds due to changes in people live, work, entertain and travel patterns. The interaction between various elements and objects, resulting from IoT, lead to complex relationships with many actors and a concept called ecosystem that can be adopted in complex situations. Suggested ecosystems for IoT are as follows:

- IDC proposed ecosystem
- CompTIA proposed ecosystem
- BI Intelligence proposed ecosystem
- IEEE and EricssonProposed Ecosystem [29, 30]
- Ecosystem from IoT Tree of Life proposed by ARM [31]
- Postscapes proposed ecosystem.

17.6   IoT-Based Smart Distribution Grid

The Internet of Things is expanding in all areas of society, including energy, transportation, manufacturing, health, etc., through the physical and virtual connection of objects and the use of existing and evolving communication and information technologies. The existence and development of IoT technology as a safe, fast and more accurate platform compared to other technologies, has strengthened this belief and opened a variety of research and engineering paths for researchers and engineers.

17.6.1   Introducing Smart Grid

As the energy demand increased, power companies faced many problems, including electricity losses, energy shortages, and environmental pollutants [1]. Power distribution systems should be smarter because of major reasons such as increasing demand for electricity, expanding the use of modern communication and information technologies in the electricity industry, inefficiency of network capacity development, restructuring in the electricity industry, reducing dependence on fossil energies, environmental issues, penetration of renewable energy sources and energy storages [32].

Since there is still no standard and precise definition of smart grid, smart grid is typically defined as a system that allows power companies to remotely control and command grid equipment in a real or near real time. In smart grid, by establishing communication between grid components and consumers with software platform, in addition to two-way data transfer from the grid to the consumer and vice versa, energy flow is also transferred bi-directionally between the consumer and the grid [33]. The US Department of Energy has introduced the following features for smart grids:

- Ability to actively participate in consumers
- Ability to adapt the grid to a variety of products and storage of electrical energy
- Providing the necessary power quality for different levels of consumption
- Applied optimization of equipment and efficient operation
- Ability to troubleshoot and healing, and stability against possible damage
- Telecommunication and cyber security [33].

17.6.2   Smart Grid Architecture

The Smart Grid Architecture Model (SGAM) is used to manage complexities in the smart grid. This architecture includes domains, areas, and layers of collaboration. Each part of this architecture is explained as follows [34].

Domains consider the energy conversion chain and include the following.

(1) Generation (both renewable and non-renewable generation)
(2) Transmission (infrastructure and organizations for long-distance power transmission)
(3) Distribution (infrastructure and organizations for electricity distribution to customers)
(4) Distributed Energy Resources connected to the distribution networks
(5) Customer premise (producer and final consumer of electricity, including industrial, commercial, residential facilities, and production in the form of photovoltaics, storage in electric vehicles, batteries, and small turbines).

The hierarchy of power system management and control in smart grid architecture varies with zones, including the following:

1. Process (physicals and chemical transfer of energy and equipment required)
2. Field (equipment for protection, control, and monitoring of power system processes)
3. Station (geographical aggregation level for equipment area, data aggregation)
4. Operations (management and control operations of the power system in the relevant area)
5. Economic organizations (Enterprise) (processes and infrastructure, for example, asset management, staff training, customer relationship management, billing)
6. Market (energy, trade, wholesale, retail).

Finally, layers of collaboration are defined in the smart grid architecture model as a major requirement for distributed systems. Layers of collaboration, encompasses various sections such as business (Business View on Smart grid information Exchange), functions (use of functions and services independent of their physical implementation), information (object information or data model for interoperability), communications (protocol for the transfer of information between equipment) and physical components (power system equipment, protection and control devices, control center infrastructure and network) [34].

17.6.3 IoT-Based Smart Distribution Grid

The Internet of Things is a new concept in information and communication technology, in which objects and equipment are connected to the Internet and can be controlled and managed by applications on smartphones and computers. Assuming that the objects and equipment mentioned are the objects and equipment of the distribution grid, the IoT-based smart distribution grid will emerge as the most modern smart distribution grid [20].

17.6.4 IoT-Based Smart Grid Architectures

Existing architectures for IoT-based smart grids include:

(1) Three-layer architecture: the IoT-based three-layer smart grid architecture is based on IoT features. This architecture consists of three layers of perception, network, and application.
(2) Four-layer architecture: a four-layer architecture for IoT-based smart grids is based on smart grid information features and communication systems. This architecture consists of terminal layers, field network layer, telecommunication layer, and main central system layer.
(3) IoT-based smart grid architecture for energy efficiency: improving energy efficiency in buildings is an essential aspect of smart grids. Smart energy is an important research topic in IoT. The four objectives of implementing

this system include energy-saving, mobile control and monitoring, automatic location-based control, and the use of a cloud computing platform for data storage and computing.

(4) Web-based architecture for IoT-based smart grids: One of the proposed architectures for IoT-based smart grid is web-enabled smart grid architecture. In the Web of Things, the web browser acts as an interface to the services required by IoT.

(5) The latest measurement architecture for IoT-based smart grids: The latest smart gauge meter is the closest to home, that is, the part that interacts with consumers. This architecture has three main components: a network of sensors and operators, server, and user interface.

17.6.5 IoT-Based Smart Grid Communication Infrastructure

The communication infrastructures of smart grid include Home Area Network (HAN), Neighborhood Area Network (NAN), and Wide Area Network (WAN). Figure 17.4 shows the smart grids based on the infrastructure of these three networks [35].
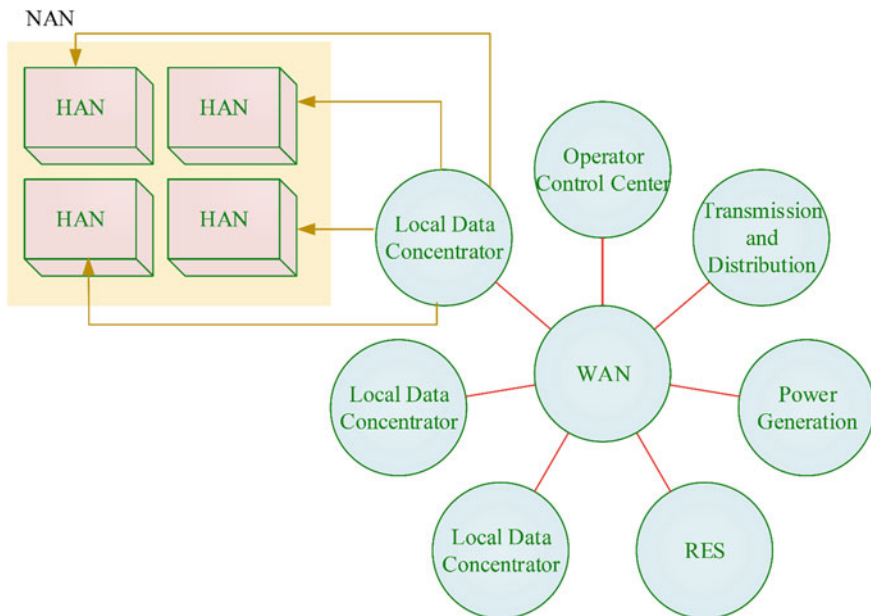

Fig. 17.4 Smart grid communication infrastructure [35]

17.6.6 IoT Applications in Power System Distribution

In the following, the applications of IoT in the smart distribution network are discussed. These applications are new specifications and features added to the traditional distribution network which build the IoT-based smart distribution network.

(1)   Management of electric vehicles

Electric vehicles can be used as energy storages in the IoT-based smart distribution network. These devices provide environmentally friendly transportation by reducing carbon dioxide emissions. Efficient energy transfer between electric vehicles and smart grids requires exchanging information between electric vehicles, charging stations, and infrastructure.

(2)   Integrated Distributed Energy Resources (DERs)

With the expansion of the installation and operation of renewable energy generators such as photovoltaic cells and wind turbines, these resources are gradually being integrated with the power grid. Renewable energy production centers are distributed throughout the power grid, and their production depends on the location and climatic conditions. This poses challenges to the predictability and reliability of production resources. The Internet of Things predicts the availability of energy in the near future with the help of wireless sensors and by collecting real-time weather information from sensors. The Kalman filter is used to estimate conditions in IoT-based smart grids. In this case, IoT is used to sense, estimate, control, and aggregate energy resources [36].

(3)   Smart monitoring of electricity distribution network

Monitoring, Protection, and Distributed control Systems have made it possible to access power grid information. Monitoring systems can be based on IoT. In the monitoring system, the Phasor Measuring Device (PMU) is used as a network information acquisition device, and the control center can automatically and manually control and protect the network with network distributed information by analyzing the information received from this device.

(4)   IoT-based power system theft detection

Electricity theft is a major problem in the grid worldwide, which is illegal and should be banned. Electricity theft means using electricity without any contract with the supplier. In this method, in order to eliminate power theft, its location is determined so that the necessary actions can be taken against the violators.

(5)   Smart distribution post

Due to the increase in distributed generation, there is a need to increase component information in medium voltage (MV) and low voltage (LV) networks. Several MV/LV smart posts have been designed to manage fluctuations while maintaining network quality and reliability. These models are built to overcome specific problems of distribution networks such as voltage harmonics, resonance, and peak load reduction.

(6)   Smart Street Lighting

Despite the countless brightness of passage, smart systems can affect sensors and identify the presence of individuals or vehicles to a large extent in reducing energy consumption.

(7)   Energy Storage

Renewable energies play an effective role in supplying energy due to efficiency and cost-effectiveness, and their use is increasing. Despite this process, maintaining the balance between supply and demand is a constant challenge for renewable energy providers, and the variable nature of this type of energy is an obstacle when aggregated with the network. Renewable energy sources are not able to compete with fossil fuels in reliability due to periodic production. To increase the stability of power supply from renewable energies, providers of this type of energy are equipped with Internet-based energy storage systems. Additional energy obtained from renewable sources such as solar, is stored per day. This stored energy is used whenever the demand is greater than generation or the frequency need to be adjusted. Among these systems, the Solo Energy and BYD storage system can be referred.

(8)   Demand Side Management

Demand Side Management (DSM) represents the interface between energy departments and energy consumer equipment with the aim of reducing the demand peak in the network, minimizing casualties, and increasing the use of energy storage. Internet-based management platforms (with smart energy management function at point consumption) are necessary for the successful implementation of DSM applications. In demand management, there are various options such as discounts, stimulus and motivation factors to save costs.

(9)   Interactive effects of AMI

AMI, as an infrastructure platform, contains five main station sections, a communication channel, data collection terminal, power measurement, and auxiliary equipment. This system provides a smart architecture with an automated two-way flow between smart electrical measurements, other terminal equipment, and power companies. This system can be used to support real-time acquisition, measure and analyze the electrical conditions of users as well as sending data and subjects through the communication layer. Users can be informed of their real-time usage of electricity, and using the reference price, select a wise choice of energy consumption. Meanwhile, power network companies can analyze the status of electricity and provide timely and accurate data for managerial decision making and investment analysis. This important technology is a modern marketing backup and a vital part of the smart grid.

(10)   Using IoT in wind turbines and solar cells

    (A)   Using IoT and mainly through the Wireless Sensor Network (WSN), wind data can be collected, and the output variation can be predicted in real-time as well. Through a wireless sensor network, the monitoring

center records real-time wind turbine information and sends real-time collected data to the prediction server. The result from the predictive server processing is transmitted to the wind power station and can also be transferred to the timetable server. The timing server welcomes the prediction results at the distributor station.

(B)   With the development of IoT, sensors can be installed on solar panels so that benefits such as real-time monitoring on status, real-time reforms and predict analysis, are achievable. An Internet sensor can control specific panel parameters such as energy output, temperature, tilt angle, and the original direction. These details provide the ability to monitor and modify panels to solar farms. Through real-time monitoring, the solar farm manager can see and resolve the problem in the panels with the aim of retaining the efficiency.

(11)   Asset Management

Nowadays, network operators have limited access to network assets, because only access to part of key assets (such as active power, reactive power, voltages and currents). This results in limiting operators in full understanding of conditions, analyzing problems and prediction of situation [37]. The electricity network assets are wide-scale, therefore, it needs abundant information to be managed. With this in mind, internet technology can be used widely in asset management.

(12)   Monitor Transformer Parameters

The architecture of the Master Secondary Sub-station (MSS) smart grid is shown in the IoT platform in Fig. 17.5. This system shows the monitoring of the Internet platform for the transformer. The main idea of this plan is to collect transformer information from the post (Fig. 17.6).

(13)   SCADA-based IoT integration with fog for Distribution Automation

The Distribution Automation (DA) is part of the smart grid that refers to the functional automation of the entire distribution system and is in fact a combination of SCADA and information-related information programs. Distribution Automation can combine local automation, remote control equipment, and central decision making with a flexible and cost-effective operating architecture to maintain the integrity of the distribution system characteristics of the power distribution system. Application of sensor in distribution automation includes:

- Smart measurement for consumer monitoring and control
- Line sensors for monitoring voltage resources and flow lines
- Smart electronic equipment for monitoring temperature, load, voltage, flow, and power sources.
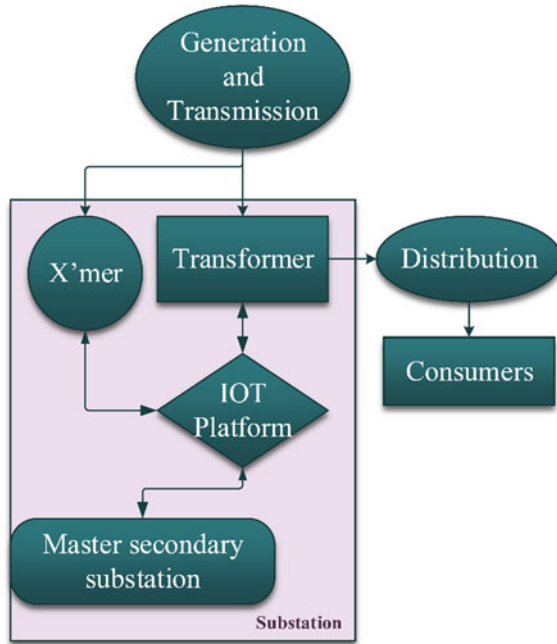
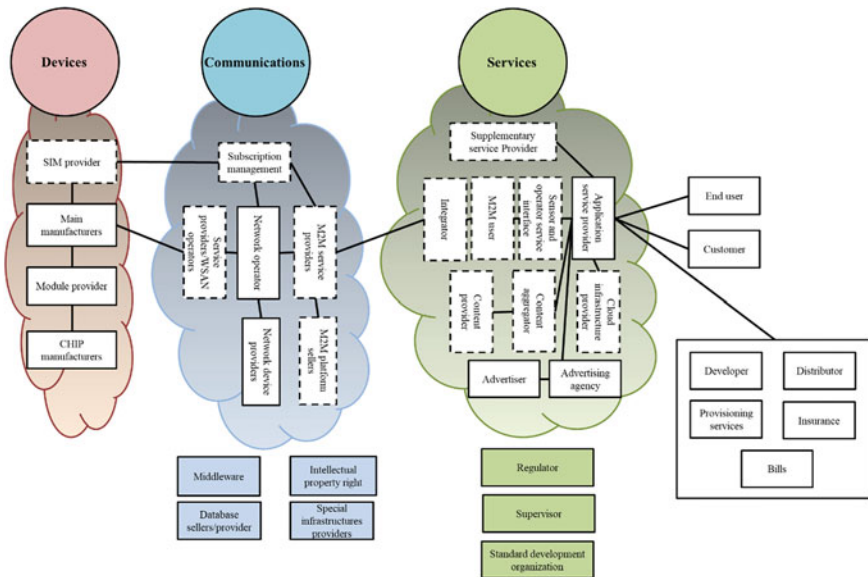Fig. 17.5 Proposed MSS system architecture based on IoT in smart grids [38]

Fig. 17.6 Maps in IoT ecosystem [39]

(14)   Prosumers

In traditional power systems, the actors can be referred to as either generators or consumers. Today, renewable energy resources, storage and Demand Response (DR) allow the consumer to generate and store energy. This leads to an emerging new type of customers known as prosumers. In fact, in smart grids, the consumer, generator, and storage are integrated, and the preconditions for microgrid formation are provided [39]. Prosumers not only consume energy but also share excess energy generated by renewable energy resources with the grid or other consumers.

17.7   New Businesses in IoT-Based Distribution Networks

Structurally, business ecosystems can generally have a star structure with a hub or a flat mesh structure. The star structure is the usual model in the United States of America. In this model, it is assumed that the ecosystem communicate with a large number of small suppliers through a central hub. Moreover, the flat model of the business ecosystem that is common in Europe is made up of a large number of small and medium enterprises, but at the same time able to match to the largest one.

A business ecosystem includes social interactions of companies and individuals with their social and economic environment, in which companies are usually competed and cooperated with their main assets (related to the physical and the virtual world of the Internet). The main assets may be hardware and software products, platforms, or standards. The focus of standards should be on connected devices, their communications, software services made on these connections or services required to provide them, warranty, as well as billing for the services.

Generally, IoT consists of three components of devices, communications, and services, which are not necessarily homogeneous, but work together with the ultimate aim of IoT. In terms of role and responsibility, in addition to the abovementioned cases, the rols related to the life cycle of the product or service, including development, distribution, supply, guarantee, and billing, should not be avoided. Other essential functions include legislation, supervision, standardization, and other institutions that directly or indirectly affect IoT [40].

17.7.1   The Conceptual Model of the Smart Grid and Its Components

The conceptual model of the smart grid is in fact the basis of the analysis of the features, use, behavior, relationships, requirements and smart grid standards. This model does not only show the ultimate architecture of the smart grid, but is also a tool for describing that architecture. The smart grid conceptual model provides
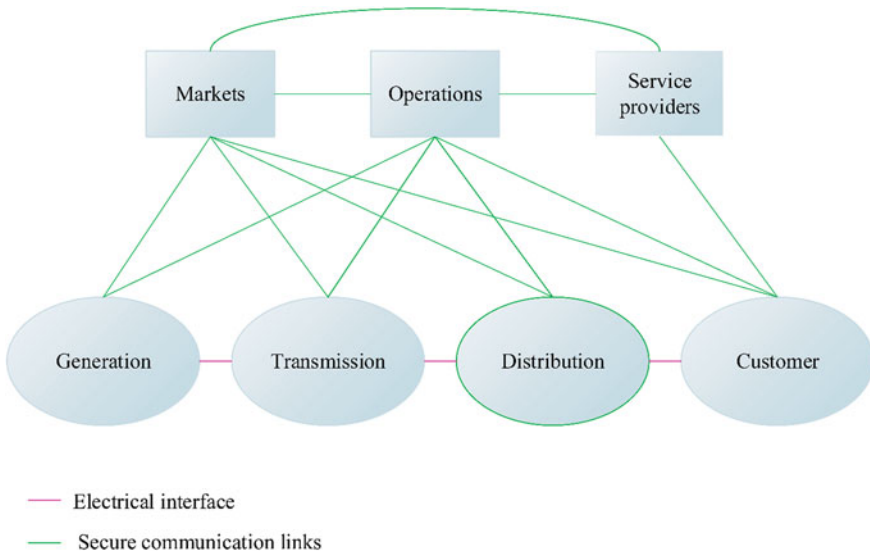
Fig. 17.7 High-level smart grid conceptual model [41]

ground for mutual analysis to develop smart grid architecture. The smart gird model is depicted in Fig. 17.7. Here, components are displayed as clouds.

The conceptual model has several components, each of which includes many applications and actors connected by the associations, with many interfaces. Actors may be devices, computer systems, software programs, or their owner organizations. The ability to decide and exchange information between actors is possible through interfaces. The tasks performed by actors inside the components forms the applications, some of them are carried out by a single actor and others in collaboration with several actors. In general, actors have similar targets. Telecommunication in a similar component may have the same characteristics and requirements. Components may also include elements of other sectors. Relationships are logical communication between actors, which creates two-way communication. At each end, there is a continuity of an interface for an actor. The interface shows electrical or telecommunication connections. In Fig. 17.7, electric relationship and telecommunication interfaces are shown with red and green lines, respectively. Each of these interfaces may be two-way. Telecommunication interfaces indicate the exchange of information between two components and the actors inside them, indicating physical connections. Still, they show logical connections in the information network of different components of the smart grid.

The following table has described the components of the conceptual model of smart grids (Table 17.5).

It is important to note that the smart grid model is not limited to a specific component, application, or specific sample. The use of the term smart grid in some cases refers only to automation distribution, while in other cases, it stands for advanced

Table 17.5 Components in the smart grid conceptual model [41]

Components	Actors
Customers	They are the final consumers of electricity. Customers may also generate, store and manage energy consumption. There are generally four types of customers in the smart grid: home, commercial, residential and industrial
Market	Operators and participants are in the electricity market
Service providers	Organizations that provide services to customers and offices
Operations	The managers of the electricity chain
Mass production	Power generators are large-scale producers. They may also store energy for later distribution
Transmission	Transmits mass-generated electricity over long distances. It can also store and generate electricity
Distribution	Distributors of electricity to and from customers. It can also store and generate electricity
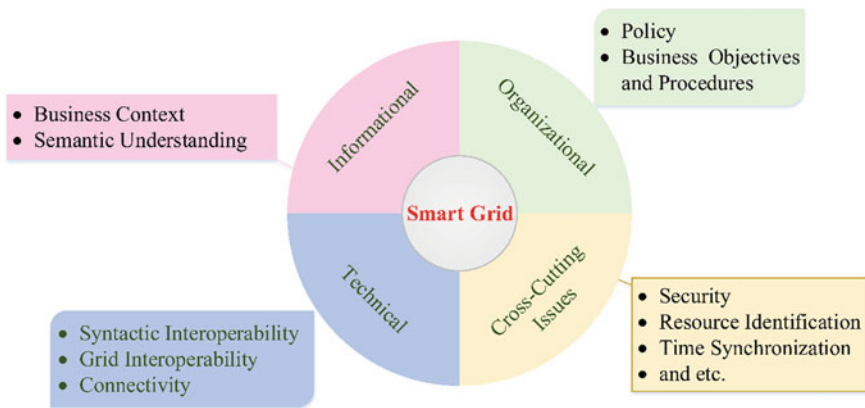
Fig. 17.8 Smart grid conceptual model and GWAC collaboration[4] framework [41]

measurement. In the conceptual model of the smart grid, it is assumed that network smartness includes a wide range of applications.

In general, the smart grid and its components, can be investigated through four dimensions including organizational, informational, technical, and mutual requirements aspects. These dimensions, as well as the energy and information flows are demonstrated in Fig. 17.8. However, gridwise architecture, the layers of this framework can be interpreted as a subset of actors, components and interfaces in the model.

---

[4] Grid Wise Architecture Council.

17.7.2   Identifying Businesses Related to IoT-Based Smart Distribution Network

To simplify the extraction of IoT-based smart grid business models, IoT business companies are divided into five general categories: Device supply companies, Communication companies, Service providers, Product/service life cycle companies, Supervision companies, and others.

17.7.3   Business Model Canvases on IoT-Based Smart Distribution Network

In the IoT-based smart distribution network, smart distribution business and IoT are merged. In fact, the variety and volume of activities in the smart grid, especially the distribution sector, are such that internet service providers (ISPs) can purely focus on works and activities in this sector. Therefore, there exist sixteen main business model canvases in the IoT-based distribution networks, listed below in accordance with Table 17.6.

1. The business model canvas of IoT device supply companies
2. The business model canvas of communication companies
3. The business model canvas of service providers

Table 17.6 IoT-based smart distribution network businesses

		Prosumers and distributed generations	Market operations
IoT-based smart distribution network businesses	Smart distribution network businesses	Aggregation	Retail
		Installation and maintenance of the network and the customer facilities	Financial services
		Storages	Network operation
		Design, manufacture, and equipment supply	Education, technology research, and human resources
	IoT businesses	Device supply companies	Communication companies
		Service providers	Companies providing product/service life cycle
		Supervision companies	Auxiliary map

4.   The business model canvas of product/ services life cycle companies
5.   The business model canvas of Supervision companies
6.   The business model canvas of IoT auxiliary companies
7.   Prosumers business model canvas and distributed generation resources
8.   Business model canvas of market-related companies
9.   Aggregator business model canvas
10. Retail business model canvas
11. The business model canvas related companies with installation, smart distribution network maintenance
12. The financial business model canvas
13. The storage business model canvas
14. Network operating business model canvas
15. The business model canvas of companies designing, manufacturing, and supplying equipment
16. Business model canvas of companies active in the field of education, technology research, and human resources.

17.7.4   IoT-Based Smart Distribution Network Problems and Challenges

Given that the IoT-based smart grid is an emerging technology and has not yet reached puberty, there are significant challenges ahead. Therefore, it is necessary to pay special attention to these challenges so that this technology can provide fine services to its consumers. In the following, the challenges in this area are discussed [36].

(1)   Different working conditions and devices with limited capabilities

IoT-based smart grid systems are subject to different operating conditions. Therefore, providing the requirements for reliability, accessibility, compatibility with hybrid communication technologies and signal coverage in adverse environmental conditions is of particular importance. IoT solutions for self-improvement and self-organization should also be considered. For example, when a set of IoT devices have difficulty communicating, the alternative path should be chosen by the IoT self-improvement feature so that the reliability of the smart grid is not compromised.

(2)   Energy Consumption

In IoT-based smart grids, IoT terminals and sensors are supported by batteries in many applications. Therefore, energy consumption of this equipment is a serious problem for the realization of IoT applications in the smart grid. Consequently, it is necessary to design suitable energy storage sources for IoT equipment and power generation equipment and energy conversion. Currently, the new generation of batteries can last more than ten; however, there are still limitations in the energy consumption of this equipment.

(3) Safety against severe environmental conditions

IoT devices are exposed to extreme electromagnetic conditions in some smart grid applications. Therefore, the protection of this equipment and the use of new technologies with the capabilities of resistance to dust, water, electromagnetic waves, vibration, and high and low temperatures in the construction of IoT devices and their chips should be considered for longer life.

(4) Communication Networks

Throughout the communication paths, from the equipment to the local network, then to the gateways, then to the central server, and finally to the cloud, different communication protocols are used every time. Furthermore, the reliability and speed of communication are of a lot of importance. Therefore, despite compression techniques and various networks, IoT-based smart grid systems should be provided with comprehensive network support.

(5) Data Fusion

IoT equipment In IoT-based smart grids, resources and storage, bandwidth, processing, and battery capacity are limited. Therefore, IoT devices cannot transfer all the data to the gateway for data collection because it requires a lot of bandwidth and energy consumption. In general, the only optimal solution is to use the data synthesis process to filter and collect only helpful information from multiple IoT devices. This will increase productivity and save energy and bandwidth.

(6) Congestion

Congestion causes packets to be delayed and lost, both of which are essential parameters in the performance of an IoT-based smart grid. Because some smart grid applications are sensitive to latency, it is crucial to minimize communication latency in these systems. For many IoT-based smart grid systems, more simultaneous messages should be sent from multiple devices without delay or loss of packets. This does not mean increasing bandwidth, but rather minimizing the messages sent by IoT devices to each HAN gateway, for which the number of nodes and gateways must be carefully selected.

(7) Ability to cooperate and integrate packages

Interoperability is defined as the ability of two or more heterogeneous networks/devices to exchange information and use the information exchanged in a standard function. IoT-based smart grid systems consist of a large number of different IoT devices and gateways that differ in specifications, functionality, and resources, as well as communication stacks and protocols. Lack of interoperability and coordination of devices is a severe obstacle to IoT-based smart grids. One of the proposed solutions to help achieve smart grids is to convert proprietary protocol networks to IP-based networks.

(8)   Big Data control

In addition to creating higher costs associated with storing and processing large volumes of data, the integration of IoT technology with the smart grid imposes a more significant burden on IoT communication networks. Information in the smart grid includes energy consumption, customer load demand, recorded data of advanced meters, power line errors, etc. Using bandwidth and high data rates, as proposed by LTE, increases the ability to carry data but creates bottlenecks elsewhere. As a result, power utilities need to design systems with better capabilities for storing, managing, and processing collected data.

(9)   Need for standardization

Standardization is essential for compatibility, interoperability, reliability, and security. Although research on IoT and IoT standardization has been ongoing, no specific IoT-based standardization activities have been conducted to date. Although the standardization of IoT data collection, under the name One M2M, is underway, it has not been well received, and the energy industry views it as an added burden and unsuitable for limited devices. The OMA standard for LWM2M[5] has become more popular due to its simplicity.

De facto standards have appeared organically on the web with the widespread use of what are commonly referred to as open-source or open-access software components. Although these standards may eventually be applied to IoT-based smart grid systems, security issues still require more immediate solutions which are not covered by these standards.

(10)   Security issues

Extensive use of IoT technology in smart grids can lead to various security vulnerabilities. Since the monitoring and control of IoT-based smart grid systems is done in the open Internet, and this space has no more security than Internet-based security and lower security than managed mobile and fixed networks, Therefore, it is more vulnerable to cyber-attacks. An attacker can upset the real-time balance between energy production and energy consumption by altering data generated by smart objects or sent by power utilities, causing significant financial losses to the power utility and customers. At present, probabilistic analysis in the IoT-based smart grids has been proposed and considered to increase security. Security considerations that should be prioritized for IoT-based smart grids include:

- Limited resources
- Privacy
- Trust management
- Authentication and access permission
- Data integrity
- Cyber-attacks
- Scalability

---

[5] Lightweight M2M.

- Reliability
- Identification.

17.8 Conclusions

This chapter gives an overview of IoT and its associated business models. In general, IoT is a concept to describe a not-so-distant future in which physical objects connect to the World Wide Web and interact with other objects. In order to implement IoT, it is necessary to go through four stages of data collection, data transmission through the communication network, evaluation and estimation of data, and meeting the needs of users. Nowadays, IoT has entered various fields and has the ability of making all such systems smart. Therefore, topics with major priority, such as existing architectures, operating systems, data collection to above issues, storage, management and processing, networking, platform, technologies, and IoT security, were discussed in this chapter.

Due to the effects of IoT elements on each other and their interactions, and also due to the pervasiveness of this concept in other areas such as health, agriculture, etc., different ecosystems have been proposed in order to identify and study more actors and their relationships in IoT. After introducing the IoT technology, the smart grid, actually the most modern type of IoT-based smart grid, and related concepts are considered. Also, this chapter gives information on the architecture of the smart grid, its infrastructure and components, and in particular, the smart distribution network. The effects of IoT on the distribution network include the management of electric vehicles (EVs), aggregation of distributed energy resources (DERs), smart distribution substations, demand-side management (DSM), DR, and many other factors that increase the efficiency of the distribution network and the entire power system.

In the latter part of the chapter, the IoT business ecosystem and the conceptual model of the smart grid, besides their businesses, are investigated. In fact, by extracting the businesses of each of them and further combining them, the business model canvas related to the IoT-based smart distribution network was obtained. Finally, the problems and challenges of the IoT-based smart distribution network were pointed out and described.

References

1. A. Zakaria-zadeh, Energy and load management modeling in Iran smart metering systems (In persian), Iran Energy Efficiency organization
2. H. Arasteh, V. Hosseinnezhad, V. Loia, A. Tommasetti, O. Troisi, M. Shafie-khah, P. Siano, IoT-based smart cities: a survey, in *16 IEEE International Conference on Environment and Electrical Engineering (EEEIC)* (Florence, Italy, 2016)
3. A. Afuah, *Business Models: A Strategic Management Approach* (McGraw-Hill, 2003)
4. F. Betz, Strategic business models. Eng. Manag. J. **14**, 21–28 (2002)
5. R. Amit, C. Zott, Value creation in E-business. Strateg. Manag. J. **22**(6–7), 493–520 (2001)

6. P. Timmers,Business models for electronic markets. Electron. Mark. **8**(2) (1998)
7. E.M. Roche, Place to space: migrating to E-business models. J. Glob. Inf. Technol. Manag. **4**, 70–71 (2001)
8. H. Chesbrough, R.S. Rosenbloom, The role of the business model in capturing value from innovation: evidence from xerox corporation's technology spin-off companies. Ind. Corp. Chang. **11**(3), 529–555 (2002)
9. E. Faber, P. Ballon, H. Bouwman, T. Haaker, O. Rietkerk, M. Steen, Designing business models for mobile ICT services, in *16th Bled Electronic Commerce Conference* (2003)
10. M. Rappa, Business models on the web: managing the digital enterprise, in *North Carolina State University* (2001)
11. S. Shafer, H. Jeff Smith, J.C. Linder,The power of business models. Bus. Horiz. **48**(3), 199–207 (2005)
12. T. Nordlund, M. Tallberg, H. Hämmäinen, Scenarios for management of digital homes, in *Telecommunication Techno-Economics* (2007)
13. A. Osterwalder, Y. Pigneur, *Business Model Generation: A Handbook for Visionaries, Game Changers, and Challengers* (Wiley, 2010)
14. B. Demil, X. Lecocq, Business model evolution. in search of dynamic consistency. Long Range Plan. **43**(2–3), 227–246 (2010)
15. H. Meier, R. Roy, G. Seliger, Industrial product-service systems-IPS2. CIRP Ann. Manuf. Technol. **59**(2), 607–627 (2010)
16. J. Gao, Y. Yao, V.C.Y. Zhu, L. Sun, L. Lin, Service-oriented manufacturing: a new product pattern and manufacturing paradigm. J. Intell. Manuf. **22**(3), 435–446 (2009)
17. J. Forrest et al., *Systems Science: methodological Approaches* (2013)
18. A. Leitão, P. Cunha, F. Valente, P. Marques, Roadmap for business models definition in manufacturing companies. Procedia CIRP **7**, 383–388 (2013)
19. C.M. DaSilva, P. Trkman, Business model: what it is and what it is not. Long Range Plan. **47**(6), 379–389 (2014)
20. M.B. Dehnavi, Internet of things technologies (In Persin), General Department of Communications and Information Technology of Qom Province
21. M.H. Amini, H. Arasteh, P. Siano,Sustainable smart cities through the lens of complex interdependent infrastructures: Panorama and state-of-the-art, in *Sustainable Interdependent Networks II: From Smart Power Grids to Intelligent Transportation Networks, Studies in Systems, Decision and Control*, vol. 186 (Springer International Publishing, 2019), pp. 45–68
22. L. Min, K.A. Alnowibet, A.F. Alrasheedi, F. Moazzen, E.M. Awwad, M.A. Mohamed,A stochastic machine learning based approach for observability enhancement of automated smart grids, Sustain. Cities Soc. **72** (2021)
23. M. Zarei, *Applications of the Internet of Things* (ICT Research Institute)
24. M. Boland,IoE and IoT getting everything to happen, in *Cisco Systems* (IoT Asia, Singapore, 2014)
25. S. Li, L. Da Xu, S. Zhao, The internet of things: a survey. Inf. Syst. Front. **17**(2), 243–259 (2014)
26. A. Torkaman, M.A. Seyyedi, Analyzing IoT reference architecture models. IJCSSE **5**(8), 154 (2016)
27. H. Cai, B. Li, L. Jiang, A. Vasilakos, IoT-based big data storage systems in cloud computing: perspectives and challenges. IEEE Internet Things J. **4**, 75–87 (2017)
28. S.H. Verma, Y. Kawamoto, Z. Fadlullah, H. Nishiyama, N. Kato, A Survey on network methodologies for real-time analytics of massive IoT data and open research issues. IEEE Commun. Surv. Tutor. **19**, 1457–1477 (2017)
29. A. Riahi Sfar, E. Natalizio, Y. Challal, Z. Chtourou,A roadmap for security challenges in internet of things. Elsevier J. Digit. Commun. Netw. **4**(2), 118–137 (2017)
30. H. Yeganeh, H. Sabaei, M. Dindoost, Analysis of communication technologies with the aim of identifying IoT-related orientations in the field of communication technology (In Persian). Res. Inst. Commun. Inf. Technol. (2015)

31. A. Gupta, R.K. Jha, A survey of 5G network: architecture and emerging technologies. IEEE Access **3**, 1206–1232 (2015)
32. S. Parhoudeh, A. Baziar, P.E. Lopez, F. Moazzen,Optimal stochastic energy management of smart city incorporating transportation system and power grid. IEEE Trans. Ind. Appl. (2020)
33. S.M. Banifatemeh, M. Rabbani, S Ebrahim-Nejad, *Smart Grid—The Future of Power Industry* (In Persian) (Noon, 2015)
34. C. Danekas, C. Neureiter, S. Rohjans, M. Uslar and D. Engel,Towards a model_driven-architecture process for smart grid projects, in *Springer Conference Paper* (2014)
35. D. Baimel, S. Tapuchi, N. Baimel,Smart grid communication technologies. J. Power Energy Eng 1–8 (2016)
36. Y. Saleem, N. Crespi, M. Rehmani, R. Copeland,Internet of things-aided smart grid: technologies, architectures, applications T prototypes and future research direction. IEEE Access (2019). arXiv:1704.08977
37. K. Billewicz, P. Wroclawska, Possibility of internet of things technology implementation in smart power grids. Energetyka **5** (2016)
38. R.V. Jadhav, S.S. Lokhande, V.N. Gohokar, Monitoring of transformer parameters using internet of things in smart grid. in *International Conference on Computing Communication Control and Automation (ICCUBEA)* (2016), pp. 1–4
39. S. Grijalva, M.U. Tariq, Prosumer-based smart grid architecture enables a flat, sustainable electricity industry, in *ISGT Conference* (2011), pp. 1–6
40. O. Mazhelis, H. Warma, S. Leminen, P. Ahokangas, P. Pussinen, M. Rajahonka, R. Siuruainen, H. Okkonen, A. Shveykovskiy, J. Myllykoski,Internet of things market, value networks, and business models: state of the art report, in *Computer Science and Information Systems Reports. TR, Technical reports* (2013)
41. Electric Power Research Institute (EPRI), Report to NIST on the smart grid interoperability standards roadmap (2009)

Chapter 18
Modeling the Energy Storage Systems in the Power System Studies

Mohammad Reza Sheibani, Golam Reza Yousefi, Habibollah Raoufi, and Niki Moslemi

Abstract Today, energy storage systems (ESSs) have become attractive elements in power systems due to their unique technical properties. The ESSs can have a significant impact on the growth of the presence of renewable energy sources. Growing the penetration of ESSs, in addition to creating different capabilities in the power system, will also lead to challenges. Therefore, the development of the ESSs and their operation requires accurate studies. The focus of this chapter is on modeling the ESSs in the power system studies. For this purpose, different storage technologies are studied at the first section. In this section, by investigating the characteristics of the different ESS technologies, the characteristics of each of them that should be considered in modeling are assessed. Studies show that similar modeling for all ESS technologies will affect the accuracy of the results. After that, the modeling methodologies of the ESSs will be presented. For this purpose, the proposed models are presented for ESS expansion planning and operation planning. In the expansion planning studies, the capacities and location of the ESSs are usually determined. The storage capacities include the power and energy capacities of the ESSs. In the operation planning studies, the status and amount of charge and discharge of the ESSs are determined at any time. The needful formulations for modeling the behavior of ESSs in each of the expansion and operation planning studies will be studied in this section. For this purpose, in addition to reviewing the proposed methods in the previous studies, the necessary suggestions will be provided.

M. R. Sheibani (✉) · H. Raoufi · N. Moslemi
Power Systems Operation and Planning Research Department, Niroo Research Institute (NRI), Tehran, Iran
e-mail: msheibani@nri.ac.ir

H. Raoufi
e-mail: hraoufi@nri.ac.ir

N. Moslemi
e-mail: nmoslemi@nri.ac.ir

G. R. Yousefi
Department of Electrical and Computer Engineering, Isfahan University of Technology, Isfahan, Iran
e-mail: yousefi@cc.iut.ac.ir

18.1   Introduction

In the past years, electrical energy was produced by the conventional fossil fuel power plants with relatively high generation capacity and transported and delivered to consumers through transmission systems and distribution networks. Planning and decision making in such integrated system was done by the power system operator. Nowadays, power systems due to recent changes, such as the restructuring, distributed and renewable generation integration and micro-grids emergence, encounter with new challenges. The issues pertaining to system security, stability, output power fluctuations of renewable energy resources, reliability and energy transfer difficulties are the most critical ones. The energy storage systems (ESSs) are one of the available equipment that can help power system decision makers to solve these challenges. The ESSs by adding flexibility and controllability to different levels of the power systems can play an important role in achieving the power systems planning goals [1–5].

In this book chapter, the modeling of the ESSs in the power system studies is investigated. First, the important features of the ESSs are discussed. Then, the types of the ESSs used in the power systems are introduced. Afterwards, the applications of the ESSs in the power systems are reviewed. Then, some effective characteristics of the ESSs are modeled. Finally, a proposed formulation for the ESSs modeling in the power systems studies is presented.

18.2   Introduction of Energy Storage Systems

In this section, to introduce the ESSs, at first the most critical technical and economic characteristics of the ESSs in the planning studies are discussed. Then different technologies of the ESSs are reviewed and finally, the application of the ESSs in different levels of the power systems is studied.

18.2.1   Technical and Economic Characteristics

Operational and economic characteristics of the ESSs are the main specification to decide to utilize these elements in the power systems. A number of these characteristics are as follows.

- Power capacity: Maximum instantaneous power of charge or discharge of the ESSs [6].
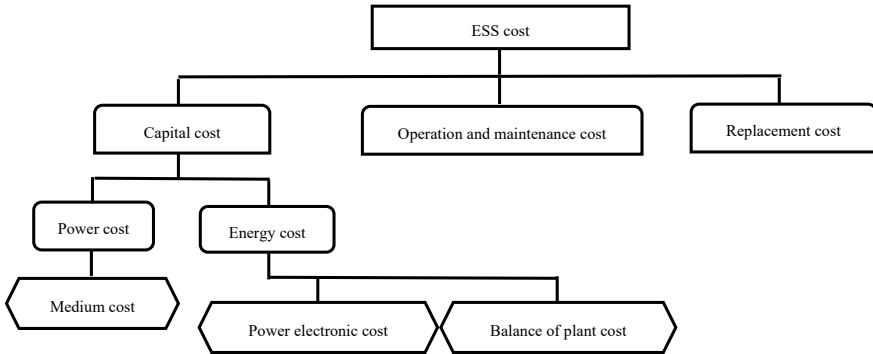
Fig. 18.1 ESS costs classification

- Energy capacity: Maximum amount of energy of the ESSs, available to charge or discharge [6].
- Life time: Life time of an ESS indicates the time span from the beginning of its utilization time. The number of cycling capacity which denotes the charging/discharging cycles of the ESS affects the life time [7].
- Energy efficiency: The ratio denoting on the amount of releasing energy during the discharging period to the amount of absorbed energy during the charging period [8, 9].
- Self-discharge: The amount of energy consumed internally by the ESS [10, 11].
- Cost: One of the key characteristics in the ESS planning studies. Figure 18.1 classifies the ESS costs into some subcategories. The ESS costs consist of capital cost, operation and maintenance cost and replacement cost [6]. The capital cost includes two terms related to power and energy costs. The first term is for storage medium and proportional to storage power capacity. The second term consists of power electronics related costs used in the ESS and costs related to balance of plant, proportional to the ESS capacity. Each ESS needs to be replaced completely or partially after its lifetime expires and the replacement cost is considered to state this matter [12].

18.2.2   Classifications

The ESSs, depending on their types of technology, store electrical energy and deliver it to consumers through an energy conversion procedure [29]. According to this principle, the ESSs can be classified from different aspects. One of the most conventional classifications is done according to energy storage techniques. Electrical energy can be stored in the form of four kinds of energies: mechanical, electrical, chemical and thermal. Figure 18.2 presents a classification of the ESS technologies. Brief description of each ESS technology is as follows.
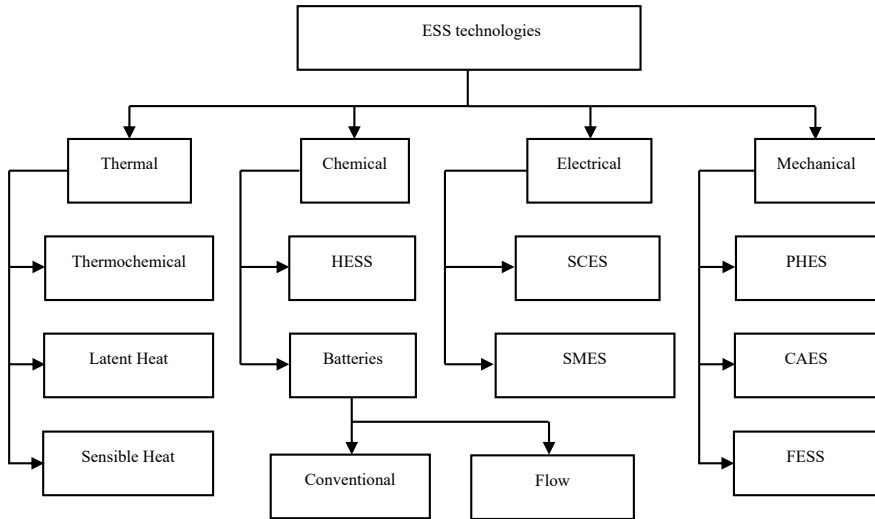
Fig. 18.2 ESS types classification

- Mechanical energy storage system: In this technology, energy is stored in the form of potential energy or kinetic energy. Pumped hydroelectric energy storage (PHES), compressed air energy storage (CAES) and flywheel energy storage (FES) systems are the most significant types.

  - Pumped hydro energy storage: PHES is the oldest, largest and most dominant form of the ESS. It consists of two water reservoirs with different elevations. During the charging process water from lower reservoir is pumped up to the upper one. In the discharging process, the water is released from the upper reservoir and flows through hydro turbines connected to generators and electrical energy is generated [13].
  - Compressed air energy storage: CAES is the second largest ESS technology used in the power systems. In this technology, compressed air is stored in a high pressure. During the discharging process, compressed air is released through a turbine and produced electrical energy [14].
  - Flywheel energy storage: In this storage system, electrical energy is stored in the form of kinetic energy. In the flywheels, a rotating mass is turning around a shaft. During the charging process, the system works as a motor, and in discharging process it works as a generator and converts kinetic energy to electrical [15].

- Electrical energy storage system: In this technology, electrical energy is stored in electric or magnetic fields. Super capacitors energy storage (SCES) and superconducting magnetic energy storage (SMES) are the known types.

- Super capacitor energy storage system: In these devices, energy is stored in the electric field. It operates same as the conventional capacitor. To increase the capacitance, super capacitors use polarized liquid layers and porous material on the surface area of electrodes [16].
- Superconducting magnetic energy storage: In this type of storage, energy is stored in the magnetic field produced by DC current circulating through the superconducting coil. To reduce resistive losses, the coil is kept in at low temperature superconducting state, by means of helium or nitrogen cooling systems [17].

- Chemical energy storage: In this technology, electrical energy is stored in the form of chemical energy. Different types of batteries are presented below [7, 18].

  - Lead-acid (LA)
  - Nickel-metal hybrid (Ni-MH)
  - Lithium-ion (Li-ion)
  - Nickel–cadmium (Ni–Cd)
  - Sodium-sulfur (NA-S)
  - Flow battery energy storage: This type of electrical energy storage is a relatively new method. Flow batteries principle of operation is similar to conventional batteries, based on reversible electrochemical reactions, with the difference that, to start reaction, electrolytes stored in two separate tanks are pumped to cell. To obtain specific level of output voltage, cells can be used in series, parallel or combined configurations. Vanadium redox (VRB), polysulphide bromide (PSB) and zinc bromine (ZBB) are the best known types of these batteries [19, 20].
  - Hydrogen energy storage (HESS): In this chemical energy storage technology, during charging process, hydrogen produced from water electrolysis is compressed and stored. To create energy from hydrogen, during the discharging process two conventional methods are used: internal combustion engine and fuel cell [21].

- Thermal energy storage: In this type of the ESSs, energy can be stored in the form of thermal energy. There are three types of storage: reversible chemical reaction heat storage, latent heat storage and sensible heat storage [22, 23].

  - Chemical reaction heat storage: in this energy storage technology, electrical energy is stored and released through a reversible chemical reaction.
  - Latent heat storage: In this technology, energy is absorbed and stored as latent heat during phase transition, and released during the reverse transition.
  - Sensible heat storage: In this storage technology, heat is stored as temperature growth with no phase transition.

18.2.3 Applications in Power Systems

The ESSs due to their ability to be charged by excessive energy absorption and inject it to the system during the discharging process are utilized in different levels of the power systems. Table 18.1 represents the characteristics and applications of the ESSs in the power systems [7, 14, 15, 20, 24–28]. Some applications of the ESSs are presented in the following.

- Renewable energy resources integration growth: The most significant issue in the renewable energy resources integration is their accessible and unlimited nature. Decrease pollution and fossil fuel consumption are the other advantages of renewable energy resources integration. During recent years, many countries through adopting various persuasive policies, like investment financial supports and tax incentives, try to extend these resources utilization. However, these power generation resources lead to some difficulties. One of the most important difficulties is due to their unpredictable and variable nature, such as wind speed and solar radiation which result in output power of these resources. These factors affect reliability, power quality and stability. The ESSs by eliminating the aforementioned difficulties enhance the penetration level of these resources [29–31]. This realizes by renewable energy resources adaption to consumption, output fluctuation smoothing, and supportive resources procurement beside renewable energy resources [32, 33]. The ESSs supporting the renewable energy resources typically have 100 kW–40 MW power capacity and a few seconds to several minutes' response time [13]. According to Table 18.1, PHES, CAES and batteries are the most appropriate technologies for this case.

- Load levelling and peak shaving: The ESSs can be charged by purchasing electric energy, available during off-peak periods. The stored energy can be used or sold during peaking periods. The ESSs with seasonal or weekly energy storage capability can extend this concept to long term. The system suitable for this task must have several MWs power storage capacity and a few minutes response time [13]. According to data presented in Table 18.1, PHES, CAES, batteries, TES, and HES are the most appropriate technologies for this case. The other ability of the ESSs, resulting in their operational strategies, is the peak shaving concept, which leads to energy arbitrage, by means of inexpensive power purchasing and saving during off-peak periods and selling it at peak hours and high prices [34, 35]. The system suitable for this task must have 100 kW–100 MW power storage capacity and a few minutes response time [13]. According to Table 18.1, the ESS technologies suitable for this case are the same as the load leveling application.

- Power quality improvement: The ESSs have an effective role to improve power quality indices such as transient phenomena like voltage sag and swells and protect sensitive electrical devices [36]. The ESSs suitable for power quality improvement must have up to 1 MW power storage capacity and a quarter of a cycle response time [13]. According to Table 18.1, FES, batteries, SMES, and SCES are the most appropriate technologies for this application.

Table 18.1 The specifications of the ESSs

Energy storage technology		Capital cost	Energy rating (MWh)	Power rating (MW)	Cycling capability	Response time	Life (years)	Energy efficiency (%)	Application category
Mechanical	FESS [15]	400–800 ($/kWh)	0.025–5	0.1–20	1×10^5–1×10^7	<1 Cycle	20	85	Power quality Voltage regulation
	CAES [7]	2–50 ($/kWh)	2860	5–300	1×10^4–3×10^4	Sec-min	20–40	41–75	Integration of renewable re-sources Peak shaving Load leveling Spinning reserve Transmission upgrade deferral Black start
	PHES [25]	5–100 ($/kWh)	400–5000	10–5000	2×10^4–5×10^4	Sec-min	40–60	65–80	Integration of renewable re-sources Peak shaving Load leveling Transmission upgrade deferral reserve
Electrical	SCES [21]	7200 ($/kWh)	0.01	0.05–0.25	5×10^5–1×10^6	<1/4 Cycle	8–17	65–90	Power quality Voltage regulation

(continued)

Table 18.1 (continued)

Energy storage technology			Capital cost	Energy rating (MWh)	Power rating (MW)	Cycling capability	Response time	Life (years)	Energy efficiency (%)	Application category
		SMES [20]	560–740 ($/kWh)	0.015	1–100	1×10^4–1×10^5	<1/4 Cycle	20	80–95	Power quality Spinning reserve Voltage regulation Load following
Chemical	Batteries	Lead-acid [15]	200–600 ($/MWh)	0.001–40	0.05–10	200–1800	<1/4 Cycle	5–15	70–80	Power quality Integration of renewable re-sources Peak shaving
	Flow batteries	Li-ion [19]	900–1300 ($/kWh)	0.0015–50	0.015–50	1500–3500	¼ cycle-sec	14–16	78–88	Load leveling Spinning reserve
		Ni–Cd [15]	400–2400 ($/kWh)	6.75	45	3500	¼ cycle-sec	13–20	72	
		Na-S [25]	260–300($/MWh)	0.4–244.8	0.05–34	2500	<s	10–20	75–87	Transmission upgrade deferral
		VRB [21]	600 ($/kWh)	2–120	0.2–12	1000–13,000	<1/4 Cycle	10–20	65–88	
		ZBB [19]	500 ($/kWh)	0.1–4	0.1–2	2000–2500	<1/4 Cycle	5–10	65–85	Black start Voltage regulation Load following
		PSB [21]	131–303 ($/kWh)	0.005–120	0.1–15	3000	20 ms	15	60–75	

(continued)

Table 18.1 (continued)

Energy storage technology	Capital cost	Energy rating (MWh)	Power rating (MW)	Cycling capability	Response time	Life (years)	Energy efficiency (%)	Application category
HESS [21]	0.6–1 ($/kWh)	120	0.3–50	2×10^4	¼ cycle-sec	15	35–42	Integration of renewable re-sources Peak shaving Load leveling Black-start Transmission upgrade deferral Spinning reserve Load following
Thermal [43]	0.1–100 ($/kWh)	Up to 2000	0.1–200	–	Slow response	5–40	50–100	Peak shaving Load leveling Transmission upgrade deferral Black star

- Transmission upgrade deferral: Optimally located ESSs and their effective operation can delay or even in some cases avoid investment in transmission system upgrade. The ESSs do this by means of congestion relief through transmission lines [37, 38]. The ESSs suitable for this task must have 10–100 MW power storage capacity and less than a minute response time [13]. According to Table 18.1, CAES, batteries TES, and HES are the most appropriate technologies for this case.
- Ancillary services procurement: The ESSs due to their rapid response time are able to provide some ancillary services such as voltage regulation and load following, in order to mitigate the voltage and frequency instabilities issued by renewable energy resources integration [33, 39]. The ESSs with short term power supply ability can provide reserve capacity, in the form of spinning, non-spinning and supplemental reserve for the power system. The ESSs, providing reserve power capacity within the power system, can be used to restore the power system after a collapse. This ability is called black start capability [40]. The ESSs, providing voltage regulation typically have several MWs power capacity and a few milliseconds response time [13]. According to Table 18.1, SMES, SCES, flywheels and batteries are suitable for this application. The ESSs used for the load following typically have several MWs power capacity and a few seconds response time [13]. Table 18.1 shows that SMES, HESS and batteries are good candidates for this case. The ESSs used for spinning reserve procurement typically have several MWs power capacity and few seconds response time [13]. SMES, HESS, CAES and batteries are suitable for this application. The ESSs, providing black start capability typically have more than 40 MWs power capacity and up to one minute response time [13]. TES, HESS, CAES and batteries are suitable for this case.

18.3 Modeling the ESS's Specifications

In this section, some of the main specifications of the ESSs are investigated. Also, how they are modeled in power systems' studies is examined.

18.3.1 State of Charge

The state of charge (SOC) is an important feature that determines the amount of energy stored in the ESSs. The SOC limitation between the minimum and maximum stored energy allowed for the ESSs is one of the important constraints in the ESS operation studies. Indeed, the SOC is a critical specification in the energy management decisions for the ESSs [41].

The SOC of an ESS is usually defined as the ratio of its current stored energy ($E(t)$) to the nominal energy capacity (E^{nominal}) as follows [41]:

Table 18.2 The properties of the SOC estimation methods [41, 44]

Method	The basis of the method	Mathematical methods
Direct measurement	Calculating the physical properties of the ESSs such as the voltage and impedance	– Open circuit voltage method – Terminal voltage method – Impedance method – Impedance spectroscopy method
Book-keeping estimation	Integrating the discharging current over time	– Coulomb counting method – Modified Coulomb counting method
Adaptive systems	Adjusting the SOC for different discharging conditions	– BP neural network – RBF neural network – Support vector machine – Fuzzy neural network – Kalman filter
Hybrid methods	Combining different estimation methods	– Coulomb counting and EMF combination – Coulomb counting and Kalman filter combination – Per-unit system and EKF combination

$$SOC(t) = \frac{E(t)}{E^{\text{nominal}}} \tag{18.1}$$

In (18.1), the SOC is calculated as per unit. In the power systems studies the $E(t)$ and E^{nominal} are measured in watt-hours (Wh). However, in a large number of power system studies, the SOC is defined as the current energy in terms of Wh [42, 43].

Estimating the SOC for the ESSs, especially chemical ESSs, is relatively complex [41]. Different methods have been proposed to estimate the SOC. The common classification of these methods is as follows:

1. Direct measurement
2. Book-keeping estimation
3. Adaptive systems
4. Hybrid methods.

The properties of these methods are summarized in Table 18.2.

18.3.2   Depth of Discharge

The depth of discharge (DOD) is usually defined to determine the level of discharging which an ESS is allowed to go to that level. According to this definition for the DOD, the SOC of the ESS is limited as follows:

$$(1 - \text{DOD}) \times E^{\text{max}} \leq \text{SOC}(t) \leq E^{\text{max}} \qquad (18.2)$$

where the E^{max} is the energy capacity of the ESS.

Due to the effect of DOD on the lifetime of the ESSs, especially batteries, it is recommended that they not be fully discharged. Therefore, many battery manufacturers determine a maximum recommended DOD for optimal performance of the battery.

In the above definition, the DOD is applied to limit the minimum SOC. However, in some studies the minimum DOD is specified to limit the maximum SOC [45]. Thus, the SOC is limited as follows:

$$(1 - \text{DOD}_{\text{max}}) \times E^{\text{max}} \leq \text{SOC}(t) \leq (1 - \text{DOD}_{\text{min}}) \times E^{\text{max}} \qquad (18.3)$$

According to the above constraint, the DOD specifies the ESS's operation range in the SOC.

Due to the significant effect of the DOD on the ESS's operation life time and on the other hand its storage capability, determining the optimal DOD value is one of the main challenges of the studies in the field of the ESSs, especially batteries. Increasing the DOD usually reduces battery life time but increases storage capacity. For example, if a NaS battery is operated at 100% DOD, the life cycle number will be 2500 cycles, while at 50% DOD the life cycle number rises up to 7000 [46]. But for 50% DOD, half of the energy capacity of the battery will be unused.

18.3.3 Efficiency

In the storage process, some energy is lost which leads to reduced storage efficiency. The energy flow in a sample ESS is shown in Fig. 18.3. Equipment related to the charging and discharging processes imposes losses on the ESS. The efficiency of the charging and discharging processes (η_{ch} and η_{dis}) are usually considered individually. If the self discharge of an ESS is ignored, the ESS efficiency, which is commonly known as round-trip efficiency (η_{rt}), is defined as the product of the charging and discharging efficiencies as follows.
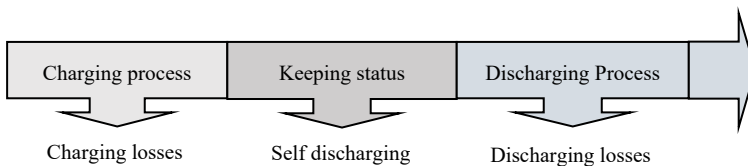
Fig. 18.3 The energy flow of a sample ESS

$$\eta_{\mathrm{rt}} = \eta_{\mathrm{ch}} \times \eta_{\mathrm{dis}} \tag{18.4}$$

It is usually assumed that charging and discharging efficiencies are equal. Therefore, the following relationship will be established [47].

$$\eta_{\mathrm{ch}} = \eta_{\mathrm{dis}} = \sqrt{\eta_{\mathrm{rt}}} \tag{18.5}$$

The self discharge can be ignored for PHES, CAES, and Li-ion batteries, but this assumption is not true for all the ESS technologies. For example the daily self discharge of the Na-s battery, SCES, and FESS is about 20%, 30%, and 100%, respectively [48]. In this case, the self discharge must be considered in calculating the SOC. Thus, the SOC at any time step (t) is determined as follows [49]:

$$\mathrm{SOC}(t) = (1 - \mathrm{SDR}) \times \mathrm{SOC}(t-1) + \eta_{\mathrm{ch}} \times E_{\mathrm{in}}(t) - \frac{1}{\eta_{\mathrm{dis}}} \times E_{\mathrm{out}}(t) \tag{18.6}$$

where SDF is self discharge rate and $E_{\mathrm{in}}(t)$ and $E_{\mathrm{out}}(t)$ are the input and output energies of the ESS.

18.3.4 Life Time

Life time is an important indicator in the ESS's operation and expansion planning studies in power systems. In addition to the time duration limit (life time), the ESSs also face the limitation of charge and discharge cycles (cycle life).

Completion of authorized charge and discharge cycles may occur earlier than the allowable storage time duration limit. Therefore, in the planning studies, the ESSs' life time and the limitation of the charge and discharge cycles are simultaneously considered.

DOD has a significant effect on the cycle life of the ESSs. Therefore, the cycle life of the ESSs is usually determined for a given DOD. The cycle life of a li-ion battery against DOD is plotted in Fig. 18.4 [50]. It can be seen that for a DOD of 10%, the cycle life is 30000 cycles, but when DOD reaches 80%, the cycle life will be 5000. Therefore, the decision to determine DOD in the operation planning of the ESSs is very important and effective.

In some studies the relationship of the cycle life (*CL*) and DOD is modeled as follows [47, 50]:

$$\mathrm{CL} = a_1 + a_2 e^{a_3.\mathrm{DOD}} + a_4 e^{a_5.\mathrm{DOD}} \tag{18.7}$$

where a_1–a_5 are the fitting constants that can be determined based on the information of the ESSs provided by the manufactures [51].

Fig. 18.4 Cycle life a li-ion battery versus DOD
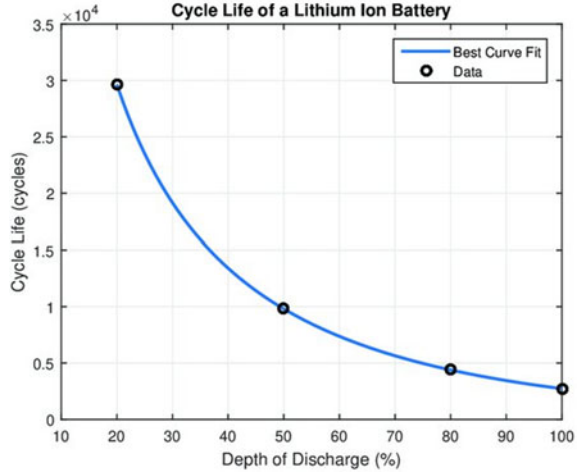
18.4 Modeling the ESS in the Power System Studies

The expansion and operation planning are the main decisions about the ESSs. These decisions can be made from different perspectives. Power system planners usually seek to minimize costs, but the ESS's owners seek to maximize profits.

In the following, a number of conventional modeling for the ESSs planning is presented.

18.4.1 ESSs Expansion Planning from the Power System Planner's Point of View

It is assumed that the system planner intends to determine the optimal capacity of the ESSs. Expansion planning for the other elements of the power system, such as energy resources and transmission lines, is usually done at the same time. In addition to energy arbitrage, the ESSs also have the ability to provide ancillary services. In this section, spinning reserve is considered as an example of ancillary services.

The objective function of an ESS expansion planning problem is as follows:

$$
\min\left(\left(\overbrace{AC^s}^{1} + \overbrace{AC^{s,o}}^{2} + \overbrace{AC^{s,O\$M}}^{3}\right) + \left(\overbrace{AC^{e,i}}^{4} + \overbrace{AC^{e,o}}^{5} + \overbrace{AC^{e,O\$M}}^{6}\right)\right) \quad (18.8)
$$

where terms 1, 2, and 3 model the annualized investment cost, annualized operation cost, and annualized operation and maintenance cost of the ESS, respectively. Also,

terms 4, 5, and 6 model the annualized investment cost, annualized operation cost, and annualized operation and maintenance cost of the other elements of the power system such as energy resources and transmission devices, respectively.

Annualized investment cost and operation cost of the ESS can be determined as follows:

$$AC^s = \overline{P^s} \times \text{AC}^{p,s} + \overline{E^s} \times \text{AC}^{e,s} + \overline{E^s} \times \text{AC}^{r,s} \tag{18.9}$$

$$AC^{s,o} = \sum_{d=1}^{D} \frac{365}{D} \sum_{t=1}^{T} \left(P_{dt}^{s,\text{ch}} \times \text{MC}^{s,\text{ch}} + \left(P_{dt}^{s,\text{dis}} + R_{dt}^{s,\text{dis}} \times D_{dt}^{s,\text{dis}} \right) \times \text{MC}^{s,\text{dis}} \right) \tag{18.10}$$

where $\overline{P^s}$ and $\overline{E^s}$ are the power and energy capacities of the ESS, respectively; $\text{AC}^{p,s}$, $\text{AC}^{e,s}$, and $\text{AC}^{r,s}$ are the annualized investment cost of the power interface unit, the annualized investment cost of the storage unit, and the annualized replacement cost of the storage unit, respectively; d is the time period index; t is the time step index; D is the number of time period in each year; T is the number of time step in each time period; $P_{dt}^{s,\text{ch}}$ is the charging power of the ESS at time step t in time period d; $P_{dt}^{s,\text{dis}}$ is the discharging power of the ESS at time step t in time period d; $R_{dt}^{s,\text{dis}}$ is the spinning reserve service providing by the ESS at time step t in time period d; $\text{MC}^{s,\text{ch}}$ is the charging marginal cost of the ESS; $\text{MC}^{s,\text{dis}}$ is the discharging marginal cost of the ESS; $D_{dt}^{s,\text{dis}}$ is the spinning reserve delivery request indicator at time step t in time period d (1 means spinning reserve delivery is requested and 0 means spinning reserve delivery is not requested).

The number of time periods is usually determined based on the storage technology and the power system characteristics. For example, four sample days can be considered as the representative of different seasons. Also, the time step can be considered hourly. Thus, the number of time period and time step will be 4 and 24, respectively.

The constraints of the ESS are as follows [52, 53]:

– **Power balance constraint**:

$$\sum_{t=1}^{T} \eta^{\text{ch}} \cdot (P_{dt}^{s,\text{ch}}) = \sum_{t=1}^{T} \frac{1}{\eta^{\text{dis}}} \cdot (P_{dt}^{s,\text{dis}} + R_{dt}^{s,\text{dis}}) \qquad \forall d \tag{18.11}$$

This equation is used to balance the charging and discharging power at each time period d, considering the charging and discharging efficiencies of the ESS.

– **State of charge calculation**:

$$\text{SOC}_{dt} = (1 - \text{SDR}) \times \text{SOC}_{dt-1} + \eta_{ch} \times E_{\text{in},dt} - \frac{1}{\eta_{\text{dis}}} \times \left(E_{\text{out},dt} + R_{dt}^{s} \right) \quad \forall t, \forall d \tag{18.12}$$

where SOC_{td} is the SOC of the ESS at time step t in time period d; $E_{in,dt}$ is the input energy of the ESS at time step t in time period d; $E_{out,dt}$ is the output energy of the ESS at time step t in time period d.

This equation sets the ESS state of charge, at the end of time period t as a function of its SOC at the end of the previous time period and the charging or discharging that took place during the time period.

– **State of charge constraint**:

$$(1 - DOD_{max}) \times \overline{E^s} \leq SOC_{dt} \leq (1 - DOD_{min}) \times \overline{E^s} \qquad \forall t, \forall d \quad (18.13)$$

The minimum and maximum limitation of the SOC is applied with this relationship.

– **Storage power constraint**:

$$0 \leq P_{dt}^{s,ch}, P_{dt}^{s,dis}, R_{dt}^{s,ch}, R_{dt}^{s,dis} \leq \overline{P^s} \qquad \forall t, \forall d \quad (18.14)$$

– **Charging power constraint**:

$$0 \leq P_{dt}^{s,ch} \leq \overline{P^s} \cdot ch_{dt} \qquad \forall t, \forall d \quad (18.15)$$

where ch_{dt} is the ESS charging status indicator at time step t in time period d (1 means charging and 0 means not charging).

– **Discharging power constraint**:

$$0 \leq P_{dt}^{s,dis} + R_{dt}^s \leq P_n^s \cdot dis_{dt} \qquad \forall t, \forall d \quad (18.16)$$

where dis_{dt} is the ESS discharging status indicator at time step t in time period d (1 means discharging and 0 means not discharging).

In Eqs. (18.15) and (18.16) the power of the ESS during the charging and discharging should be lower than the maximum power capacity of the ESS.

– **Simultaneous charging and discharging prevention constraint**:

$$ch_{dt} + dis_{dt} \leq 1 \qquad \forall t, \forall d \quad (18.17)$$

Using this equation, the ESS wouldn't be allowed to be charged and discharged at the same time.

– **Spinning reserve provision constraint**:

$$0 \leq R_{dt}^{s,ch}, R_{dt}^{s,dis} \leq 10.MSR^s \qquad \forall t, \forall d \quad (18.18)$$

$$0 \leq R_{dt}^{s,ch} \leq P_{dt}^{ch} \qquad \forall t, \forall d \quad (18.19)$$

where MSR^s is the maximum sustained ramp rate of the ESS.

ESS can provide spinning reserve in the charging and discharging statues. In the charging statues, the ESS can readily reduce its charging power and consequently reduce the overall system load.

To solve the problem, the constraints of the other elements of the system must also be established.

The presented formulation can be extended to determine the location of the ESSs. For this purpose, the power grid should be considered in the formulations.

18.4.2 ESSs Expansion Planning from the Investor's Point of View

The objective function of the ESS expansion planning from the investor's point of view is maximizing the profit as follows:

$$\max \left(\left(\overbrace{AR^s}^{1} \right) - \left(\overbrace{AC^s}^{2} + \overbrace{AC^{s,o}}^{3} + \overbrace{AC^{s,O\$M}}^{4} \right) \right) \tag{18.20}$$

where the annual revenue of the ESS is obtained by term 1 as follows.

$$AR^s = \sum_{d=1}^{D} \frac{365}{D} \sum_{t=1}^{T} \left(\left(P_{dt}^{s,\mathrm{dis}} + R_{dt}^{s,\mathrm{dis}} \times D_{dt}^{s,\mathrm{dis}} \right) \times \rho_{dt}^{e} + \left(R_{dt}^{s,\mathrm{dis}} \right) \times \rho_{dt}^{\mathrm{sr}} \right) \tag{18.21}$$

where ρ_{dt}^{e} and ρ_{dt}^{sr} are the energy and energy prices at time step t in time period d, respectively. If the ESS capacity is relatively small and has no effect on the market price, The ESS can be considered price taker and ρ_{dt}^{e} and ρ_{dt}^{sr} are considered as the input of the model. Otherwise, the ESS must be considered price maker. In this case, the prices will be determined within the model.

18.4.3 ESSs Operation Planning

In the operation planning of an ESS, the SOC of the ESS is determined for each time step in the intended time period. To model the system operation planning problem, it is sufficient to eliminate the investment costs in the expansion planning problem. Therefore, the objective function of the ESS operation planning problem from the system operator's point of view is as follows.

$$\min\left(\overbrace{C^{s,o}}^{1} + \overbrace{C^{e,o}}^{2}\right) \qquad (18.22)$$

where

$$C^{s,o} = \sum_{t=1}^{T} P_t^{s,\mathrm{ch}} \times \mathrm{MC}^{s,\mathrm{ch}} + \left(P_t^{s,\mathrm{dis}} + R_t^{s,\mathrm{dis}} \times D_t^{s,\mathrm{dis}}\right) \times \mathrm{MC}^{s,\mathrm{dis}} \qquad (18.23)$$

and $C^{e,o}$ is the operation cost of the other elements in the power system. The constraints of the operation planning problem are the same as the relationships (18.11)–(18.19) for the intended time period.

The objective function of the ESS operation planning problem from the owner's point of view is as follows.

$$\max\left(\overbrace{R^{s}}^{1} - \overbrace{C^{s,o}}^{2}\right) \qquad (18.24)$$

where

$$R^{s} = \sum_{t=1}^{T} \left(\left(P_t^{s,\mathrm{dis}} + R_t^{s,\mathrm{dis}} \times D_t^{s,\mathrm{dis}}\right) \times \rho_t^{e} + \left(R_t^{s,\mathrm{dis}}\right) \times \rho_t^{\mathrm{sr}}\right) \qquad (18.25)$$

18.5   Conclusion

In present chapter, the modeling of the ESSs in the power systems studies was investigated. Different ESS technologies were classified and introduced. Also, the main characteristics of the ESSs that are effective in their planning were introduced and modeled. These characteristics consisted of SOC, DOD, efficiency, and life time. Afterward, the ESS planning problems were formulated. For this purpose, the ESS planning problems were divided to two categories: ESS expansion planning and ESS operation planning. The ESS expansion and operation planning problems were modeled from the point view of the system planner and investor.

References

1. S. Gill et al., Maximising revenue for non-firm distributed wind generation with energy storage in an active management scheme. IET Renew. Power Gener. **7**(5), 421–430 (2013)
2. Y. Zheng et al., Optimal allocation of energy storage system for risk mitigation of Discos with high renewable penetrations. IEEE Trans. Power Syst. **29**(1), 212–220 (2014)
3. T. Basbous et al., Optimal management of compressed air energy storage in a hybrid wind-pneumatic-diesel system for remote area's power generation. Energy **84**, 267–278 (2015)
4. M.R. Sheibani, A. Moshari, Operation planning of a microgrid considering the resiliency in the presence of energy storage systems, in *10th Smart Grid Conference (SGC)* (2020)
5. M.R. Sheibani et al., Energy storage system expansion planning in power systems: a review. IET Renew. Power Gener. **12**, 1203–1221 (2018)
6. M. Leahy, An investigation into the energy storage technologies available, for the integration of alternative generation techniques. Energy Storage Report, 2007. Department of Physics, University of Limerick (2007)
7. E. Rodrigues et al., Energy storage systems supporting increased penetration of renewables in islanded systems. Energy **75**, 265–280 (2014)
8. X. Luo et al., Modelling study, efficiency analysis and optimisation of large-scale adiabatic compressed air energy storage systems with low-temperature thermal storage. Appl. Energy **162**, 589–600 (2016)
9. W.W. Wang, L.B. Wang, Y.L. He, The energy efficiency ratio of heat storage in one shell-and-one tube phase change thermal energy storage unit. Appl. Energy **138**, 169–182 (2015)
10. J. Sun et al., Investigations on the self-discharge process in vanadium flow battery. J. Power Sour. **294**, 562–568 (2015)
11. T. Tevi, A. Takshi, Modeling and simulation study of the self-discharge in super-capacitors in presence of a blocking layer. J. Power Sour. **273**, 857–862 (2015)
12. R. Dufo, J. Bernal, Techno-economic analysis of grid-connected battery storage. Energy Convers. Manag. **91**, 394–404 (2015)
13. X. Luo et al., Overview of current development in electrical energy storage technologies and the application potential in power system operation. Appl. Energy **137**, 511–536 (2015)
14. T.M.I. Mahlia et al., A review of available methods and development on energy storage; technology update. Renew. Sustain. Energy Rev. **33**, 532–545 (2014)
15. H. Zhao et al., Review of energy storage system for wind power integration support. Appl. Energy **137**, 545–553 (2015)
16. M. Mufti et al., Super-capacitor based energy storage system for improved load frequency control. Electr. Power Syst. Res. **79**, 226–233 (2009)
17. M. Sander et al., LIQHYSMES storage unit—Hybrid energy storage concept combining liquefied hydrogen with superconducting magnetic energy storage. Int. J. Hydr. Energy **37**, 14300–14306 (2012)
18. S. Koohi-Kamali et al., Emergence of energy storage technologies as the solution for reliable operation of smart power systems: a review. Renew. Sustain. Energy Rev. **25**, 135–165 (2013)
19. P.J. Hall, E. Bain, Energy-storage technologies and electricity generation. Energy Policy **36**, 4352–4355 (2008)
20. A. Poullikkas, A comparative overview of large-scale battery systems for electricity storage. Renew. Sustain. Energy Rev. **27**, 778–788 (2013)
21. G. Taljan et al., The feasibility of hydrogen storage for mixed wind-nuclear power plants. IEEE Trans. Power Syst. **23**(3), 1507–1518 (2008)
22. H. Zhang et al., Thermal energy storage: Recent developments and practical aspects. Prog. Energy Combust. Sci. **53**, 1–40 (2016)
23. Thermal energy storage, technology brief. Int. Renew. Energy Agency. IEA-ETSAP and IRENA© Technology Brief E17 (2013)
24. X. Tan, Q. Li, H. Wang, Advances and trends of energy storage technology in micro-grid. Int. J. Electr. Power Energy Syst. **44**(1), 179–191 (2013)

25. F. Gonzalez et al., A review of energy storage technologies for wind power applications. Renew. Sustain. Energy Rev. **16**, 2154–2171 (2012)
26. N.S. Hasan et al., Review of storage schemes for wind energy systems. Renew. Sustain. Energy Rev. **21**, 237–247 (2013)
27. A. Chauhan, R.P. Saini, A review on integrated renewable energy system based power generation for stand-alone applications: Configurations, storage options, sizing methodologies and control. Renew. Sustain. Energy Rev. **38**, 99–120 (2014)
28. D.O. Akinyele, R.K. Rayudu, Review of energy storage technologies for sustainable power networks. Sustain. Energy Technol. Assess. **8**, 74–91 (2014)
29. J. Barton, D. Infield, Energy storage and its use with intermittent renewable energy. IEEE Trans. Energy Convers. **19**(2), 441–448 (2004)
30. A. Zahedi, Maximizing solar PV energy penetration using energy storage technology. Renew. Sustain. Energy Rev. **15**, 866–870 (2011)
31. L.H. Koh et al., Operational adequacy studies of a PV-based and energy storage stand-alone micro-grid. IEEE Trans. Power Syst. **30**(2), 892–900 (2015)
32. G. Suvire, M. Molina, P. Mercado, Improving the integration of wind power generation into AC micro-grids using flywheel energy storage. IEEE Trans. Smart Grid **3**(4), 1945–1954 (2012)
33. C. Martinez et al., Impacts of energy storage on short term operation planning under centralized spot markets. IEEE Trans. Smart Grid **5**(2), 1110–1118 (2014)
34. A. Lamont, Assessing the economic value and optimal structure of large-scale electricity storage. IEEE Trans. Power Syst. **28**(2), 911–921 (2013)
35. R. Sioshansi et al., Estimating the value of electricity storage in PJM: arbitrage and some welfare effects. Energy Econ. **31**, 269–277 (2009)
36. S. Mohod, M. Aware, Micro wind power generator with battery energy storage for critical load. IEEE Syst. J. **6**(1), 118–125 (2012)
37. R. Poudineh, T. Jamasb, Distributed generation, storage, demand response and energy efficiency as alternatives to grid capacity enhancement. Energy Policy **67**, 222–231 (2014)
38. Y. Zhang, S. Zhu, A.A. Chowdhury, Reliability modeling and control schemes of composite energy storage and wind generation system with adequate transmission upgrades. IEEE Trans. Sustain. Energy **2**(4), 520–526 (2011)
39. G. Delille, B. Francois, G. Malarange, Dynamic frequency control support by energy storage to reduce the impact of wind and solar generation on isolated power system's inertia. IEEE Trans. Sustain. Energy **3**(4), 931–939 (2012)
40. P. Poonpun, W. Jewell, Analysis of the cost per kilowatt hour to store electricity. IEEE Trans. Energy Convers. **23**(2), 529–534 (2008)
41. M. Danko et al., Overview of batteries state of charge estimation methods. Transp. Res. Procedia **40**, 186–192 (2019)
42. F. Luo et al., Coordinated operational planning for wind farm with battery energy storage system. IEEE Trans. Sustain. Energy **6**(1), 253–262 (2015)
43. R. Fernandez-Blanco et al., Optimal energy storage siting and sizing: A WECC case study. IEEE Trans. Sustain. Energy **8**(2), 733–743 (2017)
44. W.Y. Chang, The state of charge estimating methods for battery: a review. ISRN Appl. Math. (2013). Article ID 953792
45. H. Hajipour, M. Bozorg, M. Fotuhi-Firuzabad, Stochastic capacity expansion planning of remote micro-grids with wind farms and energy storage. IEEE Trans. Sustain. Energy **6**(2), 491–498 (2015)
46. E.M.G. Rodrigues et al., Modelling and sizing of NaS (sodium sulfur) battery energy storage system for extending wind power performance in Crete Island. Energy **90**, 1606–1617 (2015)
47. J. Xiao et al., Sizing of energy storage and diesel generators in an isolated micro-grid using discrete fourier transform (DFT). IEEE Trans Sustain Energy **5**(3), 907–916 (2014)
48. A. Evans, V. Strezov, T. Evans, Assessment of utility energy storage options for increased renewable energy penetration. Renew. Sustain. Energy Rev. **16**, 4141–4147 (2012)
49. M. Ghofrani et al., Energy storage application for performance enhancement of wind integration. IEEE Trans. Power Syst. **28**(4), 4803–4811 (2013)

50. R.K. Mallan, F. Assadian, B. Fu, Analysis of on-board photovoltaics for a battery electric bus and their impact on battery lifespan. Energies. **10**(943), 1–32 (2017)
51. J. Xiao et al., Determination of the optimal installation site and capacity of battery energy storage system in distribution network integrated with distributed generation. IET Gener. Transm. Distrib. **10**(3), 601–607 (2016)
52. M.R. Sheibani, G.R. Yousefi, M.A. Latify, Stochastic price based coordinated operation planning of energy storage system and conventional power plant. J. Modern Power Syst. Clean Energy **7**, 1020–1032 (2019)
53. M.R. Sheibani, G.R. Yousefi, M.A. Latify, Economics of energy storage options to support a conventional power plant: a stochastic approach for optimal energy storage sizing. J. Energy Storage **33**, 101892 (2021)